Conference Proceedings

Contents: (click titles to navigate)

2. Emissions of regulated and unregulated pollutants from light-duty gasoline vehicles using different ethanol blended fuels
3. Air Quality and Health Benefits from Fleet Electrification in China: Future Perspectives through 2030

Air Quality and Health Impact

1. An Efficient Scheme for Urban Air Quality Estimates and Projections
2. Effects of traffic related abatement policies on Swiss air quality trends
3. Comprehensive analysis of European vehicular primary NO2 trends
4. Health impact of PM10, PM2.5 and BC exposure due to different source sectors in Stockholm, Gothenburg and Umea, Sweden
5. Impact of excess NOx emissions from diesel cars on air quality, public health and eutrophication in Europe
6. Impacts and mitigation of excess diesel-related NOx emissions in 11 major vehicle markets

Air Traffic Particles

1. Assessment of particle emissions from aircraft turbine engines: ground, cruise, and overall flight emissions
2. Impact of alternative fuels on the non-volatile particulate matter mass and number emissions of an aero gas turbine
3. Chemical composition and toxicological properties of ambient particles (PM0.25) from near-airport and urban road traffic sites

Large Scale Emission Data

1. Emission estimation based on cross-sectional traffic data
2. GNSS data-based approach to monitor real-world exhaust emissions at microscopic resolution

Update of Emission Factors for EURO 6 Diesel Passenger Cars for the HBEFA

C. Matzer[1], S. Hausberger[1], M. Rexeis[1], M. Opetnik[1], M. Ramsauer[1], O. Mogg[1] and F. Weger[1]

[1] Institute for Internal Combustion Engines and Thermodynamics, Graz University of Technology, A-8010 Graz, Austria, matzer@ivt.tugraz.at

Abstract

The HBEFA (The Handbook Emission Factors for Road Transport) provides emission factors for road vehicles on several traffic situations for different countries in Europe. The emission factors are based on simulation data for various HBEFA cycles. The simulation is done by the software PHEM (Passenger car and Heavy duty Emission Model) using emission maps created from measurement data.

The last HBEFA update 3.2 was published in July 2014 including already EURO 6 emission classes for diesel and petrol cars based on a limited amount of measured passenger cars, which were available at that time. It was noted, that especially NO_x emissions from the small measured sample may not be representative for the EURO 6 diesel car fleet. Therefore, the HBEFA version 3.3 has been produced and was released in April 2017.

For the HBEFA 3.3 in PHEM a new method to produce engine emission maps from test data ("CO_2 interpolation method") was used. With this method, it is possible to consider also measurement data where the engine load signal is not available or too inaccurate for engine map creation. This is especially useful for RDE (Real Driving Emissions) measurements, where the engine power signal in most of the cases is not available. Using RDE measurements beside chassis dynamometer test data increase the sample size of tested vehicles and improve in general the representativeness of the engine emission maps.

With the extended pool on measurement data due to additional RDE trips, also investigations like ambient temperature influence on NO_x emissions were realised. For that purpose, the measurement data of several conventional diesel EURO 6 cars at different ambient temperatures on road and on chassis dynamometer were used.

To analyse the ambient temperature effect on NO_x isolated from influences of routes and driver behaviour, separate engine emission maps with RDE data measured at different ambient temperatures were created by PHEM with the CO_2 interpolation method. With these maps the CADC (Common Artemis Driving Cycle) was simulated for each vehicle. The different results for the CADC using the maps from different ambient temperatures provide a common basis for the analysis of temperature influences on emissions. Since the CADC is representative for real world driving, the result for the temperature effects shall also be valid for real emission behaviour. The analysis showed a high sensitivity of NO_x emissions against ambient temperature, e.g. from 20 °C to 10 °C the NO_x emissions increase approximately 40 % to 50 %. This high sensitivity was the reason for further investigations based on remote sensing and finally for the implementation in HBEFA 3.3.

For HBEFA 4.1 – which is planned to be elaborated until 2019 – additional investigations regarding ambient temperatures are taken into account. Also investigations with a detailed EAS (Exhaust After-treatment System) model in the PHEM simulation are performed. The EAS simulation may improve the accuracy especially in low load cycles and cold environment since all HBEFA simulations for cars are based on EoT (End-of-Tailpipe) data so far. Special traffic situations, e.g. stop&go traffic or coasting followed by high load phases can result in relative high NO_x levels due to low conversion efficiency resulting from cool down phases of the EAS if the engine has no special heating strategies. To parametrise the SCR (Selective Catalytic Reduction) model in PHEM for such effects measurements in stop&go cycles were performed at TUG (Graz University of Technology).

Introduction

The last HBEFA (Handbook Emission Factors for Road Transport) update was published in July 2014. In the update already the EURO 6 emission classes for diesel and petrol cars based on available measurements of a few passenger cars were included, but it was noted, that especially NO_x emissions from the small measured sample may not be representative for the future EURO 6 fleet. In the meantime, several unexpected software features in diesel emission control systems were detected on one hand and the RDE legislation came in place on the other hand, which shall better control real world emission behaviour of cars.

To check and to update the EURO 6 emission factors with all vehicle emission tests at diesel EURO 6 cars collected around Europe since HBEFA 3.2, the HBEFA 3.3 has been produced. In the course of the work a first assessment of ambient temperature dependency of the NO_x emission factors was made. HBEFA 3.3 is a so-called "quick update", because only the NO_x emission factors for conventional diesel passenger cars have been revised. An update for all exhaust gas components is planned for HBEFA 4.1. Following adaptations from HBEFA 3.2 to 3.3 have been performed:

- New emission factors of EURO 6, EURO 6d-Temp and EURO 6d diesel passenger cars replace the previous emission factors of EURO 6 and EURO 6c from HBEFA 3.2.
- New NO_x emissions factors of EURO 4 diesel cars replace the old ones from HBEFA 3.2. Due to the low effect on the NO_x emission behaviour these results are not be presented in this paper, details are described in the HBEFA report (Hausberger S., Matzer C. 2017), (Keller M., et. al. 2017).
- A correction function for the influence of ambient temperature on NO_x emissions for EURO 4, EURO 5 and EURO 6 diesel cars was introduced.

The update is based on RDE (Real Driving Emissions) and chassis dynamometer measurements. For the effect of ambient temperature on NO_x emissions, also remote sensing data were used.

For HBEFA 4.1 following investigations are ongoing for further improvement of the robustness and accuracy of the emission model PHEM:

- Additional investigations regarding ambient temperature effect on NO_x emission behaviour.
- Generic CO_2 engine map calibration for the CO_2 interpolation method.
- Detailed EAS (Exhaust After-treatment System) simulation to reflect effects of low load driving conditions.

Used simulation tool and method for update of HBEFA emission factors

The emission factors are based on the simulation of a huge number of driving situations and vehicle categories with the simulation tool PHEM (Passenger car and Heavy duty vehicle Emission Model). PHEM is an engine emission map based instantaneous emission model, which has been developed by TUG (Graz University of Technology) since the late 1990's. It calculates fuel consumption and emissions of road vehicles in 1 Hz time resolution for a given driving cycle. The model has already been presented in several publications, e.g. (Hausberger S. et. al. 2009), (Zallinger M. 2010), (Rexeis M. et. al. 2009), (Luz R., Hausberger S. 2009). PHEM simulates the engine power necessary to overcome the driving resistances based on the vehicle longitudinal dynamics, losses in the drive train and power demand to run basic auxiliaries in 1 Hz over any driving cycle. The engine speed is simulated by the transmission ratios and a driver gear shift model. Then basic emission values are interpolated from the engine emission maps. Depending on the vehicle technology, the status of the EAS and dynamic effects on the emission level are considered to increase the model accuracy. With this approach, realistic and consistent emission factors can be simulated for any driving condition since the main physical relations are taken into consideration. E.g. variations in road gradients and in vehicle loading influence the engine power demand and the gear shift behaviour and thus lead to different engine loads over the cycle.

To simulate representative fleet average emissions per vehicle class, representative engine maps are necessary. PHEM produces emission maps by sorting the instantaneously measured emissions into standardised maps according to the actual engine speed and power. To produce representative engine maps from vehicle tests, many vehicles should be included and realistic driving situations should be considered. Consequently, the inclusion of PEMS (Portable Emission Measurement System) data by a newly developed methodology in addition to the chassis dynamometer data is very beneficial for a broader vehicle sample for the PHEM simulation. The new method resolves the typical issue from PEMS tests, where most often no reliable engine torque signal is available. PHEM offers the option to calculate the engine power from the measured CO_2 mass flow and engine speed based on generic engine CO_2 emission maps (Figure 1). These generic maps for different emission concepts have been acquired in a project together with Ricardo-AEA for the European Commission (Hill N., et. al. 2015). These maps contain engine speed, CO_2 flow and engine power relations for different engine technologies. Thus, only the measured engine speed and emissions are necessary to compile engine emission maps. This method, also called "CO_2 interpolation method", was already presented at the International Transport und Air Pollution Conference in Lyon 2016 (Matzer C. et. al. 2016).

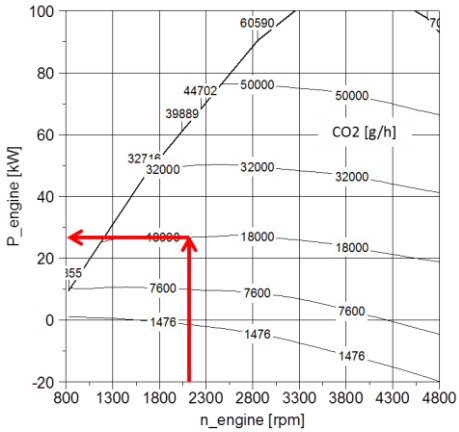

Figure 1: Example for interpolation of engine power from a generic CO_2 map.

The accuracy of the CO_2 interpolation method can be tested by comparing measurement results for cycles driven on the chassis dynamometer with simulation results based on the generic CO_2 maps for these cycles. When the test mass and road load values from the chassis dynamometer setting are used as input for the PHEM simulation, the difference to the measured CO_2 results from:

- Deviations of the vehicle specific map to the generic map.
- Differences in the generic model for losses in the gear box and the axle.
- Differences in the real auxiliary power demand to the generic data used in PHEM.

For the HBEFA 3.3 update only a few results from chassis dynamometer tests were analysed. These showed a CO_2 uncertainty of the generic diesel EURO 6 map up to 20 % using default values for auxiliary power demand and losses in the gear box and the axle. For the quick update no calibration of the generic fuel maps was applied. Deviations in the generic maps lead to inaccurate allocation of the instantaneous emissions to the instantaneous engine power and thus give less reliable emission maps. Therefor for HBEFA 4.1 a calibration of the generic maps in PHEM was developed. By calibrating the PHEM model data to meet the measured CO_2 values, a more representative generic data set can be established. The calibration of the generic or base CO_2 maps is provided for each vehicle used in HBEFA 4.1 where the required data for calibration are available from chassis dynamometer tests. The method for the map calibration is described in the following. Real world cycles including high load operating points like CADC (Common Artemis Driving Cycle), RWC (Real World Cycle) or an ERMES (European Research group on Mobile Emission Sources) cycle can be used for generic map calibration. Using the mass and road load settings from the chassis dynamometer tests PHEM recalculates the tests with the generic CO_2 map. For calibration of the generic map, the simulated CO_2 flow is compared with the measured one. To calibrate the "hot" generic maps only measurement data should be used where the engine is at operating temperature. Figure 2 shows the measured (grey points) and simulated normalized CO_2 values (black points) over normalized engine power for a single diesel passenger car in the CADC. Normalized means, that CO_2 and engine power are divided by rated

power. Since this CADC was cold started, the urban phase was not considered for map calibration. Each dot represents the CO_2 and engine power average over 20 s to avoid uncertainties regarding time alignment due to different gas delay times from engine out to the analysers in full load and idling operating points. The trend lines are described very well by linear equations. These linear equations are called “Veline” (Vehicle efficiency line) and were used already in the past at TUG, e.g. for WLTP corrections (Hausberger S., et. al. 2015) and for corrections in a HVAC (Heating, Ventilation and Air Conditioning) test procedure (Hausberger S., et. al. 2013). The Velines are similar to the well-known Willans-lines but are not restricted to a constant engine speed but to the engine speed range defined by the gear shift logics driven in the cycle. Based on the difference in the Velines functions from measured and simulated data, the calibration function can be determined.

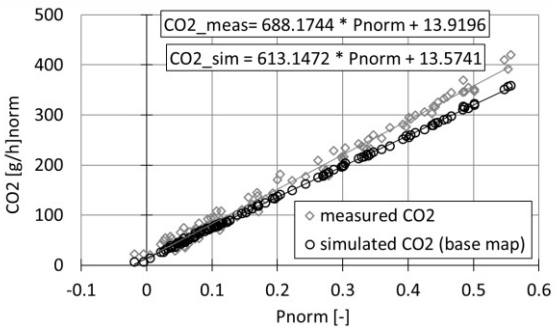

Figure 2: 20 s average of measured and simulated CO_2 and engine power on CADC using the base CO_2 map.

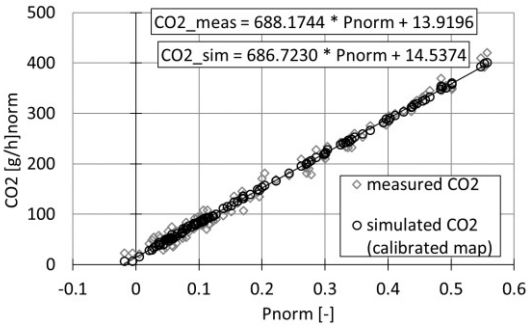

Figure 3: 20 s average of measured and simulated CO_2 and engine power on CADC using calibrated CO_2 map.

To calibrate the generic or base CO_2 map the correction could be done by adding or multiplying a correction function. Investigations showed less uncertainties if the correction function is added. For the data shown in Figure 2 the correction function reads as follows:

$CO_2\_meas(Pnorm) = 688.1744 * Pnorm + 13.9196$	…vehicle specific function	Formula 1
$CO_2\_sim(Pnorm) = 613.1472 * Pnorm + 13.5741$	…vehicle specific function	Formula 2
$\Delta CO_2\_corr(Pnorm) = CO_2\_meas(Pnorm) - CO_2\_sim(Pnorm)$		Formula 3
$CO_2\_corr(Pnorm) = CO_2\_base(Pnorm) + \Delta CO_2\_corr(Pnorm)$	…valid for Pnorm >0	Formula 4

The correction will be done only for normalized engine power >0 to have no influence on the engine drag curve where the CO_2 is zero due to trailing throttle fuel cut-off. Figure 3 shows the simulation result after map calibration. The measured data are similar to the data shown in Figure 2. After the calibration, the trend lines of the measured and simulated data are nearly congruent. Also the CO_2 dependency on engine speed was examined, but this results in less than 1 % improvement of simulated CO_2 for the investigated vehicles. Therefore, no additional calibrations over engine speed are performed. The method of CO_2 map calibration was applied to 3 diesel EURO 6 vehicles so far to test the uncertainties resulting from the generic CO_2 map method. Since for vehicles measured with PEMS only, no calibration of the map is possible, the remaining uncertainty could lead to a less reliable emission map. Table 1 shows the cycles used for map calibration as well as cycles, which were used for validation. As mentioned, the calibration and validation is performed only with cycle data where the engine worked under warm conditions. The ambient temperature was 23 °C for all cycles listed in Table 1.

Table 1: Diesel EURO 6 vehicles used for the calibration of the generic diesel CO_2 map.

ID	Segment	Odometer [km]	Rated engine power [kW]	Used cycle for calibr.	Simulated cycles
Veh_a	C-Segment	34000	81	CADC	1x WLTC, 1x CADC
Veh_b	C-Segment	1300	96	RWC	2x WLTC, 1x RWC
Veh_c	N1-III	6000	132	Ermes	2x WLTC, 1x ERMES, 2x RWC

The results for CO_2 and NO_x are shown in Figure 4 and Figure 5 for the mentioned cycles.

For all 3 vehicles the base CO_2 map underestimates the measured CO_2. As expected, the CO_2 deviations between measurement and simulation is decreasing after calibration, independent which cycle for calibration is used. The CO_2 map calibration influences also the NO_x map creation using the CO_2 interpolation method. For these vehicles the NO_x simulation with the calibrated maps result consequently in higher NO_x. This is referable to the "poorer" CO_2 maps used for the CO_2 interpolation method assuming that the measured NO_x increase with increasing engine power.

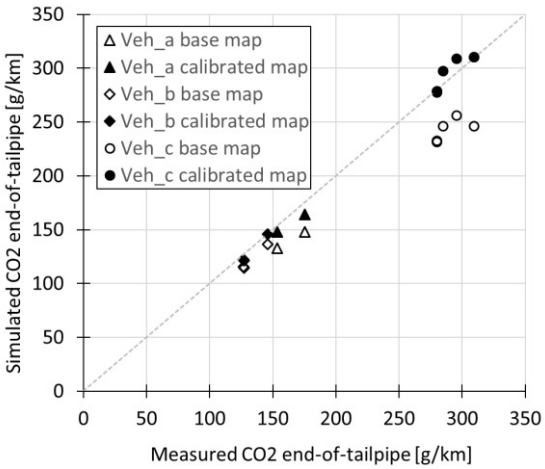

Figure 4: Comparison of simulated and measured CO_2 for 3 different diesel EURO 6 vehicles.

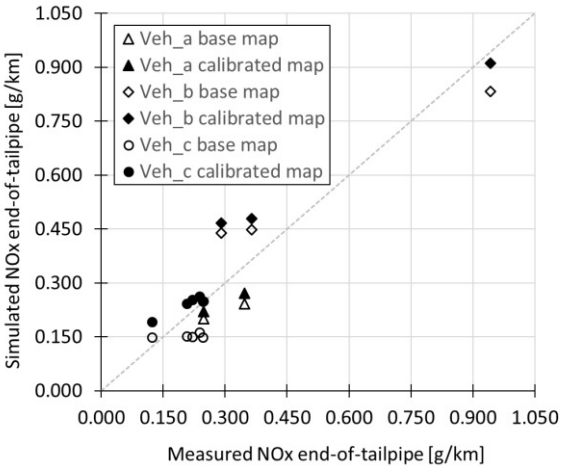

Figure 5: Comparison of simulated and measured NO_x for 3 different diesel EURO 6 vehicles.

In Figure 6 and Figure 7 the average CO_2 and NO_x deviations between simulation and measurement for the listed cycles in Table 1 are presented for each vehicle. For the simulation the generic CO_2 map (= base map, which is the same for all 3 vehicles) as well as the vehicle specific calibrated maps were used. Negative deviation means, that the simulation underestimates the measured values. Also an average deviation of all vehicles is shown, referred to as "Veh_a+b+c". After map calibration the CO_2 deviations are less than 5 %. The NO_x deviations are between -20 % to 20 % using EoT (End-of-Tailpipe) maps without any NO_x calibration. It has to be noted, that the map calibration described allocates also uncertainties in the power demand from auxiliaries to the calibration. Especially in low engine loads the auxiliaries can have a high share in the fuel consumption (correlates with CO_2 emissions), but also vary broadly over time (e.g. smart alternator control) and between vehicle models. The differences in the engine maps of the vehicles are assumed to be less pronounced than the deviations between calibrated and not calibrated data shown in Figure 4.

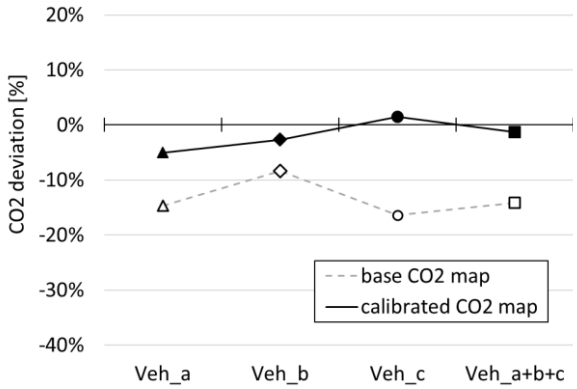

Figure 6: Average CO_2 deviations between simulation and measurement of all cycles per investigated vehicle.

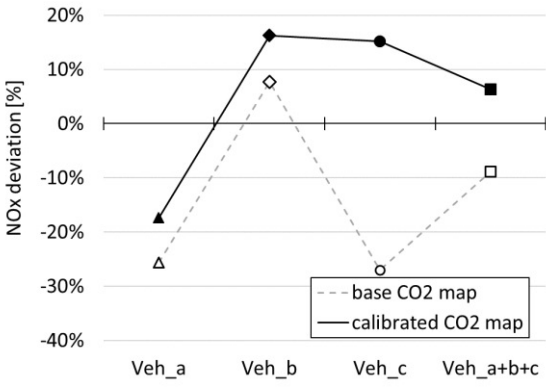

Figure 7: Average NO_x deviations between simulation and measurement of all cycles per investigated vehicle.

As mentioned above, the calibration method was not applied in the model PHEM for the quick update of passenger car NO_x emissions in HBEFA 3.3. As long as the generic CO_2 map used to produce the emission maps meets on average the CO_2 map of the measured vehicles, the error

for the average engine emission map is small since errors from single vehicles are levelled out in the average map. For the 3 vehicles investigated here the effect of the calibration of the generic engine map is an increase in simulated NO_x emissions by approximately 15 % (Figure 7). For HBEFA 4.1 it is planned to use calibrated CO_2 maps where possible.

NO_x emission factors update for HBEFA 3.3

Table 2 gives an overview on the main specifications of the vehicles available for HBEFA 3.3 and the sources of the measured data. The registration numbers refer to the number of new registrations of the particular vehicle from 2013 to 2015 according to the EU-28 CO_2 monitoring database. This is the timeframe where the EURO 6 cars have been introduced. Registration data for 2016 was not available during the work on the update of the PHEM model. The sample of measured vehicle models covers 18 % of the passenger car diesel models registered 2013 to 2015. The registration number is the basis for the weighting of the engine maps for the average engine emission map for PHEM. The registrations consider the number of new vehicles for the mentioned model as well as of variants of this model, e.g. Audi A4 Saloon or Audi A4 Avant. The assumption is that each vehicle in Table 2 represents the NO_x emission behaviour for all model variants of this vehicle.

Table 2: Diesel EURO 6 vehicle measurements used in PHEM for HBEFA 3.3 update.

Lab	Make	Model	Rated engine power [kW]	Rated engine speed [rpm]	New registrations [#]
TUG	BMW	X5	180	4000	79756
TUG	BMW	530d	180	4000	11851
TUG	Audi	A4 Allroad	180	4000	306698
TUG	Mazda	CX-5	110	4500	49514
TUG	BMW	320d	120	4000	103691
TUG	Kia	Carens	104	4000	40461
TUG	Audi	Q7	160	4000	37221
TUG	VW	Sharan	110	3500	88353
TUG	Peugeot	508 SW	88	3500	122878
EMPA	VW	Golf VII	81	3200	855277
EMPA	Mazda	CX-5	110	4500	49514
EMPA	BMW	530d	190	4000	11851
EMPA	Mercedes-Benz	GLK 220	125	3200	48060
EMPA	VW	Passat	103	4200	459372
EMPA	Renault	Scenic	96	4000	278320
EMPA	Mini	Cooper	85	4000	18994
EMPA	Mercedes-Benz	A220	125	3400	17357
EMPA	BMW	X3	140	4000	95544
EMPA	Mercedes-Benz	ML 350	190	3600	34730
EMPA	Porsche	Macan	190	4000	25615
EMPA	Peugeot	208 SW	110	3750	340831
ADAC	BMW	118d	110	4000	103691
ADAC	BMW	320d	140	4000	103691
TNO	Ford	Focus	70	3600	326974
TNO	Mercedes-Benz	C220	125	3000	57407

To produce engine emissions maps following steps were executed. The steps should give a rough overview about the update, details are described in the HBEFA 3.3 report (Hausberger S., Matzer C. 2017), (Keller M., et. al. 2017).

1. Preparation of the available modal measurement data of CADC, ERMES, WLTC (Worldwide harmonized Light vehicles Test Cycle) and RWC. Additional to the chassis dynamometer measurements also data of RDE trips have been used. The preparation includes the work for correction of time shift between emissions and load signal, removal of cold start phases and selection of measured data where the average ambient temperature was between 15 °C and 30 °C. Test data at lower temperatures were used to analyse the influences of ambient temperature on NO_x emissions as described later.
2. Engine map creation with the measurement data of each vehicle using the mentioned CO_2 interpolation method. To get one average diesel EURO 6 engine emission map, the single engine emission maps were weighted with the registration numbers listed in Table 2.
3. Calibration of the average EURO 6 engine emission map. The calibration has the target to calibrate the PHEM model, which is based on a limited sample of modal measurement data of vehicle tests to the broader sample of bag results stored in ERMES DB (database). Since the HBEFA 3.3 is a quick update for the NO_x emission behaviour, the calibration was only done for NO_x.
4. Simulation of HBEFA cycles with the average diesel EURO 6 car, which has a total vehicle mass of 1651 kg and an engine power of 99 kW.
5. Assessment of the EURO 6d-Temp and EURO 6d NO_x emission behaviour considering the conformity factors for NO_x on RDE tests.

With the PHEM parameterisation for emission behaviour of EURO 6, EURO 6d-Temp and EURO 6d diesel vehicles, emission factors for the full set of HBEFA driving cycles in combination with all road gradients have been calculated. Figure 8 shows the new NO_x emissions results as function of the average vehicle velocity for the mentioned EURO classes for 0 % road gradient. The NO_x emission results of EURO 6 from HBEFA 3.2 are plotted for comparison. The former EURO 6 emission factors of HBEFA 3.2 are between the actual EURO 6 and EURO 6d-Temp levels. When the emission factors for HBEFA 3.2 were produced, details of the RDE legislation were not defined. The update of emission factors thus improves the representativeness for EURO 6 due to the much larger sample of tested cars and reflects the recent status of the RDE legislation.

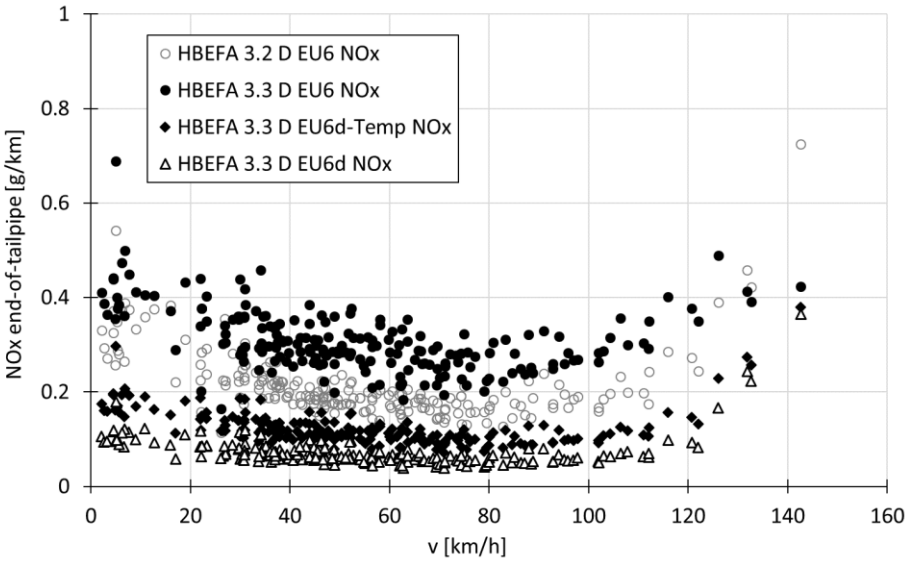

Figure 8: Old (HBEFA 3.2) and new (HBEFA 3.3) NO_x emission factors for diesel EURO 6 cars.

Effect of ambient temperature on NO_x emissions for HBEFA 3.3 and HBEFA 4.1

The NO_x formation can be described with the Zeldovich mechanism, e.g. (Hausberger S., Sams T. 2016) and depends on the temperature and the oxygen concentration at the flame front in the combustion chamber. Higher temperature and sufficient oxygen concentration result in higher NO_x emissions if all other conditions are unchanged. Both parameters can be influenced by different NO_x reduction technologies, e.g. the EGR (Exhaust Gas Recirculation). The EGR uses the properties of inert gas to reduce temperature and oxygen with the recirculation of (cooled) exhaust gas. In Figure 9 the NO_x reduction as function of the oxygen intake is shown. The maximal EGR is limited by an oxygen-available to oxygen-required ratio of 1.3, which represents the soot-emission limit (Hausberger S., Sams T. 2016).

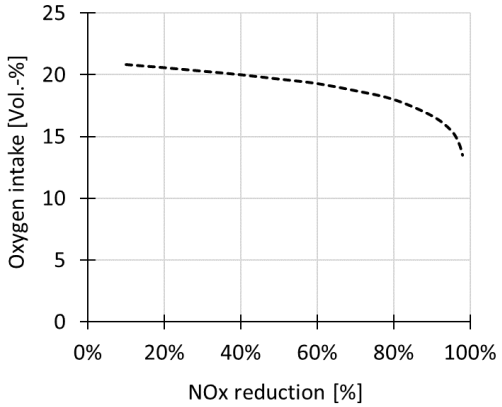

Figure 9: NO_x reduction as function of oxygen intake concentration (Hausberger S., Sams T. 2016).

For conservative technologies lower ambient temperatures result in lower temperature at the flame front and as a consequence in a lower NO_x formation but modern vehicles not necessarily maintain the EGR rates also at lower ambient temperatures. Due to the recirculation of combustion products, the water vapour concentration in the exhaust gas is increasing with the EGR rate. Consequently, lower ambient temperatures are more critical in terms of condensation effects in the EGR path at higher EGR rates. Condensation of water with particles and hydrocarbons in the distillate can cause severe problems, such as interlocking of the cooler or the intake system due to coking. Therefore, it is attractive for the OEM to reduce the EGR to save components in the EGR path. If the EGR rate is reduced at lower ambient temperatures, this results in increased NO_x. Since the type approval test is performed in a temperature range between 20 °C and 30 °C, the EGR rate is typically optimised for this temperature range. Modern diesel cars are typically equipped also with NO_x exhaust gas aftertreatment systems. Since catalytic converters are less efficient at lower temperatures on one hand and the control systems may be less efficient at lower temperatures, also the aftertreatment systems can contribute to NO_x increases at lower temperatures. E.g. the NH_3 dosing may be reduced for SCR (Selective Catalytic Reduction) catalyst while NO_x regeneration may be less frequent in case of NSC (NO_x Storage Catalyst).

The overall effect is also known as “thermal window” but until 2016 only little data were available to investigate the effect of this optimisation on the real world NO_x emissions of the vehicle fleet since almost all vehicle tests were conducted at standard conditions around 25 °C at the chassis dynamometer.

By a systematic analysis of PEMS test data as described in the following and additional chassis dynamometer tests at lower ambient temperatures, a first function for NO_x correction at lower ambient temperatures was elaborated for HBEFA 3.3. Since single vehicles show different behaviour over temperature, the results from the small test sample was seen as possibly not representative for the entire fleet. To base the correction function on a large number of vehicles a method to evaluate remote sensing data on temperature effects was elaborated in the parallel research project CONOX. The HBEFA 3.3 report (Keller M. et. al. 2017) describes the remote sensing data used.

For the investigations based on vehicle testing, measurement data of RDE and chassis dynamometer tests from 6 different diesel EURO 6 vehicles driven at different ambient temperatures have been used. Table 3 shows the investigated diesel EURO 6 vehicles.

Table 3: Diesel EURO 6 vehicle test data used for analysis of the temperature effects on NO_x.

ID	Segment	Odometer [km]	Rated engine power [kW]	Measurements at ambient temperature
Veh_1	C-Segment	5700	73	4 °C and 8 °C
Veh_2	C-Segment	1800	81	-3 °C and 10 °C
Veh_3	C-Segment	2000	100	0 °C and 23 °C
Veh_4	D-Segment	12000	88	5 °C to 23°C
Veh_5	D-Segment	5000	120	0 °C to 28°C
Veh_6	D-Segment	17100	125	8 °C and 19 °C

The NO_x emissions measured end-of-tailpipe are shown in Figure 10. Due to different routes and driver behaviour in PEMS tests, the resulting different engine load cycles overlap the effect of the ambient temperature. Thus, temperature effects cannot be gained directly by comparing PEMS results.

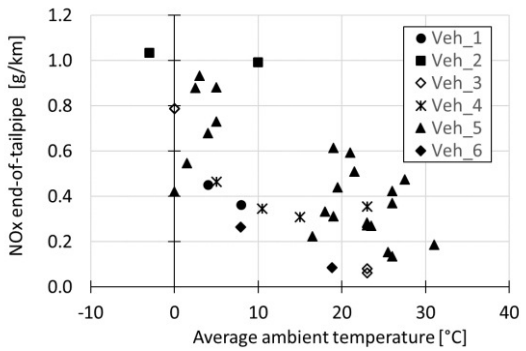

Figure 10: NO_x emissions of different RDE and chassis dynamometer tests from six different EU6 diesel cars, measured EoT.

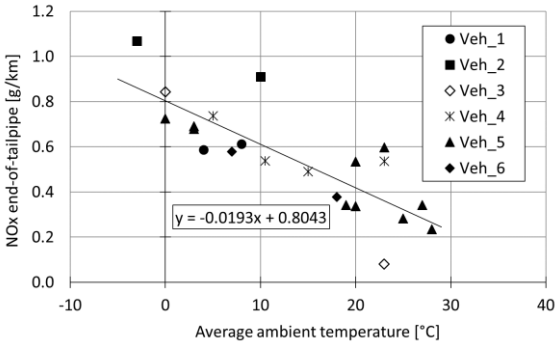

Figure 11: NO_x EoT emissions simulated with PHEM for the vehicles from Figure 10 on the CADC cycle.

To analyse the ambient temperature effect on NO_x isolated from mentioned influences, separate engine emission maps with RDE data measured at different ambient temperatures were created by PHEM using the CO_2 interpolation method. Measured trips in similar ambient temperature ranges were summarized in one map, e.g. measured trips with veh_5 at 19 °C and 21 °C results in an engine emission map at 20 °C for veh_5. With these maps for the different temperature ranges, the CADC was simulated for each vehicle with PHEM. By simulating a common cycle from all emission maps the effects of different engine load cycles is eliminated and the results provide a common basis for the analysis of temperature influences on emissions. Since the CADC is representative for real world driving as mentioned before, the result for the temperature effects shall also be valid for real emission behaviour. Figure 11 shows the result of NO_x emissions found with this method as function of ambient temperature. The trend is well described by a linear equation. The NO_x emissions increase from 20 °C to 10 °C by approximately 40 % to 50 %. This high influence was the reason for further investigations based on remote sensing to validate the effects for the vehicle fleet and also to check temperature effects for older EURO classes. Finally, similar effects were found for EURO 4 to EURO 6 in the remote sensing data (Figure 12) and correction functions were implemented in HBEFA 3.3.

The following chart shows effects for EURO 4, EURO 5 and EURO 6 diesel cars. In addition the TUG data from the vehicle tests shown above are plotted (black rhombi), which fit the remote sensing data very well. As mentioned before, the EGR is optimised for a temperature range > 20 °C, therefore only data points are plotted below this threshold.

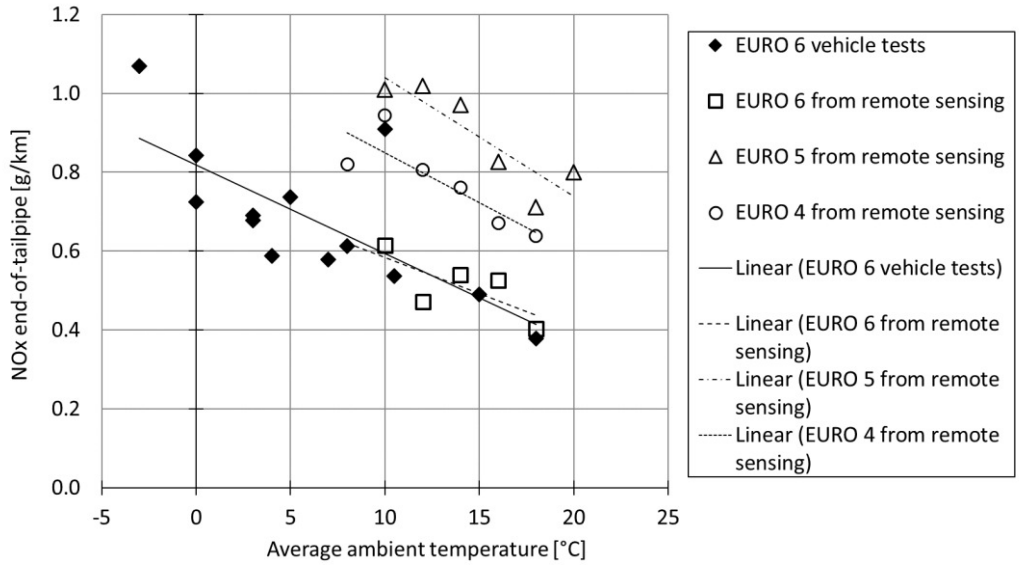

Figure 12: Preliminary NO_x correction functions for EURO 4, EURO 5 and EURO 6 diesel cars based on vehicle tests and on remote sensing data from Sweden.

These linear equations from remote sensing measurement data were used as basis for the correction in the HBEFA but have been further adjusted to remote sensing data provided from tests in Switzerland.

The final correction functions were elaborated for the following boundary conditions:

- Ambient temperature effect on NO_x emissions occurs only below 20 °C for EURO 4, EURO 5 and EURO 6.
- Ambient temperature effect on NO_x emissions for EURO 6d-Temp and for EURO 6d are limited by the boundary conditions defined in the RDE regulation (limits have to be met down to 3 °C for EURO 6d-Temp and down to -3 °C for EURO 6d). Therefore, it is assumed for the future diesel vehicles that temperature effects are relevant only below these temperature thresholds.
- NO_x does not further increase below 0 °C. The available data do not cover lower temperatures, thus no statement on the real behaviour is possible at the moment. It is assumed, that EGR is on fleet average already reduced down to almost 0 % at 0 °C, so that no further effect on NO_x occurs.

More details about the implementation of the temperature function are described in the final report for the HBEFA 3.3 (Keller M. et. al. 2017).

Effect of stop&go traffic on NO_x emissions for HBEFA 4.1

The emission factors for diesel passenger cars were simulated with PHEM in the past based on EoT emission maps, i.e. the emissions measured at end-of-tailpipe are binned into the engine map. In a cycle simulation then the emissions are interpolated from this map according to the simulated engine speed and power. PHEM offers also the simulation of the exhaust after-treatment system. Temperatures are simulated based on equations for heat transfer and energy conservation. The conversion efficiency of the catalysts can be modelled based on space velocity and temperature of the catalysts. Since the temperature of the catalysts changes rather slowly after load changes, the conversion efficiencies depend on a longer time span in front of the actual load point. Thus, the simulation of raw exhaust gas emissions and the conversion in the catalyst(s) may increase the accuracy especially in cycles where the catalysts leave the optimum temperature range. E.g. special traffic situations like stop&go traffic can result in relative high NO_x levels due to low conversion efficiency resulting from cool down phases of the EAS if the engine has no special heating strategies. As disadvantage, the setup of the detailed EAS model for each vehicle increases the effort necessary to produce emission factors.

The actual EAS for diesel vehicles include an oxidation catalyst for CO and HC reduction as well as a filter for the particulates. For NO_x reduction, a SCR catalyst or NSC or a combination of both is used. Due to the lambda (= air-fuel mixture ratio) 1 concept, for petrol vehicles only a 3-way catalyst is necessary. Some actual petrol cars use also a particulate filter.

To analyse the possible accuracy gains with a detailed EAS simulation for emission factors, one diesel EURO 6 car with oxidation catalyst, particulate filter, SCR catalyst and low plus high pressure EGR was investigated at TUG. The investigations for an EAS using NSC is still under investigation and the results will be used for the HBEFA 4.1 update. Based on these results it will be decided if also an investigation of EAS of petrol cars should be realised.

Table 4: Diesel EURO 6 measurements used for stop&go investigations.

ID	Segment	Odometer [km]	Rated engine power [kW]	Measurement at ambient temperature
Veh_I	D-Segment	1000	90	36 °C

SCR catalyst is using NH_3 to reduce NO_x to N_2 and H_2O. NH_3 is generated from AdBlue above approximately 200 °C by thermolysis and hydrolyses in the EAS. As shown in Figure 13, the NO_x reduction in a SCR catalyst is mainly a function of the temperature, which results in lower conversion efficiency for lower temperatures. The curve is only valid, if enough NH_3 for the NO_x reduction is stored in the SCR catalyst (Hausberger S., Sams T. 2016).

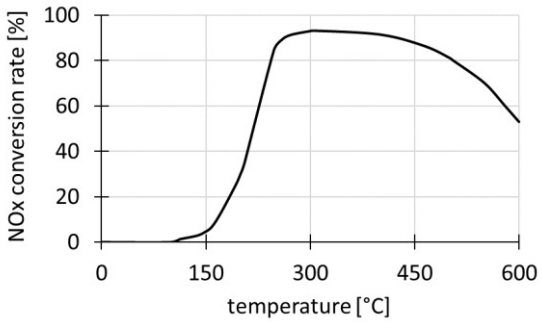

Figure 13: NO_x conversion rate as function of temperature (Hausberger S., Sams T. 2016).

In the following, the effect of stop&go traffic on NO_x emissions is presented with focus on:

- Engine heating strategies: Investigation if the vehicle has an engine heating strategy in special driving situation to prevent low conversion efficiency resulting from cool down phases.
- NH_3 storage in the SCR system: The SCR catalyst can store NH_3 to reduce NO_x emissions also in lower temperature ranges since below 200 °C no AdBlue is injected. The question is, over which time span the amount of NH_3 stored in the SCR catalyst is sufficient for a stop&go cycle driven after an usual driving cycle.
- Simulation considering the EAS: Check if a simulation of engine heating strategies and of NH_3 storage in SCR catalyst have to be implemented in the model PHEM for a sufficient accuracy. Compare the simulation accuracy with and without detailed EAS simulation.

The stop&go cycle was driven at a flat test track to have repeatable boundary conditions for the measurements. The cycle was derived from real stop&go traffic and consists of an acceleration, steady-state driving at 8 km/h, deceleration to stand still followed by a 20 s stop.

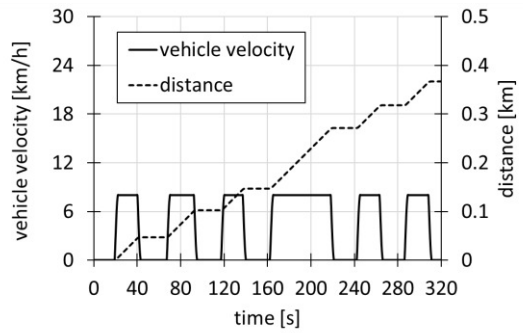

Figure 14: Defined driving profile for stop&go traffic.

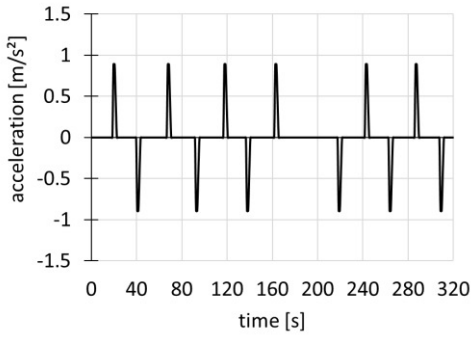

Figure 15: Defined accelerations for stop&go traffic.

The stop&go driving profile, shown in Figure 14, was driven in repetition for a duration of 27 minutes. The accelerations are between -1 m/s² to 1 m/s² (Figure 15).

Figure 16 shows the measured temperature (grey line) before SCR catalyst. It can be noticed, that the start temperature is between 250 °C and 300 °C since the vehicle was preconditioned at 80 km/h for several minutes to ensure repeatable conditions.

The measured temperature shown in Figure 16 settle down to approximately 170 °C. The trend shows no engine heating strategy at least for the first 1600 s. In the same figure is also the simulated temperature before SCR catalyst plotted (dotted black line), which also verifies the assumption that no heating strategy in the investigated time window exists since the simulation does not consider heating strategies so far.

Figure 17 shows the cumulated NO_x over time. The grey line represent the measured NO_x EoT, the dotted black line the simulated NO_x considering the EAS in PHEM. For after-treatment simulation, PHEM uses an engine-out emission map and conversion maps for the EAS. E.g. the SCR catalyst is described with a map, where the conversion efficiency is a function of space velocity and temperature before SCR catalyst. Therefore, the exhaust gas mass flow and engine out temperature have to be provided in the engine maps as input for PHEM. The mass flow and temperature maps can be derived from measurement data. The NO_x conversion map can also be derived from measurement data, if the concentration of NO_x upstream and downstream, the exhaust gas mass flow through the SCR catalyst and the temperature before SCR catalyst are available for each time step. For the investigated vehicle, all mentioned measurement data of several RDE and stop&go trips were used to produce emission and catalyst maps.

The simulated NO_x (dotted black line in Figure 17) using the after-treatment simulation in PHEM mostly fit the measured NO_x level. After 1600 s the measured NO_x level is at 233 mg/km, the simulation with after-treatment system leads to a 1 % lower NO_x level. In the same figure also a black line is plotted, showing the simulation result using the simple EoT map. For the EoT map the emissions measured end-of-tailpipe during the same trips used for after-treatment simulation (i.e. all measured RDE and stop&go cycles) are sorted in an engine map according to the engine power and engine speed using the CO_2 interpolation method. This map includes the EAS indirectly in the emission behaviour. The simulation without considering after-treatment system can lead to higher deviations between simulation and measurement. In this case the deviations results in 5 % lower NO_x after 1600 s. The time resolution is much better with the detailed EAS model since the simple EoT map is representing average temperature conditions and cannot show cool down effects.

On the other side, simulations by EoT maps are easier and faster since no EAS calibration and simulation in PHEM is necessary. The good agreement between the measurement data and the simulated data considering the EAS assume that the NH_3 storage in the SCR catalyst is sufficient since PHEM cannot consider the NH_3 storage so far. This assumption was also checked with a developed NH_3 storage model, which can be used currently as a post-processing application after measurement and/ or PHEM simulation. The model confirms that for the investigated stop&go cycle sufficient NH_3 is available, if the SCR catalyst was filled with 50 % of maximum possible NH_3 at the beginning of the test cycle. The NH_3 storage model will be presented in detail in the HBEFA 4.1 report.

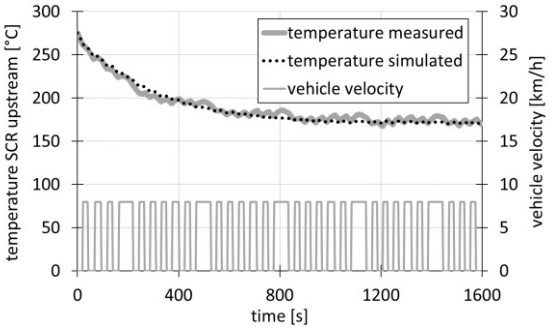

Figure 16: Measured and simulated temperature of stop&go cycle.

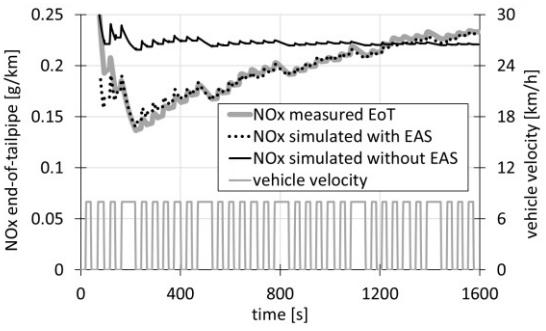

Figure 17: Measured and simulated NO_x of stop&go cycle.

Conclusion and outlook

For the HBEFA version 3.3 the new CO_2 interpolation method was used to produce the engine emission maps. With this method, it is possible to consider also measurement data where the engine load signal is not available or too inaccurate for engine map creation. This is especially useful for RDE measurements, where the power signal in most of the cases is not available. Using RDE measurements beside the chassis dynamometer test data increase the sample size of tested vehicles and improves in general the representativeness of the engine emission maps. In total the measurement data of 25 diesel EURO 6 cars were used for the update. Since the HBEFA 3.3 is a so-called quick update, only the NO_x emissions of diesel EURO 6 vehicles were updated. Based on the NO_x emissions for diesel EURO 6 vehicles also an assumption for diesel EURO 6d-Temp and EURO 6d vehicles considering the RDE conformity factor was done since no such vehicles were available so far for measurements. The RDE legislation prescribes a conformity factor of 2.1 for EURO 6d-Temp and of 1.5 for EURO 6d. This means that for a valid RDE trip, the NO_x shall not be higher than the NO_x emission limit on WLTC multiplied by 2.1 for EURO 6d-Temp, which results in 168 mg/km, and not be higher than 120 mg/km for EURO 6d. Since the RDE legislation covers a large range of driving conditions and includes also PEMS tests from independent parties, it is assumed that vehicles will meet the standards in “normal” real world cycles of HBEFA but not in stop&go and under high gradients. Consequently, the simulated NO_x emission factors decrease for the new emission standards by approximately 50 % to 70 % without considering the ambient temperature effect.

With the extended sample on measurement data due to additional RDE trips, also investigations like ambient temperature influence on NO_x emissions were realised. The measurement data of several conventional diesel EURO 6 cars at different ambient temperatures were used. To analyse the ambient temperature effect on NO_x isolated from routes and driving behaviour, separate engine emission maps with RDE measurement data at different temperatures were created and a standard CADC cycle was simulated with these maps. The investigation showed that from 20 °C to 10 °C ambient temperature the NO_x increase by approximately 40 % to 50 % for a real world cycle. This was the basis for consideration of ambient temperature effect on NO_x emissions in HBEFA 3.3.

Also an investigation regarding the effect of stop&go traffic on NO_x emissions was performed. The goal was to investigate if a detailed EAS simulation should be used in PHEM for the HBEFA 4.1 update. The simple tailpipe emission map meets the average NO_x in g/km quite accurately, but the second-by-second NO_x trend is much better if the EAS is considered in the simulation. The handling for HBEFA 4.1 is still open, further investigations are ongoing.

Acknowledgments

The HBEFA 3.3 quick update would not have been possible without the support from vehicle emission labs: EMPA (Switzerland), TNO (Netherlands) and ADAC (Germany), which provided chassis dynamometer and RDE measurement data. IVL (Sweden) and AWEL (Switzerland) also provided remote sensing data to consider the ambient temperature effects on NO_x emissions. The authors would furthermore like to thank Mario Keller (INFRAS / MK Consulting, Switzerland) for the ERMES DB management and for processing of the simulated emission factors.

Finally, the work would not have been possible without the funding from UBA Germany and UBA Austria, who set up projects as basis for the HBEFA quick update and for the HBEFA 4.1 update.

References

Hausberger S., Ligterink N., et.al.: Correction algorithms for WLTP chassis dynamometer and coast-down testing; report for DG Enterprise; TNO, Netherlands, 2015

Hausberger S., Matzer C.: Update of Emission Factors for EURO 4, EURO 5 and EURO 6 Diesel Passenger Cars for the HBEFA Version 3.3, Graz, 01. June 2017

Hausberger S., Rexeis M., Zallinger M., Luz R.: Emission Factors from the Model PHEM for the HBEFA Version 3. Report Nr. I-20/2009 Haus-Em 33/08/679 from 07. December 2009

Hausberger S., Sams T.: Schadstoffbildung und Emissionsminimierung bei Kfz Teil I und II, Skriptum IVT TU Graz, Graz, 2016

Hausberger S., Stadlhofer W., Vermeulen R., Geivanidis S., et.al.: MAC performance test procedure; Co-ordination of the pilot test phase and follow up towards the drafting of the regulatory text; Performed under Framework Service Contract ENTR/05/18, European Commission - DG Enterprise and Industry; April 2013

Hill N., Windisch E., Hausberger S., Matzer C., Skinner I., et.al.: Improving understanding of technology and costs for CO_2 reductions from cars and LCVs in the period to 2030 and development of cost curves; Service Request 4 to LDV Emissions Framework Contract; Final Report for DG Climate Action; Ref. CLIMA.C.2/FRA/2012/0006; Ricardo AEA, UK, 2015

Keller M., Hausberger S., Matzer C., Wüthrich P., Notter B.: HBEFA Version 3.3, Background documentation, Berne, 12. April 2017

Luz R., Hausberger S.: User Guide for the Model PHEM, Version 10; Institute for Internal Combustion Engines and Thermodynamics TU Graz, Graz, 2009

Matzer C., Hausberger S., Lipp S., Rexeis M.: A new approach for systematic use of PEMS data in emission simulation, 21st International Transport and Air Pollution Conference, Lyon 24. – 26. May 2016

Rexeis M.: Ascertainment of Real World Emissions of Heavy Duty Vehicles. Dissertation, Institute for Internal Combustion Engines and Thermodynamics, Graz University of Technology. October 2009

Zallinger M.: Mikroskopische Simulation der Emissionen von Personenkraftfahrzeugen. Dissertation, Institut für Verbrennungskraftmaschinen und Thermodynamik, TU Graz, Graz, April 2010

Variations of Real-world NO_x Emissions of Diesel Light Commercial Vehicles

Gerrit Kadijk, Veerle A.M. Heijne, Norbert E. Ligterink, Robin J. Vermeulen.*

Research Group Sustainable Transport and Logistics, TNO, PO Box 96800, 2509 JE Den Haag, the Netherlands, correspondence: gerrit.kadijk@tno.nl, presenter: veerle.heijne@tno.nl

Abstract

In order to gain insight into trends in real-world emissions of diesel light commercial vehicles under conditions relevant for the Dutch and European situations, fifteen Euro 6/VI and three Euro 5 light commercial vehicles (LCVs) were extensively tested on the road during the spring and summer of 2017. These measurements form the basis of the annual update of Dutch emission factors. On the road, real-world NO_x emissions of Euro 6/VI LCVs range from 30 to 1400 mg/km, on average 1 to 5 times higher than the type approval limit value. The measured average NO_x emission of the Euro 6/VI commercial vehicles in the test programs varies between 60 and 505 mg/km. In general, the difference between real-world emissions and type approval emission limit values has been growing over the years, but this trend seems reversed now with Euro6/VI LCV vehicles. For future diesel vehicles, an improvement of real-world NO_x emissions is expected with Real Driving Emission legislation. Currently the relatively expensive PEMS is foreseen as the type approval standard for on-road testing. TNO also applies a NO_x-O_2 sensor-based system with data logger (SEMS) as a NO_x screening tool.

Key-words: *Real-world NO_x emissions, light commercial vehicles, Euro 6, Euro VI, RDE, SEMS*

Introduction

Commissioned by the Dutch Ministry of Infrastructure and the Environment, TNO regularly performs test programs to determine the real-world emission performance of vehicles in the Netherlands (Kadijk et al., 2015 a,b,c & 2016 a,b,c & 2017) and (Spreen et al., 2016). The main goal of the programs is to gain insight into trends in real-world emissions of light- and heavy-duty vehicles under conditions relevant to the Dutch and European traffic situations. In 2016 and 2017 in total eighteen vehicles were tested: three Euro 5 light commercial vehicles, two Euro 6 passenger cars and thirteen Euro 6/VI light commercial vehicles (LCVs).

Based on the performed emission measurements, TNO develops and annually updates vehicle emission factors that represent real-world emission data for various vehicle types and different driving conditions. Vehicle emission factors are used for the Dutch emission inventory and air quality monitoring. TNO is one of the few institutes in Europe that perform independent emission tests for real-world conditions. Dutch emission factors are nowadays based on these on-road tests. The emission factors are one of the few independent sources of information on the growing difference between legislative emission limits and real-world emission performance of cars.

To minimize air pollutant emissions of light-duty vehicles, in 1992 the European Commission introduced the so-called Euro emission standards. Over the course of time, these standards have become more stringent. Since September 2014, all new type approved N1 Class 1 light-duty vehicles must comply with Euro 6 regulations and from September 2015 onwards all registered vehicles need to comply with the Euro 6 limits, therefore the tested vehicles are relatively early models. For the N1 Class 2 and 3 vehicles these dates are valid a year later. The standards apply to vehicles with spark ignition engines and to vehicles with compression ignition engines and cover the following gaseous and particulate emissions: CO (carbon monoxide), THC (total hydrocarbons), NO_x (nitrogen oxides), PM (particulate mass) and PN (particulate number). The focus of the test program was on compression ignition (diesel) vehicles.

As a result of the Euro emission standards, the pollutant emissions of light-duty vehicles as observed in type approval tests have been reduced significantly over the past decade. However, under real driving conditions, some emissions substantially deviate from their type approval equivalents. The real-driving nitrogen oxides, or NO_x, emissions of diesel vehicles are currently the largest issue with regard to pollutant emissions. As NO_x represents the sum of NO and NO_2

emitted, reducing NO_x emissions of vehicles is an important measure in lowering the ambient NO_2 concentration. In the Netherlands, the ambient NO_2 concentration still exceeds European limits at numerous road-side locations.

TNO regularly performs emission measurements within the “in-use compliance program for light-duty vehicles” and the “in-use compliance program for heavy-duty vehicles”. Whereas in the early years, i.e. in 1987 to 2000, many standard type approval tests were executed, in recent years the emphasis has shifted towards the gathering of real-world emission data. Real-world emission data are collected by means of:

1. Performing emission measurements on a chassis dynamometer using various non-standard driving cycles, for example driving cycles that better reflect real-world driving conditions, and;

2. Equipping vehicles with an on-board emission measurement system (PEMS and/or SEMS) to measure the emissions of the vehicles while driving on the public road.

In the Netherlands, the road tax and fuel excise duty system discourages the private ownership of diesel cars. Only 15% of the passenger cars are diesel in the Netherlands. With 8 million passenger cars, the 900,000 LCVs in the Netherlands are not negligible, since there are almost as many diesel LCVs as diesel passenger cars in the Netherlands. These LCVs are responsible for about half of the total NO_x emission of light-duty vehicles. According to the revenue office, most of the LCVs are associated with some commercial use. However, especially older vans are also used extensively in the evening and the weekend. Very likely the Euro 5 and Euro 6 LCV will be an important contributor to urban ambient NO_2 concentrations in 2020 and beyond.

Objective

The objective of this research is to assess the real-world emission performance of Euro 6/VI light commercial vehicles. For three vehicle types from the N1 Class 3 category, Euro 5 variants were tested as well.

Method

On-road testing

Emission tests were performed on the road. TNO performs real-world tests on the road with a Portable Emission Measurement System (PEMS) and/or a Smart Emission Measurement System (SEMS). PEMS equipment measures CO, CO_2, HC, NO and NO_2 emissions. SEMS is an emission screening tool which contains a data logger and a NO_x-O_2 sensor. Moreover, with SEMS NH_3 emissions are monitored. In this test program, all emission tests were performed with SEMS.

SEMS testing

Emission tests with different vehicles were performed on the road under real-world conditions. During the SEMS tests, the vehicle was loaded with a test driver, additional payload and the test equipment with a weight of approximately 5 kg.

In recent years, TNO has developed the so-called Smart Emission Measurement System or SEMS (Vermeulen et al. 2012 & 2014). SEMS is an emission screening tool that contains a data logger, a NO_x-O_2 sensor (Continental, UniNO_x) and a thermocouple temperature sensor, of which the latter two are installed in the tailpipe of the vehicle. It measures the exhaust gas temperature and the O_2 and NO_x volume concentrations in vol% or ppm. SEMS also measures geographical data, vehicle speed and logs the CAN data of the vehicle with a measuring frequency of 1 Hz. Based on the measured O_2 readings and the carbon and hydrogen content of the fuel, the CO_2 concentrations are calculated. In former projects, the accuracy and the reliability of the SEMS equipment and method has been demonstrated (2012), (2014b).

In this test program the data of the MAF (Mass Air Flow) sensor of most of the tested vehicles was used for the calculation of the NO_x and CO_2 exhaust mass flow rates [mg/km]. The quality of the air mass rate signal of the vehicle has a large influence on the accuracy of the NO_x and CO_2

mass emissions. Moreover, the NO_x-O_2 sensor is sensitive for temperature and pressure which may influence the accuracy. Calibration of the MAF sensor and the NO_x-O_2 sensor is a standard part of the test procedure.

The test and data processing procedure contains the following steps:

1. Before and after every test session the fuel tank of the vehicle is filled off at the same pump of the same filling station;
2. The measured mass air flow rate from the vehicle, the measured NO_x and O_2 concentrations are corrected based on calibration data;
3. The CO_2 volume concentration is determined from the measured O_2 volume concentration and the fuel C:H ratio;
4. The exhaust mass flow rate is determined from the vehicle Mass Air Flow signal, augmented with combustion products CO_2 and H_2O using the fuel C:H ratio and the normal air density. In case no Mass Air Flow signal is available, the exhaust mass flow rate is estimated using the fuel flow rate and the measured oxygen concentration;
5. The CO_2 and NO_x mass flow rates are determined from the measured volume concentrations and the exhaust mass flow rate.

This analysis requires three input parameters:

- the C:H ratio of the fuel, which is assumed to be 1.95 for modern market-fuel diesel;
- the ambient oxygen content of air at 20.8% for on-road conditions;
- normal air density of 1.29 kg/m^3 at standard conditions to calculate the exhaust gas density.

Performance of SEMS test equipment on a chassis dynamometer

The NO_x-O_2 sensors of the SEMS equipment and the mass air flow (MAF) sensors of most vehicles are calibrated. Independent verification with data of refills was used to determine the quality of the air flow signal of the different vehicles. The total CO_2 emissions between refills, as determined from the fuel and from the air flow signal was equal for all vehicles, within a 5% range. No systematic deviation from this 5% variation was found. It was noted that at very low concentrations of NO_x, the SEMS sensor is less accurate for transient signals. However, in the range of concentrations of the current measurements the correlation and calibration tests carried out in the last four years provide a good evidence for the accuracy of the measurements (Spreen et al., 2016b).

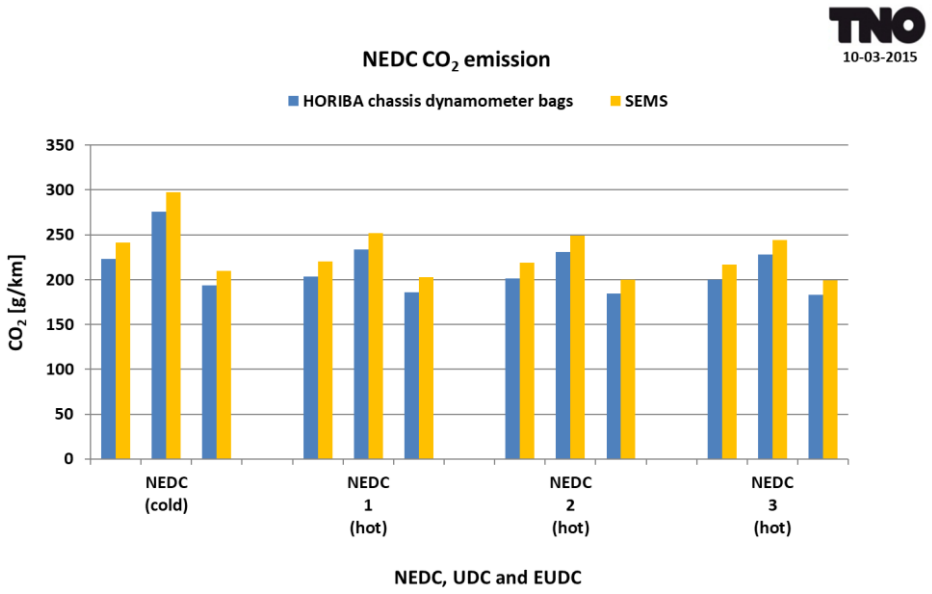

Figure 1: Example of validation CO_2 test results SEMS-chassis dynamometer of one vehicle (per test the total result and urban and extra-urban results are shown).

In order to validate the SEMS test results, over the last three years validation tests with four vehicles were performed on a chassis dynamometer. The CO_2 and NO_x test results of one vehicle are shown in Figure 1 and Figure 2. The SEMS test results are well in line with the chassis dynamometer test results. SEMS test results are partly based on (corrected) MAF data of the CAN-bus of the vehicle. In all emission tests the difference of the CO_2 emissions is 8% and the difference of the NO_x emissions is -14% to +12%. Both standard deviations for CO_2 are approximately 1%; for NO_x, these equal 8 and 12%. The results show that SEMS is a useful screening tool which yields repetitive indicative results. One should keep in mind that the accuracy of these test results is directly related to the accuracy, resolution and response time of the mass air flow signal of this vehicle type. Other vehicle types may gain different accuracies.

Although SEMS is less accurate than PEMS, the system is well suited for a quick screening of NO_x emissions of a vehicle and for measuring and monitoring over long periods of time. Its error margins are sufficiently low to identify emissions that are well beyond emission limits.

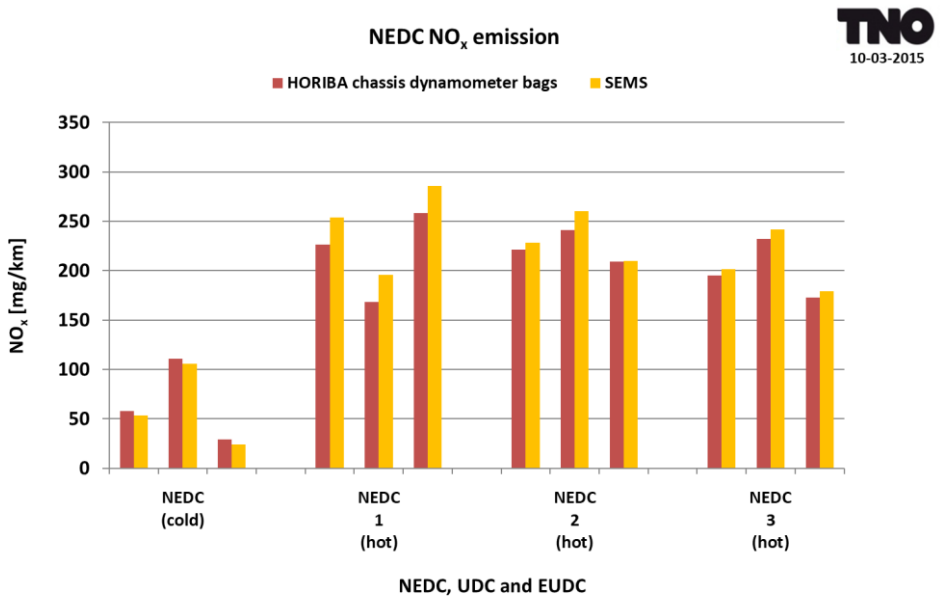

Figure 2: Example of validation NO_x test results SEMS-chassis dynamometer of one vehicle (per test the total result and urban and extra-urban results are shown).

Test routes

SEMS registers real-world conditions and real-world emissions. To be able to compare the individual real-world vehicle emissions, one Real Driving Emission (RDE) trip (with 28% payload and a hot start), an in-service conformity trip (ISC) and a delivery trip are always part of the investigation. The RDE and ISC trips consist of urban, rural and highway driving. Additionally, some other trips are driven: RDE trips with a cold start, a trip mainly containing urban driving and a trip consisting mainly of highway driving. Table 1 shows the main characteristics of the test trips. All trips start in Delft or The Hague, the Netherlands. Tests are carried out with different payloads and different driving styles.

Table 1: Specifications of SEMS test trips.

	Trip Name	Road Type(s)	Start condition	Driving style	Test Day	Payload [%]	Distance [km]	Average velocity [km/h]
1	RDE_C	Urban / rural / motorway	Cold start	Economic	1	28	74.7	43
2	Motorway	Motorway	Hot start	Regular	1	28	89.5	79
3	RDE_H	Urban / rural / motorway	Hot start	Regular	1	28	74.7	43
4	Congest_W	Motorway, evening traffic	Hot start	Regular	1	28	84.3	56
5	Congest_C	Motorway, morning traffic	Cold start	Dynamic	2	95	85.3	83
6	City	Urban	Hot start	Regular	2	95	27.8	21
7	Rural	Rural	Hot start	Regular	2	95	64.5	50
8	RDE_H	Urban / rural / motorway	Hot start	Regular	2	95	74.7	43
9	City to City	Urban / rural / motorway	Hot start	Regular	2	95	21.2	36
10	RDE_C	Urban / rural / motorway	Cold start	Regular	3	55	74.7	43
11	Short trip	Urban/rural	Hot start	Regular	3	55	4.3	28
12	Delivery trip	Urban	Hot start	Regular	3	55	17.4	12
13	ISC_H	Urban / rural / motorway	Hot start	Regular	3	55	122.7	57
14	City to City	Urban / rural / motorway	Hot start	Regular	3	55	21.2	36
	Total						837.1	

Table 2: Driver instructions of different driving styles.

Driving style		Economy	Normal	Sportive
Driving behaviour		careful	regular	dynamic
Gearshift engine speed	[rpm]	2000	2500	3500
Distance to target at start of braking	[m]	90	60	30
Delay time speed to brake pedal	[s]	30	3	0
Start-stop system active		Yes	Yes	No
Vehicle stops of 120-180 s		0	0	2
Maximum position speed pedal	[%]	80	90	100
Speed pedal activation speed		slow	normal	fast
Maximum speed on the motorway	[km/h]	110	120	140

Driving styles in on-road measurements

The test driver is given instructions for three different driving styles: ‘economic’, ‘normal/regular’ or ‘dynamic/sportive’. Some vehicles are tested with all driving styles. In Table 2 more details of the driving styles are reported.

Test vehicles

Table 3 shows the eighteen tested Euro 5, 6, and VI vehicles in the measurement program. The two M1 vehicles can be considered as N1 class 3 vehicles because they both have similar engines and aftertreatment technologies.

Table 3: Tested Euro 5, 6 and VI vehicles in 2016 and 2017.

Brand	Model	Category	Euro Class	Power [kW]	Aftertreatment	Odometer [km]	Mass empty [kg]
Peugeot	Partner	N1 class 2	6b	73	Oxicat+DPF+SCR	21,263	1,460
Renault	Trafic	N1 class 3	6b	92	Oxicat+DPF+SCR	3,200	2,065
Ford	Transit Connect	N1 class 2	6b	74	Oxicat+DPF+LNT+SCR	15,353	1,596
Volkswagen	Caddy	N1 class 2	6b	55	Oxicat+DPF+SCR	4,498	1,486
Volkswagen	Kombi Transporter	M1	6b	62	Oxicat+DPF+SCR	20,004	1,894
Mercedes-Benz	Citan	N1 class 2	6b	55	Oxicat+DPF+LNT	17	1,448
Mercedes-Benz	Vito	M1	6b	100	Oxicat+DPF+SCR	44,875	2,477
Peugeot	Expert	N1 class 3	6b	90	Oxicat+DPF+SCR	12,878	1,817
Ford	Transit	N1 class 3	5b	74	Oxicat+DPF	56,356	2,167
Ford	Transit	N1 class 3	6b	96	Oxicat+DPF+SCR	11,751	2,383
Ford	Transit	N1 class 3	VI	114	Oxicat+DPF+SCR	37152	3181
Mercedes-Benz	Sprinter	N1 class 3	5b	95	Oxicat+DPF	23,878	2,535
Mercedes-Benz	Sprinter	N1 class 3	6b	105	Oxicat+DPF+SCR	12,770	2,695
Mercedes-Benz	Sprinter	N1 class 3	VI	120	Oxicat+DPF+SCR	30,734	2,960
Volkswagen	Crafter	N1 class 3	5b	100	Oxicat+DPF	60,544	2,146
Volkswagen	Crafter	N1 class 3	6b	80	Oxicat+DPF+SCR	2,694	2,158
Volkswagen	Crafter	N1 class 3	VI	120	Oxicat+DPF+SCR	70,780	2,146
Iveco	New Daily	N1 class 3	6b	114	Oxicat+DPF+SCR	4,488	2,366

Results

All eighteen vehicles were tested on the road with SEMS. Emission and vehicle data were logged in 132 defined tests with a total distance of more than 9000 km with a measuring frequency of 1 Hz. The names of the specific trademarks and vehicle types are not mentioned in the results. These will be given in a TNO report, which is expected to be published before the end of 2017.

Overview NO_x emissions of Euro 6/VI vehicles:

Figure 3 shows the large spread in the average NO_x emissions of the executed test trips of all fifteen Euro 6/VI LCVs. A typical RDE test has an average speed of 35 – 45 km/h and average NO_x emissions in the range of 39 - 534 mg/km. Other trips with this average speed yield higher emissions (up to 1050 mg/km). The NO_x emissions in urban traffic (around an average speed of 15 km/h) are in the range of 100 – 1300 mg/km. One N1 class 2 vehicle with an LNT has in short urban trips of 4-5 km the highest urban NO_x emission around 1300 mg/km. The lowest average NO_x emissions, in the range of 50 – 500 mg/km, were measured in trips with higher average vehicle speeds (60 – 85 km/h).

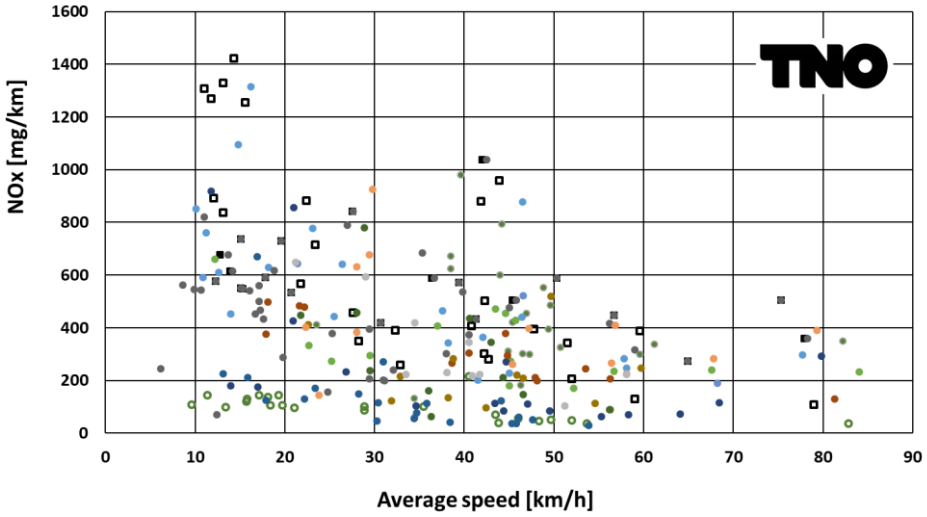

Figure 3: Average on-road NO_x emissions of different test trips with different payloads and different driving styles of fifteen Euro 6/VI light commercial vehicles.

Detailed NO_x emissions of Euro 5/6/VI vehicles:

More specific variations of NO_x emissions of the Euro 5/6/VI vehicles are shown in Figure 4 up to Figure 7. In this test program the bandwidth of the average NO_x emissions of the fifteen Euro 6/VI vehicles is 60 – 514 mg/km and the bandwidth of the average NO_x emissions of the three Euro 5 vehicles is 648 – 1498. The latter are in line with earlier TNO findings (Kadijk 2015a). The average NO_x emissions of the Euro 6/VI LCVs are substantially lower than the Euro 5 variants.

The NO_x emissions of Euro 6/VI vehicles in RDE tests, see Figure 4, are in the range of 36 to 534 mg/km and they have no direct relationship with the size of these vehicles. The performance of the applied emission control systems seems to be more decisive for the NO_x emissions.

The RDE test results of all vehicles in Figure 4 clearly show that the CO_2 emission of the vehicles is not related to the NO_x emission. The best comparison can be made with the vehicles J, K and L, which were all tested in a Euro 5, 6 and VI variant. The CO_2 emissions of each type are in a comparable range (+/- 10%) but their NO_x emissions vary with a factor 6 – 28 (600 – 2800%). Vehicle A (N1 class 2) and vehicle E (N1 class 3) already meet the Euro 6d RDE NO_x limit value in certain RDE tests with moderate conditions.

The NO_x emissions of fourteen Euro 6/VI vehicles in RDE trips with 28% payload are 36 – 534 mg/km and the NO_x emissions of HD-ISC trips with 55% payload are 38 – 448 mg/km, see Figure 4 and Figure 5. Three Euro 6/VI vehicles emit in HD-ISC tests more NO_x than in RDE tests, eight vehicles have substantially lower NO_x emissions and three vehicles have a similar performance in both tests.

The NO_x emissions in delivery trips (see Figure 6) of these fourteen Euro 6/VI vehicles are in the range of 128 – 838 mg/km and are on average substantially higher than the NO_x emissions in RDE & HD-ISC tests (36 – 534 mg/km).

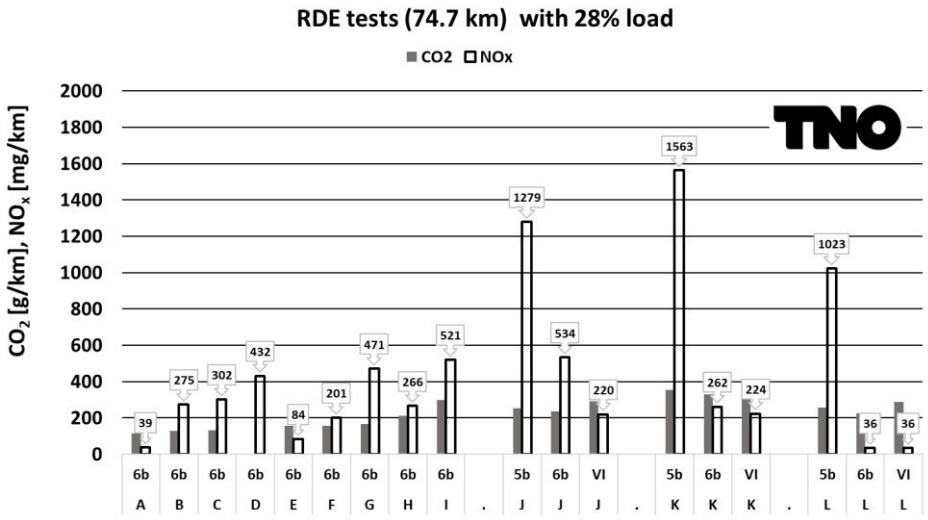

Figure 4: Average on-road NO_x and CO_2 emissions of RDE test trips of fifteen Euro 6/VI and three Euro 5 light commercial vehicles.

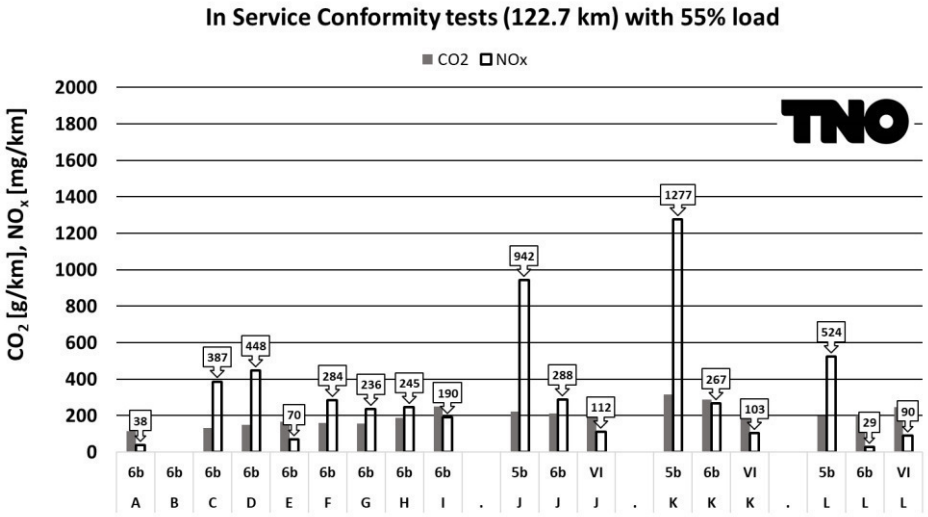

Figure 5: Average on-road NO_x and CO_2 emissions of HD-ISC test trips of fifteen Euro 6/VI and three Euro 5 light commercial vehicles.

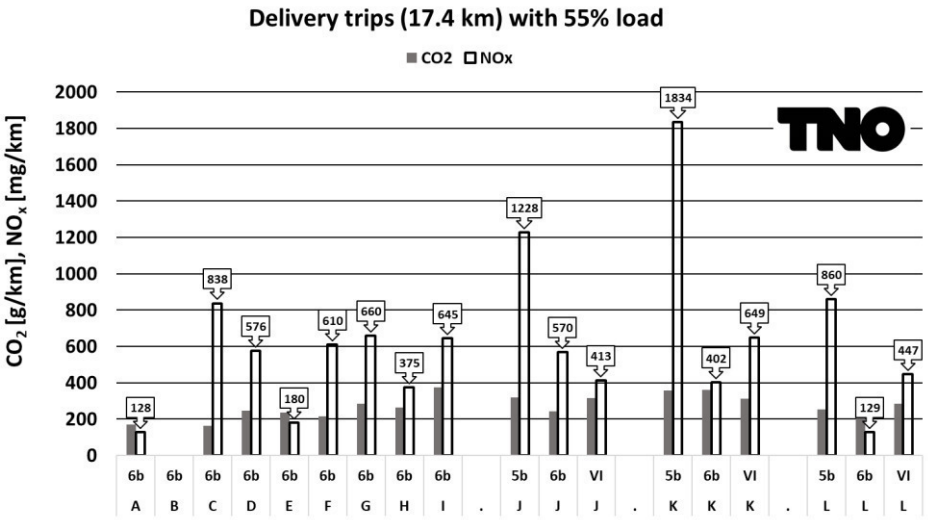

Figure 6: Average on-road NO_x and CO_2 emissions of delivery test trips of fifteen Euro 6/VI and three Euro 5 light commercial vehicles.

In Figure 7 the total average NO_x emissions of the executed test programs of all eighteen vehicles are shown. For the Euro 6/VI vehicles J, K and L the total average NO_x emissions are 60 – 560 mg/km, which is substantially lower than the total average NO_x emissions (648 – 1498 mg/km) of the Euro 5 variants of these types.

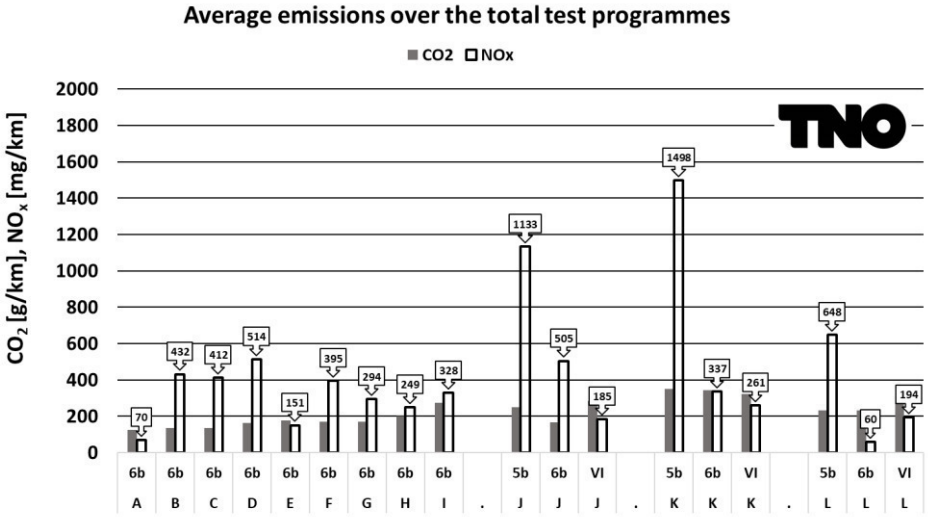

Figure 7: Average on-road NO_x and CO_2 emissions of all trips of fifteen Euro 6/VI and three Euro 5 light commercial vehicles.

The effects of different payloads and driving styles:

In Figure 8 and Figure 9 the CO_2 and NO_x results of RDE tests of eight vehicles are shown. Variations were set in payloads (28%, 55% and 95%) and three different driving styles were executed (economic, normal and sportive). The main target of these variations was to cover the whole RDE operating range with respect to payload, driving style and vehicle speeds. Since the driver instructions in terms of driving style and maximum vehicle speeds were restricted due to traffic situations, the actual execution of the RDE test may deviate.

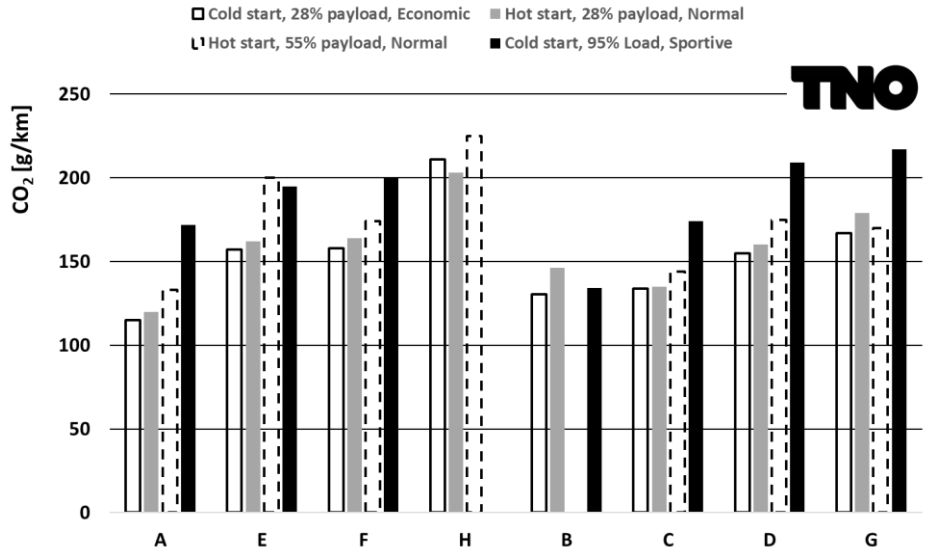

Figure 8: CO_2 emissions of RDE test trips with different payloads, driving styles and starting conditions of eight Euro 6 light commercial vehicles.

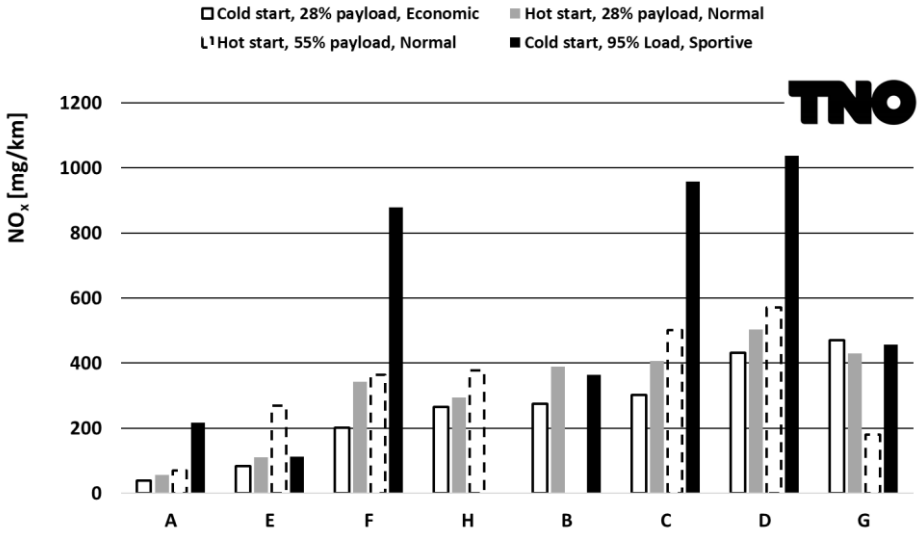

Figure 9: NO_x emissions of RDE test trips with different payloads, driving styles and starting conditions of eight Euro 6 light commercial vehicles.

The main trend of the CO_2 emission per vehicle is related to more demanding conditions of the RDE tests. Higher payloads and a dynamic driving style result for most vehicles in a CO_2 increase up to 25% to 35%, see Figure 8. In that respect, the corresponding NO_x trends in Figure 9 are more diverse. Some vehicles have very stable NO_x emissions but others range widely (up to a factor 4 to 6 for an individual vehicle). With high payloads and a sportive driving style these NO_x emissions can be 800 to 1000 mg/km. It must be noted that the emissions of these vehicles must satisfy a chassis test and are not necessarily optimized for on-road emission performance.

Cold start emissions

To evaluate the cold start, the cold start effects need to be distinguished from the normal emission behaviour. Therefore, the NO_x emissions are parameterized in terms of velocity and CO_2 using all the emission data per vehicle. This minimizes the dependency on different velocity profiles, driving behaviour and payload. Figure 10 shows the resulting instantaneous NO_x emissions as a function of velocity (x-axis) and CO_2 rate (y-axis). This Euro 6 vehicle performs better at high load when the velocity is also high. In this case, NO_x emissions do not only depend on engine load, i.e., CO_2 emission rates. The maximum CO_2 rate of 15 g/s in Figure 10 corresponds to about 75 kW power demand.

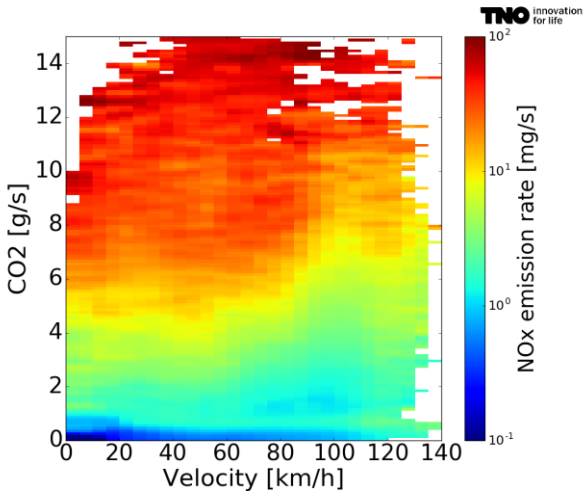

Figure 10: NO_x emissions parameterized in terms of velocity and CO_2, for one Euro 6 light commercial vehicle with SCR.

This parameterization provides a prediction for the most likely NO_x emission at a certain velocity and CO_2 emission. Applying this average emission map to the second-by-second speed and acceleration values of the recorded trips yields a prediction of the average second-by-second emissions. These predictions deviate from the actual recorded emissions. If these deviations, also called residuals, are either systematically below or above the average results, they may be attributed to specific causes other than the engine load defined by the combination of speed and acceleration.

When the NO_x residuals are calculated for the cold-start RDE trips, the time-dependent effects of the cold start will become visible, as in Figure 11. The result of the NO_x residual analysis is shown as the blue line, i.e., the extra emissions, with an error band showing the standard deviation of the underlying residual values. If there is a large spread between the values, the error band will increase. In this example, there are additional emissions (positive residual) at the start that decrease after some time, while the exhaust gas temperature is still rising. Cold starts, DPF regenerations and particular aspects of the LNT control strategy can be observed as large residuals, or differences between the average and the actual emissions.

This residual analysis shows a distinction between the LNT-equipped and the SCR-equipped vehicles. The tested SCR vehicles emit on average 0.4 g extra NO_x during the RDE cold starts which last on average about 600 seconds. In the first 300 seconds of the urban part of RDE trips with a cold start the three tested vehicles with a LNT have an average 0.05 g extra NO_x emission. This may be explained by the fact that the NO_x absorption of an LNT typically starts at 80-100 °C while the light-off temperature of SCR catalysts is 150-200 °C.

When the extra NO_x emissions due to a cold start are spread out over the (on average) 29 km urban driving in an RDE test, they result in about 5% extra emissions (in mg/km) on the urban part of a cold start compared to a hot start RDE trip. Note that the variation between vehicles and between trips is so large that these average numbers are not representative for individual vehicles.

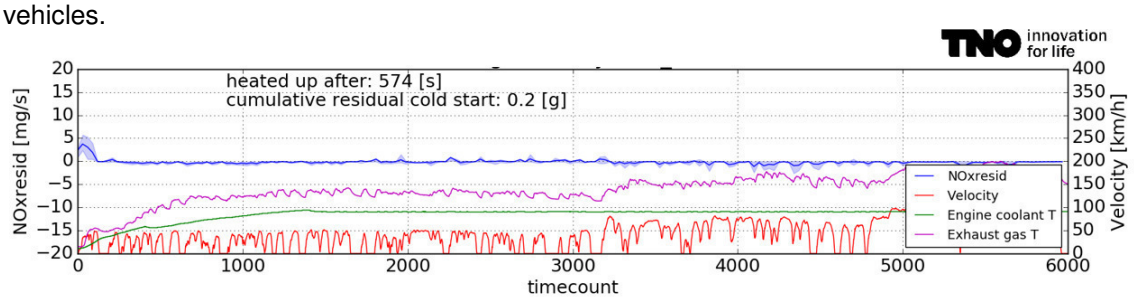

Figure 11: NO_x emission residual with respect to the average of one Euro 6 light commercial vehicle with SCR, for an RDE trip with cold start.

Emissions on different road types

Due to the increased dependency on dynamics of the emissions of Euro 6 vehicles, the necessity to distinguish between specific road types and speed limits increases. By matching the trip trajectories with map information, dependencies on road circumstances can be distilled. The test program showed that emissions on a motorway with 80 km/h speed limit are about three times lower than on an 80 km/h rural road. The reason is that on the motorway, the dynamics are minimal, whereas on rural roads much deviation in velocity takes place due to e.g. round-abouts and road crossings.

Emission dependency on ambient temperature

Similar to the cold start analysis, emission residuals can be correlated with ambient temperature after calculating the expected emissions given a certain velocity and CO_2 emission. For most vehicles, no correlation is observed within the temperature range that was covered by the test program. One of the vehicles that did show an effect is illustrated in Figure 12. In this case, the extra NO_x emission decreases with ambient temperature.

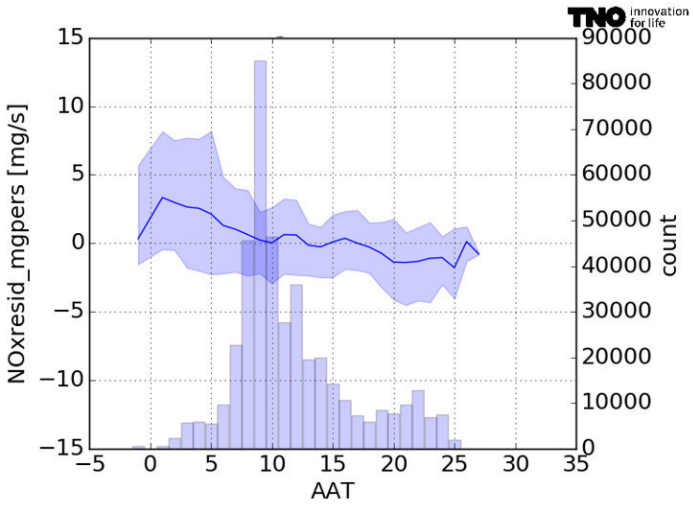

Figure 12: NO_x emission residual (blue line) versus ambient air temperature (AAT) of one Euro 6 light commercial vehicle. The amount of data per temperature bin is shown in the histogram.

Comparison of the NOx emissions of class 3 LCVs with a type-approval according the LD or the HD regime.

For LCVs in class 3, with a reference mass between 2380 and 2840 kg, manufacturers may choose for either the Euro 6 LD or the Euro VI HD regime for the emissions type-approval. Both type approval regimes differ with regard to emissions limits and test procedures. Comparing the NO_x emissions of vehicles with a Euro 6 and Euro VI type-approval there was no clear indication from the test performed that on average one regime is more effective in achieving low real-world NO_x emissions than the other. The three vehicle types tested each showed a different trend. However, the Euro 6 vehicles clearly show a larger spread in the NO_x emissions, whereas the NO_x emissions of Euro VI vehicles are more consistently low.

Discussion

What are the main emission characteristics of the tested Euro 6/VI diesel light commercial vehicles?

The test results of the fifteen tested Euro 6/VI vehicles show a variation of real-world NO_x emission from 30 to 1400 mg/km. Although the type approval emission limit values of the Euro 6 vehicles are 105 (Class II) or 125 mg/km (Class III), the average real-world NO_x emissions of all tested Euro 6/VI vehicles vary between 60 and 505 mg/km, which is substantially lower than the Euro 5 variants.

What are the main emission characteristics of the tested N1 Class III Euro 5/6/VI diesel light commercial vehicles?

Three N1 Class III vehicles were tested as Euro 5, Euro 6 and Euro VI type in the same test trips. The average measured NO_x emissions of the Euro 5 LCVs are in the range of 648 – 1498 mg/km, the Euro 6 vehicles emit on average 80 to 505 mg/km and the Euro VI vehicles emit 185 to 261 mg/km, see Figure 7. From these numbers, it seems Euro 6/VI vehicles have substantially lower NO_x emissions than Euro 5 models. The Euro VI N1 Class III vehicles which are optimized for on-road usage have on average the lowest emission. Probably the future RDE emission legislation for the light-duty vehicles will lower the on-road emissions of Euro 6 vehicles N1 class III vehicles as well.

What are the characteristics of the vehicle with the lowest real-world NO_x emissions and the vehicle with the highest real-world NO_x emissions?

The NO_x emission of vehicle L in an RDE test is 36 mg/km (conformity factor CF = 0,3) whereas vehicle I has a NO_x emission of 521 mg/km (CF = 4,2). Both vehicles have similar bodies, engines and aftertreatment technologies. These very different NO_x emissions in RDE tests are most likely

caused by the control strategy dependency on ambient temperatures, the differences in EGR and SCR system settings and adjustments.

Are the test results representative for all Euro 6/VI diesel vehicles?

The fifteen tested Euro 6/VI medium and large light commercial vehicles can be classified as main stream, and based on past sales it is estimated that these vehicle models will cover more than 65% of the Dutch Euro 6/VI LCV fleet. Most of these vehicles are equipped with SCR technology.

How can real-world NO_x emissions of Euro 6 vehicles be improved?

To improve real-world NO_x emissions, Real Driving Emission legislation (RDE) is needed. This legislation describes the test procedure and data evaluation methods for determination of real-world emission levels or Conformity Factors. It is expected that a dynamic or sportive driving style will be the most challenging condition to realize low on-road emissions in RDE tests. For two tested vehicle types it was demonstrated that NO_x emissions levels below the current limit of the chassis dyno test (125 mg/km, which represents a Conformity Factor of 1.0) can be achieved under most driving conditions.

The three Euro VI LCVs have generally low real-world NO_x emissions, with measured average NO_x emissions in the range of 185 – 261 mg/km. This in contrast to the Euro 6 variants that show a much larger spread in the real-world NO_x emissions. Two Euro 6 vehicles (A and L) already have an average measured NO_x emission of 60-70 mg/km which is lower than the Euro 6d RDE limit values with a CF 1,5. This difference between vehicles with LD Euro 6 and HD Euro VI type approvals may be attributed to the fact that for heavy-duty engines and vehicles on-road emissions tests, to check the in-service conformity, are mandatory as of 2014.

How can SCR-technology on the tested Euro 6/VI vehicles be assessed?

In order to assess SCR-technology, it is benchmarked with two other technologies. From 1988 onwards the three-way catalyst technology on petrol engines has been applied. Currently the engine control systems and the three-way catalyst technologies on petrol engines are well developed and the real-world CO, THC and NO_x emissions have been reduced with 90-99%. Since 2002 the closed diesel particulate filters have entered the market and their PM-filter efficiencies of more than 99% are remarkable. Furthermore, this technology is robust against varying circumstances because all exhaust gas is filtered.

General discussion

Summarizing the current status, the available engine and aftertreatment technologies and real-world emissions of Euro 6/VI LCVs, it is clear that the next step is RDE legislation for Euro 6 vehicles. This RDE legislation will be the main actor to ensure low real-world emissions of light duty vehicles and will determine the real-world effectiveness of NO_x aftertreatment technologies.

In this project the NO_x and CO_2 emission mass rates are based on measured volume concentrations, fuel parameters, calculations and the measured air mass rates. Although the air mass rate signals of the vehicles might deviate (i.e. +/- 10%) the on-road vehicle NO_x emissions are far higher than the type approval emission limit values. Independent comparison of the CO_2 emissions with the recorded fuel consumption, based on the same signals, yields typical deviations of less than 5% for the accumulated CO_2 over a few trips.

The test results of this study proved a limited effect of payload and external circumstances, causing typically less than 15% variation per vehicle between the extreme cases. However, the NO_x emissions seem to be very dependent on the driving behaviour. The three applied driving styles cover the majority of real-world driving styles and are expected to be representative.

In conclusion, even though emission tests were executed in a realistic way, not to produce high emissions due to special test circumstances, the results were still high.

Conclusions

In several emission test programs TNO has tested fifteen Euro 6/VI Light Commercial Vehicles and three Euro 5 types. The tests were carried out on the road with mobile test equipment. In total, more than 9000 km with 1 Hz emission data were gathered. From the measurements, TNO draws the following conclusions:

1. The measured average NO_x emissions of the fifteen N1 Class II and III Euro 6/VI light commercial vehicles range from 60 to 505 mg/km, which can be marked as a huge improvement compared to Euro 5 vehicles that emit 2 to 3 times more NOx. The two vehicles with the lowest average emission (60 and 70 mg/km) seem to be RDE compliant. However, their performance just above 0 °C ambient temperature is not measured and should be checked.

2. The spread of the measured NO_x emissions of all tested vehicles is large and ranges from 60 to 1400 mg/km. On average, real-world emissions are 1 to 4 times higher than the type approval limit values of 105 and 125 mg/km. This seems to indicate that emission control technologies perform differently on the road than they do on the chassis dynamometer. Only proper RDE-legislation can improve these real driving emissions.

3. The measured NO_x emissions are partly related to the actual vehicle speed. The applied control strategies of the EGR, SCR or LNT systems in combination with driving styles seem to be more relevant.

4. Current Euro 6 diesel vehicles with low real-world NOx emissions run with active and well-functioning EGR and SCR systems. Vehicles with higher real-world emissions seem to operate with EGR, LNT or SCR systems that are inactive or partly inactive. The highest measured NOx emission of 1300-1400 mg/km is measured with a vehicle with LNT in urban trips of 4-5 km with a warm engine start.

5. The applied driving styles and payloads in this study are representative for the range of real-world driving behaviour. Due to a sportive driving style in combination with a high payload the NO_x emission may raise with a factor 4 (i.e. from 200 to more than 800 mg/km) and the corresponding CO_2 emission raises approximately 30%.

6. Three vehicle types were tested as Euro 5, 6 and VI variants. The average measured NO_x emissions of the Euro 5 LCVs are in the range of 648 – 1498 mg/km, the Euro 6 vehicles emit on average 80 to 505 mg/km and the Euro VI vehicles emit 185 to 261 mg/km. The Euro VI N1 Class III vehicles are optimized for on-road use have on average the lowest emission. Probably the future RDE emission legislation for the light-duty vehicles will lower the on-road emissions of Euro 6 vehicles N1 Class III vehicles as well.

7. Vehicles with SCR technology emit more NO_x in a trip with a cold start than vehicles with an LNT. This may be explained by the fact that the NOx absorption of an LNT typically starts at 80-100 °C while the light-off temperature of SCR catalysts is 150-200 °C.

8. The test program showed that emissions on a motorway with 80 km/h speed limit are about three times lower than on an 80 km/h rural road. The reason is that on the motorway, the dynamics are minimal, whereas on rural roads much deviation in velocity takes place due to e.g. roundabouts and road crossings.

9. There is still a difference between the NO_x emission limit and the real-world emissions of modern diesel vehicles. Previous studies have shown that vehicles that perform well during a type approval test, generally and almost with no exception have far higher NO_x emissions under real-world conditions. These Euro 6/VI LCVs do seem to turn the trend of the difference between real-world emissions and type approval emissions because the difference starts to decrease.

11. For most vehicles, no correlation with temperature is observed within the temperature range that was covered by the test program. One of the vehicles that did show an effect, the extra NO_x emission decreased with ambient temperature.

12. The new emission data will be used in 2018 to update the current Dutch emission factors for light commercial vehicles.

Acknowledgements

This work is part of the in-use compliance program of light-duty vehicles, which is financed since 1987 by the Dutch Ministry of Infrastructure and The Environment (I&M).

References

Kadijk G., Ligterink N.E., Spreen J.S. (2015a), On-road NOx and CO2 investigations of Euro 5 Light Commercial Vehicles, TNO report 2015 R10192 (30 p).

Kadijk G., van Mensch P., Spreen J.S. (2015b), Detailed investigations and real-world emission performance of Euro 6 diesel passenger cars. TNO report TNO 2015 R10702 (75 p).

Kadijk G., Ligterink N.E., van Mensch P., Spreen J.S., Vermeulen R.J., Vonk W.A. (2015c), Emissions of nitrogen oxides and particulates of diesel vehicles. TNO report TNO 2015 R10838 (16 p).

Kadijk G., Ligterink N.E., van Mensch P., Smokers R.T.M. (2016a), NOx emissions of Euro 5 and Euro 6 diesel passenger cars – test results in the lab and on the road. TNO report TNO 2016 R10083 (33 p).

Kadijk G., Vermeulen R.J., Heijne V.A.M, Ligterink N.E., Buskermolen E.G., Elstgeest M., van Heesen D., van der Mark P.J., (2017), NOx emissions of eighteen diesel Light Commercial Vehicles: Results of the Dutch Light-Duty road vehicle emission testing programme 2017. TNO report 2017 Rxxxxx, to be published in Q4-2017.

Spreen J.S., Kadijk G., Vermeulen R.J., Heijne V.A.M., Ligterink N.E., Stelwagen U., Smokers R.T.M., van der Mark P.J., Geilenkirchen G. (PBL) (2016b), Assessment of road vehicle emissions: methodology of the Dutch in-service testing programme, TNO report 2016 R11178 (86 p).

Vermeulen R.J. et al. (2012), A smart and robust NOx emission evaluation tool for the environmental screening of heavy-duty vehicles, TNO and Ministry of Infrastructure and the Environment, the Netherlands. Paper TAP conference 2012, Thessaloniki, Greece.

Vermeulen R.J. et al. (2014b), SEMS operating as a proven system for screening real-world NOx and NH3 emissions, TNO and Ministry of Infrastructure and the Environment, the Netherlands. Paper TAP conference 2014, Graz Austria.

Vermeulen R.J., et al., (2016c), The Netherlands In-Service Emissions Testing Programme for Heavy-Duty Vehicles 2015-2016 Annual Report, TNO report TNO 2016 R11270, 10 October 2016.

Comparison of regulated emission factors of Euro 6-LDV in Nordic temperatures and cold start conditions: Diesel-DI and Gasoline-DI

C. Weber[1], E. Figenbaum[1]

[1]Institute of Transport Economics, Gaustadalléen 21, 0349 Oslo, Norway
Keywords: Emission factors, Euro 6, Diesel DI, GDI.
Presenting author email: christian.weber@toi.no

Local emissions from traffic such as particulate matter (PM) and nitrogen oxides (NO_x) present a growing problem in European cites. The Scandinavian cites meet an additional challenge: Cold starts in cold temperatures cause even higher emission levels, however there is little focus on the problem in the rest of Europe. In order to fill this gap, the Institute of Transport Economics has since 2011 followed development in emissions of Euro 6 passenger cars (Hagman 2013, Weber 2015, Weber 2016).

The gasoline direct injection (GDI) technology developed was driven by the aim to meet low fuel consumption incentives, stated both by the customer and the regulation authorities. However, with in-cylinder pressures rising, while combustion gets more efficient, it is also adapting the known problems of diesel direct injection (DI) engines, such as high emission of NO_x and PM. This paper presents the results of a study of 8 diesel and 6 gasoline passenger cars.

The main findings show that the reduction in CO_2-emission in GDI-passenger cars comes at a price for the local emission factors.

Measurements were conducted at the emission laboratory of VTT in Helsinki, Finland. A chassis dynamometer is placed in a climate chamber, test temperatures were kept at +23 and -7 °C. The exhaust gasses are guided into a constant volume sampling system. The study focuses on measuring the regulated emission factors, PM, particulate number (PN), NO_x, carbon monoxide (CO) and hydrocarbons (HC). In addition, emission of CO_2 is reported. Besides the type approval cycle (NEDC), Artemis Urban and Helsinki City cycles are applied to reflect realistic city-driving conditions. Cars were chosen after availability on the market.

The total difference in emission of CO_2 of the GDI vehicles compared to the diesel vehicles is marginal, however the average size of the cars in the sample differs. When normalizing to the weight of the vehicle, the GDI group in average shows a 13 % higher CO_2-emission than the diesel cars.

Diesel cars show low emissions of PM in all tested cycles and temperatures. GDI cars show higher emission of PM than the diesel cars, although the emission factors are below the Euro 6 type approval limit value. In cold start conditions at -7 °C, however, exceedances of up to a factor 8.6 times the limit value are found.

As reported in the literature, the Euro 6 diesel vehicles show significant exceedances of the limit value, especially at -7 °C. However, as Figure 1 shows, we also found exceedances for NO_x for half of the GDI-vehicles we tested, although the temperature dependence seems to be less pronounced.

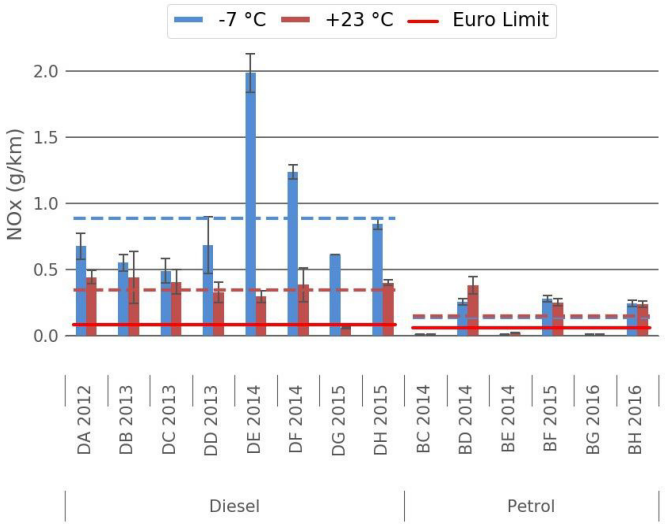

Figure 1. NO_x-emission factors for LDV tested in the Helsinki-city cycle. The dashed red and blue lines show the average values for diesel- and gasoline cars at -7 and +23 ºC, respectively. The light red line shows the type-approval limit for Euro 6 (European Parliament, 2007).

This work was part of the EMIROAD project funded by the Norwegian Public Roads Administration. The authors thank the team at VTT for good and fruitful cooperation.

European Parliament, (2007) 'Regulation (EC) No 715/2007 of the European Parliament and of the Council of 20 June 2007 on type approval of motor vehicles with respect to emissions from light passenger and commercial vehicles (Euro 5 and Euro 6)', *Official Journal of the European Union*.

Hagman, R., and Amundsen, A. H. (2013). Utslipp fra kjøretøy med Euro 6/VI teknologi. TØI rapport 1259/2013: Transportøkonomisk institutt, Oslo.

Weber, C., Hagman, R. and Amundsen, A. H. (2015) Utslipp fra kjøretøy med Euro 6/VI teknologi Resultater fra måleprogrammet i EMIROAD 2014. TØI rapport 1405/2015: Transportøkonomisk institutt, Oslo.

Weber, C. and Amundsen, A. H. (2016) Utslipp fra kjøretøy med Euro 6/VI teknologi Resultater fra måleprogrammet i EMIROAD 2015. TØI rapport 1506/2016: Transportøkonomisk institutt, Oslo.

Measurement and simulation of hybrid and plug in hybrid vehicles for the handbook of emission factors

S. Lipp[1], S. Hausberger[1], L. Schreiber[1]

[1] Institute for Internal Combustion Engines and Thermodynamics, Graz University of Technology,

Inffeldgasse 19, 8010 Graz, Austria

Email: lipp@ivt.tugraz.at

Abstract

For the upcoming HBEFA 4.1 (Handbook Emission Factors for Road Transport) the fuel consumption and emission behavior of PHEVs (Hybrid and Plug In Hybrid vehicles) shall be considered because the registration numbers of these vehicles are assumed to further increase in coming years. The following figure shows the increase of the registration numbers of passenger cars for the European Union for the first quarter of the years 2016 and 2017 with more than 60% increase of HEV's (Hybrid Electrical Vehicles) registrations.

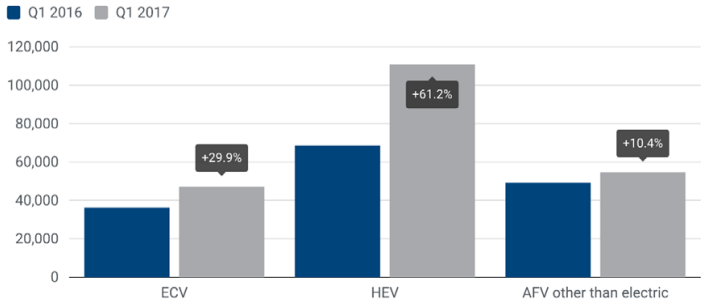

Figure 1: New passenger car registrations in the European Union (source: "ACEA", European Automobile Manufacturers Association), ECV…Electrically Chargeable Vehicles; AFV… Alternative Fuel Vehicles

The emission factors for conventional vehicles are calculated for the HBEFA with the model PHEM (Passenger car and Heavy duty Emission Model). PHEM simulates the power demand and the engine speed based on the equations for longitudinal dynamics and calculates fuel flow and emissions from engine maps in 1Hz resolution over driving cycles (see chapter 3). The model PHEM shall be used also for HEVs and PHEVs (Plug in Hybrid Vehicles) to provide emission factors comparable to the data for conventional vehicles.

For conventional vehicles the input data for PHEM is elaborated based on vehicle data and emission test data collected in the ERMES (European Research group on Mobile Emission Sources) group. The ERMES database collects vehicle emission tests in real driving situations. The ERMES database is used also as a basis for the hybrid vehicles but covers so far only three PHEVs.

The simulation approach in PHEM for HEV allocates the demanded propulsion power to the combustion engine and to the electric motor according to a generic control strategy. The control strategy is using inter alia the SOC (state of charge) of the battery and the actual power demand in the algorithm. High SOC leads typically to prefer electric driving. Due to the larger battery and the high electric power, the SOC has a main influence on the emissions and fuel consumption especially for PHEVs. The SOC is the main parameter determining if the PHEV is driving with the electric motor (charge depleting mode) or if it is driving as "normal HEV", i.e. in charge sustaining mode. Emissions in charge depleting mode are almost zero (vehicle is driven as EV) while at lower SOC the emissions are rather like from a conventional HEV. Thus, an assessment of typical SOC levels in the various traffic situations of the HBEFA is a fundamental prerequisite for representative PHEV emission factors.

The actual SOC depends on the SOC at the start of the trip, on the trip length and on the driving conditions up to an actual situation. Thus, typical SOC levels will be on average quite different for different traffic situations e.g. in residential areas compared to highway driving. The paper describes the

simulation method for HEV and PHEVs in PHEM and a statistical approach to calculate representative emission factors for PHEVs.

In addition, the actual RDE (Real Driving Emissions) legislation for PHEVs may change the way the electric range is considered in the evaluation methods for PEMS (Portable Emission Measurement Systems) tests on PHEVs. The evaluation method may influence the RDE emission levels of these vehicles in future. To consider PHEV's for the next HBEFA update some steps had to be carried out.

1. Data collection PHEV's

The first step was the data collection for PHEV's because in contrast to conventionally driven vehicles the database for this technology in ERMES was quite small. The measured data are important for the later explained simulation of those vehicles to validate the simulation model.

Emissions of two PHEV's were measured at TUG. One PHEV was equipped with a petrol-engine and one with a diesel-engine. Both vehicles were measured regarding RDE on the street and the petrol-PHEV was measured on the chassis dynamometer at TUG. For the diesel PHEV the measurement on the test bed was not possible because it was a permanent 4-wheel driven car and the test bed handles only one driven axis. The same diesel car without hybrid-technology was also tested in house, so the emissions between both technologies for the same vehicle could be compared.

Table 1**:** Specifications of the tested vehicles

Vehicle data	**veh1**	**veh2**	**veh3**
	PHEV diesel	PHEV petrol	conv. diesel
P_{engine} [kW]	190	110	160
n_{idle} [U/min]	840	750	840
n_{rated} [U/min]	4000	5750	4000
mass approval [kg]	2520	1598	2050
battery capacity [kWh]	17.3	8.8	-
electrical power [kW]	85	75	-
number RDE tests	6	3	14
number cycles test bed	-	18	-

Figure 1 shows the measured NO_x and CO_2 emissions for vehicle 1 (diesel PHEV). 3 RDE-trips had a start SOC of 100%, one of 85% and two trips where driven with a unknown status, that means that the condition after driving one RDE route with a known start SOC was the starting condition for the following trip with unknown start SOC. The RDE driving was carried out in the "Auto-mode" of the car. Since the overall RDE trip on the "Ries-route" is approx. 80 km, the SOC at test start does not dominate the average emissions over the entire trip. Also the driving style influences the engagement of the combustion engine and thus the resulting emissions.

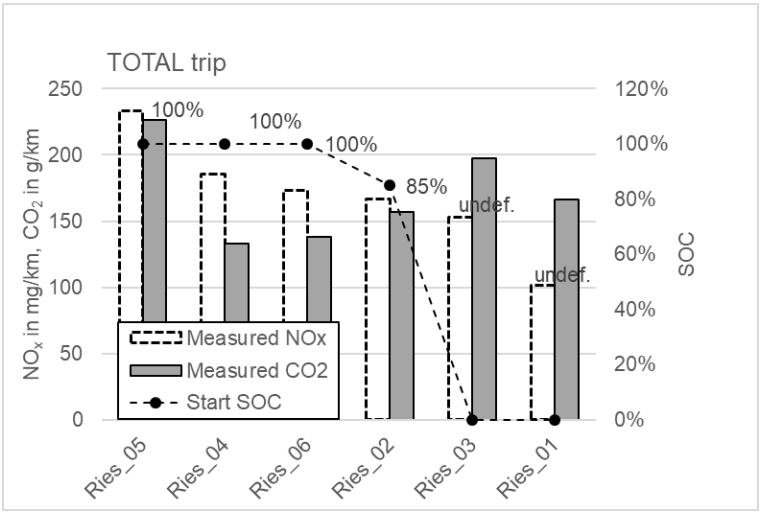

Figure 2: Measured NO_x and CO_2 of the diesel PHEV (vehicle 1)

The test data of the vehicles was used to calibrate the generic HEV control strategy in the model PHEM to reproduce the average real world behavior.

2. PHEV simulation model for HBEFA

The idea behind the HBEFA is to give a detailed assessment of emissions depending on the traffic situations at a local level. The shares of traffic situations and vehicle fleet compositions can be defined on a larger scale (for example Austria). Therefore single emission factors for different vehicle-categories (passenger cars, motorcycles etc.), vehicle-technologies (diesel, petrol, hybrid etc.) and emission-concept (EURO 5, EURO 6, etc.) have to be provided as input data to the HBEFA. For a systematic assessment of the emission factors, representative vehicle models for the simulation are necessary.

The vehicle models shall represent average European vehicle specification for the single vehicle class. For these vehicles, the model PHEM simulates emission factors (g/km) based on average emission maps for a set of pre-defined driving cycles. Each driving cycle represents a traffic situation (e.g. main road, urban, dense traffic, 2% road gradient). The model PHEM provides the emission factors of all vehicle classes as input to the HBEFA. In HBEFA the detailed emission factors are weighted to calculate fleet average values. The averaging in HBEFA allows several different levels of detail.

For diesel and petrol passenger cars representative simulation models are available from the work for HBEFA 3.3 up to EURO 6d. For the next update (HBEFA 4.1) representative models shall be elaborated also for hybrid and plug-in-hybrid vehicles. An existing hybrid model in the simulation tool PHEM was used as basis for the actual work. The existing model was calibrated with measured data and an average PHEV EURO 6 vehicle model was developed. This vehicle model was used for the calculation of a first set of emission factors for the HBEFA cycles. A final data set for HBEFA 4.1 is planned for spring 2018.

The vehicle specifications of the average PHEV model for PHEM are based on the registration statistic from the most sold PHEV's in Europe for the year 2016. Table 2 shows the data used for the definition of the specifications of the average PHEV for PHEM.

Table 2: Statistic of the 10 most sold PHEV'S in Europe in the year 2016 ("EAFO" 2017)

Ranking	Make	Model	number of registrations 2016	Share in %
1	Mitsubishi	Outlander PHEV	21328	21.77
2	VW	Passat GTE	13248	13.52
3	VW	Golf GTE	11351	11.59
4	Mercedes	C350e	10231	10.44
5	Volvo	XC90 PHEV	9586	9.78
6	BMW	330e	8702	8.88
7	Audi	A3 e-tron	6894	7.04
8	BMW	225xe Active Tourer	5915	6.04
9	BMW	X5 40e	5393	5.5
10	BMW	i3 Rex	5322	5.43
Sum			97970	100

Based on this statistic an average PHEV EURO 6 was defined

Table 3: Specifications of the average PHEV

Parameter	Unit	Value
Curb weight (DIN)	kg	1738
Fuel consumption (Type approval)	l/100 km	1.81
Power combustion engine	kW	123
Power electrical engine	kW	79
Type of electrical engine	-	PMSM
Battery capacity	kWh	8.8
Battery voltage	V	314
Electrical range	km	43

Vehicle number 2 was selected for testing after the specifications in Table 3 were elaborated to meet the average specifications as good as possible. Thus mainly vehicle 2 was used to validate and calibrate the generic hybrid model in PHEM.

3. PHEV simulation for HBEFA in PHEM

PHEM is an instantaneous emission model based on equations of vehicle longitudinal dynamics and engine emission maps, which has been developed by TUG since the late 1990's. It calculates the fuel consumption and emissions of road vehicles in 1Hz for a given driving cycle based on the vehicle longitudinal dynamics and emission maps (Figure 3). The engine power demand is calculated in 1Hz for the cycles from the driving resistances and losses in the transmission line. The engine speed is simulated by the tire diameter, final drive and transmission ratio as well as a driver gear shift model. Base exhaust emissions and fuel flow are then interpolated from engine maps. To increase the accuracy of the simulated emissions transient correction functions are applied to consider different emission behavior under transient engine loads. Furthermore, models for the efficiency of exhaust gas after treatment systems are implemented. The temperatures of catalytic converters are simulated by a 0-dimensional heat balance and from the heat transfer between exhaust gas and the catalysts material and from the exhaust line to the ambient. The exhaust system model from PHEM is described in (Rexeis, 2009). A driver model is implemented to provide representative gear shift maneuvers.

Since the vehicle longitudinal dynamics model calculates the engine power output and speed from physical interrelationships, any imaginable driving condition can be illustrated by this approach. For simulation of emission factors PHEM offers a predefined set of "average vehicles" representing average vehicles for all relevant vehicle categories, which are also used for the emission factors from HBEFA.

Since 2010, the option for a detailed simulation of HEV and BEV vehicles is included in PHEM, e.g. (Lutz, 2011), (Renhart, 2010).

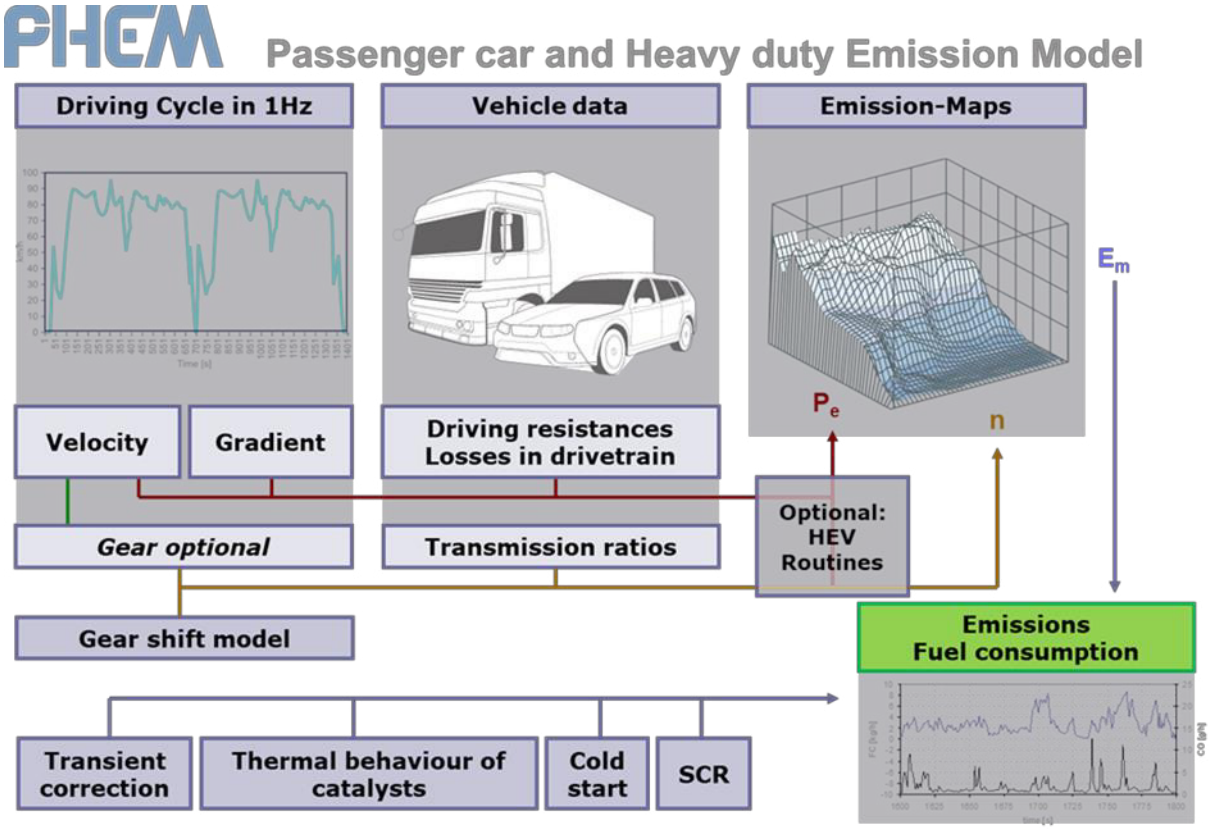

Figure 3: PHEM calculation scheme (source: "PHEM User Guide, 2017")

For the hybrid simulation additional input parameter are necessary. Table 4 shows the common input parameter for the emission simulation in PHEM. Table 5 shows the additional input parameter for the hybrid simulation. In PHEM, a parallel hybrid vehicle is modeled.

Table 4: General model input parameters for PHEM

Module	Input parameter General	
VEH	* Vehicle mass	* Rolling resistance coefficients
	* Loading	* Engine data
	* Red. mass wheels	* Transmission parameters
	* Wheel diameter	* Gear ratios
	* Drag coefficient	* Power demand auxiliaries
	* Cross sectional area	
MAP	* Engine map (fuel consumption, emissions, …)	
FLD	* Full load and drag curve	
DRI	* Driving cycle with gradient	

Table 5: HEV model input parameters for PHEM

Module	Input Parameter Hybrid	
BAT	* Open circuit voltage	* Number of cells
	* SOC – Minimum	* Internal resistance
	* SOC – Maximum	* Battery capacity
EMO	* Efficiency map electric engine and generator	
	* Full load curve electric engine and generator	
STE	* Hybrid characteristic given via control curve	

The module “STE” describes the hybrid control strategy between electrical and conventional driving for the vehicle. The aim of the strategy is to minimize emissions and fuel consumption. The following effects are simulated in the control strategy:

1. Recuperation of braking energy up to a predefined maximum SOC
2. Engine stop at zero power demand as long as SOC is above predefined minimum value
3. Electric driving as long as SOC is above minimum value.
4. Shifting the load point of the combustion engine in areas with more efficiency by generation of electric energy up to the maximum SOC
5. The selection between electric driving, electric assistance, power generation and driving with combustion engine only is based on a comparison of the efficiencies of the three possible modes in each computation step.

The efficiency chain of the electrical and the conventional powertrain is important for the operating strategy. A so-called efficiency factor K_e is calculated for point 5. Of the control strategy. The equation for K_e is:

$$K_e = \frac{W_{electric}}{\Delta m_{fuel}}$$

$W_{electric}$ ..... energy from or to battery in kWh

Δm_{fuel} ..... difference in fuel consumption compared to pure combustion engine operating in kg

$$K_{e\_assist} = \frac{W_{electric\_taken}}{\Delta m_{fuel}}$$

$$K_{e\_charge} = \frac{W_{electric\_stored}}{\Delta m_{fuel}}$$

The efficiency factor for the assisting should be as small as possible and for the generating, the value should be as big as possible. The limits for the K_e factors are defined in the STE function (Figure 4). Assisting is allowed only for K_{e_assist} values below the threshold curve, generation of electric energy is allowed for $K_{e\_generate}$, above the thresholds, otherwise no efficiency increase in comparison to only conventional driving with the combustion engine is given.

The vertical line in Figure 4 is a schematic picture of the decision making process in a time step “t”. In this case “generating” would be selected since it has the larger distance to the threshold curve.

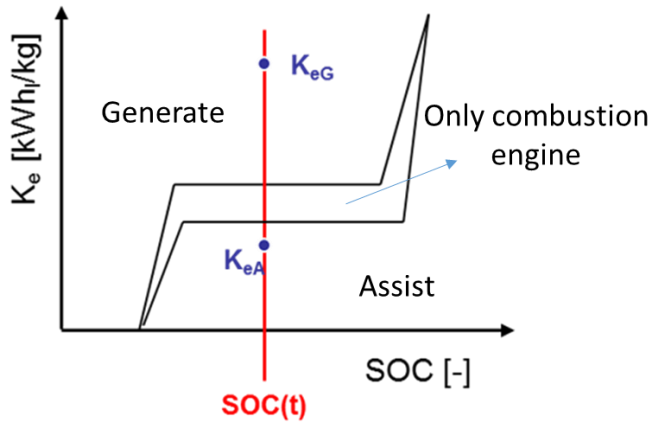

Figure 4: Operating control curve (STE curve) for the hybrid strategy in PHEM.

The dependency of the STE curve on SOC ensures that towards SOC Min “generating” is preferred and that SOC Min is not exceeded. Toward SOC Max consequently “electric drive” is preferred to keep capacity in the battery free for possible regeneration at braking events.

The position of the horizontal STE function is computed from real world cycle simulations in a way, that the fuel saved by electric driving outweighs the fuel needed to generate electric energy on board. Therefore the cycle is simulated in three operation modes: only combustion engine driven, only assisting and only generating. Then the efficiency factors are calculated and plotted over the cumulated electrical

energy. The K_{e_assist} values are sorted starting with the smallest values and the $K_{e\_generating}$ are sorted inverse starting with the biggest value. The intersection of both curves gives the vertical height of the operating curve like shown in an example in Figure 5. The intersection can be interpreted as the amount of electric energy that can be efficiently spent for assisting or electric driving from the battery since it has been produced with a lower extra fuel consumption compared to the fuel saved by electric motor engagement.

The intersection efficiency value is quite robust against variations in the cycles used and has a similar level for all HEV and PHEV configurations. More details are described in (Lutz, 2011).

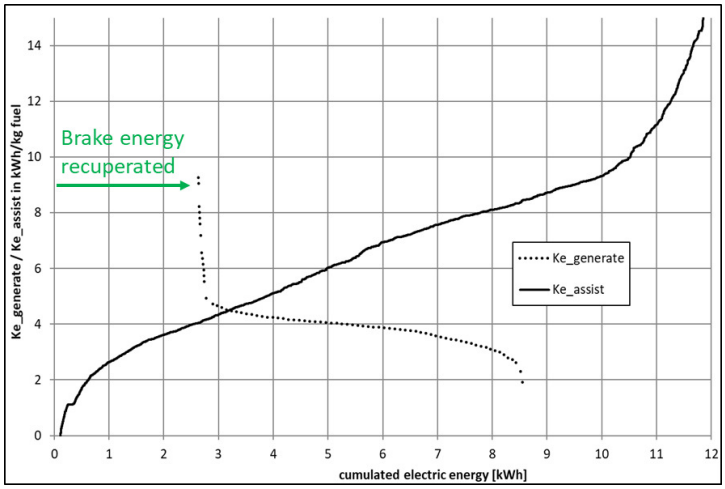

Figure 5: Determination of the operating curve

The steps explained above as well as the validation of the resulting PHEV model are described in (Schreiber, 2017) and lead to the base hybrid vehicle model in PHEM for the HBEFA simulation.

For the following analysis HBEFA cycles representative for the average traffic situation in Austria were considered. Each cycle has a weighting factor according to his share in the total vehicle mileage. The big unknown factor for PHEV's is the share of electric driving in the cycles, which is run with electricity taken from the grid. Electric driving situations using energy provided by brake energy recuperation or by on board electricity generation is simulated by PHEM in a realistic way in the charge sustaining mode for HEVs. The share driven with electricity from the grid depends certainly on how the battery is recharged by the user and which driving distance distribution is following recharging events. Detailed information on this data is hardly available. Regarding the electrical driving share, we thus made different investigations described in more detail in the following.

For a well-defined and easily applicable consideration of the share driven with electricity from the grid, following approach is used:

The emission factors for the PHEV are simulated in all 257 HBEFA cycles (traffic situations) with road gradients from -6% to +6% for:

a) charge depleting mode resulting in pure electric driving as long as the electric motor has sufficient power,

b) charge sustaining mode, i.e. as a HEV without charging from the grid

The emission factors are the weighted average from the emission factors from a) and from b) as follows:

$$E_{PHEV} = \frac{K_{EV}}{100} \cdot E_{EV} + \left(1 - \frac{K_{EV}}{100}\right) \cdot E_{HEV}$$

E_{PHEV} ..... Weighted emission factors including driving with electricity from the grid in g/km

K_{EV} ..... share driven with electricity from the grid in %

E_{EV} ..... Emission factors with electric driving mode in g/km

E_{HEV} ..... Emission factors with HEV charge sustaining mode in g/km

The emission factors E_{EV} and E_{HEV} are calculated by PHEM as described before. For the share driven with electricity from the grid (K_{EV}) different scenarios are developed.

Version 1) constant K_{EV}

Version 2) K_{EV} depending on the average speed of the cycle based on German statistics

Version 3) K_{EV} depending on the average speed based on simulated trip distributions.

For the version 3, the dependency between electrical driving share and cycle velocity was elaborated by defining and simulating typical mission profiles with different start SOC's with the average hybrid model in PHEM. The aim of these simulations was to produce a representative matrix of electrical driving shares per traffic situation. The steps carried out are described in more detail in the following. For version 3 instead of a speed dependency also a dependency on urban/road/motorway situation is possible but would result in sharp steps of emission factors between the situations.

Version1: Constant electrical driving share

For K_{EV} two versions are implemented for a sensitivity analysis:

K_{EV} = 0% and K_{EV} = 35%

Figure 6 shows the CO_2 emissions over the average cycle speed for the average PHEV for K_{EV} = 0% and for the average petrol vehicle EURO 6 (based on interim HBEFA 4.1 results). For Figure 6, only cycles with road gradient from 0% are shown.

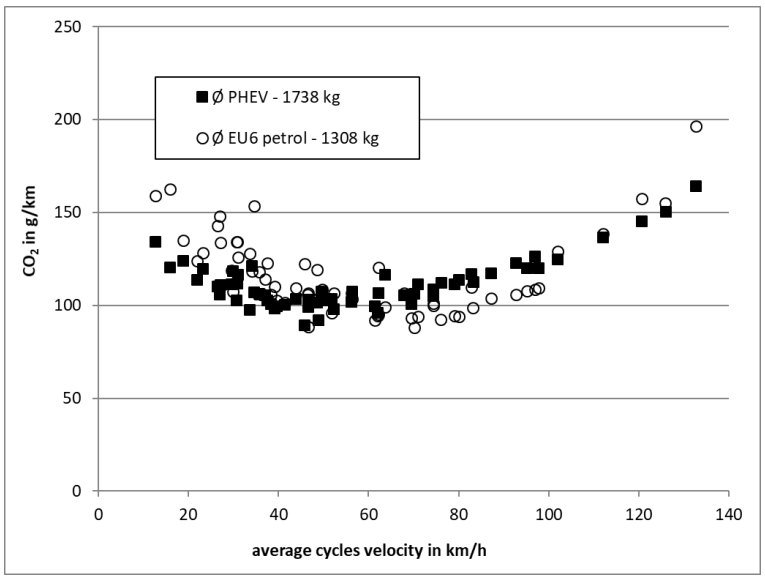

Figure 6: CO_2 emissions from the average PHEV with K_{EV} = 0% and from the average petrol EURO 6 vehicle

Without charging the PHEV from the grid, the saving potential of CO_2 for the PHEV especially is given for cycles with lower average speeds representing urban driving. In these cycles, the recuperated energy during braking of the vehicle is quite high and the stored energy is used for electric driving saving CO_2. For cycles with higher average cycle speeds and less braking events this potential gets lower and so, the CO_2 emissions of PHEVs and conventional cars are similar. It has to be mentioned that the average petrol vehicle EURO 6 is built from five cars representing rather small vehicles. The mass of the simulated petrol vehicle is about 400 kg lower than the mass of the average PHEV. The higher weight leads to higher driving resistances for the PHEV and thus to disadvantages in cruising phases compared to the petrol driven vehicle. To which extent PHEV technology will be used also in future rather in the larger vehicle segments is open. The additional costs for the technology support the assumption that few PHEVs will be found in small vehicles also in future.

Figure 7 shows the results for K_{EV} = 35%. In that case the CO_2 tailpipe saving potential form PHEV's is much bigger.

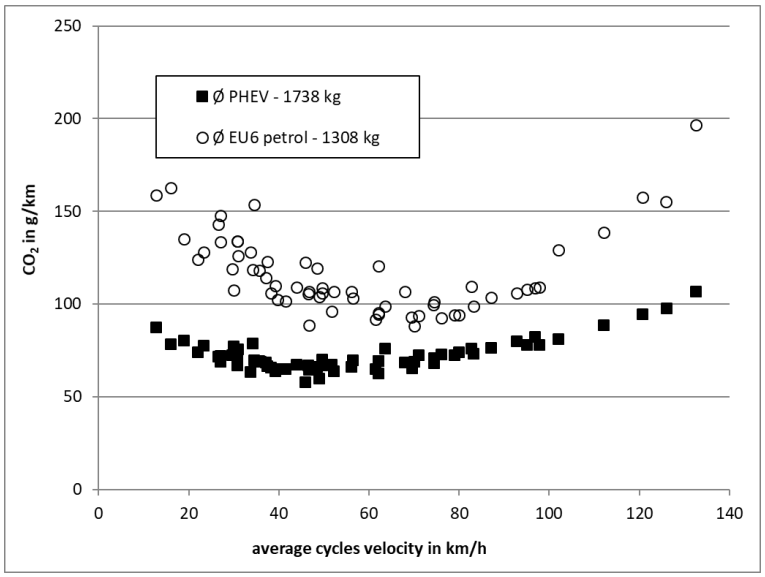

Figure 7: CO_2 emissions for the average PHEV and petrol EURO 6 vehicle with 35% electrical share

For the WTW (Well To Wheel) emissions also the emissions during the production process for the respective energy form (for example the production of the electricity to charge the battery of a PHEV) are taken into account. The electrical energy consumption for PHEV's from the grid in kWh/km are result from the simulation in the EV-mode. The WTW emissions were then calculated using the following equation:

$$CO_{2\_WTW} = \frac{K_{EF}}{100} \cdot EC_{EV} \cdot K_{CO_2} + \left(\left(1 - \frac{K_{EF}}{100}\right) \cdot \frac{FC_{HEV}}{\frac{\eta_{Gasoline}}{100}} \right) \cdot 3.153$$

EC_{EV}..... electric energy consumption from the grid in kWh/km

FC_{HEV} ..... Fuel consumption with electric driving mode in g/km

K_{CO2}..... emission factor of the electricity mix for Europe in gCO_2/kWh

$\eta_{Gasoline}$..... efficiency of petrol manufacturing in %

For the emission factor of the electricity mix 480 g/kWh was used for illustration, the efficiency factor for the production of petrol was set to 82% to produce the well-to-wheel results in Table 6.

Table 6: Simulated TTW- and WTW emissions for version 1

	tank-to-wheel gCO_2/km	**well-to-wheel** gCO_2/km	**fuel consumption ttw** l/100km
Ø EU 6 petrol	123.45	150.55	5.30
Ø EU 6 PHEV 0% el. Driving	117.59	143.40	5.05
Ø EU 6 PHEV 35% el. Driving	76.43	122.20	3.28

With 35% share of electric driving with electricity from the grid the TTW emissions from the PHEV are approx. 40% lower compared to the conventional gasoline vehicle, although the PHEV represents a larger vehicle segment. The WTW emissions are in this case 20% lower from the PHEV. A PHEV, which is hardly recharged from the grid, provides only minor CO_2 reductions compared to conventional vehicles due to the higher weight.

Version 2: Variable electrical driving share DLR

In version 2, the share of electric driving from electric energy from the grid was computed based on a dataset from DLR (Deutsches Zentrum für Luft- und Raumfahrt, KIT Karlsruher Institut für Technologie) from a final report "LADEN2020". For an electrical range of PHEVs of 40 km a matrix where the electrical driving share in % per distance class over the driven distance in km per class was given, was used. Based on this matrix a linear function between average speed and electrical driving share was computed. Therefore, we assumed an average speed per distance class. The function for average speed per distance class is based on the assumption that shorter distances are driven with lower average speeds (i.e. an increasing extra-urban driving with increasing distance). Figure 8 shows the resulting function between the electrical driving share and the average cycle speed. Since a simple linear dependency between speed and trip distance was used, also the share in electric driving over vehicle speed is a linear function. Possibly this approach underestimates electrical driving shares of PHEVs on highways.

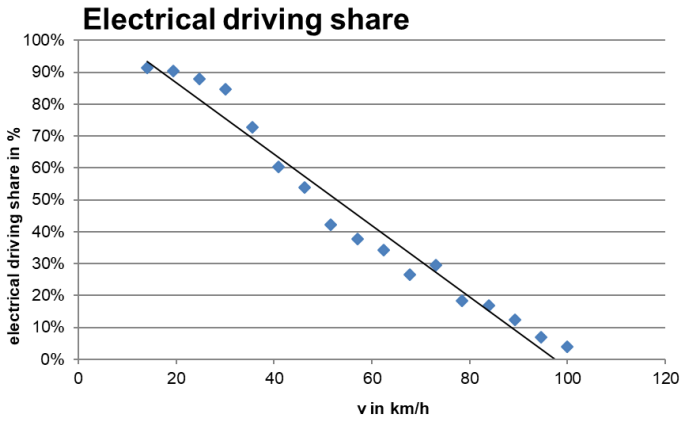

Figure 8: Electrical driving share over average speed in version 2

Using the function shown in Figure 8 instead of the constant 35% electrical driving share for all cycles the weighted average CO_2 emissions from the PHEV are quite similar (Table 7).

Table 7: Simulated results TTW- and WTW emissions for version 2

	tank-to-wheel gCO_2/km	**well-to-wheel** gCO_2/km	**fuel consumption ttw** l/100km
Ø EU 6 petrol	123.45	150.55	5.30
Ø EU 6 PHEV version 2	81.34	122.15	3.49

Version 3: Variable electrical driving share TUG

The aim of version 3 was the production of a representative matrix for electric driving shares per traffic situations for different start SOC's.

The first step was the elaboration of typical mission profiles for PHEV's and to simulate them with different start SOC's. Standard driving cycles with driven distances between 20 to 300 km were defined based on the relevant HBEFA cycles. For each road category (urban, rural and motorway) one cycle was defined and urban, road and motorway was mixed as function of the distance of the total trip.

The differentiation between the three road-categories was made in the evaluation by using the driven velocity. Urban driving means v<=50 km/h, rural means v>50 km/h <=90km/h and motorway is defined for velocities bigger than 90 km/h.

For the shortest standard cycle with 20 km distance a specific distribution with 1/3 urban, 1/3 rural and 1/3 mw was chosen. The urban driving was split into two sections, one at cycle start and the other at cycle end. For the longer standard cycles, up to 100 km, the urban distance was kept constant and only the rural and motorway parts where extended in a way that the driven distance for both parts is nearly the same. For the 200 km and the 300 km cycles the 100 km cycle was sequenced twice and three times. Figure 9 shows the velocity distribution for the 20 km standard cycle.

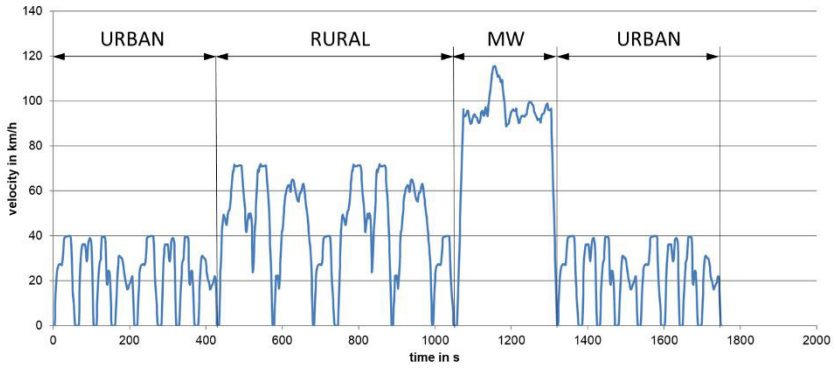

Figure 9: 20 km standard cycle

A matrix of 6 typical mission profiles with 20, 40, 60, 100, 200 and 300 km with four different start SOC's from 20,40,60 and 80% where simulated with the average PHEV in PHEM which has an electrical range of approx.. 40km, depending on the driving cycle, loading and auxiliary power demand. In the PHEV model described before, a SOC lower than 20% leads to a charge sustaining mode and no further energy consumption from the grid. The share of electric driving thus can be computed for each simulation result in the trip for the seconds with zero fuel consumption until SOC drops the first time to 20%. Also later in a cycle electric driving occurs but is fed by energy produced on-board in the HEV mode. The aim of the simulation was to produce a matrix of electric driving shares per traffic situation (length of the trip and start-SOC). Table 8 shows the results. As expected, the share driven with electricity from the grid (K_{EV}) decreases with increasing trip distance. Increasing distance again is linked to higher average speeds.

Table 8: Shares of electrical driving with electric energy from the grid over velocity and distance for different SOC's

velocity in km/h	**0-50**	SOC 20	51%	51%	47%	47%	43%	29%
		SOC 40	96%	93%	79%	63%	52%	35%
		SOC 60	96%	93%	90%	83%	61%	40%
		SOC 80	97%	95%	92%	90%	69%	46%
	50-90	SOC 20	6%	5%	8%	13%	13%	9%
		SOC 40	88%	87%	62%	39%	28%	19%
		SOC 60	88%	87%	88%	78%	45%	30%
		SOC 80	87%	87%	89%	89%	60%	40%
	>90	SOC 20	18%	23%	24%	25%	12%	8%
		SOC 40	23%	25%	24%	25%	12%	8%
		SOC 60	23%	25%	25%	25%	12%	8%
		SOC 80	26%	26%	25%	26%	13%	9%
distance km			**20**	**40**	**60**	**100**	**200**	**300**

To get a dependency between electrical driving share and average speed (or road category), the distance- and the start SOC-distribution is needed. While statistics on trip distance distributions exist for several countries, no data on SOC distributions at trip start is available yet. Figure 10 shows the SOC-distribution which is based on estimations at TUG. It is expected, that the battery of a PHEV is charged in future quite regularly and so most of the time the start SOC is quite high. We expected a start SOC from 80% for 40% of the rides. Lower start SOC's are expected more rarely. These assumptions can be replaced by statistical data easily in future.

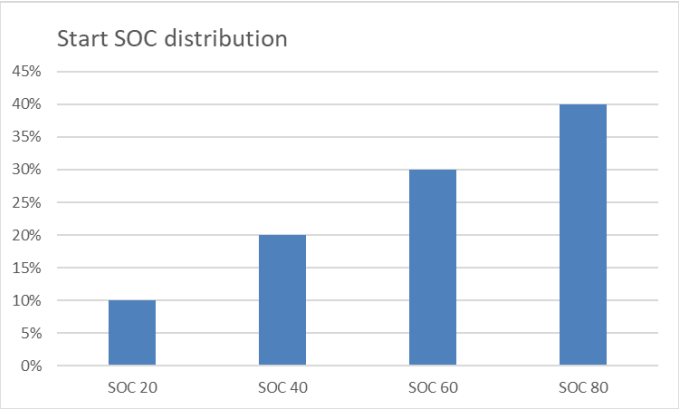

Figure 10: Start SOC-distribution assumed for version 3

The distance distribution was calculated based on a distribution given in (DLR, 2017) as shown in Figure 11. It is important to note, that for emission factors in [g/km] the shares of the distance classes in the total distance driven are needed. In this unit (share in km) longer distances have a higher weighting than in the frequently shown unit (share in trips).

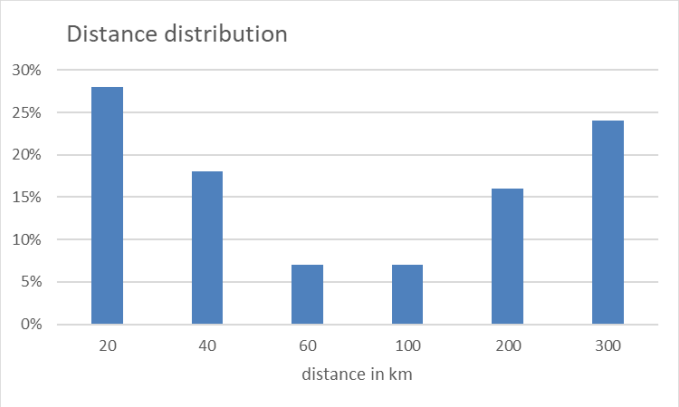

Figure 11: Distance distribution used for version 3

The probability for both distributions (SOC and distance shares) multiplied with the matrix from Table 8 leads to the equation between electrical driving share and average cycle velocity used for version 3. Figure 12 illustrates the equation found from version 3. For speeds below 40 km/h a constant share was assumed (urban average) and also for cycles with average speeds above 110 km/h a constant value (motorway average) was fixed.

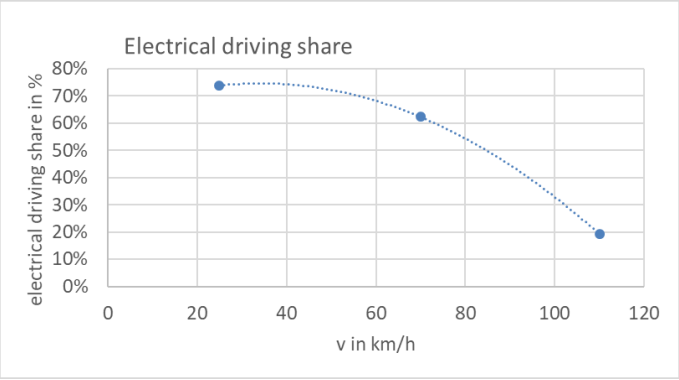

Figure 12: Electrical driving share over average speed version 3

For the average PHEV version 3 leads to the lower TTW and WTW CO2 emissions than version 1 and 2 (Table 9). The WTW emissions from the PHEV are in this scenario 25% lower compared to the

gasoline car, TTW emissions are almost 50% lower. With higher shares of renewable energies in the power plant mix, the WTW emissions of the PHEV could be further reduced. Certainly also renewable fuels for the combustion engine of the HEV or PHEVs could significantly contribute to further CO_2 reductions in future.

Table 9: Simulated results for TTW- and WTW emissions for version 3

	tank-to-wheel gCO_2/km	**well-to-wheel** gCO_2/km	**fuel consumption ttw** l/100km
Ø EU 6 petrol	123.45	150.55	5.30
Ø EU 6 PHEV version 3	65.79	114.17	2.82

Similar to the CO_2 emissions also the pollutant emissions from the PHEV were simulated with PHEM for electric drive mode (charge depleting) and for HEV mode (charge sustaining). Table 10 shows the results for the charge sustaining mode and the mix-mode, where charge sustaining and charge depleting were mixed together according to version 3 for the electrical driving share (K_{EF}). With a reasonable charging ("Mix") of PHEVs emissions can be reduced compared to the charge sustaining mode by approx. 50&. This however needs a sufficient recharging infrastructure for regular charging at home and occasional charging at target locations of longer trips (only 10% of the trips start with an SOC at charge sustain limit).

Table 10: Results for emissions and fuel consumption version 3

	NOx mg/km	**PN** #/km	**CO2** g/km	**fuel consumption** l/100 km
Charge Sustaining Mode	27.44	5.95E+08	118.97	5.11
Mix	12.92	3.19E+08	66.23	2.84

4. Conclusion and outlook

It is expected that the number of hybrid and plug-in-hybrid vehicles in the near future will increase. So an estimation of emission factors and fuel consumption of these vehicle-technologies is demanded. For the next update of HBEFA it is foreseen to introduce PHEVs as new vehicle category. For providing emission factors for hybrid and plug-in-hybrid vehicles, a representative simulation model had to be elaborated which represents the emission behavior of those vehicles in real traffic. An average model of a PHEV EURO6 car for the simulation model PHEM from TUG was elaborated based on actually available PHEVs on the market. The simulation tool PHEM calculates for the PHEV electric energy consumption and emissions for any driving cycle and for any state of charge of the battery at trip start.

For representative emission factors from PHEVs the share of electric driving with energy from the grid is necessary. With this share the real world emission factors can be weighted from PHEM results for empty battery (charge sustaining mode, no energy from the grid used) and full battery (charge depleting mode, electric driving purely with energy from the grid).

The electrical driving shares most likely are different for different traffic situations. A literature review showed an electrical driving share for PHEVs of 60% for the year 2020 in case of a well-established charging infrastructure. For a more flexible approach, a trip matrix was simulated with PHEM for the PHEV model with different distances, traffic situations and SOC levels at trip start. From the results, the share of electric driving with grid energy can be computed for given distributions for the shares of trip distance classes and start SOC-classes. The latter is based on estimations at TUG yet since no statistical data was found. The result shows on average approx. 50% share of electric driving with energy from the grid when the traffic situations are weighted for trip distance.

The matrix also allows to compute a dependency between the electrical driving share and the average trip velocity. With this function representative emission factors for PHEVs can be computed for all traffic situations. The method was used to calculate PHEV emission factors with the model PHEM for all 257 HBEFA cycles successfully. For the final HBEFA 4.1 data set assumptions made for the SOC distribution at trip start may be updated if any data source can be found.

Abbreviations

ACEA	European Automobile Manufacturers Association
EAFO	European Alternative Fuels Observatory
ERMES	European Research group on Mobile Emission Sources
EV	Electric vehicle
DLR	„Deutsches Zentrum für Luft- und Raumfahrt“ with KIT, „Karlsruher Institut für Technologie“
HBEFA	Handbook Emission Factors for Road Transport
HEV	Hybrid Electric Vehicle
K_{EV}	share of the trip distance of a PHEV driven with electricity from the grid [%]
PEMS	Portable Emission Measurement System
PHEM	Passenger car and Heavy duty Emission Model
PHEV	Plug in Hybrid Electric Vehicle
PMSM	Permanent Magnet Synchronous Motor
RDE	Real Driving Emissions
SOC	State of Charge
TTW	Tank To Wheel
WTW	Well To Wheel

References

“EAFO” [Onine] Available under: http://www.eafo.eu/vehicle-statistics/m1. [accessed: 29-Mai-2017]

Luz R., Hausberger S., Rexeis M., et al.: Optimisation tool for Hybrid Electric Recuperation and Operation Strategies. Endbericht des Projektes „HERO“ finanziert im Rahmen der 2. Ausschreibung der Programmlinie a3plus des Forschungs- und Technologieprogramms iv2splus. Graz, 30.5.2011

Renhart W., Magele C., Hausberger S., Zallinger M., Luz R.; Recent NiMH-battery Modeling Supported by Finite Element Thermal Analysis, 20. Symposium on Power Electronics, Electrical Drivers, Automation and Motion (SPEEDAM), Pisa, 14.-16.06.2010

Rexeis M.: Ascertainment of Real World Emissions of Heavy Duty Vehicles; PHD at University of Technology Graz; 2009

„PHEM User Guide“ S. Hausberger, M. Rexeis, und R. Luz, „PHEM User Guide“. Institut für Verbrennungskraftmaschinen, TU Graz, 2017.

Schreiber L.: Abbildung eines durchschnittlichen Plug-In-Hybridfahrzeuges für die Fahrzeugsimulation (Simulation of a representative PHEV); Master Thesis at University of Technology Graz; 2017

A novel approach for NOx emission factors of diesel cars in HBEFA (Version 3.3)

M. Keller[1], S. Hausberger[2], C. Matzer[2], Ph. Wüthrich[3] and B. Notter[3]

[1] MK Consulting GmbH, CH-3012 Bern/Switzerland (mario.keller@mkconsulting.ch)
[2] Institute for Internal Combustion Engines and Thermodynamics, TU Graz, A-8010 Graz/Austria
[3] INFRAS, CH-3012 Bern/Switzerland

Context and objective

The Handbook Emission Factors for Road Transport (HBEFA) provides emission factors for all current vehicle categories (cars, light commercial vehicles, heavy goods vehicles, urban buses, coaches and motor cycles). The first version of HBEFA (HBEFA 1.1) was published in December 1995. Since then every 4 to 5 years HBEFA-updates were developed taking into account the newest technological developments in emission behavior of the vehicles, new or adapted regulations, new methodologies in emission measurement and modelling, changes in the fleet compositions and driving behavior etc. In the context of 'Dieselgate' it became evident that the NOx emission factors for diesel cars of the HBEFA version 3.2 which was published in 2014 were underestimated. Therefore, it was decided to produce a "quick update" of these factors (and only these factors), since a regular update is scheduled for end of 2018/early 2019. The results (software and documentation) are published as version HBEFA 3.3 (www.hbefa.net, Keller et al. [2017]).

Originally the focus was set on the newest concept Euro-6. Work was started under the assumption that the emission factors up to Euro-5 would not need to be adapted, since the emission factors of the HBEFA were always based on real world emission measurements over non-regulatory driving cycles which reflect a realistic driving behaviour. As a result, Euro 5 diesel car emission factors already have been significantly higher than the emission limit value (0.18 g/km). The values in the version HBEFA 3.2 (2014) – weighted over all traffic situations for example for Germany – are close to 0.7 g/km, i.e. ca. 4 times higher than the limit value. However, after the emission control failures of diesel cars became public several investigations and measurement programs in different countries were performed (BMVI/KBA 2016, MEEM 2016, CTA 2016, DfT 2016). The results indicate that also other factors influence the emission behaviour of the vehicles, one of them is the ambient temperature. As a consequence, this influence is now taken into account not only for Euro-6, but also for earlier concepts.

The emission factors of earlier HBEFA versions had to rely almost exclusively on emission measurements performed on chassis dynamometers in manufacturer-independent laboratories (as ADAC, EMPA, JRC, LAT, TNO, TRL, TUG etc.). In general, standardized real world driving cycles were used to get comparable data from different laboratories. These emission measurements (measured second-per-second) are a crucial input to build the engine maps out of which the PHEM (Passenger car and Heavy duty Emission Model) of the TU Graz eventually calculates the emission factor (in g pollutant/km) for the different traffic situations and vehicle concepts which are then integrated in HBEFA. This approach is also used for version HBEFA 3.3. However, it does not (yet) integrate the influence of ambient temperature. Therefore, additional data sources were analysed.

One of the sources are on-road measurements. These will become more prominent in the future particularly due to the Real-Driving Emissions (RDE) regulation which is expected to improve the effectiveness of emissions control in the real world. PEMS (Portable Emission Measurement System) measurement campaigns were also started by independent third parties to monitor emission behaviour of the vehicles. Collecting and analysing such data will continue also for future HBEFA versions.

An additional measurement technique in monitoring air quality is remote sensing (RS). This method monitors the on-road emissions by determining the concentration of certain pollutants in the exhaust plumes of vehicles passing at particular locations and assigns the emission levels out of the concentrations to individual vehicles (see e.g. AWEL 2017, Borken-Kleefeld 2013, Chen et al. 2016). While tests on chassis dynamometers as well as on-road tests with PEMS provide emission data for individual vehicles, remote sensing delivers information on a much wider set of

vehicles resp. a whole fleet passing by at singular locations, hence giving indications about fleet emissions overall. Therefore, remote sensing can be seen as complementary approach to the classical measurement techniques. It is particularly valuable for identifying the influence of factors which are difficult to be captured by measuring individual vehicles, as e.g. deterioration with increasing mileage or age or the influence of ambient temperature.

Hence, for the version HBEFA 3.3 a two-step procedure was applied: (i) "base emission factors" were generated by the PHEM model relying on tests on chassis dynamometers as well as on-road tests with PEMS, (ii) correction factors for mileage as well as for ambient temperature were derived from remote sensing data (RSD).

"Base emission factors"

Approach: the PHEM model

The "base emission factors" (i.e. the g pollutant / km, differentiated by traffic situation and vehicle type) are provided by the PHEM Model, developed by the TU Graz. The term "base emission factors" means that other influencing factors (as e.g. age-dependent deterioration or ambient temperature) are not yet taken into account.

Details about PHEM are described in a separate TU Graz report (TUG 2017). In short: PHEM calculates the fuel consumption and emissions of vehicles based on the vehicle longitudinal dynamics and on engine emission maps. For each second PHEM computes for each vehicle the actual engine power to overcome the driving resistances and the losses in the drive train. A driver model simulates the corresponding gear shift behaviour to calculate the actual engine speed. With engine speed and engine power the emissions are taken from engine maps. A transient correction module adapts the emission levels from the engine maps to the actual driving cycle. Additional modules take into account the behaviour of specific technologies. The model results are 1 Hz courses of engine power, engine speed, fuel consumption and emissions of different pollutants – for each cycle and differentiated vehicle types, i.e. for each 'subsegment' and driving pattern according to the HBEFA definitions. These values then can be aggregated for the full cycle which results in the familiar emission factors (in g/km).

"Base emission factors" of diesel cars Euro 6

At the time when HBEFA 3.2 was developed (2013/14) modal measurements of only 5 EURO 6 cars were available as basis for the PHEM model. Additional uncertainties were due to the fact that these vehicles were premium class vehicles, hence not representative for the fleet. Further uncertainties were due to the unknown shares of NOx control technologies. Additional measurements of another 12 vehicles as "bag values" (i.e. not on a second-by-second basis) were available for calibrating the emission level. In the meantime (for HBEFA 3.3) the number of available Euro-6 vehicles resp. measurements with comparable real world cycles, particularly in the so-called CADC cycle (Common Artemis Driving Cycle), could be increased up to 25. This is still a limited sample size but nevertheless contributes to decrease the uncertainty.

Figure 1 shows on one side the NOx emissions as empirical basis from chassis dynamometer tests in the CADC for typical driving patterns (urban, rural and motorway and an overall average) which were available for developing HBEFA 3.2 and later for 3.3, and on the other side the emission factors derived by the PHEM model for comparable average driving patterns as provided by HBEFA for Germany. The two data sets shown in Figure 1 (CADC and EF) are not directly comparable since the underlying driving behaviour is not the same. But the figure illustrates that the available empirical basis determines the emission factors of HBEFA: The new measurements (CADC) indicate that the previous sample (i.e. the basis for HBEFA 3.2) was indeed not representative and underestimated the average emission level of the Euro-6 diesel cars significantly particularly in the urban and rural driving (e.g. ca. 0.2 instead 0.35 g NOx/km in urban driving). This underestimation hence was transferred to the HBEFA emission factors. The new value of 0.35 g NOx/km is approximately the result for the overall average emission factors according to HBEFA 3.3. This means that the new "base emission factor" of Euro-6 diesel cars is about 4-5 times higher than the limit value for Euro-6 (0.08 g/km).

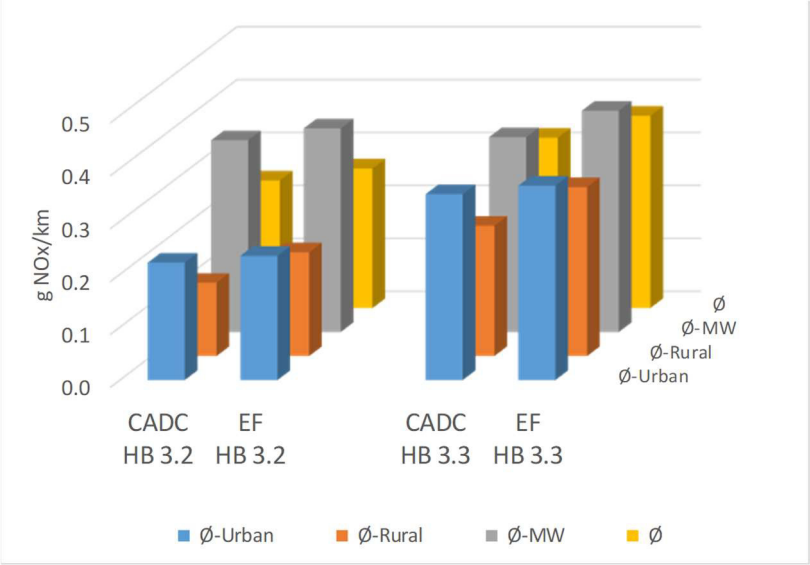

Figure 1: Comparison between the NOx "base emission factors" for Euro-6 vehicles according to the available measurements (CADC cycle) and the NOx emission factors modelled by PHEM in the context of the HBEFA versions 3.2 resp. 3.3. These factors do not yet take into account further corrections for e.g. ambient temperature.

"Base emission factors" of diesel cars Euro-6d1 and Euro-6d2

The previous version HBEFA 3.2 distinguished between a first generation of Euro-6 vehicles (labelled as 'Euro-6') and vehicles which were expected to enter the market based on a more stringent emission regulation in 2017/18 (labelled as 'Euro-6c'). The new HBEFA version 3.3 adjusts the segmentation of the Euro-6 vehicles to the adapted regulation which will require on-road emission testing with PEMS equipment (RDE tests). This will be introduced in two stages differentiating as usual between new type approvals (TA) and new registrations. In addition, the "conformity factors[1]" will be tightened for NOx from 2.1 (in stage 1) to 1.5 (in stage 2), and the relevant temperature range will be lowered to 3°C (in stage 1) and to 0°C (in stage 2). The introduction of two stages will be as follows:

Table 1: Introduction date for Euro-6 stages 'd1' and 'd2'

	For new type approval	For all new registrations
Stage d1 (or 'EU6d-Temp/RDE')	Sept. 2017	Sept. 2019
Stage d2 (or 'EU6d/RDE')	Jan. 2020	Jan. 2021

Since the vehicles approved according to Euro-6d1 and Euro-6d2 are not yet available on the market the new standards (limit values including conformity factors) are taken as guides for assuming the new emission levels. Since some of the vehicles tested do in fact already reach these low emission levels one can assume that in future these values should be attainable.

"Base emission factors" of diesel cars Euro-4 and Euro-5

The empirical basis for determining the base emission factors of the previous concepts Euro-4 and Euro-5 has not changed significantly even if the number of measurements has increased

[1] Conformity factors basically mean higher limit values since the official standard (0.08 g NOx/km for Euro-6) is multiplied by these factors. Translated into real terms this means limit values for on-road tests of 0.168 g/km in stage 1 and 0.12 g/km in stage 2

since. The average emission values in the CADC cycle remain more or less at the same level. Hence the emission factors of Euro-5 in HBEFA 3.3 are the same as in HBEFA 3.2. Also for Euro-4 the empirical basis is basically the same. However, the emission factors of Euro-4 were developed in 2009/2010. They were used for HBEFA 3.1 and remained unchanged since then. The calculation model PHEM has been adapted in the meantime. For consistency reasons the NOx emission factors Euro-4 were adapted as well (TUG 2017). However, the impact is not very significant: only the motorway emission factors are higher while urban and rural traffic situations remain at roughly the same level.

Deterioration effects

The emission values underlying the new emission factors for Euro-6 are deferred from comparatively new vehicles. A certain deterioration over the lifetime resp. the mileage of the vehicles may occur. Empirical information on such effects however is difficult to obtain since the same vehicle would have to be measured regularly over a considerably long period (e.g. every 30'000 km). Remote sensing data have the potential to isolate this effect since the emission levels monitored resp. the underlying fleet can be split up by registration years, hence providing information about a potential deterioration. Figure 2 shows the emission levels (in g NOx per kg fuel) monitored in a remote sensing campaign in Zurich/Gockhausen in 2016 (AWEL 2017) as a function of their age (as a proxy for mileage). The figure shows for the Euro-6 vehicles not a deterioration with age but rather an improvement. This is in line with the measurements presented in Figure 1 where the early Euro-6 vehicles show a very low level of emissions since they were premium class vehicles while the present new registrations on average show higher emissions. For Euro-5 a similar "sample effect" can be excluded. The "base emission factor" of the Euro-5 vehicles was not derived from 'new' Euro-5 vehicles but from a vehicle sample which is well distributed with respect to age. Therefore, deterioration is already included and should not be taken into account additionally. The situation is different for the Euro-6 vehicles: the new "base emission factors" are derived from a sample of still comparatively new vehicles. Hence a deterioration may well occur. The assumption is that a correction similar to the observed effect for Euro-5 vehicles (according to Figure 2) can be attributed to the Euro-6 vehicles as well. The effect is moderate and corresponds to a linear increase of the base emission factor up to 20% at a cumulative mileage of 150'000 km (assuming a yearly mileage of 15'000 km/a over 10 years).

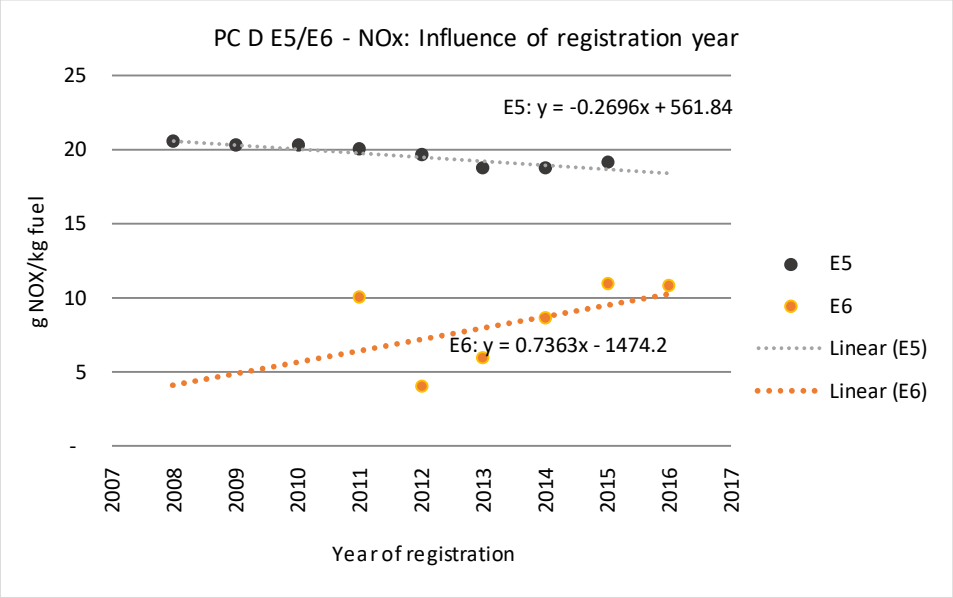

Figure 2: NOx emission levels of Euro-5 and Euro 6 diesel cars, measured 2016 in Zurich, as a function of their age.

There are indications that deteriorations are also an issue for previous concepts (≤ Euro-4) [Chen et al. 2016]. But for the time being (i.e. HBEFA version 3.3) no deterioration effects are taken into account for the earlier diesel concepts.

Influence of ambient temperature on NOx emissions

Ambient temperature appears to be a significant factor influencing the emissions as the results of several measurement campaigns indicate. For example, in the German investigation project (BMVI/KBA 2016) several vehicles were measured at 10°C in addition to the normal test temperature of ca. 20 – 25°C. Figure 3 shows the emission results of 12 Euro-5 resp. 24 Euro-6 diesel cars measured in 3 NEDC[2] cycles (1. 'standard NEDC' with cold start, 2. 'Hot NEDC' driven after the NEDC with a cold start, and 3. 'Hot NEDC at 10°C'). These measurements indicate a significant influence of the ambient temperature. However, the diagram shows a substantial heterogeneity, in the sense that some vehicles show hardly any difference while others show a substantial increase. On the average, the increase for these samples are roughly 15-20% for the Euro-5 vehicles and ca. 80% for the Euro-6 vehicles (comparing the 'NEDC hot at 10°C' to the 'NEDC hot after cold'). These values obviously depend very much on the samples which are not necessarily representative for the fleets, and the NEDC cycle is not representative for real world driving either.

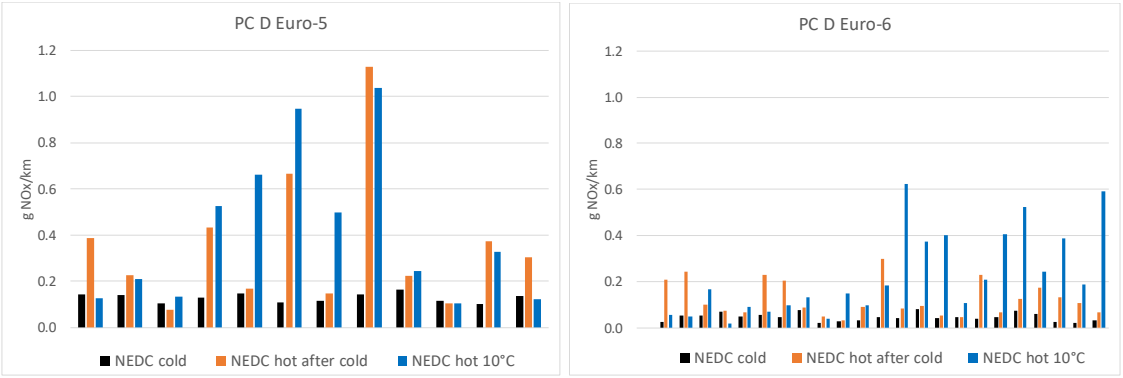

Figure 3: Results of varying NEDC tests at different ambient temperatures (Source: BMVI/KBA 2016)

A significant influence of the ambient temperature on the NOx emissions is also shown in the regular Swiss measurement programs for the updates of HBEFA which are commissioned by the Swiss Federal Office of Environment. EMPA measured several diesel cars in different cycles (IUFC[3] and WLTC[4]) and at different temperatures. Figure 4 shows for the Euro-5 vehicles an increase of a factor close to 2 if ambient temperature drops from the normal test temperature of ca. 23°C down to -7°C (from ca. 0.8 g NOx/km up to 1.5 g/km). The relative increase of the Euro-6 vehicles is even higher leading to an increase form ca. 0.3 g/km up to 0.75 g/km. Noticeable is the fact that a further temperature reduction below the -7°C level (Euro-5 vehicles) does not increase the emission level further.

[2] NEDC: New European Driving Cycle
[3] IUFC: "Inrets – urbain fluide court» (particularly designed for cold start behaviour)
[4] WLTC: Worldwide Light duty Test Cycle

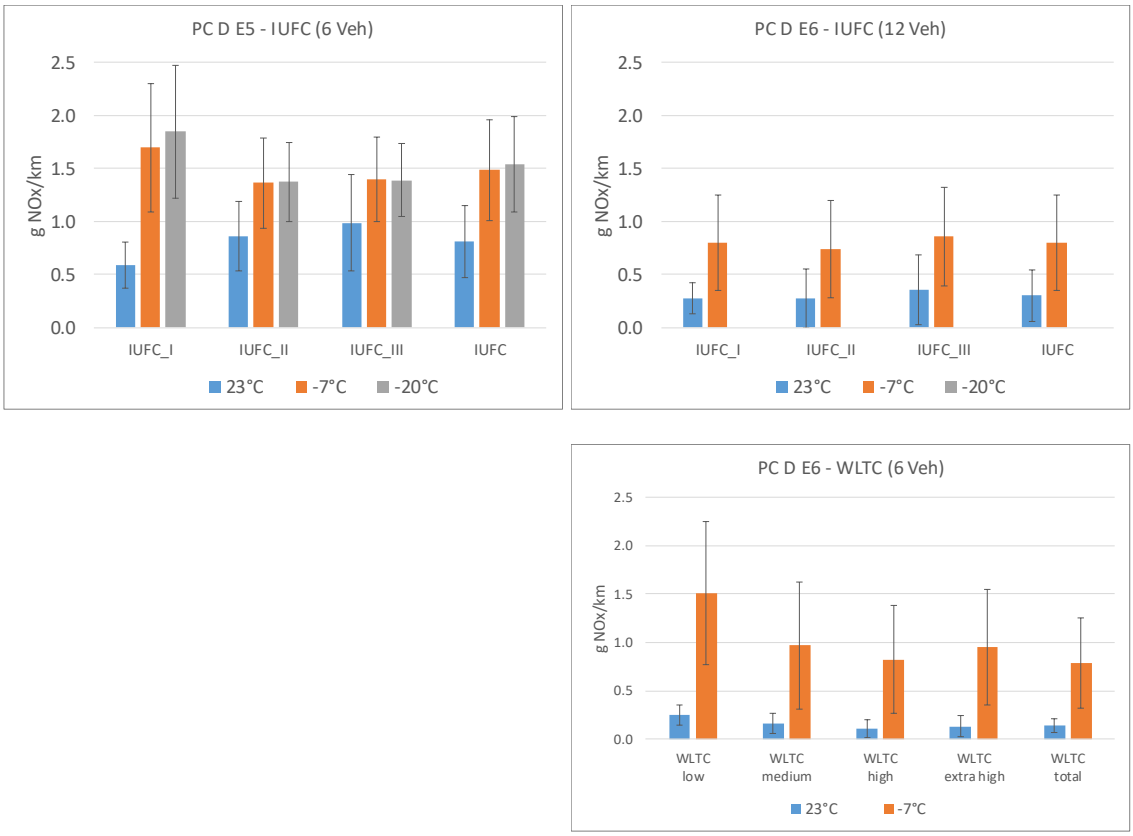

Figure 4: Results of IUFC and WLTC tests at different ambient temperatures (Source: EMPA measurement programs)

This has a technical background (see e.g. BMVI/KBA 2016, DfT 2016). A widely used technology for control of NOx emissions generated during combustion is exhaust gas recirculation (EGR). This technique reduces peak combustion temperatures and in turn reduces formation of NOx. The amount of EGR which can be used is dependent on ambient temperature. At low temperatures moisture condensation may lead to a build-up of deposits and in turn can lead to preventing the EGR from operating correctly and – according to manufacturers – possibly influence proper operation of the vehicles. State of the art technology for NOx control on Euro 5 diesel vehicles is a combination of EGR with control of the fuel injection timing to influence the combustion process. For Euro 6 vehicles additional exhaust after-treatment is used, either a lean NOx trap (LNT) or selective catalytic reduction (SCR). Ambient temperature influences the temperature of the after-treatment systems and thus can also impact the efficiency with which LNT and SCR exhaust NOx after treatment control can work. Both technologies have optimum temperature windows for effective operation and do not convert NOx below approx. 200°C.

Correction factors for ambient temperatures

For HBEFA the question was and still is how to capture this influence of ambient temperature. Since singular measurements do not provide an ideal basis for building an appropriate average it was again referred to the remote sensing monitoring method. Recent measurement campaigns in Sweden (Göteborg, Sjödin et al. 2017) and Switzerland (Zurich/Gockhausen, AWEL 2017) performed in 2016 register data about concentrations and individual vehicle types as well as the ambient temperature. Even if the measurements cover a limited temperature window between 10 and 20°C they allow to derive a quantitative dependency. Figure 5 shows the results of the analysis: the emission levels at temperatures below 20° were set in relation to the average of the emission level measured at the RS station above 20°C which corresponds to the normal temperatures of laboratory tests from which the base emission factors are derived. These functions are transformed into the format visualised in Figure 6 where ratios below 100% from Figure 5 were limited to 100% since it is unlikely that between approximately 18° and 20°C lower emissions occur than above 20°C. These functions are applied in HBEFA version 3.3 as

temperature correction factors. For e.g. 0°C this means an increase of 41% in NOx emissions for Euro-4 cars, of 78% for Euro-5 and 92% for Euro-6 vehicles. Below 0°C no further reduction is assumed – in line with the measurements presented in Figure 4. For the concepts Euro-6d1 and Euro 6d2 there are no empirical data available; it was assumed that the necessary corrections will be minimal or zero expecting that the RDE regulations will be effective also with respect to ambient temperature.

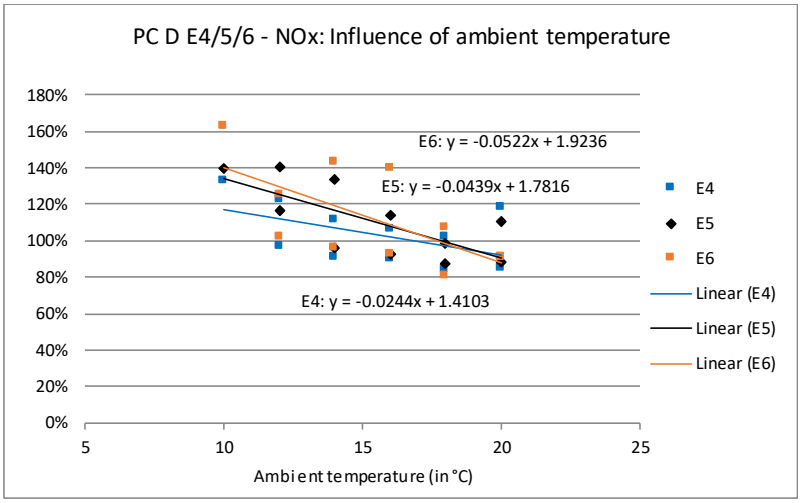

Figure 5: Influence of ambient temperature on NOx emissions compared to levels at ≥20°C (Sources: Measurement in Göteborg (Sjödin et al. 2017) and Switzerland (Zurich/Gockhausen (AWEL 2017)

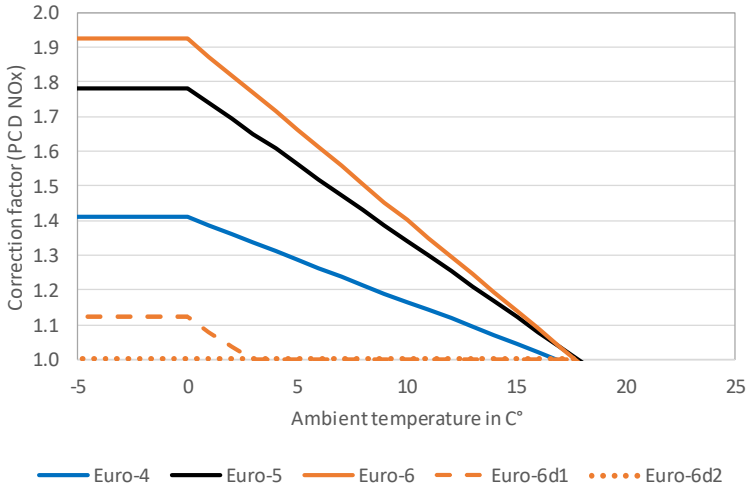

Figure 6: Correction functions for ambient temperature <20°C for hot NOx emission factors of diesel cars used in HBEFA version 3.3.

Impact of ambient temperature

Taking into account the ambient temperature as influencing factor is new for the hot emissions – but not new for the cold start and evaporation emissions. Therefore, HBEFA contains already country-specific distributions of ambient temperatures. For example, for Germany HBEFA assumes temperatures as shown in Figure 7 which depicts temperature distributions for four typical seasonal days; the black line corresponds to an average daily traffic variation which is used as weighted factor. Based on these assumptions the weighted temperature distributions can be calculated, as illustrated as cumulative distributions in Figure 8. Weighting the temperatures with the correction factors of Figure 6 the average correction factors can be derived as shown in Figure 9 for all HBEFA countries.

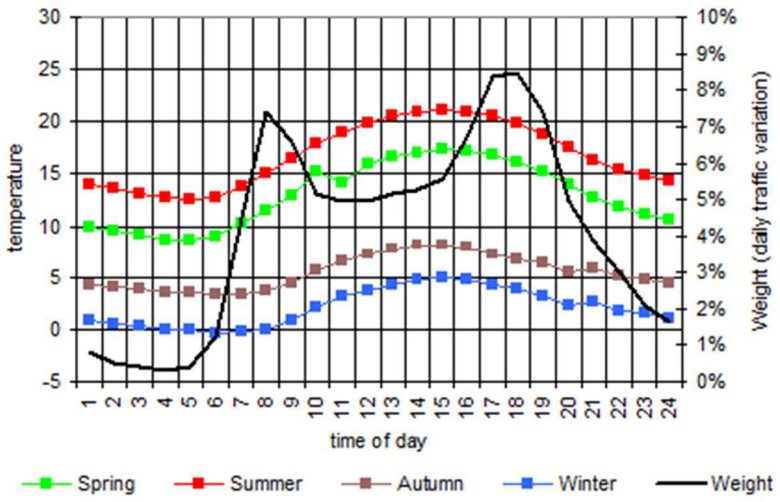

Figure 7: Temperature distributions for 4 typical seasonal days and a typical daily traffic variation (Example Germany)

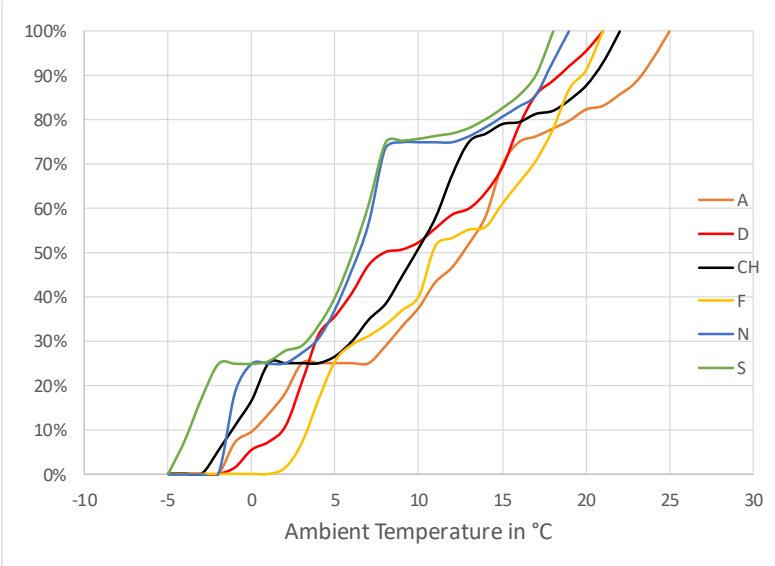

Figure 8: Cumulative temperature distributions as assumed in HBEFA for the different countries

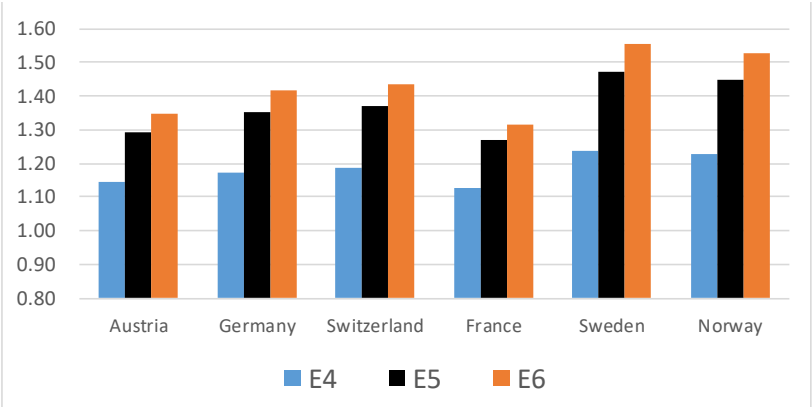

Figure 9: Average ambient temperature correction factors for NOx of diesel Euro-4/-5/-6 cars in the different countries

Results

The new emission factors and comparison HBEFA 3.3 vs. 3.2

Figure 10 displays the new average NOx emission factors for diesel cars of the different concepts and compares them with the previous values of HBEFA version 3.2. All values refer to average driving over all road categories (weighting for Germany). Since HBEFA 3.3 includes a slight deterioration over mileage the values are shown for vehicles with an assumed cumulative mileage of 50'000 km. As the figures indicate the new values result in an overall increase by 24% for Euro-4, by 34% for Euro-5 and by 92% for Euro-6. The newer concepts corresponding to the future RDE regulation Euro-6d1 and 6d2 are assumed to remain at a similar levels as already expected in HBEFA 3.2, i.e. close to the limit values (including RDE conformity factors). The figure also shows the impact of the new corrections for ambient temperature for the different concepts.

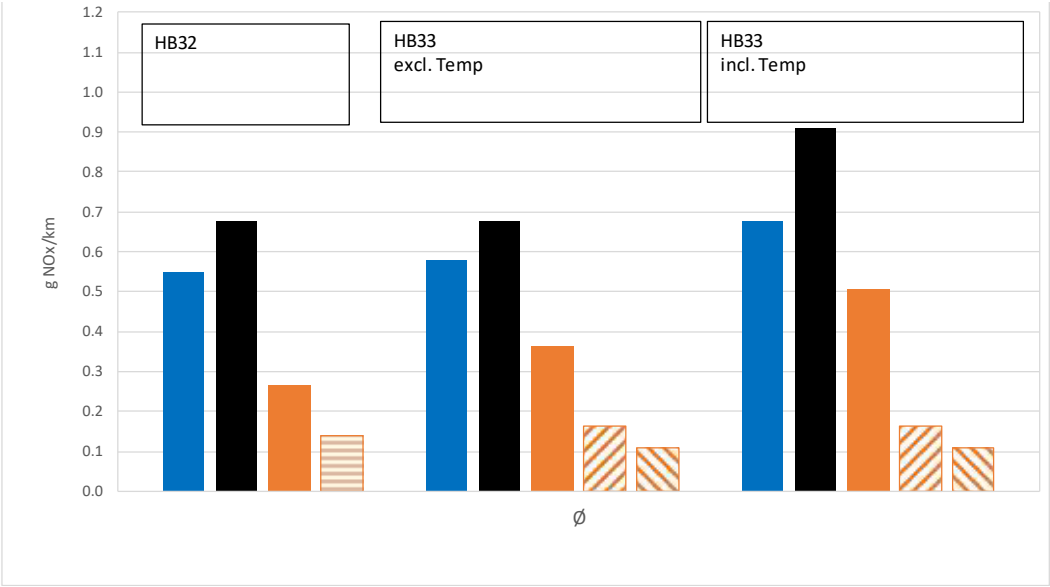

Figure 10: NOx emission factors of the diesel cars Euro-4/-5/-6 in HBEFA 3.2 vs. HBEFA 3.3 excluding resp. including the effect of ambient temperate (Ø all road categories)

Comparison with on-road measurements

Figure 11 compares the old and new HBEFA emission factors with on-road measurements from different sources (BMVI/KBA 2016, DfT 2016, DUH/EKI 2016). Some of the data did not disclose the ambient temperature when the measurements were taken; some tests were driven during the summer months hence do not necessarily capture the representative temperature distribution.

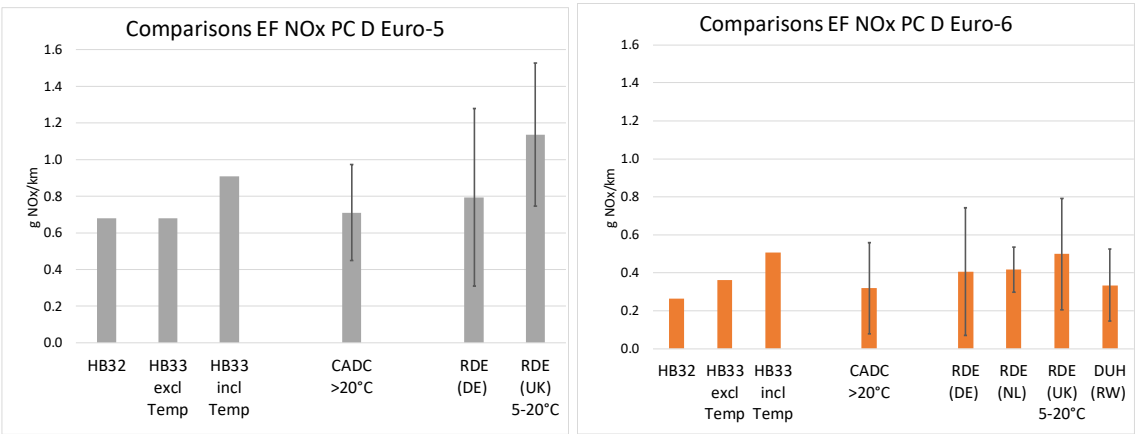

Figure 11: Comparison of HBEFA emission factors (diesel cars, Euro-5 and Euro-6) with real world (RW) measurements (average values +/- standard deviations per campaign).

The variation of the measurement results between vehicles within the same campaigns is remarkably high, leaving a considerable uncertainty range. Overall one can conclude that the new emission factors fit better to the real world measurements than the previous ones.

Impact on the emission factor development 2000-2030 (Germany)

Finally, the following two figures show the fleet weighted emission factors for the years 2000 up to 2030 in Germany, once for the diesel car fleet (Figure 12) and once for the overall car fleet (Figure 13). The figures show the average values for all road categories. The overall emission factor in 2015 is 25% higher than assumed in the previous version, the difference raises up to 47% in 2020 and then continuously drops down again so that the values in 2030 are almost at the same level as expected in version 3.2. The emission factors for urban roads are very similar to the overall averages.

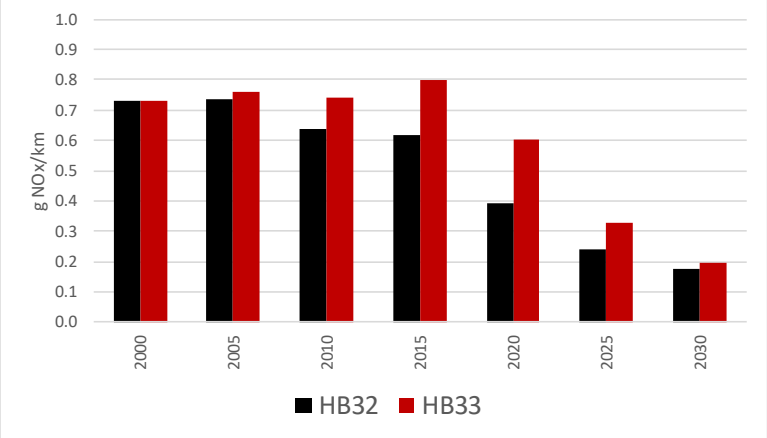

Figure 12: Weighted NOx emission factors for the German diesel car fleet in HBEFA 3.3 vs. 3.2

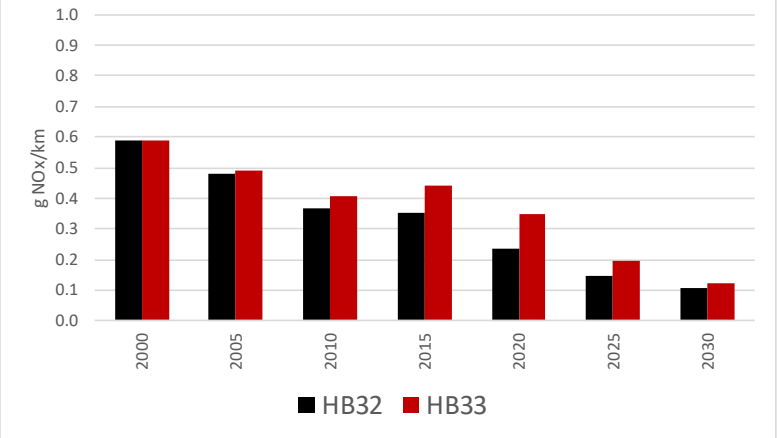

Figure 13: Weighted NOx emission factors for the German total car fleet in HBEFA 3.3 vs. 3.2

References

AWEL 2017, Amt für Abfall, Wasser, Energie und Luft der Baudirektion des Kantons Zürich, RSD Messungen 2016, Auswertung und Bericht, 21. April 2017.

Borken-Kleefeld 2013, Guidance note about on-road vehicle emissions remote sensing, commissioned by ICCT, July 2013.

BMVI/KBA 2016, Bericht der Untersuchungskommission „Volkswagen» des Bundesministeriums für Verkehr und digitale Infrastruktur und des Kraftfahrt-Bundesamtes, 2016.

Chen et al. 2016, Yuche Chen and Jens Borken-Kleefeld, NOx Emissions from Diesel Passenger Cars Worsen with Age, *Environ. Sci. Technol.*, 2016, 50 (7), pp 3327–3332.

CTA 2016, Centre de Technologie Avancée (Wallonie), Résultats de l'évaluation des rejets athmosphériques par les véhicules légers Diesel, mandaté par le Ministre wallon de l'Environnement (Wallonie), Mons/Wallonie, Juin 2016.

DfT 2016, Department of Transport (UK), Vehicle Emissions Testing Programme, April 2016.

DUH/EKI 2016, NOx- und CO2-Messungen an Euro 6 Pkw im realen Fahrbetrieb, Hintergrundpapier, Emissions-Kontroll-Institut der Deutschen Umwelthilfe e.V., Berlin, 07. September 2016.

DUH/EKI 2017, NOx- und CO2-Messungen an Euro 6 Pkw im realen Fahrbetrieb, Wintermessungen September 2016 – März 2017, Emissions-Kontroll-Institut der Deutschen Umwelthilfe e.V., Berlin, 07. 29. März 2017.

EMPA 2013, Emission measurements PC Euro-5 (internal document).

EMPA 2015, Emission measurements PC Euro-6 (internal document).

EMPA 2016, Pilotprojekt Vergleichsmessungen Remote Sensing - PEMS - Rollenprüfstand im Auftrag des Bundesamts für Umwelt BAFU, EMPA-Bericht Nr. 5214010202.01, 28.10.2016.

Keller et al. (2017), Keller, M., Hausberger, S., Matzer, Wüthrich, Ph., Notter, B., HBEFA 3.3 - Background documentation, 25. April 2017, www.hbefa.net.

MEEM 2016, Ministère de l'Environnement, de l'Énergie et de la Mer (France), Rapport final de la commission indépendante mise en place par la Ministre Ségolène Royal après la révélation de l'affaire Volkswagen, Contrôle des émissions de polluants atmosphériques et de CO2 mené sur 86 véhicules, 29 juillet 2016.

Sjödin et al. 2017, Sjödin, Å., Jerksjö, M., Fallgren, H., Salberg, H., Yahya, M.-R., Wisell, T., Lindén, J. (2017) On-Road Emission Performance of Late Model Diesel and Gasoline Vehicles as Measured by Remote Sensing, IVL Report B2281, June 2017.

TUG 2013, Update of Emission Factors for EURO 5 and EURO 6 vehicles for the HBEFA Version 3.2, Report No. I-31/2013/ Rex EM-I 2011/20/679, 06.12.2013 (www.hbefa.net).

TUG 2017, Update of Emission Factors for EURO 4, EURO 5 and EURO 6 Diesel Passenger Cars for the HBEFA Version 3.3, Report No. I-09/17/ CM EM 16/26/679, 01.06.2017 (www.hbefa.net).

Assessment of risks for elevated NO_x emissions of diesel vehicles outside the boundaries of RDE

P. van Mensch[1], N.E. Ligterink[1],R.F.A. Cuelenaere[1], G. van Grootveld[2]*

[1] Research Group Sustainable Transport and Logistics, TNO, PO Box 96800, 2509 JE The Hague, the Netherlands, presenting author: pim.vanmensch@tno.nl
[2] Ministry of Infrastructure and the Environment, The Hague, the Netherlands.

Abstract

The expectation is that RDE (Real Driving Emissions) legislation will bring major improvements in the emission performance of light-duty vehicles for a large part of vehicle usage on European roads. However, a number of special, but not necessarily uncommon situations fall outside the boundaries for the test and vehicle conditions specified within the RDE legislation, or even outside the In-Service Conformity (ISC) specification. If the effectiveness of emission control strategies would be focused on low emissions in normal use situations inside the RDE boundaries, elevated emissions due to different emission control strategies might occur in situations that are outside the scope of the current vehicle legislation, but still part of normal vehicle use. The aim of this paper is to provide an overview of driving and vehicle conditions with possibly elevated emissions. In addition, the paper aims to identify possible technical abatement measures and aims to provide guidance on how to detect situations with elevated emissions.

The situations with possibly elevated emissions are related to 'ambient and road conditions', 'trip composition', 'driving behaviour' and 'vehicle conditions'. A technical reason for higher emissions at low temperatures can, for example, be a modified EGR rate to reduce the risk of condensation in the inlet manifold and EGR intercooler. However, in some situations a different emission control strategy may be the result of efforts to optimize the strategy to comply with the RDE legislation rather than having low emissions in all real-world conditions. These identified situations can occur in countless combinations during real-world driving.

Observed high vehicle emissions in normal use in monitoring programs are the start of an investigation, which may branch out in many directions. The In-Service Conformity RDE test is one of these directions, where specific test conditions may be needed. Tampering of vehicles is another avenue of investigation, as well as poor maintenance. But the issues with elevated emissions, not covered by the RDE test protocol and the vehicles eligible for in-service confomity testing should remain in the picture. Moreover, the acceptable elevation levels and the test protocols should be investigated further.

Keys-words: *Light Duty Vehicles, ISC, RDE, Real-world NO_x emissions, Euro 6, Monitoring, Risk-based testing, boundary conditions, elevated emissions, diesel vehicles.*

Introduction

With RDE (Real Driving Emissions) legislation a new chapter in emission testing has started for light-duty vehicles (Cuelenaere, 2016). RDE legislation poses new and more complex engineering targets for manufacturers. The expectation is that RDE will bring major improvements in the emission performance of light-duty (LD) vehicles for a large part of vehicle usage on European roads. However, a number of special, but not necessarily uncommon situations fall outside the boundaries for the test and vehicle conditions specified within this legislation. If the effectiveness of emission control strategies would be focused on low emissions in normal use situations inside the RDE boundaries, elevated emissions due to different emission control strategies might occur in situations that are outside the scope of the RDE test conditions and vehicle selection.

A focus on emission reductions under RDE conditions only, might be in conflict with the general principle in emission legislation set out in article 5(1) of the Euro 5/6 regulation: "*The manufacturer shall equip vehicles so that the components likely to affect emissions are designed, constructed and assembled so as to enable the vehicle, in normal use, to comply with this Regulation and its implementing measures.*"

An alternative interpretation of current study is the investigation what a *defeat device* would be, as stipulated in article 5(2) of the same regulation. With on-road RDE testing, a defeat device is

no longer the possible cause of the difference between laboratory and on-road tests. It cannot be expected that manufacturers are held to the same standard on a RDE test as in other circumstances. On the other hand, *normal use* extends beyond the vehicle state and boundaries as prescribed in the RDE legislation.

The Ministry of Infrastructure and the Environment in the Netherlands has requested TNO to identify potential risks for elevated emissions in situations which are common across Europe but are not covered by RDE legislation (van Mensch, 2017). The goal of the ministry is that under all real world circumstances the emissions are as low as possible. To reach this situation it is important to know why elevated emissions occur outside the boundaries and also to know how these emissions in practice can be reduced. This information might lead to a widespread implementation of state-of-the-art technology outside the boundaries to reduce the emissions. The aim of this paper is to provide an overview of driving and vehicle conditions with possibly elevated emissions. In addition, the paper aims to provide guidance on how to detect such situations and identifies possible technical abatement measures.

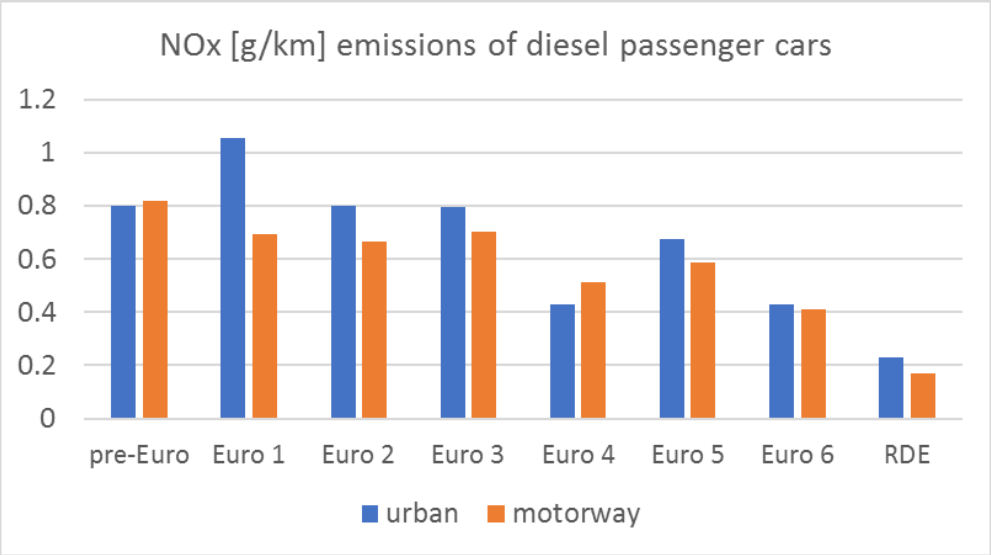

Figure 1 The NO_x emissions of diesel passenger cars, including the preliminary estimate of vehicles under RDE legislation, as used for Dutch air quality prognoses.

The overview of special situations with possibly elevated emissions and the proposed guidance for assessment are meant for type approval authorities and other third parties which perform tests. Charting the variations could be the basis for risk-based monitoring and surveillance programs and for the development of technologies to reduce the emissions outside the boundaries. Insights from these programs can help to secure low emissions in various real-world circumstances.

In this paper the focus is solely on diesel-powered light-duty vehicles and NO_x emissions. Emissions from petrol-powered vehicles, in particular the particulates emissions from direct fuel injection engines, may be relevant as well but are outside the scope of this paper.

The situations with possibly elevated emissions are related to ‘ambient and road conditions’, ‘trip composition’, ‘driving behaviour’ and ‘vehicle conditions’.

Examples of situations outside the RDE boundaries with possibly elevated emissions

RDE legislation will cover the majority of European driving conditions. However, RDE test conditions were never meant to cover all situations that might occur when driving on European roads. The general thinking was that each boundary condition with respect to temperature, dynamics, altitude gain, and other aspects would cover 95% of all kilometres driven on European roads. However, as conditions outside the 95% interval for each parameter can occur in countless

combinations during real- world driving, eventually much less than 95% of all driving may be within the combined boundaries of RDE.

Here a few examples of use cases are described where such combinations are relevant. The review by TüV Hessen inspired TNO to describe these use cases. They also clearly illustrate that these situations, although they can be considered outside the scope of "normal driving", are not rare and can constitute a significant part of the annual mileage of various groups of vehicle users.

Family on holiday

A family of four or five going on a summer holiday has a fully packed car, so they may need a roof box to carry all the luggage. They drive for extended periods at high speed on European highways to their holiday destination. On a hot summer day, the air-conditioning may be at full blaze, the cool box plugged in to the 12-volt system, and maybe a window is partly open to have some fresh air in the hot and packed car. One or two DVD players may be running in the back seat to keep the kids entertained. The combination of additional weight, the air drag of the roof rack and open windows, the long periods of high speed driving, and the high use of auxiliary power is outside the RDE boundaries in many ways. The total distance driven under these conditions easily amounts to 10 to 20% of the vehicle's annual mileage. Moreover, during a one hour stop at the motorway restaurant, with the car fully exposed to the sun, the car will become very hot and temperatures may exceed 35 ˚C. Such conditions lie outside the RDE boundary for soak in both the temperature range and soak period.

German business driving

Long distance driving on the German motorway, with speeds above 145 km/h, is quite normal for many drivers, who spend many hours on the road for work. On the autobahn without speed limits this is normal practice. Such driving lies outside RDE, both in velocity and in duration. This means that for the share of German cars with the highest annual mileages, and therefore a substantial contribution to the total distance travelled in Germany, a large part of their driving is not covered at all by RDE.

Trailer or caravan towing

Towing a heavy trailer or caravan may be the reason to buy a high-powered car or van. This driving is well within the capabilities of the car. On the motorway driving with a trailer or caravan occurs at a lower velocity than is prescribed in RDE as motorway velocity. But the engine load can be substantially higher than covered in the RDE. Towing uphill adds further to the load. Hence, the extent to which trailer and caravan towing lies outside the RDE boundaries can be substantial.

Winter period

At -10 ˚C with roads often (potentially) covered with ice or snow, cars drive slowly and carefully to avoid slipping off the road. Prior to driving, the engine is kept running for several minutes to defrost the windows and warm the cabin. Not only the ambient temperature and idling are outside RDE boundaries, but also the snow on the road would not be appropriate for an RDE test. The slow driving will also be outside the RDE boundaries for urban and motorway driving. Still, in many parts of Europe, this situation is a familiar winter scene.

Maintenance on an older vehicle

A vehicle with 160,000 km or more on the odometer will typically have had several owners, many maintenance services, and possibly a number of replacement parts. Even with the best intentions of the owner and the garage the vehicle may not perform up to the emission standards. In the case of NO_x emissions this may go unnoticed in the periodic inspection. In principle, the car manufacturer sets the standard for servicing and maintenance. High emissions can arrive from shortcomings in this standard, but also from irregularities in use and maintenance.

Trade-off between low NO_x emissions and other vehicle aspects

In many cases NO_x reduction is not achieved by an isolated single change to a vehicle. There

often is a certain trade-off between achieving low NO_x emissions and other aspects of engine and vehicle design. To minimize such trade-offs efforts may be made to optimize the emission control strategy in order to fulfil with the RDE legislation rather than to achieve low emissions under all real-world conditions. The following aspects are examples which can be in competition with the application of NO_x reduction technologies. These examples are not necessarily applied or even considered by a manufacturer.

Fuel economy and particle emissions

Some examples:

- Regenerations of the NO_x storage catalyst cause an increase in fuel consumption;
- Use of an enhanced fuel injection strategy. This can lead to an improved fuel economy, lower particle emissions and lower combustion noise. However, it can also cause increased NO_x emissions due to higher combustion flame temperatures;
- The use of EGR (Exhaust Gas Recirculation) can lead to a fuel penalty as EGR causes an increase in soot emissions. Due to this increase the DPF (Diesel Particulate Filter) may cause higher backpressures and a need for more frequent regeneration, both leading to a higher fuel consumption.
  Cooling is needed as well for EGR. In order to have sufficient cooling at high engine loads and EGR rates additional heat exchange may be needed. However, for a low fuel consumption, the effective heat exchange on the vehicle is often minimized, especially for passenger cars.

Engine and catalyst durability

Some examples:

- EGR causes contamination within the engine and the EGR system itself. With higher EGR rates, the contamination will be higher as well.
- Every regeneration of the NO_x storage catalyst cause deterioration of the catalyst

Investment and usage costs

Costs are involved to reduce NO_x emissions, both in terms of investments and additional costs throughout the vehicle's lifetime during usage. Some examples:

- Investments:
  - In order to reach low emissions in real-world circumstances enhanced emission control strategies are needed, such as a NO_x storage catalyst or an SCR (Selective Catalytic Reduction). The choice of certain technologies can vary for different types of cars.
- Vehicle lifetime costs:
  - EGR causes contamination within the engine and EGR system. Also extra and more persistent particle emissions are produced. This will increase the maintenance costs. Moreover, engine malfunctions can lead to (costly) compensation claims or recalls.
  - An SCR system needs urea. If more NO_x needs to be converted, more urea is needed. Technically an SCR catalyst can be developed to convert very high levels of NO_x emissions. However, this will have an effect on the costs for the user since the urea consumption will be high as well.

The aforementioned aspects should not be considered a license to switch off emission control systems when the vehicle is operated in conditions which are not covered by the RDE legislation. At minimum, the vehicles should make the best possible use of the applied technologies on the vehicle. If the technologies are partly or fully deactivated under conditions not covered by RDE, clear justification and evidence should be supplied by the vehicle manufacturer.

Possible situations with elevated emissions which are not covered by RDE legislation

RDE conditions were never meant to cover all situations that might occur when driving on European roads. The general thinking was that each boundary condition would cover 95% of the full range of normal use. This means that 95% of all kilometres driven on European roads is expected to occur within the 0 to 30 ˚C range of RDE. The same applies for driving dynamics,

altitude gain, and other aspects. Hence, eventually much less than 95% of all driving may be within the combined boundaries and therefore be covered by RDE. It is in part the independent testing which should seek out the critical boundaries of RDE testing to achieve the maximal coverage possible with RDE testing.

The aforementioned 95% coverage of driving conditions implies another important complexity of RDE regulation. It means that it is accepted that elevated emissions occur in circumstances which only seldom occur in normal driving. This however does not mean that for translating RDE requirements to engineering targets these circumstances may be considered as situations for which no rules apply. A focus on emission reductions under RDE conditions only, might be in conflict with the general principle in emission legislation set out in article 5(1) of the Euro 5/6 regulation: "*The manufacturer shall equip vehicles so that the components likely to affect emissions are designed, constructed and assembled so as to enable the vehicle, in normal use, to comply with this Regulation and its implementing measures.*"

Instead, therefore, these exceptional circumstances should be considered as situations where for good reasons some leeway may be given. These exceptional circumstances and the reasons for elevated emissions can be put in perspective by applying limits on the accepted increase of emissions.
In this chapter, a range of situations with possibly elevated emissions is identified. This is to be considered a non-exhaustive overview. The identified situations are listed, divided in the categories as described below. These categories are related to several parts of the RDE legislation. Each category is described in a separate paragraph:

- Ambient and road conditions;
- Trip composition;
- Driving behaviour;
- Vehicle conditions.

For each identified situation with possibly elevated emissions, the aspects below are considered. The assessment of these aspects is based on expert judgement of the authors, augmented with input from the stakeholder consultations:

- The possible emission behaviour in the identified situations and examples of possible technical reasonings for this behaviour:
    - Next to expert judgement and inputs from stakeholder consultation reflecting future technologies in line with RDE, this report is also based on experiences with current technology and the problems encountered with high emissions;
    - In several public statements manufacturers have motivated certain choices regarding the balance between engine protection and emission control;
    - Given the fact that RDE is not in place, this a is non-exhaustive overview;
- Possible technical mitigation options and some examples;
    - This also is non-exhaustive overview;
- The identified situations can occur in countless combinations during real-world driving. The combined impacts have not yet been assessed.

<u>Ambient and road conditions</u>

The RDE legislation contains several requirements for ambient and road conditions. Important requirements are related to ambient temperature and to driving at altitude. It is possible that elevated emissions occur outside the ambient temperature boundaries of RDE legislation. This risk is also present for the effect of a higher altitude. However, given the relatively wide RDE scope on ambient and road conditions, it depends on the common conditions in specific member states how relevant these situations are.
For ambient and road conditions, the following possible situations with potentially elevated emissions are identified:

- Driving or conditioning in ambient temperatures lower than -7 ˚C;
    - Under cold ambient conditions the temperature is possibly not the only reason of an invalid RDE test, the boundaries for driving behaviour can be a reason as well. As the road can be covered with snow and ice, certain speed requirements may not be met;
- Cold start in ambient temperatures lower than -7 ˚C;

- Driving in ambient temperatures higher than 35 ˚C;
- Driving at altitudes higher than 1300 meter.

In Table 1 the identified situations are elaborated in more detail.

Table 1_possible ambient and road conditions with potentially elevated emissions

Situation	**Possible behaviour (B) and examples of the technical reasoning (R) for elevated emissions**	**Examples of possible technical abatement options**
T_{amb} < -7 ˚C during driving or conditioning	**B:** Modified EGR rate ***R:*** *Reduce the risk of condensation in inlet manifold and EGR intercooler* ***R:*** *Lower internal contamination of the engine* **B:** No AdBlue injection **R:** Insufficient heat in exhaust gas for urea conversion to ammonia **R:** Urea crystallization in SCR manifold **B:** Adapted injection strategy **R:** Compensation for low intake air temperature and improve fuel economy	Feasibility of the following measures is already shown in heavy-duty vehicles: **+** Alternative or additional emission control system/ strategy, e.g. NO_x storage catalyst for low exhaust temperatures, gaseous ammonia in SCR system, closed coupled SCR/DPF, or water injection[1] **+** Improved temperature management, like improved insulation and rerouting air flow **+** (Mild) hybridization to avoid long idling periods which cool down the catalyst **+** Improved fuel injector quality to reduce soot emissions
Cold start at T_{amb} < -7 ˚C	**B:** Alternative cold start strategy without fast warm-up of catalysts **R:** Focus on engine warm-up instead of catalyst warm-up and to improve combustion stability and avoid misfire	Same as above-mentioned **+** Electric catalyst heating
T_{amb} > 35 ˚C and Altitude: >1300 meter	**B:** Modified EGR rate and different engine operation (e.g. different air/fuel ratio) **R:** Avoid overheating of engine **R:** Lower air density → lower air intake **R:** Lower oxygen level (only relevant at high altitudes) **R:** Lower internal contamination **B:** No or limited NO_x regenerations in NO_x storage catalyst → NO_x is passing the catalyst unconverted **R:** Catalyst temperature too high for proper NO_x storage or limited possibilities for regeneration due to higher engine loads.	**+** Alternative or additional emission control system/strategy e.g. SCR, or water injection **+** Improved design for temperature management, like an improved EGR cooler, two-stage EGR cooling and an increased engine cooling capacity **+** (Mild) hybridization for electric boost to assist engine during firm accelerations **+** Improved fuel injector quality to reduce soot emissions

Trip composition

The RDE legislation contains several requirements for the composition of a valid RDE trip setting boundaries on the duration of the trip, the sequence of urban, rural and motorway driving, the minimum trip length and the number and duration of vehicle stops.

Based on the trip composition requirements, augmented with some non-specified conditions, the following possible situations with potentially elevated emissions are identified:

- More than 15 seconds of idling after initial engine start, more than 90 seconds of vehicle

[1] Water injection is still in development stage, with possible durability issues.

stop in the cold start period and more than 300 seconds of idling:
    - The limitation of idling to a maximum of five minutes in the RDE test is a restriction of the test with respect to normal use. For example, many motorists keep the engine idling for long periods at movable bridges where vehicles must wait for the passage of ships. Other examples are taxis which are waiting for passengers, traffic jams or waiting for traffic lights in urban rush hour. Having this restriction of five minutes idling in the test could mean after longer idling periods emissions may go up to typical engine out levels;
    - The same risk applies to the maximum of 15 seconds idling after engine start. For example, it is not unusual for motorist to set the navigation, or to remove ice from the car windows, after they have started the engine;
- Deviating trips or trip sections in time and/or distance and a deviating sequence of the road sections compared to the RDE trip:
    - In real-world circumstances the variations in trip composition are almost infinite. By prescribing the trip composition, there is a potential risk that vehicles are optimized towards the specific trip composition and/or duration. Moreover, emissions may be higher in specific road sections which are not evaluated separately, like the rural and/or the motorway part. An example of this (for a vehicle not type-approved under RDE legislation) is shown in Figure 2 where the emission performance during rural driving varied strongly;
- Manual switch-off of the engine during an RDE trip or in real life multiple times:
    - By doing so, an optimized vehicle may 'think' that the test just started, while the vehicle is, for example, at the end of the urban or somewhere in the rural part;
- Total cumulative positive altitude gain of > 1200 meter per 100 km:
    - In some countries, it is difficult to drive a valid trip due to this boundary condition. Even in moderately hilly regions the cumulative altitude gain can be substantial;
- A difference of more than 100 meters in altitude between the end and the beginning of the trip:
    - This might be relevant when mainly up- or downhill driving occurs during trips in regions with mountains.

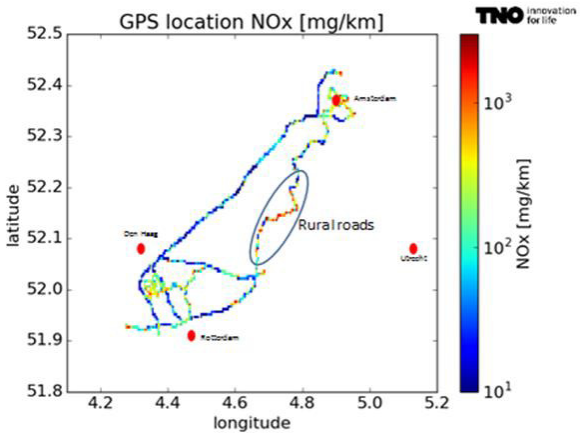

Figure 2: Emission measurement results of a modern Euro-6 diesel passenger car plotted on a real-world trip (Cuelenaere, 2016).

Possible behaviour of the above-mentioned first three main bulletpoints are: modified EGR rate and/or AdBlue injection, uncontrolled or missing regenerations in NO_x storage catalyst, application of poor quality or lower volume catalysts and/or alternative temperature management. If such behaviour is observed for the mentioned situations it is likely that efforts are made to optimize the emission control strategy in order to comply with the RDE legislation rather than achieving low emissions under all real-world conditions.

For the situations which are related to the latter two main bulletpoints, elaborates in more detail concerning the situations with an altidue gain or altitude difference.

Table 2_possible situations with potentially elevated emissions related to altitude gain or altitude difference

Possible behaviour (B) and examples of the technical reasoning (R) for elevated emissions	**Examples of possible technical abatement options**
Uphill driving: **B:** Modified EGR rate and different engine operation (e.g. different A/F ratio) **B:** No or limited NO_x regenerations in NO_x storage catalyst → NO_x is passing the catalyst unconverted **R:** Engine power needed **R:** Avoid overheating of the engine: cntrol strategies focused on reducing temperature **R:** Lower internal contamination **R:** Temperatures in engine and exhaust outside normal operation range **R:** Catalyst temperature too high for proper NO_x storage or limited possibilities for regeneration due to higher engine loads **Downhill driving:** **B:** No or limited AdBlue injection **B:** No regeneration in NO_x storage catalyst **R:** Insufficient heat in exhaust gas from motoring	**Uphill driving:** **+** Alternative or additional emission control system/ strategy e.g. SCR or water injection6 **+** Improved design for temperature management, like an improved EGR cooler two-stage EGR cooling and an increased engine cooling capacity **+** (Mild) hybridization for electric boost to assist engine during firm accelerations **+** Improved fuel injector quality to reduce soot emissions **Downhill driving:** **+** Alternative or additional emission control system/ strategy, e.g. gaseous ammonia in SCR system, closed coupled catalyst/DPF **+** Apply higher EGR rates **+** Improved temperature management, like improved insulation of the SCR and/or NO_x storage catalyst **+** Throttling or by-passing motoring exhaust gas flow in catalyst

Driving behaviour

The RDE legislation contains several requirements for the driving behaviour to prevent a valid RDE trip from consistently being driven extremely aggressive or extremely smooth. An important aspect for the evaluation of driving behaviour is related to driving dynamics. A high value for $v * a_{pos}$, the product of vehicle speed and (positive) acceleration, is commonly used as an indicator for high(er) dynamics of a trip, while a low value for RPA, the relative positive acceleration, is an indicator for the lack of dynamics in a trip. Other aspects which are used to evaluate driving behaviour are related to vehicle speed, e.g. maximum speed or average speed.

Based on the requirements for driving behaviour, augmented with some non-specified conditions, the following possible situations with potentially elevated emissions are identified:

- High engine loads due to high driving dynamics or motorway driving at high vehicle speeds:
    - Driving dynamics: Higher $v * a_{pos}$ (speed multiplied with positive acceleration) values than allowed according to the RDE legislation (EC/2016/646).
        - As described in the report regarding driving behaviour, the limits for $v * a_{pos}$ cover normal driving behaviour quite well. (Ligterink, 2017), However, as driving behaviour and power-to-mass ratios of vehicles differ substantially, it is not necessarily unusual that higher driving dynamics occur during real-world circumstances.
    - Motorway driving at speeds higher than 145 km/h for relatively long periods:
        - This situation is particularly relevant for some German motorways without speed limitations. On these motorways, the vehicles are frequently operated for extended periods at speeds higher than 145 km/h;

- Traffic congestion on the motorway:
    - These traffic jams can cause an invalid RDE trip due to the RDE limitations of maximum test duration, minimum required distance and required average speed. Therefore, congestion is not very well covered within the RDE;
- Urban driving with an average speed lower than 15 km/h:
    - Stop-and-go traffic is frequently observed in densely populated areas with high traffic density. Stop-and-go urban traffic is generally associated with high emissions;
- Disable traction control and/or ESP (Electronic Stability Program). Or, enable special driving modes such as sportive or off-road modes:
    - These very specific kinds of systems may be disabled by aggressive/sportive motorists. In addition, drivers often have the possibility to choose different driving modes, like 'eco' or 'sportive'. In particular for traction control and ESP, it is not clear from the RDE legislation if these specific modes are covered.

In Table 3 the identified situations are elaborated in more detail.

Table 3 possible situations with potentially elevated emissions related to the driving behaviour.

Situation	**Possible behaviour (B) and examples of the technical reasoning (R) for elevated emissions**	**Examples of possible technical abatement options**
$v * a_{pos}$ [95] > RDE limit & motorway driving at > 145 km/h	**B:** Modified EGR rate and different engine operation (e.g. different A/F ratio) **B:** No or limited NO_x regenerations in NO_x storage catalyst → NO_x is passing the catalyst unconverted **B:** Modified AdBlue injection **R:** Engine power needed **R:** Avoid overheating of the engine: control strategies focused on reducing temperature **R:** Lower internal contamination **R:** Temperatures in engine and exhaust outside normal operation range **R:** Catalyst temperature and/or space velocities too high for proper NOx storage or limited possibilities for regeneration due to higher engine loads	**+** Alternative or additional emission control system/ strategy like water injection **+** Improved design for temperature management, like an improved EGR cooler, two-stage EGR cooling and an increased engine cooling capacity **+** Improved fuel injector quality to reduce soot emissions **+** Improved design SCR or NO_x storage catalyst to allow for higher space velocities and extra AdBlue injection (in case of SCR) **+** (Mild) hybridization for electric boost to assist engine during firm accelerations
Traffic congestion on the motorway & v_{avg} urban driving < 15 km/h	**B:** No or limited AdBlue injection **B:** No regeneration in NO_x storage catalyst **R:** Insufficient heat in exhaust gas	**+** Alternative or additional emission control system /strategy e.g. gaseous ammonia in SCR system, closed coupled catalyst/DPF **+** Apply higher EGR rates **+** Improved temperature management, like improved insulation of the SCR and/or NO_x storage catalyst **+** Improve fuel injector quality to reduce soot emissions **+** (Mild) hybridization to avoid long idling and low load periods which cool down the catalyst

Disable traction control and/or ESP or select special mode	Efforts to optimize the emission control strategy in order to comply with the RDE legislation rather than achieving low emission under all real-world conditions.	Efforts to optimize the emission control strategy for all reasonable real-world conditions

Vehicle condition

The RDE legislation contains several requirements for the condition of the test vehicle prior to or during the RDE test. These requirements are for example related to the usage of auxiliary devices, payload and precondition. Apart from this specified conditioning, the vehicle must be in a proper state. Hence, a proper maintenance record should be available. Moreover, the vehicle should not have active OBD (On-Board-Diagnostics) errors.

Based on the set specifications for vehicle conditions as described in the RDE legislation and in Regulation (EC) No 692/2008 regarding emissions from light passenger and commercial vehicles (Euro 6)), augmented with some non-specified conditions, the following possible situations with potentially elevated emissions are identified:

- Towing a trailer or caravan, or using a roof rack or bicycle rack:
  - A typical but not exclusively Dutch situation, a family car towing a caravan. The total mileage of this type of driving is limited. It is not the vehicle conditions as such that exclude towing a caravan from valid RDE testing, but the boundaries for driving behaviour and the evaluation tools. The motorway speed requirement, that the RDE trip shall properly cover a range between 90 and at least 110 km/h and shall be above 100 km/h for at least 5 minutes, cannot be met. Moreover, the evaluation tools will simply exclude most events, because of the high CO_2 emissions;
- Driving a convertible with the roof open:
  - This can have a significant effect on the aerodynamics of the vehicle, in particular during highway driving;
- Fuel quality;
- Vehicle conditions with the result that the vehicle may be excluded from In-Service-Conformity (ISC) RDE testing, such as:
  - Odometer > 100.000 km:
    - For ISC testing the mileage of the vehicle should not exceed 100.000 km. However, according to Reg. 692/2008, the useful life of a vehicle is set to 160.000 km. Moreover, in real-world the lifetimes of modern vehicles are in general much higher. A mileage exceeding the RDE boundary of 100.000 km as such should not be a sufficient reason for elevated emissions;
  - Expired maintenance interval:
    - An expired maintenance interval is not a valid reason to have elevated emissions, except when there is a problem with the emission control system;
  - Non-intrusive OBD (On-Board-Diagnostics) error:
    - A non-intrusive OBD error is not a valid reason to have elevated emissions when this error is not related to the emission control system;
- Vehicle conditions which the vehicle may recognize as being RDE tested, such as:
  - OBD connected;
  - Rear window open or removed taillight;
  - Exhaust back pressure and/or load on the trailer hook due to PEMS installation;
  - A preconditioning of the vehicle which differs from the procedure in the legislation: ‘driven for at least 30 minutes, then engine off for 6 to 56 hours’.

In Table 4 the identified situations are elaborated in more detail.

Table 4: Possible situations with potentially elevated emissions related to vehicle conditions.

Situation	**Possible behaviour (B) and examples of the technical reasoning (R) for elevated emissions**	**Examples of possible technical abatement options**
Towing a	**B:** Modified EGR rate and different	**+** Alternative or additional emission

trailer or caravan, or using a roof rack or bicycle rack	engine operation (e.g. different A/F ratio) **B:** No or limited NO_x regenerations in NO_x storage catalyst → NO_x is passing the catalyst unconverted **B:** Modified AdBlue injection **R:** Engine power needed **R:** Avoid overheating of the engine: control strategies focused on reducing temperature **R:** Lower internal contamination **R:** Temperatures in engine and exhaust outside normal operation range **R:** Catalyst temperature and/or space velocities too high for proper NO_x storage or limited possibilities for regeneration due to higher engine loads	control system/ strategy like water injection6 **+** Improved design for temperature management, like an improved EGR cooler, two-stage EGR cooling and an increased engine cooling capacity **+** Improved fuel injector quality to reduce soot emissions **+** Improved design SCR or NO_x storage catalyst to allow for higher space velocities and extra AdBlue injection (in case of SCR) **+** (Mild) hybridization for electric boost to assist engine during firm accelerations
Convertible with roof open & Fuel quality & Vehicle not valid for ISC emission testing & Potential test recognition	**B:** Modified EGR rate and/or AdBlue injection **R:** Efforts to optimize the emission control strategy in order to comply with the RDE legislation rather than achieving low emissions under all real-world conditions.	**+** Efforts to optimize the emission control strategy for all reasonable real-world conditions **+** The application of catalysts with an enhanced durability (related to ISC)

General testing principles to identify elevated emissions

This section provides some general testing principles for the detection of (situations with) possible elevated emissions. However, a sound test procedure and data analysis should be more comprehensive. The paragraphs below provide a starting point only.

Risk based testing within the boundary conditions

Risk based testing is meant to recognize the situations where elevated emissions may or are expected to occur. In an ideal situation, the first step would be to drive a regular RDE test with sufficient variation in driving behaviour. This RDE trip shall be compliant with the set boundary conditions. In the second step the trip data is analysed, and situations with clearly elevated emissions can be identified. A second RDE test is driven as a third step. Also this test shall be compliant with the boundary conditions. However, the trip should be designed such that situations where elevated emissions occur hold a prominent position in the test. For example, when a vehicle seems to have elevated emissions at low speed urban driving, these conditions can be emphasized during the RDE test.

As an alternative, when only one test can be executed, the risk of failure can be estimated based on the applied emission control technologies. For example, a vehicle with SCR may find low-power driving conditions difficult to cope with. Such driving conditions can be emphasized during

the RDE test.

'Non-RDE-compliant' and additional specific real-world testing

A more extensive method of testing would be to drive one or more extra on-road tests in addition to a regular RDE trip. This method is meant to assess the vehicle's emission performance outside the scope of the RDE boundary conditions. The first step would be to drive a valid RDE trip which fulfils the RDE criteria. If all is well, the vehicle is be compliant with the emission limits. The second step is to drive an additional extended real-world trip where the situations outside the scope of the RDE legislation are assessed.

For example, this trip may include the aspects which were identified in the previous chapter:

- 5 minutes idling after initial engine start;
- Multiple idling phases of more than 10 minutes;
- Multiple firm accelerations at different vehicle speeds;
- Testing in residential areas with speeds < 15 km/h;
- A motorway trip with congestion;
- A complete test with a caravan or trailer;

Depending on the common ambient and road conditions in specific member states, the following aspects might be interesting to include in the test:

- Testing at ambient temperatures lower than -7 ˚C or higher than +35 ˚C;
- Testing at altitudes higher than 1300 meters;
- Testing with an altitude difference of more than more 100 meters between start and end;
- Testing at the German highway at speeds > 145 km/h for more than 3% of duration of motorway driving.

To identify possible efforts which are made to optimize the emission control strategy in order to comply with the RDE legislation rather than achieving low emissions in all real-world conditions, the following trip and vehicle aspects, for example, may be added:

- a random sequence different from U/R/M with deviating distance shares for one or more road sections. For example, a more than one hour test drive at the highway or a one-and-a-half-hour test drive in an urban area;
- Manually switch off the engine multiple times during idling phases;
- Switch off ESP and traction control for 10 minutes at each road type;
- OBD connected for some periods during the tests;
- Testing a vehicle with:
    - the rear window opened;
    - a removed taillight;
    - a mileage of more than 160.000 km;
    - an expired maintenance interval;
    - some active OBD errors.

When the trip data is analysed, it is important to check if the elevated emissions only occur during a specific situation, or that this situation works as a trigger. When it has worked as a trigger, emissions remain high during 'RDE compliant' situations as well (e.g. hysteresis in the system).

Another possible testing method is to use repetitions of short cycles, or parts of routes. Many emission control strategies contain an aspect of history or delay. This may in part be legitimated, for example, with a cold start or catalyst buffer. But in principle, the repetitions of short cycles, or parts of routes are a good method to examine history effects. A repetition of the same (short) route, with the same driving, should without history effects lead to similar emissions. Large variations, above the RDE limits, in the results of repeated trips are an indication of a complex emission control strategy warranting further investigations.

Monitoring

As an alternative for testing, monitoring is a very suitable method to detect high emissions in various real-world situations. With monitoring, emissions are measured during regular use of the vehicle throughout a period of multiple days, weeks or even months. All kinds of real-world circumstances can occur in these longer periods. In an ideal situation, multiple vehicles of the same model are monitored. By doing so, the effect of different types of usage and driving behaviour can be assessed.

In the data analysis the situations where elevated emissions arise can be detected. Moreover, it can be determined if these elevated emissions occur one-off or repeatedly in relation to conditions that are inside or outside of the RDE boundaries.

Usually, the equipment used for monitoring is different than for regular on-road measurements. For official RDE testing a PEMS (Portable Emissions Measurement System) is used. The RDE legislation contains a full description of the PEMS equipment, its required quality and the measurement procedures. However, as a PEMS is expensive equipment, takes up quite some space and has an autonomy which is limited to a few hours, and requires an operator it is not suitable for monitoring purposes. Therefore, a small sensor based data acquisition system is more practical for monitoring purposes. Moreover, such a system does not necessarily need to measure all regulated emission constituents. Instead, it can be limited to the most important parameters. As an example, depending on the situation, it can be sufficient to measure only NO_x and CO_2 for diesel engines.

Compared to PEMS testing, monitoring can be rather cost effective. However, for legislative purposes PEMS equipment is required. Therefore, monitoring can also be used as a screening method to detect high emitting vehicles or situations with elevated emissions. When further investigation of a monitored vehicle is needed, PEMS equipment can be installed.

Discussion

There are several initiatives to monitor the emissions of vehicles on the road. For example, remote emission sensing initiatives are started across Europe. Very likely, high emissions are observed for a variety of vehicles in a variety of situations. This may trigger the In Sevice Conformity RDE testing by independent parties, as foreseen by the European Commission. However, high emissions, as shown above, may also occur outside the framework of RDE legislation, and are not reproduced in RDE tests. This requires, very likely, a different follow-up by the type-approval authorities. Moreover, the cause and the mechanism of these occurances of high emissions should be understood from the monitoring studies, such that the results can be reproduced in additional testing, in multiple vehicles.

In summary, observed high vehicle emissions in normal use in monitoring programs are the start of an investigation, which may branch out in many directions. The In-Service Conformity RDE test is one of these directions, where specific test conditions may be needed. Tampering of vehicles is another avenue of investigation, as well as poor maintenance. But the issues with elevated emissions, not covered by the RDE test protocol and the vehicles eligible for in-service confomity testing should remain in the picture. Moreover, the acceptable elevation levels and the test protocols should be investigated further.

The European Commission has asked the type-approval authorities to keep track of technology options to reduce emissions, to ensure the best available technology is applied. (COMM 2017) In principle the type-approval tests are the domain of type-approval authorities. Problems with real-world emissions will likely evolve over time. Both the indications of elevated emissions, as evidence for unacceptable emission levels in particular situations, require a larger commitment from a larger community to monitor emissions, develop test procedures outside the realm of RDE, and to set the acceptable limits. Hopefully, this work is a starting point in this development.

References

RDE legislation: EC/2016/427, EC/2016/646, EC/2017/1154 amending Euro-5/6 legislation (EC/2007/715) with relevant articles 5.1 and 5.2 (accessible through http://eur-lex.europa.eu)

COMM 2017, Notice of the European Commission C(2017) 352 final.

Cuelenaere, Rob F.A., Ligterink, Norbert E., Assessment of the strengths and weaknesses of the new Real Driving Emissions (RDE) test, TNO report 2016 R11227, 27 September 2016.

Ligterink, Norbert E., Spreen, Jordy S., Cuelenaere, Rob F.A., Chase car study: driving behaviour in the Netherlands, Belgium, France and Germany, TNO report 2017 R10436, 31 March 2017.

Mensch, P. van, Cuelenaere, Rob F.A., Ligterink, Norbert E., Assessment of risks for elevated NO_x emissions of diesel vehicles outside the boundaries of RDE; Identifying relevant driving and vehicle conditions and possible abatement measures, TNO report 2017 R10862, 3 July 2017.

Plume Chasing NO_x RDE Measurements to Identify Manipulated SCR Emission Systems of Trucks

D. Pöhler[1], T. Adler[1], C. Krufczik[1], A. Mossyrsch[2], M. Horbanski[1], J. Lampel[1], L. Tirpitz[1], and U. Platt[1]*

Affiliation of authors, include e-mail address for corresponding author (Arial 9).[style: Affiliation]
[1] Institute of Environmental Physics, University of Heidelberg, Heidelberg, 69120, Germany, denis.poehler@iup.uni-heidelberg.de
[2] Camion Pro e.V., München, Germany

Abstract

This study investigates the real driving emissions (RDE) of nitrogen oxide (NO_x) from German and foreign trucks on German highway. NO_x emissions have significantly be reduced for EURO V (2000mg/kWh) and EURO VI (400mg/kWh) trucks. This is achieved with SCR emission cleaning systems using AdBlue®. Nowadays AdBlue® emulators are available which turn of the SCR system to save AdBlue® and thus increase the NO_x emission. We apply the plume chasing / sniffer emission measurement principle with our newly developed NO_x ICAD + CO_2 measurement system to derive the NO_x RDE from a measurement in the emission plume of the trucks. From the observed NO_x emission values a group of 23% of the trucks show significantly enhanced NO_x emissions and potentially apply illegal AdBlue® emulators. Almost all trucks in this group are foreign trucks from Eastern Europe. The total effect of these potential manipulations are estimated to additional 7.000t of NO_x per year only on the German highway. Additionally theses trucks cause a financial damage, as lower toll rate apply for low emission trucks which in these cases would be without any reason. The observations are also analysed for NO_x RDE of all trucks.

Introduction

Vehicles, especially Diesel, are the most relevant NO_x (NO + NO_2) source in urban areas which cause large environmental problems. Thus vehicle NO_x emissions are regulated in the EU with the EURO Norms. Especially new trucks (> 3,5t) and busses (>3,5t) had to reduce significantly NO_x emissions in Europe over the last two decades to improve air quality, as they are one of the largest NO_x source. Allowed emissions reduce from 5000mg /kWh for EURO III (since 1.10.2000) to 400mg/kWh for EURO VI (since 1.1.2013), see Figure 1.

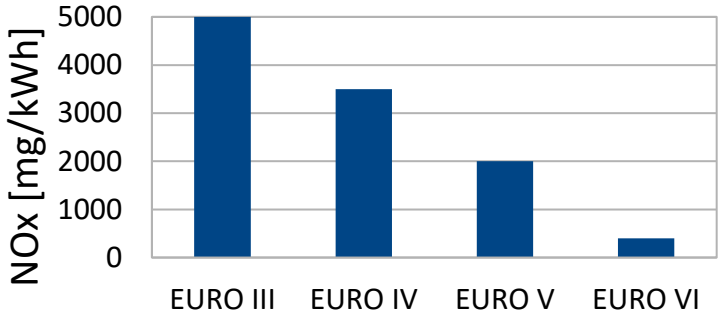

Figure 1: NO_x Emission Norm limit for trucks (>3,5t) and busses (>3,5t).

Trucks achieve these low emissions with complex emission after treatment systems. All EURO VI and most EURO V trucks use the SCR (Selective Catalyst Reduction) system (Figure 2). The water- urea solution AdBlue® is injected to the exhaust gas, so that AdBlue® is consumed.

The reduction of NO_x in the exhaust gas works over two steps in the SCR catalyst. First, the urea solution will form Ammonia (NH_3) at warm temperatures in a so called Thermolysis and Hydrolysis reaction. In the second step, Ammonia react with NO_x to Nitrogen and Water (via Standard and Fast- SCR reactions). These systems are very effective to reduce NO_x up to ca. 90%. However they do not work if the SCR catalyst is cold. Thus the system is typically switched off after motor start until the catalyst reached its working temperature of few hundred degrees. Additionally

Ammonia itself is an air pollutant. It should not pass the emission system and thus a precise injection of the urea solution is required. The motor electronic should assure the correct function of the SCR system, like correct injection and AdBlue® solution. The electronic should give an alarm if it is not working properly and can even reduce the driving capability.

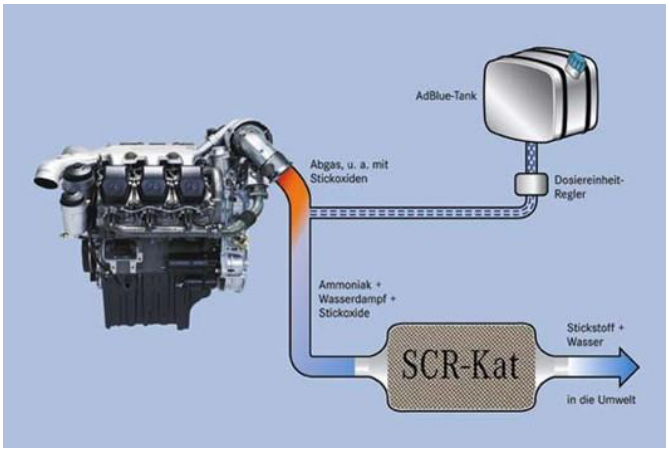

Figure 2: SCR system to reduce NO_x by injecting AdBlue® urea solution to the exhaust gas.

So far only few investigations of NOx RDE are available (e.g. Kleinebrahm, 2008, TNO 2014, TNO, 2016). They typically focus on the emissions of new trucks. We know only one study explicitly including RDE of an aged truck (TNO, 2016). From these studies it is known that NO_x RDE of truck are for EURO VI agree well to the EURO Norm (e.g. TNO 2014, TNO, 2016). For EURO V larger discrepancies are observed (e.g. TNO 2014, TNO, 2016), but for driving conditions like on a highway, they show emission values also within the EURO Norm (Kleinebrahm, 2008; TNO 2014, TNO, 2016).

AdBlue® Emulators

The AdBlue® consumption is a non-ignorable cost factor for trucks and busses. The consumption is typically 1,5l per 100km. AdBlue® can be bought cheap (~0,20€/l) in very large quantities, however for trucks operating on long range transport without the possibility to refuel AdBlue® at their depot, need to by the more expensive AdBlue® at petrol stations for ~0,55€/l. For a truck the total cost for AdBlue® can sum up to 1000 to 2000€ per year and some operators like to reduce these costs.

Since some time so called AdBlue® emulators or AdBlue® killers are available online. Even if these tools are illegal to operate in a truck in Europe they can be bought for less than 50€ over several online platforms. These systems turn off the SCR system in order to reduce the AdBlue® consumption and thus save money. This can lead to significantly increased NO_x emissions even to levels of EURO I trucks (as new trucks are not optimised for low NOx emission without SCR). At the beginning these tools were a small electronic box which was connected to the motor electronic to cheat it and switch off the SCR system. These electronic boxes can be found, to detect such illegal manipulations, however there small size allow many very hard to find locations in a truck. Newer AdBlue® emulators are even a pure software manipulations. This means that to the truck motor electronic a modified software is uploaded which will turn off the SCR system. In this case no illegal connected hardware can be found. Even more these systems allow various settings which make them very difficult to detect. For example often they are configured, that the SCR systems works at small speeds (AdBlue® consumption is low anyway), and only it is turned off at higher speed. This makes the observation in a control almost impossible.

To our knowledge there is so far no study investigating the effect of AdBlue® emulators on the NO_x RDE, and also no investigation of how often such emulators are applied based on emission measurements.

Real Driving Emissions (RDE) of NOx with the Plume Chasing Principle

To uncover AdBlue® emulators, Real Driving Emission (RDE) measurements can be used, as manipulated trucks and busses have much higher NO_x emissions. The main problem is that RDE with standard PEMS (Portable Emission Measurement Systems) are not practical for control purposes. Also optical emission measurements over a street (where the vehicle passes the light beam for a measurement) are not reliable to detect the emission of an individual vehicle, as emissions vary significantly on a few second base and a snap shot may give wrong results for an individual vehicle (Bütler, 2016). Reliable emissions require the measurement over at least few minutes. We apply a different approach to investigate NO_x RDE, the plume chasing / sniffing vehicle method (Figure 3 and Figure 4) like also applied by Chui et al., 2016.

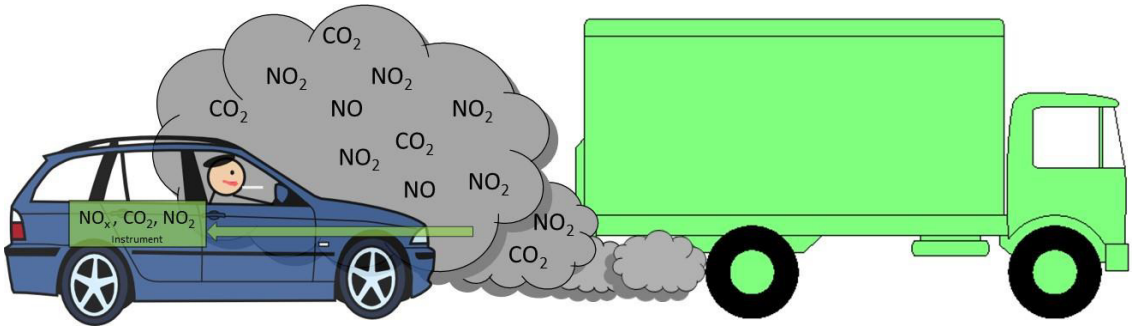

Figure 3: Plume chasing measurement configuration where a measurement car is driving behind the investigated truck in the emission plume. With a sniffer the air in the plume is sampled and analyzed by the ICAD NO_x + CO_2 instrument.

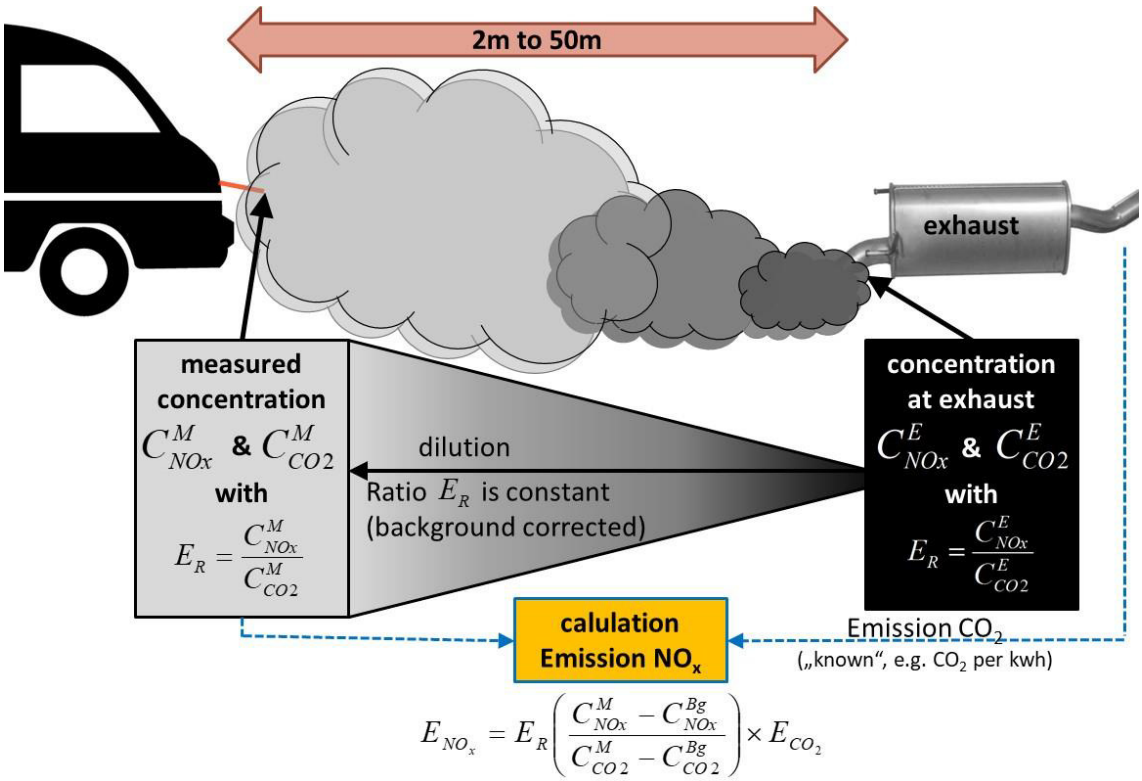

Figure 4: Plume chasing measurement principle. The vehicle emissions will be diluted in the plume, but the ratio E_R of NO_x / CO_2 of the emission gas will stay the same (if background CO_2 and NO_x concentration are considered). Thus with the measurement of the ratio the NO_x emission can be calculated.

The measurement is based on a gas observation in the diluted emission plume of the investigated vehicle. A sniffer in a following car samples the air of the plume which is analysed in a NO_x-ICAD + CO_2 –instrument. The observation is based on the principle that the emission of a vehicle consist of several gases. The emissions of CO_2 are well defined over the fuel consumption as it arises from the oxidised carbon in the fuel. For trucks and busses the CO_2 emission per kWh of the engine can be well estimated over the engine efficiency. Thus the CO_2 emission is relative constant per kWh and can be used as reference gas. We apply an efficiency of 40%, which is a very optimistic energy efficiency of a truck and corresponds to a best case emission calculation (with lower efficiency a higher emission factor would be calculated). The emissions like NO_x do not have such a fixed relation and depend mainly on the formation in the engine and the emission cleaning system. Thus from the ratio of NO_x to CO_2 concentration the emissions of NO_x can be calculated without the need to measure the emission gas flux. The calculation is just based on the measured concentrations and known CO_2 emission (see Figure 4). As the calculation just rely on the relative concentration $E_R = NO_x / CO_2$, it does not require to measure this concentration ratio in the emission pipe, but can also be in the diluted plume with lower concentrations of NO_x and CO_2, as the ratio (E_R) will not be changed. For the estimation of the emission ratio E_R in the diluted plume the background concentration of NO_x and CO_2 in the background air needs to be considered. The quantification of the background concentration can be very important, as the concentration in the diluted plume maybe close to the background concentration, especially for CO_2. Thus the background concentrations on the street should be measured regularly. Fortunately three factors make this background measurement relative easy. First, vehicles typically do not drive constantly with the same engine power, in periods when the engine is in idle, no emissions arise and the background data can be determined from these periods. Second, even if some emissions are present in the period of the background measurement, it will have no influence on the result, as long as the emission ratio E_R does not change to much. The reason is that a remaining concentration in E_R just cancel out. Third, if individual vehicles are investigated they are first approached and later a change to another vehicle is performed. Thus before and after the measurement background concentrations are observed. However still the plume sampling should be optimised, to measure higher concentrations of the emission, as than the error of the background correction plays a minor role. Optimising the sampling for plume changing is thus still topic of current investigations.

The key for successful plume changing / sniffer car measurements of NO_x is the NO_x measurement instrument. A very fast, precise and vibration robust measurement instrument is required without interferences to other gases present in large concentrations in the emission plume. This can typically not be achieved with currently available commercial NO_x instruments like CLD. We apply the new developed ICAD NO_2 / NO_x instrument, developed by us and now available by the University of Heidelberg Spin-off Airyx GmbH (Figure 5). It is an optical instrument directly measuring NO_2 concentration by its characteristic differential absorption features. The total NO_x is observed, as the NO is converted to NO_2 before entering the measurement cell. The measurement with 2 seconds time resolution has an accuracy of ~0.5ppb.

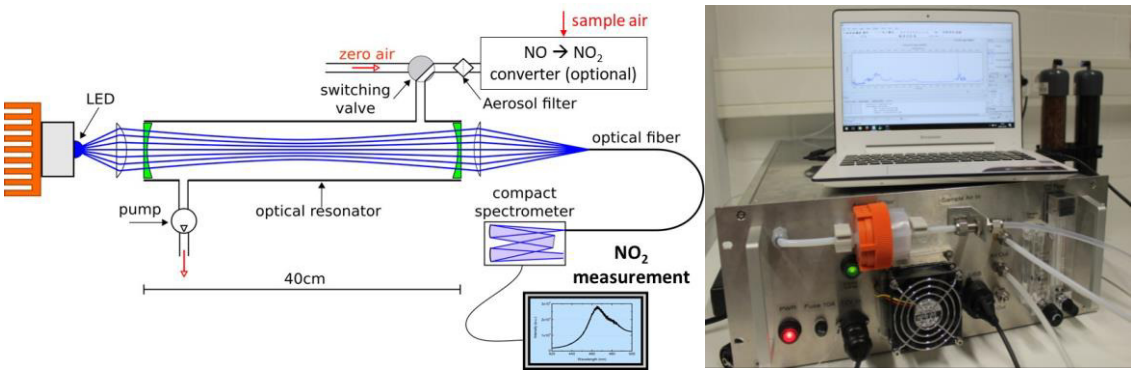

Figure 5: ICAD NO_x + CO_2 instrument used for plume changing studies. This mobile instrument can easily be operated in a car. As it is not sensitive to vibrations and has a power consumption of only ~30W. With its fast measurement (2 seconds) and high accuracy it is ideal for plume chasing observations.

The ICAD NO_x instrument is combined with an IR CO_2 sensor. For the plume chasing measurements, the gas concentrations in the emission plume are measured for several minutes. Afterwards the data are averaged over the time when air was sampled inside the emission plume. This was defined if the CO_2 concentration is 30ppm above background level. From the average emission ratio, the NO_x emission factor is calculated and compared to the EURO standard.

To validate our NO_x emission measurement system based on plume chasing, we performed intercomparisons with a well-accepted PEMS system on EURO 6 diesel cars. The derived NO_x emissions over a distance of 31km were compared and agreed within ±5% or ±10mg/km, what is better than the accuracy of both systems. If only very short measurement periods are compared the difference increase, but for two minutes the difference is still only ±32.5mg/km. Thus the accuracy is enough for most emission studies, especially if vehicles with much higher emissions should be identified. Similar intercomparisons for truck emissions are currently performed.

Observation of Manipulated SCR Emission Systems

We performed a study of NO_x RDE of more than 250 randomly chosen trucks on German highways. The NO_x emissions of each truck were typically measured between 5 to 10 minutes. Due to the measurement on the highway, warm summer weather conditions and the measurement time we can mainly exclude that SCR emission cleaning system were not working due to a cold SCR system. The main target of the study was to investigate potentially manipulated emission systems with AdBlue® emulators. For most trucks the brand, the model name, the country of registration and its EURO class could be determined and used in a statistical analysis.

The country of origin were: Germany (21%), Poland (29%), Bulgaria (8%), Czech Republic (8%), Baltic Countries (7%), Romania (5%), Slovakia (4%), Hungary (4%), Turkey (3%), Slovenia (2%) and other (9%). 50,4% of the trucks had a clear EURO class label and thus allow precisely to be classified as EURO VI, EURO V or EURO IV truck. We could not get additional information from the other trucks via the number plate due to data security. Other indications were used to classify these trucks, e.g. the presence of an AdBlue® tank indicate that it is at least a EURO V truck and was thus further investigated like a EURO V truck even if it could also be a EURO VI truck. As a EURO VI truck would have even lower emission, it should still fulfil the EURO V emission factors. With these additional classifications in total 69% of the measured trucks could be assigned to a EURO emission class. These are 39,4% EURO VI, 58,3% EURO V and 2,3% EURO IV. To perform statistical analysis, the trucks were classified according to their derived NO_x emission values, e.g. for EURO V trucks emissions below 500, 500 to 1000, 1000 to 1500 mg/kWh and so on, see Figure 6. The histograms of the NOx emission derived for EURO V and Euro VI are shown in Figure 6 and Figure 7 respectively. They are separated for German and foreign trucks.

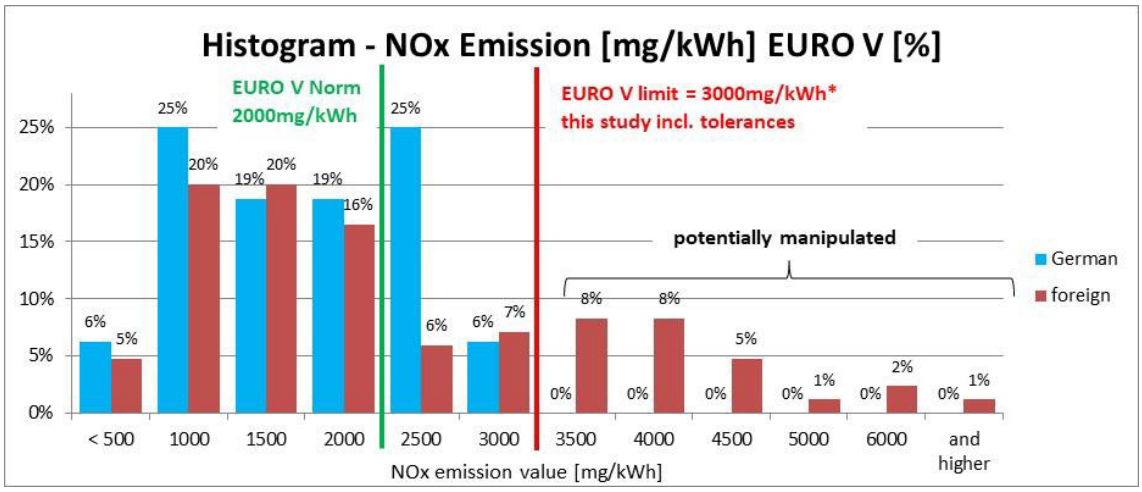

Figure 6: Histogram of derived EURO V NO_x emissions of trucks.

For EURO V (Figure 6) we found that most of the trucks show emissions below or close to the EURO Norm of 2000mg/kWh. We could not observe a German truck with much higher emissions, however between the foreign trucks several show much higher values. We define for EURO V a

limit to classify trucks with correct working emission system of 3000mg/kWh. This includes an additional tolerance to the EURO Norm of +1000mg/kWh. This large safety margin was chosen as the measurement was only over few minutes and does not represent the whole driving cycle for an emission test. Also we wanted to make sure only to classifiy trucks as defective which clearly show much higher emission values. However we would expect for driving on the highway due to its constant driving property optimal conditions for a good working engine and emission cleaning system. Lower emissions at these conditions are well known for trucks (Kleinebrahm, 2008; TNO, 2014; TNO 2016). Thus, the large tolerance is already a very conservative value. Trucks above this limit are classified as non-correct working emission cleaning system and are potentially manipulated with AdBlue® killers. For EURO V we find only foreign trucks in this group with emissions up to 10.000mg/kWh.

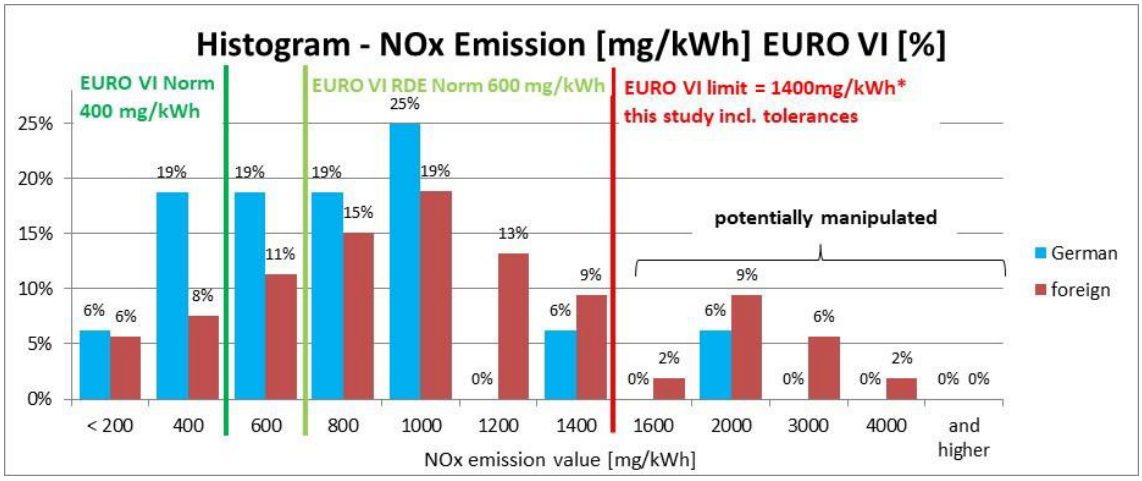

Figure 7: Histogram of derived EURO VI NO_x emissions of trucks.

For EURO VI (Figure 7) the emissions are typically lower like expected and emissions were classified in different groups than for EURO V. For EURO VI there is not only the EURO Norm with 400mg/kWh, but also the EURO VI RDE Norm with 600mg/kWh which is already higher to account for more difficult conditions on the street than in the lab. Most EURO VI trucks were not below this RDE emission Norm, but close with emissions below 1000mg/kWh. Again it can be observed, that EURO VI trucks from Germany show lower emissions than foreign trucks which show emissions up to 4000mg/kWh. We defined for EURO VI a limit to classify trucks with correct working emission system of 1400mg/kWh. This includes again an additional tolerance to the EURO Norm of +1000mg/kWh. Trucks above this limit are classified as non-correct working emission cleaning system and are potentially manipulated with AdBlue® killers. For EURO VI we find mostly foreign trucks in this group and one German truck (causing the 6% in the histogram).

Table 1: Percentage of trucks with exceeding NOx emissions (above EURO Norm limit + 1000mg/kWh) and thus potentially manipulated with AdBlue® emulators.

	potentially manipulated with AdBlue® emulators		
origin	EURO V	EURO VI	all
Germany	0 %	6,9 %	2,7 %
Foreign	25,6 %	18,9 %	22,7 %

The observed exceeded emission values can be summarised that 18,9% of the EURO V and EURO VI trucks show values above the limit which already included large tolerances to the EURO Norm of +1000mg/kWh. Trucks with emissions above the limit are classified with defective emission cleaning system and potentially manipulated with AdBlue® emulators, but we cannot exclude that also other factors may result in these high emissions. These suspicious trucks were almost exclusively foreign trucks were 22,7% had exceeded emissions (see Table 1). These are almost exclusively trucks from Eastern Europe, as these were the dominating group of foreign trucks. Only one German truck was observed with exceeding emissions what corresponds to 2,7% of the German trucks. The difference between German and foreign trucks cannot be explained by older or other trucks, as we compare same EURO type trucks with each other. Emissions above the defined limit could be observed for EURO V and EURO VI trucks. That the

percentage of potentially manipulated EURO V trucks is higher than for EURO VI may be due to the simpler technical implementation of AdBlue® emulators to these systems. The much smaller percentage of potentially manipulated German trucks may be caused due to stronger regulations and fines. The country of origin of these potentially manipulated trucks can be further analysed. They originated from all eastern European countries except from Czech Republic. However the amount of investigated trucks per country are too small for significant statistics.

Comparison of estimated EURO class with Toll Statistics

The available toll statistics of trucks on German highways includes the amount of different EURO classes and separation to German and foreign origin (Bundesamt für Gütervekehr, 2017).

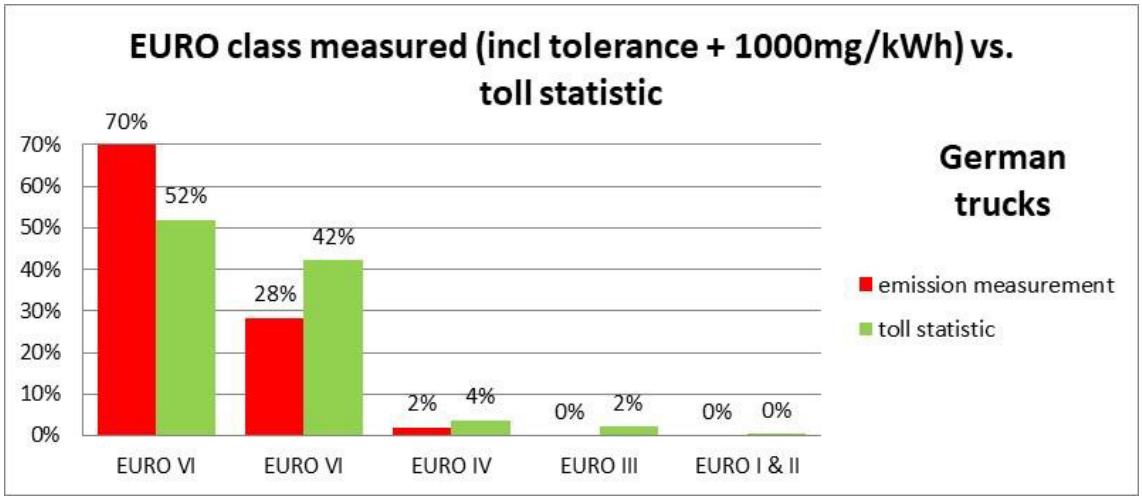

Figure 8: Comparison of statistical derived EURO class of the investigated trucks purely on the measured NO_x emission value including a tolerance of +1000mg/kWh in comparison to the EURO Norm versus the EURO classes according to the toll statistic just for the German trucks.

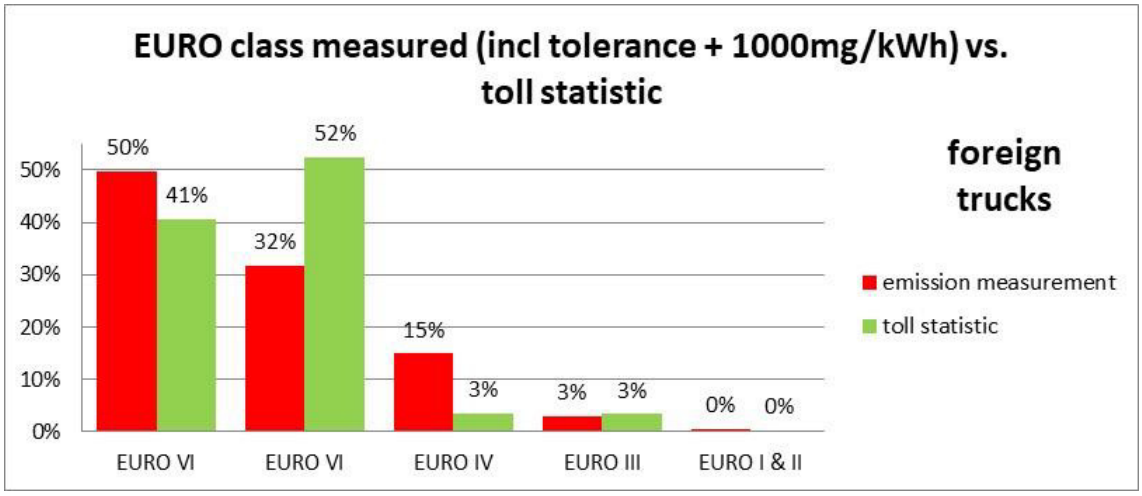

Figure 9: Like Figure 8 but for foreign trucks.

These data can be used to compare with the observed emission data of this study. Therefore we derive an estimated EURO class of the investigated trucks purely on the measured NO_x emission. The advantage is than in this case all measured trucks can be included even if no clear EURO classification due to labels could be performed. The truck was accounted to EURO VI if its emission was below the EURO VI Norm (400mg/kWh) + the tolerance of 1000mg/kWh resulting in 1400mg/kWh. The same was done for the other EURO Norms. Afterwards the percentage of the different observed EURO classes in the study is compared to the toll statistics. Due to the large tolerance we expect that on average the trucks will be assigned to better EURO classes than they are in reality, and this could be observed for German trucks (Figure 8). 70% of the trucks were accounted as EURO VI even if from toll statistics only 52% of the German trucks should

have this EURO class. Thus we observe on average less trucks with older EURO classes than statistically should be present, e.g. we did not classify any truck of EURO III and older, and only half as EURO IV like expected.

A different picture is observed for foreign trucks (Figure 9). Here we classified much more trucks as EURO IV (15%) according to the NO_x emission value, in comparison to the toll statistic of 3% in this group. As the investigated trucks were chosen randomly, the difference can only be explained that foreign trucks more often have a defective emission system potentially due to AdBlue® emulators. Only this may explain why statistically we classify much more trucks to older EURO norms.

Analysing RDE NO_x Emission Values

The derived NOx emission data can also be used to investigate RDE of trucks on highways for the real truck fleet (not for new trucks). If we include all trucks with classified EURO Norm, the average emission is shown in Table 2. This includes also the trucks with potentially manipulated emission system. Also here a significant higher emission on average for foreign trucks is observed.

Table 2: Derived average NO_x RDE of the different trucks including also potentially manipulated trucks [in mg/kWh].

origin	EURO IV	EURO V	EURO VI
All countries	2134	1941	929
Germany	1671	1449	662
Foreign	2597	2032	1016

German EURO IV and EURO V trucks show here lower NO_x emissions than the EURO IV and V norm. This is expected from previous publications (Kleinebrahm, 2008; TNO, 2014; TNO, 2016), where it was shown that trucks show especially at driving conditions on the highway lowest emissions. However for EURO VI trucks this was not observed and maybe RDE of EURO VI are higher than so far expected. But this analysis also includes potentially manipulated trucks what may increase the average derived emission value. Still the data may indicate that EURO VI RDE emission of used trucks may be on average much higher than so far expected. This may be due to ageing of the emission cleaning system or that the systems may not work always under optimal conditions.

The separation of trucks with potential manipulations and those without to analyse purely the NOx RDE of non-manipulated trucks is difficult, as a clear threshold for the separation in emission is unknown. We applied the same threshold like before with EURO norm + 1000mg/kWh tolerance. Trucks with emissions below that value are accounted as correctly working, and those above as defective. If we apply this, than on average correctly working EURO VI trucks would have NO_x emissions of 745mg/kWh and above of 1791mg/kWh. For EURO V 1548mg/kWh and 3752mg/kWh respectively. The emissions of the correctly working trucks are estimated to high if the tolerance is chosen to large. If we use this separation and the derived percentage of potentially manipulated trucks we can estimate the additional NO_x emission due to these potential manipulations using the toll statistic of the amount of different trucks on the German highway (Bundesamt für Gütervekehr, 2017). We calculated an additional NO_x emission of about 7.000 t NO_x per year only for the German highway.

Next Steps

This study shows that plume chasing / sniffer measurements of NO_x with the mobile NO_x ICAD + CO_2 system can derive NO_x RDE values of trucks on the highway. The measurements can be used to effectively identify potentially manipulated vehicles. Further developments of the measurement system are currently performed and still needed to improve and simplify the measurements and data analysis. The measurement system will be commercially available from Airyx GmbH, a spin-off from the University of Heidelberg. Several measurement projects to further quantify the measurement accuracy of this technique and to investigate AdBlue® emulators are currently planned. They should be combined with direct truck controls by police or federal office

for goods transport. So far the implementation of these observations for official controls was not possible, as authorities did not accept it as official measurement. Here a change is required that new technologies can effectively support emission controls in the future.

Acknowledgements

This work was supported by EXIST Forschungstransfer Project (FKZ: 03EFGBW121), Camion Pro e.V. and Zweites Deutsches Fernsehen (ZDF).

References

Bundesamt für Gütervekehr, Mautstatistik für Juli 2017 (2017), https://www.bag.bund.de/DE/Navigation/Verkehrsaufgaben/Statistik/Mautstatistik/mautstatistik_node.html.

Bütler, T. (2016), Pilotprojekt Vergleichsmessungen Remote Sensing - PEMS – Rollenprüfstand, Empa-Bericht Nr. 5214010202.01.

Chui F.L., A. Rakowska, T. Townsend, P. Brimblecombe, T.L. Chan, Y.S. Yam, G. Močnik, Z. Ning (2015), Evaluation of diesel fleet emissions and control policies from plume chasing measurements of on-road vehicles, Atmos. Environ., 122, 171-182.

Kleinebrahm, M. et al. (2008), On-Board Measurements of EURO IV / V Trucks, Final Report, a research project of the Federal Environmental Agency (FKZ: 204 45 144). Germany: TUV NORD Mobilität.

TNO (2014), The Netherlands In.Service Emission Testing programme for Heavy-Duty 2011-2013, TNO 2014 R10641.

TNO (2016), The Netherlands In-Service Emissions Testing Programme for Heavy-Duty Vehicles 2015-2016 – Annual report, TNO 2016 R11270.

Analysis of tail-pipe emissions of a plug-in hybrid vehicle and its average emissions for different test cycles

S. I. Ehrenberger, J. Qiao, M. Konrad, F. Philipps

Institute of Vehicle Concepts, German Aerospace Center, Stuttgart, 70569, Germany, simone.ehrenberger@dlr.de

Abstract

In order to assess the correlation of tail-pipe emissions with different impact factors, a PHEV is evaluated with real-driving emission RDE tests and on our chassis dynamometer. Apart from analysing the energy consumption of the vehicle and the resulting carbon dioxide (CO2) emissions, the main pollutants mainly analysed are, amongst others, carbon monoxide (CO), nitrogen oxides (NO_x) and particles. PHEV direct emissions strongly vary depending on the operating strategy. We compare the results of test with different modes in RDE tests and with the results from the dynamometer. Using this information, we evaluate the differences in emissions for the phases urban, rural and motorway driving of the test cycles.

Keywords: plug-in electric vehicle, dynamometer test, real-driving emissions

Introduction

The electrification of passenger cars is seen as one instrument towards mitigation of local air pollution and climate change (European Commission, 2011). Nevertheless, up to now the market share of electric vehicles (EV) falls short of expectations in many European countries. Therefore, plug-in hybrid vehicles (PHEV) can be seen as a transition technology towards a fully electrified vehicle fleet, as they combine the advantage of locally emission free driving in certain areas without cutting the total vehicle range. However, knowledge on real-world driving, energy consumption and tail-pipe emissions of PHEV under different driving conditions still has to be improved.

PHEV direct emissions strongly vary depending on the operating strategy. We compared the emissions of various measurements with parameters like ambient temperature, catalyst temperature, air-fuel-ratio and others. First results have been presented in Kugler et al. (2016). In this paper, we present result of on-road emission measurements with a portable emission measurement (PEMS) device. We compare the results of these real-driving emission (RDE) tests with the results for the WLTC tested on the dynamometer. Main focus of this analysis is the range of overall emissions and energy consumption in different driving modes and battery states. Additionally, we consider the influence of the electric range on the absolute emissions for different driving situations which are “urban”, “rural” and “motorway”.

Set-Up for PHEV Emission Tests

In order to assess the correlation of tail-pipe emissions with different impact factors, two different gasoline PHEVs are tested on our chassis dynamometer and on-road. Apart from analysing the energy consumption of the vehicle and the resulting carbon dioxide (CO2) emissions, the pollutants mainly analysed are, amongst others, carbon monoxide (CO), nitrogen oxides (NO, NO2) and particles as particle number (PN). The vehicle characteristics of the tested EURO6 compliant PHEV are listed in Table 1.

Table 1: Technical characteristics of the tested PHEV

Internal combustion engine	**135 kW**
Electric motor	65 kW
System power	185 kW
Electric range	40 km
Fuel consumption (NEDC)	1,9 l/100km
CO2 emission (NEDC)	44 g/km
Curb weight	1735 kg

Apart from exhaust emissions, data of the on-board-diagnostics (OBD) have been logged in order to evaluate the potential influence of parameters like catalyst temperature or air-fuel-ratio on the pollutant forming process.

Main goal of the tests is to evaluate the range of possible emissions from PHEV vehicles under different driving conditions. Therefore, RDE tests using one representative route which meets the requirement of the RDE directive (European Commission 2017) are performed. In order to evaluate the energy efficiency and the emissions as close to real life as possible, the tests have been performed with air condition turned on. Additionally, the worldwide harmonized light vehicles test procedure (WLTP) has been applied using the corresponding test cycle WLTC. The tests have been conducted in different modes according to the SAE standard on measure the electric range of hybrid electric vehicles (SAE 2010) and at different ambient temperatures. The tests at -7°C have the same vehicle conditions as at 23°C. Cold starts are performed after vehicle charging and are driven with a charge depleting driving mode (CD mode). In addition to the CD mode tests, the results for the tests with charge sustaining (CS) mode are analyzed. These tests are represents the situation where the electric range of the vehicle is exceeded and the driver uses the car as a common gasoline hybrid vehicle. Nevertheless, the vehicle recuperates the braking energy in this mode, and the electric driving share in this case is notable.

In case of PHEV, various factors determine the energy consumption and the formation of local emissions. Apart from the state of charge (SOC) of the battery which strongly influences the use of the internal combustion engine (ICE), other aspects like the selected driving mode, the ambient temperature, the used secondary consumers and the driving behavior

In order to assess the potential range of energy consumption and emissions, the RDE compliant route was operated in various driving modes. For the RDE tests the following modes have been chosen:

- Maximum electric drive in the eco mode with 100% SOC at the beginning of the test
- Hybrid driving in the comfort mode with 100% SOC at the beginning of the test
- Hybrid driving in the comfort mode with 0% SOC at the beginning of the test
- Most dynamic mode with 0% SOC at the beginning of the test

The first and the last modes span the potential range of energy consumption and emissions of the PHEV.

Energy Consumption of PHEV RDE Tests

The usage of the electric energy in hybrid vehicles depends strongly on the operating strategy of the car which results, for example, from the selected driving mode, the state of charge from the battery or the ambient temperature. The possibility to choose a driving mode leads to different electric driving ranges according to the chosen mode. For three of the analyzed RDE tests, the vehicle internal energy flows have been measured.

The ambient temperature varies between 24 - 28 ° C. This of course has an influence on the energy consumption for example on the AC. By using the measurement of the engine speed, the fuel flow and the current to the ignition coils it was possible to find the selections of the ride that where driven without the combustion engine. These parts are marked red in Figure 1. Blue is the fraction of the distance covered by the internal combustion engine.

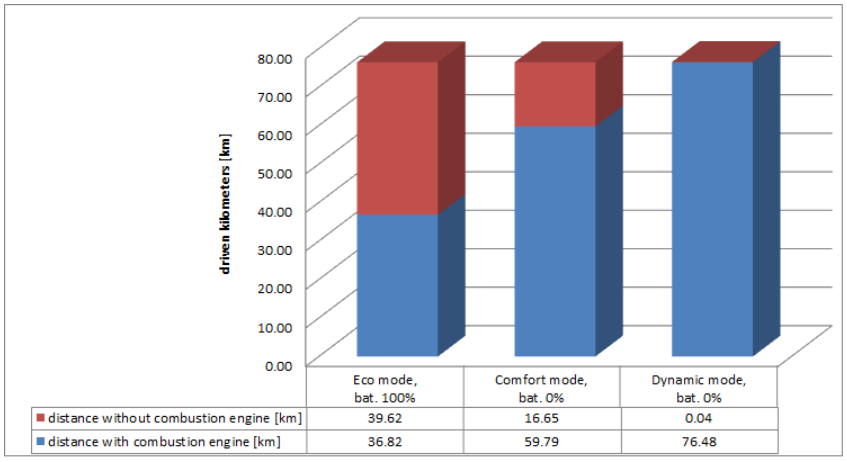

Figure 1: Overview of the electric and combustional driven range depending on the driving mode

Figure 2 intents to provide an overview of the energy content used for the route. Blue is the energy content from the used fuel. The energy balance from the high-voltage system is shown in red. The energy content from the used fuel (density corrected and a calorific value of 8760 kWh/m³) and the used energy from the high voltage battery are shown. It includes the propulsion power conversion losses, HV-AC, the 12V power transmission and the current into the drive converter.

In the case that during the ride the HV battery gets loaded by recuperation or from the combustion engine the energy that is in the end of the measurement in the battery will enter as negative energy value into to graphic. As a result the energy balance on the HV system has to consider the vehicle specific working strategy.

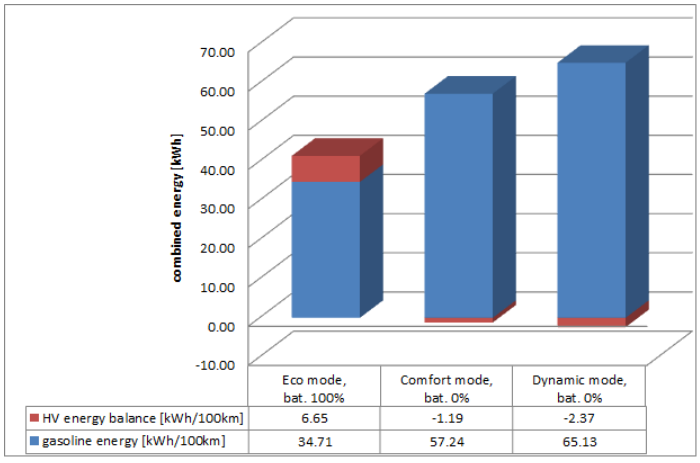

Figure 2: combined energy used for the RDE drive dependent on the driving mode

Results of PHEV RDE Tests

The RDE tests have been performed under similar weather conditions and fulfil the requirements of the RDE directive. Figure 3 shows the cumulative emissions of four RDE measurements. The engine speed indicates the use of the ICE which is zero during phases of electric driving. The tests with a SOC of 100% at the beginning have a long period of electric driving. The ICE starts only in moments of certain acceleration and when the SOC reaches its lowest level. For both tests with full battery starts, this state is reached after more or less the same distance, although the eco mode test is slightly more energy efficient. The use of the ICE is directly linked to the CO_2 emissions which are in these two cases almost identical.

In the eco-mode and comfort mode with full battery start, the operation strategy is quite similar. In contrast to that, the dynamic driving mode causes considerably higher CO_2 emissions. The larges fuel consumption does not imply higher pollutant emissions, as Figure 3 shows. The test in the eco mode with high shares of electric driving in the beginning has higher CO emissions than the other tests. Also the particle formation after the maximum electric range is reaches a high level.

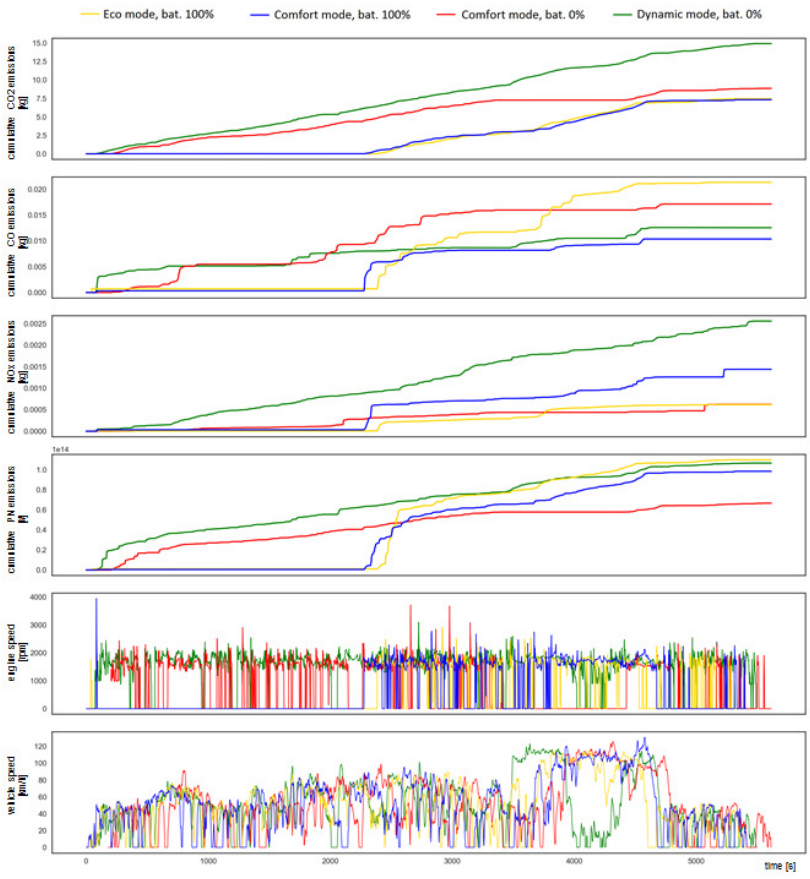

Figure 3: Cumulative emissions, engine speed and vehicle speed of RDE tests

The vehicle speed shows that the RDE test is not reproducible, although the route remains the same. Nevertheless, the three speed categories can be identified easily. In case of hybrid vehicles, the potential of recuperating and storing energy during driving adds variable vehicle behaviour to the test set-up. For example, during the test in the hybrid comfort mode which started with 0% SOC, the battery has been charged partially and the energy is used during the motorway phase of the test.

Average Emissions of the PHEV

The results of the tests have been evaluated according to the average emissions for each speed category. These figures represent the average mass of emissions per kilometre for urban, rural and motorway driving.

Additionally to the RDE tests, standardized driving cycles have been measured. The WLTC has been tested on a dynamometer according to the requirements regarding the use of auxiliaries, temperature, conditioning etc. The standard temperature for these tests is 23°C. The cycle has been started as cold start with full battery and repeated until the battery has reached a constantly low SOC. For the tested PHEV, the third repetition represents a test in the charge sustaining mode as the test starts with 0% SOC.

Both the dynamometer and the RDE test have been evaluated according to the emission in different road categories. In case of the RDE test, the classification into “urban”, “rural” and “motorway” driving results from different speeds during the tests. For the WLTC, the four cycle phases have been separated and assigned to the road categories. Figure 4 and Figure 6 show the results for the three categories and the average total emission figures. The CO_2 emissions for the dynamic driving mode are higher than in other modes.

Clearly, the battery SOC determines the absolute CO_2 emissions (Figure 5). Generally, the higher the electric share, the lower the gasoline consumption and the CO_2 emissions. In motorway conditions, the ICE is turned on at a certain speed, independently from the SOC. In addition to the test at 20 to 30°C, the WLTC has been measured at -7°C. The conditioning has been equal to the 23°C test, but the PHEV is driven mostly with the ICE in the first cycle, although the SOC is 100% and heating is turned off. This affects the average emissions in the urban and rural part of the cold start test which are much higher compared to the mainly electric driven cold start test at 23°C. In most cases, the gasoline consumption and the CO_2 emissions of the motorway driving are higher than in the urban and rural phases, but higher shares of electric driving, e.g. due to the recuperated energy in the RDE test with comfort mode, can turn around this finding. The NEDC emissions are slightly higher than the official standard value. As these figures are calculated with the artificial formula for hybrid vehicles, they are not comparable to the other tests.

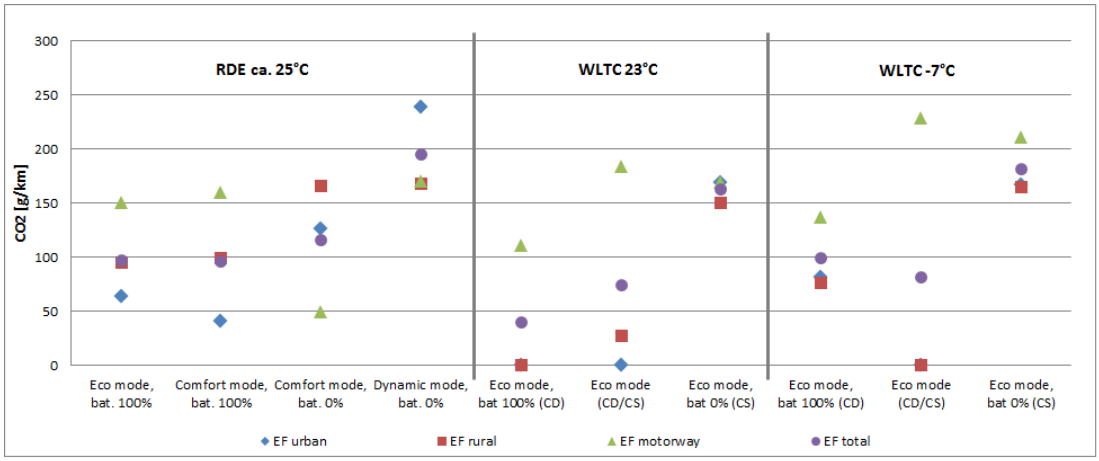

Figure 4: Comparison of CO_2 emissions of RDE, WLTC and NEDC tests

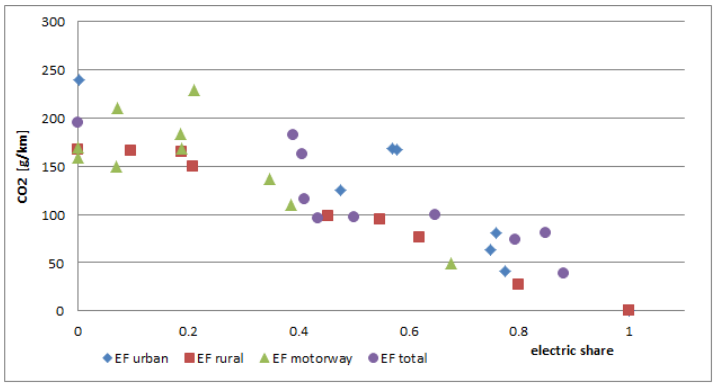

Figure 5: Relation between CO_2 emissions and share of electric driving

The emission figures for CO and NO_x show that the PHEV emissions are lower than the legal limits (Figure 6). The only exception are the tests at -7°C which indicate different emission characteristics of the ICE or the exhaust gas treatment at lower temperatures. But the particle number exceeds the legal limits in many cases. In general, the average emissions of the RDE test are similar to the WLTC tests. The average pollutant emissions are less related to the speed or road category. In general, CO and PN emissions show fewer differences between the three categories "urban", "rural" and "motorway" than the CO_2 or NO_x emissions. The test in the dynamic mode shows high NO_x emissions in the urban part of the RED test which is mainly driven in the first third of the test and influenced by cold start motor behaviour. At -7°C, cold start emission have a high influence on the average emissions of driving cycle, especially in the urban phase. At this temperature, the variance of average emissions in the three categories is generally higher.

Unlike for CO_2 emissions, the correlation between pollutant emissions and share of electric driving is not visible (Figure 7). Apart from the ambient temperature, the driving conditions in the moment of ICE starts strongly influence the absolute emissions. Figure 7 also depicts the higher average electric driving share in the urban road category, while the motorway in average goes along with lower electric shares. This is due the forced ICE use at higher speeds and the recuperated energy in driving situation with phases of breaking and slowing down. This recuperated energy is used for electric driving until the SOC reaches is lowest level again.

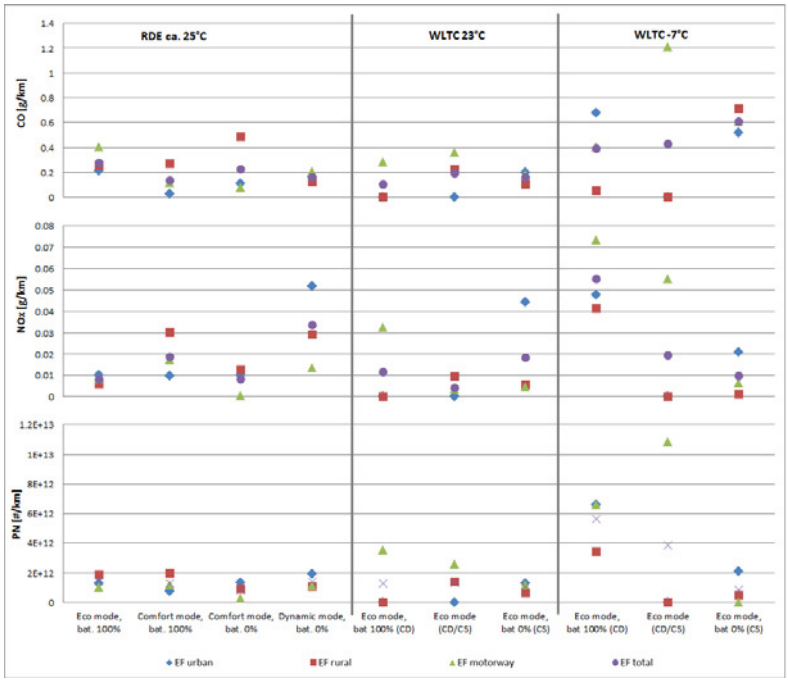

Figure 6: Comparison of pollutant emissions of RDE, WLTC and NEDC tests

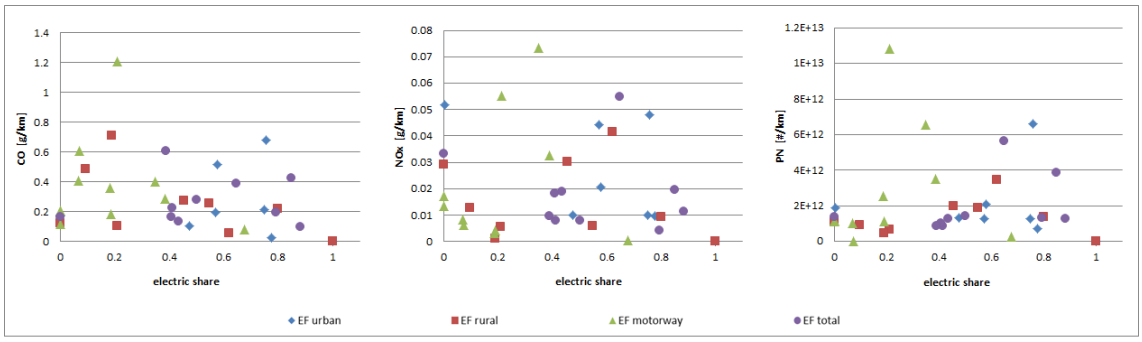

Figure 7: Relation between pollutant emissions and share of electric driving

Conclusions

The test presented in this paper have shown that the CO_2 emission strongly correlate with driving mode and battery SOC of the PHEV. Compared to the results of the WLTC and RDE teste, the calculated NEDC results are much lower. In case of pollutants, the CO and NO_x emissions are generally below the legal limits. Particle number, however, is above the allowed limit. The test at an ambient temperature of -7°C show a notably different operation strategy and emission formation that the measurements at moderate temperatures. Future works will apply the same test set-up with other PHEVs in order to validate these findings and in order to narrow down the potential range of PHEV emissions to a more realistic level. So far the test have clearly shown that the standard CO_2 emissions for a PHEV as well as approaches for calculating the pollutant emissions as a function of electric driving share do not reflect the real life emissions of such vehicles.

References

European Commission. 2017. Commission Regulation (EU) 2017/1154 of 7 June 2017 Amending Regulation (EU) 2017/1151 Supplementing Regulation (EC) No 715/2007 of the European Parliament and of the Council on Type-Approval of Motor Vehicles with Respect to Emissions from Light Passenger and Commercial Vehicles (Euro 5 and Euro 6) and on Access to Vehicle Repair and Maintenance Information, Amending Directive 2007/46/EC of the European Parliament and of the Council, Commission Regulation (EC) No 692/2008 and Commission Regulation (EU) No 1230/2012 and Repealing Regulation (EC) No 692/2008 and Directive 2007/46/EC of the European Parliament and of the Council as Regards Real-Driving Emissions from Light Passenger and Commercial Vehicles (Euro 6). http://eur-lex.europa.eu/legal-content/EN/TXT/?uri=CELEX:32017R1154.

Kugler, Ulrike, Simone Ehrenberger, Mascha Brost, Holger Dittus, and Enver Doruk Özdemir. 2016. “Real-World Driving, Energy Demand and Emissions of Electrified Vehicles.” Journal of Earth Sciences and Geotechnical Engineering.

SAE. 2010. “Recommended Practice for Measuring the Exhaust Emissions and Fuel Economy of Hybrid-Electric Vehicles, Including Plug-in Hybrid Vehicles.” Society of Automotive Engineers.

Particle Number Emissions of Euro6 Light Duty Vehicles

P. Dimopoulos Eggenschwiler, D. Schreiber and A. Liati

[1]Automotive Powertrain Technologies Laboratory, Empa Swiss Federal Laboratories for Material Science and Technology, Dübendorf, 8600, Switzerland
Keywords: Particle Number, Euro6, Passenger Cars, Gasoline DI, IDI, Diesel, CNG
Presenting author email: panayotis.dimopoulos@empa.ch

Abstract

Particle number emissions of Euro 6 light duty vehicles have been measured on the chassis dynamometer. The study involved six gasoline (two with direct, DI, and four with intake pipe, IDI, fuel injection), one natural gas (CNG) and six Diesel powered vehicles. The main distinction among the Diesel vehicles was the exhaust aftertreatment system. All vehicles have been tested on a series of different driving cycles, NEDC, WLTC, CADC and the IUFC for assessing mainly the cold start emission behaviour. Particle number measurements have been performed with different instruments in parallel, counting all particles larger than 10nm, as well as all particles larger than 23nm.

All vehicles had particle emissions below the current Euro 6b limit on the NEDC cycle, while a limited number among them exceeded the future Euro 6c limit. The highest particle emissions have been measured on the DI gasoline vehicles. Surprisingly, the difference to the IDI gasoline vehicles was smaller than expected and this on all tested cycles.

The lowest particle numbers have been emitted by the Diesel vehicles equipped with a DOC/DPF system. The DOC/DPF/SCR vehicles had higher while the DOC/NSC/DPF ones the highest particle emissions of all Diesel vehicles. Particle emissions of the Diesel vehicles increased by almost two orders of magnitude during and immediately after active DPF regenerations.

Particle number emissions of the CNG vehicle have been in between the Diesel and the gasoline vehicle emissions. Regarding only the cold start, particle emissions of the CNG vehicle have been by far the lowest of all vehicles.

The present study is, to our current knowledge, one of the very few studies comprising a sufficient number of Euro 6 state-of-the-art vehicles measured in different driving cycles. Moreover, assessing numbers of ultrafine particles (>10nm and <23nm) is an additional novelty.

Introduction

In recent years a particle number (PN) standard was introduced for Diesels (Light Duty vehicles since 2011, Heavy Duty engines since 2014). A major effect of this standard was the wide use of Diesel Particle Filters (DPFs) in practically all new Diesel vehicles. Following several research investigations [Mathis et al., 2005, Schreiber et al. 2007, Giechaskiel et al. 2014a] reporting high particle number emissions of gasoline vehicles, in particular those utilizing Direct Injection (DI) for the fuel introduction in the combustion chamber, a standard for the PN emissions of DI gasolines was introduced, effective from 2014. The PN limit though was higher than for Diesels and only after September 2017, Diesels and DI gasolines have to respect identical limits.

In general the particles in the exhaust are considered to exhibit a tri-modal number distribution characterized by the nucleation mode (~20nm), comprising volatiles, droplets and smaller solid agglomerates, the accumulation mode (~70nm), consisting mainly of solid agglomerates (soot) and condensed volatiles, and the coarse mode (~1000nm), including larger agglomerates also formed during the path along the exhaust, [Giechaskiel et al. 2014b]. Most particles, by mass, reside in the accumulation mode, while by number sometimes the nucleation mode can dominate [Kittelson 1998]. The development and magnitude of nucleation mode particles is depending on a series of engine, fuel and sampling parameters [Giechaskiel et al. 2014a, b, c and references therein]. In order to avoid the complications introduced by the variability of the nucleation mode regarding the volatile or solid nature of the particles, the European legislation introduced a particle number (PN) method based on the thermal pretreatment of the aerosol for measuring only the accumulation mode. This is achieved by directing the exhaust gas through a volatile particle remover (VPR) upstream of the particle counter, as well as by tuning the sensitivity of the particle counter accordingly. Thus, the particle number counters (PNC) used are counting 50%±12% (cut-off size, d50%) of particles at 23 nm and >90% at 41 nm. Thus, possible solid particles, smaller than 23nm, are not counted.

Morphological particle properties (size, shape, surface area, internal structure) of DI gasoline engines based on electron microscopy have been investigated by a limited number of studies. [Barone et al. 2012] showed that primary particles range between 7 and 60 nm in diameter, which turned out to be somewhat wider than the size range of diesel particulates [Lapuerta et al. 2007, Liati et al. 2010, 2012 and 2013].

The present study shows preliminary results of particle number measurements on the chassis dynamometer of six gasoline (two with direct, DI, and four with intake pipe, IDI, fuel injection), one natural gas (CNG) vehicle, and six Diesel powered vehicles.

Specific attention was given in counting all particles higher than 10nm. The vehicles have been tested at two different international established driving cycles the (still valid) certification, NEDC cycle and the IUFC cycle for assessing the effects of the cold start.

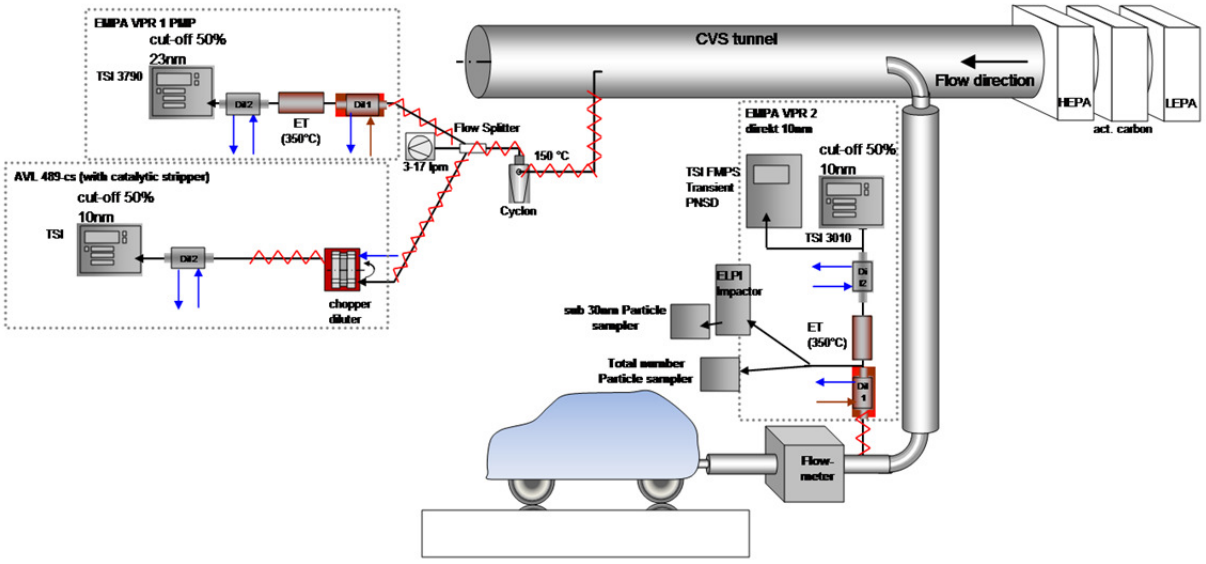

Figure 1: Experimental Setup on the chassis dynamometer at Empa.

Measurement setup

The setup of the particle number measurement was chosen so that an additional counting system (AVL498-cs) with a 10nm counting efficiency of 50% was connected at the CVS-tunnel in parallel with the PMP compliant counting system (23nm counting efficiency of 50%). The AVL System was specially developed for sub-23nm particle counting and was equipped with a catalytic stripper.

In order to assess the influence of the CVS system in the sub-23nm particle number, a third sub-23nm counting system was connected directly to the tail pipe.

For additional information on the transient particle number size distribution a TSI FMPS was connected in parallel to the particle number counter (PNC) of the third counting system. Fig. 1 shows a schematic of the entire setup as used in the Empa chassis dynamometer.

The PMP compliant system was equipped with a first heated injector pump dilution an Evaporation Tube (ET) heated at 350°C and a second cold injector pump dilution. A PNC model TSI CPC 3790 with counting efficiency of 50% for particles with a diameter of 23nm (cut-off 23nm) was connected at this VPR. The DF of this VPR could be extended with a third dilution. The Particle Total Reduction Factor (PTRF) from this VPR was calculated from calibration measurements with diffusion flame soot at 30, 50 and 100nm.

The VPR connected at the tail pipe was a similar system with a PNC model TSI CPC 3010 (cut-off 10nm) and the DF of this VPR could be extended also with a third dilution. For this VPR the PTRF was calculated from calibration measurements with diffusion flame soot at 10, 30, 50 and 100nm.

The AVL system was also calibrated with diffusion flame soot at 10, 30, 50 and 100nm.

Results and discussion

In Fig. 2 particles larger than >23nm from all measured vehicles are summarized in terms of particle number. For the NEDC cycle the lowest particle numbers have been emitted by the Diesel DOC/DPF vehicles. The Diesel DOC/DPF/SCR vehicles emitted on average 2.5 times more particles (in respect to the Diesel DOC/DPF ones). The CNG vehicle emitted on average 5 times more particles (in respect to the Diesel DOC/DPF vehicles). The Diesel DOC/NSC/DPF emitted on average 13 times more particles (in respect to the Diesel DOC/DPF vehicles). The gasoline MPI emitted on average 110 times more particles (in respect to the Diesel DOC/DPF vehicles). The gasoline DI emitted on average 105 times more particles (in respect to the Diesel DOC/DPF vehicles).

The relations described above were similar for particles larger than >10nm (Fig 3). There is though only one striking difference to the particles larger than 23nm: The gasoline MPI emitted on average 60 times more particles, while the gasoline DI emitted on average 65 times more particles in respect to the DOC/DPF diesels.

This rather shows that gasolines and diesels are more similar in their emission behaviour in the smallest particle range, i.e. between 10nm and 23nm.

In the particle number emissions of Diesel vehicles the effect of the active DPF regeneration has to be taken into account. Active regenerations of the DPF result in increased particle number emissions during and directly after regeneration before new soot cake is built up. For the assessment of the influence of active regenerations on the overall particle emission characteristics a reasonable active regeneration frequency has to be assumed. Active regenerations are more frequent, should the vehicles be used predominantly in city driving modes and less frequent, should the vehicles be used predominantly in highway driving.

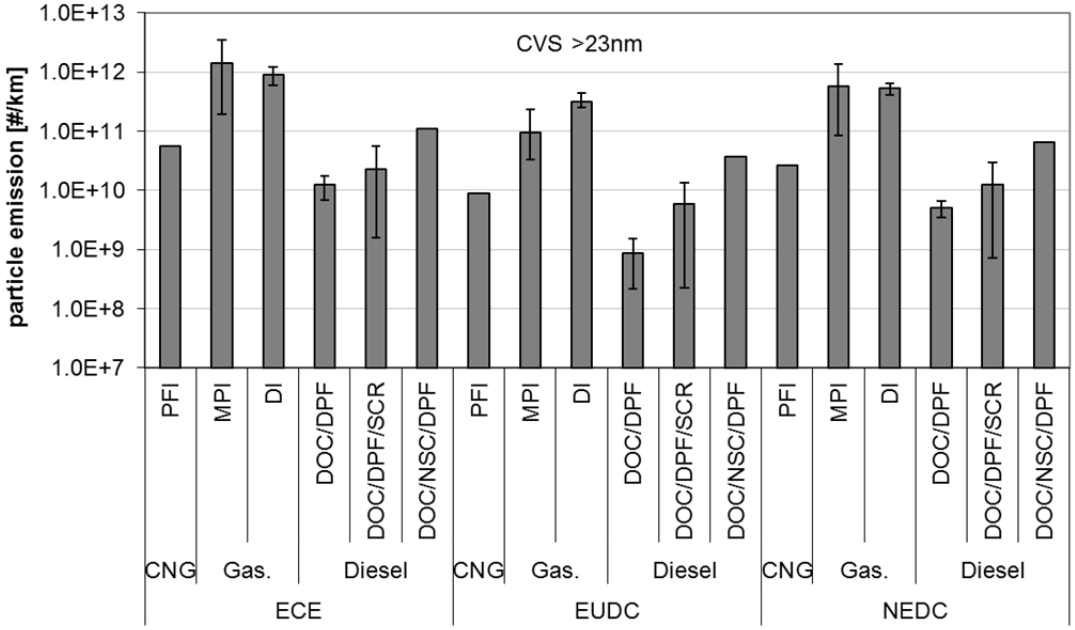

Figure 2: Particle emission overview of all powertrain technologies investigated in this study at the NEDC cycle measuring all particles at the CVS >23nm; in the Diesels no active regeneration has been accounted for.

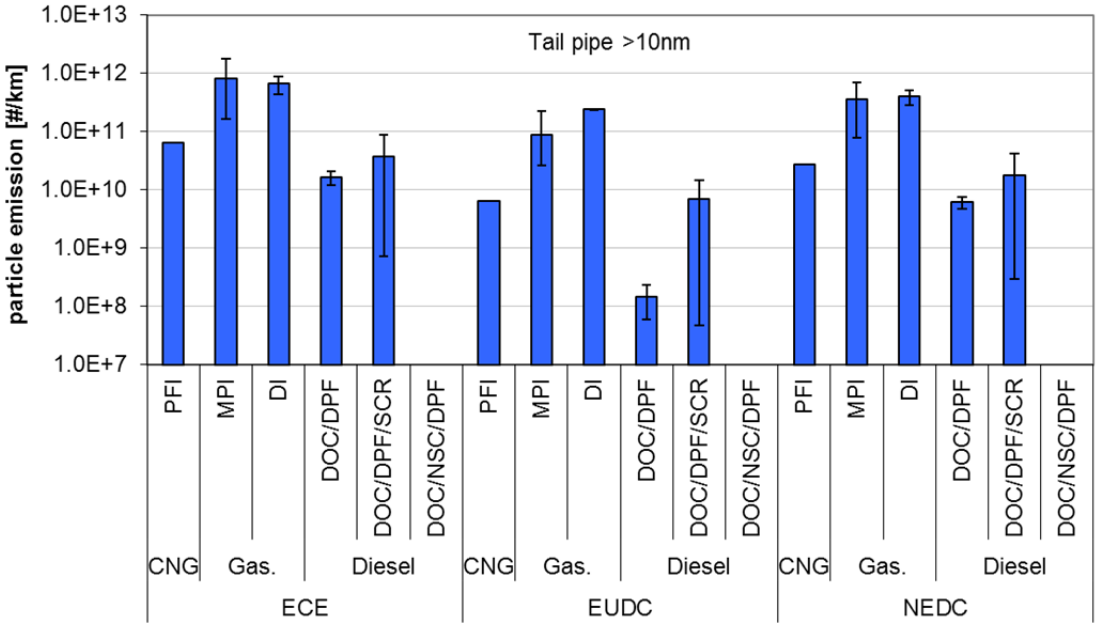

Figure 3: Particle emission overview of all powertrain technologies investigated in this study at the NEDC cycle measuring all particles at the tail pipe >10nm; in the Diesels no active regeneration has been accounted for.

We considered 3 active regenerations per 1000km as a reasonable average assumption. Based on this assumption and using the increased particle emissions as measured on the chassis dynamometer the conclusion is

- Active DPF regenerations lead to an increase of the average particle number emissions per km of the Diesel vehicles by a factor of 10.

The particularities of the cold start have been studied by using the IUFC cycle, consisting of 3 consequent repetitions of the identical mainly low load cycle. The IUFC cycle has been performed with all vehicles at 23°C. The results are shown in Figs 4 and 5.
In the first repetition of the IUFC cycle at 23°C the lowest particle numbers have been emitted by the CNG vehicle. The Diesel DOC/DPF vehicles emitted some 12 times more particles (in respect to the CNG vehicle). The Diesel DOC/DPF/SCR vehicles emitted 8 times more particles (in respect to the CNG vehicle). The Diesel DOC/NSC/DPF emitted 10 times more particles (in respect to the CNG vehicle). The gasoline MPI emitted on average 40 times more particles (in respect to the CNG vehicle). The gasoline DI emitted on average 40 times more particles (in respect to the CNG vehicle). All these trends were identical when comparing also particles >10nm; comparison of Figs. 4 and 5.

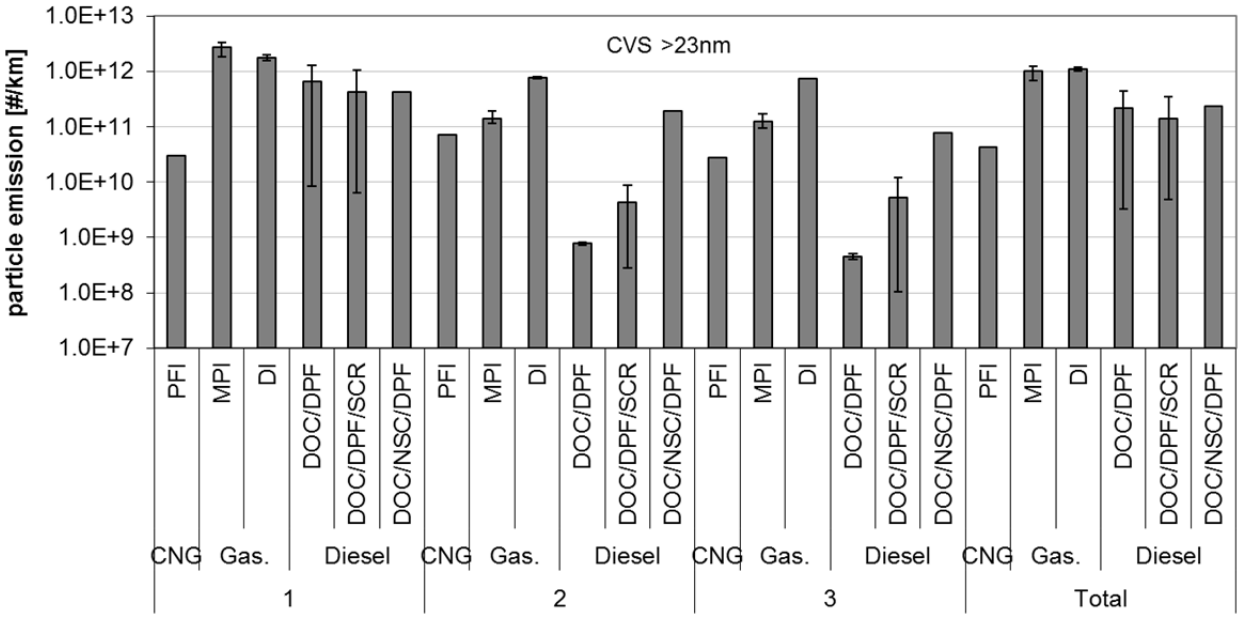

Figure 4: Particle emission overview of all powertrain technologies investigated in this study at the IUFC cycle at 23°C measuring all particles at the CVS >23nm; in the Diesels no active regeneration has been accounted for.

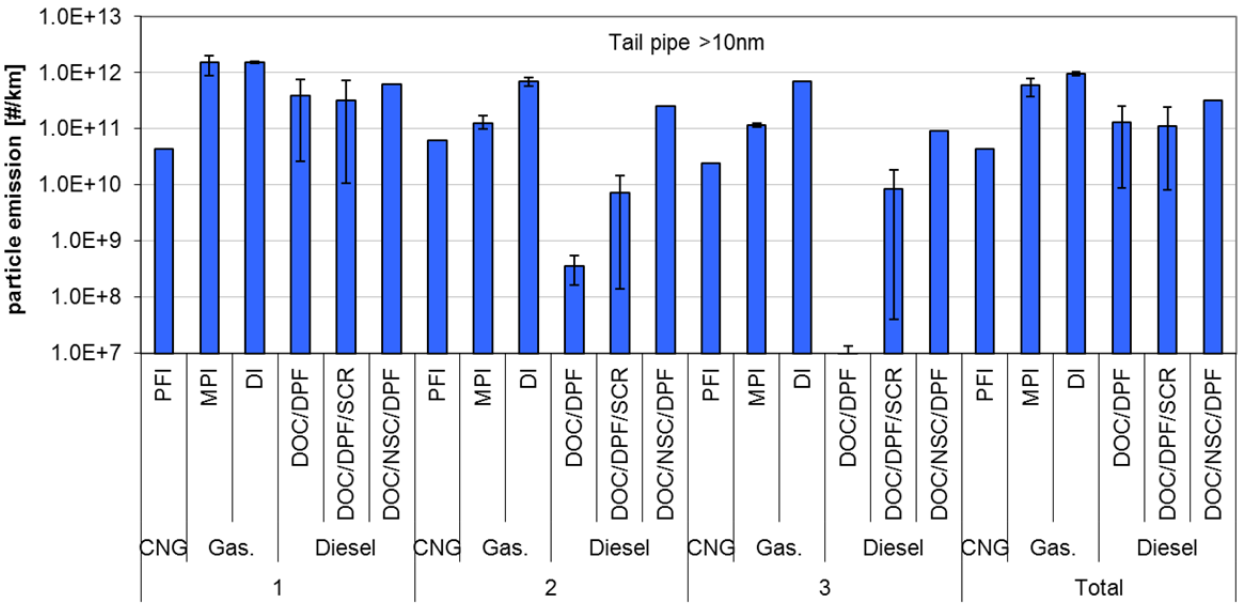

Figure 5: Particle emission overview of all powertrain technologies investigated in this study at the IUFC cycle at 23°C measuring all particles at the CVS >23nm; in the Diesels no active regeneration has been accounted for

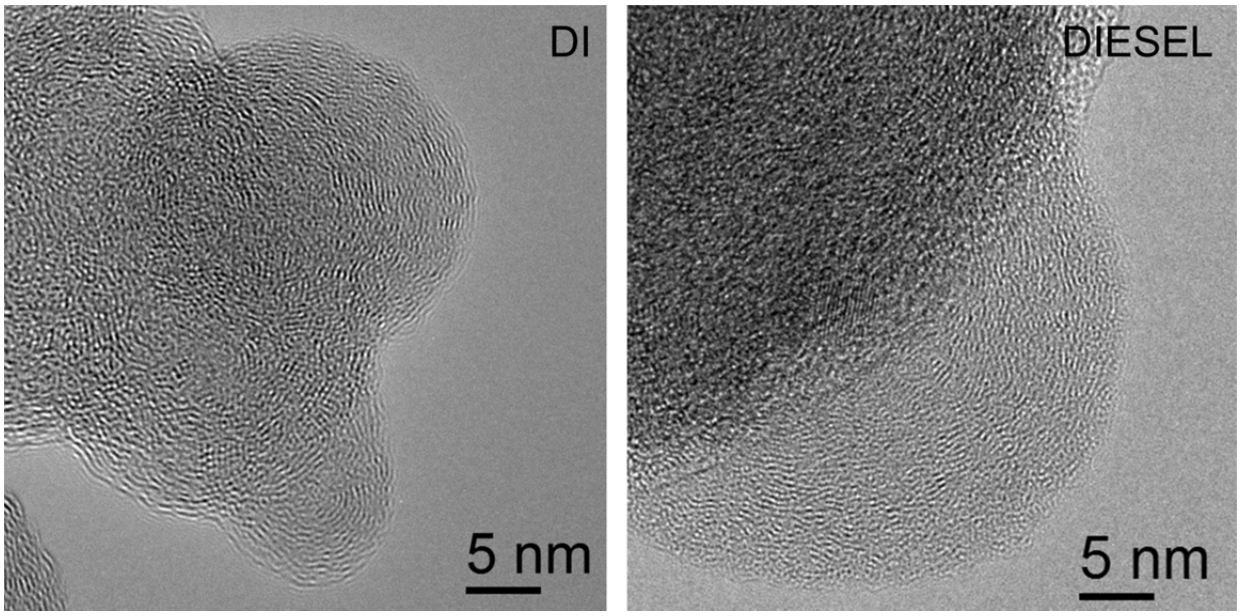

Fig. 6: Representative HRTEM images of soot from Diesel and DI vehicle exhaust exhibiting a graphene-dominated nanostructure

Following the first repetition of the IUFC the subsequent two repetitions resulted in warming up of the engines and aftertreatment systems. This led to decreasing particle emissions, the Diesel DOC/DPF vehicles exhibiting the steepest decrease. This changed the relations among the particles of the different vehicle classes, though not fundamentally. For the entire IUFC cycle the main findings can be summarized as follows: The lowest particle numbers have been emitted by the CNG vehicle. The Diesel DOC/DPF vehicles emitted some 4 times more particles (in respect to the CNG vehicle). The Diesel DOC/DPF/SCR vehicles emitted 3 times more particles (in respect to the CNG vehicle). The Diesel DOC/NSC/DPF emitted 6 times more particles (in respect to the CNG vehicle). The gasoline MPI emitted on average 20 times more particles (in respect to the CNG vehicle). The gasoline DI emitted on average 22 times more particles (in respect to the CNG vehicle). All these trends were identical when comparing also particles >10nm; comparison of Figs. 4 and 5.

Investigation of solid particle exhaust by (high resolution) transmission electron microscopy (HRTEM) for Gasoline and Diesel vehicles during the NEDC and WLTC cycles, emphasizing on sub-23nm sizes, revealed the presence of different types of particles: pure soot, soot coexisting with ash, and to a smaller extent pure ash (compounds of Ca, P, Mg, Zn, Fe, S, O) [s. details in Liati et al., submitted]. More detailed studies on morphology indicate that DI and Diesel soot show similar primary soot particle size ranges (mainly ~5 to ~25 nm) DI soot showing a higher size variability. Internal structural characteristics of primary soot particles (graphene length and curvature, degree of crystallinity) between DI and Diesel are also similar, the DI soot demonstrating a tendency to more immature nanostructures, i.e. higher reactivity (Fig. 6).

Conclusions

In this project, particle emissions of six Gasoline, one CNG and six Diesel vehicles were examined. All vehicles were according to the current standard of Euro 6b. The particle number emissions of all vehicles have been measured using different measurement analytics in parallel.

Taking into account all particles >23nm during the NEDC cycle and no active DPF regeneration:

- The lowest particle numbers were emitted by the Diesel DOC/DPF vehicles. Taking these as a reference then:
- The Diesel DOC/DPF/SCR vehicles emitted on average 2.5 times more particles,
- The CNG vehicle emitted on average 5 times more particles,
- The Diesel DOC/NSC/DPF emitted on average 13 times more particles,
- The gasoline MPI emitted on average 110 times more particles,
- The gasoline DI emitted on average 105 times more particles

The differences among the vehicle technologies become smaller when taking into account particles >10nm, in particular concerning emissions of the gasoline vehicles, which are 50 times higher than those of the Diesel DOC/DPF.

Diesel DPFs have to be periodically regenerated. Considering 3 active regenerations per 1000km (a reasonable assumption) and using the increased particle emissions during and directly after an active regeneration as measured (section 3.2.2) the conclusion is

- Active DPF regenerations lead to an increase of the average particle number emissions of the Diesel vehicles per km by a factor of 10.

A different ranking in respect to particle emissions is observed when taking into account only cold start emissions:

- The lowest particle numbers were emitted by the CNG vehicle.

In respect to the particle emissions of the CNG vehicle in cold start conditions:

- The Diesel DOC/DPF vehicles emitted some 12 times more particles,
- The Diesel DOC/DPF/SCR vehicles emitted 8 times more particles,
- The Diesel DOC/NSC/DPF emitted 10 times more particles,
- The gasoline MPI emitted on average 40 times more particles,
- The gasoline DI emitted on average 40 times more particles,
- All these trends were identical also when comparing particles >10nm.

Acknowledgements

The authors gratefully acknowledge the support of the Swiss Federal Office for the Environment for the present work by the "Sub-30nm-PM" project.

References

[Mathis et al. 2005]: Comprehensive particle characterization of modern gasoline and diesel passenger cars at low ambient temperatures, Atmosp. Environ. 39, 107-117, 2005

[Schreiber et al. 2007]: Particle Characterization of Modern CNG, Gasoline and Diesel Passenger Cars. SAE 2007-24-0123

[Giechaskiel et al. 2014a]: Review on engine exhaust sub-23 nm solid particles, JRC Science and Policy Reports, JRC 90365, EUR 26653 EN, doi: 10.2790/22597, 2014

[Giechaskiel et al. 2014b]: Engine Exhaust Solid Sub-23 nm Particles: I. Literature Survey, SAE2014-01-2834, doi:10.4271/2014-01-2834, 2014

[Kittelson 1998]: Engines and Nanoparticles: A Review," J. Aerosol Sci. 29, 575-588, 1998

[Giechaskiel et al. 2014c]: Engine Exhaust Solid Sub-23 nm Particles: II. Feasibility Study for Particle Number Measurement Systems SAE2014-01-2832, doi:10.4271/2014-01-2832, 2014

[Barone et al. 2012]: An analysis of direct injection, spark ignition (DISI) soot morphology, Atmosp. Environ. 49 268-274, 2012

[Lapuerta et al. 2007]: Effect of engine operating conditions on the size of primary particles composing diesel soot agglomerates, J. Aerosol. Sci. 38 (4) 455-466, 2007

[Liati et al. 2010]: Characterization of Particulate Matter deposited in diesel particulate filters: visual and analytical approach in macro- micro- and nano-scales, Comb. Flame 157, 1658-1670, 2010

[Liati et al.2012]: Microscopic investigation of soot and ash particulate matter derived from biofuel and diesel: implication for the reactivity of soot, J. Nanop. Res. 14 (11) 1-18, 2012

[Liati et al.2013]: Variations of diesel soot reactivity along the exhaust aftertreatment system based on the morphology and nanostructure of primary soot particles, Comb. Flame 158 (9) 1837-1851, 2013

Dilution effects on ultrafine particle emissions from Euro 5 and Euro 6 diesel and gasoline vehicles

C. Louis [a,b], Y. Liu, S. Martinet [a], B. D'Anna [c], A. M. Valiente [c], A. Boreave [c], B. R'Mili [c], P. Tassel [a], P. Perret [a], M. André [a]

[a] Univ Lyon, IFSTTAR, AME, LTE, F-6975 Lyon, France
[b] French Environment and Energy Management Agency, ADEME, 49004 Angers, France
[c] IRCELYON, UMR 5256 CNRS, Université de Lyon, 69626 Villeurbanne, France

Link to publication: https://doi.org/10.1016/j.atmosenv.2017.09.007

On-road measurements of particles from tire-road contact

B. Muresan[1], L. Lumière[1], A. Guilloux[1], V. Cerezo[1], K. Deboudt[2] and S. Khardi[1]*

[1] Ifsttar, 14-20 Boulevard Newton, Champs sur Marne, Marne la Vallée F-77447, France, bogdan.muresan-paslaru@ifsttar.fr
[2] LPCA, Université du Littoral Côte d'Opale, Dunkerque, 59140, France

Abstract

The emission dynamics and grain size distributions of particles from tire-road contact (TCP) were investigated by means of on-road measurements. The investigation involved series of measurements carried out in urban and peri-urban environments. The measurements had three main objectives: i) to test the feasibility of on-road measurements, ii) to find clear determinants for particulate concentrations measured at the rear of the wheel (RWP) and iii) to formulate tracers for TCP based on number-weighted grain size distributions. On-road measurements overall provided access to useful information on RWP and TCP emission dynamics. Firstly, the vehicle speed as well as accelerations and decelerations had a significant influence on RWP concentrations. Hence, adapting vehicle dynamics by taking into account identified relationships could yield benefits in terms of local RWP level reduction. Secondly, TCP emissions exhibited a large sub-micrometric fraction that concentrated in the 0.050 µm - 0.250 µm range but, due to local atmospheric blanks loading with sub-micrometric particles (partly from exhausts), did not markedly increase RWP levels. Finally, from differences in grain size distributions recorded on different road sections, the sum of number-weighted contributions in the 0.03-0.10 µm range divided by this in the 1-2.5 µm range was proposed as a near-wheel tracer of TCP emissions.

Keywords: *particles, tire-road contact, on-road measurements, determinants, tracers.*

Glossary: NEP: non-exhaust particles from road traffic. The NEP includes particles from resuspension, wear of vehicles (including from engine) and infrastructure parts.

RWP: rear-of-wheel particles. The RWP includes all the particles collected a few centimeters behind the front passenger wheel. Depending on road sections and the local traffic conditions, RWP consist of different proportions of NEP and exhaust particles.

TCP: tire-road contact particles. The TCP regroup all the particles produced or (re)-mobilized (including the vehicle-induced resuspension) by the passage of the tire. TCP concentrations were typically calculated in sectors where exhaust particle levels were low and under free-flowing traffic conditions by subtracting local atmospheric blanks from RWP concentrations.

Introduction

In urban areas, non-exhaust particles (NEP) from road traffic account for a significant fraction of ambient particles (Grigoratos and Martini, 2014). The origins of road traffic NEP are multiple: i.e. from the resuspension of the dust as well as the wear of vehicles' (i.e. tires, braking system, clutch, engine belts and metal sheets) and roads' (asphalt concrete, guardrails) parts (Thorpe and Harrison 2008). For 20 years, NEP have been increasingly studied and it is now admitted that the atmospheric load of micrometric NEP is comparable to that for exhaust particles (Querol et al., 2001; Lenschow et al., 2001). In urban environments, NEP are thought to stand for a few tens of percent to up to 90% of PM_{10} (i.e. a particle category having a D_{50} of 10 µm) (Harrison et al., 2001; Lenschow et al., 2001; Querol et al., 2004; Omstedt et al., 2005; Thorpe et al., 2007; Johansson et al., 2007). The emission factors found in Copert 4, EMEP / EEA and PIARC databases as well as in the literature (Abu-Allaban et al., 2003; Ketzel et al., 2007; Bukowiecki et al., 2010) are from below 5 mg/km/vehicle to 50 mg/km/vehicle for passenger cars and from 100 mg/km/vehicle to over 1000 mg/km/vehicle for heavy duty vehicles. Taking mean values of 25 mg/km/veh and 400 mg/km/veh for passenger cars and heavy duty vehicles, NEP emissions stand for 2.5 kg and 40 kg per 100,000 km traveled, respectively. The resuspension and wear (from tire, brake and road surface) contributions usually found in the literature are around 50 / 50 for passenger cars and 75 / 25 for heavy duty vehicles, in this order. Yet, these rough ratios should only be considered as indicative since these depend on many variables among which: vehicle dynamics, tire and road surface properties, meteorological conditions.

There have been many attempts to identify tracers for NEP emissions (Sternbeck et al., 2002; Weckwerth, 2001; Snilberg et al., 2005; Gertler et al., 2006). Yet, because of the diversity of sources, in-situ transformations and the interactions with exhaust or other ambient particles, most of the proposed tracers are still equivocal (Thorpe and Harrison, 2008; Rhuel et al., 2010). Among tracers, researches mainly focused on metallic (Jj et al., 2006; Querol et al., 2007; Denier et al., 2007) or organic (Hildemann et al., 1991; Di Tullio et al., 2008; Kumata Hidetoshi et al., 1997) chemicals starting early nineties (Rogge et al., 1993). Besides, despite NEP may comprise a significant proportion of ultrafine or nanometric particles, most of the researches that aimed at finding NEP-specific tracers focused on micrometric particular categories (i.e. mainly PM_{10} and $PM_{2.5}$). The same is true for current emission factors, which exclusively involve mass-weighted measurements. This overall limits the amount of knowledge relating to the whole NEP grain size distributions and discourages the use of sub-micrometric particles for investigating in-situ NEP transformations or discriminating among particular sources. In this study, we explored the possibility of on-road NEP number-concentration measurements and of monitoring changes in NEP grain size distributions. The NEP under consideration are the tire-road contact particles (TCP) that originate from both the tire and the asphalt concrete wears as well as resuspension. Hence, several TCP measurement campaigns were conducted on-road (see below) and gained data was used to:

- i) probe the real-world emission dynamics of (sub-)micrometric TCP in urban and peri-urban environments,
- ii) find clear determinants for TCP emissions as a function of vehicle dynamics and road surface contamination with dust,
- iii) formulate tracers for TCP that base on both the micrometric and sub-micrometric fractions their grain size distributions.

The difficulty of these objectives comes from the wide variety of interactions between TCP and ambient particles and because TCP size distributions are also likely to change according to many factors including, but not limited to: meteorological and traffic conditions, ambient pollution with particles, driving style, variations in tires' texture and road surface characteristics. All these factors render the TCP identification and related emission dynamics studies complex, yet, extremely challenging with respect to vehicles' instrumentation and test carried on-road.

Materials and method

Particulate concentrations were monitored a few centimeters behind the front passenger wheel (Figure 1). Unless otherwise stated, given concentrations consist of non normalized values (dN

or dV). The recorded rear-of-wheel particles' (RWP) signals were obtained in the real traffic by using the Ifsttar institute's service vehicles. Overall, 8 vehicles were implemented, including 7 passenger cars and a van. The tires used during on-road measurements were in the mid-price range and differed in wear rate, pressure, load and brand. The results proposed herein come from two measurement series that are quite representative of RWP concentration signal evolutions and involved a fully instrumented vehicle. This vehicle gave access to several key parameters related to the engine functioning and vehicle dynamics. Parameters included, but were not limited to: engine pace and acceleration, fuel consumption, wheel and ground speeds, brake pressure and steering angle. All data was obtained at 10 Hz frequency and continuously recorded by on-board computers.

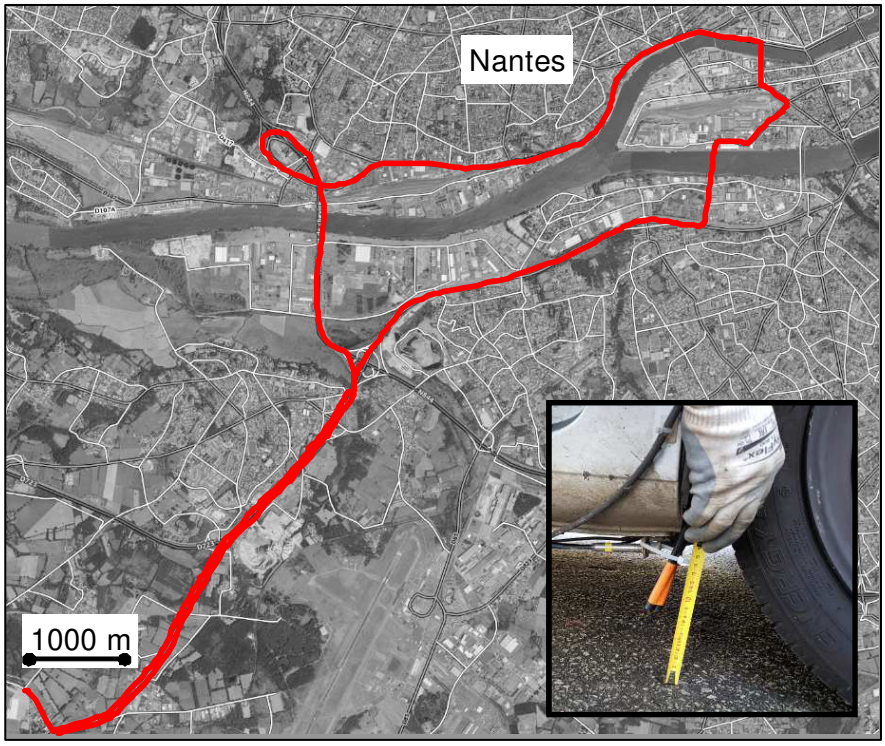

Figure 1. Route taken during on-road RWP measurements. The setting for air intake is showed as a photograph.

RWP concentrations were measured by two aerosol spectrometers: the model 1.108 and/or the model G1.371 analyzers from Grimm. These two analyzers are autonomous thereby allowing mobile RWP measurements in the 0.35-22.5 µm and 0.01-35.15 µm size intervals, respectively. Analytical principles for measurements are dynamic light-scattering for model 1.108 and a combination of dynamic light-scattering and electrical mobility for model G1.371. The frequencies for measurements are 6 s in 15 channels and 1 min in 41 channels, respectively. The associated count and mass ranges are 1-3 10^6 #/L (optical analyzers), 3,000-10^9 #/L (electrical sensor) and 1 µg/m^3-100 mg/m^3. The instruments are factory-calibrated and their responses are regularly checked against these of another fully calibrated 1.108 model and an electrical low pressure impactor (ELPI®). Mean reproducibilities equal ±3% (optical analyzers) and ±8% (electrical sensor). By including the potential losses on walls of the antistatic tubing conveying RWP to the analyzers, the average uncertainties on measurements over all accessible sizes are < 20%: typically in 10-15% range.

The air intake of analyzers was set behind the front passenger wheel (i.e. circa 7 cm from the road surface and 15 cm from the tire, Figure 1). Antistatic tubing was used in order to convey sucked RWP to analyzers placed on the rear seats of the vehicles. The sample flow rates equaled 1.2 L/min ± 5%, which corresponded to a RWP tubing-transit time of 5-7 s (depending on the vehicle). The inlet of the tubing faced downward: in a manner perpendicular to RWP streamlines, as previously identified during test track measurements. This was thought to limit the variations in the sample flow rate and grain size distribution caused by changes in the 3-dimensional air flow pattern around the inlet.

In order to minimize the contribution of exhaust particles from the surrounding traffic and to increase the traffic conditions' consistency, on-road measurements were carried out between 11 AM and 5 PM by following a same route that runs in urban and peri-urban areas (Figure 1). This allowed examining RWP and TCP emission dynamics over a wide range of speeds: from below 30 km/h to almost 90 km/h. The route taken was 25 km long and the overall weather conditions were fine: clear skies with low winds (wind speed < 25 km/h) and no rain (previous rains took place *circa* 2 weeks before measurement series). The temperature and moisture percentage of air ranged from 5°C to 14°C and from 60% to 90%, respectively. Depending on traffic conditions and analyzers' response, one or two runs were necessary in order to achieve full datasets. The course gathered several road types (country roads, ring roads, highways metropolitan streets, restricted-speed streets), which involved various traffic situations and specific driving conditions (stops at traffic lights, crossing roundabouts and crossroads, passing junctions). Along with weather conditions and road surface characteristics (i.e. apparent macrotexture, dryness and visible dust contamination), driving conditions and traffic situations were recorded by hand by vehicle's co-pilot. This information served to classify road sections according to near-wheel air contamination with specific particle categories and thus better account for observed variations in RWP and TCP levels (Table 1).

Table 1: Classification criteria for road sections as a function of near-wheel air contamination with specific particle categories

Atmospheric blanks	Vehicles were kept at standstill or, where not feasible, at speeds < 10 km/h (data obtained during the travel at the level of each road type)
Uncontaminated road sections	No visible contamination of road surface and local atmosphere (most of the road types but a certain highway section)
Contaminated road sections	Apparent road surface impregnation with dustfall and local dust resuspension (a highway section located near a stone quarry exit)
Road sections with low exhaust levels	Roads located in open and/or barely trafficked sectors (may include highway, country road, ring road and some metropolitan streets)
Road sections with high exhaust levels	At the level of major junctions, series of traffic lights, confined urban and in heavily trafficked sectors (most metropolitan streets, certain highway and ring road sections)

Results and discussion

The influence of ground speed

The figure 2 shows the temporal evolution of the total RWP concentration in 0.35 µm to 22.5 µm range ($\Sigma RWP_{0.35\text{-}22.5}$) for the first measurement series. This specific category of micrometric particles was firstly considered because of the higher measurement frequency of optical analyzers and because RWP were initially thought having diameters greater than 0.5 µm (Grigoratos and Martini, 2014).

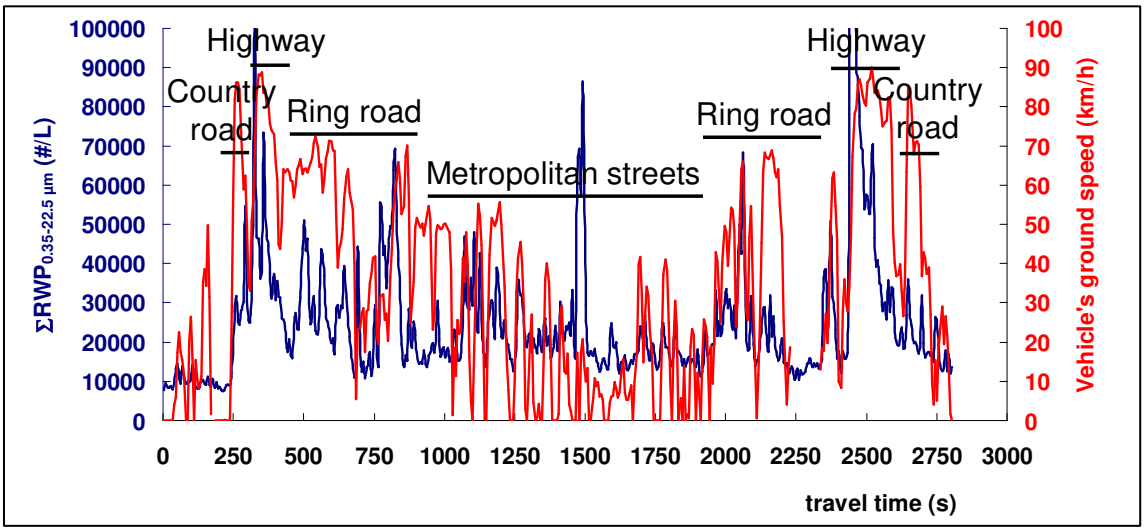

Figure 2. Evolutions of number-weighted $\Sigma RWP_{0.35\text{-}22.5}$ concentration (blue signal, left hand scale) and vehicle's ground speed (red signal, right hand scale) against travel time for the first measurement series.

Unless stated otherwise, atmospheric blank concentrations were measured during the travel when the vehicles were at the standstill or moved at speeds below 10 km/h. This provides an estimation of local urban and peri-urban atmosphere loadings with particles. Depending on the crossed geographical sectors and particle size categories, blank values in the 0.35 µm to 22.5 µm interval accounted for < 10% to 65% of the measured concentration (average of 22%). The highest contributions were determined for sub-micrometric RWP especially in these urban sectors where vehicle stopped at traffic lights and received the exhaust emission from the surrounding cars. The averaged $\Sigma RWP_{0.35\text{-}22.5}$ values of local blanks ranged from < 10,000 #/L to 12,000 #/L, which represented less than 3 % of peaked RWP concentrations. This first observation shows that concentration of micrometric RWP significantly (i.e. at $a < 0.05$ level) differed from blanks and underwent sudden and sharp variations (Figure 2). It also demonstrates that micrometric RWP number-concentrations can be successfully monitored on-road.

The $\Sigma RWP_{0.35\text{-}22.5}$ signal exhibited large variations, which were broader for micrometric sizes of particles. Depending on the situation, high concentrations episodes lasted for less than 10 s to over 1 min. There likely are many causes to these variations. To begin with, one can readily notice the resemblance between the ground speed and $\Sigma RWP_{0.35\text{-}22.5}$ evolutions. The highest speeds often accounted for increased $\Sigma RWP_{0.35\text{-}22.5}$ values: $\Sigma RWP_{0.35\text{-}22.5}$ (#/L) = 14,400 exp(0.012 v) ($r = 0.58$) where v is the ground speed in km/h. Such a positive correlation was also observed for particular volume: $\Sigma RWP_{0.35\text{-}22.5}$ ($\mu m^3/L$) = 4200 exp(0.016 v) ($r = 0.42$). These two correlations involved more than 450 measurements and thus are significant at $a < 0.01$ level. This highlighted that recorded $\Sigma RWP_{0.35\text{-}22.5}$ levels were, at least partly, be driven by the vehicle dynamics through ground speed. One possible mechanism is the increase in shearing stresses that developed at the tire-road surface interface. Other mechanisms for micrometric RWP remobilization and/or production may be: i) a modification in the hydrodynamic patterns of air flows surrounding the vehicle; ii) the rising in tire temperature that jeopardizes its rubber matrix; ii) a stronger destabilization of the road surface granular matrix caused by the brutal increases in the pressure of air confined between the tire and the road surface's micro-texture. As a matter of fact, in the 0.35-22.5 µm range, ratios of sub-micrometric to super-micrometric RWP concentrations were significantly lower when driving than at standstill: 20 at 100 km/h vs. 40 at standstill. Such a marked decrease occurred as soon as reaching 20-30 km/h; yet, beyond this range, it linearly increased with ground speed. This demonstrates that, despite being minimal, RWP developed a broader coarse fraction than atmospheric blanks. This coarse fraction could be further characterized in order to follow TCP dissemination into the nearby environmental compartments.

The influence of accelerations and decelerations

The ground speed, yet, only partially accounted for the highest concentrations. A more localized observation of recorded signals highlighted that RWP concentration peaks also occurred during accelerations (at t = 310 s, 800 s, 2040 s, 2440 s, etc.) and more casually during decelerations (at t = 270 s and 550 s) (Figures 2). In this section, the variability of RWP concentrations and related changes in their grain size distribution were discussed for a series of acceleration and deceleration episodes.

Figure 3 displays changes in RWP grain size distribution during two acceleration episodes (starting at t = 237 s and t = 309 s) and a deceleration episode (from t = 350 s to t = 410 s). As previously mentioned, acceleration episodes accompanied a rise in $\Sigma RWP_{0.35\text{-}22.5}$ values. This also corresponded to an increase in the mean diameter of particles constitutive of $\Sigma RWP_{0.35\text{-}22.5}$. Indeed, in the first moments of accelerations, relatively higher contributions of micrometric RWP (i.e. > 2 µm in diameter) were recorded. However, after 10 s to 15 s of acceleration (i.e. at speeds exceeding 50 km/h), the contribution of micrometric RWP declined and particles < 0.5 µm in diameter became even more predominant. As with accelerations, decelerations also increased $\Sigma RWP_{0.35\text{-}22.5}$ values and RWP mean diameters measured behind the wheel. The initial micrometric particles, yet, were smaller with a mean diameter falling in the 1 µm to 2 µm range. Depending on the road surface structural and mechanical characteristics as well as on its contamination degree with dust, the initial class of RWP can either be replaced by coarser particles (up to 10 µm in diameter) or progressively flushed out thereby increasing the share of sub-micrometric particles. To explain changes in the RWP size distribution, one could possibly

consider tire temperature. As a matter of fact, when the vehicle starts accelerating or braking, the temperature of tire is lower than at the end of the maneuver. Its rubber matrix passes from a more rigid (thus more abrasive) state, during which coarser particles are ejected, to a smoother state that favors the development of polishing processes. Further research is yet needed so as to ascertain the role of rubber temperature on RPW production rates.

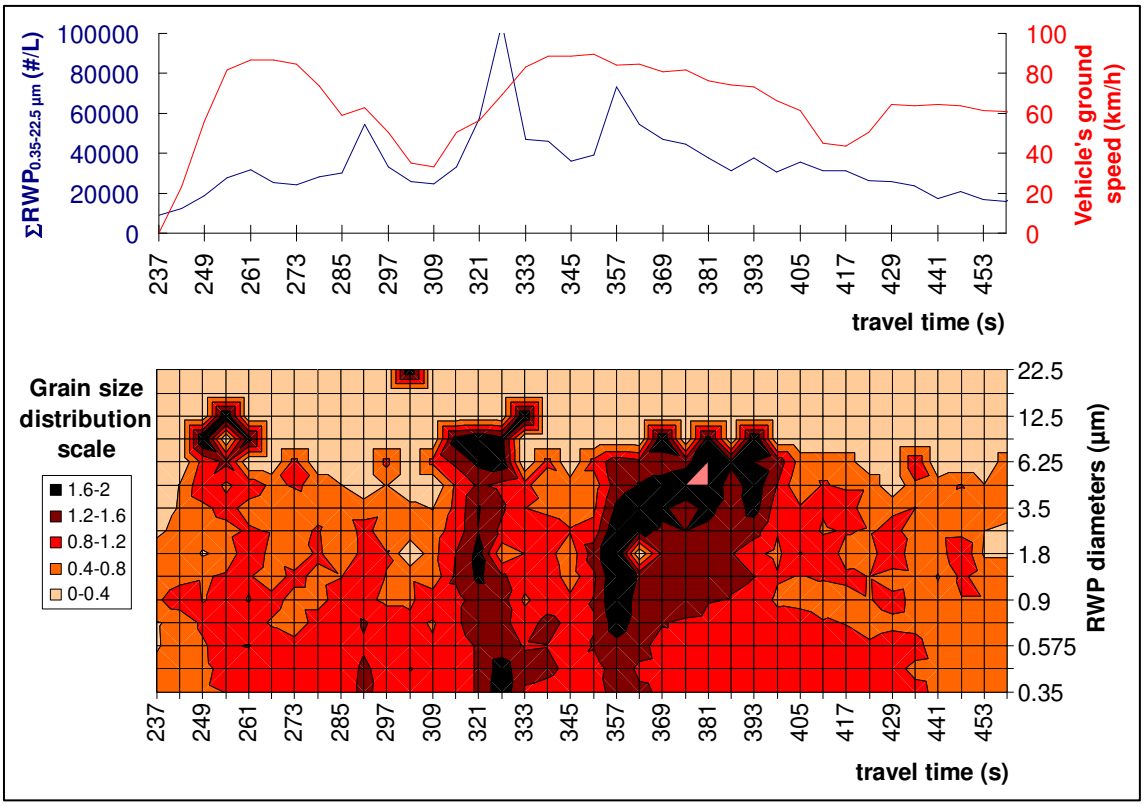

Figure 3. Top panel: Evolutions of number-weighted $\Sigma RWP_{0.35\text{-}22.5}$ concentration (blue signal, left hand scale) and ground speed (red signal, right hand scale) against travel time. Bottom panel: Evolution of standardized $\Sigma RWP_{0.35\text{-}22.5}$ grain size distribution against travel time. Standardized data is given using arbitrary units with increasing values from light to dark red tones.

Among crossed sectors, the ring roads regrouped relatively high speed driving situations (limits of 70 km/h or 90 km/h) with series of accelerations and decelerations during heavy traffic episodes. This resulted in substantial $\Sigma RWP_{0.35\text{-}22.5}$ concentration peaks (up to 45,000-50,000 #/L vs. 20,000-25,000 #/L for metropolitan roads and 25,000-35,000 #/L for highways), which superimposed to a relatively higher concentration baseline (up to 15,000-17,000 #/L vs. 12,000-13,000 #/L for metropolitan roads and 17,000-20,000 #/L for highways). As a comparison, metropolitan streets accounted for smaller $\Sigma RWP_{0.35\text{-}22.5}$ peaks and lower concentration baseline values; but also exhibited more frequent accelerations / decelerations events. In this view, traffic fluidization policies in urban areas may yield more substantial benefits on micrometric RWP levels reduction than strengthening speed limitations. At higher speeds (i.e. typically beyond 70 km/h; when driving in free-flowing traffic on highways or ring roads), due to the exponential increase in $\Sigma RWP_{0.35\text{-}22.5}$ values with ground speed, it is nevertheless speed limitation policies that would provide broadest decreases in micrometric RWP levels.

Near-wheel air levels of nanometric particles

The sum of RWP concentrations over a wide range of particle sizes (i.e. from 0.01 µm to 35.15 µm; $\Sigma RWP_{0.01\text{-}35.15}$) and the associated grain size distributions were monitored during the second measurement series and were displayed in figure 4.

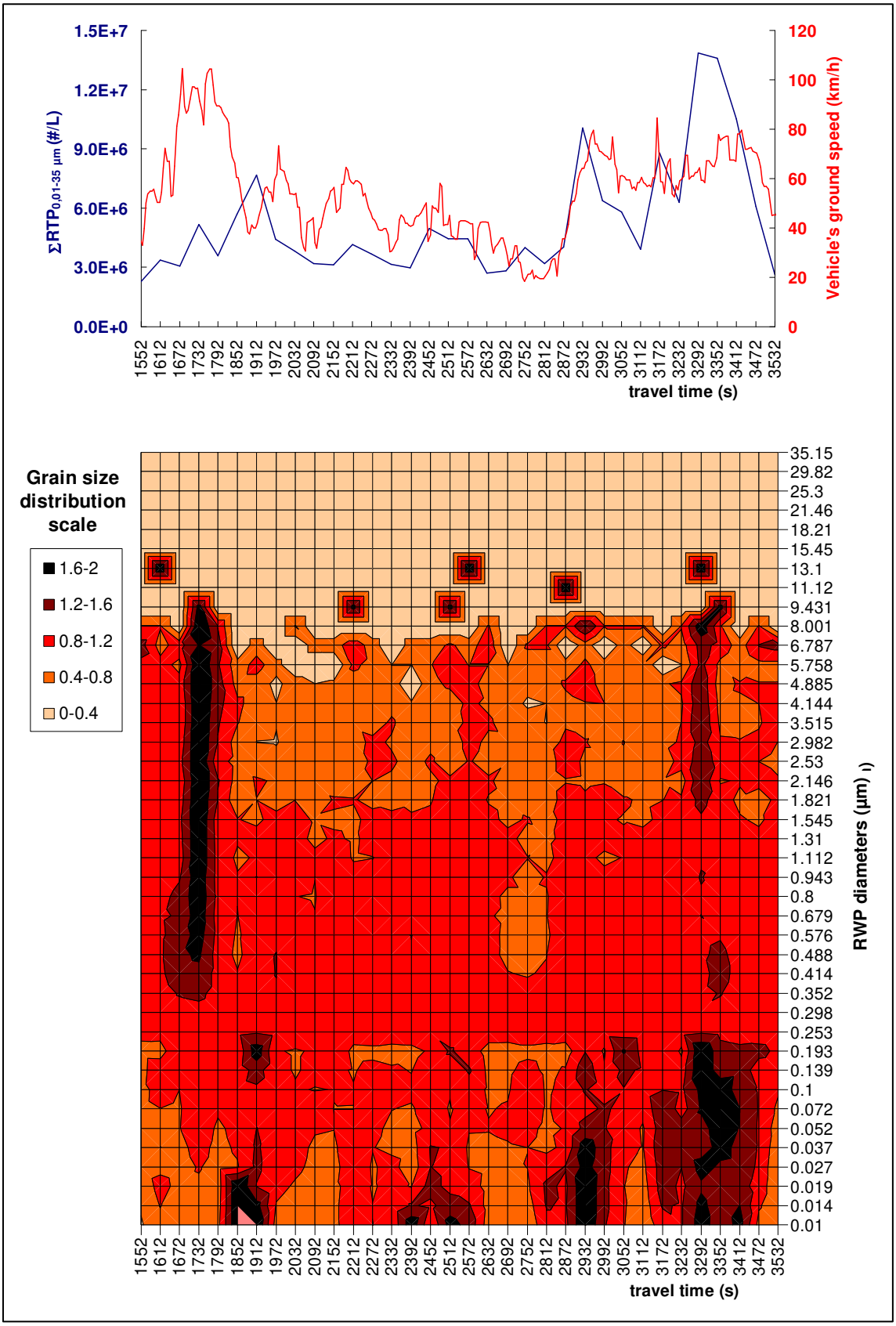

Figure 4. Top panel: Evolutions of number-weighted $\Sigma RWP_{0.01\text{-}35.15}$ concentration (blue signal, left hand scale) and ground speed (red signal, right hand scale) against travel time. Bottom panel: Evolution of standardized $\Sigma RWP_{0.01\text{-}35.15}$ grain size distribution against travel time.

Standardized data is given using arbitrary units with increasing values from light to dark red tones.

Measurements involved the same instrumented vehicle and driver as previously and the same course was followed. As mentioned before, because of the large number of monitored sizes, the time step for measurements equaled 1 min (instead of 6 s for the first measurement series). Hence, gained data could not give access to sharp concentration variations. It instead provided a more averaged view of $\Sigma RWP_{0.01\text{-}35.15}$ peak series and enduring signal patterns. Knowing this, several localized episodes of high nanometric particulate concentrations were observed. These primarily accounted for exhaust particles from adjoining vehicles. This is the case at major junctions (at t = 1850 s), during rapid series of stops at traffic lights (from t = 2350 s to t = 2600 s) or in heavily trafficked or confined urban sectors (from t = 2900 s to t =3000 s). According to table 1, these were identified as "uncontaminated road sections with high exhaust levels". Unlike these episodes, other situations were dominated by micrometric and super-micrometric TCP (e.g. at t = 1700 s, which was classified as "contaminated road sections with low exhaust levels"). Finally, high concentrations of coexisting nanometric and super-micrometric particles were encountered (at t = 3150 s and t = 3450 s). These accounted for situations where the levels of exhaust particles and TCP were balanced and thus were classified as "contaminated road sections with high exhaust levels".

Let us consider situations associated to "contaminated road sections with low exhaust levels" (e.g. at t = 1700 s when the road surface contamination with dust originated from a nearby stone quarry). At those times, a stripe of pronounced RWP concentrations, ranging from 0.4 µm to 10 µm in diameter, were observed (Figure 4). Considering that the preceding sections were "uncontaminated road sections with low exhaust levels", most of the increase in RWP levels at t = 1700 s can be attributed to vehicle-induced dust resuspension, so to TCP. However, despite being notable, the increase in number-weighted $\Sigma RWP_{0.01\text{-}35.15}$ concentration was limited: i.e. from (2.5-3.0) 10^6 #/L to (5.2-6.0) 10^6 #/L. TCP only moderately contributed to the loading of the rear-to-wheel air with nanometric particles. This is consistent with the results by Kwak et al. (2014) who found no enhancement of ultrafine particles at constant speeds. Our measurements showed that this was primarily due to the broad and relatively steady proportion of < 0.25 µm particles of local atmospheric blanks. Actually, atmospheric blanks accounted for most of the < 0.25 µm particles in sampled air. The latter occupied 37%-94% (average of 75%) of the finest RWP and overall buffered the extra contribution of small particles from tire-road contact. Hence, after discarding the contribution of atmospheric blanks and by excluding from calculations "road sections with high exhaust levels", averaged $\Sigma TCP_{0.01\text{-}35.15}$ values were 8 times higher on highly "contaminated road sections" than on other sections. The highest discrepancy corresponded to particles around 0.080-0.200 µm (above a factor 12) and 2-4 µm (close to a factor 9). This suggests that despite the limited influence of road surface contamination on nanometric RWP concentrations, the same contamination considerably increased ambient levels of certain TCP size categories. This, nevertheless, should be further validated by using test benches or test tracks with various types of road surfaces, tires as well as degrees of dust contamination.

The search for grain size distribution-based TCP tracers

The "uncontaminated road sections with high exhaust levels" (Table 1) accounted for a larger proportion of 0.03-0.10 µm particles than "uncontaminated road sections with low exhaust levels" (Figure 5). The numbered concentrations of particles in this size interval stood for 15%-16% and 11%-13% of the total concentrations, respectively. Furthermore, the same "uncontaminated road sections with high exhaust levels" also showed a lower proportion of 1-2.5 µm size particles than in the absence of notable traffic (i.e. of a factor of 3.2-4.9; 3.9 on average). Interestingly, in the latter size range, the variabilities of all number-weighted grading curves were lower (Figure 5). Hence, in an attempt to discriminate between exhaust particles and TCP at the rear of the wheel, one may divide (upon subtracting atmospheric blanks) the sum of number-weighted contributions in the 0.03-0.10 µm range by this in the 1-2.5 µm range. These average ratio values for "uncontaminated road sections with high exhaust levels" and "uncontaminated road sections with low exhaust levels" were 6500 and 1300, respectively. The same ratio equaled 1700 and 4300 on "contaminated road sections" for low (at 1700 s) and high exhaust particle levels (at t = 3150 s and t = 3450 s). The proximity between ratio values for "road sections with low exhaust levels" either contaminated with dust or not, along with the intermediary value for "contaminated road sections with high exhaust levels", suggests a relative robustness of the proposed ratio. Its relevance must nevertheless be more thoroughly validated on different road surfaces and under various driving conditions.

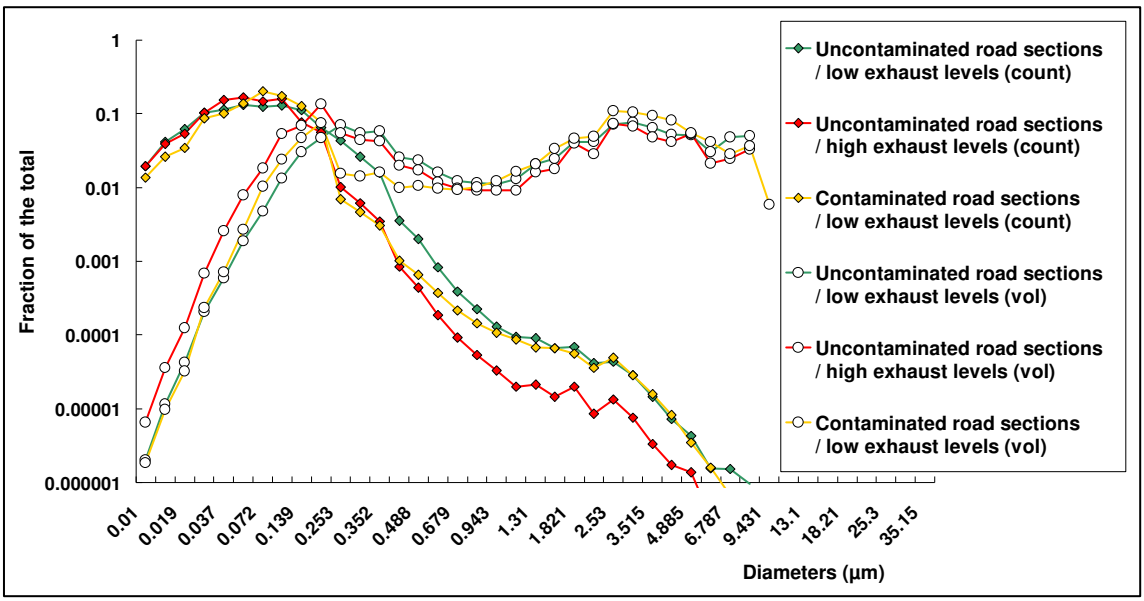

Figure 5. Number- (filled symbols) and volume- (empty symbols) weighted grading curves for RPM during the second measurement series. Data in graph is given, in the presence and absence of significant contaminations of road surface with dust or near-wheel air with exhaust particles. Local atmospheric blanks were preliminarily subtracted.

As for volume-weighted concentrations, grain size distributions showed (upon local atmospheric blanks' subtraction) two maxima around 0.15-0.25 µm and 2.5-5 µm (Figure 5). These two ranges for TCP are also typical of ambient exhaust particles' accumulation and coarse modes. Hence, compared to the tailpipe exit where nucleation and accumulation modes prevail, it is likely that exhaust particles (whenever detectable) measured on-road at the rear of the wheel underwent notable differentiation processes. As with the number-weighted size distributions, the differences in size distributions rather came from maxima's amplitudes than positions. Ratios among grain size categories must therefore be carefully used and continuously re-evaluated according to the local characteristics of road surface and traffic. Overall, the grading curve for "road sections with high exhaust levels" was highest at sizes below 0.2 µm then, beyond 1 µm, displayed lower values than for "road sections with low exhaust levels" either contaminated or not (Figure 5). Hence, TCP could be discriminated from exhaust particles by calculating (upon discarding local blanks) the ratio of the sum of volume-weighted contributions of particles < 0.2 µm to this > 1 µm. Through this approach, the ratio values for "uncontaminated road sections with high exhaust levels" and "uncontaminated road sections with low exhaust levels" averaged 0.58 and 0.16, respectively. However, the ratio value calculated for "contaminated road sections with high exhaust levels" (0.59) fell close to "uncontaminated road sections with high exhaust levels". The lack of discrimination for particulate mixtures could be solved by reducing the sub-micrometric size interval to below 0.1 µm. Under these circumstances, the averaged ratios for "uncontaminated road sections with high exhaust levels", "uncontaminated road sections with low exhaust levels" and "contaminated road sections with high exhaust levels" were 0.17, 0.03 (0.05 on "contaminated road sections with low exhaust levels") and 0.11, respectively.

Overall, for these sections where both the road surface was notably contaminated with dust and the near-wheel air was loaded with exhaust particles ("contaminated road sections with high exhaust levels"), the percentages of TCP derived by either using number-weighted or volume-weighted data were comparable: i.e. 41%-47% (the rest being from exhausts). The relatively good agreement between the both values is encouraging with respect to future identifications of TCP through the use of relevant size distribution ratios. However, the robustness of these ratios must be more thoroughly evaluated in the presence of various sources of particles or with particles of different maturation degrees. Moreover, due to their local importance, the role of exhaust particles and gazes deposited onto the road surface then remobilized as TCP represent another future field of researches. This is especially the case when considering how exhaust particles / gazes incorporate into roads' most superficial molecular layers, locally evolve (Adachi and Tainosho, 2004) and potentially modify the TCP production rate during tire-road contact. Ultimately, the study of interactions between the newly produced TCP and ambient particles

(including exhaust particles) may provide insight about how TCP take part in atmospheric pollutants' dissemination or in their local deposition.

Acknowledgements

This project was financially supported by ADEME "The French Environment and Energy Management Agency" fund through the "Physical Characterization of the Non-Exhaust Particle Emissions by Road Vehicles" project (Captatus) (grant number 1566C0016). The authors also gratefully thank L. Suard from Ifsttar for his help in preparing and making vehicles available.

References

Abu-Allaban M., J.A. Gillies, A.W. Gertler, R. Clayton and D. Proffitt (2003), Tailpipe, resuspended road dust, and brake-wear emission factors from on-road vehicles, *Atmospheric Environment*, 37, 5283-5293.

Adachi K., Y. Tainosho (2004), Characterization of heavy metal particles embedded in tire dust, *Environment International*, 30, 1009-1017.

Bukowiecki N., P. Lienemann, M. Hill, M. Furger, A. Richard, F. Amato, A.S.H. Prévô, U. Baltensperger, B. Buchmann and R. Gehrig (2010), PM10 emission factors for non-exhaust particles generated by road traffic in an urban street canyon and along a freeway in Switzerland, *Atmospheric Environment,* 44, 2330-2340. https://doi.org/10.1016/j.atmosenv.2010.03.039

Denier van der Gon H.A.C., J.H.J. Hulskotte, A.J.H. Visschedijk and M. Schaap (2007), A revised estimate of copper emissions from road transport in UNECE-Europe and its impact on predicted copper concentrations, *Atmospheric Environment*. 41, 8697-8710

Di Tullio A., S. Reale, M. Ciammola, L. Arrizza, P. Picozzi and F. De Angelis (2008), Characterization of Atmospheric Particulate: Relationship between Chemical Composition, Size, and Emission Source, *Chemistry and Sustainability*, 1, 110–117.

Geller M.D., L., Ntziachristos, A., Mamakos, Z., Samaras, D.A., Schmitz, J.R., Froines and C., Sioutas (2006), Physicochemical and redox characteristics of particulate matter (PM) emitted from gasoline and diesel passenger cars, *Atmospheric Environment*, 40, 6988-7004.

Harrison R.M., J. Yin, D. Mark, J. Stedman, R.S. Appleby, J. Booker and S. Moorcroft (2001). Studies of the coarse particle (2.5–10 ⌟ m) component in UK urban atmospheres, *Atmospheric Environment*, 35, 3667-3679.

Hildemann L.M., G.R. Markowski and G.R. Cass (1991), Chemical composition of emissions from urban sources of fine organic aerosol, *Environmental Science and Technology*, 25, 744-759.

Ketzel M., G. Omstedt, C. Johansson, I. During, M. Pohjolar, D. Oettl, L. Gidhagen, P. Wahlin, A. Lohmeyer, M. Haakana and R. Berkowicz (2007), Estimation and validation of PM2.5/PM10 exhaust and non-exhaust emission factors for practical street pollution modeling, *Atmospheric Environment*, 41, 9370-9385.

Kumata H., H. Takada and N., Ogura (1997), 2-(4-Morpholinyl)benzothiazole as an Indicator of Tire-Wear Particles and Road Dust in the Urban Environment*, Molecular Markers in Environmental Geochemistry*, ACS Symposium Series, 291–305.

Kwak J., L. Sunyoup and L. Seokhwan (2014), On-road and laboratory investigations on non-exhaust ultrafine particles from the interaction between the tire and road pavement under braking conditions, *Atmospheric Environment*, 97:195-205. http://dx.doi.org/10.1016/j.atmosenv.2014.08.014

Lenschow P., H.-J. Abraham, K. Kutzner, M. Lutz, J.-D. Preuß and W. Reichenbächer (2001), Some ideas about the sources of PM10, *Atmospheric Environment*, 35, 23-33.

Querol X., A. Alastuey, S. Rodriguez, F. Plana, C.R. Ruiz, N. Cots, G. Massagué and O. Puig (2001), PM10 and PM2.5 source apportionment in the Barcelona Metropolitan area, Catalonia, Spain, *Atmospheric Environment*, 35, 6407-6419.

Querol X., A. Alastuey, C.R. Ruiz, B. Artiñano, H.C. Hansson, R.M. Harrison, E. Buringh, H.M. ten Brink, M. Lutz, P. Bruckmann, P. Straehl and J. Schneider (2004), Speciation and origin of PM10 and PM2.5 in selected European cities, *Atmospheric Environment*, 38, 6547–6555.

Querol X., M. Viana, A. Alastuey, F. Amato, T. Moreno, S. Castillo et al. (2007), Source origin of trace elements in PM from regional background, urban and industrial sites of Spain, *Atmospheric Environment*, 41, 7219-7231.

PIARC (2015), Road tunnels: vehicle emissions and air demand for ventilation, *Technical Committee C.4 Road Tunnel Operation*, R05EN, 87 pp, ISBN: 978-2-84060-269-5.

Rogge W.F., L.M. Hildemann, M.A. Mazurek, G.R. Cass and B.R.T. Simoneit (1993). Sources of fine organic aerosol. 3. Road dust, tire debris, and organometallic brake lining dust: roads as sources and sinks, *Environmental Science and Technology*, 27, 1892–1904.

Ruehl C.R., W.A. Ham and M.J. Kleeman (2010), Temper ature-induced volatility of molecular markers in ambient airborne particulate matter, *Atmospheric chemistry and physics discussion*, 10, 20329-20353.

Schauer J.J., G.C. Lough, M.M. Shafer, W.F. Christensen, M.F. Arndt, J.T. DeMinter and J.S. Park (2006), Characterization of metals emitted from motor vehicles, *Research Report*, 133, 1-76.

Snilberg B., T., Myran, N., Uthus and E., Erichsen (2005). Characterization of road dust in Trondheim, Norway. *Repport*, 19 pp, Available at: https://www.vegvesen.no/_attachment/61346/binary/14042.

Sternbeck J., Å. Sjödin and K. Andréasson (2002), Metal emissions from road traffic and the influence of resuspension—results from two tunnel studies, *Atmospheric Environment*, 36, 4735-4744.

Thorpe A.J., R.M. Harrison, P.G. Boulter and I.S. McCrae (2007), Estimation of particle resuspension source strength on a major London Road, *Atmospheric Environment*, 41, 8007-8020.

Thorpe A., R.M. Harrison (2008), Sources and properties of non-exhaust particulate matter from road traffic: A review, Science of the Total Environment, 400, 270-282.

Weckwerth, G. (2001), Verification of traffic emitted aerosol components in the ambient air of Cologne (Germany), *Atmospheric Environment*, 35, 5525–5536.

Texture influence on road dust load

Joacim Lundberg, Göran Blomqvist, Mats Gustafsson and Sara Janhäll*

Swedish National Road and Transport Research Institute (VTI), SE-581 95, Linköping, Sweden.
*Presenting author email: joacim.lundberg@vti.se

Background

One of the main sources of PM (Particulate Matter) in the urban environment is the traffic. Traffic contributes not only to exhaust emissions, but also to direct emission from abrasion wear of pavements, tyres and brakes as well as emission from suspension of available road dust on the road surface. This dust is partially stored in the road surface macro texture. Dust accumulate on the surface due to several different mechanisms and transport phenomena's (e.g. Denby et al., 2013). Examples of transport mechanisms affecting the road dust load and thus the storage in the texture include precipitation, evaporation, turbulence from traffic, wetting of the road surface binding particles to it, sanding and crushing of the sand etc.

The road surface texture is known to affect several other traffic and environmental related aspects, such as having an impact on both friction (e.g. Kogbara et al., 2016), road noise emissions (e.g. Sandberg and Ejsmont, 2002) and rolling resistance (e.g. Sandberg et al., 2011, Ejsmont et al., 2016) and thus fuel consumption (e.g. Andersen et al., 2015).

Regarding PM emissions, it is known that traffic will generate direct emissions from abrasion wear of pavements (e.g. Gustafsson et al., 2009) as well as from tyre (Thorpe and Harrison, 2008) and brake wear (Grigoratos and Martini, 2015). Another important aspect is how the traffic causes suspension of dust stored on the road surface (Kupiainen et al., 2016). Despite this knowledge, little is still known regarding how the texture influences the potential dust storage, the transport of dust on the surface as well as the suspension of this dust.

Earlier studies have shown a negative dependency between PM10 emissions and the road surface macro texture (described as Mean Texture Depth, MTD), when applying a controlled amount of dust to the surface, and introducing suspension by using an enclosed container in which wind shear was applied by a rotating blade (Blomqvist et al., 2011, China and James, 2012). In addition, China and James (2012) also performed photo analyses on how the mean aggregate size distribution of the pavement affect the PM10 emissions, as well as a corrected aggregate size mode. The results indicated an association between PM10 emissions and the relative frequency between different type of texture features, in this case nearly flat narrow-to-medium and deep-narrow features. Similar analysis was done by Amato et al. (2013) where photo analysis was used to estimate the mean aggregate size of the pavements, although without the correction that China and James (2012) performed in their investigation. Amato et al. (2013) found a negative power law dependency for the road dust loading and the mean aggregate size of the pavement, when taking into account masking effects of other factors (e.g. construction activities). Blomqvist et al. (2011) however, showed that the macro texture had a larger influence on the emissions than the pavement maximum stone size.

In other studies, where no artificial dust was applied to the surface, however, a positive correlation between the surface texture (measured as Mean Profile Depth, MPD) and the actual dust load in a city street (Blomqvist et al., 2013) was found.

Objective

The objective of this study was to investigate the connection between pavement texture and the maximum dust load retention at a low speed.

Methods

Road Simulator

The VTI circular Road Simulator (RS, see Figure 1), was used to investigate the maximum dust load retention at a low speed, and the connection to the road surface texture. The RS is a

machine with four operational axles, allowing for up to four different tyres to be mounted, which runs over a circular pavement track. This track consists of 28 pavement slabs. In this study summer tyres were used and 14 different pavement types was used, using 2 slabs per pavement type (described in Table 1). The RS was operated at 10 km/h for 300 laps, corresponding to 1200 tyre passages. The speed was selected on the suspicion of too efficient cleaning effect from the tyre passages would be achieved at higher speeds. The axle load was set to 450 kg.

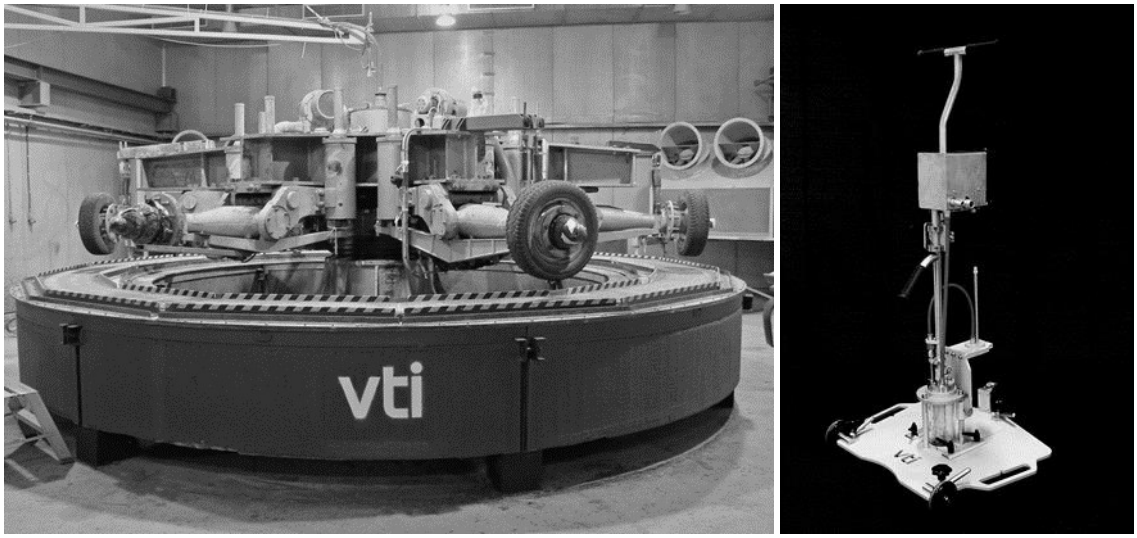

Figure 1: The VTI circular Road Simulator (left) and the VTI Wet Dust Sampler (WDS).

Texture measurement and calculation

The texture was measured using a laser device mounted on one of the axles of the RS with a sampling frequency of 32 kHz. The macro texture both in form of mean profile depth (MPD) and the inverted mean profile depth (MPDn) were calculated using the steps described in Trafikverket (2015), which follows the same requirement regarding hardware and calculation method as in ISO 13473-1 (1997). The MPDn is calculated in a similar manner as MPD, with the difference of using the depth instead of the peak relative to the base level (Lundberg, 2012), see Figure 2. This was done after the 1200 tyre passages on the dust laden track and after thorough cleaning of the texture.

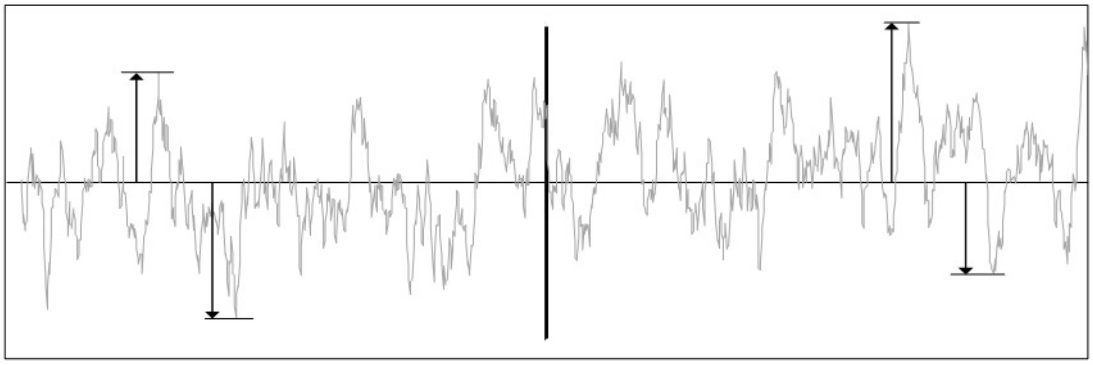

Figure 2: Simulated texture data for presentation purposes (upscaled). The peak and the depth used for calculation of MPD and MPDn in a segment (divided by the vertical line) relative to the base line is illustrated by the arrows.

Materials

The pavements used in the RS for the investigation is presented in Table 1.

The mineral aggregate dust used was a type of granite (“Skärlunda”) found in Sweden, used as filler in surface course mixes. The size distribution was determined using laser granulometry

analysis and is presented in Figure 3. The laser granulometry was performed at VTI using a Malvern Mastersizer 3000, and a Hydro EV with glass container of 600 ml as sample vessel.

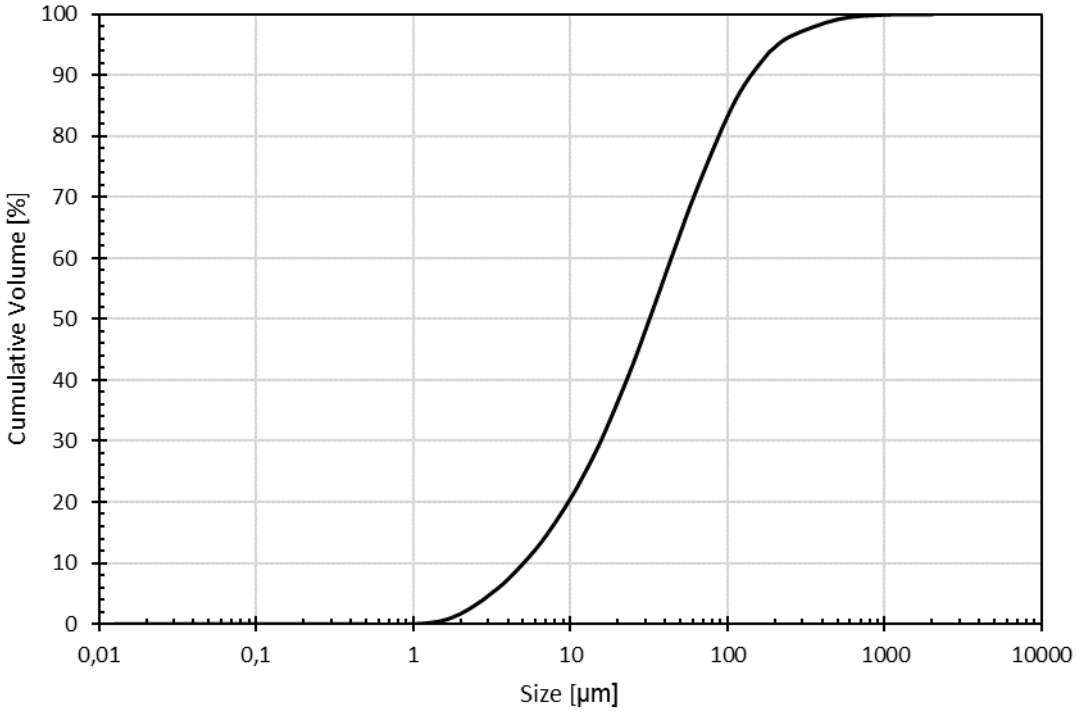

Figure 3: Size distribution from the laser granulometer analysis. Average distribution based on three measurements.

The dust was weighed and applied manually until the texture was estimated to be filled to its maximum, forming a flat surface. The amount of applied dust is given in Table 1. After the application, the tyres were lowered on to the surface until the load of 450 kg was achieved. The road surface, after manual application of the road dust, prior to and after the 1200 tyre passages is seen in Figure 4.

Figure 4: Road surface after application of dust (top figures) and after 1200 tyre passages with residual dust left in the road surface texture (bottom figures).

Dust Sampling

To assess the dust load, sampling was done using a Wet Dust Sampler (WDS, Figure 1). The WDS is a VTI developed sampling method with the basic principle of operation to flush a given small circular surface with water forming a dust sample directly transferred to a bottle, allowing further analysis (Jonsson et al., 2008). This method is used by VTI to investigate and follow up the road dust loads and how different road operation strategies effect the dust load (e.g. Gustafsson et al., 2017). For each asphalt slab in the RS, 5 samplings were performed and stored in a large bottle. On 3 selected slabs, 6 samplings were performed, 5 stored in a large bottle and 1 stored in a small separate bottle. An example on the resulting surface is shown in Figure 5.

Figure 5: Example on road surface after WDS sampling. In the right figure, 6 samplings were performed, divided into 5 sampling stored in a large bottle and 1 sampling stored in a small bottle.

Dust sample evaluation

The dust sampled by the WDS was analysed using turbidity. Turbidity is an optical method where light is scattered by particles suspended in water, which is used as an indicator for

particle sediment concentration. A HI88713 ISO Turbidity Meter by Hanna Instruments were used. The turbidity meter has a FNU range of 0 – 1000 with a resolution of 0.01 for 0.00-9.99, 0.1 for 10.0 – 99.9 and 1 for 100 – 1000. The accuracy is ± 2% of reading in addition to stray light. Three measurements were performed per WDS sample, and the average turbidity was calculated, with the resulting values presented in Table 1.

Results and Discussion

Texture

As can be seen in Figure 6, there is a positive linear correlation between the clean texture and the difference between clean and the residual dust left in the texture (i.e. dust load) for both texture parameters. The correlation between the dust load and the texture was larger for MPDn (R2 = 0.99) and for MPD (R2 = 0.77). This result agrees with the previous observation that increasing texture indicates a potential increase of dust load, while also introducing a new parameter likely of interest, MPDn, which is based on the valleys of the texture, rather than the stone peaks as for the MPD. This measure might be of further interest for characterisation of the road surface and the pavement's dust storage capabilities. These results reinforce the need of taking the road surface characteristics into account when discussing road dust and the potential of road dust resuspension.

Table 1: Applied dust and the resulting texture and turbidity values. SMA = Stone Mastic Asphalt and the numbers 11, 8 and 6 denotes the maximum aggregate size in mm.

Slab	Pavement type	Applied Dust [g]	MPD [mm]		MPDn [mm]		Turbidity [FNU]	Std. Dv. [FNU]
			Clean	Residual Dust	Clean	Residual Dust		
1	SMA 11	268.5	1.45	1.04	2.60	0.59	732	7.8
2	SMA 11	412.4	1.51	0.86	2.20	0.57	753	26.8
3	SMA 8	161.9	0.94	0.70	1.18	0.45	383	1.2
4	SMA 8	156.1	1.06	0.75	1.55	0.53	334	7.1
5	SMA 8	172.4	1.09	0.79	1.19	0.47	379	8.2
6	SMA 8	185.2	1.04	0.70	1.69	0.51	465	17.2
7	SMA 8	177.5	1.13	0.83	1.32	0.47	384	32.6
8	SMA 8	156.5	1.06	0.78	1.08	0.44	346	10.1
9	SMA 8	187.1	1.15	0.85	1.40	0.44	491	14.1
10	SMA 8	157.3	1.20	0.86	1.70	0.49	484	3.6
11	SMA 8	155.4	0.99	0.83	1.12	0.51	457	14.4
12	SMA 8	139.9	0.95	0.77	1.12	0.51	336	17.7
13	SMA 8	145.6	0.87	0.67	1.53	0.46	343	14.6
14	SMA 8	168.7	1.11	0.79	1.57	0.58	423	7.1
15	SMA 6	146.8	1.05	0.85	1.20	0.51	326	6.7
16	SMA 6	147.8	0.89	0.77	0.94	0.53	312	12.7
17	SMA 6	147.6	0.87	0.71	0.91	0.47	323	1.7
18	SMA 6	153.2	1.09	0.74	1.05	0.43	401	12.0
19	SMA 6	132.1	0.99	0.80	0.90	0.46	277	4.5
20	SMA 6	130.3	0.73	0.65	0.82	0.41	269	2.6
21	SMA 6	143.5	0.87	0.75	0.90	0.47	388	10.0
22	SMA 6	127.8	0.78	0.70	0.97	0.48	332	1.2
23	SMA 6	167.9	1.24	0.98	1.58	0.53	472	4.8
24	SMA 6	172.1	1.14	0.89	1.38	0.46	452	12.5
25	SMA 6	148.7	0.95	0.67	0.98	0.45	423	4.8
26	SMA 6	124.3	0.95	0.74	1.16	0.44	291	8.5
27	SMA 6	173.0	1.00	0.75	1.64	0.50	434	2.6
28	SMA 6	135.3	0.90	0.68	1.34	0.52	368	18.4

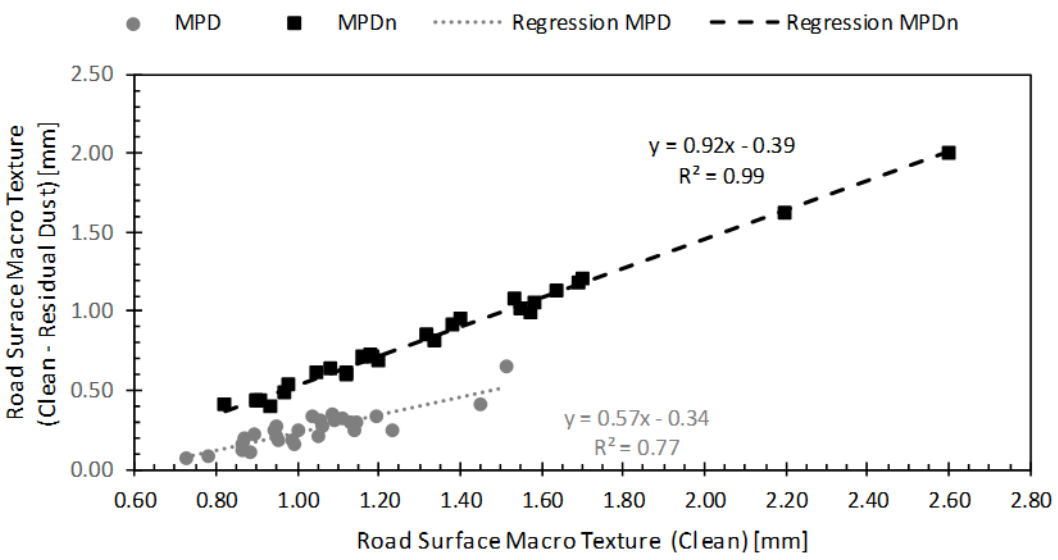

Figure 6: Comparison clean texture and difference between clean and texture filled by residual dust (the stored dust).

Turbidity

As can be seen in Figure 7, there is a positive linear correlation between the amount of dust calculated as the difference between clean texture and the residual dust left in the texture after tyre passages (both MPD and MPDn) for the road dust proxy turbidity in the WDS samples. As for the texture, the largest correlation is found for MPDn (R2 = 0.71) than for MPD (R2 = 0.63). It can also be noted that the largest turbidity values are relatively close to the maximum range limit of 1000 FNU.

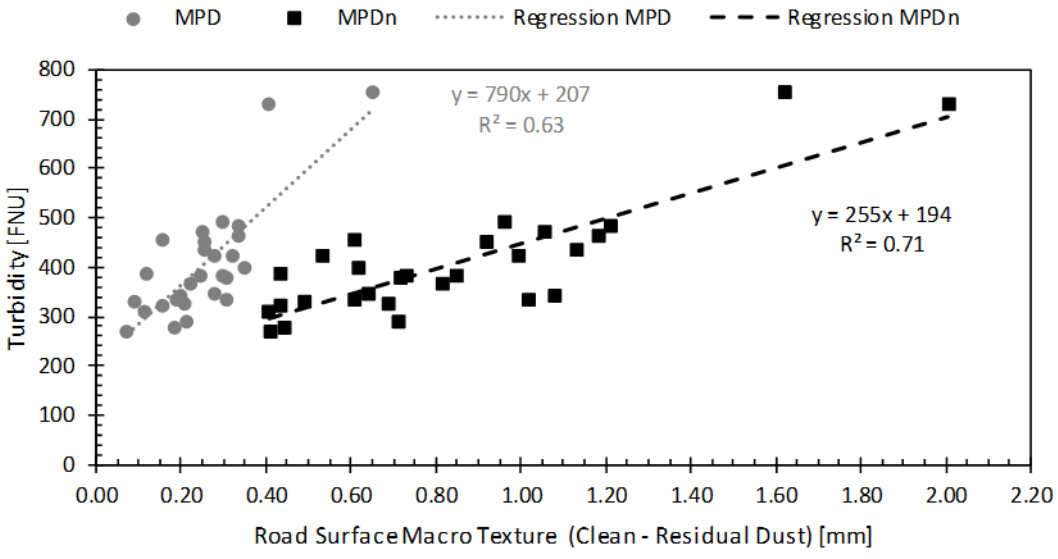

Figure 7: Comparison between two texture measures and the turbidity of the sampled dust.

Figure 8 (a and b) shows that the turbidity follows reasonably the amount of applied dust (before tyre passages). For both cases, a small positive correlation is found between the part of texture filled with dust and the applied dust which is expected. A possible explanation that the trend is not very clear could be due to not taking the shape of the texture into account. In this case an average value has been calculated based on the largest depth/peak available in the segment. This will not consider the other possible shapes of the texture and their different abilities to store dust. In Figure 12, some examples of different texture shapes which probably will affect the

possibility to store dust. This will likely also affect the possibility of suspension of the dust by traffic, since the tyre will likely not be able to reach the bottom in most cases, or the shear due to wind will not be able to erode the stored particles, which is also indicated by China and James (2012).

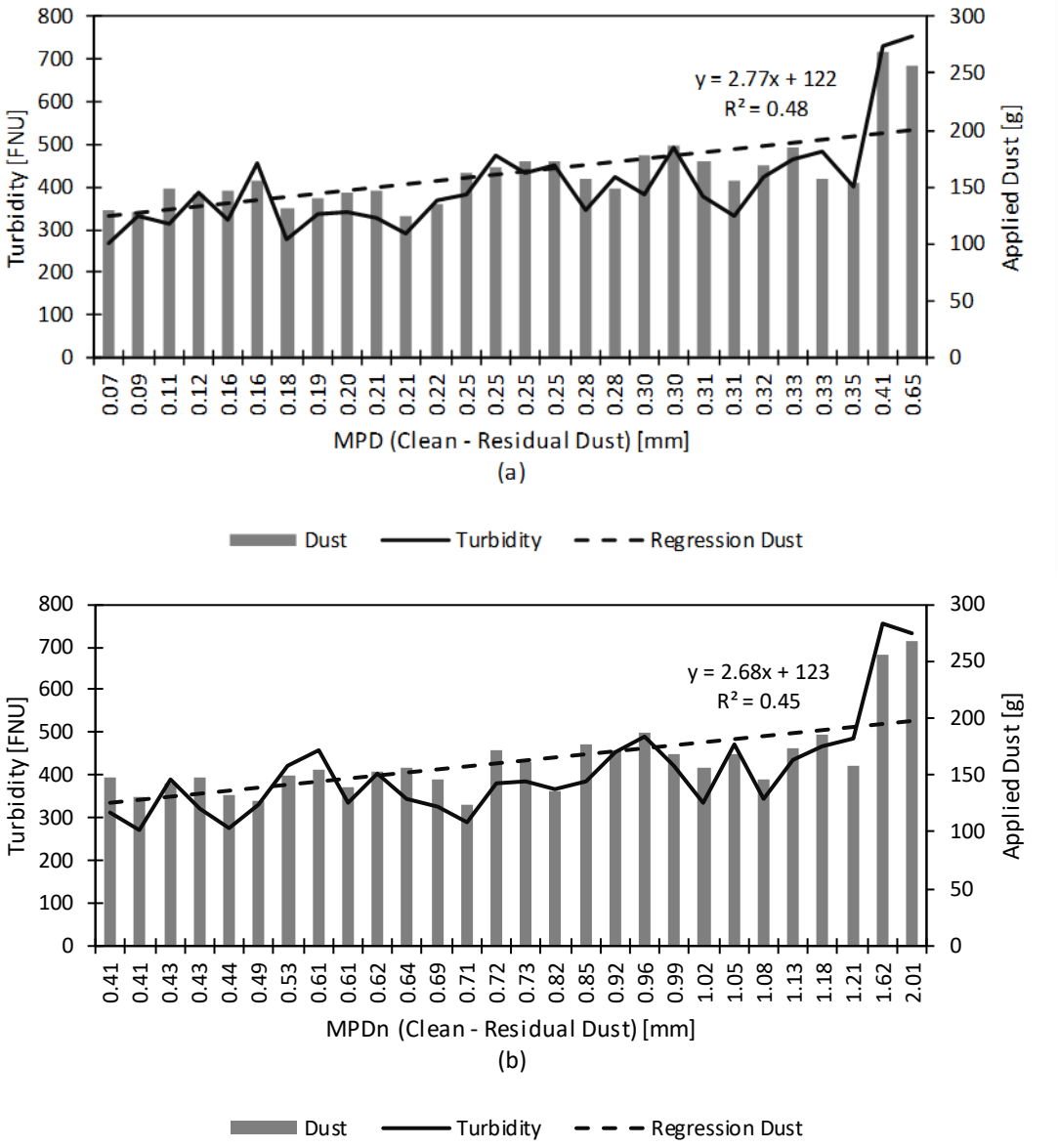

Figure 8: Turbidity and applied Dust vs Residual Dust texture for (a) MPD and (b) MPDn.

Pavement type and texture

Another interesting result from the investigation is the comparison between the pavement types based on the largest aggregate size (11 mm, 8 mm and 6 mm respectively in this case) and the clean texture (Figure 9) as well as for the dust stored in the texture after the tyre passages (clean – residual texture, Figure 10). As can be noted, for all four cases, a relation can be seen between the largest aggregate size and the texture. For the clean texture (Figure 9), only a small difference is seen between the 8 mm and 6 mm sizes, while a larger difference can be seen for the dust stored in the texture after tyre passages (Figure 10). For all four cases, the largest stone size (11 mm) has the highest texture. The implication of this is that increasing stone aggregate size results in an increased dust storage potential.

The results seemingly imply a disagreement with previous studies in which Amato et al. (2013) observed decreasing dust loads with increasing mean aggregate sizes. An important difference though, is that the WDS aims to sample the total road dust load, while the dry vacuum cleaner

device used by Amato samples the suspendible PM10 from the road surface. A deep texture has a higher potential to accumulate dust, while also, more efficiently, protecting accumulated dust from suspension forces depending on the geometrical features of the texture as presented by China and James (2012). Taking this into account, the results are not contradictory to the observations by Amato et al. (2013).

Also Blomqvist et al. (2011) and China and James (2012), observed decreasing PM10 emissions with an increasing road surface macro texture (MTD) when applying wind shear to induce suspension. A later observation by Blomqvist et al. (2014) based on WDS measurements showed increasing dust loads with increasing road surface macro texture (MTD).

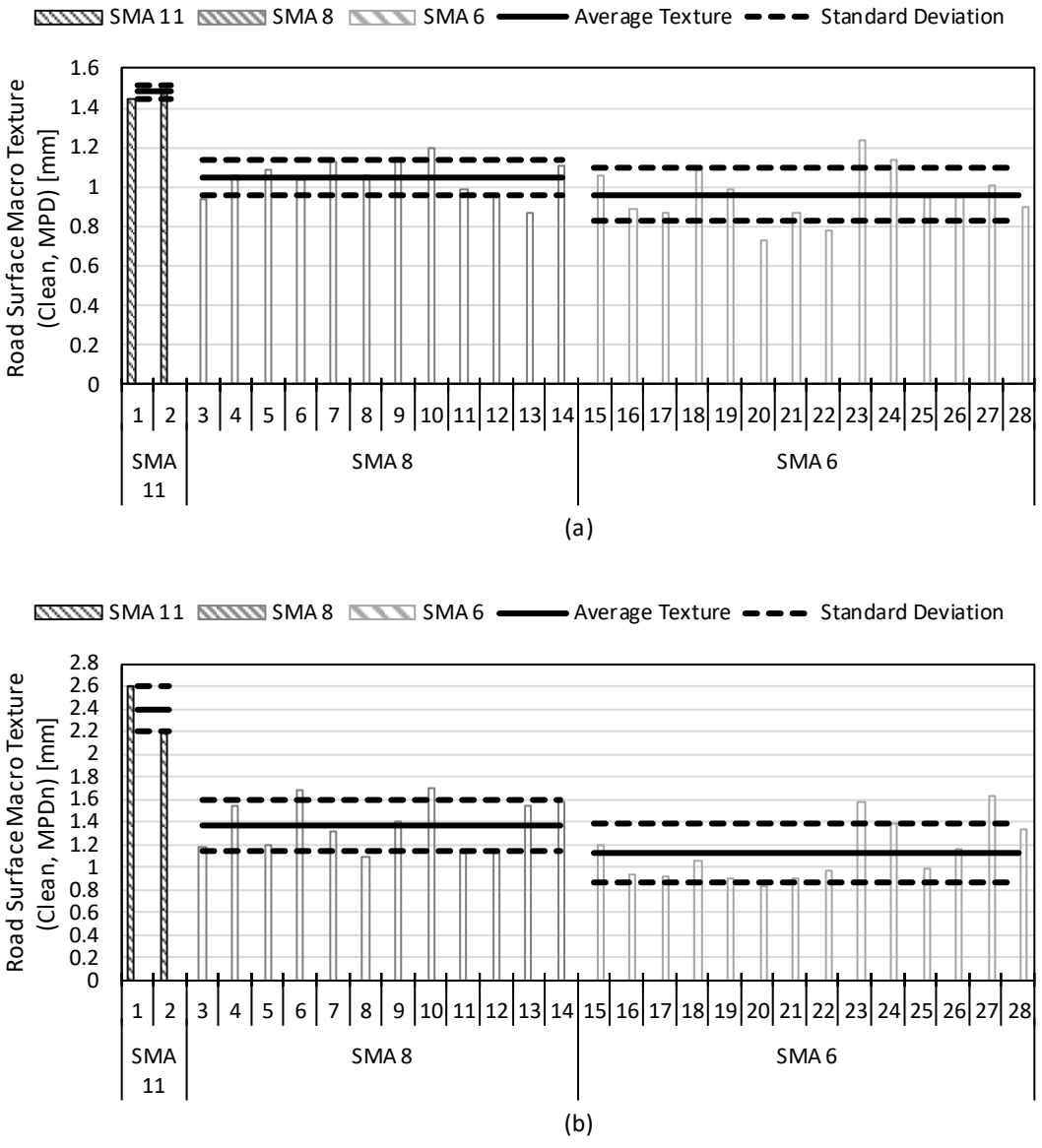

Figure 9: Road surface macro texture (clean) divided into groups based on pavement type (maximum aggregate size) with the average texture for each group for (a) MPD and (b) MPDn.

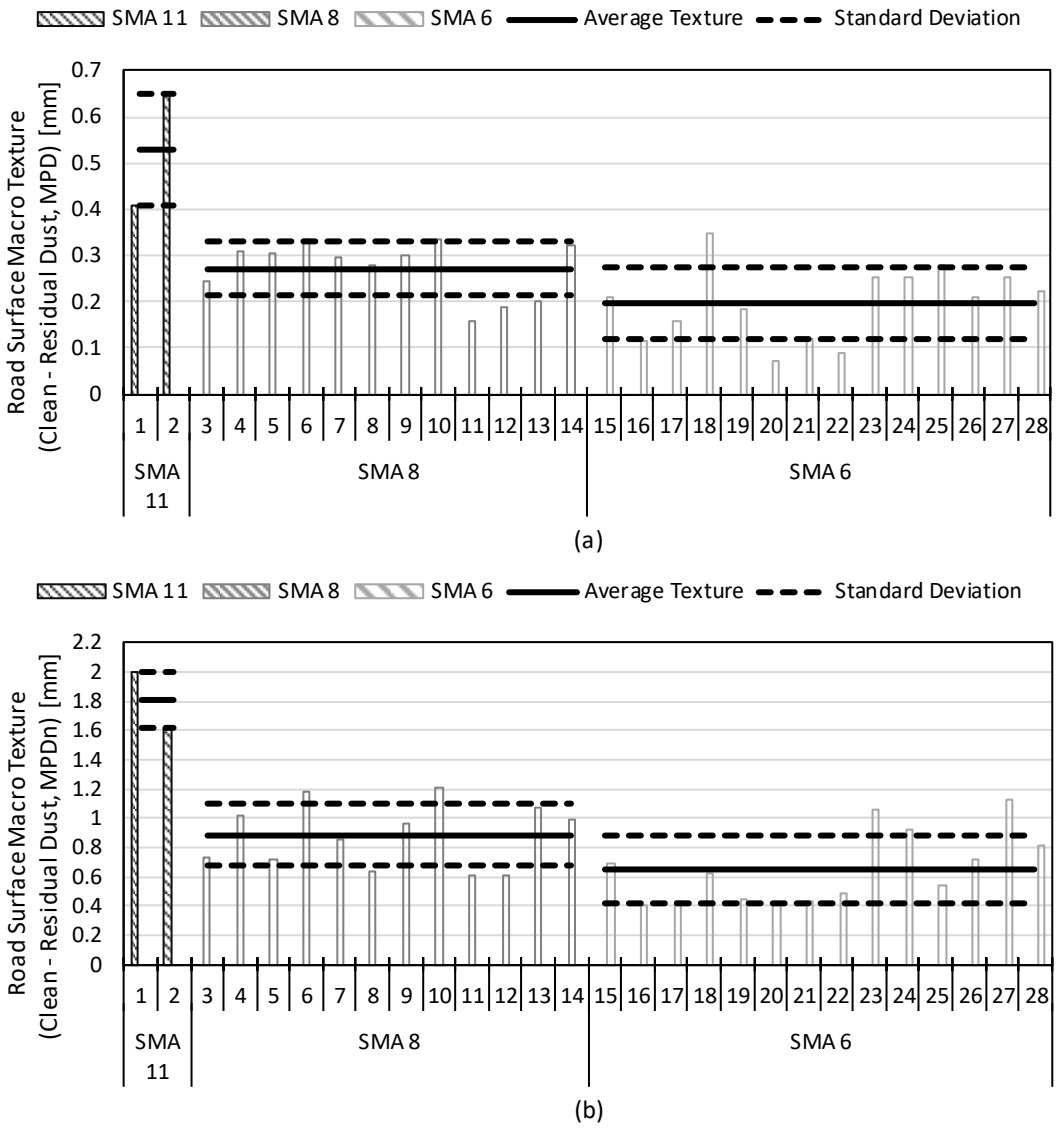

Figure 10: Road surface macro texture (clean – residual dust) divided into groups based on pavement type (maximum aggregate size) with the average texture for each group for (a) MPD and (b) MPDn.

Similar results for the three groups are seen when comparing against turbidity results instead of texture results (Figure 11).

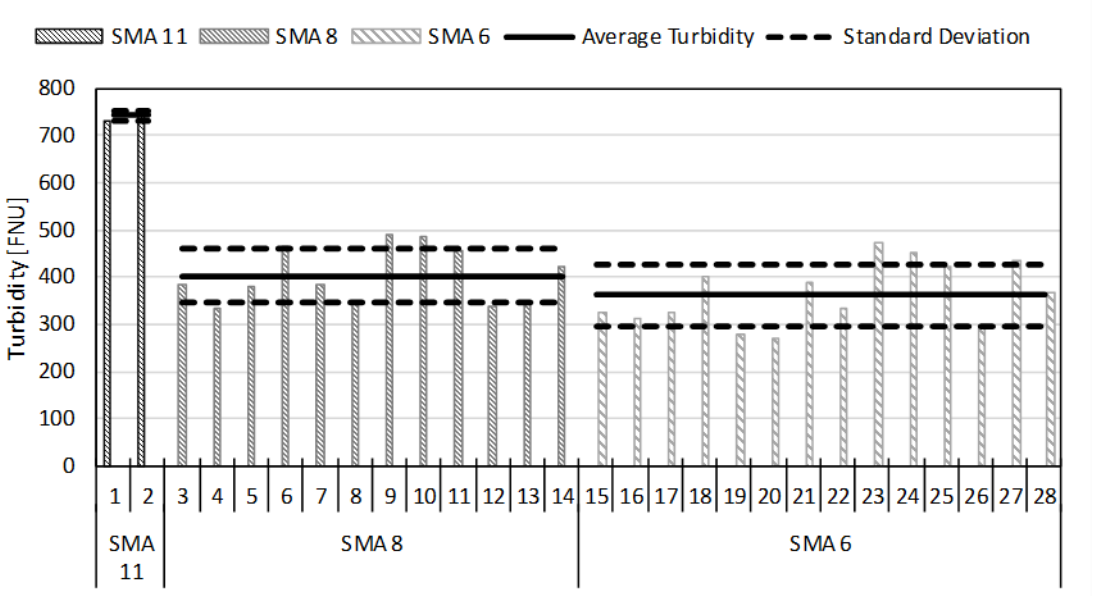

Figure 11: Turbidity divided into groups based on pavement type where the number denotes largest aggregate size.

Conclusions

The results presented in this paper have increased the understanding on how the road surface macro texture impacts on the potential dust load. The results show that:

1. An increased aggregate size implies a higher potential dust load. The correlation to texture is likely to better and more detailed describe the potential dust load in comparison to the largest aggregate size.

2. The road surface macro texture measure MPD is probably insufficient to accurately describe the potential maximum road dust load, which is shown by the comparison to the newly introduced MPDn. In this case, MPDn was found to better describe the residual dust stored in the texture.

3. The turbidity follows the amount of residual dust in the texture in comparison to the total applied dust.

Future work

The results presented in this paper have shown the potential available to develop more ways to use macro texture data to determine the space available for dust load storage. One can suspect though, that other measures than those presented are required to more accurately describe other aspects of the problem, such as how much of the road dust will have the potential to be suspended depending on the texture itself, such as very narrow texture valleys versus very wide, as indicated in Figure 12.

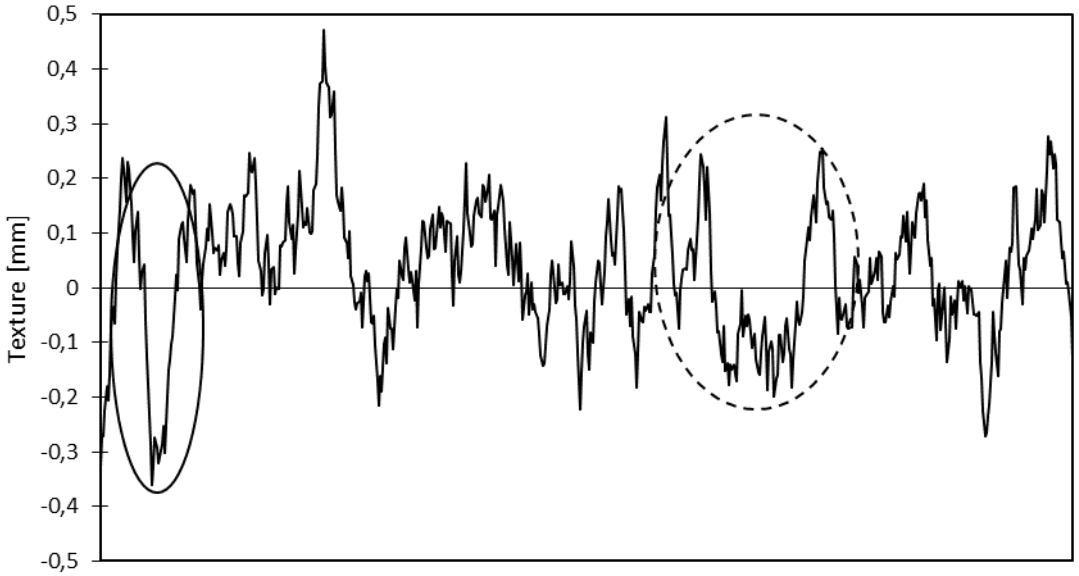

Figure 12: Simulated texture data for presentation purposes (upscaled). The dashed shape shows an example of a wide texture allowing for more dust to be stored, while the solid shape shows a narrower texture, allowing for less dust to be stored.

Other aspects related to macro texture and dust load, although not investigated in this specific paper, is how the texture changes over time. In this investigation, with only 1200 tyre passages with summer tyres, one can assume that the impact on the texture is very low, especially considering a constant climate where no other road surface damaging processes are present. Also, the low speed used in this investigation is likely to affect the results. An increased speed would reduce the residual dust stored in the texture, due to the increased shear by wind, causing more dust to be suspended. Future investigation should focus on the relation between the retention of dust in the texture and the speed of the passing tyres. Also, to further investigate the dust load relation to speed, experiments should be made concerning how many tyre passages are required at a constant speed to reach a steady-state dust load in a laboratory setting. Another important aspect is differences in dust removal potential between summer tyres, non-studded winter tyres and studded tyres.

Concerning tyre types, the road surface texture development is also of future research interest, since studded tyres increase the texture, while summer tyres and non-studded winter tyres reduce it. In combination with the seasonal temperature changes, the tyre type usage causes an annual cycle in texture development and thus also the road dust load potential. This is of course of special interest in countries where studded tyres are used (the Nordic countries, some states in the U.S.A., Canada, Russia etc.). Another possible investigation of interest is to compare tyre settings (e.g. tyre pressure) and the effect on road dust retention.

In reality, several more complex processes will have an impact on the transport and accumulation processes of road dust, such as the metrological conditions, the traffic properties, the properties of the dust itself, the surface course, the process of cementation of stored dust in the texture thus not being available for suspension etc. Further research is required for all these suggested processes and how they, together with road surface texture affects road dust load and emissions.

Another interesting aspect for further investigation is the connection between road surface macro texture and its effect on abatement activities such as e.g. street sweeping and washing activities. It is likely that texture influences the effect of activities as well as when, where and how these abatement measures would be planned and carried out, especially if combined with knowledge obtained from the suggested investigations above.

Acknowledgements

The authors would like to sincerely thank and acknowledge Dennis Hydén and Tomas Halldin for operation of the RS, Carl Södergren for help with sampling (VTI) and Peter Andrén (Datamani) for raw data processing.

This work was carried out in a PhD program financed by the Swedish Transport Administration and VTI.

References

Amato, F., Pandolfi, M., Alastuey, A., Lozano, A., Gonzalez, J. C. & Querol, X., (2013), Impact of traffic intensity and pavement aggregate size on road dust particles loading, Atmospheric Environment, 77, 711-717.

Andersen, L. G., Larsen, J. K., Fraser, E. S., Schmidt, B. & Dyre, J. C., (2015), Rolling Resistance Measurement and Model Development, Journal of Transportation Engineering, 141, 04014075.

Blomqvist, G., Gustafsson, M., Bennet, C. & Halldin, T., (2011), PM10 supension of road dust is depending on the road surface macro texture, European Aerosol Conference (EAC).

Blomqvist, G., Gustafsson, M., Janhäll, S. & Lundberg, T, (2014), PM10 emissions and road surface dust load is influenced by road surface macro texture, NOSA.

Blomqvist, G., Gustafsson, M. & Lundberg, T., (2013), Road surface dust load is dependent on road surface macro texture, European Aerosol Conference (EAC).

China, S. & James, D. E., (20129, Influence of pavement macrotexture on PM10 emissions from paved roads: A controlled study, Atmospheric Environment, 63, 313-326.

Denby, B. R., Sundvor, I., Johansson, C., Pirjola, L., Ketzel, M., Norman, M., Kupiainen, K., Gustafsson, M., Blomqvist, G. & Omstedt, G., (2013), A coupled road dust and surface moisture model to predict non-exhaust road traffic induced particle emissions (NORTRIP). Part 1: Road dust loading and suspension modelling, Atmospheric Environment, 77, 283-300.

Ejsmont, J. A., Ronowski, G., Świeczko-Żurek, B. & Sommer, S., (2016), Road texture influence on tyre rolling resistance, Road Materials and Pavement Design, 18, 181-198.

Grigoratos, T. & Martini, G., (20159, Brake wear particle emissions: a review, Environ Sci Pollut Res Int, 22, 2491-504.

Gustafsson, M., Blomqvist, G., Gudmundsson, A., Dahl, A., Jonsson, P. & Swietlicki, E., (2009), Factors influencing PM10 emissions from road pavement wear, Atmospheric Environment, 43, 4699-4702.

Gustafsson, M., Blomqvist, G., Janhäll, S., Johansson, C., Järlskog, I., Lundberg, J., Norman, M. & Silvergren, S., (2017), Driftåtgärder mot PM10 i Stockholm: utvärdering av vintersäsongen 2015–2016, VTI rapport, Linköping: Statens väg- och transportforskningsinstitut (VTI) [In Swedish with English summary].

ISO 13473-1, (1997), Characterization of pavement texture by use of surface profiles - Part 1: Determination of Mean Profile Depth, Genève, Switzerland: International Organization for Standardization (ISO).

Jonsson, P., Blomqvist, G. & Gustafsson, M., (2008), Wet Dust Sampler: Technological Innovation for Sampling Particles and Salt on Road Surface, Seventh International Symposium on Snow Removal and Ice Control Technology, Transportation Research Circular E-C126, 102-111.

Kogbara, R. B., Masad, E. A., Kassem, E., Scarpas, A. & Anupam, K., (2016), A state-of-the-art review of parameters influencing measurement and modeling of skid resistance of asphalt pavements, Construction and Building Materials, 114, 602-617.

Kupiainen, K., Ritola, R., Stojiljkovic, A., Pirjola, L., Malinen, A. & Niemi, J., (20169, Contribution of mineral dust sources to street side ambient and suspension PM10 samples, Atmospheric Environment, 147, 178-189.

Lundberg, T., (2012), Kontrollmetod för nya vägbeläggningar, Linköping: Statens väg- och transportforskningsinstitut (VTI) [In Swedish with English summary].

Sandberg, U. & Ejsmont, J. A., (2002), Tyre/Road Noise Reference Book 1st Edition, INFORMEX Esjmont & Sandberg Handelsbolag, Kisa.

Sandberg, U., Haider, M., Conter, M., Goubert, L., Bergier, A., Glaeser, K.-P., Schwalbe, G., Zöller, M., Boujard, O., Hammarström, U., Karlsson, R., Ejsmont, J. A., Wang, T. & Harvey, J. T., (2011), Rolling

Resistance - Basic Information and State-of-the-Art on Measurement methods, In: SANDBERG, U. (ed.), Linköping: Statens väg- och transportforskningsinstitut (VTI).

Thorpe, A. & Harrison, R. M., (2008), Sources and properties of non-exhaust particulate matter from road traffic: a review, Sci Total Environ, 400, 270-82.

Trafikverket, (2015), Vägytemätning Mätstorheter, TDOK 2014:0003, Borlänge: Trafikverket [In Swedish].

Wear particle emissions from cement concrete pavement

Mats Gustafsson[1], Göran Blomqvist[1], Lars Kraft[2]*

[1] National Swedish Road and Transport Research Institute (VTI), SE-58195 Linköping, Sweden, mats.gustafsson@vti.se
[2] Swedish Cement and Concrete Institute, SE-100 44 Stockholm, Sweden

Introduction

In Nordic countries, where studded tyres are used, road surface wear is a problem causing rutting, high maintenance costs and high emissions of inhalable particles (PM_{10}) (Gustafsson et al., 2009; Jacobson & Wågberg, 2007). PM_{10} is regulated according to an EG air quality directive (EG, 2008) and limit values are not to be exceeded in EU member states. Standard asphalts are adapted to be wear resistant and less PM_{10} emitting through durable constructions, including wear resistant and coarse aggregates and high aggregate content, but alternatives to asphalt are of high interest to further reduce the wear (Gustafsson et al., 2009; Gustafsson & Johansson, 2012). Cement concrete road surfaces have certain advantages over conventional asphalt. Generally lower wear, light absorption and fuel consumption as well as lower maintenance costs are the most important ones (Silfwerbrand, 2014). However, concrete pavements are more expensive to build. As wear is generally lower for concrete pavements, it is reasonable to expect that also the formation of inhalable wear particles is lower. In this work, the emission and properties of PM_{10} generated by studded tyres from a concrete pavement construction was compared to that of an asphalt pavement with the same aggregates, using the VTI road simulator (RS) (Gustafsson et al., 2009).

Methods

VTI Circular Road Simulator (RS)

The road simulator (Figure 1) consists of four wheels that run along a circular track with a diameter of 5.3 m. A separate motor is driving each wheel and the speed can be varied up to 70 km/h. An eccentric movement of the vertical axis is used to slowly side shift the tyres over the full width of the track. Any type of pavement can be applied to the simulator track and any type of tyre can be mounted on the axles. An internal air cooling system in the hall is used to temperate the simulator hall to below 0°C to simulate winter conditions. During tests, there is no forced ventilation of the simulator hall and the cooling system is turned off not to contaminate the tests.

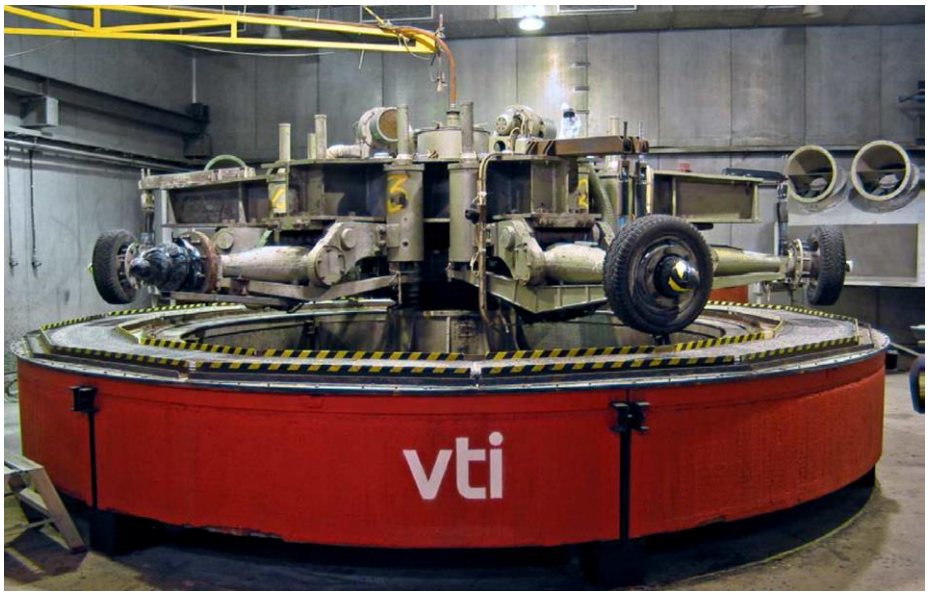

Figure 1: The VTI circular road simulator.

Materials

A reference studded tyre type set (Nokian Hakkapeliitta 7) was used for each pavement test. The concrete was mixed and 28 sector slabs for each test in the road simulator were cast at Betongindustri AB in Linköping, Sweden. After casting, a retarder was applied upon the surface of the concrete slabs in a similar manner as Swedish concrete highway surfaces are prepared. That is for removal of mortar and exposure of the aggregates in order to improve the initial wear resistance and friction. After the surface preparation of the slabs they were moistened and cured under plastic at ~ 20°C and RH ~ 50 %.

The reference stone mastic asphalt (SMA 16) slabs were mixed and manufactured at VTI in Linköping. All pavements used the same wear resistant granite rock aggregates (Figure 2).

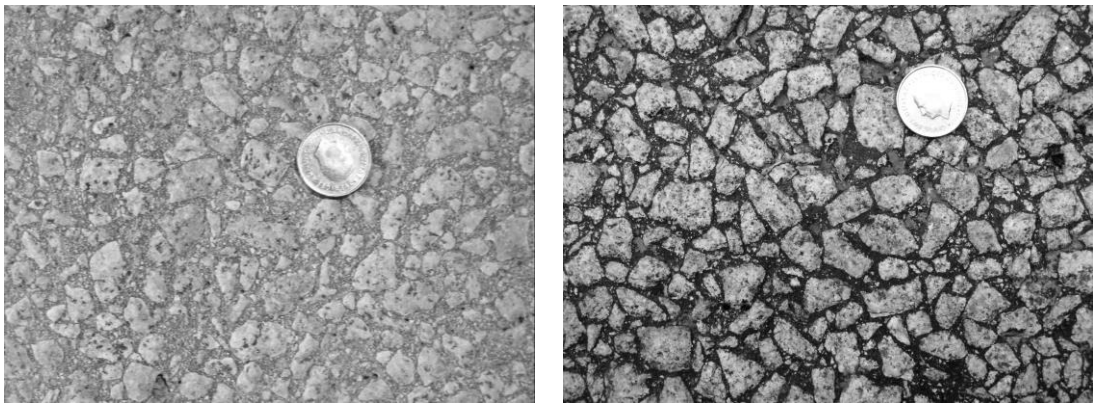

Figure 2: Pavements tested in the CRS. Cement concrete (left) and Stone mastic asphalt (right). Diameter of coin is about 25 mm. Notice the higher aggregate surface density in the asphalt pavement.

Test procedure

Before a test, the simulator hall and the CRS is thoroughly cleaned using high pressure water. The room is then left to dry up and cooled to around 0°C. A large filter fan device is used to clean the air from remaining particles. Tyre inflation pressure and axle load were controlled before the test. The cooling and the filter fan is turned off just before the test and the machine then runs at 30, 50 and 70 km h^{-1} for 1.5, 1.5 and 2 hours is a sequence.

Particle measurement set-up

During the tests, PM_{10} was measured using a tapered element oscillation microbalance TEOM 1400 (RP), particle size distributions using an aerosol particle sizer APS 3321 (TSI Inc.) and a scanning mobility particle sizer SMPS 3080 (TSI inc.). Using a 12-stage cascade impactor (Decati) connected to an aerosol splitter from the PM_{10} inlet of the APS, particle were sampled for element analyses using PIXE (particle induced x-ray emission) (Shariff et al., 2002).

Results

In Figure 3 PM_{10} and number concentration time series from the road simulator tests are shown. The concrete and asphalt pavements produce similar PM_{10} concentrations at 30 km/h, but at 50 and 70 km/h the concrete emits higher amounts pf PM_{10}. The peak appearing as the simulator accelerates to 70 km/h is caused by deposited dust on and around the machine, that is suspended at the increased speed. The number concentration for the asphalt is clearly speed dependant, with higher concentrations at higher speeds. The concrete, though, reacts in a different way. Initially, the number concentration seems speed dependant, but when speed is increased to 70 km/h, only a small peak results followed by a fast decrease in concentration levelling out at a level only marginally higher than at 30 km/h and only a fourth of the concentration produced by the asphalt. This behaviour has been repeated also in later tests of concrete in the road simulator.

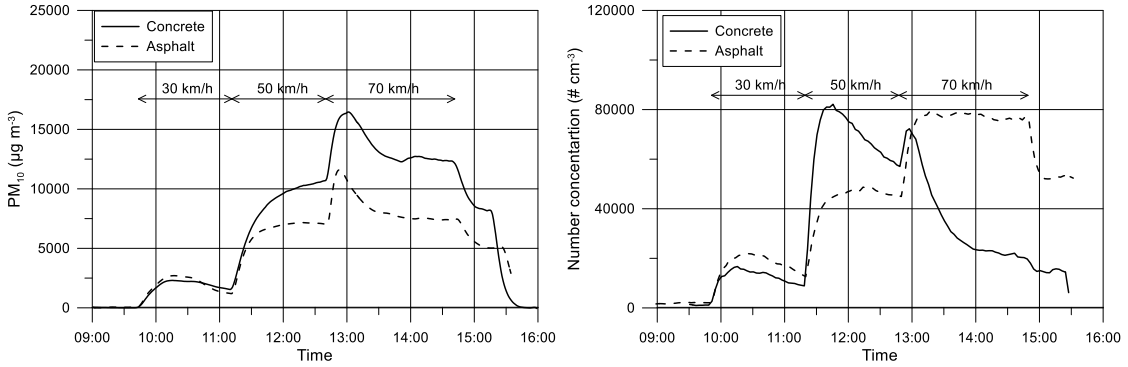

Figure 3. Time series of PM_{10} (left) and particle number (right) concentration during tests in the VTI RS.

The particle mass size distributions (Figure 4, right) reveal that PM_{10} has a mass peak at around 4 µm for concrete and at around 3-4 µm for the asphalt (at 70 km/h). It should be noted that the decrease against coarser fractions is caused by the PM_{10} inlet cut-off A relatively high share is below 2.5 µm, thereby also contributing to fine particle ($PM_{2.5}$) emissions. Ultrafine particles dominated the particle number size distribution (Figure 4, left). The unimodal distribution of the asphalt particles peak at 20 nm, while concrete particles peak at a slightly finer diameter. An interesting feature is the small number peak at 150-200 nm appearing only for the concrete particle size distribution. The ultrafine particles at 20 nm are likely to be formed from friction heat and are to some extent volatile (Dahl et al, 2006). The particles at 150-200 nm seem to be related to wear of the concrete and, since the cement binder is the only difference between the asphalt and concrete pavements, it is likely that these particles are produced from wear of cement.

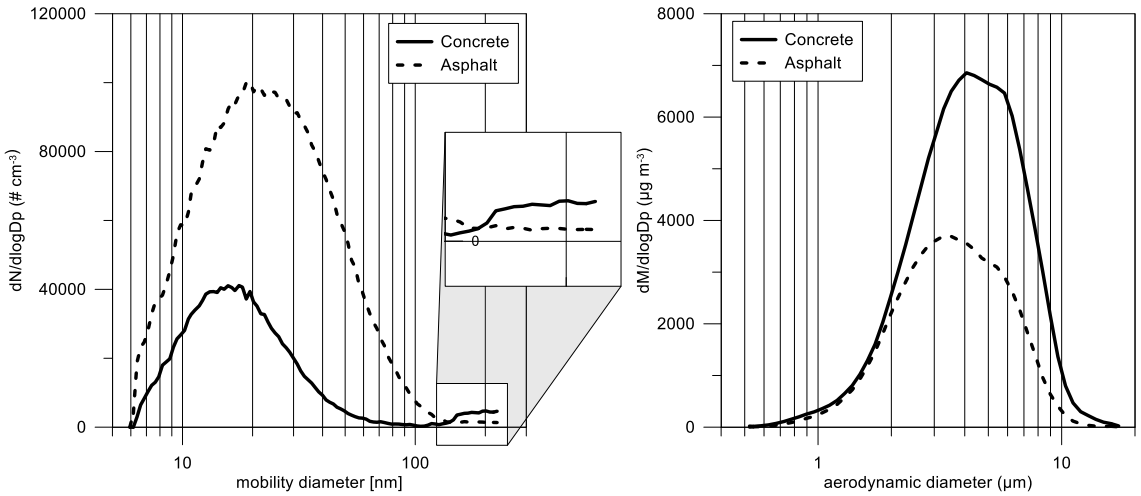

Figure 4. Number and mass size distributions when testing concrete and asphalt in the VTI road simulator. Mean distributions 15 minutes before simulator stop (at 70 km/h).

Bulk analyses of PM_{10} from both material samples reveal that dominating elements are Si, K, Ca and Fe, with smaller contributions of S, Ti, Cu, Mn and Zn (Table 1), reflecting their mineral origin. An abundance of calcium in PM_{10} from concrete, indicates a contribution from the calcium-rich cement binder. On the other hand the asphalt PM_{10} contains relatively more S and tracers, like Cr and Cu, than the concrete.

Table 1: Bulk elemental content in PM_{10} from concrete and asphalt wear (%)

Element	Asphalt	Concrete	Element	Asphalt	Concrete
Si	73.49	61.93	Ni	-	-
P	0.23	-	Cu	0.35	0.03
S	1.39	0.49	Zn	0.18	0.17
Cl	0.11	0.11	As	-	-
K	13.79	10.88	Se	0.01	-
Ca	4.51	19.78	Br	-	-
Ti	0.38	0.40	Rb	0.09	0.06
V	-	-	Sr	0.07	0.09
Cr	0.24	-	Zr	0.03	0.02
Mn	0.09	0.14	W L	0.48	0.33
Fe	4.57	5.56	Pb L	-	0.00

A size resolved analyses reveals how the elements are distributed in different sizes (Figure 5). In the coarser fractions above ca 1 µm, the particle composition is rather stable, indicating a common source or combination of sources. Here, the higher abundance of Ca in the concrete samples is obvious, mainly at the expense of Si and K. Asphalt has a small contribution of S in the coarser fractions that might be related to bitumen. S is abundant in fractions below 1 µm in the asphalt sample, where Si dominate in the concrete. Also, Cr is present in these fractions in the asphalt PM_{10}. It should be kept in mind, though, that the sample amounts at the finest fractions are very small and the analyses more uncertain.

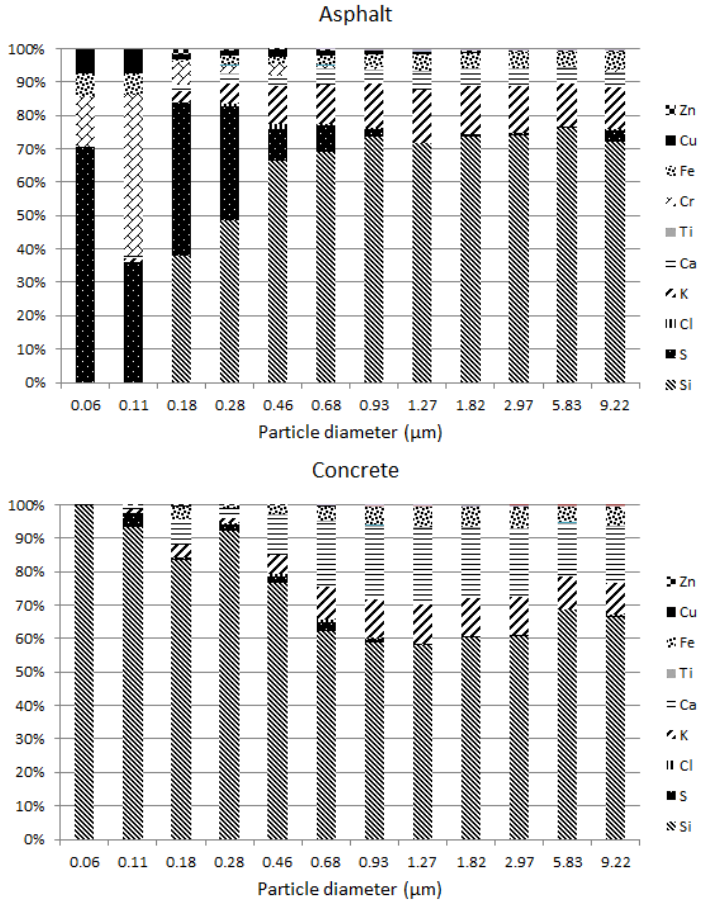

Figure 5. Size resolved elemental composition of PM_{10} from asphalt (top) and concrete (bottom) pavement.

Discussion and conclusions

Road pavement wear as a source for PM_{10} pollution is a matter of great concern, especially in Northern countries with high frequency of studded tyres. Current pavement development towards higher wear resistance therefore also considers lower PM_{10} emissions. Except for asphalt development, also the PM_{10} emission properties of alternatives to standard asphalt pavements are investigated. Mixing of rubber with the bitumen phase, exchanging rock aggregates for slag and using porous pavements are examples of investigations conducted during the last ten years or so, most of which are summarized in (Gustafsson & Johansson, 2012). Since cement concrete pavements are known to be able to wear less and offer longer timespans between maintenance resulting in lower maintenance costs, it has also been expected that the PM_{10} emissions should be lower and cement concrete be a suitable pavement when low PM_{10} emissions are requested.

This investigation shows that cement concrete asphalt might wear less in total (Gustafsson et al., 2015), but the PM_{10} emission is actually higher, due to that the cement binder contributes to a higher degree to PM_{10} than do the bitumen binder in asphalt. The lower surface aggregate density in the concrete is likely to contribute to this result. The results from this test therefore do not indicate that concrete pavements are a suitable abatement measure to use for reduction of PM_{10} emission in winter climate when studded tyres are used.

Particle mass size distributions of PM_{10} is similar to previous investigations (Gehrig et al., 2010; Gustafsson & Johansson, 2012) and the distributions do not differ much between asphalt and concrete. Chemically, the concrete pavement contains more calcium than the asphalt mainly on expense of silica and potassium, while asphalt contains relatively more sulphur and tracers like copper and chromium.

While the mass concentration for both asphalt and cement concrete increases with speed, the particle number concentration (mainly consisting of the ultrafine particle fraction) reacts differently. At the test with cement concrete the concentration declines markedly with time during 50 and 70 km/h. The ultrafine particle fraction has previously been suggested to originate in evaporating and condensing softening oils from tyres. They have also been shown to be more heterogenic than the coarse fraction and also partly volatile (Dahl et al., 2006). The results from this study therefore suggest that an interaction between studs and bitumen might be a more likely source, since the binder is the only parameter differing between the combinations of tyres and pavements tested. Less ultrafine particles seem to form in the interaction between studs and cement. Since the ultrafine size fraction also might be important from a health point of view (Ibald-Mulli et al., 2002; Möller et al., 2005), the reduced emission is a beneficial outcome for the concrete pavements.

Further development of concrete construction and cement binder recipes is needed to reduce wear particle emissions to levels in line with or lower than emissions from standard asphalts with equally wear resistant rock aggregates.

References

Dahl, A., Gharibi, A., Swietlicki, E., Gudmundsson, A., Bohgard, M., Ljungman, A., Blomqvist, G., & Gustafsson, M. (2006). Traffic-generated emissions of ultrafine particles from pavement-tire interface. *Atmospheric Environment, 40*(7), 1314-1323.

EG. (2008). Europaparlamentets och rådets direktiv 2008/50/EG om luftkvalitet och renare luft i Europa.

Gehrig, R., Zeyer, K., Bukowiecki, N., Lienemann, P., Poulikakos, L. D., Furger, M., & Buchmann, B. (2010). Mobile load simulators - A tool to distinguish between the emissions due to abrasion and resuspension of PM10 from road surfaces. *Atmospheric Environment, 44*(38), 4937-4943.

Gustafsson, M., Blomqvist, G., Gudmundsson, A., Dahl, A., Jonsson, P., & Swietlicki, E. (2009). Factors influencing PM10 emissions from road pavement wear. *Atmospheric Environment, 43*(31), 4699-4702. doi:10.1016/j.atmosenv.2008.04.028

Gustafsson, M., & Johansson, C. (2012). *Road pavements and PM10. Summary of the results of research funded by the Swedish Transport Administration on how the properties of road pavements influence emissions and the properties of wear particles. Trafikverket, Report 2012:241.* (ISBN: 978-91-7467-432-3). Retrieved from http://vti.diva-portal.org/smash/get/diva2:674206/FULLTEXT01.pdf

Gustafsson, M., Kraft, L., & Silfwerbrand, J. (2015). *Wear and particle generation of three pavement alternatives, a reference concrete, an experimental photocatalytic concrete, and a standard asphalt pavement*. Paper presented at the 3rd International Conference on Best Practices for Concrete Pavements, Bonito, Brazil.

Ibald-Mulli, A., Wichmann, H. E., Kreyling, W., & Peters, A. (2002). Epidemiological evidence on health effects of ultrafine particles. *J Aerosol Med, 15*, 189 - 201.

Jacobson, T., & Wågberg, L. (2007). *Utveckling och uppgradering av prognosmodell för beläggningsslitage från dubbade däck samt en kunskapsöversikt över inverkande faktorer*. Retrieved from Linköping, Sweden: http://vti.diva-portal.org/smash/get/diva2:670344/FULLTEXT01.pdf
Möller, W., Brown, D. M., Kreyling, W. G., & Stone, V. (2005). Ultrafine particles cause cytoskeletal dysfunctions in macrophages: Role of intracellular calcium. *Particle and Fibre Toxicology, 2*.
Shariff, A., Bülow, K., Elfman, M., Kristiansson, P., Malmqvist, K., & Pallon, J. (2002). Calibration of a new chamber using GUPIX software package for PIXE analysis. *Nucl. Instr. and Methods in Phys. Res., B 189*, 131-137.
Silfwerbrand, J. (2014). *The advantages of concrete pavements in tunnels*. Paper presented at the 12th International Symposium on Concrete Roads, Prague, Czech Republic.

Non-exhaust PM_{10} traffic emissions, road dust loading and the impact of dust binding – application of the NORTRIP emission model

Bruce Rolstad Denby[1], Mats Gustafsson[2], Göran Blomqvist[2], Sara Janhäll[2], Michael Norman[3], Christer Johansson[3,4]

[1] Norwegian Meteorological Institute. PO BOX 43 Blindern, 0313 OSLO, Norway (bruce.denby@met.no)
[2] Swedish National Road and Transport Research Institute, Sweden
[3] Environmental and Health Protection Administration of the City of Stockholm, Sweden
[4] Department of Applied Environmental Science, Stockholm University, Sweden

Introduction

Non-exhaust emissions of particulate matter (PM) from traffic are a significant air pollution problem in many urban areas (Amato et al., 2014), particularly in countries where studded tyres and winter sanding are used (Gustafsson et al., 2008; Norman and Johansson, 2006). Road dust suspension is often worst in spring when road surfaces dry out and road dust that is accumulated during the wet and frozen winter period are suspended into the air. The processes governing these emissions are complex, dependent not only on traffic, tyre and pavement characteristics but also on meteorological conditions and winter time road maintenance activities.

Over the past years the NORTRIP road dust emission model has been developed to describe these emissions (Denby et al., 2013a, 2013b, Norman et al., 2016; Denby et al., 2016). The model includes a range of processes governing road dust surface loading, PM emissions and surface moisture conditions. It solves the mass balance equations for dust loading and surface moisture and predicts the direct and suspended emissions of both dust and salt. The aim of the model is to support the effective implementation of measures for controlling road dust emissions and as such must adequately describe the processes governing these emissions.

Road dust loading is one of the important prognostic variables of the model, as it defines the amount of dust available for suspension. To date, this parameter has never been directly verified by measurement, only through inference by the ability of the model to reproduce enhanced road dust concentrations in spring. In recent years the road dust loading has been measured on streets in Stockholm using the wet dust sampler developed at VTI (The Swedish National Road and Transport Research Institute). This paper presents a comparison between the modelled and measured road dust loading on two streets in Stockholm for three winter seasons. In addition the impact of dust binding, as calculated by the model, is presented and compared to observational estimates available for one of the periods.

Sites and measurements

Measurements of kerb side and urban background PM_{10} concentrations have been carried out for a number of years at several sites in the city of Stockholm. Since 2011 additional measurement data, including road dust loading, have been gathered and road maintenance activities such as dust binding and cleaning have been monitored with the aim of assessing the impact of these activities on the PM_{10} concentrations. Five streets in Stockholm have been monitored during this period and two of these, Hornsgatan and Sveavägen, have been selected for modelling as they provide the best available traffic and meteorological data. Information concerning these measurement campaigns can be found in (Gustafsson et al., 2013; 2014; 2015; 2016; 2017).

One of the measurements undertaken was the road dust loading, measured using the wet dust sampler (WDS). The WDS is a device for repeatable sampling of road dust loading (Jonsson et al., 2008). It uses time controlled washing of a specific circular surface with high pressurized distilled water overlapped and followed by moving the water and dust sample into a sample bottle using an air pump, Figure 1.

These measurements are only carried out once or twice a month as they require road lane closures and intensive manual sampling and analysis. Normally, samples from six sampling spots are aggregated into one larger sample to improve the representability of the surface area. Samples, containing both road dust and any dissolved salts from the road surface are sieved (180 µm), filtered, weighed, burned and weighed again to obtain the inorganic dust load (DL180) and organic content. Samples are taken before filtering for size distribution and after filtering for ion content.

Figure 1. The wet dust sampler (WDS) in the laboratory (left) and in the field (right). (Photo: Mats Gustafsson, VTI).

In addition to the road dust sampling, ambient PM_{10} concentrations were measured at street level and at an urban background roof top site. Meteorological data, used in the modelling, was measured at street level (temperature and humidity), at roof top (wind speed and direction) and at a nearby measurement site (global radiation and precipitation). Information concerning the traffic and street configuration for these two streets is provided in Table 1.

Table 1. Site traffic and road data for the winter season 2013-2014

	Traffic ADT (veh/day)	Number of lanes	Speed (km/hr)	HDV (%)	Studded tyre share (%)	Canyon width / height (m)
Hornsgatan	20 000	4	42	3	31	23 / 25
Sveavägen	22 000	4	38	4.5	48	33 / 25

The NORTRIP model

The NORTRIP model is a coupled road dust/salt and road surface moisture model. It is based on the physical processes that govern the mass balance of water/ice/snow and of dust/salt on the road surface. Included in the model are process descriptions for the energy balance of the road surface, the surface temperature, the impact of salt and acetates on vapour pressure and

melting as well as processes governing the emission and build-up of dust and salt on the road surface.

Road dust emissions and loading are the result of road wear by studded tires as well as contributions from tire and brake wear. These wear sources are each specified with their own size distribution in the model. For road wear almost all of the particles are smaller than 200 µm and the fraction of PM_{10} in this wear is taken to be 28% (Snilsberg et al., 2008) in the model. Friction sanding may also contribute with its own size distribution. Emissions are described as 'direct emissions', the result of wear during dry conditions that are directly emitted or are quickly suspended to the air, and 'suspended emissions', resulting from the build-up of road dust on the surface during wet periods and the subsequent suspension of this dust loading during dry periods. It is the interaction between road surface conditions, dust loading and suspension that makes such a coupled model necessary.

Input data required by the model includes hourly traffic and meteorological data as well as road maintenance activity data for salting, dust binding, cleaning and snow ploughing. Emission factors for exhaust are also included in order to determine the total PM_{10} emissions due to traffic. Conversion of emission data to concentrations, for comparison with measurements, is carried out using NO_X as a tracer. With knowledge of NO_X emission factors and measured NO_X concentrations then a dispersion factor linking emissions and concentrations can be defined and the conversion of PM_{10} emissions to PM_{10} concentrations can be made.

Dust binding is modelled by the impact of dust binders on the surface vapour pressure. The application of salts and acetates lead to a vapour pressure depression on the surface allowing, in the model, water to condense on the surface at a lower atmospheric humidity than 100%. The vapour pressure curves for a number of salts and CMA (calcium magnesium acetate) are shown as a function of solution in Figure 2. When atmospheric and surface temperatures are the same then these curves indicate the relative humidity at which a salt or acetate solution will absorb water from the atmosphere. For example $MgCl_2$ has the largest vapour pressure depression, being able to absorb water from the atmosphere at a relatively low relative humidity of 33%. When the atmospheric humidity is lower than these depression levels then the dust binder will remain dry. Similarly if surface temperatures are higher than atmospheric ones then the dust binder will be less effective since vapour pressure on the surface will increase with temperature.

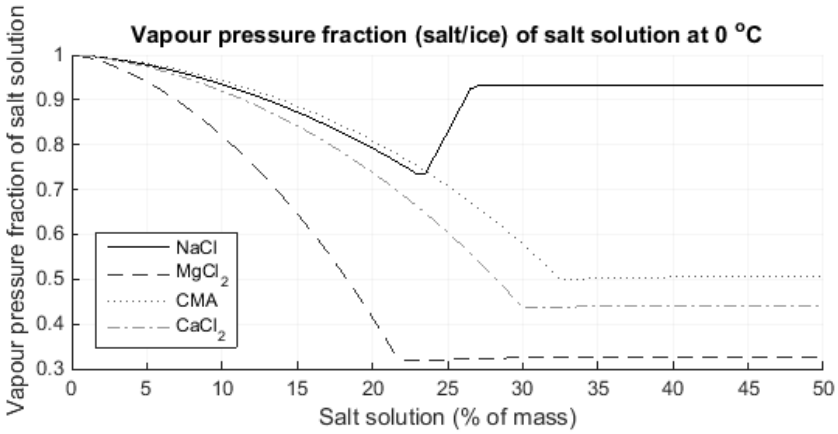

Figure 2. Vapour pressure depression curves applied in the model to simulate dust binding for NaCl, $MgCl_2$, CMA and $CaCl_2$.

The model has been extensively described and assessed in Denby et al. (2013a, 2013b) and the reader is referred to these papers for more details.

Results

Modelled concentrations

The model is applied for three, eight month periods covering the winter seasons of 2011-2012, 2012-2013 and 2013-2014. During these periods ambient air concentrations and road dust loading measurements are available on the two roads Hornsgatan and Sveavägen. Only for one season and one road (Hornsgatan 2011-2012) was friction sanding applied.

Before looking at the road dust loading results, the modelled concentrations are compared to observed net concentrations of PM_{10} (traffic site minus urban background site) for the period 2012-2013 (Figure. 3). The other years show similar results and these are statistically summarized in Table 2. The model successfully represents the observed concentrations for most of the period, including the wet/frozen period from December to February and the spring peak in March. The model tends to underestimate, for 2012-2013, concentrations in April and May.

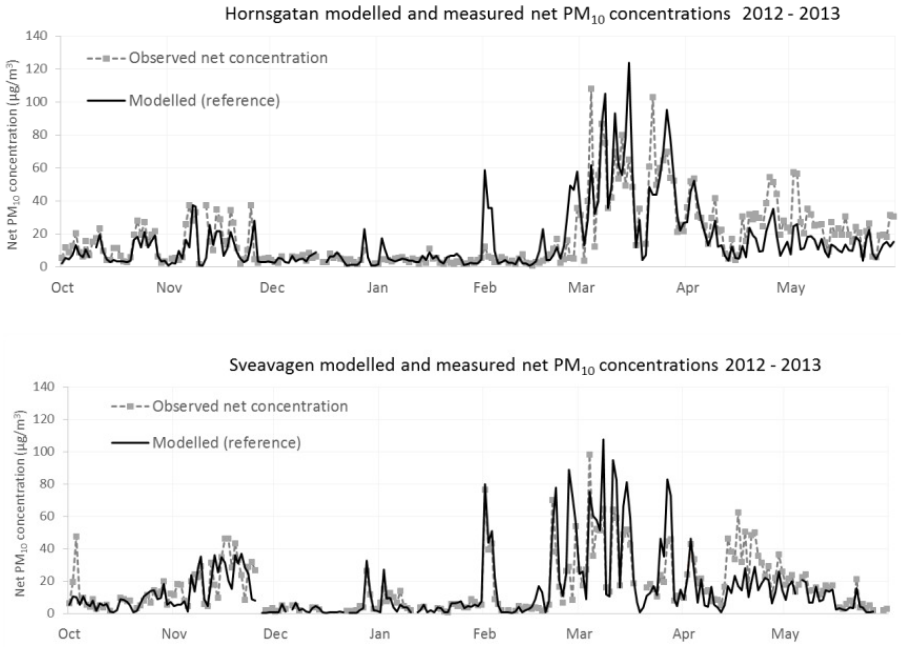

Figure 3. Net modelled and observed daily mean PM_{10} concentrations for Hornsgatan (top) and Sveavägen (bottom) for the modelling period 2012-2013.

In Figure 4 the source and emission process contributions to the model calculations for the period 2013-2014 on Hornsgatan are shown, other years give similar results. The source contributions are dominated by road wear and the emission process contribution is dominated by direct emissions. Only 22% of the total emissions during this period are the result of suspension.

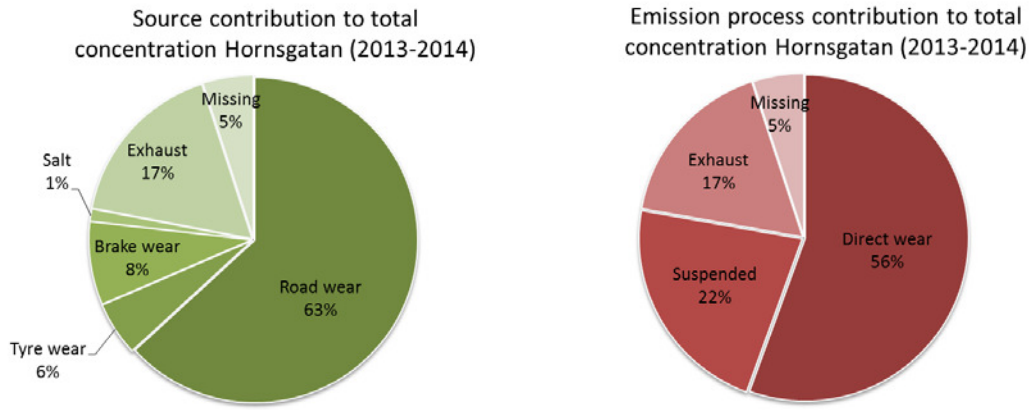

Figure 4. Source contribution (left) and emission process contribution (right) to the modelled PM_{10} concentrations for Hornsgatan 2013-2014. 'Missing' indicates the difference between the mean modelled and observed concentrations.

Table 2. Selected statistics for the three years of modelling. Mean net concentrations (with background concentrations subtracted) and number of exceedance days using total concentrations (including background concentrations) are shown.

PM_{10} dataset	Observed/modelled mean net concentration ($\mu g/m^3$)	Observed/modelled total days with daily mean > 50 $\mu g/m^3$	Daily mean net/total R^2
Hornsgatan 2011-2012	18.2 / 17.9	43 / 44	0.40 / 0.65
Hornsgatan 2012-2013	20.4 / 19.9	46 / 37	0.61 / 0.78
Hornsgatan 2013-2014	18.1 / 17.6	33 / 33	0.34 / 0.60
Sveavägen 2011-2012	17.9 / 16.5	32 / 34	0.34 / 0.60
Sveavägen 2012-2013	20.3 / 21.6	41 / 38	0.59 / 0.74
Sveavägen 2013-2014	14.7 / 15.2	23 / 29	0.16 / 0.49

Modelled dust loading

In Figures 5 – 7 the modelled (DL_{200}) and measured (DL_{180}) road dust loading is shown. Measurements made in the in- and between wheel track regions of the road are shown separately. The measurement data shows a large variation between the two sampling regions, particularly for Hornsgatan which has been shown to have quite different surface textures and dust loadings on the different road regions (Blomqvist, et. al 2013). This also indicates the need for modelling the two regions of the road separately. At this stage the model treats the road as one single surface and the individual effects of e.g. tire and vehicle wake turbulence, different driving behaviour (changing lanes) in the different streets, or the possible effects of different textures is not taken into account (Gustafsson et al., 2013; 2014; 2015). The model best reproduces surface dust loading for Sveavägen, which has a smoother and more consistent surface, also reflected in the lower dust load. On Hornsgatan, with a consistently higher dust load, the model reproduces best the wheel track measurements.

In the model calculations the efficiency of cleaning for the removal of dust was set to a very low value and this process contributes little to the removal of dust (Figure 8). This was necessary in order to reproduce the observed concentrations and supports previous measurement analysis

that cleaning seems to have little impact on the PM_{10} concentrations (Amato et al., 2010; Gustafsson et al., 2013; 2014; 2015).

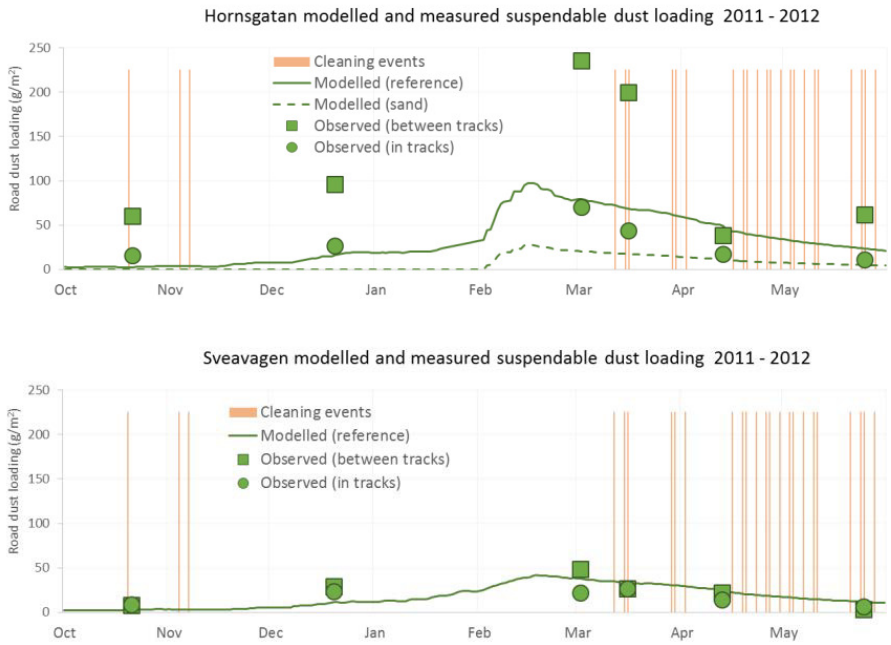

Figure 5. Measured and modelled road dust loading for the period 2011-2012 on Hornsgatan (top) and Sveavägen (bottom). In track (circle) and between tracks (squares) measurements are shown separately. Also shown are the cleaning events undertaken. For this year cleaning was undertaken with a wet vacuum cleaner.

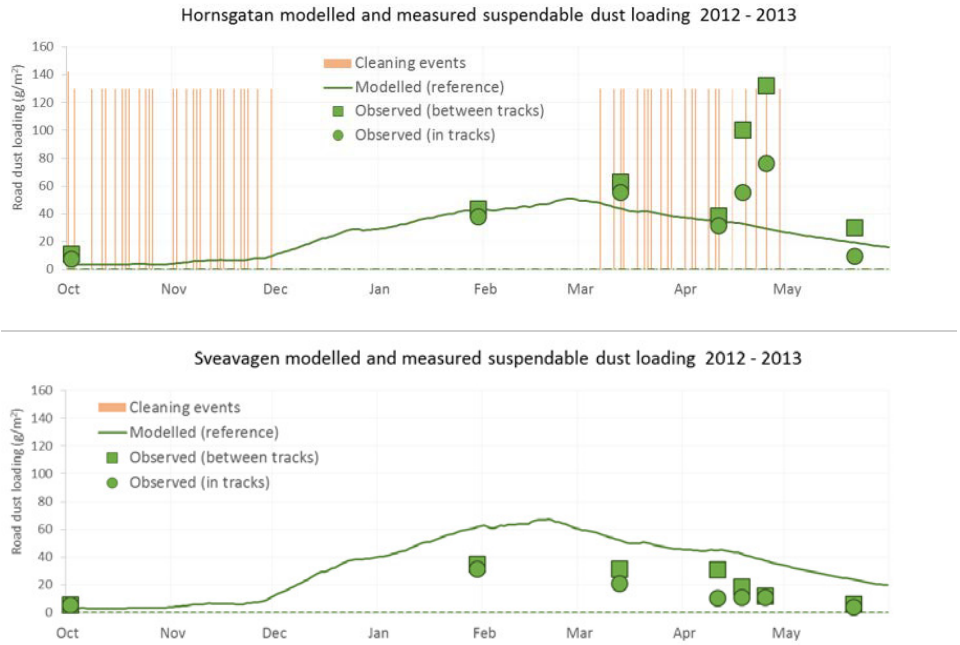

Figure 6. As in Figure 5 but for the period 2012-2013. No PM_{10} abatement cleaning was carried out on Sveavägen during this season.

Two sensitivity studies were implemented for the season 2013-2014 (Figure 7). The first removed the road dust sink term associated with drainage (no drain) and the second assumed that all road dust generated was retained on the road surface (all retained), so that there were no 'direct' emissions, only emissions through suspension. The first represents uncertainty in the drainage process and the second the maximum possible loading obtainable given the calculated road wear.

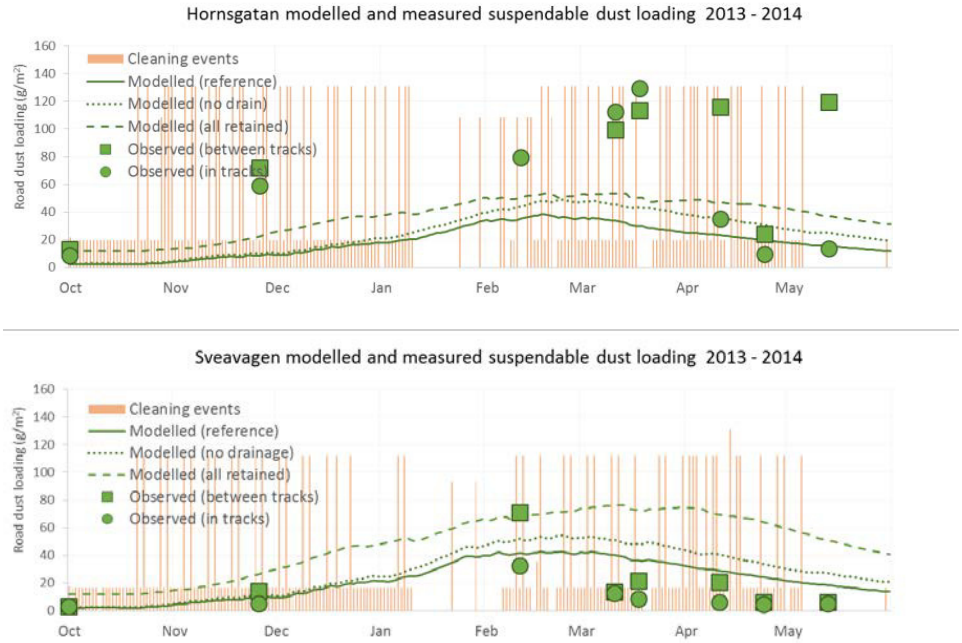

Figure 7. As in Figure 5 but for the period 2013-2014. For this year cleaning was undertaken with a dry vacuum cleaner, large cleaning bars, and the smaller cleaning bars represent regular sweeping activities. The dashed and dotted lines represent a model sensitivity study, see text for details.

In Figure 8 the contribution of the different processes governing the road dust loading is shown for the 2013-2014 season on both roads. For the current model application the production of road dust through the retainment of wear is balanced mostly by the removal through suspension and drainage. Spray, at low speeds, is not significant and cleaning has been set to a low efficiency.

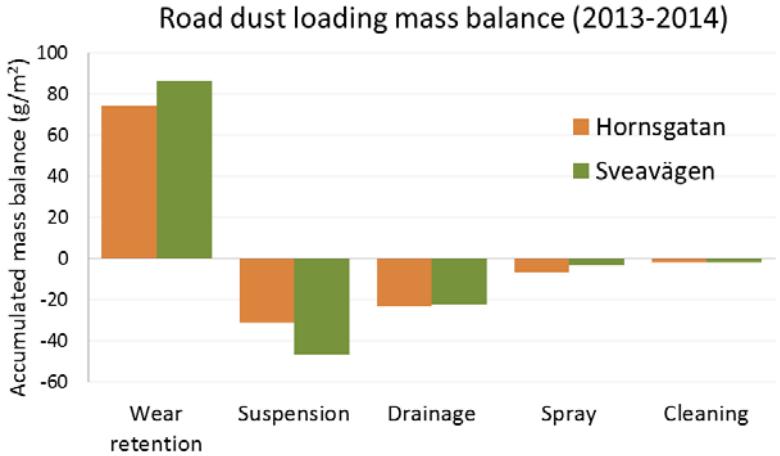

Figure 8. Modelled road dust loading mass balance for the winter season 2013-2014.

Modelled dust binding

To assess the impact of dust binding during the spring period of 2012, observed concentrations of PM_{10} on Hornsgatan were compared to a similar reference street, Folkungagatan, where dust binding was not applied. The reduction of local PM_{10} concentrations due to dust binding on dust binding days, after correction for differences between the two streets, was found to be 43% of the net concentration (Gustafsson et al., 2013). The same spring period was also modelled and the results are presented in Figure 9. The result of the modelling, Figure 9 top, underestimates the amount of CMA loading on the surface during this period when compared to measurements. However, it is uncertain exactly how much CMA was actually applied. Other periods modelled for CMA show a good correspondence between observed and modelled CMA loading. The impact on PM_{10} concentrations is also shown, Figure 9 bottom. This is found to be significant and the average reduction of net PM_{10} concentrations during dust binding days was found to be 36%. This is similar to the observed estimate of 42% made from observations.

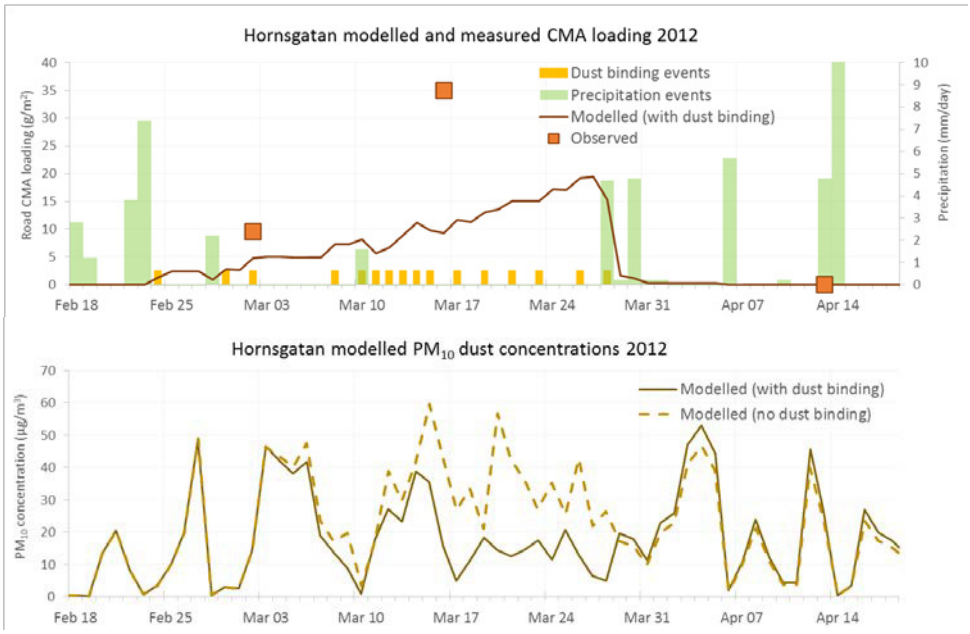

Figure 9. Calculations using NORTRIP assessing the impact of dust binding on Hornsgatan during the spring period of 2012. The top figure shows the CMA application and the build-up of CMA on the street during this period. The bottom figure shows the net modelled daily mean concentrations with and without dust binding. The average modelled reduction in PM_{10} emissions due to dust binding, on dust binding days, was found to be 36%.

Discussion and conclusions

Modelling road dust emissions and road dust loadings is a challenging task. In this paper we show the first comparison of modelled and measured road dust loadings for two roads in Stockholm. For one of the roads, Sveavägen, the model fairly successfully reproduces the observed road dust loading but for the other road, Hornsgatan, the results are less satisfactory. The results for Hornsgatan are influenced by the variable surface texture, which results in large measurement differences between the in- and between wheel track regions of the road surface. The NORTRIP model does not currently distinguish between these regions and does not contain a description of the impact of surface texture on the road dust removal processes.

Despite this, the PM_{10} concentrations are reasonably well modelled for both roads for the three years shown, as they have been for previous years (Denby et al, 2013b). Since the model calculates suspended contributions to the total concentrations of around 20 - 25% for these roads during these periods, an error in the calculated road dust loading of 100% will only lead to a 10% error in the calculated total concentrations, similar to other uncertainties in the model.

Modelling of the impact of dust binding for one street and one season was compared to observational estimates. The modelled reduction of net PM_{10} concentrations due to dust binding was found to be 36% and the observed estimate was very similar at 42%. Though the model successfully predicted this reduction during this period, when observations were available for comparison, other periods modelled showed less impact of dust binding as this is dependent on the atmospheric and road conditions during the period.

In order to advance the modelling more information is needed concerning the wet removal processes of drainage and vehicle spray. Across street measurements of road dust (Gustafsson et al., 2015) indicate significant build-up of dust at the curbside and between lanes. A single track model, as NORTRIP currently is, cannot represent this distribution so the development of a multi-track description of the model would be necessary. This will be able to account for differences between in- and between-wheel track processes (suspension, spray) and will also allow the redistribution of accumulated dust that occurs during cleaning. In addition to the multi-track modelling the effect of road surface texture on road dust processes such as drainage, spray, cleaning, suspension needs to be addressed if a more universal application of the model is to be implemented.

Aknowledgements

This work was supported by the Nordic Council of Ministers, the Traffic Office at the City of Stockholm and the Norwegian Road authorities.

References

Amato F., Querol X., Johansson C., Nagl C., Alastuey A. (2010). A review on the effectiveness of street sweeping, washing and dust suppressants as urban PM control methods. *Sci Total Environ.* 2010 Jul 15;408(16):3070-84. doi: 10.1016/j.scitotenv.2010.04.025

Amato F, Cassee FR, Denier van der Gon HAC, Gehrig R, Gustafsson M, Hafner W, Harrison RM, Jozwicka M, Kelly FJ, Moreno T, Prevot ASH, Schaap M, Sunyer J, Querol X. (2014). Urban air quality: The challenge of traffic non-exhaust emissions. *Journal of Hazardous Materials*; 275: 31-36.

Blomqvist, G., Gustafsson, M. & Lundberg, T., 2013. Road surface dust load is dependent on road surface macro texture. *Extended abstract presented at the 2013 European Aerosol Conference,* September 1–6, 2013 in Prague Czech Republic.

Denby, B.R. , M. Ketzel, T. Ellermann, A. Stojiljkovic, K. Kupiainen, J.V. Niemi, M. Norman, C. Johansson, M. Gustafsson, G. Blomqvist, S. Janhäll, I. Sundvor, (2016) Road salt emissions: A comparison of measurements and modelling using the NORTRIP road dust emission model, *Atmos. Environ.*, Volume 141, September 2016, Pages 508-522, ISSN 1352-2310, http://dx.doi.org/10.1016/j.atmosenv.2016.07.027

Denby, B.R., Sundvor, I., Johansson, C., Pirjola, L., Ketzel, M., Norman, M., Kupiainen, K. , Gustafsson, M., Blomqvist, G. and Omstedt, G. (2013a). A coupled road dust and surface moisture model to predict non-exhaust road traffic induced particle emissions (NORTRIP). Part 1: road dust loading and suspension modelling. *Atmos. Environ.* 77, 283-300. http://dx.doi.org/10.1016/j.atmosenv.2013.04.069

Denby, B.R., Sundvor, I., Johansson, C., Pirjola, L., Ketzel, M., Norman, M., Kupiainen, K. , Gustafsson, M., Blomqvist, G., Kauhaniemi, M. and Omstedt, G. (2013b). A coupled road dust and surface moisture model to predict non-exhaust road traffic induced particle emis-sions (NORTRIP). Part 2: surface moisture and salt impact modelling. *Atmos. Environ.,* 81, 485-503. DOI: http://dx.doi.org/10.1016/j.atmosenv.2013.09.003

Gustafsson, M., Blomquist, G., Gudmundsson, A., Dahl, A., Jonsson, P., Swietlicki, E., 2008. Factors affecting PM10 emissions from road pavement wear. *Atmos. Environ.,* 43, 4699-4702.

Gustafsson, M. ,G. Blomqvist, C. Johansson and M. Norman (2013). Operational measures against PM10 pollution in Stockholm – evaluation of winter season 2011–2012. *VTI report 767* (In Swedish). http://www.vti.se/sv/publikationer/driftatgarder-mot-pm10-pa-hornsgatan-och-sveavagen-i-stockholm---utvardering-av-vintersasongen-20112012/

Gustafsson, M., G. Blomqvist, S. Janhäll, C. Johansson and M. Norman (2014). Operational measures against PM10 pollution in Stockholm – evaluation of winter season 2012–2013. *VTI report 802* (In Swedish). http://www.vti.se/sv/publikationer/driftatgarder-mot-pm10-i-stockholm--utvardering-av-vintersasongen-20122013/

Gustafsson, M., G. Blomqvist, S. Janhäll, C. Johansson and M. Norman (2015). Operational measures against PM10 pollution in Stockholm – evaluation of winter season 2013–2014. *VTI report 847* (In Swedish). http://www.vti.se/en/publications/operational-measures-against-pm10-pollution-in-stockholm-evaluation-of-winter-season-20132014/

Gustafsson, M., Blomqvist, G., Janhäll, S., Johansson, C., Norman, M., & Silvergren, S. (2016). Driftåtgärder mot PM10 i Stockholm : utvärdering av vintersäsongen 2014-2015.

Gustafsson, M., Blomqvist, G., Janhäll, S., Järlskog, I., Johansson, C., Lundberg, J., Norman, M., & Silvergren, S. (2017). Driftåtgärder mot PM10 i Stockholm : utvärdering av vintersäsongen 2015-2016

Jonsson P, Blomqvist G, Gustafsson M. (2008). Wet Dust Sampler: Technological Innovation for Sampling Particles and Salt on Road Surface. *Seventh International Symposium on Snow Removal and Ice Control Technology, Transportation Research Circular E-C126*: 102-111.

Norman, M., I. Sundvor, B.R. Denby, C. Johansson, M. Gustafsson, G. Blomqvist, S. Janhäll, (2016) Modelling road dust emission abatement measures using the NORTRIP model: Vehicle speed and studded tyre reduction, *Atmos. Environ.*, Volume 134, June 2016, Pages 96-108, ISSN 1352-2310, http://dx.doi.org/10.1016/j.atmosenv.2016.03.035.

Norman M., Johansson C. (2006). Studies of some measures to reduce road dust emissions from paved roads in Scandinavia. *Atmos. Environ.,* 40, 6154-6164.

Snilsberg, B., Myran, T., Uthus, N. (2008). The influence of driving speed and tires on road dust properties. In: B. Snilsberg: Pavement wear and airborne dust pollution in Norway. Characterization of the physical and chemical properties of dust particles. Doctoral Thesis. Trondheim, Norwegian University of Science and Technology. (Doctoral theses at NTNU, 2008:133).

PACLA (PArticle CLAssifier): A Novel Approach for Quantification and Differentiation of Primary Particulate Matter (PM) Emitted by Road and Railway Transport

J. Rausch[1,2], T. Zünd[1], M. Meier[1,2], D. Jaramillo Vogel[1,2], R. Locher[3] and K. Kammer[4]*

[1]Particle Vision GmbH, c/o Fri Up, Annexe 2, Passage du Cardinal 11, Fribourg, 1700, Switzerland, juanita.rausch@particle-vision.ch

[2]Department of Earth Sciences, University of Fribourg, Fribourg, 1700, Switzerland

[3]Institute of Data Analysis and Process Design (IDP), Zurich University of Applied Sciences (ZHAW), Winterthur, 8400, Switzerland

[4]Federal Office for the Environment (FOEN), Bern, 3003, Switzerland

Introduction

Particulate Matter (PM) is an important air quality parameter due to its environmental and health impact. From PM_{10} measurements according to DIN EN12341, no conclusions can be drawn about the contribution of the diverse sources. Following a new sampling and analytical approach, the proportions for the PM_{10} main sources, regarding primary particles, can be determined. This approach is based on a selective sampling for coarse and fine mode particles, which are subsequently analyzed on their morpho-chemical properties by automated scanning electron microscopy (SEM) coupled with energy dispersive X-ray spectroscopy (EDX). Due to the complexity of the multidimensional SEM/EDX results a statistical software for particle classification was developed and used for data interpretation.

Sampling

Coarse mode sampling (Sigma-2 passive sampler)

The coarse mode ($PM_{10-2.5}$) was sampled passively on boron substrates with the Sigma-2 passive sampler (VDI 2119:2013) (Fig. 1).

Figure 1: Left image: Sigma-2 passive sampler; right image: adhesive surface with different substrates. Boron (lower right corner) and carbon pad (upper right corner) for REM/EDS analysis. Glass plate (left) for light microscopy.

Fine mode sampling (SKC Airchek3000)

The fine mode ($PM_{2.5}$) was collected actively on polycarbonate filters using the AirChek 3000 air pump system (Fig. 2).

Figure 2: SKC Airchek3000 air pump system (left) and sampling housing with polycarbonate filter (right).

Analytical Methods:

Automated single particle SEM/EDX analysis coupled to the PArticle CLAssifier PACLA

All 32 collected samples were analyzed by automated SEM/EDX. Analyses were run with a FEI XL30 SFEG microscope at the University of Fribourg (Switzerland) using an acceleration voltage of 20 keV. Compositional data obtained by SEM/EDX was ZAF corrected. Automated SEM/EDX analysis is able to produce detailed chemical and morphological data of a significant number of single particles (Fig. 3), which can be used for source apportionment studies.

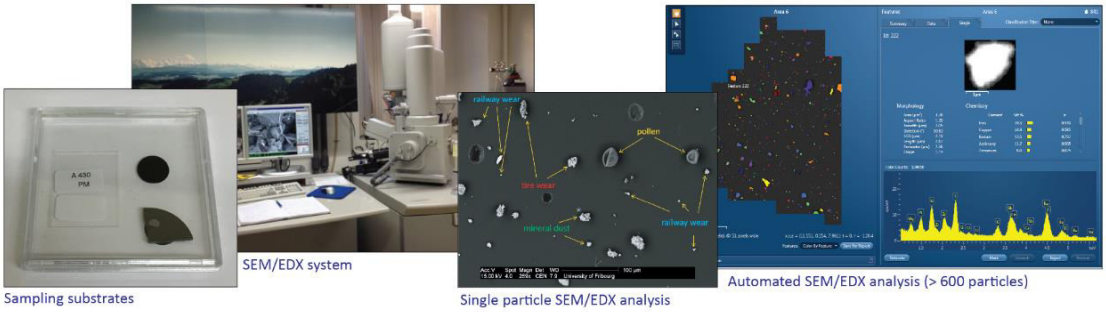

Figure 3: Automated Scanning Electron Microscopy (SEM) coupled with Energy Dispersive X-ray spectroscopy (EDX).

However, a major issue of this method is the time-consuming data treatment and interpretation. To deal with this issue we developed a particle classifier [1] able to classify homogeneous and mixed particles based on their chemical composition. It was trained with SEM/EDX results of > 55000 single particles from different environments (83 samples).

The performance of the SEM/EDX analyses and of the subsequent clustering with PACLA was tested on standard glasses (Fig. 4). For particle classification a two-stage procedure is applied. The first stage is a rule-based filter grouping particles consisting of the same elements with a content ≥ 5 wt.%, into so called main classes. In the second stage, a robust model-based clustering method using the R package tclust is applied to each main class resulting in subclasses (Fig. 5). Outliers are excluded automatically and hence have no effect on the shape of the subclasses. The above-mentioned training of single particles from different environments delivered 465 subclasses within 227 main classes. The subclasses were manually verified and assigned to known substances (Fig. 6).

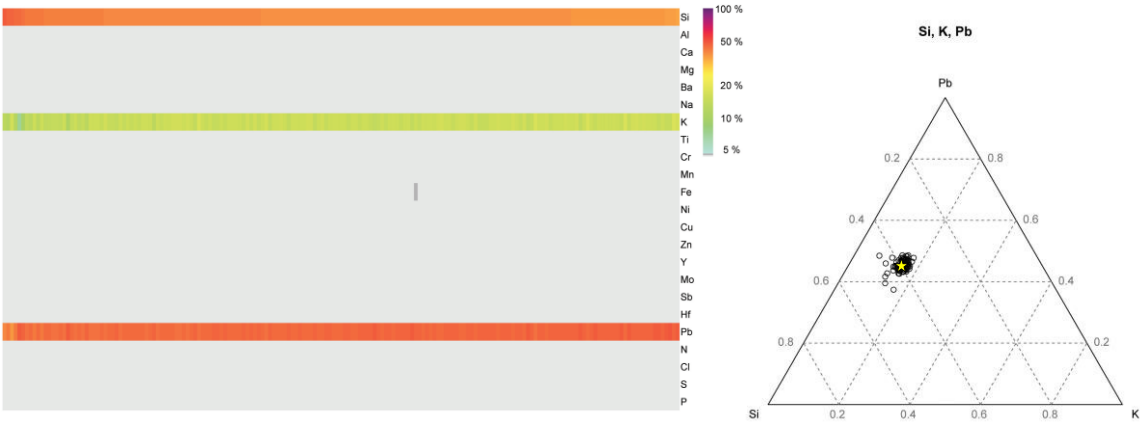

Figure 4: Left: Heatmap showing composition of a standard glass consisting of 44.7 wt.% Pb, 39.6 wt.% Si and 14.8 wt.% K. EDX spectra were obtained from > 500 single particles ranging from 1 to 15 µm. Right: Ternary diagram showing the Si, Pb, K proportion in the same standard glass measurement (yellow star shows glass composition).

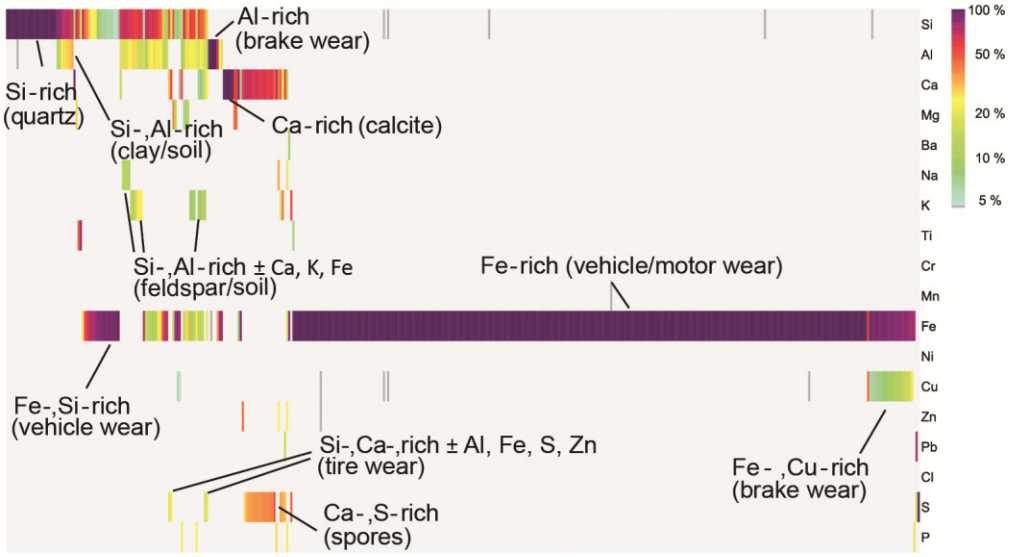

Figure 5: Heatmap showing typical classes and subclasses for a road traffic site.

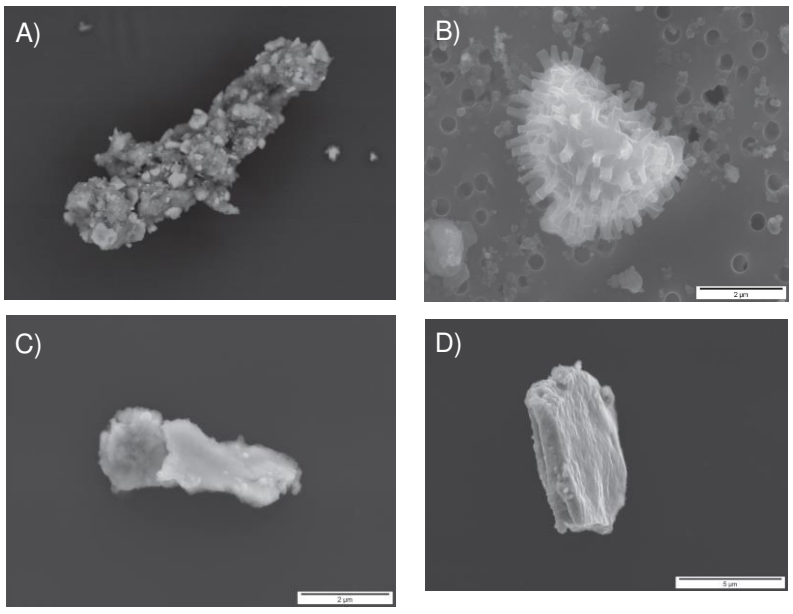

Figure 6: Typical particles found close to road and railway lines. A) tire wear (C, Si, Ca ± Al, Fe, K, S, Zn), B) biogenic particle (spore) (C, N ± K, P, Ca, S), C) iron-rich brake wear (Fe, Cu ± C, Zn) and D) railway wear (Fe ± Si, C).

Carbon and secondary particles

A determination of elemental carbon from road and railway traffic (pantograph ablation) was not performed in this pilot project. However, it could be implemented in a future study since newly developed boron substrates enable the semi-quantitative analysis of the element carbon. Due to limitations in SEM/EDX methodology, secondary particles were neither considered. It is, therefore, important to note that the results mentioned in this case study are "only" based on the primary particles emitted, excluding the elementary carbon.
This restriction is not of great relevance for the assessment of the railway traffic particles, since, in the case of purely electric operation, only volatile compounds are created via the braking process with composite brakes, which can lead to the emission of secondary particles.
In the case of road traffic, it is known to emit nitrogen oxides (NOx) and volatile organic compounds (VOC), which are converted to a large percentage into secondary particles (nitrates, organic mass etc.). However, due to their delayed formation away from the source, they cannot longer be allocated quantitatively to any source.

Context of case study

The MFM-U (Monitoring Flankierende Massnahmen Umwelt) project was launched in 2003 by the Swiss authorities to monitor and control the environmental impact of freight traffic crossing the Swiss Alps. Within the frame of this project, the portion of PM_{10} emitted from a specific highway and railway segment in the Alpine north-south axis (Altdorf, Reuss valley, Canton of Uri, Switzerland) was studied in a pilot project between September and October 2016 [2]. The aim was to characterize, quantify and differentiate the non-exhaust primary particulate matter and study the lateral dispersion of the emitted pollutants. For this purpose, a transect consisting of two emission and two immission sites, located between the A2 highway and the AlpTransit railway line, was deployed (Fig.7). Passive [3] and active sampling was performed during 4 weeks in sampling periods of one week.

Results and discussion

The morpho-chemical results of the particulate matter were evaluated with the recently developed particle classifier PACLA, which enables the classification of airborne particles based on their chemical composition and size. In addition, the particle classifier allows to plot the concentration of each chemical class along transects (Fig. 7), thus, facilitating the recognition of their emission point and dispersion trends. Chemical fingerprints were compared to reference samples, and in the case of a positive match, they were assigned to a specific source (e.g. railway, road traffic, biogenic, geogenic etc.).

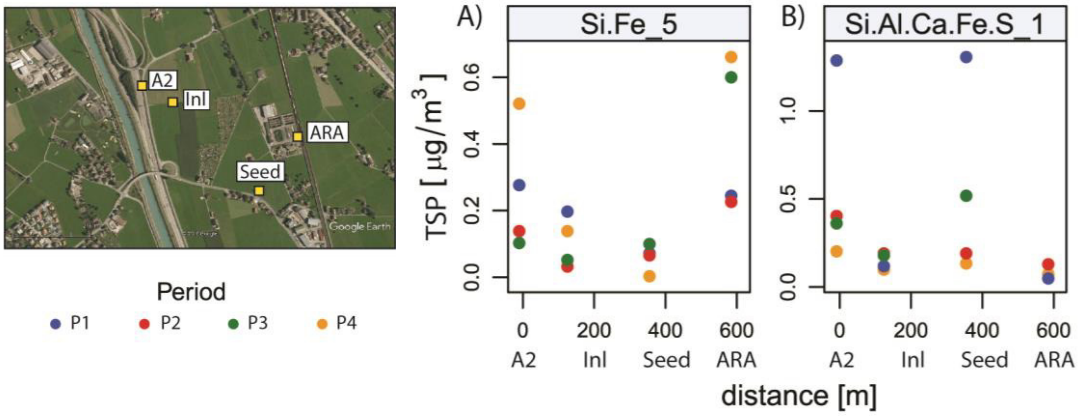

Figure 7: A) TSP transect plot of the subclass Si.Fe_5 (railway, wheel and vehicle wear) and B) Si.Al.Ca.Fe.S_1 (tire wear). Inset map: location of sites.

This study shows that the emissions of railway and road traffic are in part very similar (e.g. Fe-rich particles). However, road traffic emissions are by far more heterogeneous consisting of at least 47 different chemical subclasses. The PM_{10} concentrations of non-exhaust primary particles

emitted by the road and railway traffic obtained in this study are mainly dictated by the Fe-rich particles (13-52 % of measured PM_{10}). In the case of road traffic, tire wear plays an additional important role (22-38 %). The most relevant groups regarding the PM_{10} mass of particles emitted by railway and road traffic are summarized in Table 1. The low concentration of brake wear measured along the railway can be explained by the fact that the studied railway segment is lacking curves and inclination.

Table 1: PM_{10} relevant chemical classes of railway and road emissions (oxygen is not considered).

Emission source	Composition	Typical size (µm)
railway transport		
railway/wheel wear	Fe ± Si, Ca	0.1-10
overhead line wear	Cu	0.1-2.5
pantograph wear	C	0.1-2.5
brake wear	Fe, C ± Cu, Zn	0.1-2.5
road transport		
vehicle wear	Fe ± Si	0.1-2.5
brake wear	Fe ± Cu, Zn, Ca, Cr, Al, Si, S	0.1-2.5
tire wear	C, Si, Ca, Al ± Na, K, Fe, S, Zn	1-100
soot agglomerates	C	0.01 0.5

After successful identification of the different particle sources it is possible to compare the contribution of the different pollutants and natural sources at the studied sites, as shown in figure 8. The transect measurements reveal that the contribution of the coarse particles ($PM_{10-2.5}$), from both sources (i.e. railway and road traffic), to the immission sites, is generally low and strongly dependent on wind velocities, as well as, prevalent wind direction. At higher wind speeds these particles are transported longer distances in the wind direction, while under low wind speeds they sediment near the source. For this specific geographic location, it must be noted that the wind often blows along the valley axis and, thus, parallel to the A2 highway (A2 site), respectively to the Alp Transit railway line (ARA site), making a lateral particle spread unlikely.

The higher concentration of mineral particles at the emission sites along the A2 and the railway line are interpreted to result from the resuspension of previously sedimented particles due to strong airstreams generated by the passing vehicles and trains.

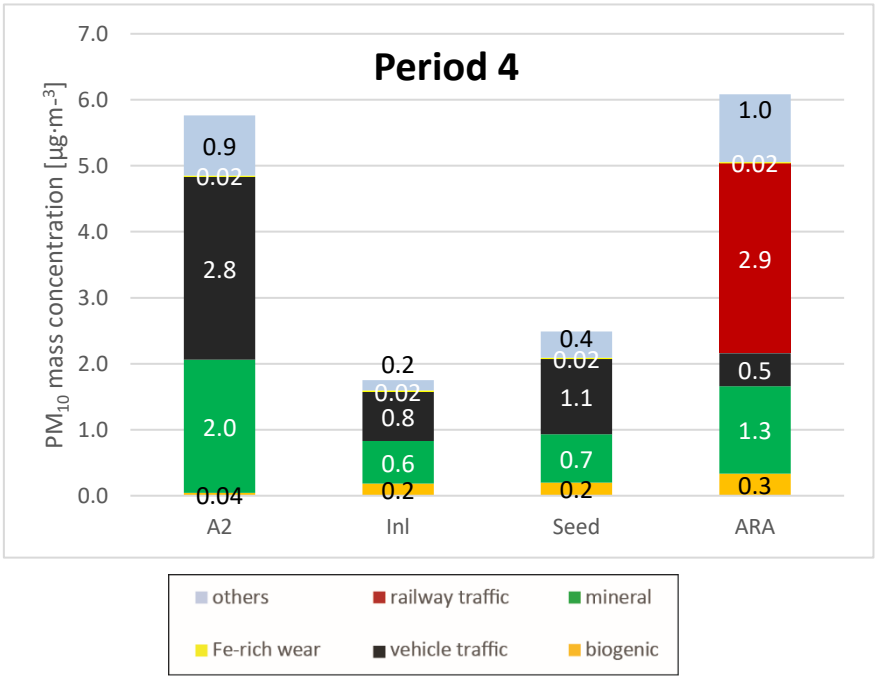

Figure 8: Bar diagram showing the concentration of the main sources (i.e. mineral, biogenic, vehicle, railway traffic and others) at the 4 studied sites during period 4. The category "Fe-rich wear" (bright yellow) represents a background concentration.

$PM_{2.5}$ particles show a completely different transport behaviour. They are finely dispersed in the air independent of the wind conditions. Thus, it can be generalized that $PM_{2.5}$ particles measured away from the emitting source mainly represent a background concentration.

Even though the mass concentration of $PM_{2.5}$ is in general low at all studied sites, a high number concentration of Fe-rich particles was observed at the A2 and ARA sites in all four studied periods. This behaviour is related to the small mass of fine dust (cubic relationship between decrease of the mass of a particle in comparison to its diameter decrease).

This implies that the mass concentration is not a meaningful parameter for such small but potentially harmful particles since it underestimates the occurrence of these respirable particles.

References

[1] The particle classifier (PACLA) was developed in collaboration with the Institute of Data Analysis and Process Design (IDP) at the Zurich University of Applied Sciences (ZHAW) and the Department of Geosciences at the University of Fribourg (Switzerland), and was financially supported by the Swiss Commission for Technology and Innovation (CTI project 16675.1 PFIW-IW).

[2] The case study was performed on behalf of the Swiss Federal Office for the Environment (FOEN). The complete report can be downloaded under the following link: https://www.bafu.admin.ch/dam/bafu/de/dokumente/daten-karten/externe-studien-berichte/bestimmung-des-pm10-anteils-aus-dem-schienen-und-strassenverkehr-im-urner-reusstal-altdorf-kt-uri.pdf.download.pdf/Bericht_MFM-U_Pilotprojekt_2016_V1.31.pdf

[3] Sigma-2 passive sampling method: VDI, VDI2119:2013-06, Beuth Verlag, 10772, Berlin, Germany, 2013

Particle and gaseous emissions from a dual-fuel marine engine

K. Lehtoranta[1], T. Murtonen[1], H. Vesala[1], P. Koponen[1], P. Karjalainen[2], L. Ntziachristos[2], N. Kuittinen[2], J. Alanen[2],T. Rönkkö[2], J. Keskinen[2], M. Aurela[3], H. Timonen[3]

[1] VTT Technical Research Centre of Finland, Espoo, Finland

[2] Tampere University of Technology, Tampere, Finland

[3] Finnish Meteorological Institute, Helsinki, Finland

Corresponding author email: kati.lehtoranta@vtt.fi

Introduction

The emissions from ships can be a significant source of air pollution in coastal areas and port cities and can have negative impact on human health and climate (Eyring et al. 2010; Corbett et al. 2007; Viana et al. 2014).

The International Maritime Organization (IMO) has implemented regulations to reduce emissions from ships. So far, these regulations consider only emissions of nitrogen oxides (NO_x) and sulphur oxides (SO_x). Limitations are set globally while stricter limits exist for special emission control areas. Since January 2015 the allowed sulphur content in marine fuel oils is limited to 0.1 % in sulphur emission control areas (SECAs). The global limit, at the moment, is 3.5 % S, with a stricter regulation of 0.5 % S coming in 2020. This sulphur decrease can be achieved either with decreasing the fuel sulphur level or by using exhaust after-treatment (like scrubbers).

Although no global emission limits for particulate matter (PM) emitted by ships exist, the SO_x regulation is expected to have an indirect impact on particle emissions, i.e. by decreasing the fuel sulphur level this would also decrease the formation of sulphate particle emissions.

The limits for NO_x emissions are set for engines depending on the engine maximum operating speed and are divided into three categories (Tiers I, II, III). The strictest (Tier III) applies for ships operating in NO_x emission control areas (NECAs). This increases the use of emission control technologies, selective catalytic reduction (SCR) being the most prevailing and effective NO_x abatement technology.

One way to achieve the needed low levels of NO_x and SO_x, without any after-treatment technologies on-board, is to use natural gas as a fuel by proper engine modification or as an option for new engines. So far only few studies have addressed the particle and gaseous emissions from gas powered ship engines (Anderson et al. 2015).

In the present study, we investigated the gaseous and particle emissions from a dual-fuel marine engine utilizing natural gas as the main fuel. For comparison, the engine was also operated with a liquid diesel fuel.

Experimental

The engine was a Wärtsilä Vasa 4R32, a four-cylinder medium-speed diesel engine that was modified to run with natural gas in dual fuel mode. The maximum power for this engine was 1400 kW. In addition to natural gas, which was used as main fuel, a pilot liquid fuel was needed to operate the engine. The natural gas was from Nordstream and was high in methane content (>95%). The pilot (liquid) fuel was marine gas oil (MGO) which was of road diesel quality (EN 590:2009) with very low sulphur level. For comparison, the engine was also operated with MGO as pilot and main fuel. Engine oil type was Shell Argina XL 40.

The engine was tested in various modes from 30% to 85% of full load. Main experiments were conducted on 40% and 85% loads which were selected to represent the conditions at open sea (85%) and at harbour areas (40%). The amount of pilot fuel in normal condition was 1% of total fuel flow at 85% load and 4% of total flow at 40% load.

Particle mass (PM) and number (PN) concentrations were studied. PM was measured following the ISO 8178-1:2006 standard. According to this, the PM is determined as material collected on

a filter following dilution of exhaust gas with clean, filtered air to a temperature higher than 42 °C and less than or equal to 52 °C, as measured at a point immediately upstream of the filter. A dilution ratio of 10 and sampling times of 5-30 minutes were used. Samples were collected on TX40HI20-WW filters (Ø 47 mm). The PN measurement method originated from the PMP (Particle Measurement Programme) work and considered non-volatile particles with a diameter greater than 23 nm. A Dekati® Engine Exhaust Diluter (DEED) was utilized for exhaust conditioning. The system consists of two ejector diluters and an evaporation tube between the two dilution units. The dilution factor of the DEED system is 100. The temperature of the first ejector is ~200 °C and the temperature at the outlet of the DEED unit is below 35 °C. Airmodus A23 Condensation Particle Counter (CPC) was used after DEED for counting all aerosol particles larger than 23 nm.

The PM filters were further analysed for anions and organic and elemental carbon. Anions, including sulphates, were analysed by electrophoresis from water and isopropanol mixture extracts. The OC/EC samples were collected on quartz filters and the analysis was performed by a thermal optical method. The analysis method is divided into two phases. In the first phase, the sample is heated in helium atmosphere with a certain temperature ramp, and the released organic carbon is oxidized to CO_2 and further reduced to CH_4, which is measured by a flame ionization detector (FID). In the second phase, the sample is heated in helium/oxygen atmosphere over a second temperature ramp. During this phase, the EC and the pyrolyzed OC are oxidized to CO_2 and yet again reduced to CH_4 and measured with FID. The measured CH_4 concentrations in the two phases are then used to calculate the OC/EC content of the sample.

In addition, elemental analysis was conducted from the PM filters. Samples were extracted in micro oven by using nitric acid and hydrofluoric acid and analysed by using inductively coupled plasma mass spectrometry.

The gaseous emission measurement setup consisted of a chemiluminescence detector (CLD), used to measure nitrogen oxides (NO_x: NO, NO_2) and a non-dispersive infrared (NDIR) analyser to measure carbon monoxide (CO) and carbon dioxide (CO_2). Hydrocarbon components were measured from a dry sample gas with an online gas chromatograph (GC - Agilent Micro). In addition, FID was utilized in part of the tests, to measure the total hydrocarbon (THC) level. Aldehyde samples were collected from diluted exhaust gas by using the DNPH (dinitrophenyl hydrazine) cartridges. Sulphur dioxide (SO_2) was measured with FTIR (Fourier Transform Infrared spectroscopy).

Results and Discussion

Gaseous Emissions

No SO_2 was detected in the exhaust gas when utilizing either of the fuels. The sulphur level in the natural gas distributed in Finland (Nordstream) is approximately 1 ppm. Analysis of the MGO fuel led to a fuel sulphur content of 6 ppm. The lubricating oil sulphur content was 6500 ppm. Even in MGO case if all the sulphur from the fuel and lube oil would end up to SO_2 in the exhaust, this would mean SO_2 levels below 2 ppm in the exhaust gas. Consequently, with the natural gas use the SO_2 level would be even lower. With the FTIR we are able accurately measure only levels above 2 ppm.

The nitrogen oxides, carbon dioxide and carbon monoxide emissions are presented in Figure 1. As expected, there are significant differences in these emission components between the natural gas use and MGO use. Lower levels of NO_x were measured with natural gas (i.e. dual fuel mode) compared to the diesel fuel only. In addition, the CO_2 emissions were lower with natural gas use, which is due to the fact that the natural gas is mainly composed of methane that has a higher H/C ratio compared to diesel.

However the CO and hydrocarbon (see Table 2 also) emissions were higher with the natural gas use compared to MGO use. These results are in line with other studies (Hesterberg, Lapin, and Bunn 2008; Liu et al. 2013; Anderson, Salo, and Fridell 2015; Lehtoranta et al. 2017). CO and HC levels were found to greatly depend also on the engine load since significantly higher emission levels were measured at the lower load mode of 40 %. These types of engines (ship engines) are usually optimized to be utilized at higher loads near 75-90% that is typical operation at open sea.

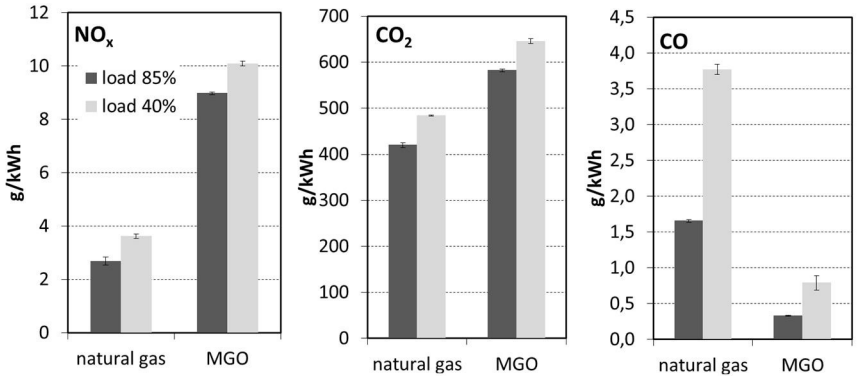

Figure 1: NO_x, CO_2 and CO emissions at two different engine loads with natural gas and MGO fuels. Error bars show the standard deviation of five measurements the minimum.

Since natural gas is mainly composed of methane one could expect to have some methane emissions if small quantities of gas escape from the combustion process. This was found to be true in present study also. The main HC component found in the exhaust gas was methane when natural gas was used as a fuel. Methane content in the natural gas was 96.4 mol-%. Comparing the methane emission to the total hydrocarbon emission resulted to nearly the same value i.e. 96,7 % at engine load of 85% and 96,5 % at engine load of 40% (see Table 1).

Table 1: Portions of methane, ethane and propane in natural gas and exhaust gas (when natural gas is used as a fuel).

	CH_4 %	**C_2H_6 %**	**C_3H_8 %**
Natural gas	96,4	2,3	0,35
Exhaust gas			
load 85%	96,7	2,2	0,29
load 40%	96,5	2,3	0,13

Ethane and propane were also found from the engine exhaust when running on natural gas. Ethane and propane also exist in the natural gas (see Table 1). In addition, although not shown in the table, small amount of ethylene was found from the exhaust gas.

No methane, ethane or propane were detected from the engine exhaust when running on diesel (MGO in this case). However the FID measurement resulted to THC level of 0.37 g/kWh at 85% engine load when running on MGO fuel, constituting likely only of longer chain hydrocarbon components (Table 2).

The methane emission level in DF mode, when utilizing natural gas as a fuel, was relatively high at 85% load and 40% load produced even higher methane and total hydrocarbon emissions (see Table 2). However, one should note that these might not be typical hydrocarbon emission values for the modern DF engines in production today. Since the test engine in our case was an older engine modified to run with natural gas (in DF mode) it might not be the best representative of the natural gas engines produced today. Nevertheless, since the modification was done in year 2016 utilizing state-of-the-art components it is not expected to be very different from today's engines.

The methane emission of 5.6 g/kWh at 85% engine load was also larger than what was measured on board a LNG ship (Anderson, Salo, and Fridell 2015) that reported THC values of 1.1-2.4 g/kWh at engine loads of 72-90%. The difference might be due to different engine sizes. The engine on board (Anderson, Salo, and Fridell 2015) was a 7600 kW engine with larger cylinder and lower speed meaning there is more time for the combustion compared to the engine in present study. Also, the combustion chamber design is probably different which could mean differences in the natural gas amounts escaping the cylinder.

Table 2: Methane, ethane and propane emissions with natural gas use and THC emission with MGO use.

	load %	CH_4 *g/kWh*	C_2H_6 *g/kWh*	C_3H_8 *g/kWh*
Natural gas	**85**	5,6	0,24	0,05
	40	13,8	0,62	0,05
		THC *g/kWh		
MGO	**85**	0,37		
	40	0,53		

** FID measurement*

This study agrees what was also pointed out by Anderson et al. (2015): the methane emission is important to consider since methane has a high global warming potential (GWP). Methane emissions could be reduced by engine optimization (e.g. by better fuel mixing conditions, combustion chamber design, reducing crevices) (Järvi 2010; Hiltner, Loetz, and Fiveland 2016). One option could also be the use of oxidation catalysts. But, further research is needed, since the highly active catalysts capable of oxidizing methane are deactivated even by very small amounts of sulphur (Ottinger et al. 2015; Lehtoranta et al. 2017).

Formaldehyde can be emitted from large bore natural gas engines as a product of incomplete combustion, mostly due to partial oxidation events in the engine (Mitchell and Olsen 2000; Olsen and Mitchell 2000). Formaldehyde is a toxic compound and hazardous even in small concentrations. The formaldehyde concentration was higher when using natural gas (40 ppm at 85% load) compared to MGO (2 ppm at 85% load). Oxidation catalyst is one way to effectively decrease the formaldehyde level (Lehtoranta et al. 2017).

Particle emissions

The particle emissions results of both PM and PN showed significantly lower levels when utilizing natural gas as the main fuel compared to MGO fuel (see Figure 2). The engine load was also found to have a significant effect on PM formation. At 40% load the PM emission was found to be higher for both fuels. We note that with the natural gas use a higher fraction of MGO pilot fuel was utilized at lower loads which could end up producing higher PM emissions compared to higher load mode of 85%.

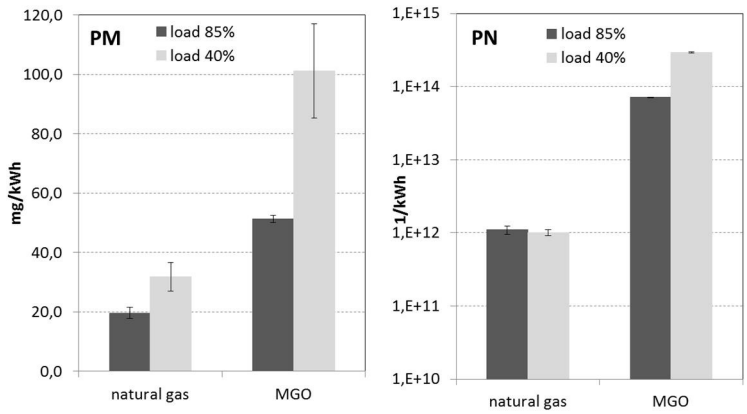

Figure 2: PM and PN emissions at two different load modes (40% and 85%) with natural gas and MGO fuels. Error bars show the standard deviation.

The PM collected was also analysed for organic and elemental carbon. The elemental carbon content is a good proxy for black carbon (Aakko-Saksa et al. 2016). The International Maritime Organisation (IMO) is currently evaluating the needs for regional and global control of BC, and work is launched to establish a methodology for BC measurements in shipping environment. BC emissions into atmosphere increase global warming directly by affecting radiative forcing of atmosphere and indirectly by increasing ice melting through deposition on ice and snow. These are of concern in the Arctic where ship traffic and consequently the ship emissions are anticipated to increase.

The organic carbon was found to be the main component in all cases studied while the elemental carbon was practically found only when utilizing MGO and not with the natural gas use (see Figure 3). This indicates that utilizing the natural gas as fuel could be one way to suppress the BC emissions and its impacts on global warming

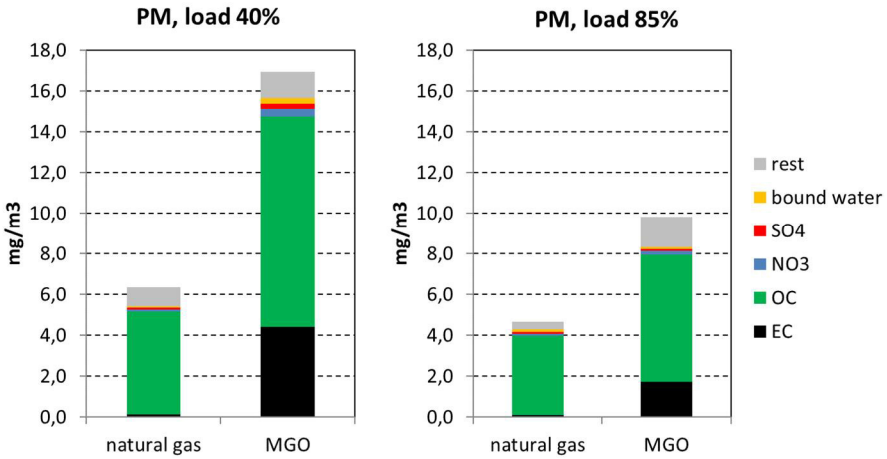

Figure 3: PM composition.

In addition, anions (sulphates and nitrates) were analysed from PM filters. Results are included in Figure 3 and show how these anions are in very minor role in contributing to particle mass both in natural gas and MGO case. The water content in the graphs has been calculated assuming hydrated sulphate (H_2SO_4. 6.5 H_2O). The 'rest' is calculated by subtracting the other components (shown in the Figure 3) from the total PM. This 'rest' includes then also the metals originating from the fuel and/or the lube oil. Metals were also analysed and the results are collected in Figure 4. The x-axis shows all the metals analysed. In case of some of the metals the result is missing indicating that the result was below the detection limit.

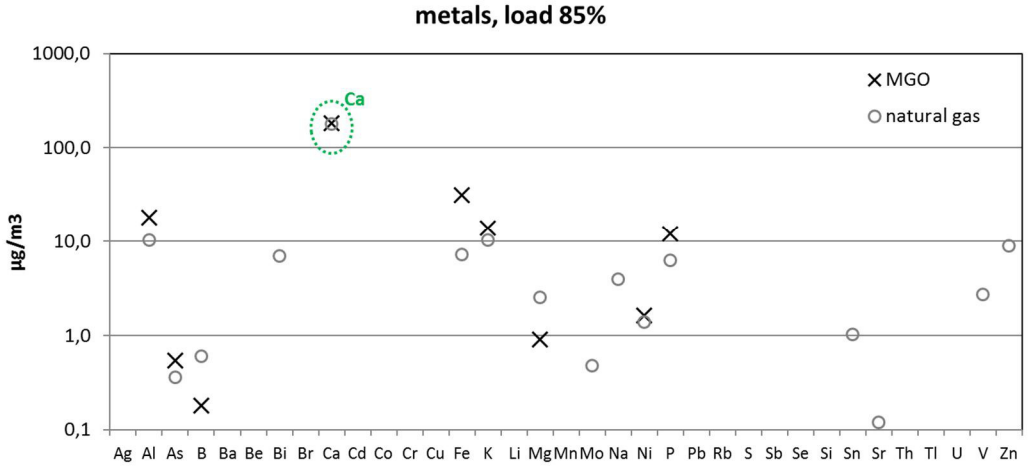

Figure 4: Metals analyzed from PM. Note that the vertical axis is logarithmic.

Metal analysis (outsourced) were conducted from the MGO fuel and lube oil samples. Practically, all the metals analysed from the MGO fuel resulted to level that was below the detection limit. In the lube oil, calcium was found to be the most abundant with a level of app. 17 000 ppm while sulphur level was app. 6500 ppm, zinc 430 ppm, phosphorous 380 ppm. And the rest of the metals were in minor roles with levels well below 100 ppm. As seen from the Figure 4, the lube oil contributes to the PM since calcium was also found to be the most abundant metal in the PM filters. Furthermore, the lube oil can contribute also to the OC levels in PM emission. Previous studies have also suggested that lubricating oil may (significantly) contribute to the particles emitted by natural gas engines (Jayaratne et al. 2012; Bullock and Olfert 2014; Anderson, Salo, and Fridell 2015; Alanen et al. 2015).

Particle number emission for natural gas was found to be significantly lower (98-99%) than for the MGO (see Figure 2). The elemental carbon and the fuel related ash/metals were mainly missing from the natural gas engine exhaust likely had an effect also on the observed PN. One should also note that the PN measurement consider (only) non-volatile particles with a diameter greater than 23 nm. If the smaller nanoparticles and the volatiles are considered the PN result might be different.

Even though IMO is not directly regulating shipping induced particle emissions, there are concerns related these emissions due to their environmental and health effects. In Europe, the emissions from inland waterway vessels are regulated. European emission standards for engines used in new non-road mobile machinery (NRMM) have been structured as gradually more stringent tiers known as Stage I...V standards. Stage III A standard introduced emission limits (CO, HC+NO_x, PM) for engines used in inland waterway vessels, also. Additionally, emission limits for inland waterway vessels have been significantly tightened under the Stage V regulation – including also PN limit coming into force in 2020. This PN limit is $1*10^{12}$ 1/kWh over a certain test cycle including several steady-state modes with different weighting factors. The PN measured in present study at both 40% and 85% load modes, when natural gas is utilized as fuel, is very close to this limit. This indicates that the usage of natural gas as fuel for inland waterway vessels could be one way to comply with the Stage V regulation. Also, bearing in mind that the test engine in present study is not the best representative of the engines produced today but there could be room to optimize the combustion process further to reach lower particle emission levels.

Conclusions

The usage of natural gas as an energy source can lead to significantly lower NO_x, particulate and CO_2 levels. In present study, CO_2 was found to be 25-28% lower with the natural gas use than with the MGO use. Also lower levels of NO_x emissions were achieved with the natural gas use compared to MGO use. This is most probably due to lower temperature combustion of natural gas. However, the CO and HC emissions were higher with the natural gas use. Methane is the principal hydrocarbon species emitted by natural gas combustion. Since methane is a potential greenhouse gas, its emissions should be minimized in order not to compromise the climate benefit gained from the CO_2 decrease.

The particle emission studies indicated that the PM level is lower with the natural gas use compared to MGO use. PM composition studies showed that practically no elemental carbon (black carbon) was found when utilizing natural gas. This can reduce the BC emissions impacts on global warming. The OC part was found to be the most dominant part in the PM composition in all cases studied. Metals concentrations in the exhaust emissions were also analysed and indicated that the lubricating oil contributes to the PM. Particle number emission with the natural gas use was found to be significantly lower than with the MGO use. The lower particle (and NO_x) emissions indicate that the usage of the natural gas instead of present marine fuel oils can improve the air quality.

One should note that the comparison of natural gas usage and liquid fuel oil usage in present study is made utilizing MGO fuel of very high quality. However, lower quality fuels are commonly utilized in ships today. These fuels include heavy fuel oil, marine diesel oil, hybrid fuels (low-sulphur residual marine fuel oils). It has been shown in other studies that, in general, the fuels of lower quality (e.g. fuels with higher sulphur levels) are expected to produce higher PM levels also (Aakko-Saksa et al. 2016; Leonidas Ntziachristos et al. 2016; L. Ntziachristos et al. 2016; Zetterdahl et al. 2016). This means that if one compares the emissions of liquid marine fuels and natural gas usage, in general, e.g. the decrease in PM levels achieved by the usage of natural gas is even higher than what is shown in this paper where we compared natural gas and MGO usage.

In addition to the present results, studies of particle size, volatility and secondary aerosol formation would give more detailed information about the particle emissions of a dual fuel engine utilizing natural gas as a fuel. Studies done in parallel with the present study answers to this need and will be published in near future.

Acknowledgements

This work was conducted in the framework of the HERE project funded by Tekes (the Finnish Funding Agency for Innovation), Agco Power Oy, Dinex Ecocat Oy, Dekati Oy, Neste Oyj, Pegasor Oy and Wärtsilä Finland Oy. Sami Nyyssönen, Jarmo Kuusisto and Jarno Martikainen from VTT are acknowledged for running the engine and handling the fuels.

References

Aakko-Saksa, Päivi, Timo Murtonen, Hannu Vesala, Päivi Koponen, Sami Nyyssönen, Harri Puustinen, Kati Lehtoranta, et al. 2016. “Black Carbon Measurements Using Different Marine Fuels.” *28th CIMAC World Congress* Paper 068.

Alanen, Jenni, Erkka Saukko, Kati Lehtoranta, Timo Murtonen, Hilkka Timonen, Risto Hillamo, Panu Karjalainen, et al. 2015. “The Formation and Physical Properties of the Particle Emissions from a Natural Gas Engine.” *Fuel*. doi:10.1016/j.fuel.2015.09.003.

Anderson, Maria, Kent Salo, and Erik Fridell. 2015. “Particle- and Gaseous Emissions from an LNG Powered Ship.” *Environmental Science & Technology* 49 (20): 12568–75. doi:10.1021/acs.est.5b02678.

Bullock, Dallin S., and Jason S. Olfert. 2014. “Size, Volatility, and Effective Density of Particulate Emissions from a Homogeneous Charge Compression Ignition Engine Using Compressed Natural Gas.” *Journal of Aerosol Science* 75 (September): 1–8. doi:10.1016/j.jaerosci.2014.04.005.

Corbett, James J., James J. Winebrake, Erin H. Green, Prasad Kasibhatla, Veronika Eyring, and Axel Lauer. 2007. “Mortality from Ship Emissions: A Global Assessment.” *Environmental Science and Technology*. doi:10.1021/es071686z.

Eyring, Veronika, Ivar S.A. Isaksen, Terje Berntsen, William J. Collins, James J. Corbett, Oyvind Endresen, Roy G. Grainger, Jana Moldanova, Hans Schlager, and David S. Stevenson. 2010. “Transport Impacts on Atmosphere and Climate: Shipping.” *Atmospheric Environment* 44 (37): 4735–71. doi:10.1016/j.atmosenv.2009.04.059.

Hesterberg, Thomas W., Charles A. Lapin, and William B. Bunn. 2008. “A Comparison of Emissions from Vehicles Fueled with Diesel or Compressed Natural Gas.” *Environmental Science and Technology*. doi:10.1021/es071718i.

Hiltner, Joel, Andy Loetz, and Scott Fiveland. 2016. “Unburned Hydrocarbon Emissions from Lean Burn Natural Gas Engines - Sources and Solutions.” *28th CIMAC World Congress* Paper 032.

Jayaratne, E. R., N. K. Meyer, Z. D. Ristovski, and L. Morawska. 2012. “Volatile Properties of Particles Emitted by Compressed Natural Gas and Diesel Buses during Steady-State and Transient Driving Modes.” *Environmental Science and Technology* 46 (1): 196–203. doi:10.1021/es2026856.

Järvi, Arto. 2010. “Methane Slip Reduction in Wärtsilä Lean Burn Gas Engines.” *26th CIMAC World Congress* Paper 106.

Lehtoranta, Kati, Timo Murtonen, Hannu Vesala, Päivi Koponen, Jenni Alanen, Pauli Simonen, Topi Rönkkö, et al. 2017. “Natural Gas Engine Emission Reduction by Catalysts.” *Emission Control Science and Technology* 3 (2): 142–52. doi:10.1007/s40825-016-0057-8.

Liu, Jie, Fuyuan Yang, Hewu Wang, Minggao Ouyang, and Shougang Hao. 2013. “Effects of Pilot Fuel Quantity on the Emissions Characteristics of a CNG/diesel Dual Fuel Engine with Optimized Pilot Injection Timing.” *Applied Energy*. doi:10.1016/j.apenergy.2013.03.024.

Mitchell, Charles E., and Daniel B. Olsen. 2000. “Formaldehyde Formation in Large Bore Natural Gas Engines Part 1: Formation Mechanisms.” *Journal of Engineering for Gas Turbines and Power* 122 (4). American Society of Mechanical Engineers: 603–10. doi:10.1115/1.1290585.

Ntziachristos, L., E. Saukko, K. Lehtoranta, T. Rönkkö, H. Timonen, P. Simonen, P. Karjalainen, and J. Keskinen. 2016. “Particle Emissions Characterization from a Medium-Speed Marine Diesel Engine with Two Fuels at Different Sampling Conditions.” *Fuel* 186 (December): 456–65. doi:10.1016/j.fuel.2016.08.091.

Ntziachristos, Leonidas, Erkka Saukko, Topi Rönkkö, Kati Lehtoranta, Hilkka Timonen, Risto Hillamo, and Jorma Keskinen. 2016. “Impact of Sampling Conditions and Procedure on Particulate Matter Emissions from a Marine Diesel Engine.” *28th CIMAC World Congress* Paper 165.

Olsen, Daniel B., and Charles E. Mitchell. 2000. “Formaldehyde Formation in Large Bore Engines Part 2: Factors Affecting Measured CH[sub 2]O.” *Journal of Engineering for Gas Turbines and Power* 122 (4). American Society of Mechanical Engineers: 611–16. doi:10.1115/1.1290586.

Ottinger, Nathan, Rebecca Veele, Yuanzhou Xi, and Z Gerald Liu. 2015. “Desulfation of Pd-Based Oxidation Catalysts for Lean-Burn Natural Gas and Dual-Fuel Applications.” *SAE Tech. Pap. Ser.* SAE paper. doi:10.4271/20l5-0l-0991.

Viana, Mar, Pieter Hammingh, Augustin Colette, Xavier Querol, Bart Degraeuwe, Ina de Vlieger, and John van Aardenne. 2014. “Impact of Maritime Transport Emissions on Coastal Air Quality in Europe.” *Atmospheric Environment* 90 (June): 96–105. doi:10.1016/j.atmosenv.2014.03.046.

Zetterdahl, Maria, Jana Moldanová, Xiangyu Pei, Ravi Kant Pathak, and Benjamin Demirdjian. 2016. “Impact of the 0.1% Fuel Sulfur Content Limit in SECA on Particle and Gaseous Emissions from Marine Vessels.” *Atmospheric Environment* 145: 338–45. doi:10.1016/j.atmosenv.2016.09.022.

Maritime Emissions for Different Emission Reduction Scenarios in the Arctic

M. Winther[1], J.H. Christensen[1], I. Angelidis[1], E.S. Ravn[2]*

[1]Department of Environmental Science, Aarhus University, Roskilde, 4000, Denmark, mwi@envs.au.dk
[2]Ravn Consult, Frederiksberg, 2000, Denmark

Abstract

This paper presents spatially distributed emission inventories for the Arctic area above 58.95N. For the historical years 2012-2016 inventories are based on satellite AIS data, ship engine power functions and technology stratified emission factors. Emission projections are made for the years 2020, 2030 and 2050 based on the robust five-year weighted historical data for ship traffic, updated traffic growth rates and emission factors. The emission projections include a Baseline emission scenario and two additional SECA and HFO ban scenarios. For 2012*[2013, 2014, 2015, 2016]* the following total results are calculated for fuel consumption: 4.8*[5.1, 6.3, 6.6, 5.4]* MTonnes; SO_2: 81*[84, 108, 60, 53]* kTonnes; NO_x: 320*[339, 429, 432, 361]* kTonnes and BC: 0.71*[0.73, 0.86, 0.65, 0.56]* kTonnes. In the Baseline scenario for the forecast years 2020*[2030, 2050]* the following total results are calculated for fuel consumption: 5.7*[5.8, 6.3]* MTonnes; SO_2: 17*[17, 18]* kTonnes; NO_x: 371*[318, 247]* kTonnes and BC: 0.43*[0.44, 0.47]* kTonnes. The introduction of a fully covering SECA zone or a complete ban of HFO use in the inventory area are both very efficient means for the reduction of SO_2. In all scenario years the calculated SO_2 emissions for the SECA and HFO ban scenarios become almost half of the emissions calculated for the Baseline scenario. The emission reduction potential for BC is, however, less promising; in 2020*[2030, 2050]* the HFO ban and SECA emissions are 8 %*[9 %, 12 %]* and 3 %*[3%, 3 %]* smaller, respectively, than the Baseline results.

Keywords: Ships, scenarios, EGCS, HFO, MDO/MGO, fuel consumption, SO_2, NO_x, BC

1. Introduction

Navigation is one of the most important local sources of emissions in the Arctic area. Navigation emissions are characterized by the fact that the air pollutants formed during ship engine combustion are being injected directly into the Arctic environment along the vessels route at low vessel chimney heights. Hence, the emission deposition from vessels sailing in the arctic area becomes relatively large compared to the total emissions emitted by these vessels (e.g. Corbett et al., 2010; Winther et al., 2014). In this respect the emissions of black carbon (BC) are of particular interest. It is well known that BC has global warming properties due to its ability to absorb light over reflective surfaces e.g. snow covered surfaces and due to its darkening effect when deposited to snow and ice surfaces (e.g. Quinn et al., 2008; Flanner, 2007, 2009).

This paper presents spatially distributed emission inventories for SO_2, NO_x and BC for the Arctic area above 58.95N made in the DANCEA project “Emissions from shipping in the Arctic from 2012-2016 and updated emission projections until 2050”. The project was carried out by Department of Environmental Science at Aarhus University on behalf of the Danish Environmental Protection Agency. The emission estimates for the historical years 2012-2016 are based on satellite AIS data, ship engine power functions and technology stratified emission factors. The emission projections for the years 2020, 2030 and 2050 are made based on the robust five-year weighted historical data for ship traffic, updated traffic growth rates and emission factors. The emission projections include a Baseline emission scenario and two additional SECA HFO ban scenarios. In the SECA scenario, the existing SECA zones (i.e. America and North Sea/Baltic

Sea SECA's)[1] are expanded to cover the entire inventory area. In the HFO ban scenario, the use of HFO by ships is prohibited all across the inventory area.

The full list of emission components included in the project are the short lived climate forcers SO_2, NO_x, CO, NMVOC, PM, BC and OC and the greenhouse gases CO_2, CH_4 and N_2O. For further details please refer to Winther et al. (2017).

2. Ship activity data

2.1 Ship activity data for 2012-2016

The ship activity data provided by the Danish Maritime Authority (DMA) in this project are based on AIS signals received from terrestrial base stations and from satellites equipped with AIS receivers. The data represent the years 2012-2016, divided into 0.5° longitude x 0.225° latitude grid cells, and on a monthly resolution. The ships are classified into 14 ship types and 16 ship lengths (LPP: length between perpendiculars) categories (intervals of 25 m) and data for total sailed distance and average sailing speeds are provided stratified into the different ship types/LPP/average speed combinations that have been recorded in the individual cells.

Table 1 shows the engine type, fuel type by origin, assumed engine life time and total sailing distances for 2012-2016 for the vessel types included in this study.

Table 1: Engine type, fuel type by origin, assumed engine life time and total sailing distances for 2012-2016 for the vessel types included in this study.

	Engine			Total sailing distance (km x 10^3)				
Vessel type, V	Type, k [c)]	Origin fuel type, f	Life time	2012	2013	2014	2015	2016
Crude oil tanker	SS	HFO	30	1439	1435	1554	1695	1970
Oil/chemical tanker	SS	HFO	30	10778	10940	11608	12699	11480
Ro-ro passenger ship	MS/HS[a]	HFO, MDO/MGO[b]	30/10[a]	15202	12727	14261	15970	18326
Gas tanker	SS	HFO	30	861	742	855	1006	1010
Container ship	SS	HFO	30	5884	5478	5516	5436	5234
General cargo ship	SS	HFO	30	29893	28020	30287	33894	33958
Bulk carrier	SS	HFO	30	4493	4663	4860	4869	4727
Ro-ro cargo ship	MS/HS[a]	HFO, MDO/MGO[b]	30/10[a]	3243	2716	2671	2752	2776
Passenger ship	MS/HS[a]	HFO, MDO/MGO[b]	30/10[a]	10064	10475	11610	13818	14852
Fast ferry	MS/HS[a]	HFO, MDO/MGO[b]	30/10[a]	187	197	271	324	762
Support ship	MS/HS[a]	HFO, MDO/MGO[b]	30/10[a]	13095	13537	17098	17984	15290
Fishing ship	MS		20	28984	31817	38679	46254	38243
Other ship	MS/HS[a]	HFO, MDO/MGO[b]	30/10[a]	5751	8915	11162	11546	6831
Total				129873	131661	150431	168247	155458

[a)] High speed engines and life time = 10 years for design power < 1000 kW. [b)] MDO/MGO for design power < 4000 kW. [c)] SS/MS/HS: Slow speed (2-stroke), Medium speed/High speed (4-stroke),HFO: Heavy Fuel Oil, MDO/MGO: Marine Diesel Oil/Marine Gas Oil.

Although a limited number of Exhaust Gas Cleaning Systems (EGCS) for SO_x scrubbing has been installed on board ships globally until now, the preferred choice from ship owners/charterers has been to switch fuel from HFO to MDO/MGO instead of using EGCS in order to comply with the

[1] American ECA: south of 60N extending up to 200 nautical miles from coasts of the United States, Canada and the French territories. North Sea/Baltic Sea ECA: Outer boundaries are the North Sea south of 62N and east of 4W and the English Channel east of 5W and north of 48°30'N. These areas are also designated NECA areas in which ship engines constructed after 1.1.2016/1.1.2021 must comply with IMO Tier III standards, for American/North Sea-Baltic Sea NECA's, respectively.

0.1 % fuel sulphur limits for HFO in SECA's, which entered into force from 1.1.2015 (e.g. Danish EPA, 2017). Consequently, in this project for 2015 and 2016 we assume that the fuel type being used is MDO/MGO inside SECA's and HFO outside SECA's for ships using HFO by origin.

Figure 1 shows the distance sailed per ship type in 2012-2016 (left figure) and total distance sailed per month 2012-2016 (right figure). Please note the different scales on the two graphs.

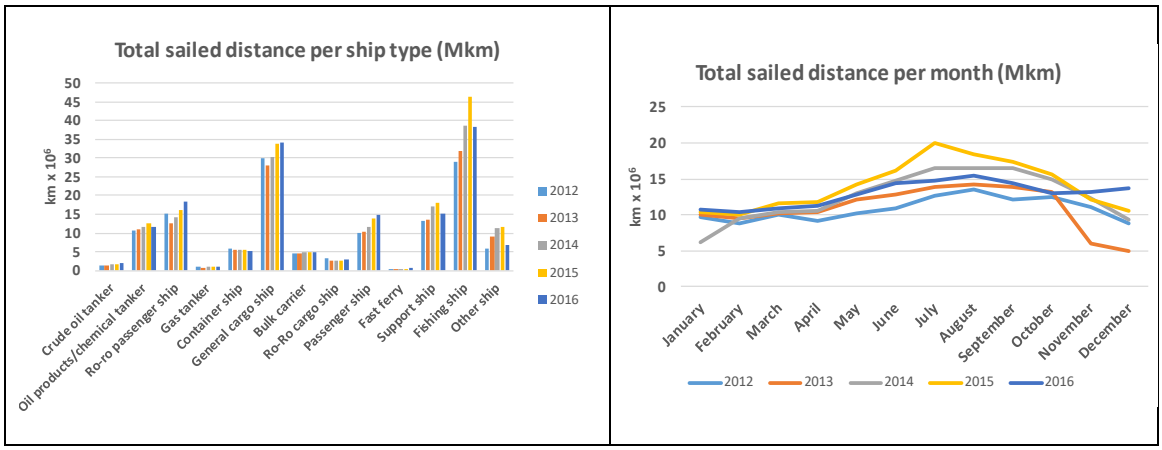

Figure 1: Distance sailed per ship type and total distance sailed per month in 2012-2016

In 2016, most of the sailed distance in the area (percentage shares in brackets, derived from Figure 1) is done by fishing ships (25 %), general cargo (22 %), passenger ships (sum: 22 %), support ships (10 %) and tankers (sum: 9 %). For fishing vessels, the transport development per month is variable, whereas for the remaining most busy ship categories, the traffic maximum is reached during the warmest months of the year (not shown). Figure 2 shows the total spatial distribution of ship traffic for all ships in 2016 based on the AIS dataset.

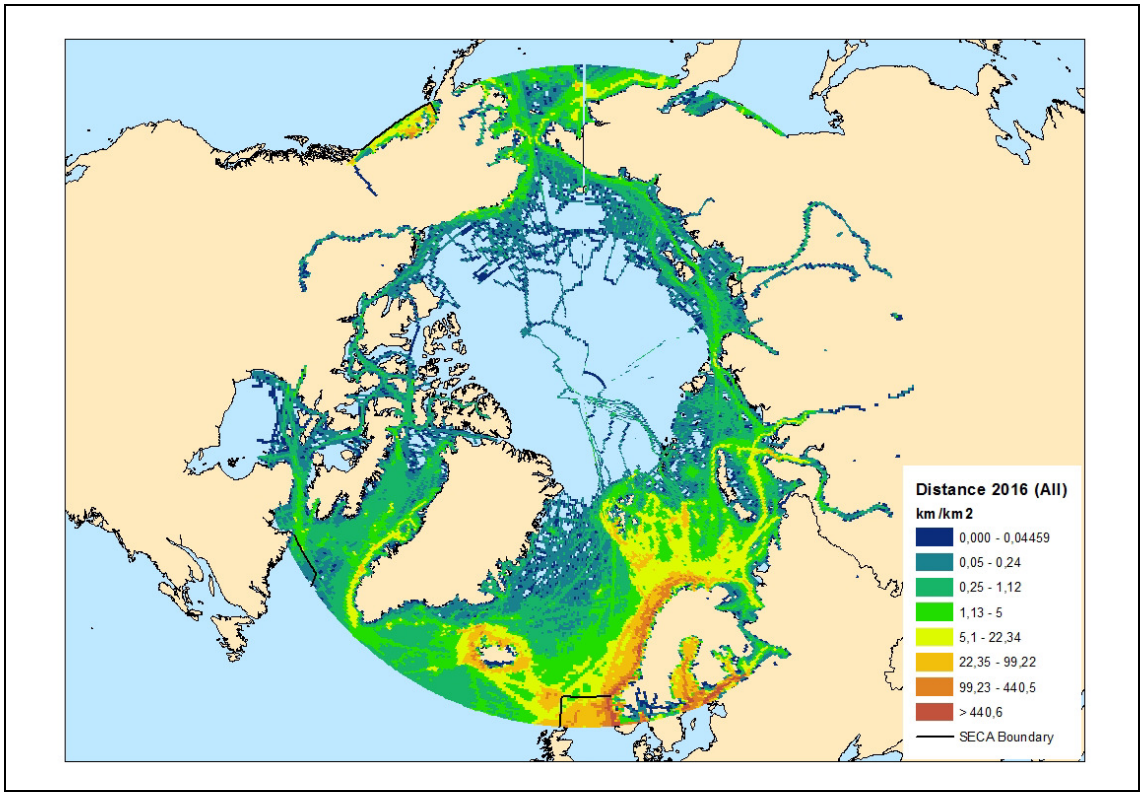

Figure 2: Spatial distribution of ship traffic for all ships in 2016

2.2 Activity data projections for 2020, 2030 and 2050

A weighted and consolidated ship activity data set for the midpoint year 2014 is created in this project based on the five-year (2012-2016) ship activity data provided by DMA. The consolidated traffic weighted ship activity data are used in order to obtain a more robust basis for the projection of ship activity data, thus avoiding inexpedient temporal and spatial specific fluctuations in traffic records, and in order to achieve a uniform grid cell reference system for the emission projection calculations. Due to the nature of data processing in DMA, the grid cell references differ from year to year in DMA data.

To obtain uniform distance sailed and kWh's produced by main engines and auxiliary engines, the grid cell specific share of the year x month x ship type x LPP x speed value combination in DMA data (stratified data record), projected into the appropriate uniform grid cell, is summed up for this specific uniform grid cell and stratified data record combination. The uniform grid cell sum is subsequently divided by five (the number of inventory years in DMA historical data).

Uniform main engine loads are obtained by weighing the main engine load for each stratified data record with the share of produced main engine kWh's projected into the appropriate uniform grid cell, and subsequently divide by the sum of produced main engine kWh's being projected into the uniform grid cell.

The traffic scaling factors used in this study for traffic projections are derived from traffic growth factors in the Corbett et al. (2010) business as usual (BAU) scenario[2] by referring our study's ship types to the Corbett et al. (2010) ship types and by using modified Corbett traffic growth factors evolved from 2014. The EEDI factor expresses the percentage reduction in fuel consumption for ships globally modelled from EEDI fuel efficiency regulations agreed by Marpol 83/78 Annex VI and mandatory from 1st January 2013 for new built ships larger than 400 GT. For further explanations regarding the estimations of the EEDI factors, see Winther et al. (2014).

Table 2 shows the vessel type specific traffic scaling factors between the weighted midpoint base year ("2014w") and the forecast years 2020, 2030 and 2050. The traffic scaling factors are used to estimate the traffic levels by ship type in the forecast years shown in Table 2 and Figure 3.

Table 2: Traffic scaling factors for the years 2020, 2030 and 2050 used in this study.

Vessel type	Traffic scaling factors			Total sailing distance (km x 10^3)				EEDI factor (%)		
This study	2020	2030	2050	2014w	2020	2030	2050	2020	2030	2050
Crude oil tanker	1.30	1.71	2.62	1618	2103	2768	4238	2.33	11.00	28.66
Oil/Chemical tanker	1.30	1.71	2.62	11501	14943	19667	30115	1.86	8.76	22.84
Ro-ro passenger ship	1.04	1.14	1.43	15297	15932	17488	21809	0.33	5.67	18.67
Gas tanker	1.30	1.71	2.62	895	1163	1530	2343	2.01	9.47	24.67
Container ship	1.19	1.71	3.86	5510	6571	9436	21244	2.02	9.53	24.83
General cargo ship	1.02	1.07	1.21	31211	31758	33375	37888	1.07	5.06	13.20
Bulk carrier	1.09	1.29	1.85	4722	5142	6078	8725	2.17	10.22	26.62
Ro-ro cargo ship	1.02	1.07	1.21	2831	2881	3028	3437	0.33	5.67	18.67
Passenger ship	1.04	1.14	1.43	12164	12668	13905	17341	0.33	5.67	18.67
Fast ferry	1.04	1.14	1.43	348	362	398	496	0.33	5.67	18.67
Support ship	1.14	1.32	1.69	15401	17538	20360	26043	0.33	5.67	18.67
Fishing ship	1	1	1	36795	36795	36795	36795	0.00	0.00	0.00
Other ship	1	1	1	8841	8841	8841	8841	0.33	5.67	18.67
Total				147134	156698	173669	219317			

[2]The Corbett BAU scenario originates from the Second IMO GHG Study 2009 (Buhaug et al., 2009).

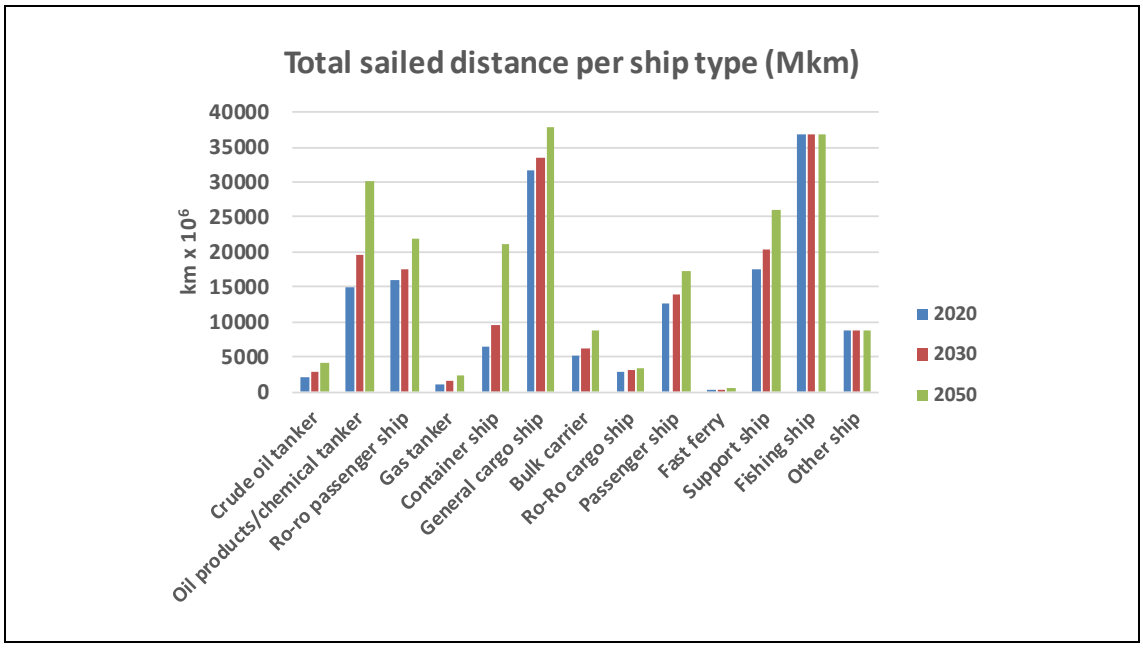

Figure 3: Total distance sailed per ship type projected for the years 2020, 2030 and 2050.

3. Emission scenarios

3.1 Description of scenarios

This project includes a Baseline emission projection scenario and two additional SECA and HFO ban scenarios. The baseline scenario forms the basis for the SECA and HFO ban scenarios.

All three scenarios use the traffic activity projections explained in Chapter 2.2 and further the scenarios assume an increasing amount of LNG fuel used as a substitution for HFO in the inventory area throughout the projection years. The scenarios use the "low case" LNG fuel share of total marine fuel consumption being 2 %, 4 % and 8 % in the years 2020, 2030 and 2050, respectively, as described in the IMO 3rd GHG study published by IMO (2015).

The baseline scenario assumes an increase in the use of EGCS for SO_2 emission abatement in the case of ships using HFO with a high content of sulphur. In the baseline scenario inside the existing SECA zones (i.e. America and North Sea/Baltic Sea SECA's) the fuel type switches from HFO to MDO/MGO for ships using HFO by origin (c.f. Table 1) and not having an EGCS installed (c.f. chapter 3.2). Outside the existing SECA's the latter ships use 0.5 % HFO.

In the SECA scenario, the existing SECA zones (i.e. America and North Sea/Baltic Sea SECA's) are expanded to cover the entire inventory area. The SECA scenario takes on board the baseline shares of LNG fuel consumption and EGCS installations. Further in the SECA scenario, the fuel is shifting from HFO to MDO/MGO outside the existing SECA areas by ships using HFO by origin (c.f. Table 1) and not using EGCS. The emission impact of using EGCS is further assessed in a model run involving higher shares of EGCS installations on board ships.

In the HFO ban scenario, no use of HFO by ships is allowed at all in the inventory area. The HFO ban scenario includes the consumption of LNG as assumed in the baseline scenario. The remaining part of the HFO consumption not being substituted by LNG is assumed to switch to MGO/MDO in the entire inventory area.

3.2 Projections of EGCS installations

The projections of EGCS installed on board ships in 2020, 2030 and 2050 are made based on EGCS installation cost effectiveness (CE) functions from IMO (2016a), global ship fleet engine size data from Danish Shipping, general assumptions of average life time of ships and expert views from Danish Shipping, Danish Maritime Authority and Danish Maritime.

IMO (2016a) finds the share of ships for which EGCS are cost-effective (CE) to use as a function of installed main engine power (>5 MW) for new build installations and retrofit installations during dry dock visits, respectively. The CE probability functions are based on economic considerations that include annualized capital and operational expenditures weighted up against saved fuel cost.

IMO (2016a) also points out other barriers for the installation of EGCS on board ships. These include regulatory barriers (discharge of washwater being constrained or prohibited), technical or operational barriers (space limitations on board ships, ship stability, Tier III compatibility), installation capacity in ship yards and other barriers (e.g. split incentive between owner/charterer).

Danish Shipping and DMA believe global EGCS installation shares between 25 % and 30 % of the global fleet (>5 MW) in 2050 to be realistic, taking into consideration fuel price differences, fuel availability concerns and the demand for more climate-friendly fuels. Danish Maritime regards twice as high global EGCS installation shares to be more realistic. Based on these expert views, we choose a global EGCS share of 28 % as end target for 2050 to include in the baseline and SECA scenarios, and double (56 %) EGCS shares as input for a "high case EGCS" sensitivity model run included in the SECA scenario.

We produced an unadjusted (i.e. regardless of other barriers) EGCS installation distribution by combining the IMO (2016a) new build and retrofit CE probability curves with the main engine size distribution of the global fleet. For all ships, an assumed average lifetime of 30 years roughly gave the number of new build ships each year, and estimated dry dock visits every five year roughly gave the number of ships in dry dock visit each year. Subsequently the unadjusted EGCS installation distributions for 2020, 2030 and 2050 are iteratively downscaled so that the sum of EGCS installations in 2050 match 28 % and 56 % of the global fleet in 2050. The scaling factor that we use can be interpreted as the sum of additional barriers for EGCS installations expected by the stakeholders consulted in our project. In 2020*[2030, 2050]* the percentage share of ships with EGCS installed are 14 %*[20 %, 28 %]* and 18 %*[38 %, 56 %]* for Baseline and SECA high case EGCS model runs, respectively.

Figure 4 shows the fraction of ships with EGCS installed as a function of the installed ship main engine power. These fractions are used as input for the emission calculations made in the project.

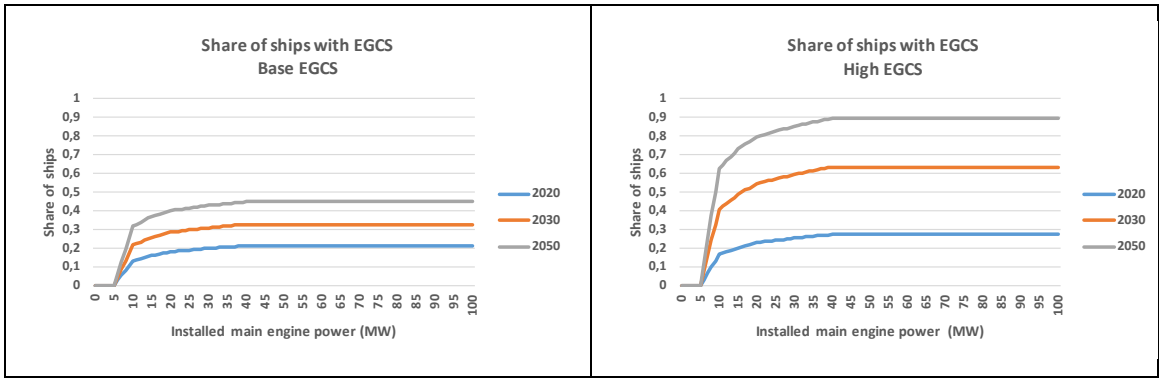

Figure 4: Share of ships with EGCS as a function of the installed ship main engine power.

3.2 Sulphur content of the fuels

Based on MARPOL Annex VI fuel sulphur regulations, IMO sulphur monitoring data (IMO, 2016b), and scenario definitions (chapter 3.1) the following sulphur content of fuels are used in the project.

HFO fuelled ships with EGCS
In the current inventory (Baseline and SECA scenarios), the ships with EGCS installed are assumed to continuously be using HFO with a fuel sulphur content of 2.45 % (Fs = 2.45 %), as monitored by IMO (2016b) for 2015. By assumption, the EGCS sulphur removal efficiency is equivalent to Fs = 0.1 %. EGCS systems are included in the emission projections from 2020+.

HFO fuelled ships without EGCS
Inside SECA's, the ships without EGCS using HFO by origin (historical years 2015/2016, and all scenario years) are assumed to shift fuel from HFO to MDO/MGO (c.f. Chapter 2). Outside SECA's - in historical years as well as in Baseline forecast years – ships without EGCS continue to use HFO with Fs corresponding to the IMO monitoring levels for 2012-2015, 2.45 % for 2016-2019 and 0.5 % from 2020 onwards (Tables 3 and 4). Outside SECA's, in the SECA and HFO ban scenarios these ships are assumed to shift fuel from HFO to MDO/MGO.

MDO/MGO fuelled ships
For MDO/MGO outside SECA's, the fuel sulphur content used in the present inventory reduces from 0.14 % in 2012 to 0.08 % in 2015 (monitored by IMO, 2016b). Inside SECA's, the fuel sulphur content is 0.1 % for 2012-2014 and 0.08 % from 2015 (Tables 3 and 4).

Table 3: Sulphur content of fuels used in the present inventory for 2012-2016.

Fuel/Area	2012	2013	2014	2015	2016
HFO SECA	1	1	1	Fuel shift to MDO/MGO	
HFO outside SECA	2.51	2.43	2.46	2.45	2.45
MDO/MGO SECA	0.1	0.1	0.1	0.08	0.08
MDO/MGO outside SECA	0.14	0.13	0.12	0.08	0.08

Table 4: Fs and removal efficiency equivalent Fs eq. of fuels used in the present inventory for 2020, 2030 and 2050.

	Fuel/Area	Area	Fs (2020, 2030, 2050)	Comment
Baseline	HFO (with EGCS)	SECA	2.45 %	Fs eq. = 0.1 %
	HFO (with EGCS)	Non SECA	2.45 %	Fs eq. = 0.1 %
	HFO (without EGCS)	SECA	(0.1 %)	Fuel shift to MDO/MGO
	HFO (without EGCS)	Non SECA	0.5 %	-
SECA scenario	HFO (with EGCS)	SECA	2.45 %	Fs eq. = 0.1 %
	HFO (without EGCS)	SECA	(0.1 %)	Fuel shift to MDO/MGO
All scenarios	MDO/MGO		0.08	-
	LNG		0	-

3. Emission factors

The specific fuel consumption factors (sfc) and NO_x emission factors (g/kWh) for HFO and MDO/MGO used in the calculations are classified according to engine type and engine production year. For LNG, the source of sfc and emission factors is IMO (2015). Figure 5 shows the fuel related NO_x emission factors for the whole inventory area derived from the Baseline scenario results. The decreasing emission factor trend is the result of gradually more NO_x emission efficient diesel engines entering into the global fleet, predominantly ruled by the Tier III regulations for new engines in the NECA areas from 2016 (America) and 2021 (North Sea/Baltic Sea). For further details please refer to e.g. Winther et al. (2014).

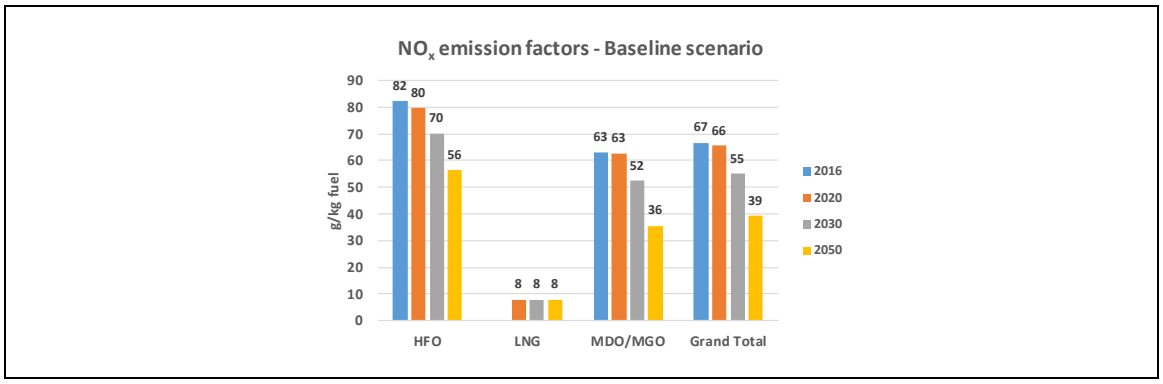

Figure 5: Fuel related NO_x emission factors (g/kg fuel) for the whole inventory area for 2016, 2020, 2030 and 2050

The BC emission factors for HFO and MDO/MGO used in this project are taken from Aakko-Saksa et al. (2016). The main motivation for using this source is that the level of the emission factors measured by Aakko-Saksa et al. (2016) are in good accordance with recent findings from an international research project on maritime BC emissions, bringing together experts from engine manufacturers, measurement laboratories, emission inventory compilers and policy experts (e.g. ICCT, 2014 and 2016). ICCT (2016) suggest that shifting from conventional HFO to distillate fuels such as MGO can reduce BC emissions, and further conclude that the general BC emission levels for ship engines are much lower than the often cited Corbett factor of 0.35 g/kg fuel regardless of fuel type. The emission factors from Aakko-Saksa et al. (2016) for HFO, IFO and MDO used in the present study are shown in Table 5. The emission factors are measured with the filter smoke number (FSN) method representing an engine load of 75 %.

Table 5: Emission factors for BC used in the present project.

Fuel type	EFBC (g/kg fuel)
HFO (Fs =2.5 %)	0.155
IFO[3] (Fs = 0.5 %)	0.065
MDO/MGO (Fs = 0.1 %)	0.056
LNG	0.00155

In the case of EGCS, an average 40 % reduction of the BC emissions for HFO is assumed (i.e. 0.093 g/kg fuel) based on the available data from the literature (ICCT (2015; Lack and Corbett (2012); Johnson et al. (2016)) For LNG, a BC emission factor of 0.00155 g/kg fuel (Table 5) is used, derived as 1 % of the BC emissions for HFO as suggested by ICCT (2015). The emission factors are transformed from g/kg fuel to g/kWh by multiplication with sfc/1000.

3. Calculation method

For each inventory year, X, and for each combination of ship type, engine type, fuel type and LPP length interval, the work produced by the ship engine during the sailing distance, D, and the vessel average speed, V, is calculated as:

$$W_{S,f,k,l}(X) = P_{S,f,k,l} \cdot (100 - EEDIf_S(X))/100 \cdot D_{S,l}(X)/V_{S,l} \quad (1)$$

Where W = Engine work produced in kWh, S = ship type, f = fuel type, k = engine type, l = LPP length interval, P = Engine power in kW, D = Distance in NM and V = Vessel average speed in knots provided by DMA (Section 2.1), EEDIf = Energy Efficiency Design Index factor (Table 2).

[3] IFO (Intermediate Fuel Oil) is a fuel type, which is likely to be commercially available as a substitute for high sulphur HFO fuels, when the global 0.5 % fuel sulphur limits come into force in 2020.

The engine power is estimated with the SHIP-DESMO model (Kristensen, 2012) by using ship type, LPP and vessel average speed as input parameters.

The fuel consumption and the emissions are calculated as:

$$E_{S,i}(X) = \sum_{f,k,l} W_{S,f,k,l}(X) \cdot EF_{i,f,k}(X) \cdot LAF_i \quad (2)$$

EF_i = Fuel consumption or emission factor in g/kWh and LAF = engine load adjustment factor.

The input engine load for the engine load adjustment functions is calculated for each data record in the traffic data as the ratio between main engine kW produced by the specific ship type/LPP class at the specific sailing speed and the design power for the specific ship type /LPP class.

The engine load adjustment functions for specific fuel consumption (sfc) and NO_x are taken from IMO (2015) based on Starcrest (2014). For BC the engine load adjustment factors comes from Corbett and Lack (2012).

3. Results

Table 6 shows the sailed distance, engine kWh's produced, total fuel consumption (by mass and energy), BC, NO_x and SO_2 emission results calculated for the inventory area in 2012-2016 and Baseline, SECA and HFO ban scenario results calculated for 2020, 2030 and 2050.

Table 6: Results calculated for the inventory area in 2012-2016 and scenario results calculated for 2020, 2030 and 2050

Scenario	Year	Distance km x 10^6	Power kWh x 10^6	Fuel kTonnes	Fuel TJ	SO_2 Tonnes	NO_x Tonnes	BC Tonnes
-	2012	129.8	23558	4768	199168	81224	320105	708
-	2013	131.7	25129	5050	211151	84115	339249	727
-	2014	150.4	31636	6287	263118	108211	428740	859
-	2015	168.2	33006	6582	279165	59842	431636	652
-	2016	155.5	27335	5407	229223	52660	360819	556
-	2016 uniform	147.1	28106	5522	233976	57074	368359	535
Baseline	2020	156.7	29679	5664	240115	16976	371126	432
Baseline	2030	173.7	31406	5775	245208	16883	317669	438
Baseline	2050	219.3	35135	6310	268933	17757	246870	470
SECA	2020	156.7	29679	5664	241820	9019	371126	418
SECA	2030	173.7	31406	5775	246882	9073	317669	424
SECA	2050	219.3	35135	6310	270682	9597	246870	455
HFO ban	2020	156.7	29679	5664	242440	8881	371126	399
HFO ban	2030	173.7	31406	5775	247792	8870	317669	397
HFO ban	2050	219.3	35135	6310	272068	9289	246870	414

In 2016, the largest shares (percentage values in brackets) of fuel consumption (by mass), BC, NO_x and SO_2 are calculated for fishing ships (45 %, 33 %, 39 %, 7 %) followed by passenger ships (21 %, 22 %, 18 %, 25 %), general cargo (10 %, 16 %, 13 %, 22 %), tankers (10 %, 12 %, 14 %, 21 %), bulk carriers (4 %, 6 %, 5 %, 12 %) and container ships (3 %, 4 %, 5 %, 7 %).

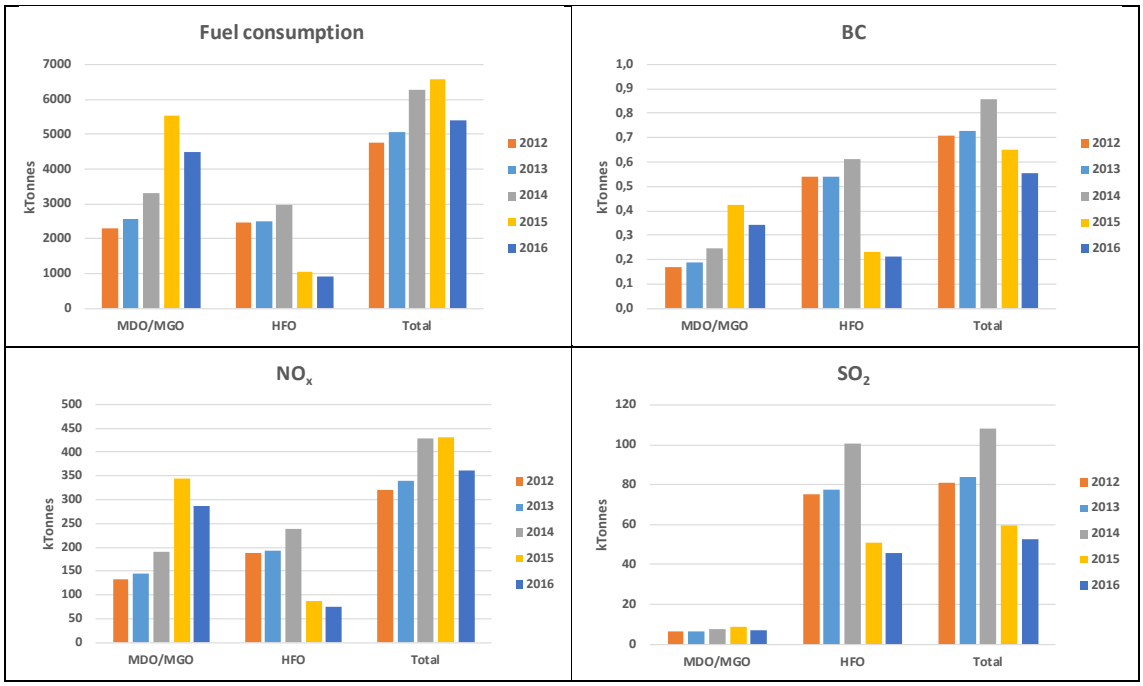

Figure 6: Total fuel consumption (by mass), NO_x, SO_2 and BC emissions in 2012-2016.

For the years 2012-2016, the total NO_x emissions levels are quite similar to the fuel consumption levels (Figure 6). In 2015 and 2016, the calculated SO_2 emissions drop significantly due to the stricter fuel sulphur regulations in SECA's from 1.1.2015 causing a fuel switch from HFO to MDO/MGO in SECA's by ships using HFO by origin (c.f. chapter 2.1). The latter fuel switch also brings significant BC emission reductions due to the lower BC emission factors for MDO/MGO compared to HFO.

The SO_2 emission reductions in the SECA areas from 2012 to 2016 are clearly visible from Figure 7. Although less visible, BC emission reductions in the SECA areas also appear from Figure 7.

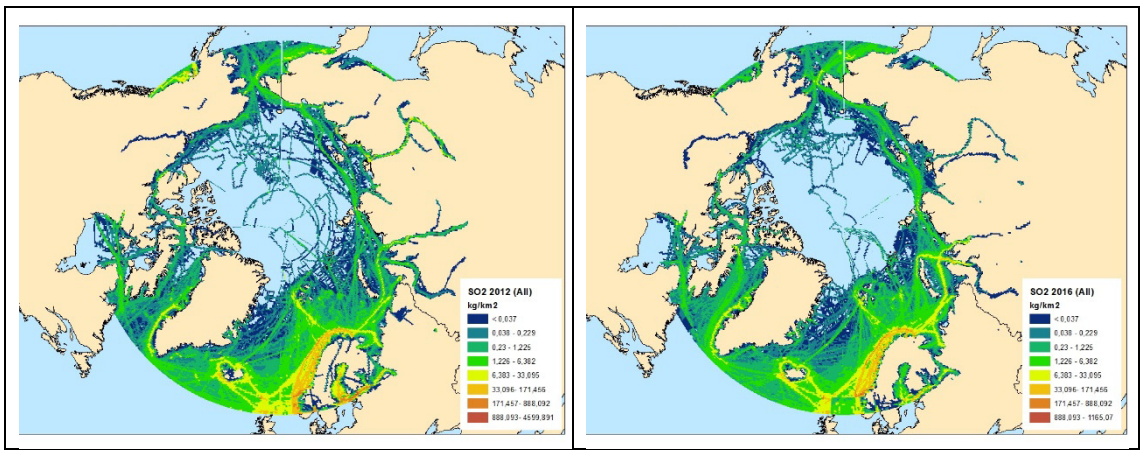

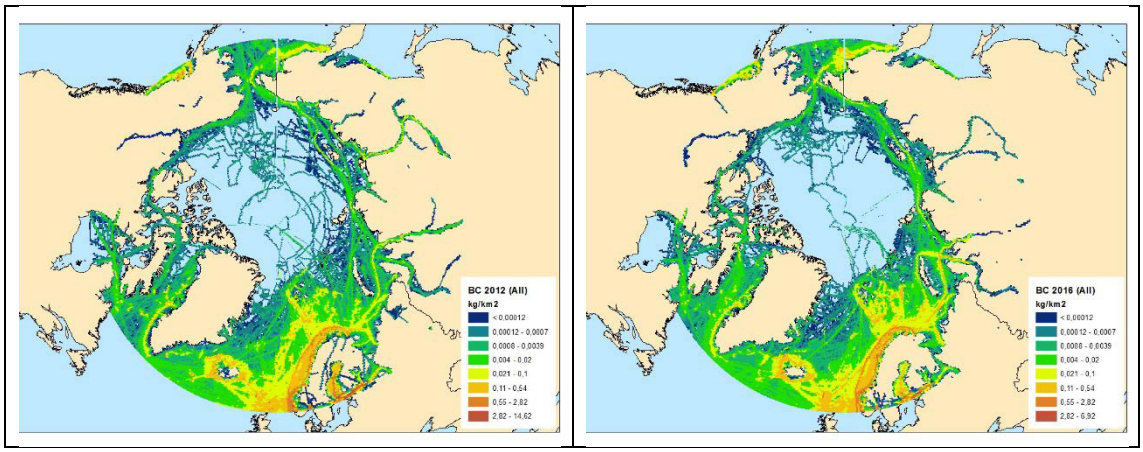

Figure 7: Spatial distribution of SO_2 and BC emissions for all ships in 2012 and 2016

The most convenient way to assess the emission results for the Baseline BAU scenario is to explain the emission development from today's emissions calculated by using the consolidated (five-year weighted average) ship activity data and the uniform grid system used to project the ship activity data and emission factors for 2016 (the so-called uniform gridded 2016 inventory).

The following percentage changes between the uniform gridded 2016 results and the Baseline BAU results for the forecast years 2020, 2030, 2050, respectively (results in brackets) are calculated for fuel consumption(+3 %, +5 %, +14 %), BC(-19 %, -18 %, -12 %), SO_2 (-70 %, -70 %, -69 %) and NO_x (+1 %, -14 %, -33 %).

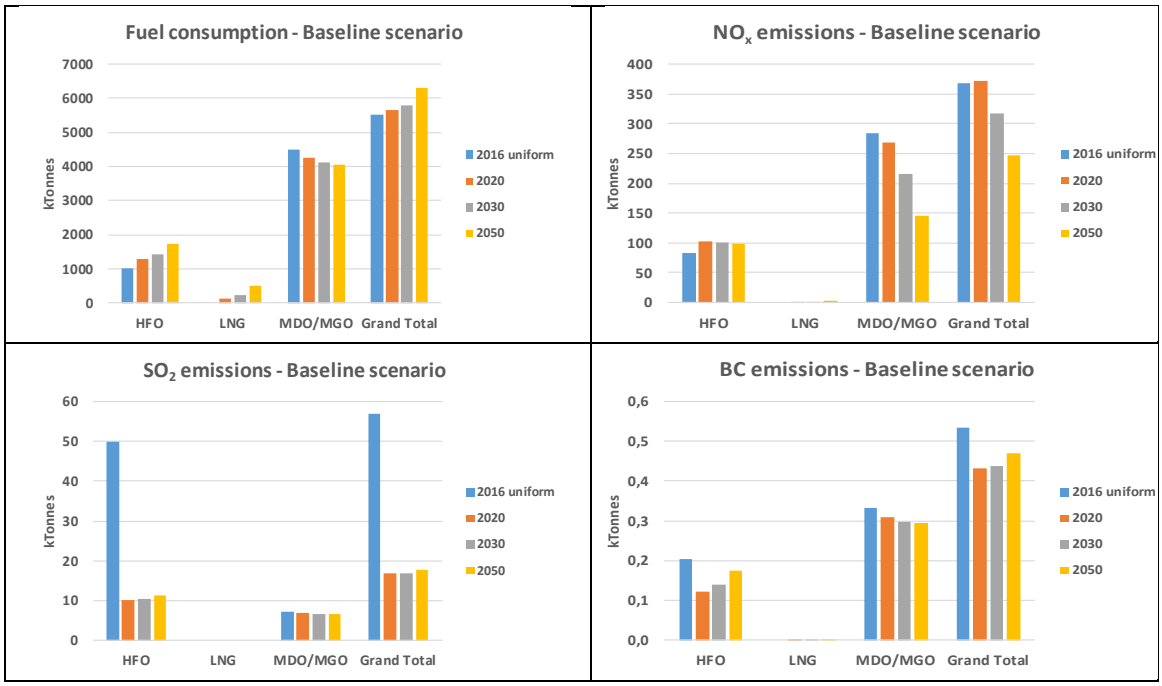

Figure 8: Total fuel consumption (by mass), NO_x, SO_2 and BC emissions calculated for 2016 (uniform gridded) and 2020, 2030 and 2050 in the Baseline BAU scenario.

The NO_x emission reductions during the forecast period (Figures 8 and 9) is due to the decrease in NO_x emission factors (Figure 5). The spatial NO_x emission reductions are most significant for the North SEA/Baltic Sea SECA area (Figure 9) where new engines installed on board ships from 1 January 2021 must comply with the most stringent Tier III NO_x emission standards. For SO_2 and BC, the major reason for the emission reductions from 2016 (uniform gridded) to 2020 shown on Figure 8 is the reduction of the HFO fuel sulphur content from 2.45 % in 2016 to 0.5 % in 2020 and the consequently reduced emission factors.

Despite the increase in total fuel consumption from 2020 onwards, the total emissions of SO_2 are almost stable during the forecast period due to the increasing amount of HFO being used in combination with EGCS (Figure 8). Also the gradually increased LNG fuel consumption assumed in the Baseline scenario plays an important role in the emission explanation for SO_2. The emissions of BC increase somewhat due to higher BC emission factors for HFO in combination with EGCS compared with the emission factors for the fuel being replaced (MDO/MGO inside SECA's, 0.5 % HFO outside SECA's).

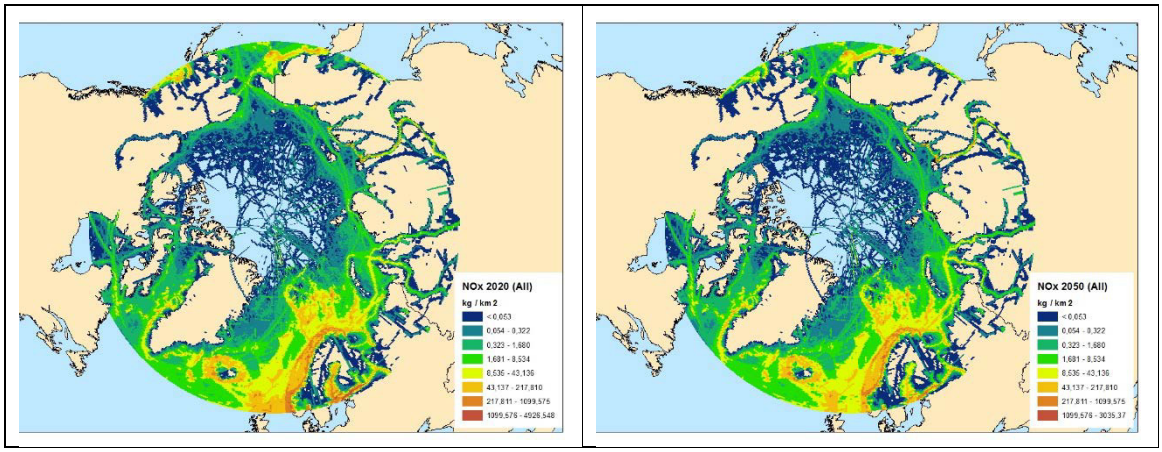

Figure 9: Spatial distribution of NO_x emissions for all ships in 2020 and 2050 calculated in the Baseline BAU scenario

The fuel consumption and NO_x emission totals are the same for the Baseline, SECA and HFO ban scenarios due to equal sfc and NO_x emission factors for HFO and MDO/MGO and similar LNG shares of total fuel consumption per forecast year assumed in all three cases.

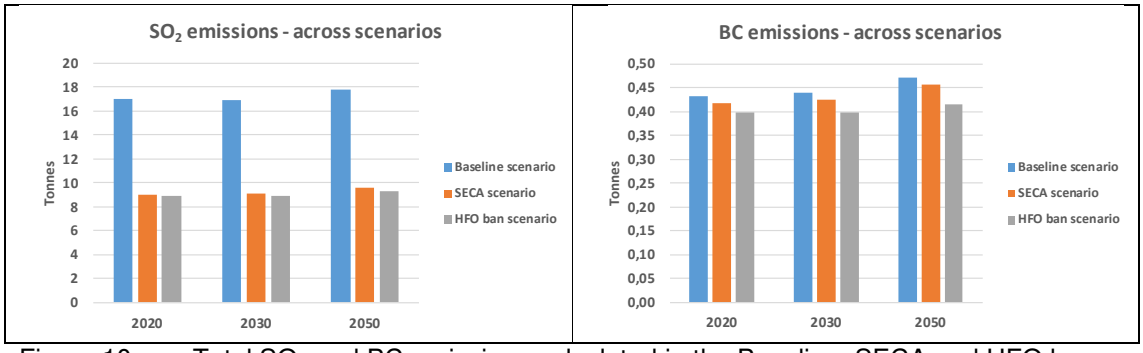

Figure 10: Total SO_2 and BC emissions calculated in the Baseline, SECA and HFO ban BAU scenarios.

In all scenario years, the calculated SO_2 emissions for the SECA and HFO ban scenarios are almost half of the emissions calculated for the Baseline scenario (Figures 10 and 11) for the following reasons. In the SECA scenario HFO is only used by ships in combination with EGCS and the remaining 0.5 % HFO used outside the original SECA area, and not being replaced by LNG, is being replaced by MDO/MGO. In the HFO ban scenario all HFO consumption by ships not being replaced by LNG is replaced by MGO/MDO.

For BC in 2020*[2030, 2050]* the HFO ban and SECA emissions are 8 %*[9 %, 12 %]* and 3 %*[3%, 3 %]* smaller, respectively, than the Baseline results. Apart from LNG with similar fuel consumption shares assumed in all scenarios, in the HFO ban scenario only MDO/MGO fuel is used with a correspondingly low BC emission factor. In the SECA scenario, HFO fuel in combination with EGCS is used with a relatively higher BC emission factor. However, in the SECA scenario, the BC emissions from MDO/MGO replacing 0.5 % HFO are smaller than the emissions from 0.5 % HFO used in the Baseline scenario due to the level of the BC emission factors.

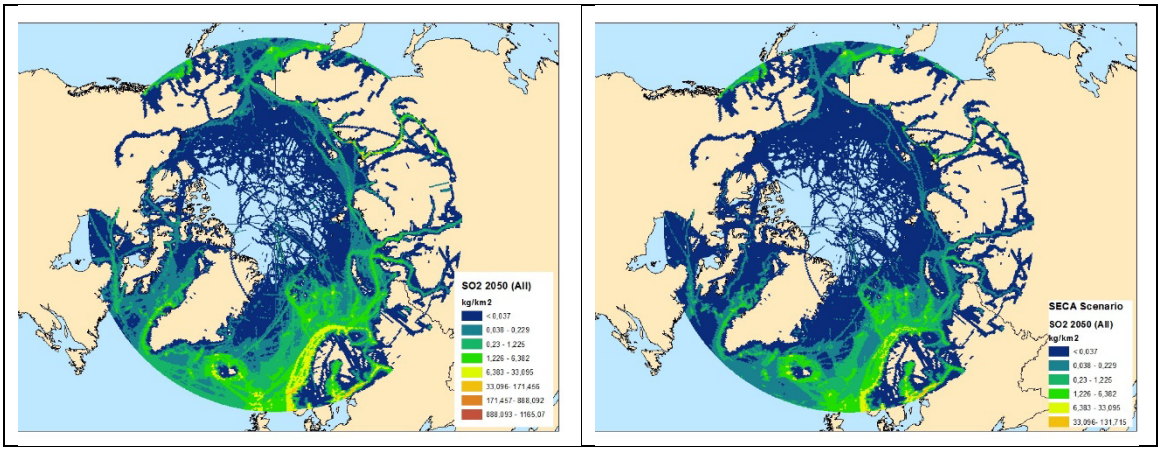

Figure 11: Spatial distribution of SO_2 emissions for all ships in 2050 calculated in the Baseline and SECA scenarios.

Figure 12 shows the fuel type specific results for the baseline EGCS shares assumed in the SECA (and Baseline) scenario and the high EGCS shares used in the "high case EGCS" model run. Emission results are only shown for SO_2 and BC, for the fuel types MDO/MGO and HFO, given that the use of EGCS is assumed to have no impact on fuel consumption and NO_x emissions, and that results for LNG remain unchanged in the two calculation situations. As predicted by the calculation assumptions, the total fuel consumption of HFO increases with the number of EGCS installed in a given projection year and the total fuel consumption of MDO/MGO correspondingly decreases (Figure 12). The BC and SO_2 emission differences between the baseline and high EGCS share calculations are rather small. For the high share EGCS model run, the total emissions of BC*[SO_2]* increase by 1 %*[0 %]*, 6 %*[2 %]* and 9 %*[3 %]* in 2020, 2030 and 2050, respectively, compared with the emissions obtained using the baseline shares of EGCS installed.

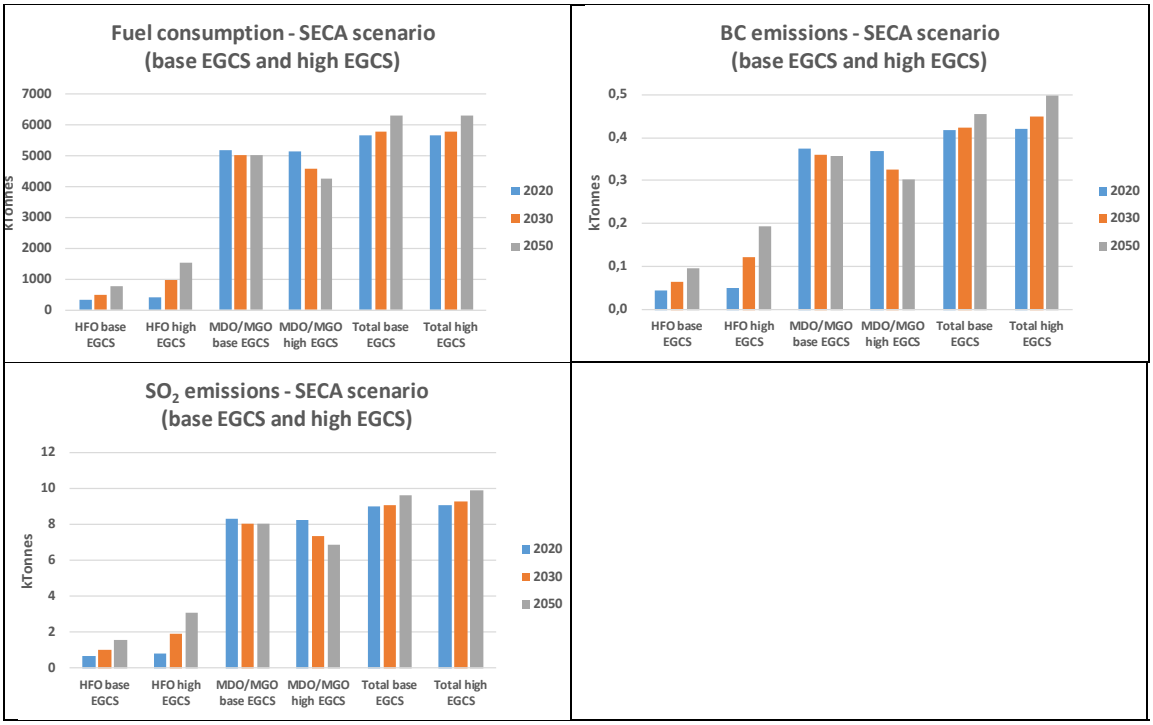

Figure 12: Total fuel consumption (by mass), SO_2 and BC emissions calculated in the SECA scenario.

4. Conclusions

This paper presents spatially distributed emission inventories for the Arctic area above 58.95N. For the historical years 2012-2016 inventories are based on satellite AIS data, ship engine power functions and technology stratified emission factors. Emission projections are made for the years 2020, 2030 and 2050 by using the robust five-year weighted historical data for ship traffic, updated traffic growth rates and emission factors. The emission projections include a Baseline emission scenario and two additional SECA and HFO ban scenarios. In the SECA scenario, the existing SECA zones (i.e. America and North Sea/Baltic Sea SECA's) cover the entire inventory area. In the HFO ban scenario, the use of HFO by ships is prohibited all across the inventory area.

For 2012*[2013, 2014, 2015, 2016]* the following total results are calculated for fuel: 4.8*[5.1, 6.3, 6.6, 5.4]* MTonnes; SO_2: 81*[84, 108, 60, 53]* kTonnes; NO_x: 320*[339, 429, 432, 361]* kTonnes and BC: 0.71*[0.73, 0.86, 0.65, 0.56]* kTonnes. In the Baseline scenario for the years 2020*[2030, 2050]* the following total results are calculated for fuel consumption: 5.7*[5.8, 6.3]* MTonnes; SO_2: 17*[17, 18]* kTonnes; NO_x: 371*[318, 247]* kTonnes and BC: 0.43*[0.44, 0.47]* kTonnes.

The following percentage changes between the uniform gridded 2016 results and the Baseline BAU results for the forecast years 2020, 2030, 2050, respectively (results in brackets) are calculated for fuel consumption(+3 %, +5 %, +14 %), BC(-19 %, -18 %, -12 %), SO_2 (-70 %, -70 %, -69 %) and NO_x (+1 %, -14 %, -33 %).

The introduction of a fully covering SECA zone or a complete ban of HFO use in the inventory area are both very efficient means for the reduction of SO_2. In all scenario years the calculated SO_2 emissions for the SECA and HFO ban scenarios are almost half of the emissions calculated for the Baseline scenario. The emission reduction potential for BC is less promising; in 2020*[2030, 2050]* the HFO ban and SECA emissions are 8 %*[9 %, 12 %]* and 3 %*[3%, 3 %]* smaller, respectively, than the Baseline results.

Bearing in mind the scarcity of BC measurement data from EGCS systems, and hence higher uncertainties on results, this project calculate small total emission increases for the more widespread use of EGCS in the high share EGCS model run compared with baseline shares of EGCS installed. In 2020*[2030, 2050]*, the total BC emissions increases become 1 %*[6 %, 9 %]*.

In all areas, the emission factors for BC are still very uncertain, and the obtained emission results for this component must be regarded with care. Hence, due to the level of impact from the different factors that influences the emissions of BC from ship engines, additional measurement research is needed in this field. In this way, BC formation is influenced by many variables such as fuel properties (e.g. hydrogen/carbon ratio), fuel blend composition for lower sulphur hybrid fuels (residual and light fraction blends), engine type, engine IMO Tier standard and engine load (e.g. ICCT, 2016). Any new data arriving on BC emission factors will be carefully assessed in future shipping emission projects for possible inclusion in updated emission inventory calculations.

Acknowledgments

Daniel Lack, Air Quality and Climate Consulting, must be thanked for providing engine load specific data for BC emissions used in this study. Also many thanks to Jens Peter Hansen, Alfa Laval, for discussions related to EGCS emission reduction rates and to Per Winther Kristensen, Danish Shipping, Palle Kristensen, DMA and Michael Prehn, Danish Maritime, for providing views on global EGCS deployment rates for shipping in the forecast years.

References

Aakko-Saksa, P., Murtonen, T., Vesala, H., Koponen, P., Nyyssönen, S., Puustinen, H., Lehtoranta, K., Timonen, H., Teinilä, K., Hillamo, R., Karjalainen, P., Kuittinen, N., Simonen, P., Rönkkö, T., Keskinen, J.,

Saukko, E., Tutuianu, M., Fischerleitner, R., Pirjola, L., Brunila, O.-P. and Hämäläinen, E. (2016), Black carbon measurements using different marine fuels, 28th CIMAC world conference, Helsinki 6-10 June, 2016.

Buhaug, Ø., Corbett, J.J., Endresen, Ø., Eyring, V., Faber, J., Hanayama, S., Lee, D.S., Lee, D., Lindstad, H. and Mjelde, A. (2009), Second IMO Greenhouse Gas Study 2009, IMO, London.

Corbett, J.J., Lack, D.A., Winebrake, J.J., Harder, S., Silberman, J.A. and Gold, M. (2010a), Arctic shipping emissions inventories and future scenarios, Atmos. Chem. Phys., 10, 9689–9704, doi:10.5194/acp-10-9689-2010.

Flanner, M.G., Zender, C.S., Randerson, J.T. and Rasch, P.J. (2007), Present-day climate forcing and response from black carbon in snow, Journal of Geophysical Research-Atmospheres, 112, D11202, doi:10.1029/2006jd008003.

Flanner, M.G., Zender, C.S., Hess, P.G., Mahowald, N.M., Painter, T.H., Ramanathan, V. and Rasch, P.J. (2009), Springtime warming and reduced snow cover from carbonaceous particles, Atmos. Chem. Phys., 9, 2481–2497, doi:10.5194/acp-9-2481-2009.

ICCT (2015), Database for marine black carbon emissions reduction strategies and technologies. Available at: www.theicct.org.

IICT (2016), Workshop summary: Third Workshop on Marine Black Carbon Emissions: Measuring and Controlling BC from Marine Engines, September 7–8, 2016, Environment and Climate Change Canada, Vancouver, British Columbia, Canada. Available at: http://www.theicct.org/events/3rd-workshop-marine-black-carbon-emissions

IMO (2015), Third IMO GHG Study 2014, Smith, T.W.P., Jalkanen, J.P., Anderson, B.A., Corbett, J.J., Faber, J., Hanayama, S., O'Keeffe, E., Parker, S., Johansson, L., Aldous, L., Raucci, C., Traut, M., Ettinger, S., Nelissen, D., Lee, D.S., Ng, S., Agrawal, A., Winebrake, J.J., Hoen, M., Chesworth, S. and Pandey, A. (2015), International Maritime Organization, (IMO) London, UK, April 2015. Available at: http://www.imo.org/en/OurWork/Environment/PollutionPrevention/AirPollution/Documents/ Third Greenhouse Gas Study/GHG3 Executive Summary and Report.pdf

IMO (2016a), Assessment of fuel availability – final report, 186 pp., IMO Marine Environment Protection Committee, MEPC 70/INF.6.

IMO (2016b: Air pollution and Energy Efficiency – Sulphur monitoring for 2015, 7 pp., IMO Marine Environment Protection Committee, MEPC 69/5/7.

Johnson, K., Miller, W., Durbin, T., Jiang, Y., Yang, J., Karavalakis, G. and Cocker, D. (2016), Black Carbon Measurement Methods and Emission Factors from Ships, 184 pp., Report prepared for: International Council on Clean Transportation, Report Prepared by: University of California, Riverside, December 2016.

Kristensen, H.O. and Lützen, M. (2012), Prediction of Resistance and Propulsion Power of Ships. Technical University of Denmark and University of Southern Denmark. Project no. 2010-56, Emissionsbeslutningsstøttesystem. Work Package 2, Report no. 04.

Lack, D., Lemer, B., Granier, C., Baynard, T., Lovejoy, E., Massoli, P., Ravishankara, A. R. and Williams, E. (2008), Light absorbing carbon emissions from commercial shipping, Geophys. Res. Lett., 35, L13815, doi:10.1029/2008GL03390, 2008.

Lack, D., Corbett, J., Onasch, T., Lerner, B., Massoli, P., Quinn, P.K., Bates, T.S., Covert, D.S., Coffman, D., Sierau, B., Herndon, S., Allan, J., Baynard, T., Lovejoy, E., Massoli, P., Ravishankara, A.R. and Williams, E. (2009), Particulate emissions from commercial shipping: Chemical, physical and optical properties, Journal of Geophysical Research, Vol. 114, D00F04, doi:10.1029/2008JD011300.

Lack, D. and Corbett, J.J. (2012), Black carbon from ships: a review of the effects of ship speed, fuel quality and exhaust gas scrubbing, Atmospheric Chemistry and Physics Discussions 12, 3509e3554. Available at: http://dx.doi.org/10.5194/acpd-12-3509-2012

Quinn, P.K., Bates, T.S., Baum, E., Doubleday, N., Fiore, A.M., Flanner, M., Fridlind, A., Garrett, T.J., Koch, D. and Menon, S. (2008), Short-lived pollutants in the Arctic: their climate impact and possible mitigation strategies, Atmos. Chem. Phys., 8, 1723–1735.

Starcrest (2013), Port of Los Angeles Inventory of Air Emissions – 2012. Available at: http://www.portoflosangeles.org/pdf/2012_Air_Emissions_Inventory.pdf.

Winther, M., Christensen, J.H., Plejdrup, M.S., Ravn, E.S., Eriksson, Ó.F., and Kristensen, H.O. (2014), Emission inventories for ships in the arctic based on satellite sampled AIS data, *Atmospheric Environment*, *91*, 1-14. Available at: 10.1016/j.atmosenv.2014.03.006

Winther, M., Christensen, J.H., Angelidis, I. and Ravn, E.S. (2017), Emissions from shipping in the Arctic from 2012-2016 and emission projections for 2020, 2030 and 2050. Aarhus University, DCE – Danish Centre for Environment and Energy, 118 pp., Scientific Report from DCE – Danish Centre for Environment and Energy (in press).

CO_2 emissions of the European Heavy Duty Truck Fleet, a Preliminary Analysis of the Expected Performance Using VECTO Simulator and Global Sensitivity Analysis Techniques[1]

N. Zacharof[1], G. Fontaras[1], B. Ciuffo[1], A. Tansini[1], T. Grigoratos[1] , I. Prado[1] and K. Anagnostopoulos[1]*

[1]European Commission Joint Research Centre, Ispra, Via E. Fermi 2479, 21027, Italy

*Corresponding Author: georgios.fontaras@ec.europa.eu

Abstract

The new approach for the certification of CO_2 emissions Heavy Duty Vehicles in the EU foresees the use of vehicle simulation in order to calculate and then assign the respective emission and fuel consumption values to each vehicle. For this reason the European Commission developed the Vehicle Energy Consumption Tool (VECTO). VECTO initially will be used for monitoring CO_2 emissions and fuel consumption from HDVs, while in the future it will assess the progress to reach CO_2 targets that will be established in the near future. Setting such targets for Heavy Duty Vehicles is not a simple task as a multitude of factors and parameters affecting the CO_2 emissions of the actual fleet need to be considered. The study attempts a first investigation of the problem by means of a global sensitivity analysis on VECTO. The most important input parameters for running VECTO were sampled either from fleet-data based distributions or, in cases where the latter were not available, from random distributions respecting the expected boundaries for modern tractor-trailer vehicles (Class 5 vehicles). More than 2000 simulation cases were developed and run in VECTO over the official driving cycles. Results showed an almost normal distribution of the fuel consumption both over the long haul and the regional delivery cycle with an average fuel consumption of 31.8 and 32.7 l/100km, respectively. The specific fuel consumption was estimated at 1.65 and 2.5l/100tonne-km. Finally in order to facilitate calculations by other users simplified regression models are provided where only a limited number of variables is necessary for calculating fuel consumption.

1 Introduction

In May 2017 a new approach for the certification of CO_2 emissions in EU has been voted (COM/2017/0279 2017). This new approach foresees the use of vehicle simulation in order to assign CO_2 and fuel consumption values to Heavy Duty Trucks sold in the European market. In a second step these values will be monitored in order to quantify with higher accuracy the green-house gas emissions emitted from the Heavy Duty transport activity and assess the progress made in reaching the established targets for a more sustainable transport sector (European Commission 2017a).

The certification and monitoring process is founded on the Vehicle Energy Consumption Tool (VECTO) (European Commission 2017c), which is the official tool for estimating CO_2 emissions from Heavy Duty Vehicles (HDV). The tool runs with some predetermined parameters, such as the vehicle's payload that depends on the vehicle class and the intended use in order to ensure

[1] The views expressed in this paper are purely those of the authors and shall not be considered as an official position of the European Commission under any circumstance

comparable results between vehicles of the same class. However, users can modify a series of parameters that characterize the vehicle and define its fuel consumption and CO_2 emissions.

In parallel to the above the European Commission is considering the introduction in the future of CO_2 targets to be based on the CO_2 monitoring mechanism. One difficulty in proposing specific targets is the lack of a clear picture regarding the fuel consumption and CO_2 emissions of European trucks today. In addition, even if one could accurately calculate the CO_2 performance of existing vehicles using VECTO, there are several uncertainties induced by the inputs used to run the model and the model's operation itself. Further to this, it is essential that any CO_2/fuel consumption values that will be officially attributed to the vehicles, maintain a close connection to what drivers will experience in reality in order to be representative and not undermine the associated policy initiatives.

In order to investigate the uncertainties associated with the VECTO CO_2 estimates a wide-scale sensitivity analysis on class 5 trucks (tractor-trailer vehicles) was performed. Class 5 trucks account for most of the CO_2 emissions of the HDV sector. More than 2000 simulation cases were defined and executed for the purpose. The current study focuses on the sensitivity of VECTO to certain, user-defined, parameters which characterize the most relevant vehicle characteristics affecting CO_2 emissions and tries to provide some estimate of the uncertainty that should be taken into account when establishing future CO_2 targets. The results of the detailed sensitivity analysis were used to derive simplified regression models that can be used in cases that limited info is actually available about the vehicles.

2 Methodology

2.1 Input parameter description

VECTO can run in two modes: Engineering and Declaration mode. In engineering mode, the user is free to adjust most of the simulation parameters, while Declaration mode, intended for official certification purposes, has a predefined set of simulation parameters. Predefining these parameters in official simulations ensures that vehicles are simulated under the same conditions producing comparable results. The study utilized the Declaration mode from VECTO and focused on HDV Class 5 which accounts for the majority of the vehicles that were included in the first version of the European HDV CO_2 monitoring legislation.

The main parameters that vary in Declaration mode, related to the mission profile (Luz et al. 2014), are the payload and the driving cycle, with VECTO applying three[2] types of payload: empty, reference and full. Empty and full payload reasonably correspond to empty and fully loaded vehicles, while reference payload is considered a representative payload value for the vehicle class. The driving cycles are distance based, meaning that a vehicle runs a certain distance with an allocated target speed, which the vehicle attempts to reach. The target speed varies throughout the cycle in order to simulate real world conditions (European Commission and TUG 2017). In this sense the cycle's average target speed, as well as the acceleration and deceleration events, described as transient conditions, become fundamental in calculating fuel consumption. Table 1 presents the reference payload values for Class 5 vehicles by driving cycle.

Table 1: Reference payload in kg by driving cycle (European Commission and TUG 2017).

Vehicle	Long haul	Regional delivery
Class 5	19300	12900

[2] At the time of the study VECTO performed calculations for 3 payload values. The simulated payloads are reduced to two in VECTO version 3.2.0.940: low load and reference load.

Figure 1 presents the target speed profile and the mean target speed of the driving cycles that were used in the analysis. A closer examination of the speed profile shows that the long haul cycle has the lowest number of acceleration/deceleration events, while the regional delivery and the municipal utility are more transient cycles. Especially in the municipal utility, the most transient conditions and stop events are observed at low speeds.

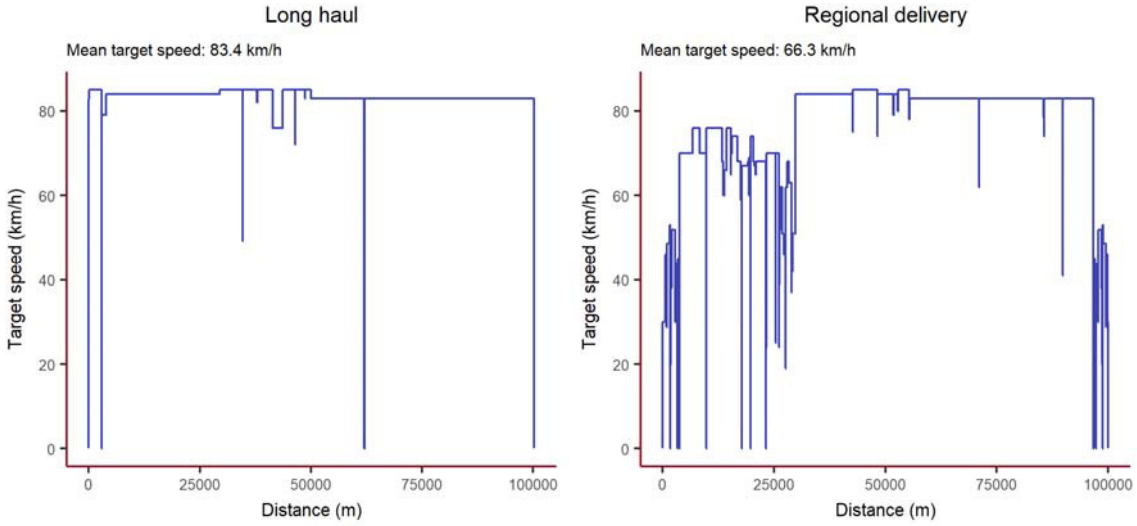

Figure 1: Target speed profile of driving cycles used in the study.

Initially, the user-defined parameters were screened (European Commission 2017b) and set the value range for each vehicle class. VECTO vehicle input parameters can be in the form of tabulated data, scalar values and categorical data, i.e. data that describe qualitative values instead of numeric ones. Figure 2 presents an example of the VECTO input data types.

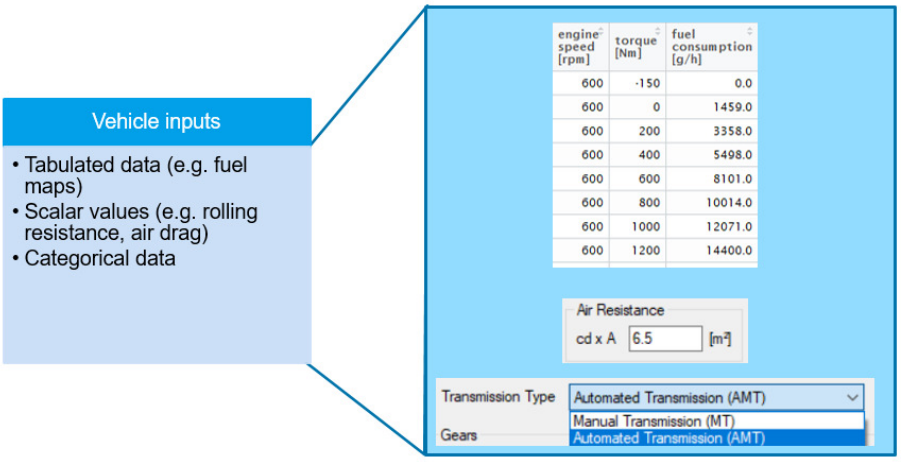

Figure 2: VECTO input data types and example of each data type.

The records of the tabulated data can be expressed in the form of loss-value, like e.g. torque in and torque out of the gearbox or efficiency unit or in absolute quantities. For the analysis a series of

multipliers were calculated and applied on the baseline values. This approach was applied for the following input data: fuel maps, gearbox torque loss maps and axle efficiency maps.

Since only few pre-existing fuel consumption maps were available, their modified versions used for the purposes of the study were produced by an extended Willans model (Guzzella and Onder 2009); a description of the model can be found in Sorrentino et al. (2015) and Zacharof et al (2017). The maximum engine power output curve plays an important role in VECTO operations. For defining the engine full load curve and further modifying it, a normalized generic full load curve was used as described by Hausberger et al. (2009). Regarding the gearbox torque loss and the axle efficiency map, no official input was available so the generic VECTO maps were used and modulated as previously described.

In a similar approach for the scalar inputs, the analysis used an internal JRC database to retrieve the range of possible values and calculate the sales-weighted mean and standard deviation. Table 2 presents the user-defined tabulated and scalar parameters, along with the minimum and maximum boundaries considered in the distributions from which the values were sampled. The table also presents the arithmetic mean modifier for the tabulated data and the sales-weighted mean for the scalar inputs.

Table 2: VECTO user-defined tabulated and scalar parameters with minimum, maximum and mean values

Input parameter	**Parameter ID**	**Class 5**		
		max	**min**	**mean**
Curb vehicle weight (kg)	cWv	8330	7016	7635
Gross vehicle weight (t)	gVw	40	16	28
Drag area (m^2)	CdA	6.50	4.20	5.32
Rolling resistance (kg/t)	RRC	6.30	4.60	5.46
Displacement (cc)	D	12901	10677	11994
Engine power (kW)	eP	374.9	310.0	337.7
Engine efficiency (multiplier)	eE	1.1	0.9	1.0
Gearbox torque loss and axle efficiency (multiplier)	A	1.2	0.8	1.0

Categorical data describe qualitative inputs that represent a specific technology, such as the steering pump type. The user selects a technology and VECTO applies a set of predefined parameters in order to properly simulate the technology. The analysis for the categorical data inputs applied all the supported available options of VECTO. Most of the categorical inputs correspond to auxiliary technologies and VECTO adjusts the auxiliary power load on the engine depending on the chosen technology (JRC and TUG 2016). Transmission technologies are also defined based on categorical input, with the version of the tool supporting Automated Manual Transmission (AMT) and manual transmission. By selecting one of the two transmission types, VECTO applies the respective parameters, such as gear shifting time that simulate the gearbox. Table 3 presents the categorical input parameters along with the list of the available technologies.

2.2 Uncertainty and sensitivity analysis and simplified model development

Objective of the study is to understand the variability of the fuel consumption of HDVs estimated using VECTO and to identify which parameters of the model has the main role in determining the

variability (with the possible objective to produce a simplification of the model). The first objective is achieved performing an uncertainty analysis of the model, while the second by performing a sensitivity analysis of the model.

Table 3: VECTO user-defined categorical input parameters (European Commission 2017b).

Input parameter	Parameter ID	Values
Transmission	tT	1. AMT 2. Manual
Fan	F	1. Crankshaft mounted - Electronically controlled visco clutch 2. Crankshaft mounted - Discrete step clutch 3. Hydraulic driven - Electronically controlled 4. Crankshaft mounted - On/off clutch 5. Crankshaft mounted - Bimetallic controlled visco clutch 6. Hydraulic driven - Variable displacement pump 7. Belt driven or driven via transm. - Electronically controlled visco clutch 8. Belt driven or driven via transm. - Discrete step clutch 9. Belt driven or driven via transm. - On/off clutch 10. Belt driven or driven via transm. - Bimetallic controlled visco clutch 11. Hydraulic driven - Constant displacement pump
Steering pump	sP	1. Variable displacement elec. controlled 2. Variable displacement mech. controlled 3. Dual displacement 4. Fixed displacement with elec. control 5. Fixed displacement
Electric system	eS	1. LED 2. Default
Pneumatic system	pS	1. Medium Supply 1-stage + mech. clutch + AMS 2. Medium Supply 2-stage + mech. clutch + AMS 3. Medium Supply 1-stage + visco clutch + AMS 4. Medium Supply 1-stage + mech. clutch 5. Medium Supply 1-stage + ESS + AMS 6. Medium Supply 2-stage + visco clutch + AMS 7. Medium Supply 2-stage + mech. clutch 8. Medium Supply 2-stage + ESS + AMS 9. Medium Supply 1-stage + visco clutch 10. Medium Supply 1-stage + ESS 11. Medium Supply 2-stage + visco clutch 12. Medium Supply 2-stage + ESS 13. Medium Supply 1-stage 14. Medium Supply 2-stage

LED: Light Emitting Diode
ESS: Energy Saving System
AMS: Advanced Mechatronics System

In both cases a probabilistic numerical setting was considered. In particular, a Monte Carlo framework has been used to randomly generate approximately ~2000 combinations of the input parameters listed in Table 2 and Table 3. In particular, in each combination, the parameters have been independently sampled from their distributions in order to achieve approximately ~2000 test cases for each vehicle class. In order to guarantee the best possible coverage of the

multidimensional parameter space, the Sobol low-discrepancy sequence of quasi-random numbers has been used in the analysis (Sobol 1976). 2048 parameters combinations have been used as the Sobol sequence guarantees minimal discrepancy of the sample for power of two dimension. A truncated normal distribution using the data reported in Table 2 and Table 3 (mean, standard deviation, minimum and maximum values) has been used to sample the different parameter values. Since the distributions reported in the aforementioned tables are derived using the annual vehicle sales, the distribution of the fuel consumption calculated from the model can also be considered as a proxy of the distribution in fleet fuel consumption.

Per each parameter combination VECTO was ran in Declaration mode and in each case it applied the mission profiles that are implemented in the tool as foreseen by the legislation. As already anticipated, from the results of 2048 VECTO simulations, the following analyses have been carried out:

1. Estimated probability distribution of the fuel consumption and the transport efficiency of the vehicle fleet.
2. Applied a variance-based sensitivity analysis on the simulation results
3. Produced multiparametric simplified model for calculating fuel consumption without running VECTO simulations

The analyses focused on the cases with the reference payloads. In the first analysis (1), the simulation results have been used to derive the distribution of the fuel consumption In order to provide more accuracy, the analysis separated the results by mission profile. In addition, in order to produce a more suitable comparison, the analysis also produced a probability distribution of the transport efficiency. The metric of transport efficiency metric was l/100tkm and represent the amount of fuel that is consumed in order to move 1 t of payload over 1 km.

In the second analysis (2), the simulation results have been used to identify the most influential parameters for each driving profile using the reference payload of each class. In order to achieve this objective, a global sensitivity analysis (SA) of the model has been carried out. Given the characteristics of the VECTO model, the methodology proposed by Ciuffo et al. (2013) has been adopted in the present study. More information about this methodology is provided in section 2.3. The following paragraphs describe in detail the Kriging-based approach that was applied in the second analysis (2).

Finally, in the third step (3), the investigation produced two simplified multiparametric models for calculating fuel consumption without the need to run VECTO simulations to be used in cases that only few input information is available. The simplified model is based on multilinear regression, of the most influential input parameters against the VECTO simulated fuel consumption for each mission profile. The first regression model makes use of the results of the sensitivity analysis, taking into account the input parameters that present the highest sensitivity index. The second regression model makes use of the most influential VECTO inputs, which are also publicly available. The analysis calculated the root mean squared error (RMSE) to measure the differences in each model.

2.3 Kriging-based approach for the global sensitivity analysis of model outputs

The Kriging-based approach employed in this paper is based on the findings in reported in Ciuffo et al. (2013). Given the non-negligible computation time required by VECTO, the method first derives an analytical approximation of the model and then calculate variance-based sensitivity indices on it.

2.3.1 Kriging meta-models for the SA of computationally expensive simulation models

The Kriging approach was originally developed in the geostatistics field (Matheron 1963) and can be viewed as an estimator based on the value of neighbor points. The basics of the Kriging model

can be found in Matheron (1963) and in Kleijnen (2009). In the literature, numerous studies are available to show that this class of meta-model can provide a powerful statistical framework for computing an efficient predictor of model response for applications such as simulation optimization or sensitivity analysis (Kleijnen 2009). For more information about the possible formulations of the Kriging meta-model, the interested reader can refer to Kleijnen (2009). In the present study, the DACE MATLAB toolbox (Lophaven and al 2002) was used to estimate the parameters of the Kriging meta-model from the results of the 2048 VECTO simulations.

Once the meta-model is correctly estimated, the variance-based SA can be performed based on the meta-model instead of the real model. As it will be briefly outlined in the next section the number of model executions required to compute the sensitivity indices is in general bigger than the 2048 simulations used to estimate the meta-model. From here the advantage to use a Kriging-based approach for the SA (that otherwise would have been resulted unfeasible).

2.3.2 Variance-based methods via the Sobol decomposition of variance

The variance-based method based on Sobol variance decomposition has been adopted in the present study. The original formulation of the variance-based method comes from Sobol (2001), who provided the analytical derivation and the Monte Carlo-based implementation of the concept. The latest setting for its practical application was provided by Saltelli et al. (2010). This method consists of the evaluation of two sensitivity indices, i.e., the first order sensitivity index and the total sensitivity index.

Given a model in the form $Y(X_1, X_2, \ldots, X_k)$, the first order sensitivity index for a generic factor Xi with respect to the model Y can be defined as:

$$S_i = \frac{V_{X_i}\left(E_{\mathbf{X}_{\sim i}}(Y|X_i)\right)}{V(Y)} \quad (1)$$

while the corresponding total sensitivity index is defined as:

$$S_{T_i} = 1 - \frac{V_{X_{\sim i}}\left(E_{\mathbf{X}_i}(Y|X_{\sim i})\right)}{V(Y)} = \frac{E_{X_{\sim i}}\left(V_{\mathbf{X}_i}(Y|X_{\sim i})\right)}{V(Y)} \quad (2)$$

In Equations (1) and (2), E represents the expected value and V is the variance of the distribution of the model output Y. Xi is the i-th model input, and X~i is the matrix of all model inputs except Xi. The total sensitivity index of the i-th input factor (i.e., S_{T_i}) provides the sum of first and higher order effects (interactions) of Xi. When the total index S_{T_i} is 0, Xi can be fixed to a whatever value in its range of variability without affecting the outputs' variance. It is worth to mention that $\sum_{i=1}^{r} S_i \leq 1$ and $\sum_{i=1}^{r} S_{T_i} \geq 1$, with both being equal to 1 only for perfectly additive models (no interactions).

The calculation of the variance-based sensitivity indices presented in Equations (1) and (2) can be performed in a Monte Carlo framework. In this paper we adopted the approach specified in Saltelli et al. (2007) and (2010). In this method, the contextual calculation of the two sensitivity indexes for all input factors is achieved using $N(k+2)$ model evaluations, where N is the size of the Monte Carlo experiment, and k is the number of model inputs. N can vary from a few hundreds to several thousands depending on the structure of the simulation model. Thus, although the method is more efficient than other alternative methods, it cannot be considered cheap in terms of the absolute number of model evaluations. When the model's dimension is high and the computation time required by each evaluation is not negligible, the method is still unfeasible. In the presence

case, the analysis is extended to 13 input parameters. Even considering *N*=1000 (which it is usually assumed to be needed at least to be able to verify that the number has been sufficient), the SA would require 15.000 model evaluations. Hence, a Kriging meta-model is used instead of the simulation model to carry out the variance-based SA. In fact, such approach allows cutting the cost of each single model evaluation. In addition, the SA can be carried out with a higher dimension of the Monte-Carlo experiment, allowing a better evaluation of the sensitivity indices.

3 Results and discussion

3.1 Results overview and fuel consumption distributions

Initially, the results from all the runs were analyzed and focused on the fuel consumption in order to provide an overview of a possible fuel consumption distribution for modern vehicles. Visualizing the results, a probability distribution of the fuel consumption for the examined cases is presented in Figure 3 a.

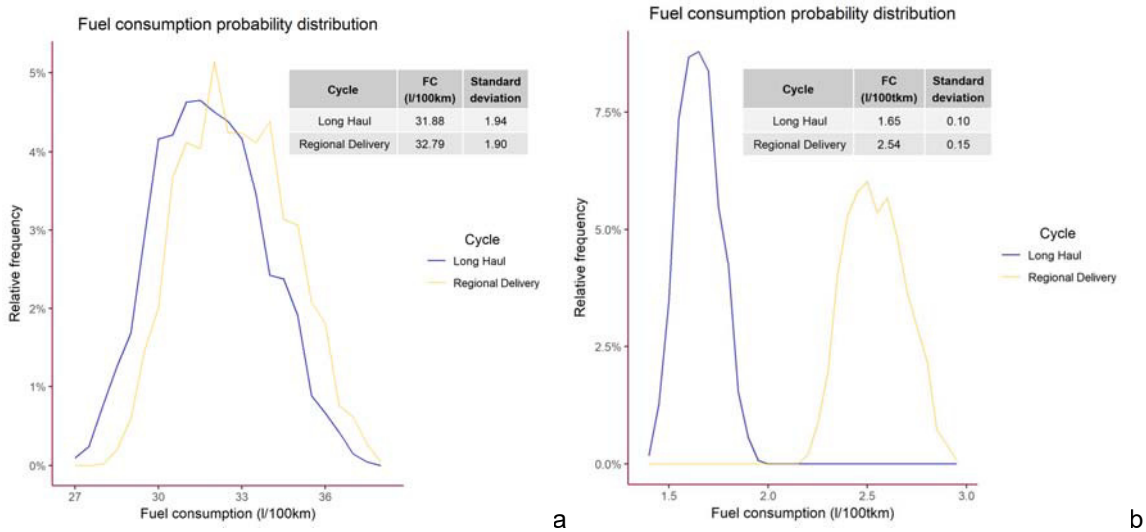

Figure 3: Probability distribution of the fuel consumption (a) and transport efficiency (b) distribution.

Results in Figure 3 are expressed in absolute fuel consumption values, which may not be comparable to each other due to differences in the payload, as the reference payload differs by driving cycle and vehicle class. For this reason Figure 3b presents the transport-efficiency probability distribution by cycle and vehicle class.

The results of the distribution probability analysis showed a Gaussian distribution of the fuel consumption values and can be considered to be representative of the 2015 vehicle fleet. Looking into the results there is an apparent divergence in the fuel and transport efficiency values which in the latter case are related to the driving cycle. Similar average fuel consumption values were observed in the long haul and the regional delivery cycle, 31.8 and 32.7 l/100km respectively. However, the payload in the regional delivery was 33.2% lower than in the long haul cycle and the follow up analysis found that the transport efficiency of the long haul cycle is higher compared to the regional delivery with the respective values to be 1.65 and 2.5 l/100tkm. The difference between the two cycles could be attributed to the slightly more transient conditions of the regional delivery.

It is worth mentioning here that the distribution in the fuel consumption derived from the 2048 parameter combinations can be considered as representative of the current fleet if no correlation exists among the different parameters. If the value achieved by a single factor in reality depends

upon the value achieved by the authors, the resulting distributions may be different. However, assuming the independence of the different parameters leads to a resulting uncertainty which is certainly higher than the actual one (because also combinations which in reality would not exist are included in the analysis). In this light the fuel-consumption distributions resulting from the present study can be considered as a worst case-scenario in terms of fuel consumption variability. In the reality, the actual fuel consumption distribution should be narrower than what is achieved here.

Future improvements on the vehicle can reduce further the fuel consumption and lower the mean fuel consumption closer to the current minimum values. The following analysis in paragraph 3.2 indicates the most significant factors for achieving this target.

3.2 Global Sensitivity Analysis

In the present section, the results of the VECTO sensitivity analysis are provided. Results are presented in terms of bar-charts showing first order and total sensitivity indices for different driving cycles. Figure 4 reports the sensitivity indices for the Long Haul and Regional Delivery cycle. In the different charts, the white bars represent the first order sensitivity indices per each parameter, while the black bar behind represents the total order indices. The visible part of the black bar represents the share of the variance in the model output (in this case the vehicle fuel consumption) explained by the interactions of each parameter with all the other parameters. In the charts, the model parameters are indicated using the labels defined in Table 2 and Table 3. In the different charts, also the 90% confidence interval per each sensitivity index is reported. This is calculated by performing a parametric bootstrapping of the meta-model evaluations used in calculating the sensitivity indices (for more information please refer to Saltelli et al.(2007)). As commonly experienced, also in this case, total order sensitivity indices achieve stability sooner than the first order ones (and the 90% confidence intervals appear significantly narrower). Since the objective of the study is the identification of the most important parameters, the total indices are those providing the necessary information and therefore the results presented in the charts can be considered acceptable for the global sensitivity analysis.

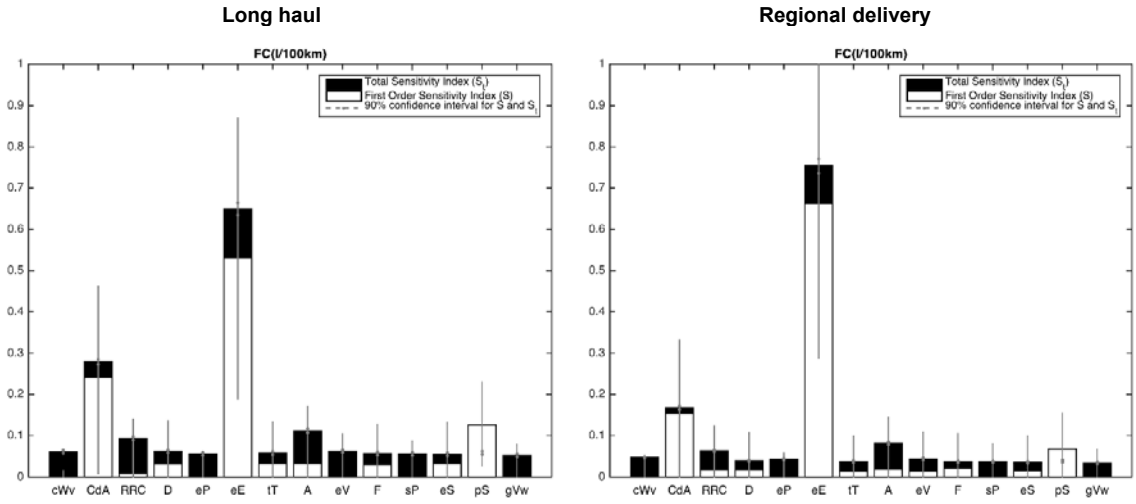

Figure 4: Sensitivity index for VECTO input parameters. Black bars behind corresponds to Total Sensitivity Index (S_t) and white bars in front to First Order Sensitivity Index (S). 90% confidence intervals for S_t and S are also reported.

An initial overview of the sensitivity analysis results showed that the engine efficiency is by far the most influential parameter in every cycle. An investigation of the cycles one by one showed that there is a differentiation in the next-more influential factors after engine efficiency.The sensitivity of the factors pointed out the drag area as the most influential factor – after engine efficiency – followed by the gearbox and axle efficiency for both cycles. It is interesting that the auxiliaries have the same impact in each cycle, but pneumatic system in both cycles stands out as more influential. The payload and the vehicle speed affect fuel consumption, but they are considered to stay stable over time; the need to transport goods remains the same, while the vehicle speed depends on the circulation regulation, and the area type and the structure of the area where the vehicle circulates.

3.3 Multiparametric simplified models

Based on the findings of the previous section the factors presenting the highest influence on fuel consumption were identified and used in order to derive simple multilinear regression models of fuel consumption. The first model included all the variables exhibiting a high sensitivity index, which are summarized in Table 4.

Figure 5 (a) presents the comparison between the simulated and the estimated fuel consumption, along with the regression formulas that were used for estimating the fuel consumption by driving cycle. The figure also presents the RMSE per driving cycle as an indicator for the dispersion of the error. The model results showed a good correlation between the VECTO and the regression fuel consumption, with relative low RMSE of 0.52 and 0.47 for the long haul and the regional delivery respectively.

Table 4 Main variables used for the extended and simple linear regression models and the corresponding share the variance accounted for. The case of a Class 5 vehicle.

Variable	**ID**	**Extended linear regression model cumulative variance share* (%)**		**Simple linear regression model cumulative variance share* (%)**	
		Long haul	**Regional delivery**	**Long haul**	**Regional delivery**
Total vehicle mass	M (t)	1	1	1	1
Air Drag area	CdA (m^2)	24	18		
Rolling resistance coefficient	RRC (-)	25	20	2	3
Engine Displacement	D (L)	28	22	5	5
Engine Power	P (kW)	29	23	6	6
Engine Peak Efficiency	E (%)	86	91		

* The cumulative variance share is calculated using only the first order sensitivity indices. Considering also the interactions, a higher share is expected to be explained by the listed variables. However information concerning the specific interaction of each parameter with any other parameter is not available in this study

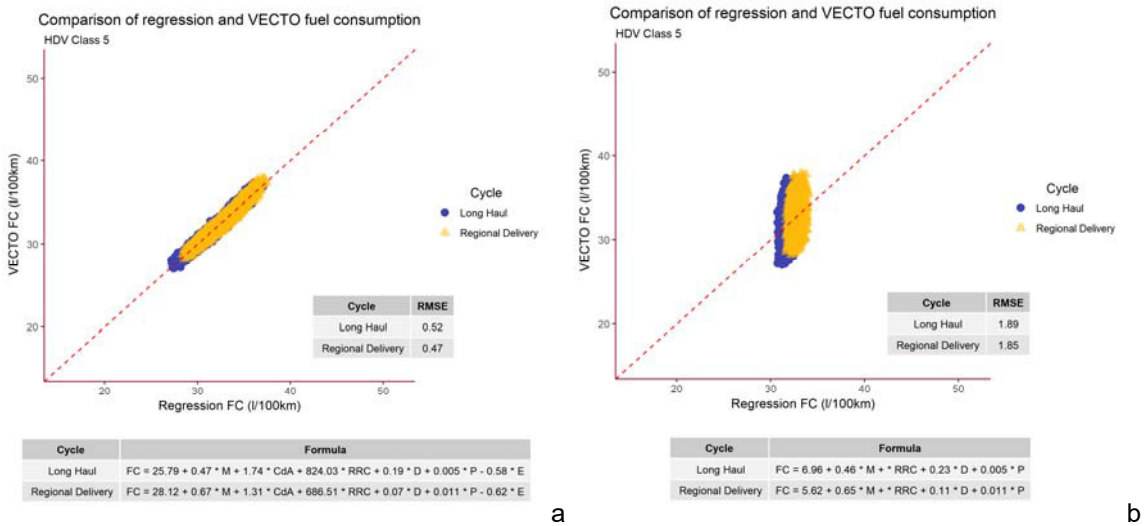

Figure 5: (a) First model - Comparison of VECTO simulated and regression fuel consumption by driving cycle. (b) Second model - Comparison of VECTO simulated and regression fuel consumption by driving cycle.

The first regression model utilized several parameters that could be difficult to find, as they rarely are publicly available. The second model proposed below uses parameters that can be found in public information documents. Figure 5 (b) presents the comparison between the VECTO simulated and regression fuel consumption, along with the regression formulas and the RMSE by cycle.The comparison of the results of the second model showed that VECTO calculations and the regression fuel consumption model are more loosely correlated with the removal of the drag area and engine peak efficiency inputs. The RMSE increased to 1.89 in the long haul cycle, 1.85 in the regional delivery (roughly 5% compared to the respective average fuel consumption value).

A comparison of the first and the second model shows clearly that the first calculates more accurately fuel consumption through the regression formulas, signifying the importance of making available parameters such as the drag area and engine peak efficiency. This attempt to create a simple formula for calculating fuel consumption showed the current limitations of such an attempt. In the future if more parameters are available it could be possible to create such a formula that anybody interested in the field could assess vehicle's fuel consumption easily and fast. In order to overcome the issue of some parameters being confidential, it could be possible for the manufacturers to provide vehicle-specific formulas to the users that would permit them to calculate their fuel consumption based on the available parameters.

4 Conclusion

The sensitivity analysis resulted in a distribution of the Class 5 HDV fuel consumption that should be representative of the 2015 vehicle fleet. Average consumptions of the order of 32l/100km were calculated. The latter should be compared against data from real operating conditions. It is expected that future technology improvements can lower further fuel consumption and converge with the minimum values of the distribution. The global sensitivity analysis indicated that the parameters with the highest impact are the engine efficiency, the drag area, the vehicle mass, the rolling resistance, and the engine characteristics. Any future initiative in the direction of reducing fuel consumption should aim at improving these factors. Finally, for simpler analyses, the simplified regression formulas could be used. The extended regression model would be more suitable, but as some input parameters are not publicly available its use may not be feasible. Thus for informing the consumers and allowing better monitoring of the vehicles' actual performance by experts it is advisable that the most important parameters affecting fuel consumption and CO_2 emissions are made available to the public.

5 References

Ciuffo, Biagio, Jordi Casas, Marcello Montanino, Josep Perarnau, and Vincenzo Punzo 2013 Gaussian Process Metamodels for Sensitivity Analysis of Traffic Simulation Models: Case Study of AIMSUN Mesoscopic Model. Transportation Research Record: Journal of the Transportation Research Board 2390: 87–98.

COM/2017/0279 2017 Proposal for a REGULATION OF THE EUROPEAN PARLIAMENT AND OF THE COUNCIL on the Monitoring and Reporting of CO_2 Emissions from and Fuel Consumption of New Heavy-Duty Vehicles. http://eur-lex.europa.eu/legal-content/EN/TXT/?uri=CELEX:52017PC0279, 2017.

European Commission 2017a COMMISSION REGULATION (EU) …/… Implementing Regulation (EU) No 595/2009 of the European Parliament and of the Council as Regards the Determination Of... https://ec.europa.eu/info/law/better-regulation/initiatives/ares-2017-1900557_en, accessed September 29, 2017.
2017b VECTO Input Parameters.
2017c Vehicle Energy Calculation Tool (VECTO).

European Commission, and TUG 2017 VECTO Manual.

Guzzella, Lino, and Christopher Onder 2009 Introduction to Modeling and Control of Internal Combustion Engine Systems. Springer Science & Business Media.

Hausberger, Stefan, Martin Rexeis, Michael Zallinger, and Raphael Luz 2009 Emission Factors from the Model PHEM for the HBEFA Version 3. Report Nr. I)20/2009 Haus)Em 33/08/679 from 07.12.2 009. Graz: TU - Graz. http://www.hbefa.net/e/documents/HBEFA_31_Docu_hot_emissionfactors_PC_LCV_HDV.pdf, 2016.

JRC, and TUG 2016 VECTO - Generic Values.

Kleijnen, Jack P. C. 2009 Kriging Metamodeling in Simulation: A Review. European Journal of Operational Research 192(3): 707–716.

Lophaven, Søren N., and et al 2002 DACE – A MATLAB Kriging Toolbox – Version 2.0.

Luz, Raphael, Martin Rexeis, Stefan Hausberger, et al. 2014 Development and Validation of a Methodology for Monitoring and Certification of Greenhouse Gas Emissions from Heavy Duty Vehicles through Vehicle Simulation. Report No. I 07/14/Rex EM-I 2012/08 699. Graz, Austria.

Matheron, Georges 1963 Principles of Geostatistics. Economic Geology 58(8): 1246–1266.

Saltelli, Andrea, Paola Annoni, Ivano Azzini, et al. 2010 Variance Based Sensitivity Analysis of Model Output. Design and Estimator for the Total Sensitivity Index. Computer Physics Communications 181(2): 259–270.

Saltelli, Andrea, Marco Ratto, Terry Andres, et al. 2007 Global Sensitivity Analysis. The Primer. Chichester, UK: John Wiley & Sons, Ltd. http://doi.wiley.com/10.1002/9780470725184, accessed September 26, 2017.

Sobol, I. M. 1976 Uniformly Distributed Sequences with an Additional Uniform Property. USSR Computational Mathematics and Mathematical Physics 16(5): 236–242.

Sobol, I. M 2001 Global Sensitivity Indices for Nonlinear Mathematical Models and Their Monte Carlo Estimates. Mathematics and Computers in Simulation 55(1). The Second IMACS Seminar on Monte Carlo Methods: 271–280.

Sorrentino, Marco, Fabrizio Mauramati, Ivan Arsie, et al. 2015 Application of Willans Line Method for Internal Combustion Engines Scalability towards the Design and Optimization of Eco-Innovation Solutions. *In* . http://papers.sae.org/2015-24-2397/, accessed November 30, 2016.

Zacharof, Nikiforos, Georgios Fontaras, Theodoros Grigoratos, et al. 2017 Estimating the CO_2 Emissions Reduction Potential of Various Technologies in European Trucks Using VECTO Simulator. SAE Technical Paper 2017-24-0018.

On-road determination of a reference CO_2 emission for passenger cars

N.E. Ligterink[1], A. Dimaratos[2], S. Doulgeris[2], D. Tsokolis[2], F. van Oosten[1], R.F.A. Cuelenaere[1], P. van Mensch[1], L. Ntziachristos[2], Z. Samaras[2]

[1]Sustainable Transport and Logistics Group, TNO, PO Box 96800, 2509 JE The Hague, The Netherlands
[2]Laboratory of Applied Thermodynamics, Department of Mechanical Engineering, Aristotle University of Thessaloniki, 54124, Greece
Keywords: on-road testing, CO_2, real-world emissions.
Presenting author email: norbert.ligterink@tno.nl

Introduction

The gap between real-world and type approval CO_2 emission values is growing, and the forthcoming WLTP is expected to have limited impact to close that gap. Laboratory tests take place in idealized circumstances, which do not capture all of the usual conditions experienced during daily driving and such a test can be optimized for attaining low CO_2 emissions. The on-road determination of CO_2 emissions, similar to the RDE legislation for pollutants, may prove able to serve as a more appropriate alternative for measuring the real-world emissions of vehicles.

Given the impact, the accuracy of a few grams per kilometre is needed to make such an on-road reference CO_2 value relevant. This accuracy is difficult to obtain with the current PEMS equipment and on-road instruments for pollutants. For example, the actual air-drag and road surface effect on rolling resistance, and the road slope are needed with high accuracy to compensate for local and ambient variations, which come naturally with on-road tests. Likewise, the battery state and auxiliaries' operation need to be incorporated in order to derive an accurate reference number, from the varying results, in a test in uncontrolled environment.

In order to correct the test variations to a reference value, substantial simulation effort is also needed. The additional CO_2 emissions associated with, for example, headwind, rough road surfaces, and battery charging, in all the different vehicle operations must be accounted for. A simulation model must be able to capture the intricate relations between vehicle operation and the external influencing factors. A reference value for a vehicle should not depend on the particular circumstances during the test. Hence modelling is essential to compensate for these variations. If possible this should be weighted over the variations encountered across Europe, or adaptable to a specific usage and location.

Both TNO and LAT have been working on this long-term goal to generate on-road reference CO_2 emission values. At TNO, new sensors and equipment is tested, validated, and calibrated, to come to a more accurate determination of the second-by-second variation in the influencing factors. LAT has been using this data to fine-tune their generic passenger car simulation model and predict the second-by-second results, , as well as the total CO_2 emissions performance. The combined effort allows for using on-road measurements into a validated simulation model, for each individual vehicle, to produce smoothed results under the same driving conditions, corrected for uneven parameters such as ambient temperature, wind intensity and direction, alternator operation etc.. The reference CO_2 emissions of an individual passenger car, with an accuracy based on the post-diction of the on-road results, will be the outcome of both testing and simulation activities and must cover all existing different vehicle variations, i.e., engine types (gasoline-MPI/GDI, diesel), powertrains - manual and automatic transmissions (hydraulic, double clutch) and vehicle sizes, configurations and topologies (incl. hybrid systems).

In this paper, the progress on this activity will be reported, including a way to more accurately determine road slope and air drag during a real-world trip, and the progress on the simulation model that incorporates these effects for an accurate prediction of the second-by-second CO_2 emissions. This will establish the baseline accuracy with which the reference CO_2 emission can be determined.

On-road variations in test conditions

Repeating on-road emission tests in the laboratory will seldom produce the same results. Installing only PEMS equipment and logging basics vehicle signals, like engine speed, are not sufficient to determine the conditions necessary to repeat a test. Moreover, repeating an on-road test is not possible given the variations in the vehicle state at the start of the test and with ambient conditions. Modelling is always needed to compare multiple real-world tests in detail. This comparison requires a multitude of additional signals at high accuracy. Measuring the alternator current, the road slope, and the actual air drag are the minimal requirements to determine the engine power demand accurately. The rolling resistance, on a variety of road surfaces and temperatures, forms another unknown factor, which will affect the power demand and engine operation.

Alternator current and voltage are easily recorded. Hence, starting with the most important aspects, road slope and air drag measurements in on-road testing are essential additions to the PEMS equipment, to understand, predict, and compare the measured results. The accuracy goals are not met, as yet. Standard equipment does not deliver the desired levels, of about twenty centimetres road incline over 100 metres, and 25 N variations in air drag, associated with about 1 m/s wind speed at 100 km/h driving. Both the incline and the air drag resolution are associated with a second-by-second accuracy in CO_2 emissions of about 5 g/km. For the average result the accuracy is expected to be better, as for example, gravitation force may have a limited net contribution in a round trip. However, large noise on the second-by-second signals will form the basis of a bias which may affect the average result.

Effect of wind on air drag

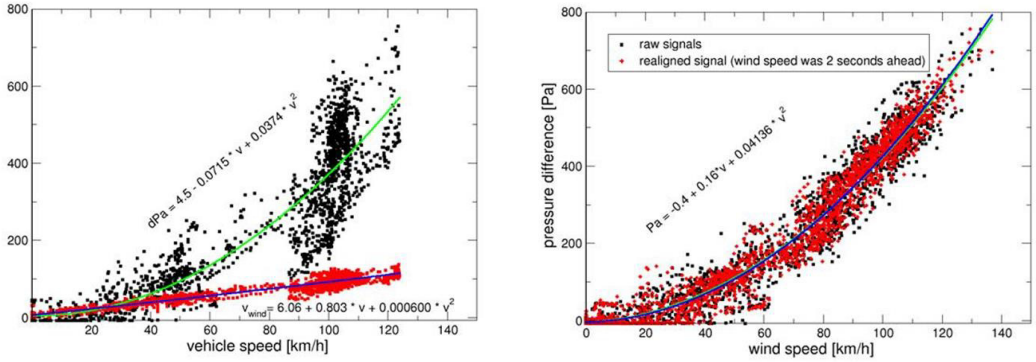

Figure 1 The left figure shows independently the pressure difference variation in black [Pa], and the wind speed in red [km/h], as function of the vehicle speed. Right, if the pressure differences are plotted against wind speed (above the vehicle), it is clear that the pressure difference fluctuations, and the corresponding air drag fluctuations, of more than 100% are correlated to the wind speed, and therefore a true phenomenon.

Simple formulas show air drag as a function of vehicle velocity alone. The implicit assumption is that other effects are limited. The air density may vary with temperature, altitude, and humidity. Air drag is proportional to the air density, and 20% variation in density across European locations and seasons is to be expected. Very likely, a greater part of the Dutch seasonal variation of 10% in fuel consumption is related to the variation in air-drag. (Ligterink 2016) Moreover, the wind may increase, or decrease the apparent air velocity over the vehicle. The effect of wind speed is instantaneous, and cannot be corrected for by altitude and weather data. Hence, TNO is looking for methods to record the effect of wind speed on the air drag fast and accurate. Two methods have been examined. One method is an anemometer attached to the roof of the car, recording the apparent wind speed near the car. The other system measures the pressure difference, while driving, between the front and the back of the car. The pressure difference is the most accurate and fastest signal. Moreover, pressure difference is already proportional to the air-drag force, while wind flow speed still has to be converted, using for example the density and compensating

for the distortion of the flow by the vehicle itself. The Buckley ABCD, or Ford, method of attaching the anemometer to a boom away from the car is not viable for driving on the public roads. (Buckley 1995) However, it should be clear that side wind and head wind may not result the same effect on air drag.

The location of the pressure sensors is key to the success of correcting the air drag for wind effects. In many locations the observed, dynamic pressure is lower due to the flow, through the Bernoulli effect. Hence, it is essential to place the sensors at forward and backward location on the car with limited flow. These locations are stagnation points. The pressure difference of a normal car at these points is associated with the air drag through an effective area of about one square metre. Hence, an air drag force of 400 N, at 100 km/h, is roughly related to a pressure difference of 400 Pa for a passenger car. The forward location has a much higher share in this pressure difference than the backward location. In the sensitivity for the location of the sensors, the forward sensor location is critical. Placing the forward sensor already 20 centimetres sideways off centre of the vehicle nose reduces the effect significantly, through two effects: lower static pressures than at the stagnation point, and reduced dynamic pressure due to the flow.

Road slope determination

In a round trip, starting and ending at the same location, no net gravitational force is added to the total work of the car. Hence, it could be concluded that road slope has limited effect on the total CO_2 emissions in a round trip. This is also reflected in simple models, like the Willans line approach, which assume a linear relation between power and CO_2 emissions. In the case of a steep downhill slope, which requires additional braking, these assumptions certainly no longer hold.

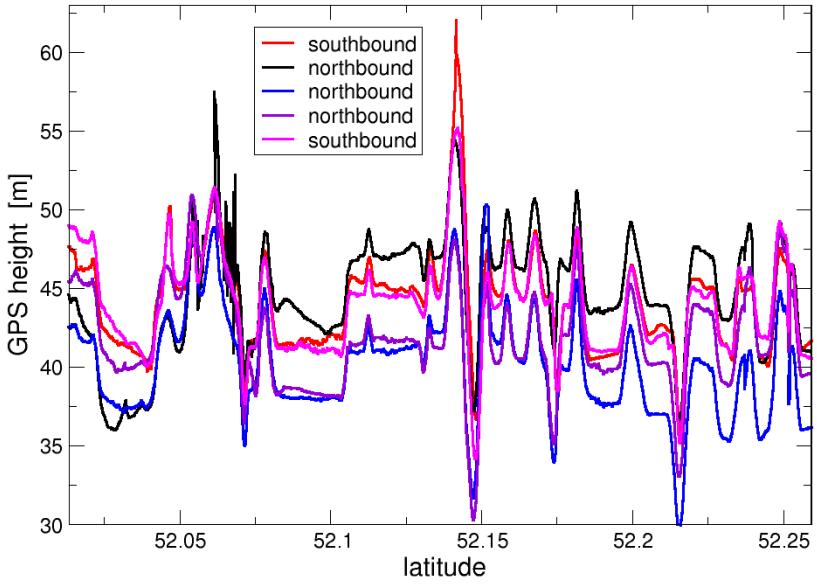

Figure 2 Repeat trips along the same route, in both directions (northbound and southbound), show substantial differences in the altitude with the Racelogic VBOX system. Absolute altitude is more poorly determined than slope, except for a few parts of the trip.

The road slope determination is important for many reasons. First of all, without an accurate road-slope determination, the second-by-second signal of fuel consumption cannot be analysed. It is one of the most important cause of variations in the power at the wheels. Other effects, all causing the variation in fuel consumption and CO_2 emissions are swamped by the effect of a few percent variation in road slope. Second, the Willans line approach, decomposing the total CO_2 emission

in a fraction proportional to the work, and the remainder as an offset associated with losses, is too simplistic to yield predictions with the required resolution. More detailed modelling requires more detailed input data on engine load, in which road slope and acceleration dominate.

The GPS signal is generally insufficient to determine the road slope accurately over distances of 100 metres or less. About 5 centimetres over 100 metres is the optimal resolution. Even systems with a accelerometers, like the Racelogic VBOX with IMU, did not meet the criteria in repeat driving along the same route. Therefore, TNO is investigating options with barometric pressure sensors. Cheap MEMS sensors with relative accuracy of a few Pascal seem promising to determine the altitude and the slope accurately. See Figure *2*.

Over the duration of a two hour trip, the barometric pressure may change slightly with the weather. In extreme cases this can result in a change of pressure corresponding to about 50 metres altitude change. With a pressure reading at the same location stationary at the beginning and the end of a test, this drift in pressure is easily compensated for.

The important aspect in developing such an approach based on barometric pressure is the placement of the sensors in, or on, the vehicles. Testing different sensors at different location show both a sensitivity for the blower and air inlet in the cabin, and the flow around the vehicle, inside and outside the cabin. The vehicle velocity is an important part in both locations. The velocity of the vehicle generates a lower pressure in and below the vehicle. The effects of vehicle velocity correspond, at best, to a misreading of the altitude by a few metres. See Figure *3*. Automatically compensating for this effect is an ongoing research. The eventual goal is a plug-and-play system which combines probably two pressure sensors and the velocity signal to correct for velocity dependencies of the pressure readings, compared to the static ambient pressure.

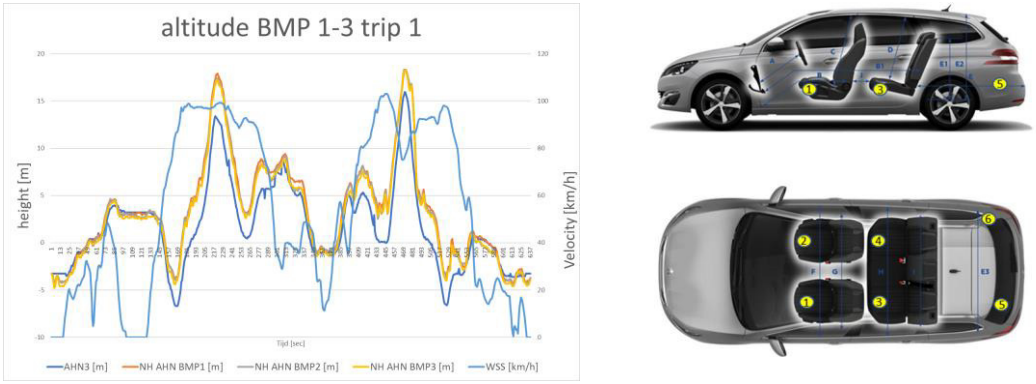

Figure 3 Different pressure sensors (BMP1-3) in the vehicle compared with the map-based altitude (ANH3). With the higher velocities, all sensors show a systematic deviation upward of a few metres, associated with a lower pressure readings.

Rolling resistance variations and determination

Overcoming rolling resistance is an important part of the power demand of a vehicle at low velocities. So far, coastdown tests and installing torque meters are the manner in which the rolling resistance is determined as part of the total driving resistance of a vehicle. An accurate determination of the altitude allows for an alternative determination of rolling resistance. On a downhill slope, the rate in which a vehicle picks up speed is a quite accurate manner to determine the driving resistance at low and moderate speeds.

If the data of the downhill velocity pick-up is plotted in a particular manner the driving resistance can be read of immediately from the gradients of the curve in the plot. If the total energy of the car: gravitational and kinetic is plotted against the distance driven, the decrease of this total energy over the distance is the driving force. In a simple test, nine repeats of the downhill run, the

average force over the run was 154 N, with a run-to-run variation of 15 N, or 10%. The altitude determination was with GPS and still adding a source of uncertainty. With the improved altitude determination and stricter test protocol, it is expected that the accuracy of this rolling resistance determination will be much better. See Figure 4.

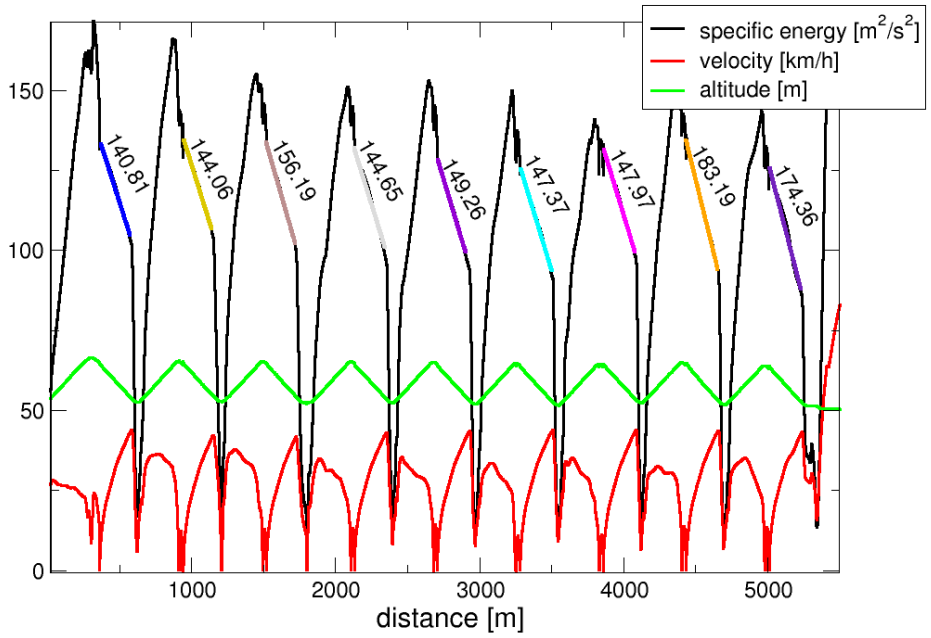

Figure 4 A repeat run with coasting down the hill shows the velocity picking up from nearly zero to 40 km/h, increasing kinetic energy but lowering the gravitational potential energy. The net effect is energy lost by driving resistance. The indicated numbers a resistance force in Newton from linear fits.

This study on rolling resistance determination will be continued once the altitude measurements have been made fit for standard on-road testing at TNO. But plotting the specific energy, i.e., the total energy per kilogram, of a vehicle is an interesting approach to avoid using finite differences of noisy signals as input to simulations. Moreover, such an approach allows for averaging over different time scales, to ensure most is made of the data with limited noise.

Development of vehicle simulation models with generic specifications

After the accurate determination of the factors influencing strongly the on-road CO_2 emissions, the vehicle simulation model is developed. All the detailed information produced by processing the on-road test data (as described above) is used as input to the model. The procedure followed for the evaluation of real world CO_2 emissions with generic simulation models developed on the basis of PEMS data and RDE recordings is described with the next steps and can be seen in Figure 5:

1. In the first step, a validated vehicle model is used to specify and investigate the difficulties and limitations of the approach. The real-world measurements are simulated with the model, which was built with input data derived by the respective OEM and the results are compared against experimental data. These simulations provide some first indications of the difficulties and the limitations of the approach. The PEMS measurements are used to back calculate the engine map of the tested vehicle. This is performed by stretching an

existing vehicle model (hereinafter called “generic model”) with partial “generic” characteristics (engine map, powertrain losses etc).

2. For the second step, the same procedure is repeated for a new developed vehicle model with generic data, such as the engine map and the powertrain losses.

3. In the third step, a comparison between the simulated CO_2 emission results for the two vehicle models is conducted that highlights any differences among them, indicating the parameters that need further calibration.

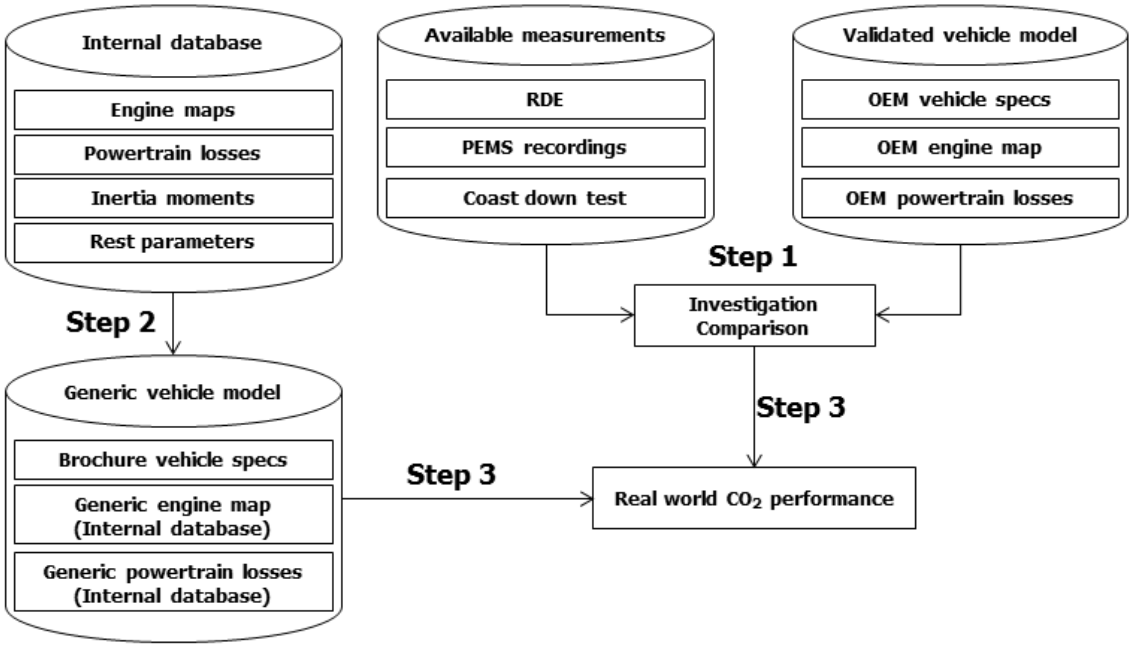

Figure 5: Schematic of the followed methodology.

The approach is applied in two vehicles, the main specifications of which can be found in Table 1. The vehicle simulation models were developed in the AVL Cruise simulation software (AVL, 2017) and validated in the context of WLTP/NEDC correlation exercise (Tsokolis et al. 2015, 2016) achieving a final error of less than 2 gCO_2/km compared to chassis dynamometer measurements. The graphical user interface of AVL Cruise, together with the main vehicle components that were used for the simulations are shown in Figure 6 and explained below:

- Component No 1 is used to describe the vehicle body, where information relevant to the test mass and the driving resistance coefficients are inserted as input.

- Component No 2 describes the internal combustion engine where its specifications (fuel, displacement, number of cylinders, etc.) for the simulated vehicle are inserted. Additionally, this component uses the fuel consumption (FC) map, the full load and the motoring curves of the engine.

- Component No 3 (group of components) includes the drivetrain and it consists of the clutch, the gearbox, the final drive, the differential and the driven wheels. The most important input parameters of this component are the gear and final drive ratios, the torque loss map of the drivetrain system and the tire dynamic radius.

- Component No 4, which consists of the generator and its pulley, the battery, the starter and the electrical consumer along with their controllers, simulates the electrical system of the vehicle.

- Component No 5, apart from the Start & Stop system, includes additional necessary modules essential for the simulation.

Table 1: Vehicle specifications used for the real-world simulations.

Vehicle	Transmission	Curb mass [kg]	Displacement [cc]	Max Power [kW]	Max Torque [Nm]
MPV	MT, 6 gears	1601	1598	100	320
C Segment	MT, 6 gears	1293	1560	88	270

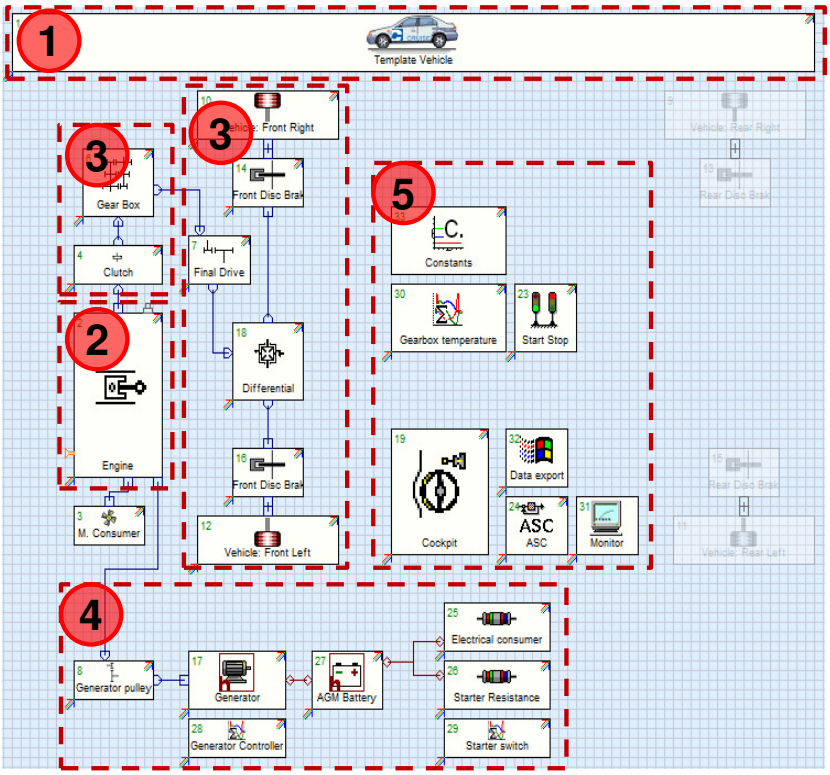

Figure 6: Graphical user interface and topology of the simulation models.

The next step, after the development of the models, is their validation against real-world data obtained with PEMS. The tests were conducted by TNO with SEMS as part of their standard on-road measurement program in the area The Hague. (Heijne 2016) The study of signals for alternator currents, and electric power usage, road incline, and air drag, described above, are not suitable yet for this investigation.

Figure 7 The vehicle with SEMS equipment in and under the car and different pressure sensors installed at the back can be operated in normal use.

The available instantaneous data from the tests include time, altitude, longitude, latitude and vehicle speed provided by the installed GPS, ambient temperature, engine coolant temperature, engine speed, intake air temperature, air flow rate, vehicle speed from the vehicle's OBD and

CO_2, CO, NO_2 and NO_x emissions from the PEMS or SEMS instrument, while fuel consumption was calculated. The vehicle with the SEMS and pressure measurement installation can be seen in Figure 7.

During the real-world validations, time, altitude, vehicle speed from the GPS, engine speed from the OBD and CO_2 emissions from the PEMS instrument, together with the calculated fuel consumption, were used. For the determination of driving resistance, the WLTP Road Load (RL) of the two vehicles was used, in order to estimate the real world RL. The driving resistance coefficients were adjusted according to vehicles' test mass. Additionally, in order to simulate alternator's power demand, the generic electrical system's model was calibrated and used in the simulations. In summary, the real-world simulations include preparation on the exact gear-shifting followed during the tests and processing of the altitude information, as shown in Figure 8, calculation of the real-world driving resistances and integration of the electrical consumptions.

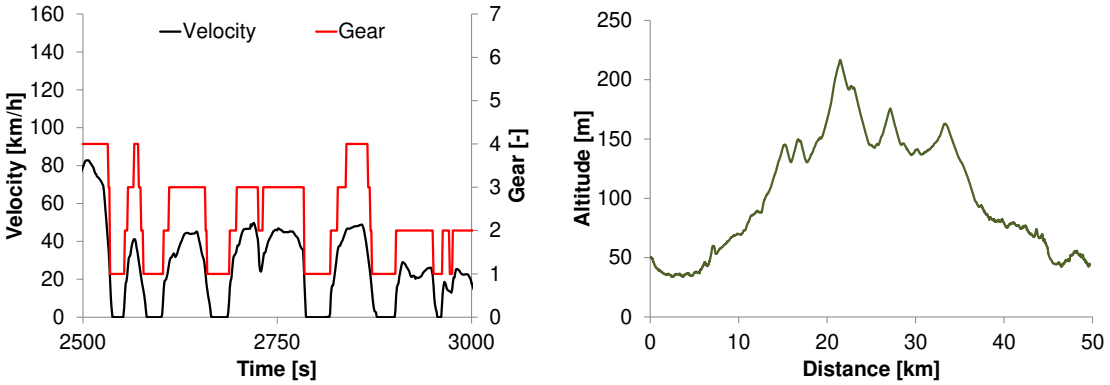

Figure 8: Example of the processed real-world gear shifting and altitude.

For the development of the vehicle simulation models with generic specifications, an internal database developed by LAT was used. This internal database consists of input data provided by automotive OEMs in the context of WLTP/NEDC correlation exercise (Tsokolis et al. 2016). Specifically, the database includes information for 18 conventional and 3 light commercial vehicles (LCV) equipped with manual or automatic transmissions. For the gasoline and diesel vehicles of the database, information related to fuel consumption engine maps, powertrain losses, inertia moments, gear shifting strategy and driving resistance coefficients are available. Figure 9 summarizes the structure of the database.

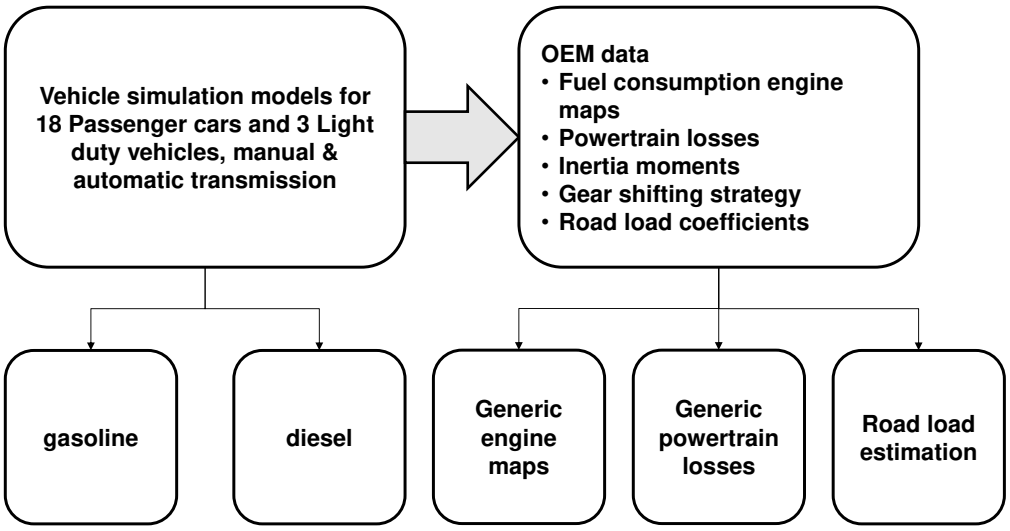

Figure 9: Contents of the internal database.

Results of the simulations

The outcome of this approach is the development of vehicle simulation models that are able to simulate the CO_2 emissions performance under real-world driving conditions. The deviation

between measured and simulated CO_2 emissions for the two vehicles is illustrated in Figure 10 and for both vehicles it is below 2.5%. In Figure 11 the comparison between simulated and experimental cumulative fuel consumption (grey and black lines respectively) for the case of the MPV is presented. It can be observed that the difference (green solid line) between simulation and measurement is within ±5% (dashed line) for the whole trip in both cases, either using OEM or generic data.

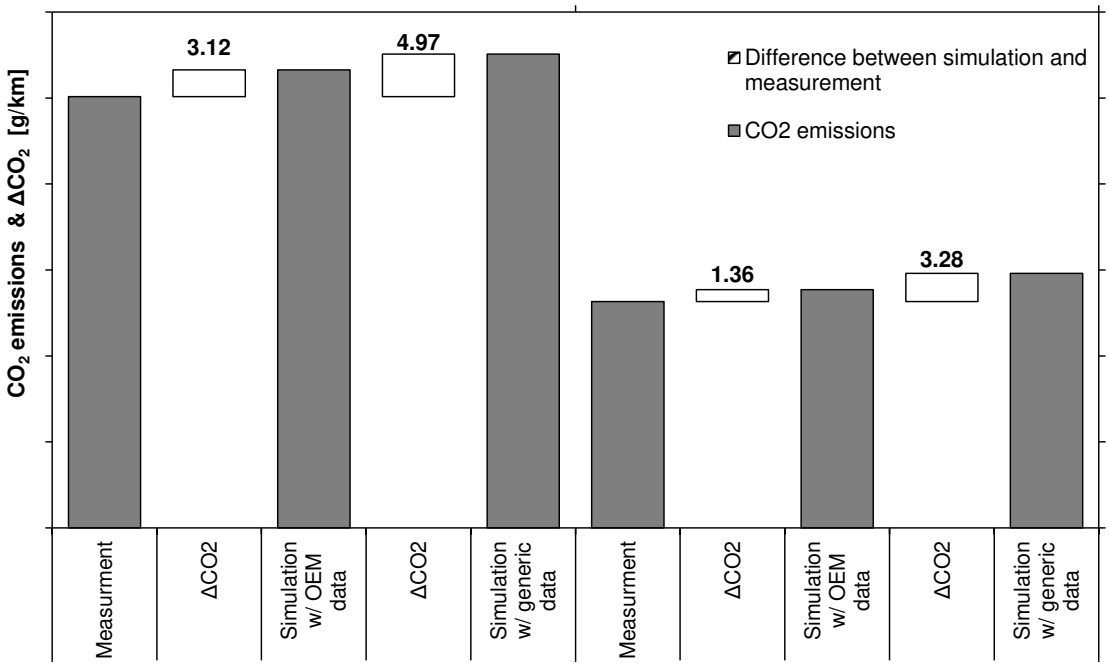

Figure 10: Comparison between simulated and measured CO_2 emissions

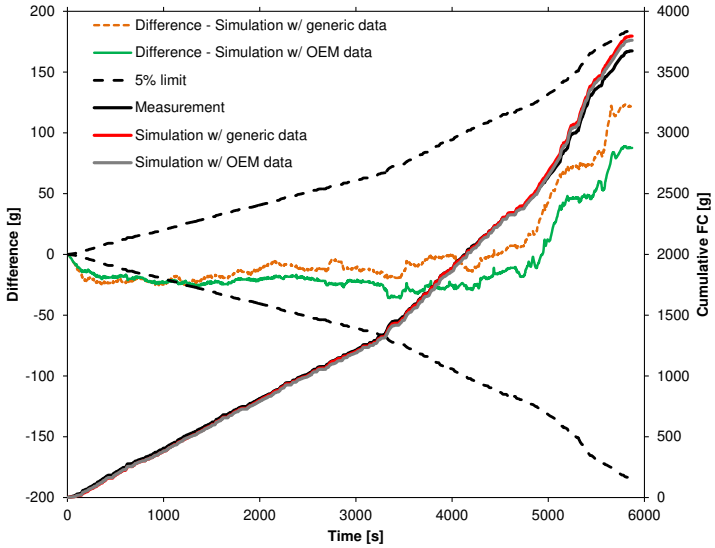

Figure 11: Comparison between simulated and experimental cumulative fuel consumption

The vehicle simulation models are used in order to identify the impact of different testing conditions on vehicle CO_2 emissions. Ambient temperature is one of the factors that influence the driving resistance of the vehicle, since air density increases with the decrease of temperature and aerodynamic drag (as represented by F_2 coefficient of road load) is proportional to air density. With the developed vehicle simulation model, a sensitivity analysis for the effect of F_2 on CO_2

emissions was conducted, which actually corresponds to the effect of ambient temperature on CO_2 emissions. Figure 12 presents the variation of CO_2 emissions as a function of F_2 and ambient temperature. CO_2 emissions increase with a decrease in temperature due to the higher air density and vice versa. The overall increase in CO_2 emissions is roughly 4% for a temperature difference of 45ºC or ~1%/10˚C.

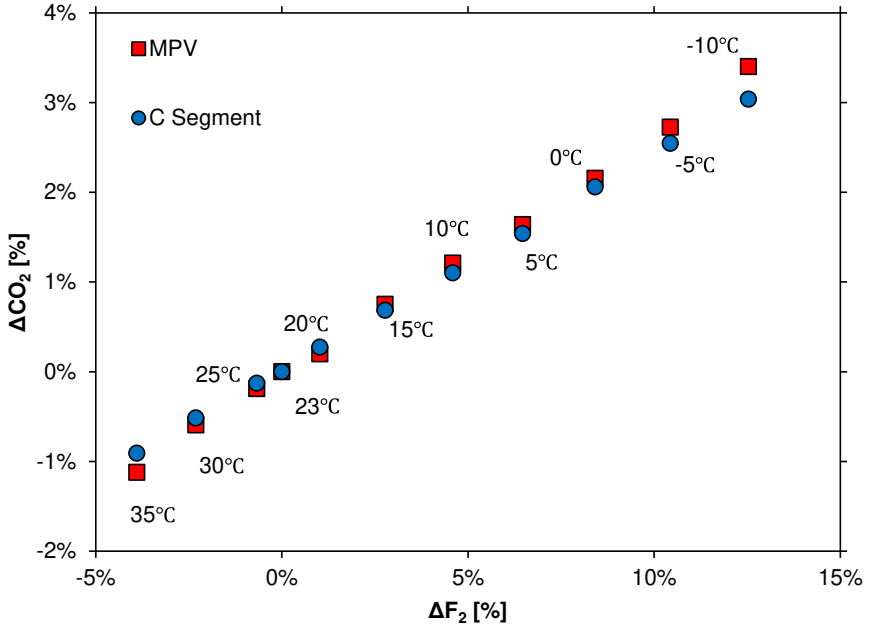

Figure 12: CO_2 emissions as a function of F_2 variation

The simulation models were also used to examine the impact of battery initial state of charge (SOC) on CO_2 emissions. The alternator is responsible for recharging the battery and cover the electrical consumption of the vehicle, taking power from the internal combustion engine. During an RDE trip, the battery will be depleted below the recharge limit, hence alternator is activated. As a result, the status of the battery before the test will affect CO_2 emissions of the vehicle. Figure 13 illustrates the change in CO_2 emissions for the various initial battery SOC levels. The analysis is conducted for up to 50% SOC, as it was assumed that below this level the engine would no start at all (the respective results are only theoretical). As can be observed in Figure 13, CO_2 emissions present a linear increase with the decrease in SOC, with different slope for the two vehicles considered in this study, which can be attributed to the different characteristics of the battery and generator of each vehicle.

Engine load is determined from the driving resistance (aerodynamic drag, rolling resistance) that is applied on the vehicle and from gravitational forces during uphill or downhill driving. Thus, essential input data that enhance the accuracy of the simulations is the altitude of the road followed during the real-world measurement. In Figure 14 simulation results with and without altitude effect are compared, where it can be seen that difference between simulated and measured CO_2 emissions is decreased when altitude is taken into consideration. The altitude is recorded via the installed GPS device and the accuracy and quality of the signal is proportional to the availability of data, the number of the satellites and the connection with the GPS device. The raw recorded signal cannot always be used directly in the simulation due to outliers or not consistent data; hence it is important to process the altitude information in order to remove such data. One possible way to correct the raw altitude recording is to obtain information of the route followed from accurate geographical maps, something that requires a good recording of longitude and latitude. Since longitude and latitude quality also depends on GPS, this method becomes complex because a correction of the vehicle position may be required. A second more efficient way to correct altitude data and obtain accurate information is to take advantage of the barometric pressure which is measured during on-road driving. Barometer data may be used in order to calculate the differential altitude from the differential pressure change in order to calculate the

road slope. A detailed study on the altitude impact will indicate the importance and the correction and accurate calculation of road grade.

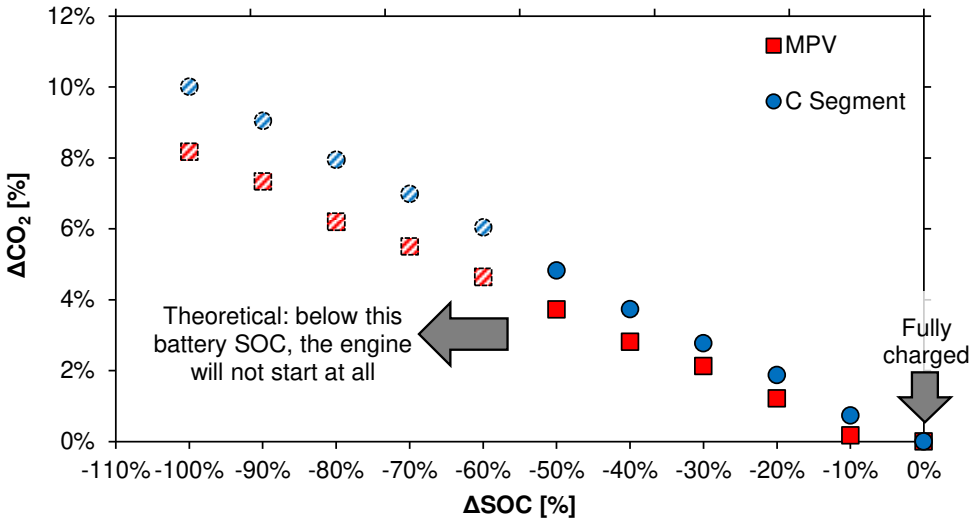

Figure 13: Impact of battery initial state of charge on CO_2 emissions

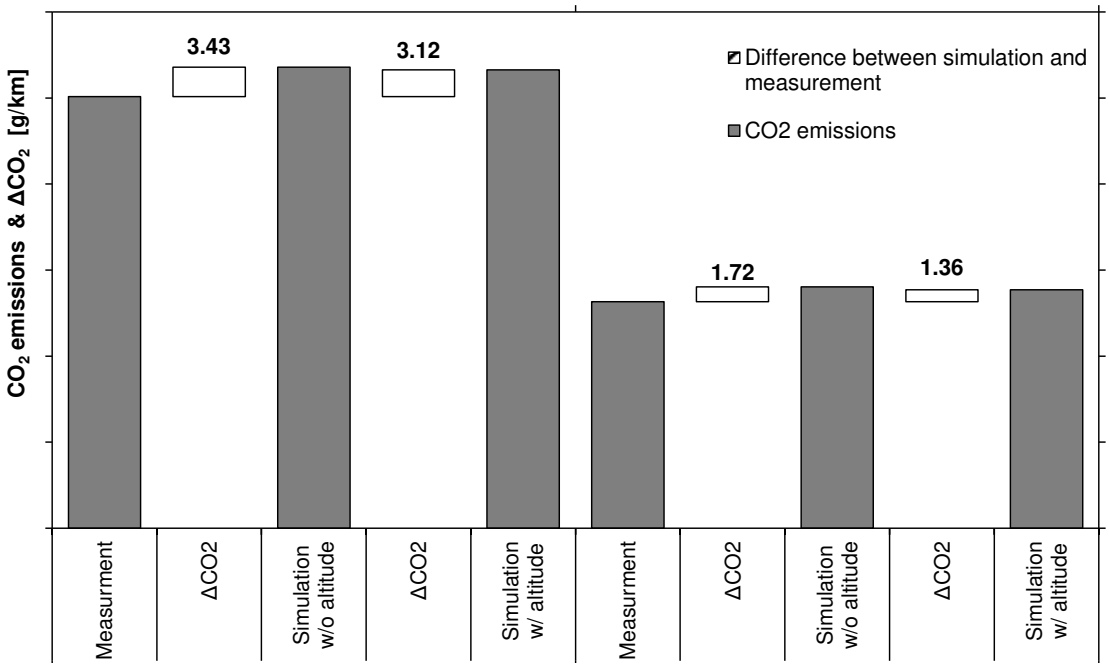

Figure 14: Effect of altitude consideration on CO_2 emissions

Conclusions

The on-road determination of CO_2 reference values for individual vehicles requires the decomposition of both the influencing factors and the effects of vehicle technology to a level that the result of an individual test can be corrected for the specific conditions and operations. It is not the intention to be able to replicate the research effort of the vehicle manufacturers for achieving high fuel efficiency. The correcting the results for test variations is more limited in its goal, but detailed simulations remain necessary, even for the 10-20 g/km which are expected to be

corrected for. The simulations require appropriate input, which has to come from new an accurate sensors and measurement principles.

Comparing the final result alone, in total trip g CO_2/km between the prediction and the measurement is not adequate for a complete assessment of real-world CO_2 emissions. There are many compensating factors which yield a good comparison for the wrong reasons. Eventually, only by comparing second-by-second results the necessary confidence can be reached that the predictions are not accidental, but arrive from the true understanding of the vehicle operation in the on-road driving conditions.

References

AVL, 2017. AVL Cruise - Vehicle System and Driveline Analysis, https://www.avl.com/cruise; [accessed on January 2017].

Buckley, F., ABCD - An Improved Coast Down Test and Analysis Method, SAE Technical Paper 950626, 1995.

Heijne, V.A.M. (Veerle) et al., NOx emissions of fifteen Euro 6 diesel cars: Results of the Dutch LD road vehicle emission, TNO report 2016 R11177.

Ligterink, N.E. (Norbert), Richard T.M. Smokers, Jordy Spreen, Peter Mock, Uwe Tietge, Supporting analysis on real-world light-duty vehicle CO_2 emissions, TNO report TNO 2016 R10419v3.

Tsokolis, D., Tsiakmakis, S., Dimaratos, A., Fontaras, G., Pistikopoulos, P., Ciuffo, B., Samaras, Z., 2016. Fuel consumption and CO_2 emissions of passenger cars over the New Worldwide Harmonized Test Protocol. Applied Energy 179, 1152-1165.

Tsokolis, D., Tsiakmakis, S., Triantafyllopoulos, G., Kontses, A., Toumasatos, Z., Fontaras, G., Dimaratos, A., Ciuffo, B., Pavlovic, J., Marotta, A., Samaras, Z., 2015. Development of a Template Model and Simulation Approach for Quantifying the Effect of WLTP Introduction on Light-Duty Vehicle CO_2 Emissions and Fuel Consumption. SAE Technical Paper 2015-24-2391.

Estimating the European Passenger Car Fleet Composition and CO_2 Emissions for 2030

D. Tsokolis[1], Z. Samos[2], S. Doulgeris[1], A. Dimaratos[1], L. Ntziachristos[1] and Z. Samaras[1]*

[1] Laboratory of Applied Thermodynamics, Aristotle University of Thessaloniki, P.O. Box 458, GR-54124, Thessaloniki, Greece, *Corresponding author: zisis@auth.gr
[2] Emisia S.A., Antoni Tritsi 21, P.O. Box 8138, GR-57001, Thessaloniki, Greece.

1. Introduction

Until recently, the decarbonisation scenarios for automotive sector in Europe, especially those for the 2020 horizon, were based on increased contribution of diesel vehicles compared to gasoline ones (Pasaoglu et al., 2012). As a result, the share of new diesel registrations in Europe increased from 31% in 2000 to 52.7% in 2015, peaking at 55.2% in 2011 (European Commission, 2017). However, after the issued notice of violation (United States Environmental Protection Agency, 2015) of the Clean Air Act (United States Environmental Protection Agency, 1970) by the United States Environmental Protection Agency to a major European automotive manufacturer in September 2015, the vehicle market scheme seems to have changed.

In March 2017, the International Council on Clean Transportation (ICCT) reported a 5-year low of new diesel registrations in France, Germany, Spain and United Kingdom, followed by final warnings from European Commission regarding national standards on NO_2 emission limits (The International Council on Clean Transportation, 2017). Additionally, Major European cities such as Paris, Berlin, Cologne, Munich, Stuttgart, Madrid, Barcelona, Liverpool, London, Oslo, Stockholm, Athens and others, have announced permanent and temporary bans in diesel vehicles by 2025, or have begun discussions to restrict diesel vehicles from entering the city centre.

On top of that, Volkswagen announces new concepts and “reinventions” on their vehicle design structure with respect to electro mobility (Blanco, 2015) and rushes to release their first I.D., a purpose built electric car, by 2020 in order to achieve their CO_2 emission targets in Europe and China (Automotive News, 2017). Other leading European automotive OEMs, such as BMW and Daimler, are expected to follow similar strategies (Cobb, 2016), especially after the governmental boost on electric vehicles development and the target of 1 million produced units by 2020, and 5 million by 2030 (Worldwatch Institute, 2016). The year-by-year increasing selling rate of electric vehicles in Europe (McKinsey & Company, 2014) and North America (International Energy Agency, 2016) indicates that the purchase decisions are changing towards a less fossil fuel dependent market. Similar trends are also observed for plug-in hybrid vehicles (International Energy Agency, 2017). Their limited electric operation combined with the hybrid system places them between conventional and full electric vehicles.

In this study, estimations for the future European vehicle fleet composition and weighted average CO_2 emissions are conducted. For the current investigation, data available from European studies were extracted to establish the baseline composition and CO_2 emissions for the year 2015 and based on historic trends and engineering judgement on their possible evolution, the future composition and CO_2 emissions for 2030 over the New European Driving Cycle (NEDC) and the new World-wide harmonized Light-duty Test Procedure (WLTP) were assessed.

2. Methodology

For the calculation of the future weighted average CO_2 emissions from passenger cars, three parameters have been taken into consideration:

i. The vehicle fleet (or market) composition.

ii. The penetration rate of the various energy efficiency technologies that are present in the vehicle fleet.

iii. The CO_2 effect of the assessed energy efficiency technologies.

The schematic of the followed methodology can be seen in Figure 1. In the next paragraphs, a detailed description of the necessary assumptions is provided.

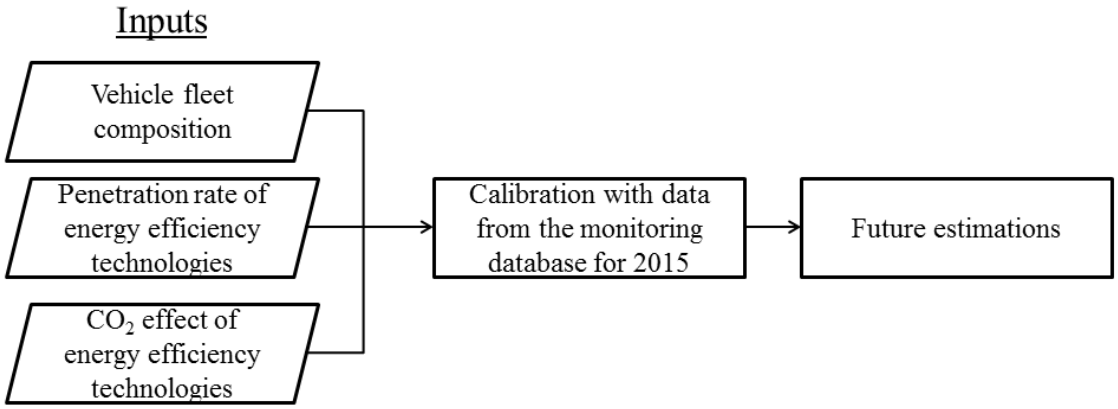

Figure 1: Schematic of the followed methodology.

2.1 Baseline vehicle fleet composition and estimation of the 2030 share

The CO_2 monitoring data for 2015 (European Environment Agency, 2016) were selected as baseline and the vehicle fleet was divided in eight segments for the investigation: small, medium and large gasoline vehicles, small, medium and large diesel vehicles, gasoline plug-in hybrid vehicles (PHEVs) and electric vehicles (EVs). Small were considered the vehicles with displacement less than 1.4l (ACEA's segments A and B), medium the vehicles with displacement between 1.4 – 2.0l (ACEA's segments B, C and D) and large the vehicles with displacement greater than 2.0l (ACEA's segments D, E and F). ACEA's B and D segments may belong in more than one clusters. Gasoline PHEVs are treated as medium-sized vehicles. The impact of vehicles fuelled by compressed natural gas, liquefied natural gas, liquefied petroleum gas, etc. is neglected assuming minimum penetration in the fleet (~1%). Fuel cell vehicles can be considered as a sub category of EVs, due to their zero tailpipe CO_2 emissions.

Due to the currently increasing importance of electric and plug-in hybrid vehicles in the market and their role for automotive OEMs to achieve fleet-level CO_2 emission targets, their penetration for the estimation of the 2030 vehicle composition was primarily taken into account. The analysis is divided in two scenarios: a pessimistic and an optimistic with respect to the presence of EVs and PHEVs; pessimistic for lower total penetration and optimistic for higher. The evolution of electrified vehicles is subjected to parameters such as macro economy, regulations, energy conservation, evolution of technology, demographics (Roland Berger, 2016). However, in the current study only the CO_2 regulatory framework was taken into consideration.

In 2015, the total penetration of PHEVs and EVs was less than 1% (European Environment Agency, 2016). The share of diesel vehicles was 52.7% and the share of gasoline vehicles was 46.7%. The detailed fleet composition for the 2015 baseline is given at Table 1.

Based on the recently established plans of major European OEMs, in favour of EVs and PHEVs, it is assumed that in 2020 the penetration rate on new sales (EVs, PHEVs) will be higher compared to the expectations and estimations until today for EU-27. The study of Pasaoglu et al. (2012) provides estimations for four different decarbonisation scenarios (reference and slightly, moderately and highly decarbonized) as regards the composition of vehicle fleet up to 2050 for EU-15[1] and EU-12[2].

[1] EU-15: Austria, Belgium, Denmark, Finland, France, Germany, Greece, Ireland, Italy, Luxembourg, Netherlands, Portugal, Spain, Sweden and United Kingdom
[2] EU-12: Bulgaria, Cyprus, Czech Republic, Estonia, Hungary, Latvia, Lithuania, Malta, Poland, Romania, Slovak Republic and Slovenia

Table 1: Share of gasoline, diesel and electrified vehicles new registrations in the baseline year 2015 (European Environment Agency, 2016).

	Gasoline vehicles			Diesel vehicles			Electrified vehicles	
	Small	**Medium**	**Large**	**Small**	**Medium**	**Large**	**PHEVs**	**EVs**
	34.7%	10.6%	1.3%	2.4%	42.6%	7.7%	0.3%	0.4%
Total	46.6%			52.7%			0.3%	0.4%

The slightly decarbonised scenario for EU-15 and the moderate scenario for EU-12 project an equal rate of 2% for both EVs and PHEVs for 2020. The moderate scenario for EU-15 and the highly decarbonised scenario for EU-12 project a total penetration of 10%, 4% for EVs and 6% for PHEVs. In this study, those rates are adopted for the pessimistic and optimistic scenario of 2020, respectively, but an equal 5% deployment of EVs and PHEVs for the optimistic case is assumed.

For the 2030 share of electrified vehicles, the "perseverant market" scenario presented by ERTRAC (ERTRAC, 2017) and Wyman (Wyman, 2015) is adopted, according to which, future CO_2 emission targets are achieved through ICE-based technology improvements and hybridization. The total penetration of electrified vehicles is 20%, which consists the pessimistic scenario in this study. For the optimistic penetration of EVs and PHEVs, it is assumed that it will reach 36% in 2030, which is actually close or equal to the highly decarbonised scenario of Pasaoglu et al. (2012), "Below 40" scenario of McKinsey (2014), "Tech 2" scenario of Cambridge Econometrics (2016) and International Energy Agency's "Blue map" scenario (2011).

The pessimistic scenario assumes limited charging infrastructures deployment and in this case, the penetration of PHEVs is expected to be higher than EVs'. A 12% rate for PHEVs is assumed, with the EVs rate being 8%. For the optimistic scenario, whereas there will be plenty of charging infrastructures in the European road network, the EVs penetration rate is higher than the respective of PHEVs, especially in the small segment. As a result, 26% of the new registrations are expected to be EVs, with the PHEVs being 10%. The percentage deployment for 2025 is estimated in order to be within the assumptions for 2020 and 2030. The penetration rates for electrified vehicles are summarized in Table 2.

Table 2: Pessimistic (Pessim.) and optimistic (Optim.) penetration of plug-in hybrid (PHEVs) and electric vehicles (EVs) until 2030.

	2015	2020		2025		2030	
	Baseline	**Pessim.**	**Optim.**	**Pessim.**	**Optim.**	**Pessim.**	**Optim.**
PHEVs	0.3%	2%	5%	5%	8%	12%	10%
EVs	0.4%	2%	5%	4%	12%	8%	26%

As regards conventional vehicles, the current decreasing trend in diesel share of new car registrations in European market (The International Council on Clean Transportation, 2017) is expected to continue. In the pessimistic scenario for 2020, it is assumed that diesel vehicles will have marginally higher share than gasoline ones, specifically 48.5% against 47.5%, while at the optimistic scenario the deployment of gasoline vehicles is higher by 4%. In this case, the share of gasoline vehicles is 47% and the share of diesel vehicles is 43%.

For the optimistic scenario of 2030, Ricardo's view on penetration rates is adopted for diesel vehicles (Jackson, 2017), which account for 15% in total. Hence, the share of gasoline vehicles is 49%. In the pessimistic scenario, new diesel registrations are assumed to be higher than the respective value in the optimistic scenario and at the same time half of what they were in the baseline year. In this case, new diesel registrations will account for a 25% of the total sales and the new gasoline registrations will account for 55%. Similarly to electrified vehicles, the percentage deployment for 2025 is estimated by the assumptions for 2020 and 2030.

In order to estimate the share of small, medium and large sizes within diesel and gasoline vehicles in 2030, the first assumption is that the small diesel segment seizes to exist already from 2020 onwards. By taking into account the historic evolution of this segment since 2011 and

extrapolating, from 2018 onwards no small diesel cars will be sold. The share of small diesel vehicles since 2011 is provided at Table 3. In addition, it is estimated that automotive OEMs will no longer produce small diesel vehicles, owing to the increased cost of the exhaust after treatment system to meet EURO 6 and RDE standards. As a result, the total vehicle cost of the small segment will no longer be affordable by the respective market.

Table 3: Share of small diesel vehicles in the market from 2011 to 2016 (European Commission, 2017).

2011	2012	2013	2014	2015	2016
6.2%	5.0%	3.9%	3.2%	2.4%	1.8%

The study of Roland Berger (2016) estimates the segment-by-segment development of new vehicle registrations until 2030. According to the study, the differentiations within the segments are in the range of 1 – 4%. Practically, the distribution is not expected to change significantly until 2030. In order to be consistent with this hypothesis, EVs are assumed to be small or medium vehicles and PHEVs medium or large.

In the pessimistic scenario of 2020, the 2015 diesel share of small vehicles is distributed to the small gasoline segment and EVs. The deployment of large diesel and gasoline vehicles increases, while the share of medium sized diesel and gasoline ones decreases. In the optimistic scenario, the share of small and large gasoline cars increases with a respective decrease in the all other segments.

In the optimistic scenario of 2030, small gasoline vehicles account for 15% of total new registrations, medium gasoline cars 33.5%, large gasoline vehicles 0.5%, medium diesels 10% and large diesels 5%. The order of 40% in small vehicles is kept by the contribution of EVs which is 26% and the share of PHEVs is distributed in the medium and large segment of gasoline vehicles. As regards the pessimistic scenario of 2030, small gasoline segment accounts for 30%, medium gasoline 24%, large gasoline 1%, medium diesel 18% and large diesel 7%. As regards the scenarios for 2025, the vehicle size composition is estimated in order to be within the 2020 and 2030 assumptions. The detailed share of diesel, gasoline and electrified vehicles can be found at Table 4 and are illustrated at Figure 2.

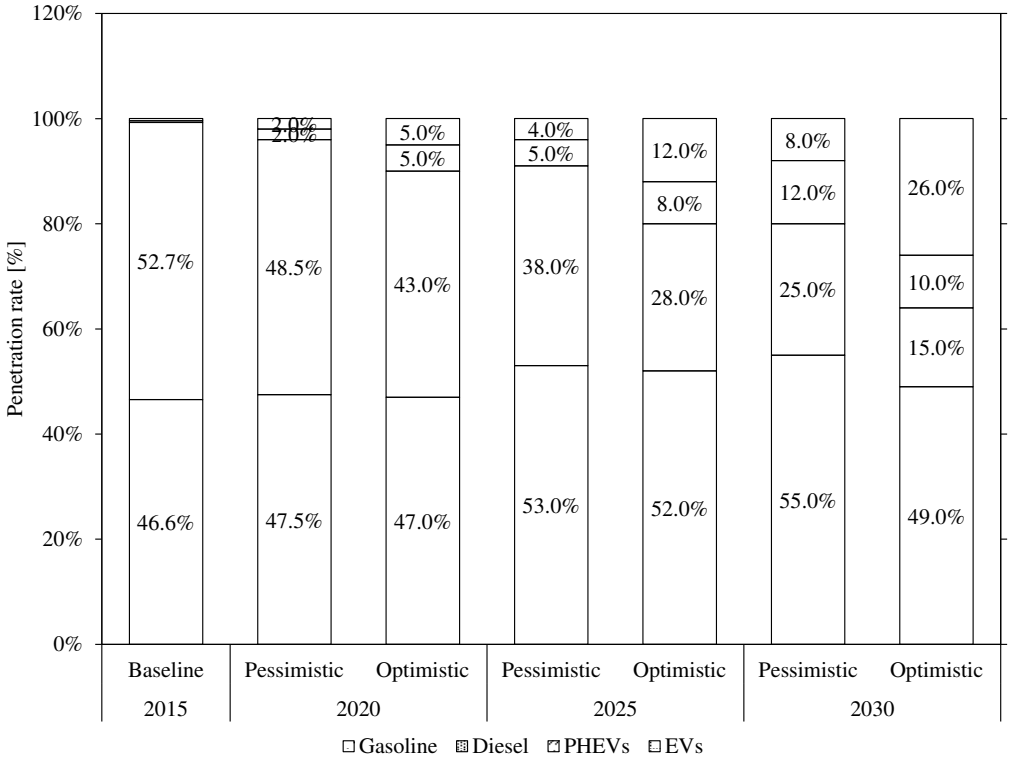

Figure 2: Share of diesel, gasoline, electric and plug-in hybrid vehicles in the baseline year 2015 and their evolution for the pessimistic and optimistic scenario until 2030.

Table 4: Composition of gasoline, diesel and electrified vehicles as a function of their segment in the baseline year 2015 and their pessimistic (Pessim.) and optimistic (Optim.) evolution until 2030.

	2015	2020		2025		2030	
	Baseline	**Pessim.**	**Optim.**	**Pessim.**	**Optim.**	**Pessim.**	**Optim.**
Small Gasoline	34.7%	37.1%	40.0%	33.0%	31.0%	30.0%	15.0%
Medium Gasoline	10.6%	8.9%	5.0%	18.5%	20.0%	24.0%	33.5%
Large Gasoline	1.3%	1.5%	2.0%	1.5%	1.0%	1.0%	0.5%
Small Diesel	2.4%	0.0%	0.0%	0.0%	0.0%	0.0%	0.0%
Medium Diesel	42.6%	40.0%	37.0%	30.0%	22.0%	18.0%	10.0%
Large Diesel	7.7%	8.5%	6.0%	8.0%	6.0%	7.0%	5.0%
PHEVs	0.3%	2.0%	5.0%	5.0%	8.0%	12.0%	10.0%
EVs	0.4%	2.0%	5.0%	4.0%	12.0%	8.0%	26.0%

2.2 CO_2 effect and penetration rate of energy efficiency technologies

The starting point for estimating the CO_2 effect of state-of-the-art energy efficiency technologies is the 21 vehicle simulation models established in the context of WLTP/NEDC correlation exercise (Tsokolis et al., 2016). The specific models were developed using the AVL Cruise software (AVL, 2017) on a basis of a generalized vehicle simulator (Figure 3) presented in detail by Tsokolis et al. (2015). It consists of the main mechanical and electrical powertrain components, together with the corresponding connections, controllers and functions, simulating the vehicle's operation. The initial dimensioning and parameterization for the various components were provided by industrial and literature sources (Tsokolis et al., 2015). The simulator, including controls and individual efficiencies, was then calibrated until the calculated fuel consumption and CO_2 emission levels matched the measured ones for the actual vehicles, tested on the chassis dynamometer. The mean CO_2 emission prediction error over the NEDC and WLTP was equal to 2 g CO_2/km, corresponding to 1.6% of the mean value, with a second-by-second R-square correlation coefficient higher than 0.9. Detailed information on the testing and the validation procedure is presented by Tsokolis et al. (2015).

In addition, for the sample of 21 vehicle simulation models, the CO_2 impact of 14 different energy efficiency technologies was assessed over the NEDC and WLTP[3], as function of the vehicle component they affect. Specifically, the applied components are related to the engine, the vehicle design, the drivetrain and the hybridization. The establishment of the technologies in the simulation models is not the same for all: some were simulated using the built-in modules of Cruise, while others were simulated by developing new functions and sub-systems or by modifying the simulator input parameters. The applications of a refined sample of technologies on different vehicle simulation models are described by Dimaratos et al. (2016) and Triantafyllopoulos et al. (2017).

Each technology variation results in CO_2 emissions reduction from less than 1% up to 31% in NEDC and from less than 1% up to 18% in WLTP depending on the impact on engine operation during the two test protocols. The summarized CO_2 effects for 12 out of 14 technologies can be seen in Figure 4. The technologies coloured with black are applied to both diesel and gasoline vehicles, while the technologies coloured with white are applied only to gasoline vehicles. The points illustrate the average of the sample and the error bars the standard deviation. The simulated sample for each technology is provided at the legend.

[3] WLTP estimations refer to vehicle configuration with the higher mass and driving resistance (WLTP-High).

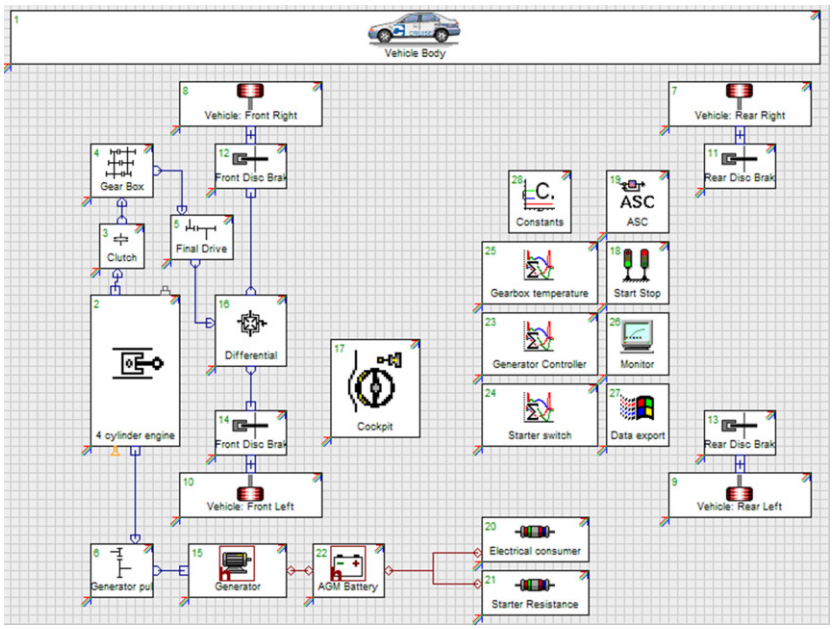

Figure 3: Topology of the AVL Cruise vehicle simulator. The simulator comprises vehicle resistances, all main powertrain components, mechanical and electrical energy consumption auxiliaries, as well as controllers for the individual systems.

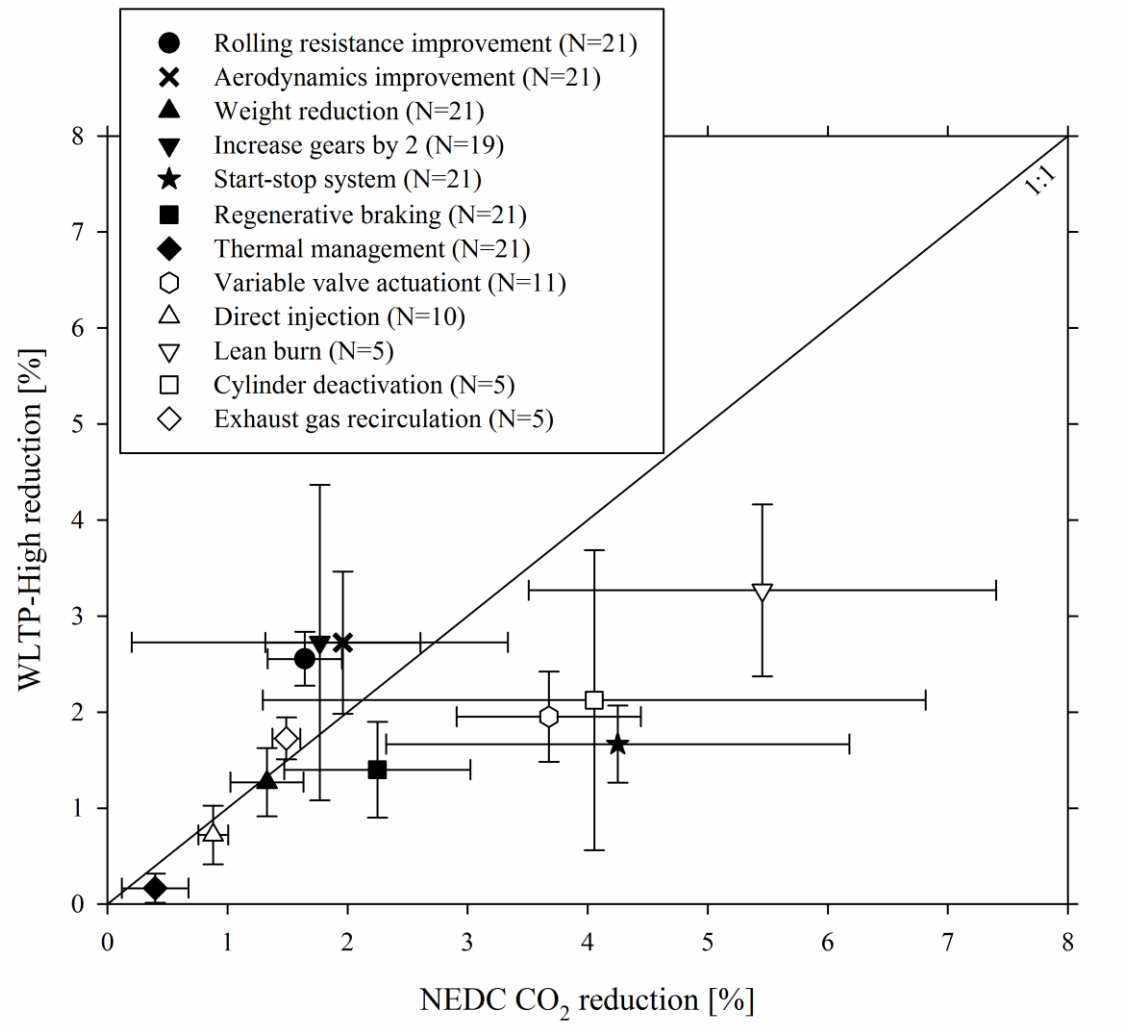

Figure 4: Summarized CO_2 effect for 12 out of 14 technologies simulated in the context of WLTP/NEDC correlation exercise.

The percentage deployment of energy efficiency technologies was extracted by the study of Ricardo, which was prepared for the Committee on Climate Change (Ricardo-AEA, 2012). In this study, a literature review is carried out on the CO_2 effect of market available energy efficiency technologies associated with road transport and assumptions made on their current and future deployment. The vehicle specific reductions from the 14 energy efficiency technologies replaced the respective values from Ricardo's study and the merged list was used in the fleet-wide calculations. The full list of the assessed technologies along with the origin of the CO_2 effect can be found in Table 5.

3. Projection of the fleet weighted average CO_2 emissions until 2030

For the calculation of the fleet weighted CO_2 emissions, apart from the vehicles' share, an average CO_2 value per segment is necessary. The average value consists of the type approval CO_2 emissions from all available models in the market. These vehicles have different specifications and built-in energy efficiency technologies and as a result, they may vary significantly in their homologation value. In order to calculate the fleet weighted average CO_2 emissions for 2030, it is necessary to calibrate the penetration rate of the market available fuel economy technologies with respect to the 2015 average CO_2 provided by the Monitoring Database and the future targets. For 2015, the average CO_2 emissions were 119.5 g/km (European Environment Agency, 2016), the 2020 target is 95 g/km and the 2030 target is assumed 65 g/km. All these values are based on the NEDC protocol.

For the calibration of the technology penetration rate in the vehicle fleet as a function of their segment, the top selling cars from the Monitoring Database for year 2015 were assessed and the sales-weighted-average CO_2 emissions were calculated for each segment of Table 4. Then, one model from those simulated in the WLTP/NEDC correlation exercise was selected and its CO_2 emissions without any energy efficiency technology were determined. The technology penetration rate was calibrated by using different shares for small, medium and large vehicles and with respect to the calculated CO_2 emissions from the simulated values with i) the fleet average CO_2 emissions of 2015, ii) diesel and gasoline average CO_2 emissions of 2015 and iii) the sales-weighted-average CO_2 emissions per segment. Basic specifications of the selected vehicles can be found in Table 6. The results from the calculations and the error in each case are presented in Table 7. The total calculated error in the fleet CO_2 emissions was calculated at -0.6 g/km.

The same procedure was followed for the 2020 target of 95 g/km and the assumed 2030 target of 65 g/km. The technology share was calibrated for those targets over the pessimistic scenario and kept constant for optimistic. However, from 2020 onwards, the contribution of PHEVs becomes significant and a more suitable type approval value should be used that follows the evolution of PHEVs technology. For this reason, Toyota's Prius was selected as the most characteristic PHEV within the segment and its type approval values were used. In addition, Toyota released two different versions of the specific model; one in 2012 and one in 2016. Thus, based on the technology evolution for these models, assumptions can be made in order to estimate future PHEV type approval CO_2 emissions in NEDC and WLTP-H.

The electric range of the Toyota Prius 2012 model is 33 km according to NEDC regulation and 23 km according to WLTP regulation. On the other hand, the electric range of the 2016 model is 55 km over the NEDC procedure and 46 km over the WLTP one. Also, the 2016 model is able to operate in electric mode up to 135 km/h, compared to the 100 km/h of the 2012 model, zeroing its CO_2 emission in charge depleting mode for both legislative driving cycles. The combined type approval CO_2 for the specific vehicles is 49 g/km for the 2012 model and 22 g/km for the 2016 model over the NEDC. Their performance in charge sustain operation can be assessed by the hybrid versions of the vehicles which are practically the same. Specifically, the 2012 Toyota Prius hybrid emits 90 g/km and the 2016 model 70 g/km. Although that no official type approval values for WLTP-H have been publically released, they can be estimated by multiplying their NEDC value with the ratio between WLTP and NEDC assessed by Tsokolis et al. (2016). Furthermore, assuming a linear evolution of the electric range of the specific vehicle models, the 2020+ model will have a 77 km range over NEDC and the 2025+ model 99km. Then, the WLTP electric range can be estimated in a similar way. Finally, the future CO_2 emissions in charge sustain operation can be calculated by assuming a constant ratio between two consecutive versions of the model. The estimated values in NEDC and WLTP-H with their assumptions for 2020, 2025 and 2030 are provided in Table 8.

Table 5: List of assessed technologies, type of applied engines and source of CO_2 effect (SI: Spark Ignition, CI: Compression Ignition).

Component	Energy efficiency technology	Engines applied	Origin of CO_2 effect
Engine	Combustion improvements	SI and CI	(Ricardo-AEA, 2012)
	Direct injection	SI	WLTP/NEDC correlation
	Lean burn	SI	WLTP/NEDC correlation
	Thermodynamic cycle improvements	SI	(Ricardo-AEA, 2012)
	Cylinder deactivation	SI	WLTP/NEDC correlation
	Downsizing	SI and CI	WLTP/NEDC correlation
	Exhaust gas recirculation	SI	WLTP/NEDC correlation
	Cam-phasing	SI	(Ricardo-AEA, 2012)
	Auxiliary systems efficiency improvement	SI and CI	(Ricardo-AEA, 2012)
	Thermo-electric waste heat recovery	SI and CI	(Ricardo-AEA, 2012)
	Variable valve actuation	SI	WLTP/NEDC correlation
	Electrical assisted steering (EPS, EPHS)	SI and CI	(Ricardo-AEA, 2012)
	Thermal management	SI and CI	WLTP/NEDC correlation
	Engine friction reduction	SI	(Ricardo-AEA, 2012)
Hybridization	Start-stop system	SI and CI	WLTP/NEDC correlation
	Regenerative braking	SI and CI	WLTP/NEDC correlation
	Torque boost	SI and CI	(Ricardo-AEA, 2012)
	Full hybrid	SI and CI	WLTP/NEDC correlation
Drivetrain	Automated manual transmission (AMT)	SI and CI	(Ricardo-AEA, 2012)
	Dual clutch transmission (DCT)	SI and CI	(Ricardo-AEA, 2012)
	Continuously variable transmission (CVT)	SI and CI	(Ricardo-AEA, 2012)
	Optimizing gearbox ratios / downspeeding	SI and CI	(Ricardo-AEA, 2012)
	Increase gears by 2	SI and CI	WLTP/NEDC correlation
	Low drag brakes	SI and CI	(Ricardo-AEA, 2012)
	Reduced driveline friction	SI and CI	(Ricardo-AEA, 2012)
	Downspeeding via slip controlled clutch and DMF removal	CI	(Ricardo-AEA, 2012)
Vehicle design	Weight reduction	SI and CI	WLTP/NEDC correlation
	Aerodynamics improvement	SI and CI	WLTP/NEDC correlation
	Rolling resistance improvement	SI and CI	WLTP/NEDC correlation

Table 6: Vehicle specifications used for the calculations of segment average CO_2 emissions.

Segment	Transmission	Curb mass [kg]	Displacement [cc]	Max Power [kW]	Max Torque [Nm]
Small Gasoline	MT, 5 gears	1102	1197	66	160
Medium Gasoline	MT, 6 gears	1300	1598	100	240
Large Gasoline	AT, 7 gears	1635	3498	200	370
Small Diesel	MT, 5 gear	1393	1248	70	190
Medium Diesel	MT, 6 gears	1465	1995	120	380
Large Diesel	AT, 8 gears	1880	2967	190	580

Table 7: Fleet and segment average CO_2 emissions for the baseline year 2015 from the Monitoring database and for the assumed technology penetration rate.

Segment	Baseline 2015 value [g/km]	Calculated value [g/km]	Error [g/km]	Error [%]
Small Gasoline	120.4	114.4	-6.0	-5.0
Medium Gasoline	133.8	136.0	2.3	1.7
Large Gasoline	152.1	140.7	-11.4	-7.5
Gasoline average	122.5	120.1	-2.4	-2.0
Small Diesel	101.3	107.1	5.8	5.7
Medium Diesel	114.7	116.0	1.3	1.2
Large Diesel	146.2	143.1	-3.1	-2.1
Diesel average	119.2	119.6	0.4	0.3
Fleet average	119.5	118.9	-0.6	-0.5

Figure 5 illustrates the evolution of NEDC and WLTP-H CO_2 emissions for the examined scenarios. ΔCO_2 between WLTP and NEDC for the 2020 pessimistic scenario remains at the same level as the 2015 baseline, since the vehicle fleet does not substantially change, and gradually decreases with time. The difference between the two type approval procedures is always greater in the pessimistic scenario rather than in the optimistic one, affected by the higher penetration of gasoline vehicles and PHEVs with the associated technologies. Nevertheless, the rate that ΔCO_2 will decrease in future will depend on the extent of adoption of technologies more effective in WLTP, such as increased gear ratios, aerodynamics and rolling resistance improvements.

The 2030 decrease in NEDC and WLTP for the optimistic scenario compared to the 2015 baseline was found 56% and 52% respectively, with the fleet average CO_2 estimated at 52 g/km and 65 g/km for the same cycles. Comparing the average CO_2 emissions of 2015 with the Monitoring Data of 2000 (15 years), the reported decrease is 31%, almost the half of what calculated for the optimistic scenario. In this case, a hypothetical future target in the order of 50 – 55 g/km cannot be justified by historic trends even with a 36% penetration of electrified vehicles.

Table 8: NEDC and WLTP CO_2 emissions for PHEVs in charge depleting (CD) and charge sustain mode (CS) until 2030.

NEDC	Electric range	CO_2 at CD operation [g/km]	CO_2 at CS operation [g/km]	Type approval CO_2 [g/km]
2015	33*	18*	90[$$]	49*
2020	55*	0*	70[$$]	21.9
2025	77[$]	0[$]	54.6[&&]	13.4
2030	99[$]	0[$]	42.6[&&]	8.6
WLTP	**Electric range**	**CO_2 at CD operation [g/km]**	**CO_2 at CS operation [g/km]**	**Type approval CO_2 [g/km]**
2015	23**	38.8[&]	104.4[&]	74.0
2020	46**	0**	81.2[&]	28.6
2025	69[$]	0**	63.3[&]	16.8
2030	92[$]	0**	49.4[&]	10.6

*: Provided by public sources

**: Assumed based on NEDC range

[$]: Linearly extrapolated

[$$]: Assumed from hybrid version of model

[&]: Calculated based on simulations

[&&]: Calculated from the ratio of the former years value

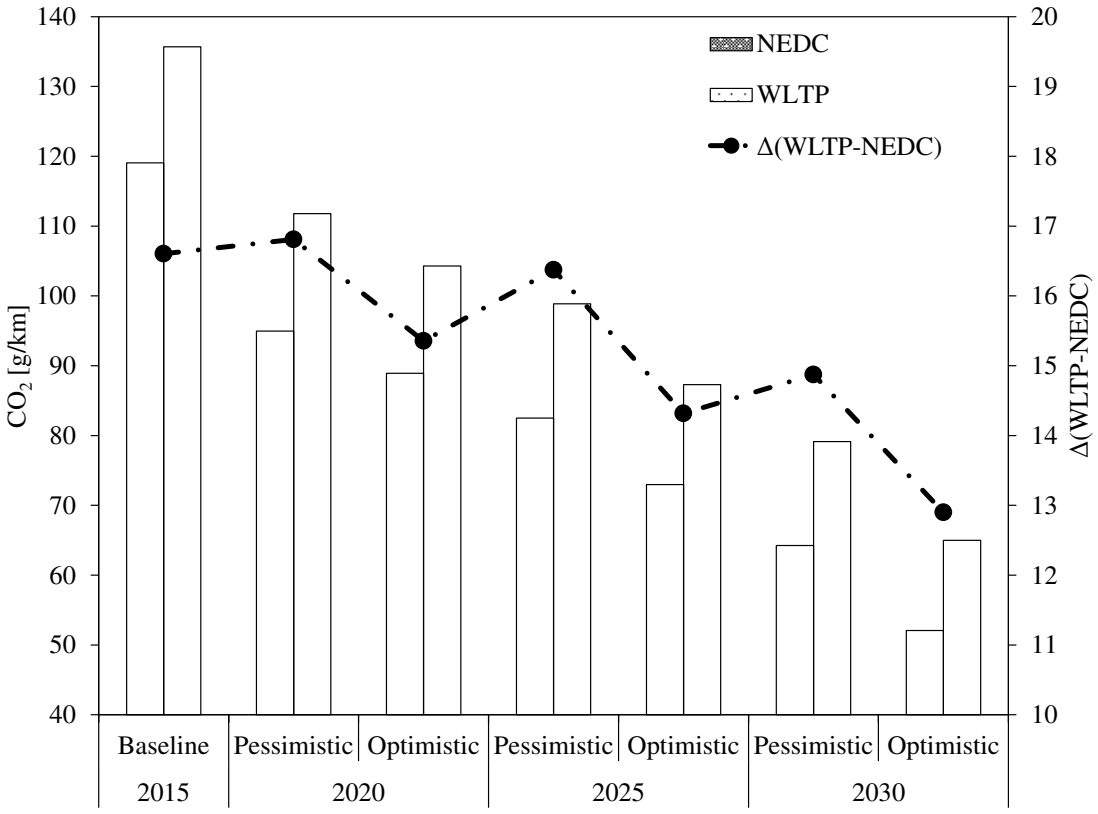

Figure 5: Evolution of NEDC and WLTP CO2 emissions until 2030 for the examined pessimistic and optimistic scenario.

4. Conclusions

In the current study, an estimation of the future vehicle fleet composition and the respective weighted average CO_2 emissions in NEDC and WLTP was conducted.

To do so, the vehicle fleet was divided in eight segments according to fuel type (gasoline, diesel), size (small, medium large) and level of electrification (plug-in hybrid vehicles - PHEVs, electric vehicles - EVs). For conventional vehicles, one validated vehicle model per segment was selected and the fleet weighted CO_2 emissions reduction was assessed in both NEDC and WLTP. The future penetration rate of energy efficiency technologies and their respective CO_2 effect was extracted from European studies, and the distribution of the vehicle fleet was assessed on the basis of historic trends, estimations and engineering judgement of the possible evolution. The CO_2 emissions for EVs were considered zero. However, if new EV sales will highly increase in the future, then their CO_2 footprint should be re-examined based on a well-to-wheel analysis. For PHEVs, the type approval fuel consumption will decrease in the future in both NEDC and WLTP. Reported WLTP CO_2 emissions will reach NEDC levels only by increasing the vehicle electric range, without any optimizations in the energy management system.

The future distribution of vehicle fleet and its average CO_2 emissions were examined using one pessimistic and one optimistic scenario related to the availability of charging infrastructures, electric range and cost for the electrified vehicles. In both scenarios, the diesel vehicles share decreases compared to the 2015 baseline, while the respective share of gasoline vehicles increases. In addition, the penetration of EVs and PHEVs increases, with their deployment percentage varying between the two scenarios and over the years. The calculated reduction for the fleet weighted CO_2 emissions in NEDC was found 45% and 55% as compared to the 2015 baseline, for the pessimistic and optimistic scenario respectively, with the WLTP reduction reaching 38% and 49%, for the same scenarios too.

Based on the analysis, the future composition of vehicle fleet cannot be predicted but rather only estimated due to its dependence on macro economy and regulatory framework, fuel and energy considerations, vehicle and powertrain technology development and customer demographics. Historic trends on the evolution of fleet-average CO_2 emissions have to be considered by policy makers in order to set the post 2020 targets for passenger cars.

References

Automotive News, 2017. VW hurries new EVs to meet CO_2 targets, http://europe.autonews.com/article/20170321/ANE/170329998/vw-hurries-new-evs-to-meet-co2-targets; [accessed on June 2017].

AVL, 2017. AVL Cruise - Vehicle System and Driveline Analysis, https://www.avl.com/cruise; [accessed on January 2017].

Blanco, S., 2015. VW CEO talks up 20 new plug-in models in Frankfurt, Autoblog, http://www.autoblog.com/2015/09/14/vw-ceo-20-new-plug-in-models-frankfurt/; [accessed on June 2017].

Cambridge Econometrics, 2016. Fuelling Europe's Future, *Final Report*.

Cobb, J., 2016. Europe Is Awakening From Diesel-Induced Sleep to Chase New Electric (Car) Dreams, http://www.hybridcars.com/europe-is-awakening-from-diesel-induced-sleep-to-chase-new-electric-car-dreams/; [accessed on June 2017].

Dimaratos, A., Tsokolis, D., Fontaras, G., Tsiakmakis, S., Ciuffo, B., Samaras, Z., 2016. Comparative Evaluation of the Effect of Various Technologies on Light-duty Vehicle CO_2 Emissions over NEDC and WLTP. *Transportation Research Procedia* 14, 3169-3178.

ERTRAC, 2017. Electrification of Road Transport Roadmap, *Final Report*.

European Commission, 2017. Regulation EC 443/2009, *Monitoring of CO_2 emissions*.

European Environment Agency, 2016. Monitoring of CO_2 emissions from passenger cars: Summary data for 2015, http://www.eea.europa.eu/data-and-maps/data/co2-cars-emission-10; [accessed on January 2016].

International Energy Agency, 2011. Electric and plug-in hybrid electric vehicles, *Technology Roadmap*.

International Energy Agency, 2016. Global EV outlook 2016: Beyond one million electric cars, *Final Report*.

International Energy Agency, 2017. Global EV outlook 2017: Two million and counting, *Final Report*.

Jackson, N., 2017. Drive trains and fuels for road transport, *12th Concawe Symposium*, 20-21 March 2017, Antwerp, Belgium. .

McKinsey & Company, 2014. Electric vehicles in Europe: Gearing up for a new phase?, *Final Report*.

Pasaoglu, G., Honselaar, M., Thiel, C., 2012. Potential vehicle fleet CO_2 reductions and cost implications for various vehicle technology deployment scenarios in Europe. *Energy Policy* 40, 404-421.

Ricardo-AEA, 2012. A review of the efficiency and cost assumptions for road transport vehicles to 2050., *Final Report*.

Roland Berger, 2016. Integrated Fuels and Vehicles Roadmap to 2030 and beyond, *Final Report*.

The International Council on Clean Transportation, 2017. Cities driving diesel out of the European car market, http://www.theicct.org/blogs/staff/cities-driving-diesel-out-european-car-market: [accessed on June 2017].

Triantafyllopoulos, G., Kontses, A., Tsokolis, D., Ntziachristos, L., Samaras, Z., 2017. Potential of energy efficiency technologies in reducing vehicle consumption under type approval and real world conditions. *Energy* 140, 365-373.

Tsokolis, D., Tsiakmakis, S., Dimaratos, A., Fontaras, G., Pistikopoulos, P., Ciuffo, B., Samaras, Z., 2016. Fuel consumption and CO2 emissions of passenger cars over the New Worldwide Harmonized Test Protocol. *Applied Energy* 179, 1152-1165.

Tsokolis, D., Tsiakmakis, S., Triantafyllopoulos, G., Kontses, A., Toumasatos, Z., Fontaras, G., Dimaratos, A., Ciuffo, B., Pavlovic, J., Marotta, A., Samaras, Z., 2015. Development of a Template Model and Simulation Approach for Quantifying the Effect of WLTP Introduction on Light-Duty Vehicle CO_2 Emissions and Fuel Consumption. *SAE Technical Paper* 2015-24-2391.

United States Environmental Protection Agency, 1970. *Summary of the Clean Air Act*, Washington D.C.

United States Environmental Protection Agency, 2015. *Notice of Violation*, Washington D.C.

Worldwatch Institute, 2016. Germany Boosts Electric Vehicle Development, http://www.worldwatch.org/node/6251: [accessed on June 2017].

Wyman, O., 2015. Future of ICE: why accelerating R&D spend is critical for future competitiveness & to reach 50g CO_2/km, *Unpublished presentation created for ERTRAC*.

Quantification of vehicle cold start effects on NO_x and NO_2 emissions using remote sensing

D.C. Carslaw[*1,2], L. Doman[1], B. Fowler[1], T. Green and R. Rose.*

[1]Ricardo Energy & Environment, Harwell, Oxfordshire, OX11 0QR, United Kingdom

[2]Wolfson Atmospheric Chemistry Laboratory, University of York, York, YO10 5DD

david.carslaw@ricardo.com

Introduction

The emission of NO_x from diesel vehicles has attracted considerable attention in recent years, in part due to the 'dieselgate' scandal in 2015. However, even before the emissions scandal there was widespread interest and concern over the emissions performance of diesel vehicles. The recent focus on diesel vehicles is related to their emissions of nitrogen oxides (NO_x) and the contribution made to exceedances of European ambient air quality standards for nitrogen dioxide (NO_2). Exceedances of the annual mean NO_2 Limit Value of 40 μg m^{-3} remain an important issue across Europe. Indeed, across 28 countries in Europe, it is estimated that NO_2 accounts for 72,000 premature based on 2012 (EEA, 2016). More generally, the emission of NO_x is associated with secondary particulate formation and ground-level ozone production as well as eutrophication.

Given the many important impacts of NO_x and NO_2 it is essential that the emissions to atmosphere are robustly quantified. In recent years there has been an increased amount of work that has shown that in the case of diesel vehicles, emissions of NO_x have not decreased as expected and are many times the Type Approval limits. However, there remains a distinct lack of research that speciates between emissions of NO and NO_2, with most work focusing on total NO_x emissions. This situation is understandable from a Type Approval perspective where limits are set for total NO_x but is not appropriate if the need is to understand the factors affecting near-road concentrations of NO_2 i.e. where the EU exceedances are most important.

More recently, the analysis of ambient data in London and across European cities suggests that the proportion of NO_x that is NO_2 from road vehicles has been decreasing or has stabilised since around 2010 (Carslaw et al., 2016, Grange et al., 2017). Such decreases have to date not been explained robustly by vehicle emission measurements – in part because of the aforementioned focus on total NO_x. However, several factors are likely important. First, as diesel vehicles age there is evidence that the amount of NO_2 they emit decreases. Second, catalyst and vehicle manufacturers have reduced the amount of platinum group metals used to produce catalysts (which would reduce NO_2 production) and third, it would be expected that improved control over SCR (Selective catalytic Reduction) systems would lead to lower NO_2 emissions. The relative importance of these factors is not well-understood.

The current work investigates some of the other potential factors that could affect the emission of NO_2 from diesel vehicles. In this study, we use comprehensive vehicle emission remote sensing measurements to quantify the emissions of NO_x and NO_2 from diesel and petrol passenger cars with hot engines and during cold start conditions. Vehicles starting with cold engines are known to have potentially very different emission characteristics compared with vehicles with hot engines but very little work is published that quantifies these differences for modern diesel vehicles. A particular focus is on how cold start conditions, which are primarily associated with short journeys in urban areas, differ from hot engine conditions.

Experimental

The instrument used in the current work was a vehicle emission remote sensing instrument manufactured by Opus. The principle of operation is extensively documented elsewhere (Burgard et al., 2006, Hallquist et al., 2013) and is only briefly considered. The version of the instrument used was the RSD 5000 with an enhanced capability to measure NO_2 and NH_3.Tailpipe ratios of CO, HC, NO, NO_2 and PM (measured by the RSD 5000 as opacity) to CO_2 are derived for each vehicle measured. Two parallel beams of IR and UV light are emitted from the Source/Detector Module (SDM) at tailpipe level and traverses each passing vehicle's exhaust plume, hitting a reflecting mirror at the opposite side of the road. The two beams are reflected back across the road, once again traversing the vehicle's exhaust plume – to be

detected at the SDM. The returning light is analysed spectrophotometrically by the detector to derive the light absorbance at various wavelengths representing the five measured gaseous pollutants.

The measured light absorbances can be converted to pollutant concentrations across the light beam path, then be converted to pollutant to CO_2 ratios, and finally to concentrations of each of the measured species in the undiluted exhaust. Calibrations were conducted every 1.5–2 h of measurements by using a certified gas mixture containing 2000 ppm NO and 12% CO_2 in N_2, 1000 ppm NO_2 in air with 15% CO_2.

A photograph of each vehicle was taken to capture the registration plate. The registration information was cross-referenced with comprehensive vehicle information databases by CDL to return data such as fuel type, engine size and Euro status. Note that CDL query vehicle manufacturer databases to ensure accurate Euro status information; albeit without identifying the different Euro 6 stages (such as Euro 6b, 6d-temp). The lack of differentiation between Euro 6 stages is unlikely to be important at this point in time because almost all vehicles sampled would not be RDE compliant.

The measurements were made on the Harwell Science Campus approximately 25 km south of the City of Oxford in south England. The campus hosts several large facilities such as the Diamond Light Source but is isolated from any major towns or cities. The nearest town (Didcot, population ca. 25,000) is 8 km from the campus. The campus itself has over 5,000 employees. The location of the campus means that the vast majority of vehicles arriving in the morning would hot engines given the distances they would have travelled. Conversely, vehicles leaving the site at the end of the day would in general have been parked most of the day and would leave with cold engines. It is likely that not every vehicle leaving the campus would do so with a cold engine. However, given the very clear 'tidal' nature of vehicle activity at this location, it is expected the vast majority of vehicles sampled leaving the campus would have been parked for many hours.

Figure 1: Location of the measurement location (shown by central circle) at the Harwell Science Campus. Note the scale at the top right of the map.

The measurements were made on Fermi Avenue at the exit point of a roundabout on flat terrain with zero gradient. The 'in-out' measurements were made on different exits from the same roundabout. We estimate that the distance travelled by vehicles at the time they are measured leaving the campus would typically be between 300-500 m. The measurements were made over 18 days from 20 March 2017 to the 20 September 2017. Because the measurement of vehicles leaving the site were performed later in the day (on average at 15:30) than those entering the site (average 07:30), the ambient temperatures were different. On average, for vehicles arriving at the site the temperature was 13°C and measurements of vehicles leaving was 19°C. The

roundabout location also ensured that the vehicle speed was similar for vehicles entering or leaving the site (35 km/h and 32 km/h, respectively).

Results

Table 1 summarizes the passenger car numbers measured over the 18 days of sampling. In total, there were 13,403 passenger cars sampled, 44% of which were diesel i.e. 5908. There were also similar numbers of vehicles entering and leaving the site for each fuel type. Table 1 also shows that there were proportionately more older petrol vehicles compared with diesel vehicles, reflecting the more recent increased uptake of diesel cars in the UK vehicle fleet.

Table 1: Numbers of passenger cars entering and leaving the Harwell Science Campus.

Euro status	Arrive (hot)		Leave (cold)	
	Diesel	Petrol	Diesel	Petrol
2	19	140	27	131
3	295	802	391	728
4	883	1235	881	1264
5	1207	1089	1145	984
6	537	547	523	567
Total	2967	3819	2941	3676

The results for petrol and diesel NO_x emissions from passenger cars are shown in Figure 2. In the case of petrol cars, the emission of NO_x is higher for all Euro classes for cold start compared with vehicles with hot engines. For Euro 3 cars, the cold start NO_x is a factor of two higher but the effect diminishes as the Euro status increases and is only 35% higher for Euro 6 vehicles. The improved cold-start performance of more Euro 4 to 6 petrol vehicles is in line with expectations and the result of better catalyst light-off approaches. For all diesel car Euro classes, there is no statistically significant difference between cold start and hot engine emissions of NO_x, except in the case of Euro 5 cars. For these vehicles, it is the hot-engine emissions that are higher than the cold-start emissions – opposite to that seen for petrol cars.

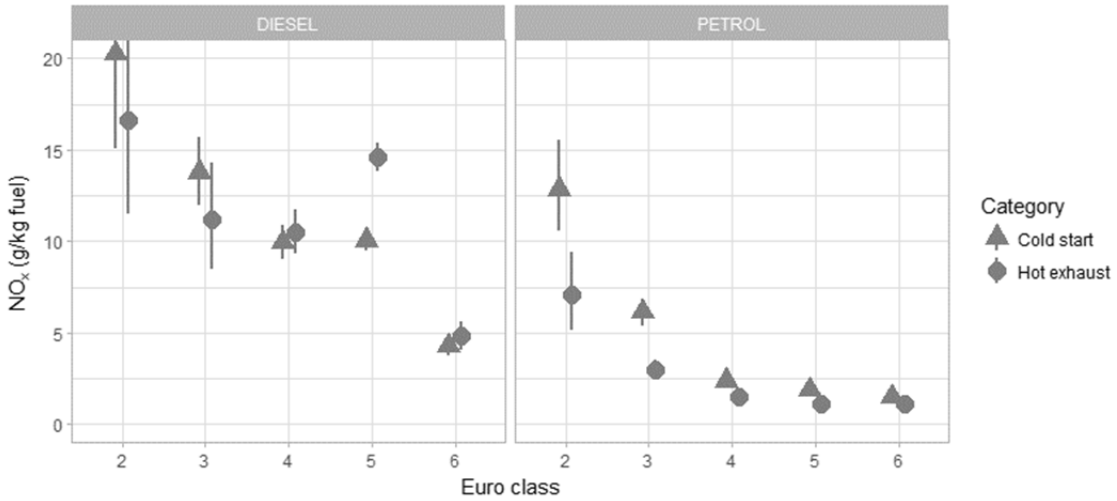

Figure 2: Emissions of NO_x from petrol and diesel vehicles split by whether vehicles are likely to have hot engines or cold starts.

Figure 3 specifically considers the variation in the NO_2/NO_x ratio for diesel passenger cars, categorised by whether a vehicle has a hot engine or is starting with a cold engine. These results indicate that for vehicles with hot engines the amount of NO_2 in the exhaust has tended to increase from Euro 3 through to Euro 6, with Euro 6 vehicles emitting about 31% of their NO_x as NO_2. However, Figure 3 also shows a markedly different behaviour for vehicles staring with cold engines. For Euro 5 and 6 vehicles, the difference between hot engined vehicles compared with cold start vehicles is large. For example, Euro 5 vehicles with hot engines emit 29% of their

NO_x as NO_2 but with cold engines emit only 12% NO_2/NO_x. The difference is larger for Euro 6 vehicles that emit 31% and 5% of their NO_x as NO_2 for hot and cold-start conditions.

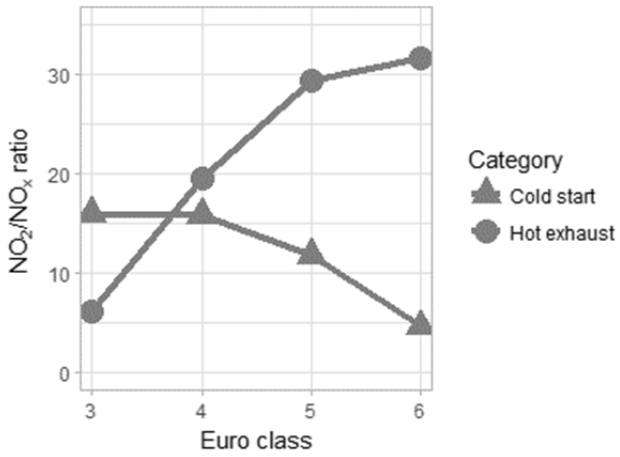

Figure 3: The ratio of NO_2/NO_x for diesel passenger cars split by whether the vehicles have hot engines or are starting with cold engines.

The results shown in Figure 3 could have important implications for urban air quality. In urban areas, trip lengths tend to be shorter than other locations and there are proportionately more cold starts. The UK National Travel Survey (NTS, 2015) for example shows that 17 % of all trips under 1 mile (1.6 km) are made by car. The proportion increases to 60% for trips between 1-2 miles and 79% for trips between 2-5 miles. It is likely however, that trips in urban areas will on average tend to be shorter than the NTS figures suggest. An increasing proportion of Euro 5 and 6 diesel cars in the fleet over time would be expected to result in fleet-average decreases in the NO_2/NO_x ratios based on the current results.

If, as is suggested in Figure 3 the NO_2/NO_x ratio has tended to decrease from Euro 4 to Euro 6 vehicles for cold starting it would have an influence on the ambient concentrations in urban areas due to the number of cold starts. As noted earlier by Carslaw et al (2016) and Grange et al. (2017), there is evidence from the analysis of ambient data in urban areas that the fleet-weighted average NO_2/NO_x emission ratio have tended to decrease or stabilise from around 2010.

Overall, there appear to be several factors that could drive a decrease in the NO_2/NO_x ratio from diesel vehicles, which include: reduced NO_2/NO_x from ageing DOC, reduced platinum group metals used in catalysts, better control of SCR systems in light and heavy-duty applications and as suggested by the current work, the effect of cold start trips. At this time, it is difficult to quantify the relative influences of these effects, which are only partially considered in emission factor methodologies.

Regardless of the attribution of the overall contribution made by these different causes, their effects will be most important close to the emission source i.e. close to roads. This is because the influence that primary NO_2 emissions have on ambient concentrations is most important close to the emission source and before the influence of the chemical production through NO + O_3 dominates as vehicle plumes disperse away from roads. However, from the perspective of exceedances of the EU annual mean Limit Value (which are dominated by locations very close to roads), the ratio of NO_2/NO_x in the exhaust of diesel vehicles is of importance.

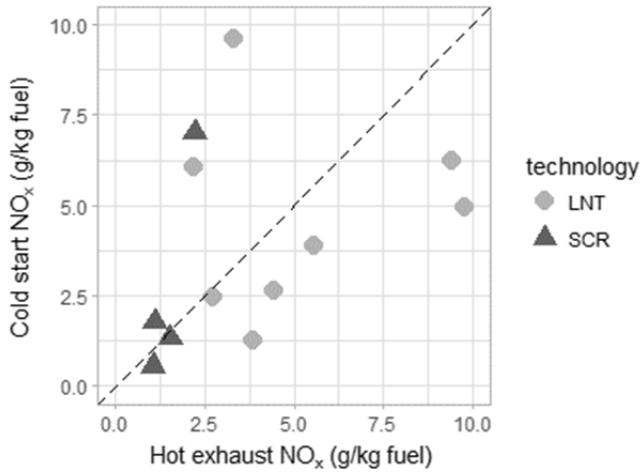

Figure 4: Hot exhaust versus cold-start emissions of NO_x for Euro 6 passenger cars split by vehicle manufacturer and the emissions control technology used.

The data for Euro 6 diesel cars can also be partitioned by the two major NO_x control technologies used: LNT (Lean NO_x Traps) and SCR. In this particular example, data are only considered if there were at least 15 measurements from a particular vehicle manufacturer and engine size. In general, the SCR-equipped vehicles perform much better than the LNT vehicles with both hot engines and cold starts, with the exception of one vehicle manufacturer. On average, the LNT-equipped vehicles emit higher emissions of NO_x with hot engines compared with cold starting, although there is a lot of scatter in the results. It should be noted that this analysis will likely need refinement to ensure that the identification of whether a vehicle uses SCR or LNT is correct and to increase the number of vehicles for which the technology used can be identified.

As noted earlier, the cold-start measurements were made with an average temperature of 19°C, which is somewhat above the annual mean temperature for London of 12°C. Under many situations it would be expected that cold starts would occur under colder ambient temperatures because they would tend to be associated with early morning commuting trips (unlike the Science Campus measurements where the cold start journey began much later in the day. Ideally it would be useful to make additional measurements under colder ambient temperatures to better understand the influence that ambient temperature has on the emissions of NO_x. Finally, work continues refining the quantification of the NO_2 emission using the RSD 5000 instrument by Opus. For this reason, it is expected that further refinements will be made to the emissions estimates in this paper.

References

Burgard, D. A., Bishop, G. A., Stadtmuller, R. S., Dalton, T. R., & Stedman, D. H. (2006). Spectroscopy applied to on-road mobile source emissions. Applied Spectroscopy, 60(5), 135A–148A.

Carslaw, D.C. and Rhys-Tyler, G. (2013). New insights from comprehensive on-road measurements of NO_x,

NO_2 and NH_3 from vehicle emission remote sensing in London, UK. *Atmospheric Environment,* Vol. 81 339-

347.

Carslaw, D.C., Murrells, T.P., Andersson, J. and M. Keenan (2016). Have vehicle emissions of primary

NO_2 peaked? *Faraday Discussions*. 189, 439-454.

EEA, European Environment Agency. Premature deaths attributable to air pollution 2016. https://www.eea.europa.eu/media/newsreleases/many-europeans-still-exposed-to-air-pollution-2015/premature-deaths-attributable-to-air-pollution

Grange, S. K., Lewis, A. C., Moller, S. J. and D. C. Carslaw (2017). Lower vehicular primary emissions of NO_2 in Europe than assumed in policy projections. *Nature Geoscience*. Accepted.

Hallquist, Å. M., Jerksjö, M., Fallgren, H., Westerlund, J., & Sjödin, Å. (2013). Particle and gaseous emissions from individual diesel and CNG buses. *Atmospheric Chemistry and Physics*, 13(10), 5337–5350. https://doi.org/10.5194/acp-13-5337-2013.

NTS (2015). National Travel Survey 2015. Available at https://www.gov.uk/government/uploads/system/uploads/attachment_data/file/551437/national-travel-survey-2015.pdf, 8 September 2016.

Thousands of snapshots vs. trips with thousands of seconds – how remote sensing complements PEMS/chassis emission measurements

J. Borken-Kleefeld[1], Y. Bernard[2], D. C. Carslaw[3], S. Hausberger[4], P. M. McClintock[5], J. E. Tate[6], G.-M. Alt[7], J. de la Fuente[8], R. A. Gentala[5], H. Jenk[9], Å. Sjödin[10], N. Vescio[5]

[1]International Institute for Applied Systems Analysis (IIASA), Schlossplatz 1, A-2361 Laxenburg, Austria
[2]International Council on Clean Transportation (ICCT), Neue Promenade 6, 10178 Berlin, Germany
[3]University of York, Department of Chemistry, Heslington, York, YO10 5DD, United Kingdom
[4]Institut für Verbrennungskraftmaschinen und Thermodynamik, TU Graz, Inffeldgasse 19/I, 8010 Graz, Austria
[5]Opus Inspection Development Center, 2104 N Forbes Blvd, Tucson, AZ 85745, Arizona, USA
[6]University of Leeds, Institute for Transport Studies, University of Leeds, Leeds, United Kingdom
[7]Kanton Zürich, Amt für Abfall, Wasser, Energie und Luft, Stampfenbachstrasse 12, 8090 Zürich, Switzerland
[8]Opus RS Europe S.L., Madrid, 28015, Spain
[9]Bundesamt für Umwelt (BAFU), CH-3003 Bern, Switzerland
[10]IVL Swedish Environmental Research Institute, P.O. Box 53021, SE-40014 Göteborg, Sweden
Keywords: emission test, real-driving, on-road, in-use surveillance, in-service conformity, type approval
Presenting author email: borken@iiasa.ac.at

Measurements on a chassis dynamometer or by portable emission measurement systems (PEMS) records thousands of instantaneous emission records per cycle/trip, but from a few individual vehicles only. Vice versa, remote sensing devices measure thousands of vehicles passing at the site(s) but each for half a second only. Thus, the two methods could complement each other: While the first can tell a lot about the emission behaviour of individual vehicles, the second captures the average of the whole class in real-driving, possibly with some limited variation of engine loads.

This paper proposes a method how to match the different data set and their results together. One important element is to translate their measurement units: The output of chassis or PEMS tests is usually given as gram pollutant per distance driven or per second. The output of remote sensing measurements is usually given as gram pollutant per kg fuel consumed. Both units are linked to each other by the (instantaneous) fuel consumption generating the pollutants emitted at the tailpipe. Both depend on the driving condition, which determines the engine load. (Jiménez, McClintock et al. 1999) suggested the engine load as common denominator for all.

Remote sensing (RS) emission rates are associated with the driving condition of the vehicle expressed e.g. as vehicle specific power (VSP), which is the engine power divided by the vehicle mass. Likewise, the emission rates measured by PEMS or on a chassis dynamometer as well as the instantaneous fuel economy can be associated with the driving condition. Thus, emission rates per VSP can be compared with each other – or aggregated over a succession of VSP states. This way the average instantaneous remote sensing emission rates per VSP can also be used to simulate any other driving cycle that is given as a succession of VSP rates.

Similarly, state-of-art emission models like PHEM are sourced by instantaneous emission factors per engine load for each vehicle class per Euro norm (Hausberger et al. 2009). They then calculate emissions per cycle (e.g. the Artemis, Ermes, HBEFA sub-cycles) as the sum of the instantaneous emissions per engine load weighted by the frequency of load's occurrence.

We here apply our method to cross-check on the results of the official inquiries into the NOx emissions from Euro 5 and Euro 6 diesel cars in Europe. Many models have been measured on variants of the NEDC and under RDE conditions, revealing excessively high NOx emissions (Bernard 2017). These results are summarized here providing the point of comparison.

The instantaneous emission rates are sourced from the collection of all available European remote sensing measurements in the so-called CONOx project (cf. paper by Sjodin et al., this issue). We first compare emission rates of the most popular vehicle models; next, to increase statistical robustness, we aggregate vehicle models that share the same engine and after-treatment within a manufacturer or a group of manufacturer; last, we compare emission rates between manufacturer groups.

This exercise demonstrates how much remote sensing measurements can i) contribute to in-service surveillance of the fleet under real-driving conditions, ii) be detailed for analysis, iii) serve as independent screening for complementary official testing.

This work was funded by Bundesamt für Umwelt (BAFU), Switzerland.

Bernard, Y. 2017. 'Fiat-Chrysler, Renault-Nissan . . . Who Might Be Next?' *International Council on Clean Transportation: From the Blogs*. January 30. http://theicct.org/blogs/staff/fiat-chrysler-renault-nissan-who-might-be-next.

Hausberger, S., M. Rexeis, M. Zallinger, and R. Luz. 2009. 'Emission Factors from the Model PHEM for the HBEFA Version 3'. TU Graz.

Jiménez, J.L., P. McClintock et al 1999. 'Vehicle Specific Power: A Useful Parameter for Remote Sensing and Emission Studies'. presented at the 9th CRC On-Road Vehicle Emissions Workshop, San Diego, April 21, 1999.

Pan-European study on real-driving NO_X emissions from late model diesel cars as measured by remote sensing

Å. Sjödin[1], D. C. Carslaw[2], J. E. Tate[3], J. de la Fuente[4], G.-M. Alt[5], J. Borken-Kleefeld[6], R. A. Gentala[7], P. M. McClintock[7], N. Vescio[7], S. Hausberger[8], Y. Bernard[9], H. Jenk[10]

[1]IVL Swedish Environmental Research Institute, P.O. Box 53021, SE-40014 Göteborg, Sweden
[2]University of York, Department of Chemistry, Heslington, York, YO10 5DD, United Kingdom
[3]University of Leeds, Institute for Transport Studies, University of Leeds, Leeds, United Kingdom
[4]Opus RS Europe S.L., Madrid, 28015, Spain
[5]Kanton Zürich, Amt für Abfall, Wasser, Energie und Luft, 8090 Zürich, Switzerland
[6]International Institute for Applied Systems Analysis (IIASA), Schlossplatz 1, A-2361 Laxenburg, Austria
[7]Opus Inspection Development Center, 2104 N Forbes Blvd, Tucson, AZ 85745, Arizona, USA
[8]Institut für Verbrennungskraftmaschinen und Thermodynamik, TU Graz, 8010 Graz, Austria
[9]International Council on Clean Transportation (ICCT), Neue Promenade 6, 10178 Berlin, Germany
[10]Bundesamt für Umwelt (BAFU), CH-3003 Bern, Switzerland
Keywords: emissions, nitrogen oxides, real-driving, on-road, diesel cars, remote sensing, Euro 5, Euro 6
Presenting author email: ake.sjodin@ivl.se

Introduction

On-road emission measurements are crucial for a comprehensive understanding of road traffic related air pollution and for evaluating the effectiveness of various road vehicle emission control policies. Despite this, after 25 years of increasingly tightened road vehicle emission standards for both light- and heavy-duty vehicles, the emphasis in the EU legislation is still not on such control mechanisms. This situation has paved the way for steadily increasing discrepancies between the levels of vehicle emissions stated by the law or in emission inventories and the real-world emissions, especially for diesel vehicles (Carslaw et al., 2011; Chen and Borken-Kleefeld, 2014; Pujadas, 2017; Rushton et al., 2016; Sjödin and Jerksjö, 2008), the worst example being the “dieselgate” scandal, disclosed in 2015 (Thompson et al., 2014).

The recent EU RDE (Real Drive Emission) regulation demands in type approval tests also on-board emission tests on HDV from EURO VI on and for cars from EURO 6-d-temp (09/2017) on. Also, in-service conformity tests can be made based on on-board emission tests. However, these are expensive and a pre-selection of makes and models may be supported by less expensive methods.

On-road emission measurements by means of optical remote sensing (Bishop et al., 1989) have been carried out in Europe since the early 1990’s (Sjödin, 1994), mainly for research purposes, and in countries such as Sweden, UK, Switzerland, Spain and France.

The present study involves the first attempt to pool the remote sensing data that has been collected across Europe since 2011 into one common database, with the primary aim to analyse the real-driving emission performance of Euro 5 and 6 light-duty diesel vehicles across the European fleet. These measurements total around 500,000 remote sensor readings, and include CO, HC, NO, NO_2, (occasionally), PM (opacity), vehicle speed and acceleration, along with detailed vehicle information retrieved from national vehicle registers, such as vehicle make, model, model year, Euro standard, weight, displacement volume and engine power.

Methods

Measurements and data overview

The data considered for the pan-European analysis carried out within this study were from remote sensing measurements carried out on various locations (in or near cities) in Spain, Sweden, Switzerland and the United Kingdom between 2011 and 2017, see Table 1. In all, more than 700,000 vehicle passages were registered in these measurements, of which close to 200,000 were diesel passenger cars with valid remote sensor readings and for which the Euro standard could be identified. The 200,000 diesel passenger car dataset was dominated by Euro 5 (39 %), followed by Euro 4 (33 %), Euro 3 (16 %) and Euro 6 (9 %). Almost 18,000 cars were Euro 6.

Table 1: Overview of the remote sensing measurements behind the analysis in this study.

Country	Measurement year(s)	Overall number of vehicle passages	Number of valid remote sensor readings (NO) for diesel passenger cars by Euro standard						
			E0	E1	E2	E3	E4	E5	E6
Spain	2015, 2017	294,861	191	343	4,038	18,741	29,246	27,144	11,007
Sweden	2016	34,944	1	3	10	55	431	3,416	2,218
Switzerland	2011-2016	212,981	92	115	680	5,148	17,311	27,858	4,139
United Kingdom	2012, 2013, 2015	173,550	111	125	894	7,381	17,979	18,718	430
Total		**716,336**	**395**	**586**	**5,622**	**31,325**	**64,967**	**77,136**	**17,794**

Remote sensing instruments

The remote sensing instruments used in the campaigns listed in Table 1 were:

- the Denver University FEAT instrument with NO_2 capability in the UK measurements in 2012 and parts of the UK measurements in 2013,
- the Opus AccuScan RSD 4600 instrument in the 2015 measurements in Spain, the 20112015 measurements in Switzerland from 2011 through 2015, and the 2015 measurements and parts of the 2015 measurements in the UK, and
- the new Opus AccuScan RSD 5000 instrument with NO_2 capability in the 2017 measurements in Spain, and in the 2016 measurements in Sweden and Switzerland.

For the remote sensing data that did not include NO_2, NO_2 emissions were estimated in order to derive NO_X emissions by applying NO_2/NO_X–fractions by Euro standard for diesel and gasoline cars derived from the remote sensing measurements including NO_2. This approach was only applied to emission data on a higher aggregated level, such as the average emissions by Euro standard presented in Figures 1 and 2, and not to emissions on an individual vehicle level or smaller subsets of vehicles, such as those presented in Tables 2-5 and Figures 3-4.

Database

An SQL Server database, accessible over the internet, was developed to host crucial (raw and refined) remote sensing data along with vehicle information. The web interface provides export and import functions as well as search queries to retrieve optimal selections of subsets of data. The database contains about 100 parameters, of which about 30 were related to vehicle information.

Emission units derived from remote sensing measurements

Remote sensing provides directly – from the ratios of pollutant to CO_2 measured in the raw vehicle exhaust – emission factors expressed as g per kg (or liter) fuel burned,. This unit has been used throughout the analysis presented in this study. A new method to convert g/kg fuel remote sensing emission factors into g/km was recently developed, based on the same pan-European remote sensing dataset as in the present study (Borken-Klefeld, 2017). It should be noted that using converted g/km instead of g/kg emission factors for the data evaluation in the present study would in some cases probably had yielded slightly different results than those presented.

Results

NO_X emissions by Euro standard

NO_X emissions in gram per kg fuel by Euro standard per country for diesel and petrol passenger cars according to the remote sensing measurements are presented in Figure 1 and 2.

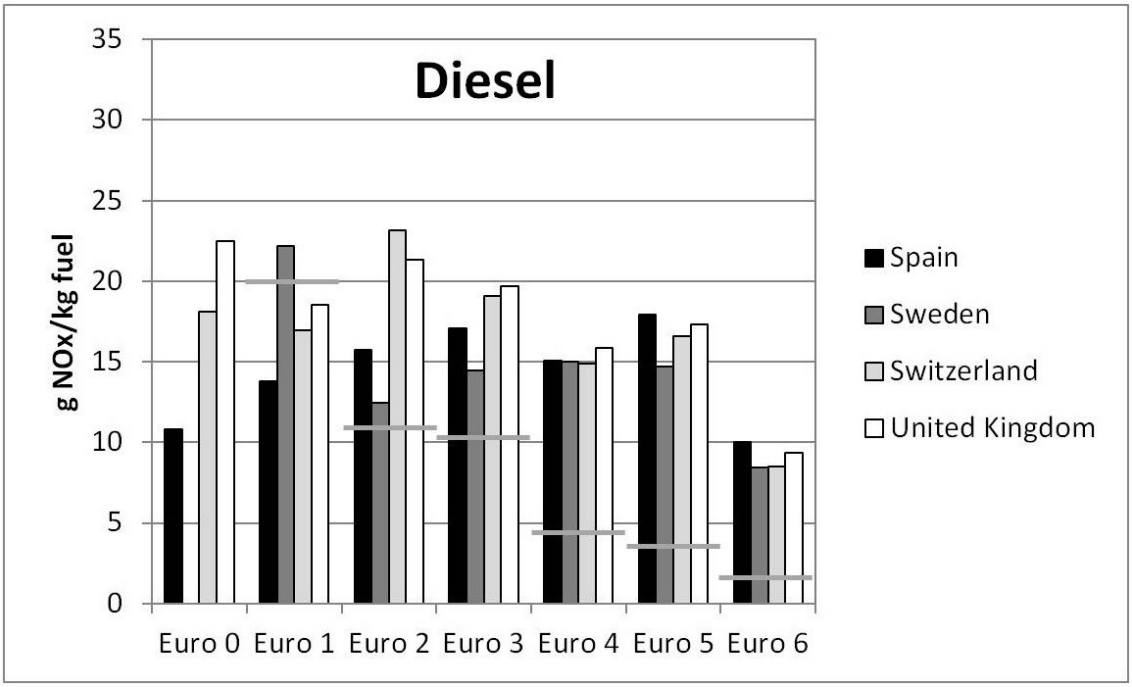

Figure 1: NO_X emissions (g per kg fuel) by Euro standard per country for diesel passenger cars according to the remote sensing measurements. The grey horizontal lines indicate the Euro standard limit value.

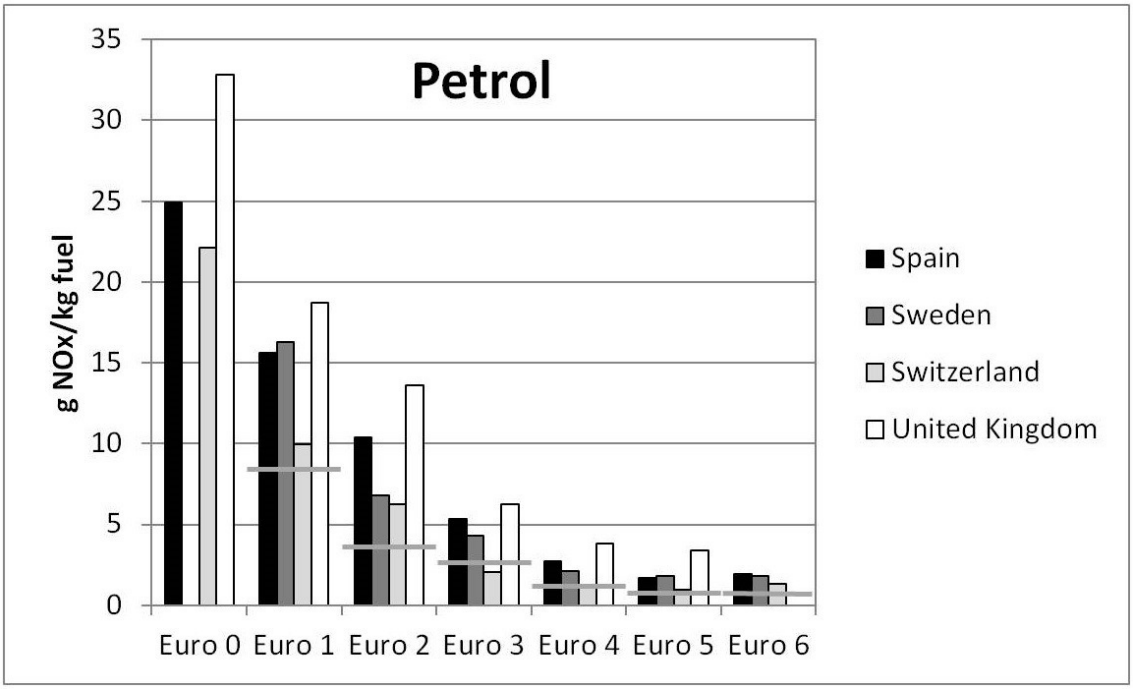

Figure 2: NO_X emissions (g per kg fuel) by Euro standard per country for petrol passenger cars according to the remote sensing measurements. The grey horizontal lines indicate the Euro standard limit value.

The trends in real driving NO_X emissions by Euro standard for passenger cars show the expected patterns, i.e. no apparent downward trend in NO_X emissions between pre-Euro cars and Euro 5 for diesel cars even though the Euro standard has been tightened more than fourfold, on the other hand the reduction in NO_X emissions from petrol cars follows the evolution of the Euro standard quite nicely.

This study presents one of the first extensive set of measurements of real driving emissions from Euro 6 passenger cars (≈18,000 measurements). It is clear from Figure 1 that the real-world NO_X emissions from diesel passenger cars have been markedly reduced with the introduction of the Euro 6 standard compared to the Euro 5 and preceding standards. Compared to Euro 4 and Euro 5 the reduction is in the order of 40%. However, on-road NO_X emissions from Euro 6 diesel passenger cars are on average still about five (5) times higher than for Euro 6 petrol passenger cars. This should be compared with the Euro 6 limits, which is 80 mg/km for diesel cars and 60 mg/km for petrol cars, i.e. virtually the same limit.

The worst and best performing makes among Euro 5 and Euro 6 diesel passenger cars with regard to NO_X real driving emissions

The highest- and lowest-emitting makes among Euro 5 and Euro 6 diesel passenger cars, respectively, with regard to NO_X real-driving emissions are presented in Tables 4-7. In order to improve the statistics, remote sensing data on NO emissions was used as a proxy for NO_X emissions for this ranking (there were much more NO data than NO_X data in the remote sensing dataset). Also due to better statistics, a top ten list was created for Euro 5 cars, whereas for Euro 6 cars it was restricted to only the top five. Also, as mentioned in the methods chapter, particularly for this analysis, using converted g/km emission factors instead of g/kg emission factors (Borken-Kleefeld, 2017) might have yielded different results than those presented.

For Euro 5, 13 of the in all 18 different makes (≈70 %) on the highest-emitting list were among the ten highest-emitting makes in two or more countries. On the lowest-emitting list, 10 of the in all 17 makes (≈60 %) were among the ten lowest-emitting makes in two or more countries. The highest-emitting Euro 5 makes emitted on average 3-4 times more NO_X than the lowest-emitting Euro 5 makes.

For Euro 6, five of the in all eleven different makes (≈45 %) on the highest-emitting list were among the five highest-emitting makes in two or more countries. On the lowest-emitting list, five of the in all ten different makes (50 %) were among the ten lowest-emitting makes in two or more countries. The highest-emitting Euro 6 makes emitted on average 5-15 times more NO_X than the lowest-emitting Euro 6 makes.

Table 2: The ten highest-emitting makes with regard to NO emissions among Euro 5 diesel passenger cars, by country. Makes occurring on the top ten list in three countries or more are marked in ***bold italics***, makes occurring in two countries are marked in *italics*.

Spain	Sweden	Switzerland	United Kingdom
Alfa Romeo	***Renault***	***Renault***	***Vauxhall/Opel***
Opel	***Nissan***	***Nissan***	***Fiat***
Skoda	***Fiat***	***Fiat***	***Chevrolet***
Porsche	*Porsche*	***Chevrolet***	***Hyundai***
Nissan	*Dacia*	***Hyundai***	***Renault***
Renault	Volkswagen	***Kia***	***Kia***
Chevrolet	***Kia***	*Dacia*	***Nissan***
Hyundai	Honda	***Opel***	*Alfa Romeo*
Kia	***Hyundai***	Jeep	*Skoda*
Suzuki	*Ford*	*Ford*	Mazda

Table 3: The ten lowest-emitting makes with regard to NO emissions among Euro 5 diesel passenger cars, by country. Makes occurring on the top ten list in three countries or more are marked in ***bold italics***, makes occurring in two countries are marked in *italics*.

Spain	Sweden	Switzerland	United Kingdom
Jaguar	***Mini***	***Jaguar***	***Land Rover***
Land Rover	***Toyota***	***Toyota***	***BMW***
Mercedes	***Land Rover***	***Land Rover***	***Volvo***
Mini	*Mazda*	***Mini***	***Jaguar***
Mitsubishi	***BMW***	***BMW***	***Mini***
Chrysler	***Mercedes***	***Volvo***	***Mitsubishi***
Subaru	***Jaguar***	*Mazda*	***Mercedes***
Toyota	***Mitsubishi***	Lancia	Honda
Citroen	***Volvo***	*Subaru*	***Toyota***
BMW	Jeep	***Mitsubishi***	Audi

Table 4: The five highest-emitting makes with regard to NO_X (NO) emissions among Euro 6 diesel passenger cars, by country. Makes occurring on the top five list in three countries or more are marked in ***bold italics***, makes occurring in two countries are marked in *italics*.

Spain	Sweden	Switzerland	United Kingdom
Dacia	***Renault***	***Renault***	Vauxhall/Opel
Renault	***Subaru***	***Nissan***	***Ford***
Nissan	Hyundai	***Ford***	Mazda
Subaru	***Nissan***	*Fiat*	Volvo
Fiat	***Ford***	***Subaru***	Volkswagen

Table 5: The five lowest-emitting makes with regard to NO_X (NO) emissions among Euro 6 diesel passenger cars, by country. Makes occurring on the top five list in three countries or more are marked in ***bold italics***, makes occurring in two countries are marked in *italics*.

Spain	Sweden	Switzerland	United Kingdom
Citroen	***Land Rover***	***Land Rover***	*Citroen*
Land Rover	Skoda	Mercedes	Porsche
Jaguar	***Volkswagen***	***BMW***	Mini
Audi	***BMW***	***Audi***	***BMW***
Volkswagen	***Audi***	***Volkswagen***	***Audi***

Ambient temperature dependence of diesel passenger cars' NO_X hot emissions

Euro 4, 5 and 6 diesel passenger cars' NO_X, NO and NO_2 hot emissions exhibited all a clear dependence of ambient temperature in the range 0 to 35 degrees C, with a minimum between 20 and 25 degrees, the most typical temperatures for legislative emission testing, cf. Figure 3.

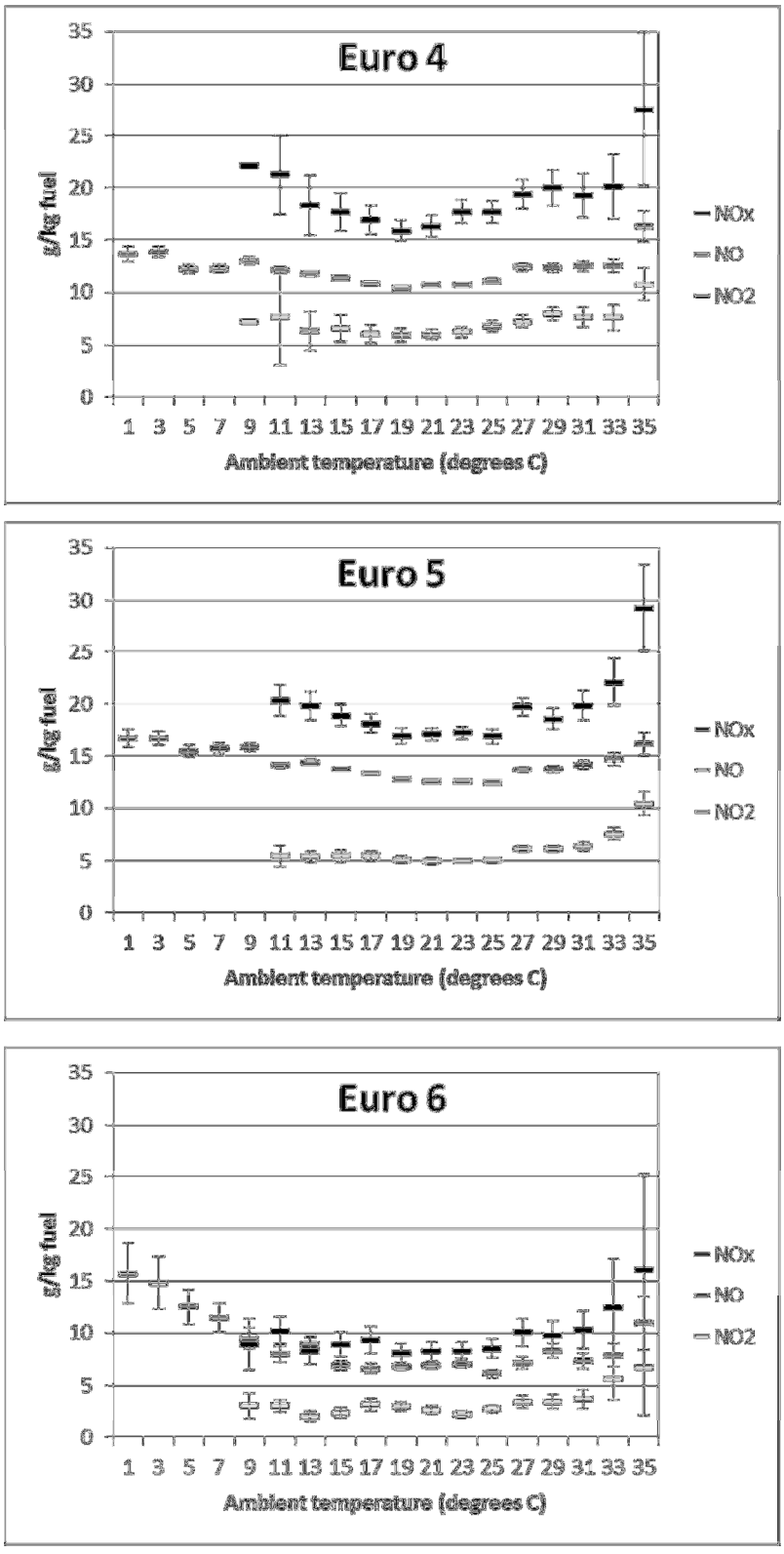

Figure 3: Ambient temperature dependence of Euro 4-6 diesel passenger cars' NO_X, NO and NO_2 emissions.

Vehicle age dependence of diesel passenger cars' NO_X emissions

The dataset comprising measurements over a six year time period enabled some analysis of the impact of vehicle age (up to 16 years) on the real driving NO_X emissions from diesel passenger cars, cf. Figure 4. A similar analysis has been made earlier for diesel cars up to Euro 4 on a subset of the data included in the present work (Chen and Borken-Kleefeld, 2016).

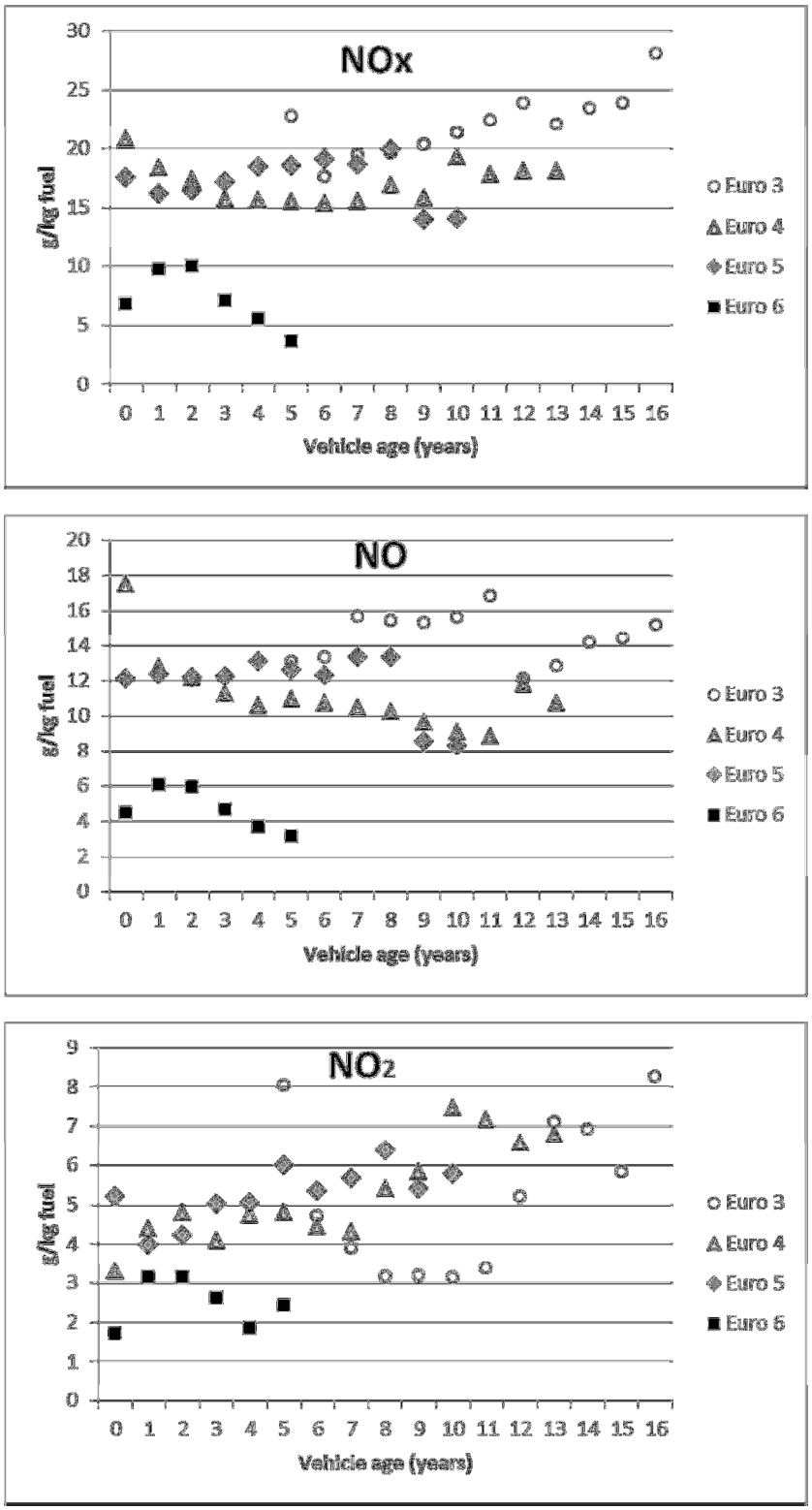

Figure 4: NO_X, NO and NO_2 emissions from Euro 3-6 diesel passenger cars as a function of vehicle age.

As apparent from Figure 4, the age dependence of diesel passenger cars' NO_X emissions is a complex matter, when considering both the different EU standards and the two components of NO_X, i.e. NO and NO_2. For instance, for Euro 3, NO_X emissions tend to increase steadily with age up to an age of 16 years, whereas primary NO_2 emissions exhibit a clearly U-shaped curve with a minimum around 8-10 years. For Euro 4, NO emissions tend to decrease and NO_2 emissions to increase with age, resulting in a rather flat emission vs vehicle age curve for NO_X. A somewhat similar behaviour can be seen for Euro 5, whereas for Euro 6 both NO and NO_2 (and thus NO_X) emissions tend to decrease with age up to five years (which was the highest age for Euro 6 cars in the analysed remote sensing dataset). Also, the age dependency of emissions may also be obscured by various other parameters contained in the analysed remote sensing dataset that influences emissions, such as ambient temperature, driving conditions and fleet composition with regard to vehicle make, etc.

Conclusions

Data pooling of remote sensing data collected over the last six years on various locations across Europe has proved to be a powerful means to analyse real driving emissions from late model diesel passenger cars. The work presented in this paper has yielded new insights into the efficiency of legislative measures to reduce on-road NO_X emissions including the various strategies used by car manufacturers to meet - more or less successfully - the legislative targets, as well as into the influence of ambient temperature and vehicle age on the emissions.

Acknowledgements

This work was part of the CONOX[1] project, sponsored by Bundesamt für Umwelt (BAFU), Switzerland. The underlying work, i.e. carrying out remote sensing measurements and associated data evaluation on a country level, was supported by various national and local authorities and other stakeholders in the involved countries. Opus Group and the Foundation of the Swedish Environmental Research Institute are particularly acknowledged for sponsoring the preparation of this paper.

References

Carslaw, D., S. Beevers, J. Tate, E. Westmoreland, M. Williams (2011), Recent evidence concerning higher NOx emissions from passenger cars and light duty vehicles, *Atmos. Environ.* 45, 7053-7063.

Chen, Y. and J. Borken-Kleefeld (2014), Real-driving emissions from cars and light commercial vehicles - Results from 13 years remote sensing at Zurich/CH, *Atmos. Environ.* 88, 157-164.

Borken-Kleefeld, J. (2017) Thousands of snapshots vs. trips with thousands of seconds – how remote sensing complements PEMS/chassis emission measurements. *TAP 2017*, Zürich, 15-16 Nov 2017.

Chen, Y. and J. Borken-Kleefeld (2016), NOx Emissions from Diesel Passenger Cars Worsen with Age *Environ Sci Technol.* 50, 3327-3332.

Pujadas, M., A. Dominguez-Saez, De la Fuente, J. (2017), Real-driving emissions of circulating Spanish car fleet in 2015 using RSD Technology, *Sci. Total Environ.* 576, 193-209.

Rushton, C., J. Tate, J., S. Shepherd (2016) NO_X Emission Performance Of Vans In Real Urban Driving and The Uptake of Euro 5 Technology Using A Remote Sensing Device. *21st Int. Symp. Transport & Air Pollution*, Lyon, 24-26 May, 2016.

Sjödin, Å. (1994) On-Road Emission Performance of Late-Model TWC-Cars as Measured by Remote Sensing, *J. Air & Waste Manag. Assoc.* 44, 397-404.

Sjödin, Å. and Jerksjö, M. (2008), Evaluation of European road transport emission models against on-road emission data as measured by optical remote sensing, *16th Int. Symp. Transport & Air Pollution*, Graz, 16-17 June, 2008.

Thompson, G. J., K. Daniel, D. K. Carder, C. Marc C., M. C. Besch, A. Thiruvengadam A. (2014) In-use emissions testing of light-duty diesel vehicles in the U.S. *Final report prepared on behalf of International Council on Clean Transportation*, May 15, 2014.

[1] "Study on comparing NO_X real driving emissions from Euro 5 and Euro 6 light-duty diesel vehicles as measured by remote sensing, PEMS and on chassis dynamometers"

Particles air pollution in diesel passenger trains, coaches, train and bus stations

V. Abramesco[1], A. Zalzberg[2], J. Czerwinski[3], A. Mayer[4] and L. Tartakovsky[1]*

[1] Faculty of Mechanical Engineering, Technion – Israel Institute of Technology, Haifa 3200003, Israel, tartak@technion.ac.il
[2] Israel Ministry of Environmental Protection, Jerusalem 95464, Israel
[3] Labs for IC-Engines & Exhaust Emission Control, Berne University of Applied Sciences, Biel, Switzerland
[4] VERT Association, TTM Niederrohrdorf, Switzerland

Introduction

Climate change and air pollution challenges lead to intensive efforts aimed at reduction of carbon footprint and mitigation of target pollutant emissions from energy conversion processes (Tartakovsky et al, 2012). Commuters' exposure to harmful pollutants is being extensively studied due to strong adverse effects the latter have on human health (Chan et al, 2002; Chuang et al, 2007; Tartakovsky et al, 2013; Abramesko & Tartakovsky, 2017). Combustion-generated particles are known as a major pollutant with well-known carcinogenic effects. The published research results showed that ultrafine particles (UFP) are more harmful to humans than larger ones because smaller particles can penetrate cell membranes and are transported within the blood stream to all human organs (Hoet et al, 2004; Knibbs et al, 2011).

Passenger turnover by rail and buses represents an absolute majority of passenger transport activity over the globe. Locomotives and buses with diesel engines are widely spread worldwide and are an important source of air pollution. Note that only 1/3 of the total length of railway lines worldwide is electrified (UIC, 2015). Pollutant emissions by locomotive and bus engines affect air quality in stations as well as inside passenger cabins. This study was aimed at investigation of air pollution by UFP inside passenger trains and buses, and a comparison with particle air pollution at bus and train stations. The gained data provide a basis for assessment of passengers' exposure to this dangerous pollutant.

Methodology

Instrumentation

The ultrafine particle number concentrations were measured by a diffusion size classifier (DiSC, Matter Engineering AG, Switzerland). This device is a small, easily portable, battery operated instrument and is therefore well suited for field measurements. The detectable particle concentrations range of this instrument is 3,000 – 1,000,000 cm^{-3} (for 20 nm particles) and 1,000 – 500,000 cm^{-3} (for 100 nm particles). The measured particles size range is 10 – 400 nm. Note that for particles < 20 nm, the DiSC generally underestimates the particle number. For particles larger than 200 nm, overestimation of the particle diameter is possible. Although DiSC is somewhat less accurate (±30%) and sensitive than other frequently used laboratory devices, such as Condensation Particle Counter – CPC (accuracy ±10%) and Scanning Mobility Particle Sizer – SMPS, it is highly applicable for field measurements due to its compactness, portability and self-contained power supply.

The instrument requires recalibration after 500 hours of operation (Fierz et al, 2008). To ensure the quality of the data collection, both the instrument operation time and Pressure Error LED signal were carefully monitored. No instrument recalibration was required upon completing the measurement program reported in this paper. To ensure the best possible accuracy of the measurements, the zero reading of the instrument was checked daily before the start of measurements. In all experiments, the sampling inlet was at the height of the breathing zone area of a sitting passenger. The sampling flow rate of the instrument was 1.5±0.1 L/min. A short Teflon tube of ~0.5 m in length and approximately 5 mm in internal diameter was connected to the sampling inlet of the instrument. The tube length was chosen to minimize particle loss (residence time ~0.4 sec), while enabling sampling at the height of the passengers' breathing zone. In all measurements, a single DiSC instrument was used. The 'ultrafine' particles measured in this work are defined as particles with a size cut of 10-400 nm.

Measurement procedure

All experiments were performed over a six-month period on various weekdays (Sunday to Friday) from 07:00 to 19:00 (Sunday is a weekday in this area). In total, 100 measurements were performed inside the carriages of passenger trains; 92 had valid results and were included in the analysis. Forty-six tests were performed in double-deck carriages, 13 in old single-deck ones, 17 in new single-deck carriages and 16 in diesel multiple-unit trains. Unfortunately, the total number of valid measurements is not sufficiently large to allow for reliable analysis of the day-to-day variance of the obtained results. Measurements inside the trains were performed on the railway route between Haifa and Tel Aviv HaShalom station (the main railway route in Israel). The route length is approximately 95 km. The duration of a one-way trip was 66-70 min. Each measurement lasted 15 min. Therefore, the authors completed the measurements in four carriages (#1, 3, 5 and 7), one-by-one, in a single one-way journey. Measurements of UFP concentrations were performed in carriages of the following types: new single-deck passenger carriages (years of production 2009-2011), old single-deck passenger carriages (years of production 1996-1997) and double-deckers. A detailed description of the investigated carriage types can be found in (Abramesko & Tartakovsky, 2017). Measurements were performed in various carriages of the train that were located at different distances from the locomotive as shown in Fig. 1. In these experiments, in each carriage, UFP sampling was performed at the next-to-door seats. Note that the studied diesel-powered passenger trains are of push-pull type. The latter means that in some journeys a locomotive is located at nose of the train and pulls it, while in other journeys it is located at the tail and pushes the train – see Fig. 1.

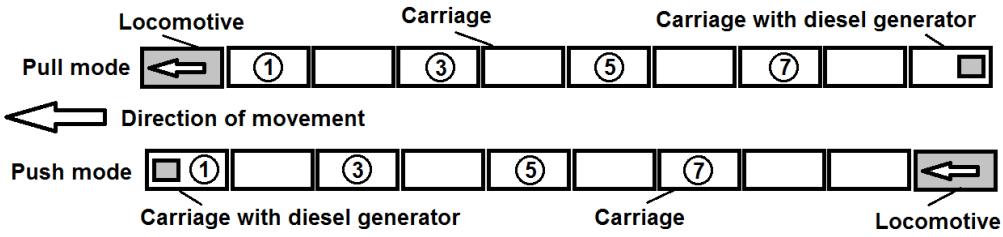

Figure 1: Scheme of measurements in passenger carriages. A digit inside a circle indicates the carriage number where measurements were performed. Carriage #1 is always located in the nose of the moving train (Abramesko & Tartakovsky, 2017).

At the train station in Tel-Aviv, measurements were performed at both levels of the station: the upper level and the platforms – Fig. 2. At the upper level, the measurements were carried out in four points: adjacent to coffee shop, near the main entrance (adjacent to the main road), on the bridge between the station and the mall (just above the highway) and outside the station on the main road adjacent to the station's entrance. The measurement points are shown in Fig. 2a. At the lower level measurements were performed in four points at platform 1 and also in four points at platforms 2-3 – Fig. 2b. They were performed at peak and off-peak hours.

The measurements of UFP concentrations inside intercity buses were performed on the route Haifa – Jerusalem. The route length is 155 km. Number of stops between final stops – 3. Average passengers' occupancy – 28. In total, 10 trips in each direction were made to complete these measurements with a total traveled distance of over 3100 km. UFP concentrations were measured in three points as shown in Fig. 3: at the second seat from the driver location (front of the bus), sixth seat (middle of the bus) and the back seat.

Measurements at Jerusalem Central Bus Station were performed in the shopping area (1st floor), food court (2nd floor), waiting (inner) area of embarkment platforms (3rd floor), embarkment platforms (3rd floor). Measurements were taken at various platforms, in order to attain a wider picture of the UFP concentrations along the different platforms. Note that the embarkment platforms of Jerusalem Central Bus Station are located inside the building, which may result in severe air pollution problems. Assessment of air pollution by UFP in this station was one of the main study objectives.

Duration of all UFP measurements performed in trains, buses, as well as the train and the bus stations was 15 min. The sampling frequency was 1 Hz. Because all studied passenger trains, buses and the respective stations are smoke-free, the issue of smoking was not investigated in our study.

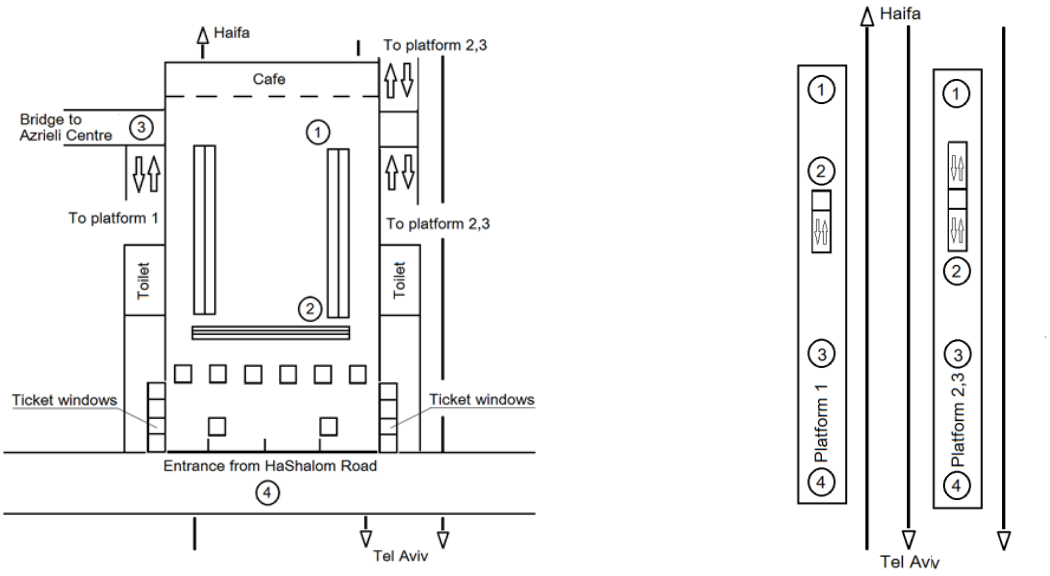

a) Upper level b) Platforms

Figure 2: Measurements scheme at the train station.

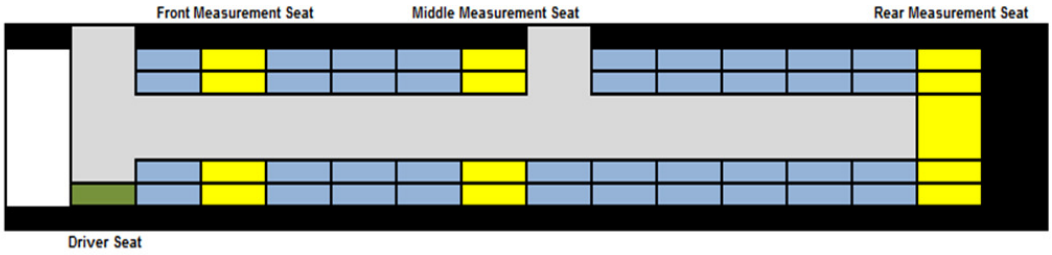

Figure 3: Measurements scheme in the intercity coach. Measurement points are highlighted by yellow.

Results and discussion

Passenger trains

Fig. 4 shows influence of the train's operating mode (push or pull) and distance from the emission source on the UFP number concentrations inside the train carriages. We show in Fig. 4 the mean values of multiple measurements performed on the same route for the same carriage type. As can be seen from Fig. 4, for all studied types of carriage, very high UFP concentrations were measured when the locomotive operated in pull mode. The measured minimal mean UFP number concentrations were 10^5 cm^{-3}. This value is higher by factors of two and 2.4 than the average UFP concentrations reported in the literature for car cabins ($4.9 \cdot 10^4$ cm^{-3}) and buses ($4.2 \cdot 10^4$ cm^{-3}), respectively (Joodatnia et al, 2013). The highest levels of the mean UFP concentrations in the pull mode were measured in carriages adjacent to the locomotive, whereas the mean UFP concentration levels in these wagons were found to be 3-$4.4 \cdot 10^5$ cm^{-3} (higher by approximately an order of magnitude than in car cabins). The UFP concentrations in all types of train carriages were substantially lower when the train operated in push mode compared to pull-mode. This clearly shows that the locomotive engine emissions are a dominant factor in train passenger exposure to UFPs. In push mode, the UFP number concentrations were lower by factors of 2.6 to 43 (depending on the carriage type) compared to pull mode. Over the entire range of studied carriage types and for all carriages for which the measurements were performed, the mean UFP concentrations in push mode did not exceed the

level of $1.2 \cdot 10^5$ cm^{-3}. In most carriages, the measured mean UFP concentrations in push mode remained lower than in an average car cabin ($4.9 \cdot 10^4$ cm^{-3}) and average bus ($4.2 \cdot 10^4$ cm^{-3}).

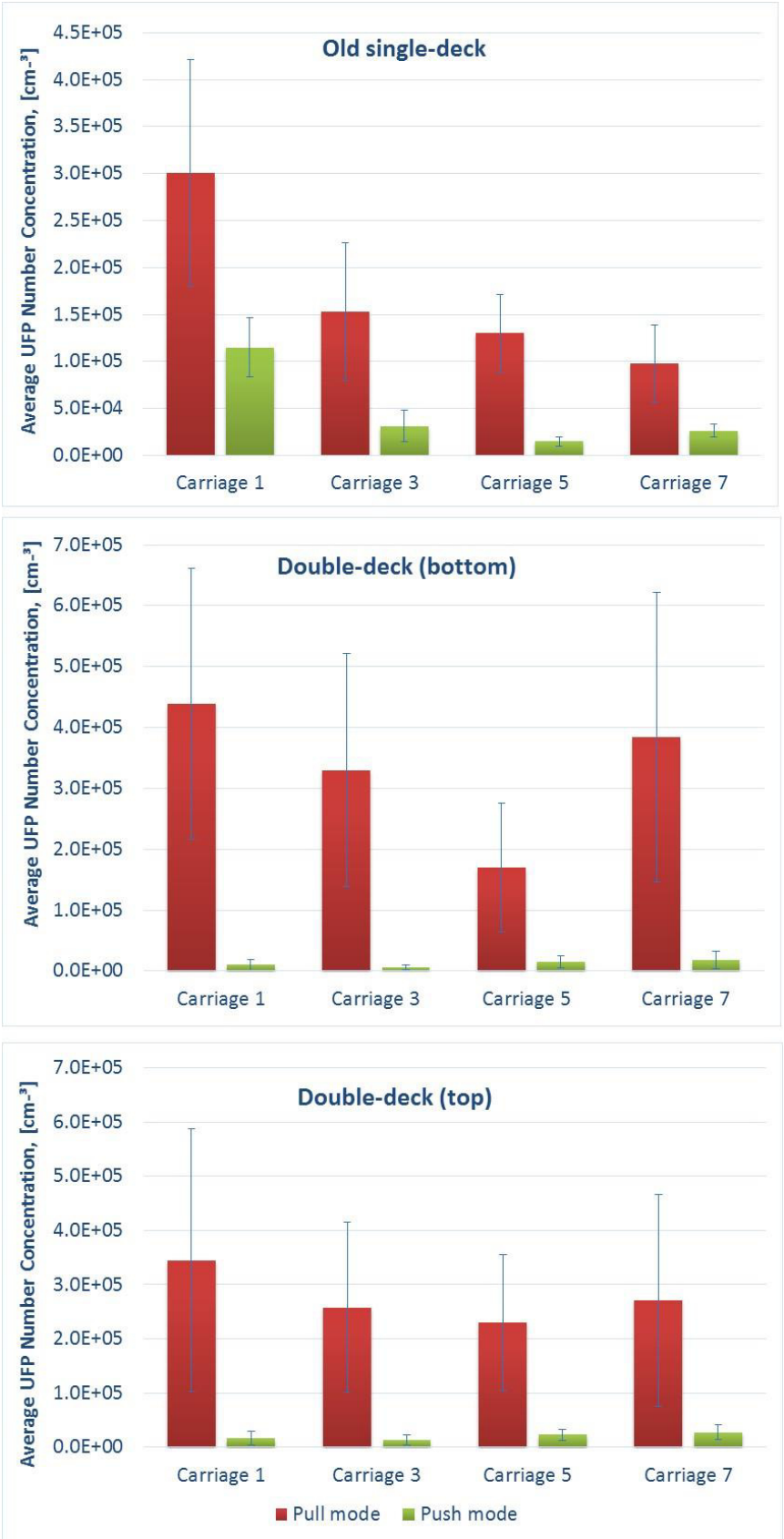

Figure 4: Influence of train operating mode on UFP concentrations inside a carriage (Abramesko & Tartakovsky, 2017).

For all investigated carriage types, the lowest average UFP NC values were measured in the middle of a train between the 3rd and 5th carriage (in a train of 9 carriages), where the joint influence of emissions from both the diesel generators and locomotive engine, together with the effects of airborne non-exhaust particles, was minimal. The mean UFP number concentrations were higher in old carriages throughout the train compared to new ones of the same type by a factor of 2-6 (Abramesko & Tartakovsky, 2017). This result confirms previously known data for road vehicles (Tartakovsky et al, 2013). Similarly to cars and buses, more UFPs penetrate the passenger compartment of older carriages through less efficient air filters, less tight doors and window sealing and leaks in the carriage structure. At the same time, we believe that the main way of particles penetration into passenger carriages is through ruptures of various sizes in the rubber connectors between the carriages – Fig. 5. Naturally, these ruptures are bigger in amount and size in older carriages.

Figure 5: Ruptures in rubber connectors between the carriages.

Train station

Fig. 6 and 7 show results of UFP measurements at the train station in Tel-Aviv. The interesting peculiarity of this station is its location between the lanes of a main highway and direct adjacency to a main city road – Fig. 8. This fact led to intensive discussions about a main source of air pollution in the station: locomotive or road vehicle emissions. Answering this question was one of important goals of the reported study.

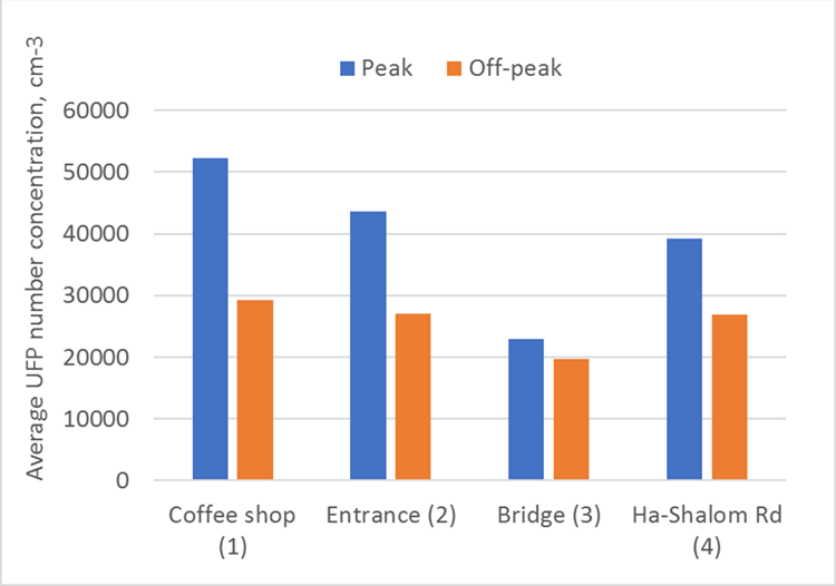

Figure 6: Measurements at the train station – upper level.

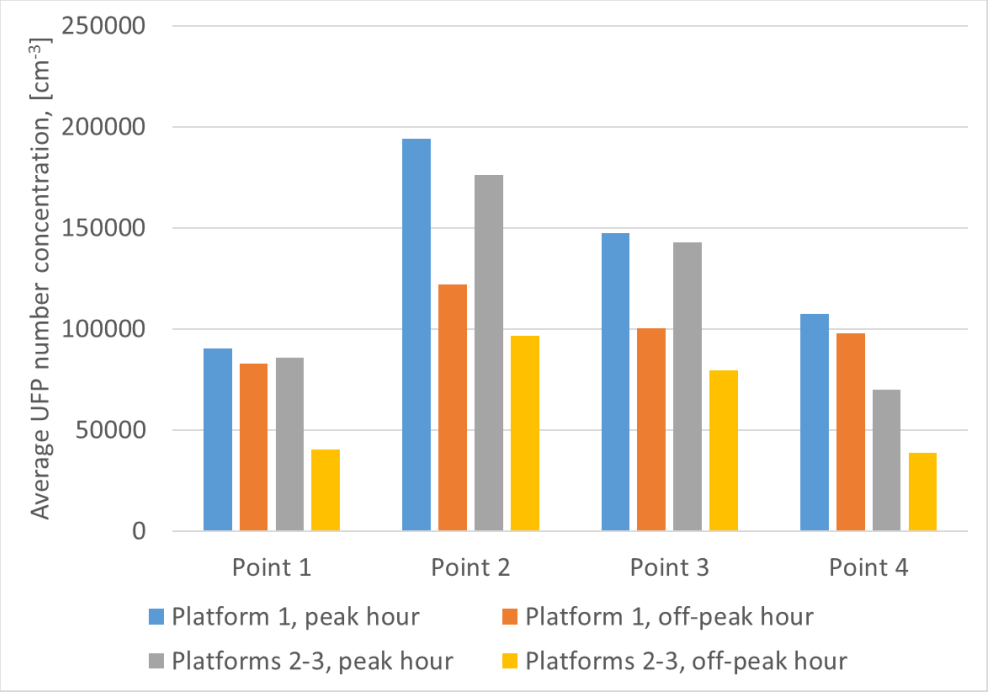

Figure 7: Mean values of UFP concentrations at platforms of the train station, cm^{-3}.

Figure 8: Two passenger trains entering Tel Aviv train station - highway from both sides of the station (Omer Simkha, 2017).

The obtained results (Fig. 6) clearly demonstrate that air pollution from the highway surrounding the train station is not a main contributor to air pollution by UFP measured inside the station. As can be seen, the mean UFP concentrations measured in the peak hours outside the station in a close proximity to the highway and the city main road are substantially lower than those inside the station. UFP concentrations measured in point 1 (coffee shop) are the highest. We explain this finding by the proximity of the measurement point 1 to the stairs connecting the upper level with the station platforms. The results of measurements at the station platforms show the highest average UFP concentrations at platform 1, especially at the platform's segments covered with the roof. It is clear that the latter makes it difficult for fresh air to recirculate, thus leading to very high UFP concentrations even during the off-peak hours (Fig. 7). A proximity to the station wall probably results in formation of stagnation zones that additionally limit air exchange rate in platform 1 area. Air pollution level at the platform segments located outside the roof (points 1 and 4) is much lower – by up to a factor of two. Somewhat lower UFP

concentrations observed at platforms 2-3 (Fig. 7) can be explained by the larger distance of these platforms from the station walls, allowing for better fresh air recirculation. As anticipated, mean values of UFP concentrations measured during the off-peak hours are substantially lower than those observed during the peak hours. Again, dependence of UFP concentrations on the daytime is found to be stronger for measurement points located inside the station (more affected by locomotive emissions).

Intercity coaches

The results of UFP measurements inside intercity coaches are shown in Fig. 9. The obtained results show that UFP air pollution inside a bus is considerably higher at the back seats. Probably, engine location in this area and possible infiltration of exhaust gases into the passengers' compartment lead to this finding. Another possible reason for higher UFP concentrations at the back seats is air circulation caused by AC. However, relevance of this hypothesis should be further checked. The mean UFP concentrations that were measured in the intercity coaches on the investigated line between Haifa and Jerusalem are quite low and lie between $1.4\text{-}1.5 \cdot 10^4$ cm^{-3}.

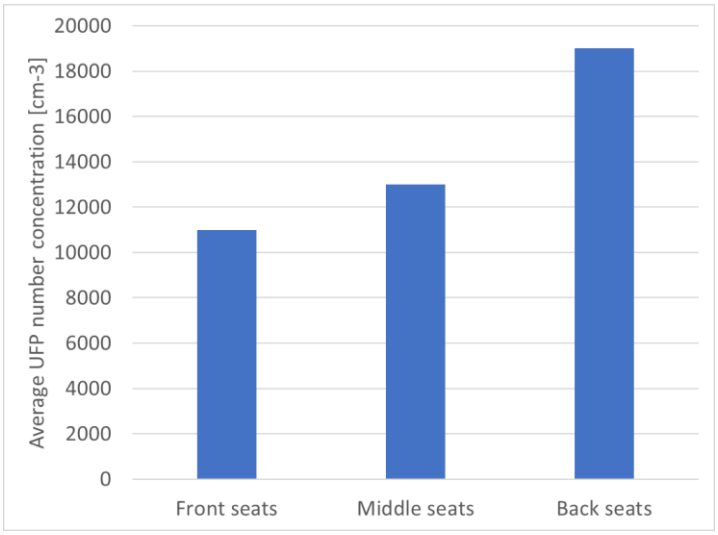

Figure 9: UFP air pollution inside intercity coaches.

Central bus station

UFP number concentrations were also measured in various areas of the Jerusalem Central Bus Station as explained in the Methodology section of this article. Measurement results are shown in Fig. 10.

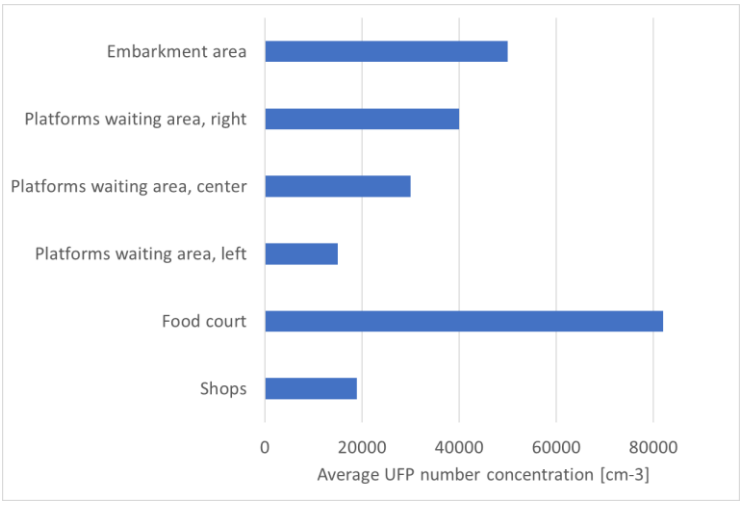

Figure 10: Mean UFP concentrations in different areas of the Jerusalem Central Bus Station.

As can be seen from a comparison shown in Fig. 10, UFP air pollution at the Jerusalem Central Bus Station was the highest in the food court. Mean UFP number concentrations measured in the food court were substantially higher than those in the embarkment area, and, higher by a factor of two or more than in the platforms waiting area. The reason of this surprising finding is in cooking that take place in a close proximity to passengers in the food court. Also, the diversity of measured UFP concentrations in the food court was higher compared to other station areas. This is a result of variation in the distance between the measuring point and the food stand where combustion-based cooking took place, wherein greater distance resulted in lower emissions. Published data (Zhang et al, 2010; Zhao et al, 2010) confirm our findings about high levels of UFP air pollution resulted from cooking activities. The obtained results further show a need in special measures to reduce UFP air pollution in the food court. Following (Zhao et al, 2010), "using up exhaust, setting up partition between cooking area with other zones and adding scuttles" can be useful in mitigation of air pollution by the cooking-generated particles.

The observed increase in UFP concentrations in the platforms waiting area from the left- to the right-side platforms is largely due to the fact that all buses leave the station through an exit near the platform designated in this article as the right one. Hence, waiting areas of the platforms located from the right side are exposed to more buses driving next to them than those located on the left side. Because of this, the platforms on the left side are exposed to less exhaust emissions and as a result, air pollution near them is lower. This finding shows a potential of further optimization of the ventilation system at the platforms waiting area. Probably, higher air exchange rates should be ensured in the area of right-side platforms.

Comparative analysis of the obtained results

Data shown in Fig. 11 summarize the all obtained results on UFP air pollution in train carriages, intercity buses, Jerusalem Central Bus Station and the train station in Tel-Aviv.

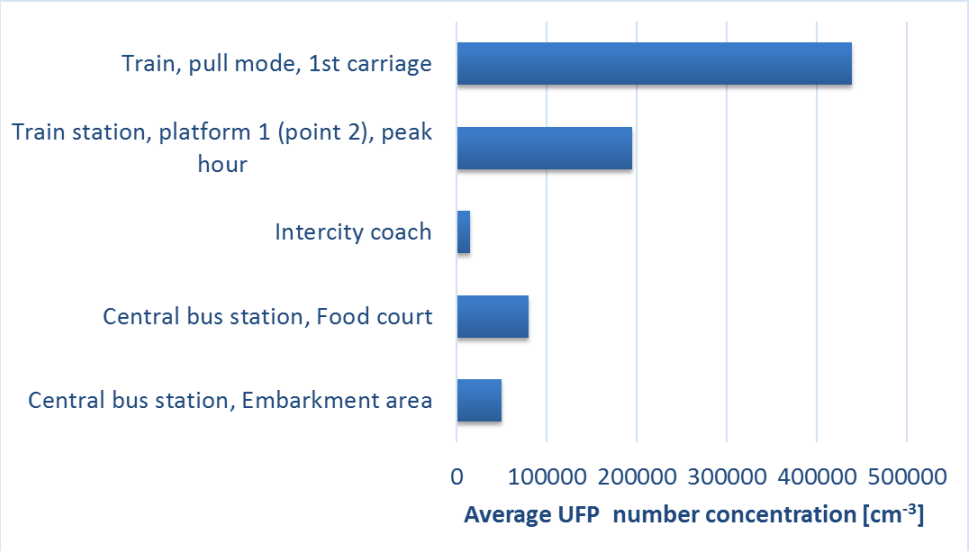

Figure 11: Comparison of measured UFP concentrations in various locations.

As clearly seen from Fig. 11, ultrafine particle concentrations in the 1st carriage of a train running in pull mode are substantially higher than those in any other studied location (factor of two higher than at the 1st platform of the train station in Tel Aviv during peak hours). Considering relatively long exposure of passengers commuting in trains to UFP air pollution, actions must be undertaken as soon as possible to reduce it. Effective measures can be undertaken at affordable costs and over a reasonable amount of time to substantially reduce passengers' exposure to air pollution inside trains (e.g., retrofitting locomotive engines with particle filters (Tartakovsky et al, 2015) or even with more effective combined NO_x-PN reduction systems (Czerwinski et al, 2014), reduction of size and number of ruptures in rubber connectors between the train carriages, using HEPA filters in the carriage HVAC system, etc.). Note that

diesel particle filters are used in nearly all diesel locomotives in Switzerland. Further research in this field can significantly contribute to reducing train passengers' exposure to harmful ultrafine particles.

Conclusions

The concentrations of UFP inside the carriages of push - pull trains are found to be dramatically higher when the train operates in the pull mode. The highest levels of mean UFP number concentrations were observed for the pull operating mode in the carriages adjacent to the locomotive. UFP concentrations in these carriages reached values of $3\text{-}4.4 \cdot 10^5$ cm^{-3} (higher by up to order of magnitude than in car cabins).

For all studied types of carriages, the lowest mean UFP concentrations were measured in the middle of the train between the 3rd and the 5th carriage (in a train of 9 carriages), where the joint influence of emissions from both the diesel generator and the locomotive engine was minimal.

High mean UFP concentrations (up to $1.9 \cdot 10^5$ cm^{-3}) were measured at the platforms of the Ha-Shalom train station in peak hours, especially at the platform segments covered by the roof. The obtained results show that train emissions are the dominant factor of air pollution measured inside the train station despite a proximity of the highway and the main city road.

The highest UFP concentrations (above $8 \cdot 10^4$ cm^{-3}) at the Jerusalem Central Bus Station were measured in the food court. This value is substantially higher than UFP air pollution in the buses embarkment area ($5 \cdot 10^4$ cm^{-3}).

Relatively low mean UFP concentrations (below $1.5 \cdot 10^4$ cm^{-3}) were measured in the intercity buses. These values are lower by a factor of up to 30 compared to first carriage in a train running in pull mode.

Measures should be undertaken to substantially reduce passengers' exposure to air pollution inside trains. Between the possible solutions, retrofitting locomotive engines with particle filters or even with more effective combined NOx-PN reduction systems, reduction of size and number of ruptures in rubber connectors between the train carriages, using HEPA filters in the carriage HVAC system, etc. can be mentioned. Further research in this field can significantly contribute to reducing train passengers' exposure to harmful ultrafine particles.

References

Abramesko V., Tartakovsky L. (2017), Ultrafine particle air pollution inside diesel-propelled passenger trains, *Environ. Pollut.* 226, 288-296.

Chan L.Y., Lau W.L., Zou S.C., Cao Z.X., Lai S.C. (2002), Exposure level of carbon monoxides and respirable suspended particulate in public transportation modes while commuting in urban area of Guangzhou, China, *Atmos. Environ.* 36, 5831-5840.

Chuang K.J., Chan C.C., Su T.C., Lee C.T., Tang C.S. (2007), The effect of urban air pollution on inflammation, oxidative stress, coagulation, and autonomic dysfunction in young adults, *Am. J Respir. Crit. Care Med.* 176(4), 370-376.

Czerwinski J., Zimmerli Y., Mayer A., Heeb N., Lemaire J., D'Urbano G. (2014), VERTdePN Quality Test Procedures of DPF+SCR Systems, SAE Technical Paper 2014-01-1579.

Fierz M., Burtscher H., Steigmeier P., Kasper M. (2008), Field measurement of particle size and number concentration with the Diffusion Size Classifier (DiSC). SAE Technical Paper 2008-01-1179.

Hoet P.H.M., Brüske-Hohlfeld I., Salata O.V. (2004), Nanoparticles - known and unknown health risks. *J Nanobiotechnology* 2,12.

Joodatnia P., Kumar P., Robins A. (2013), Fast response sequential measurements and modelling of nanoparticles inside and outside a car cabin. *Atmos. Environ.* 71, 364 - 375.

Knibbs L.D., Cole – Hunter T., Morawska L. (2011), A review of commuter exposure to ultrafine particles and its health effects. *Atmos. Environ.* 45, 2611 - 2622.

Omer Simkha (2017), Two Trains Entering Tel-Aviv HaShalom Station Headin Kfar-Saba and Haifa. https://he.wikipedia.org/wiki/%D7%A4%D7%95%D7%A8%D7%98%D7%9C:%D7%A8%D7%9B%D7%91

%D7%AA_%D7%99%D7%A9%D7%A8%D7%90%D7%9C/%D7%AA%D7%9E%D7%95%D7%A0%D7%94_%D7%A0%D7%91%D7%97%D7%A8%D7%AA/%D7%92%D7%9C%D7%A8%D7%99%D7%94/42#/media/File:Tel-Aviv_HaShalom_Station.jpg

Tartakovsky L., M. Gutman and A. Mosyak (2012), Energy efficiency of road vehicles – trends and challenges. Chapter 3 in the Edited Collection "Energy Efficiency: Methods, Limitations and Challenges", Emmanuel F. Santos Cavalcanti and Marcos Ribeiro Barbosa (editors), Nova Science Publishers, p. 63-90.

Tartakovsky L., Baibikov V., Czerwinski J., Gutman M., Kasper M., Popescu D., Veinblat M., Zvirin Y. (2013) In-vehicle particle air pollution and its mitigation. *Atmos. Environ.* 64, 320-328.

Tartakovsky L., Baibikov V., Comte P., Czerwinski J., Mayer A., Veinblat M., Zimmerli Y. (2015), Ultrafine particle emissions by in-use diesel buses of various generations at low-load regimes. *Atmos. Environ.* 107, 273-280.

UIC – International Union of Railways (2015), Railway Handbook 2015 – Energy consumption and CO2 Emissions: Focus on Vehicle Efficiency. *OECD/IEA*, Paris, France, 102pp.

Zhang Q., Gangupomu R.H., Ramirez D., Zhu Y. (2010), Measurement of Ultrafine Particles and Other Air Pollutants Emitted by Cooking Activities. *Int. J Environ Res Public Health* 7(4), 1744–1759.

Zhao K., Zhou X., Zhao, B. (2010), Cooking-generated particles' impact on indoor air quality of university cafeteria. *Build. Simul.* 3(1), 15-23.

Emissions of regulated and unregulated pollutants from light-duty gasoline vehicles using different ethanol blended fuels

Xian Wu, Jiaqian Liu, Shaojun Zhang, Xuan Zheng, Ye Wu

School of Environment, Tsinghua University, Beijing, 100084, China
Keywords: ethanol; fuel content; gaseous emissions; particle emissions.
Presenting author email: timon.wuxian@gmail.com

Vehicle emissions considerably create air pollution problems in many cities across the world. In order to reduce the air quality impact from vehicle emissions, vehicle engines and after-treatment devices have been greatly improved in past decades. In addition, biofuels have also attracted many attentions because of their possibility of reducing vehicle emissions(Karavalakis, Short et al. 2014). This study investigated the effects of different ethanol blends on the regulated emissions, gaseous air toxics and particle emissions from light-duty gasoline vehicles. Seven port fuel injection (PFI) vehicles and two gasoline direct injection (GDI) vehicles (model years from 2003 to 2015) are tested using a dynamometer under New European Driving Cycle (NEDC) and Worldwide Harmonized Light Vehicles Test Cycle (WLTC) respectively. The test gasoline samples included a China 5 gasoline fuel with 15% methyl tert-butyl ether (MTBE) content (normal fuel), a China 5 gasoline fuel with a 10% ethanol and 33% aromatics content (E1#), and a China 5 gasoline fuel with a 10% ethanol and 21% aromatics content(E2#).

In general, our measurement results indicate ethanol blended fuels (E1# and 2#) would lead to complex impacts on emission factors of regular gaseous pollutants. For example, THC emissions of E1# were 26% higher than those using normal fuel, while E2# results in no significant difference than regular fuels. For CO emissions, the ethanol blends indicated some increases using E1# and some reductions using E2#. For NOx emissions, some older vehicles (e.g. 2001-2006 model vehicles) would increases emissions when using both E1# and E2#. For some newer vehicles (e.g. 2007-2015 model vehicles), the results indicate that using ethanol blends could reduce emissions than normal fuel.

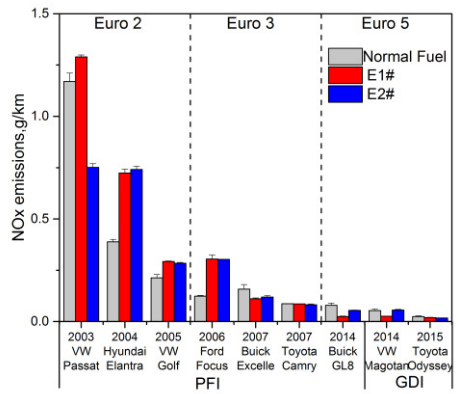

Figure 1. Average NOx emissions for all vehicles over WLTC operation

Particle mass (PM) and particle number (PN) emissions indicate increases for E1# while reductions for E2#. For example, E1# would increase PM and PN emissions by 24% and 19% than those using normal fuel. However, E2# can reduce PM and PN emissions by both 12% relative to normal fuel. The results suggest that particulate emissions from gasoline vehicles are possibly affected by oxygen and aromatics contents in the fuel.

For unregulated VOCs species, the ethanol content of E1# and E2# should no significant effect on Benzene emissions relative to normal fuel. However, toluene emissions from E1# were 41% higher than those from China 5, while E2# were 36% lower. Furthermore, ethylbenzene, m,p-xylene, and o-xylene emissions were 48%, 23% and 58% higher by using E1#. For E2#, it would increase ethylbenzene, m,p-xylene, and o-xylene emissions from a PFI vehicle by 121%, 87%, 80%, while decrease those from a GDI vehicle by 16%, 13%, 12%, respectively.

Ethanol content in fuels has a complex impact on vehicle emissions. And different ethanol blended fuels may have contrary trends. It is important to take both ethanol and hydrocarbon content into account when we choose ethanol fuels in the future.

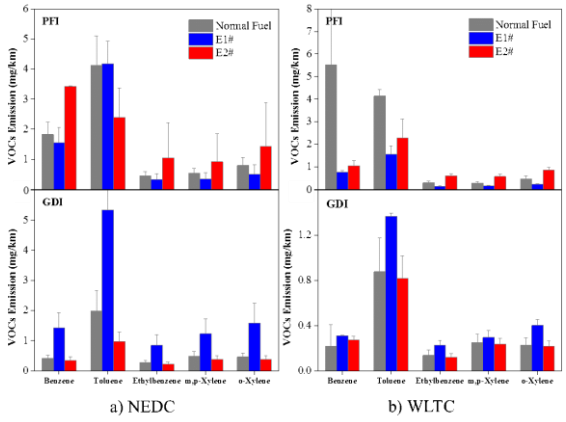

Figure 2. BTEX emissions for the 2014 Buick GL8 (PFI) and the 2014 Volkswagen Magotan (GDI) over NEDC and WLTC operation.

This work was sponsored by China National Cereals Oils and Foodstuffs Corporation (COFCO).

Karavalakis, G., et al. (2014). "Evaluating the regulated emissions, air toxics, ultrafine particles, and black carbon from SI-PFI and SI-DI vehicles operating on different ethanol and iso-butanol blends." Fuel **128**: 410-421.

Air Quality and Health Benefits from Fleet Electrification in China: Future Perspectives through 2030

Xinyu Liang [a], Ye Wu [a]
[a] School of Environment, Tsinghua University, Beijing, 100084, P. R. China.
Keywords: electric vehicle, air quality, human health, CMAQ, China.
Presenting author email: liang-xy16@mails.tsinghua.edu.cn

Electric vehicles (EVs) are rapidly promoted in China to replace conventional vehicles that are powered by liquid fossil fuels (e.g., gasoline and diesel). However, substantial concerns are attained to the environmental impact from the electrification trends alongside with the health impact due to the changes of ambient air pollutant levels (e.g., $PM_{2.5}$). In particular, some regions in China are highly dependent on coal-based power, which would emit more pollutants in the upstream processes of producing electricity than renewable and non-fossil power sources (e.g., hydro, wind, and solar). Thus, we select two of the most developed regions in China, the Jing-Jin-Ji (JJJ) and Yangtze River Delta (YRD) regions, for comparing potential air quality and health benefits from future fleet electrification. These two regions are both hubs of deploying EVs in China but differ in the cleanness of regional electricity generation. For example, the estimated shares of coal-based power are 65% for JJJ and 50% for YRD in 2030.

In this study, a mid-term future scenario through 2030 is taken into account, where 25% personal light-duty passenger vehicles, 30% light-duty trucks and 80% commercial passenger vehicles (e.g., taxis and buses) in two regions will be electrified. The Community Multiscale Air Quality (CMAQ) model enhanced is applied to simulate concentration changes of ambient air pollutants by using detailed multi-sector emission inventories as input. The CMAQ model is enhanced by the two-dimensional volatility basis set (2D-VBS) to improve simulation performance related to secondary organic aerosol (SOA) (Ke et al., 2017). The air quality simulations in these two regions are run on the hourly basis for various months (e.g., January and August) and gridded by cells of 4 km* 4 km. Furthermore, the cause-specific concentration-response functions are applied to assess the health impacts related to $PM_{2.5}$ exposure.

Results indicate that the designed scenario could reduce average $PM_{2.5}$ concentrations within the YRD region by 1.6 μg/m^3 in January and 0.7 μg/m^3 in August, respectively. By contrast, this electrification scenario would yield less reductions in $PM_{2.5}$ concentrations for the coal-rich JJJ region (i.e., 0.7 μg/m^3 in January and 0.6 μg/m^3 in August). Besides reducing ambient $PM_{2.5}$ concentrations, fleet electrification could effectively reduce ambient NO_2 concentrations, and the mitigation is more significant in the traffic-dense urban areas. For example, fleet electrification can reduce average NO_2 concentration in Shanghai by 4.8 μg/m^3 in January and 3.8 μg/m^3 in August, while less reduction will be achieved within YRD region (i.e., 2.2 μg/m^3 in January and 1.6 μg/m^3 in August). The health impact assessment suggests that future fleet electrification could reduce attributable deaths by lowering $PM_{2.5}$ exposures. For example, by considering long-term exposure health effects (e.g., stroke, Chronic obstructive pulmonary disease, Ischemic heart disease, and Lung Cancer, estimated 9600 and 3800 deaths could be avoided in the YRD and JJJ regions, respectively, in 2030. Greater reductions in mortality caused by long-term $PM_{2.5}$ exposures would occur in most populous and heavily polluted areas (i.e., Beijing, Shanghai). Therefore, our work concludes that future fleet electrification in China can improve regional air quality, indicated by reducing ambient concentrations of major air pollutants (e.g., $PM_{2.5}$), and lead to associated health benefits.

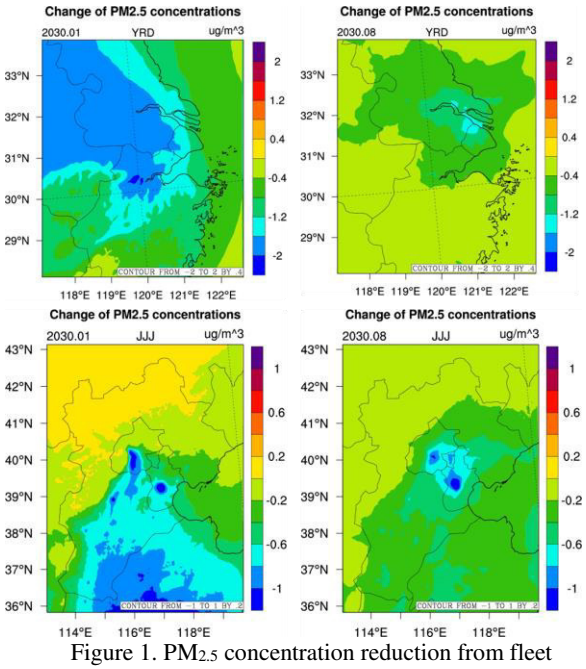

Figure 1. $PM_{2.5}$ concentration reduction from fleet electrification in January, August 2030 in YRD regions (top) and JJJ region (down)

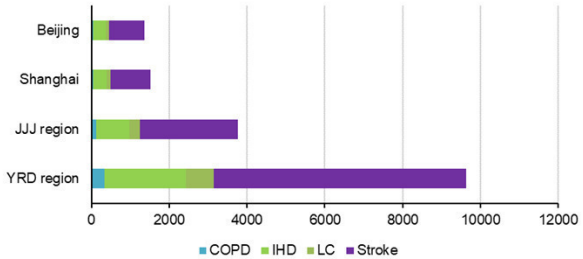

Figure 2. Mortality reduced through scenario EV in YRD, JJJ regions and two core cities in 2030

Ke, W., Zhang, S., Wu, Y., Zhao, B., Wang, S., and Hao, J. (2017) *Assessing the Future Vehicle Fleet Electrification: The Impacts on Regional and Urban Air Quality*, Environmental Science & Technology, 51 (2) :1007-1016.

An Efficient Scheme for Urban Air Quality Estimates and Projections

N. Moussiopoulos[1], L. Ntziachristos[1], E. Chourdakis[1], G. Tsegas[1] and W. Verhoeve[2]*

[1] Laboratory of Heat Transfer and Environmental Engineering, Aristotle University, Thessaloniki, 54124, Greece, moussio@eng.auth.gr
[2] EMISIA Brussels sprl, Square de Meeûs 35, B-1000, Brussels, Belgium

Keywords: air quality, ICT tools, urban background, street scale emissions.

Abstract

The application of air quality models for urban air pollution assessment is not always an easy task, as the accuracy of modelling estimates strongly depends on the availability of a variety of extensive and detailed input data. Furthermore, the resolution of typical mesoscale dispersion models is inadequate for obtaining accurate air quality estimates at the street scale. In view of these shortcomings, a new, simplified approach is proposed and validated, allowing the operational assessment of air quality at the urban and local scales without the need of extensive and detailed input data. For the verification of the method's applicability, a computational implementation has been previously incorporated as an enhancement of an existing operational Air Quality Management System and validated in a case study in Cyprus, with the results revealing a distinct performance improvement as regards the street scale. In the present work, a new validation study is performed in order to verify the applicability and transferability of the concentration increment methodology in an urban case of sufficiently different physical characteristics compared to the Cyprus one, using only minimal computational resources. The methodology is applied for a small-scale urban application in the town of Namur, Belgium, during the entire calendar year 2014. An evaluation of the application results indicates that the obtained concentration levels are in fairly good agreement with observational data, particularly with respect to the urban background levels. Concentration patterns calculated for the street scale are still within the expected range of accuracy, though exhibiting a stronger dependence on calibration parameters related to the geometry and traffic-load characteristics of the study area. Based on the so far results, the proposed scheme appears to be an appropriate tool for the fast and reliable estimation of average concentrations in urban areas and hotspots, without the need to resort to complicate physical simulations. Future work will allow assessing the system performance in a wide range of extended urban applications.

Introduction

The goal of improving air quality in order to protect human health and promote public welfare has been consistently set forward in the European Union during the past decades. Towards this goal, numerous regulations and standards, a broad suite of management tools and several monitoring networks to track progress have been established. All of these components depend on robust and up-to-date scientific and technical input, which includes an understanding of relationships between air pollutant levels and their impacts on human health, ecosystems, atmospheric visibility, and damage to materials and monuments.

The European Air Quality Directive (2008/50/EC) has introduced additional requirements for air quality assessment and management. As a result, along with air quality measurements, modelling tools should also be used by authorities and policy makers in order to assess pollutant concentrations in ambient air. It also requires that up-to-date information on concentrations of all regulated pollutants in ambient air should be readily available to the public.

In view of this emerging need, integrated informational systems known as Air Quality Management Systems (AQMS) have been developed aiming to provide technical users and policy makers with a consistent and robust environment for their regular workflows. The functional structure of a typical AQMS enables the combined application of various software modules including meteorological and chemical dispersion models, geographical information systems, databases and statistical analysis tools, in order to better simulate the complex interactions between the atmospheric, emission-related, land use and topographic parameters which affect the production, dispersion and transport of air pollutants.

Despite its versatility as an operational assessment tool, the installation and operation of an AQMS in a typical urban application requires a considerable amount of accurate input data which are often unavailable at the time of application. Additionally, the typical scales covered by the mesoscale dispersion models incorporated in the AQMS can provide reliable estimates of concentrations only down to a resolution of about 500m. This resolution is inadequate for resolving street-scale concentration maxima and therefore for accurately quantifying street-level exposure of pedestrians, drivers and residents of nearby buildings. In order to address these shortcomings, an empirical approach is presented for the improved estimation of the urban background, as well as of a street-scale concentration increment on top of the concentrations derived in the mesoscale. The methodology incorporates a functional relationship between local meteorological parameters, street characteristics and traffic emissions, calibrated on the basis of measured concentration increments in representative locations. The empirical scheme can be applied for rapid hotspot assessment and only requires a set of input data that are usually readily available from public sources.

In the frame of the present study the proposed methodology was validated in a small-scale urban application, namely for the town of Namur, Belgium, for the calendar year 2014. The results of this application indicate that the obtained concentration levels are in fairly good agreement with observational data both with respect to the urban background and street scale levels. Additional work is needed to assess the system performance for a wider range of similar extended applications.

Methodology

An advanced operational AQMS has been developed and operated by the Laboratory of Heat Transfer and Environmental Engineering (LHTEE) for meteorological and photochemical air pollutant dispersion studies, offering a range of features for nowcasting, forecasting and performing scenario calculations. The system has been in continuous operation since 2009 in the Department of Labour Inspection (DLI) of the Republic of Cyprus (Moussiopoulos et al., 2012) and since 2011 in the Organization of Planning and Environmental Protection of Thessaloniki (OR.TH.) (Moussiopoulos et al., 2011a) in Thessaloniki, Greece. The core of the AQMS consists of a mesoscale model system performing nested grid meteorological and photochemical model simulations. As expected, the accuracy of urban air quality estimates provided by the AQMS greatly depends on the availability of extensive and detailed traffic data. These include traffic counts from street counting loops or projections from traffic models, as well as fleet structure data, speed or driving pattern estimates, and others. Several large cities maintain traffic models for traffic management and planning purposes. However, the cost of maintaining a traffic model only for air quality assessment purposes cannot be justified for smaller cities and regions. Furthermore, due to their inadequate spatial resolution, the results of mesoscale models in the assessment of pollutant concentrations on the street scale are poor.

To this end, a simplified, yet scientifically robust approach is presented here, which allows the operational assessment of urban air quality, both in terms of the urban background, as well as of street-scale concentrations, without the need of detailed traffic information.The methodology presented here intends to provide high-accuracy estimates of average pollutant concentrations for arbitrary locations within an urban area, taking advantage of readily-and widely-available input data and requiring only minimal computational resources.

The overall approach involves two distinct components, the urban increment (UI) and the street increment (SI) empirical scheme, respectively. The first one is based on a statistical method which aims at the determination of an urban concentration increment on top of the regional background. The SI methodology, which constitutes the second component of the approach, aims to determine the contribution of road traffic emissions, on an hourly or daily basis, on air pollution at urban hotspots. Although both of these approaches can be used for various pollutants, so far the empirical relations have been calibrated for PM_{10} and NO_2 and, as a result, will be demonstrated here for these specific pollutants.

In order to determine the urban background increment, a piecewise functional relationship is applied following a form which has been established on the basis of certain variables known to be important (Amann et al., 2007). These variables include the level of emissions within the urban area, the size/area of the urban entity, the urban and regional background concentrations, as well as the wind speed and the atmospheric stability.

In order to fix the numerical relationship between the urban increment and the variables mentioned above, a multiple regression analysis was carried out, following the following formulation:

$$C_{i\ urban} = \omega_i + \phi_i \frac{E_{iUE}}{A_{UE} \cdot u_{avg}} + \gamma_i\ C_{i\ rural}$$

Where:

$C_{i\ urban}$ = Urban increment of pollutant *i*.

E_{iUE} = Total emission of pollutant *i* within an urban entity.

A_{UE} = Urban entity area.

u_{avg} = Urban entity average wind speed.

$C_{i\ rural}$ = Rural background concentration of pollutant *i*.

ω_i, ϕ_i, and γ_i = Multiple-regression parameters for pollutant *i*.

A separate version of the above formulation is numerically extracted for each of the seven Pasquill-Gifford stability classes (S_C = 1...7), thus taking into account the dependence of concentrations on atmospheric stability. Values of all the variables were averaged over the period identified through the stability categorisation. In this point, it should be noted that the numerical scheme was extended to provide concentration estimates on a higher temporal resolution, e.g. on an hourly basis, provided that input data in a corresponding frequency are available for the target locations. In the above formulation, it was also assumed that concentrations within the cities are influenced only by primary emissions released from low sources (Amann et al., 2007).

It should be noted that the regression analysis for the determination of the functional relationships has been performed using data from a number of large cities with high emission levels. As a result, these relationships tend to overestimate concentration increments when applied to urban areas with lower activity levels, such as Namur. In order to deal with this drawback, certain additional parameterizations were introduced in the computational scheme of the methodology.

The procedure for the determination of the street increment can be described as a three-step process, involving the selection of representative pairs of urban background and street scale locations, a multiple regression analysis for the determination of the functional relationship, and the application of the functional relation on the basis of measured or calculated urban background concentrations. The concentration sets used for the definition of the statistical relationships were derived both from measurements and from the application of the OSPM (Berkowicz, 2000) model for several traffic hot spots in the city of Thessaloniki, Greece during the calendar year 2013. More details as regards the calibration process can be found elsewhere (Chourdakis et al., 2017).

The functional relationship used for the determination of the street increment takes the form:

$$SI = [\sin(\theta) + 1] \cdot (X_1 \cdot UC + X_2 \cdot H/(W \cdot L) \cdot em/ws)$$

Where:

SI = Street scale concentration increment.

Theta = Azimuthal angle of the main street orientation.

UC = Urban background concentration.

L = Length of the road segment.

H = Average height of the buildings.

W = Width of the road segment.

ws = Wind speed.

em = Traffic emissions.

X_1, X_2: Empirical constants of the equation.

In a previous application of the methodology, a computational tool based on the approach described above was incorporated as an enhancement in the computational procedure of the AQMS operated in Cyprus, in order to enable the more accurate estimation of street-scale concentration levels in selected traffic hotspots in the cities of Nicosia, Larnaca and Limassol. The methodology was implemented as an additional operational module of the AQMS and was subsequently evaluated during a pilot period of two months. The results of the pilot application revealed a distinct improvement in the performance of the AQMS as regards the calculated street scale air quality (Moussiopoulos et al., 2017).

Application

In order to test the validity of the proposed simplified approach for air quality assessment in a typical small conurbation, a pilot application was undertaken for the Belgian city of Namur. This application case was chosen as an example of a small European city, which does not employ an official traffic model, since the associated maintenance and operational cost would be difficult to justify solely for the purposes of air quality assessment.

Namur is a small provincial city in Wallonia, Belgium, which constitutes both the capital of the province of Namur and of Wallonia. The city is confined between the rivers Sambre and Meuse and some hills. The total area of Namur is about 176 km^2, while the total population reaches 110.632 and the population density is of the order of 630 per km^2. The road traffic is characterized by congestion during the morning and noon rush hours. The weather in Namur is quite variable and dominated by a succession of cold/heat fronts. The prevailing wind direction is West by South-West. As typical for urban areas in Belgium, deterioration of air quality occurs when a high-pressure area creates an easterly flow of dry continental air combined with high temperature inversions.

The present application refers to the calendar year 2014, chosen on the basis of availability of the required data, notably with respect to measurements of regional background concentrations, as well as to the urban measurement campaign upon which the validation process is based. The aforementioned measurement campaign provided data from two mobile stations in Namur, namely Train Station and Jambes, to be used as comparison/validation of the proposed methodology. More specifically, Train Station constitutes an urban traffic station, since it is located in the centre of the city, nearby a large road. On the other hand, Jambes station could be classified as a residential urban background concentration. As a result, Train Station was chosen to be used in the validation process of the street scale application, while Jambes station was decided to play

major role in the evaluation of urban background calculations. In Figure 1, the locations of the corresponding measuring spots in the city of Namur are shown.

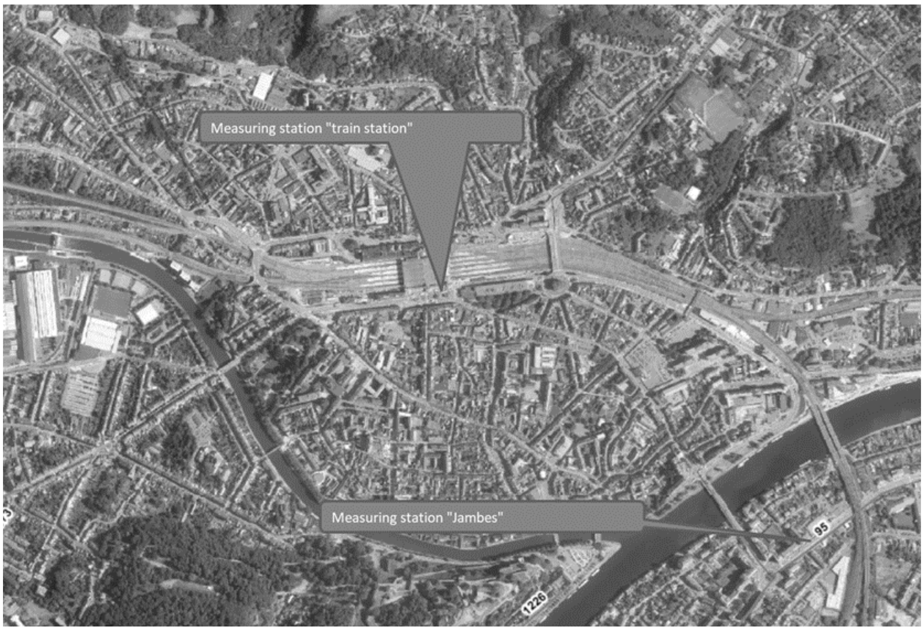

Figure 1: Location of the Train Station and Jambes measuring spots.

As regards the input data needed for the urban background application, the regional background concentrations were derived from the CAMS reanalysis results (URL1) for the entire European territory for 2014, while the required meteorological data originated from stations of the 'Weather Underground' database (URL2). Besides, estimates of the urban emissions for each city were based on the MEGAPOLI European Gridded Emission Inventory (Kuenen et al., 2010), which is a version of the TNO emissions data-set, available for the whole of Europe at a resolution of 0.0625° × 0.125° (latitude × longitude).

The final stage of the calculations involved the application of the piecewise functional relationship extracted in the previous step, in order to calculate urban concentration increments.The aggregation of these 7 different results to a single value (mean annual value) was based on an annual occurrence analysis of the 7 above-mentioned stability classes for the city of Gent, Belgium, in turn derived from a previous application (Moussiopoulos et al., 2011b) which is considered to be highly representative for the case of Namur.

In the case of the traffic application spot (Train Station), in order to obtain an estimate of street-level concentrations, an (additional) street increment was calculated and added to the urban background concentrations. For this case, urban background concentrations were derived from the results of the urban background application presented above. The geometrical characteristics (length and width of the road link, as well as average height of the buildings on the sides of the street) of the locations under consideration were estimated using orthophotography data from the "Google maps" tool, while data regarding wind speed and direction were derived from stations of the 'Weather Underground' database (URL2) for a number of spots inside the town of Namur.

The traffic data utilized in the frame of the present application originated from counting loops on the major access roads of the city of Namur. These loops measured the number of vehicles and made a distinction between light- and heavy-duty vehicles. In order to match the traffic data (only available for 2010) with the reference year 2014, the numbers were adjusted using the relative increment or decrement of light and heavy-duty traffic in the yearly emissions inventory of the Wallonia region (-6.10% for light and -17.33% for heavy duty vehicles, respectively). Figure 2 shows the location of the traffic loop used against the application spot, Figure 3 presents the geometrical characteristics of the Train Station spot

Figure *2*: Locations of the traffic loop used and the application spot.

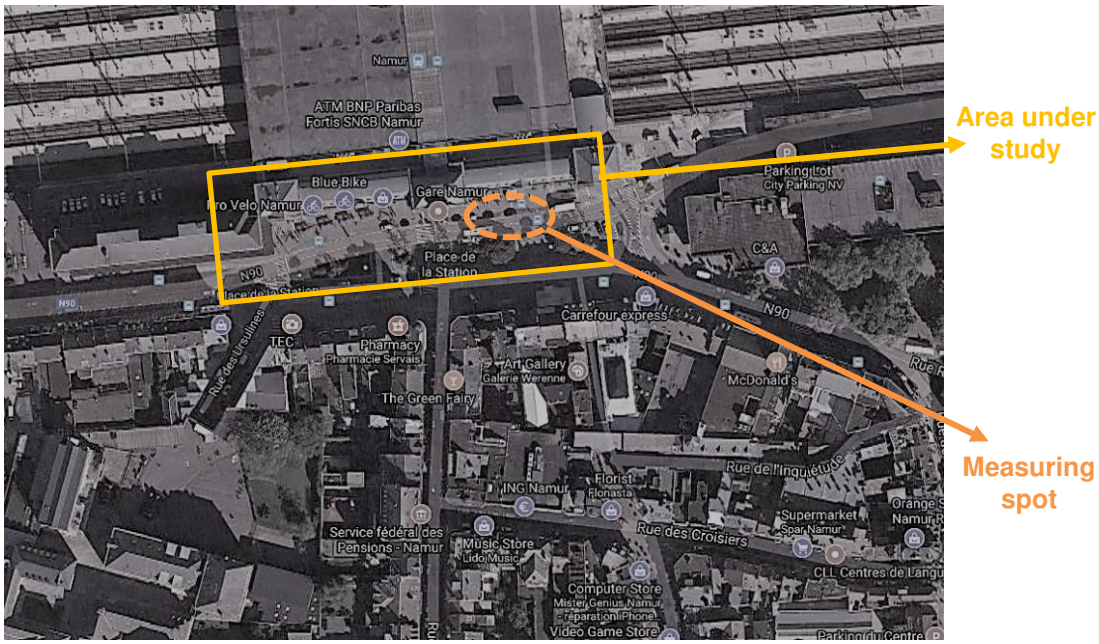

Figure 3: Location and geometrical characteristics of the Train Station spot.

Results and discussion

Table 1 depicts the urban concentrations obtained from the functional relationships of the proposed methodology in comparison with values calculated directly from available observational data.

Table 1: Results of the urban increment application (UB estimate) for the city of Namur compared to available observational data as regards the calendar year 2014 for NO_2 and PM_{10}.

Pollutant	Jambes	Train Station	UB estimate
NO_2	26	46	30
PM_{10}	18	16	14

As evidenced from Table 1, the proposed methodology provides reasonable estimates for the suburban station of Jambes, a spot which is less affected from the traffic and the rest of the human activities that occur in the city core. On the other hand, the calculated results underestimate measured concentrations at the Train Station location, which is situated inside the city core thus being heavily affected by the higher traffic loads of the nearby road. This fact leads to the conclusion that the urban increment approach is suitable for applications aiming to determine the air quality status in the suburban and residential areas of the conurbation, whereas for the assessment of air pollution levels at the street level, the utilization of an additional street-scale concentration increment is necessary.

In order to calculate concentration levels for the Train Station location, an additional street increment, on top of the urban background concentrations, was calculated by applying the corresponding part of the empirical methodology. Figures 4 and 5 present the calculated results for NO_2 and PM_{10}, respectively. In order to illustrate the apportionment on regional, urban and street-scale contributions, each hourly concentration value is represented as stacked bars indicated as RB, UB and SI, respectively.

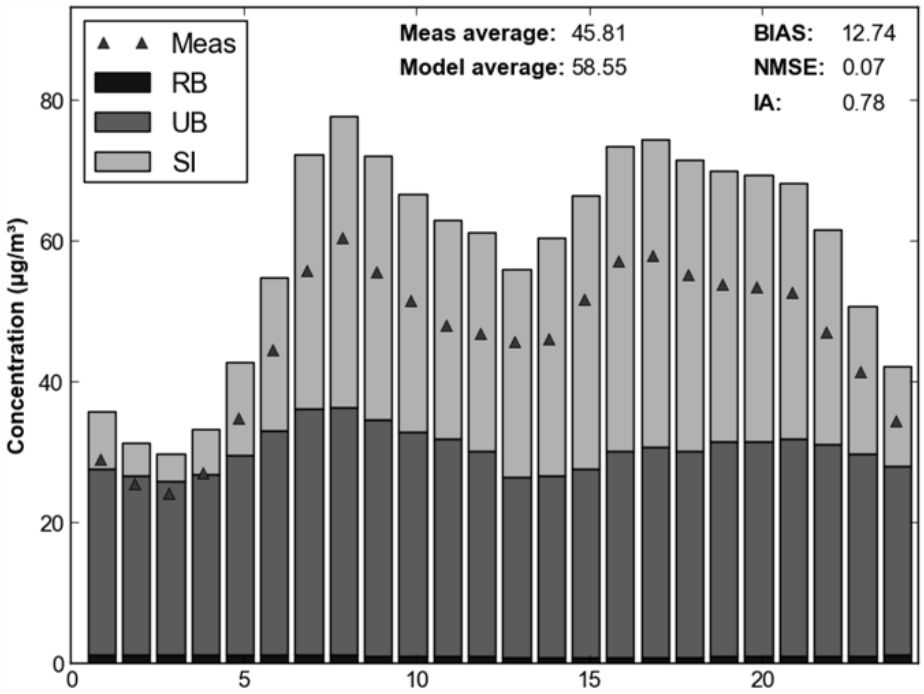

Figure 4: Average diurnal pattern of the street-level NO_2 concentrations at the site of Train Station. The Regional Background (RB), Urban Background (UB) and Street Increment (SI) contributions are indicated for each hourly concentration value.

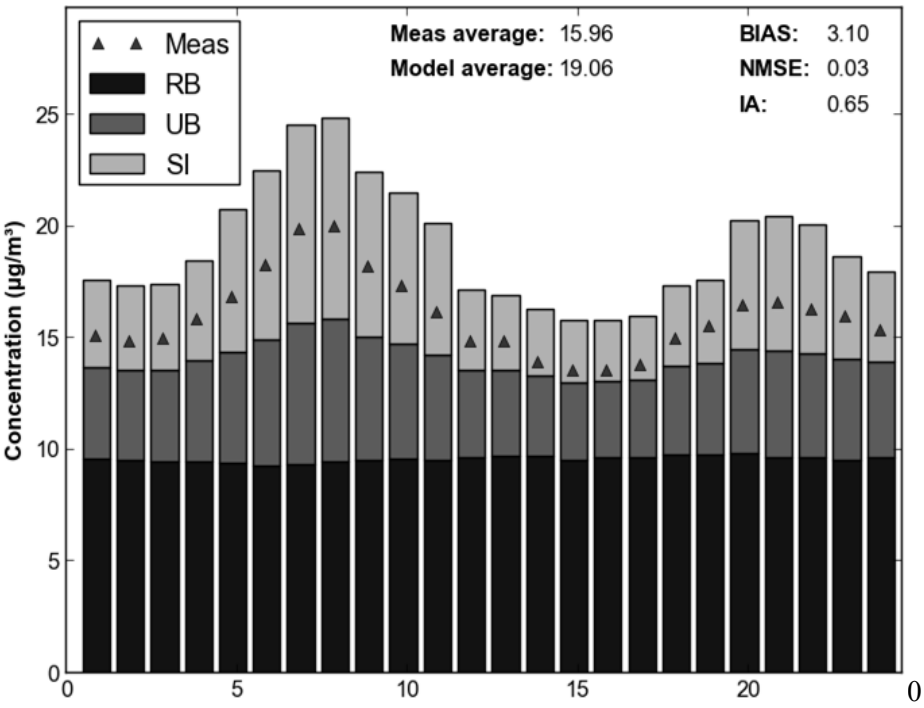

Figure 5: Average diurnal pattern of the street-level PM_{10} concentrations at the site of Train Station. The Regional Background (RB), Urban Background (UB) and Street Increment (SI) contributions are indicated for each hourly concentration value.

As evident from Figures 4 and 5, the results of the street-level application are in a fairly good agreement with the corresponding observational data, as the bias between the calculations and the measurements lies within the acceptable limits. However, the evaluation of the results should take into account two additional aspects, which introduce a number of uncertainties in the calculations. More specifically, as mentioned above, the statistical relationships used in this application were calibrated from a number of locations in the city of Thessaloniki, Greece, with certain characteristics, since they constitute street canyons with a lot of activity and correspondingly high traffic loads. This calibration bias accounts for the major part of the overestimation of the calculated concentrations.

Additionally, the traffic characteristics which were used to approximate traffic emissions in the frame of this application have originated from corresponding measurements from sites away from the Train Station location, as there were no available data for roads with similar traffic characteristics. As a result, an additional uncertainty was introduced in the calculations, since the employed data were probably not completely representative for the location under consideration. In similar future applications, where representative traffic data are not available, this drawback could be mitigated with the use of calibrated empirical factors, which will correct the statistical relationships against the available data set, in order to meet the requirements of the specific application. In the frame of the present application, though, the main goal was to explore the limits of applicability of the methodology in a case study with sufficiently different characteristics from the calibration cases in regard to the city size, street geometry and average traffic loads.

Conclusions

In an effort to supplement the performance of typical urban air quality models in calculations in the street scale, as well as in order to confront potential difficulties in conducting calculations in both the urban and street scale due to lack of the required data, a methodology for the calculation of urban background and street-scale concentration increments has been developed. Following a previous successful application of the street increment approach as an additional module of an operational Air Quality Management System in Cyprus, a new validation study was performed in order to verify the applicability of the concentration increment methodology on a case of sufficiently different physical characteristics, using only minimal computational resources. More specifically, the proposed empirical approach was applied and validated in a small-scale urban situation in the town of Namur, Belgium over a period of a calendar year. The results of this

application indicated that the obtained concentrations are in fairly good agreement with observational data with respect to the urban concentration levels. As a result, the new computational scheme is considered to be suitable for wider application in a variety of urban cases. The underlying street-scale parameterizations appear to be functional for a range of configurations as defined by city size, street geometry, traffic loads and meteorological conditions. Additional experience with the proposed modelling system is necessary to generalize the validity of the statistical relationships used to compute street increments for a wider range of extended urban applications.

Acknowledgements

It should be noted that all measured air quality data, as well as the traffic data used in the frame of this study was provided to us by the Agence Wallonne de l'iAir et du Climat (AWAC).

References

Amann M., J. Cofala, A. Gzella, C. Heyes, Z. Klimont and W. Schöpp (2007), Estimating concentrations of fine particulate matter in urban background air in European cities, *IIASA*.

Berkowicz R. (2000), OSPM - A parameterised street pollution model, *Environ Monit.*, Assess 65(1–2):323–331.

Chourdakis E., N. Moussiopoulos, F. Barmpas and I. Douros (2016), Operational application of an empirical approach for determining concentration increments at the street level, *Proceedings of the 10th International Conference on Air Quality - Science and Application*, Milan, Italy, 14-18 March.

Kuenen J., H. Denier van der Gon, A. Visschedijk, H. van der Brugh, S. Finardi, P. Radice, A. d'Allura, S. Beevers, J. Theloke, M. Uzbasich, C. Honore and O. Perrussel (2010), A Base Year (2005) MEGAPOLI European Gridded Emission Inventory (Final Version). Deliverable D1.6, *MEGAPOLI Scientific Report* 10-17, MEGAPOLI-20-REP-2010-10, 39p.

Moussiopoulos N., G. Tsegas, I. Douros, E. Chourdakis and K. Nikolaou (2011a), Development of an air quality management system for Thessaloniki, Proceedings of the 16th *International Symposium on Environmental Pollution and its Impact on Life in the Mediterranean Region* (MESAEP2011), Ioannina, Greece, 24-27 September.

Moussiopoulos N., I. Douros, G. Tsegas, E. Chourdakis and S.T. Ortiz (2011b), An approach for determining urban concentration increments, *Proceedings of the 14th International Conference on Harmonisation within Atmospheric Dispersion Modelling for Regulatory Purposes (HARMO14)* (J.G. Bartzis et al., eds), Kos island, Greece, 2- 6 October, 209-213, electronic edition.

Moussiopoulos N., I. Douros, G. Tsegas, S. Kleanthous and E. Chourdakis (2012), An air quality management system for policy support in Cyprus, Hindawi Publishing Corporation, *Advances in Meteorology* 2012, doi:10.1155/2012/959280.

Moussiopoulos N., E. Chourdakis and G. Tsegas (2017), An Air Quality Management System for Cyprus: Evaluation and Improvements, In: Karacostas T., Bais A., Nastos P. (eds) Perspectives on Atmospheric Sciences, *Springer Atmospheric Sciences*, Springer, Cham.

URL1: https://atmosphere.copernicus.eu/about-cams

URL2: https://www.wunderground.com/

Effects of traffic related abatement policies on Swiss air quality trends

Ch. Hueglin, A. Fischer, B. Schwarzenbach and L. Emmenegger

Empa, Swiss Federal Laboratories for Materials Science and Technology, Duebendorf, Switzerland
Keywords: traffic emissions, black carbon, nitrogen oxide, particle number concentration
Presenting author email: christoph.hueglin@empa.ch

During the past two decades, a number of policy initiatives have been implemented in Switzerland to reduce air pollution from road traffic. Of particular importance is the introduction of the Euro emission standards in 1995, leading to stepwise tightening of the emission limits and consequently the reduction of exhaust emissions from new vehicles. Several political actions provide financial incentives for the use of low-emission vehicles: Examples are the dependence of the federal heavy transport vehicle charge (LSVA) on the emission level of the vehicle (since 2001) and incentives for public transport companies for operating low-emission busses (since 2008).

Measurements from air quality monitoring networks allow the observation of the long-term trends of atmospheric concentrations and roadside increments of air pollutants. The trends of air pollutants such as nitrogen oxide (NO_x), equivalent black carbon (EBC, see Petzold *et al.* (2013)) and particle number concentrations (PNC) in Switzerland have been calculated and are discussed in relation to the abatement policies of air pollution from traffic.

As an example, multi-year trends of EBC have been analysed at various sites of the Swiss National Air Pollution Monitoring Network (NABEL). It was found that EBC in Switzerland is clearly declining at all site types (rural, suburban, urban and traffic sites). The annual changes are largest at the sites that are influenced by nearby road traffic emissions. The data analysis did not reveal regional differences in the temporal trends, although equivalent black carbon levels are generally higher south of the Alps compared to similar sites in the north.

At five of the sites, the light absorption of PM2.5 is measured at multiple wavelengths. This allows the calculation of the contribution of traffic (EBC_{TR}) and wood burning emissions (EBC_{WB}) to total EBC (Zotter *et al.*, 2017). Figure 1 shows the monthly concentrations of EBC_{TR} and EBC_{WB} as well as the trend lines estimated from de-seasonalized data. EBC_{TR} is significantly declining (95% confidence level) at all sites. In contrast, the contributions from wood burning emissions remained constant during the past years. The improvement in total EBC is thus entirely due to declining contributions from internal combustion engines, i.e. mainly road traffic and some off-road vehicles and stationary diesel engines.

These observations illustrate a remarkable success of the measures taken to reduce black carbon emissions from road traffic and other engines, in particular the introduction of diesel particle filters. In contrast, little progress has been made for the reduction of black carbon emissions from wood burning appliances.

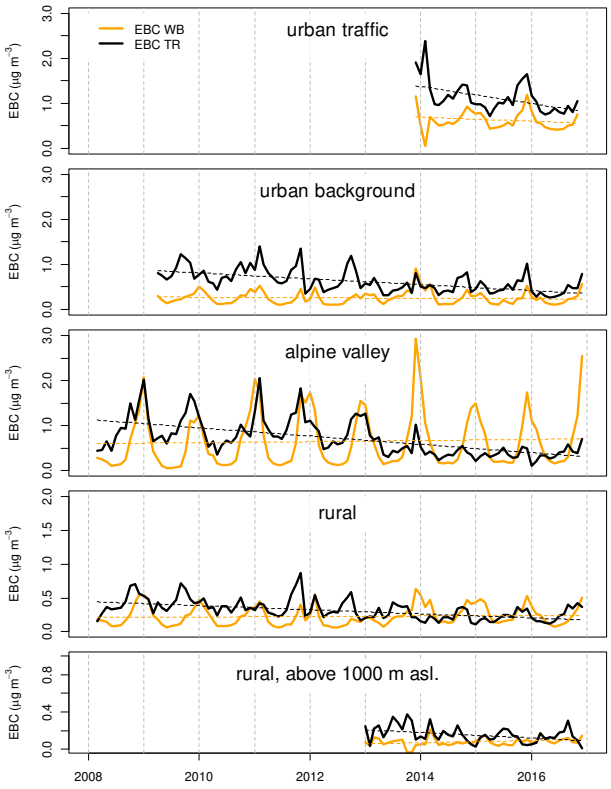

Figure 1. Time series of monthly equivalent black carbon from traffic (EBC_{TR}) and from wood burning (EBC_{WB}) at sites in Switzerland representing different environments. The broken lines indicate the corresponding linear trends.

Downward trends have also been found for other air pollutants, in particular PNC and NO_x. The achieved improvement in atmospheric NO_x concentration has, however, been limited by the known gaps between the EURO emission limits and the real world emissions of diesel vehicles.

This work was supported by the Swiss Federal Office for the Environment (FOEN).

Petzold, A., J. A. Ogren, M. Fiebig, P. Laj, S. M. Li, U. Baltensperger, T. Holzer-Popp, S. Kinne, G. Pappalardo, N. Sugimoto, C. Wehrli, A. Wiedensohler and X. Y. Zhang (2013). *Atmos. Chem. Phys.*, 13, 8365-8379.

Zotter, P., H. Herich, M. Gysel, I. El-Haddad, Y. Zhang, G. Močnik, C. Hüglin, U. Baltensperger, S. Szidat and A. S. H. Prévôt (2017). *Atmos. Chem. Phys.*, 17, 4229–4249.

Comprehensive analysis of European vehicular primary NO_2 trends

S.K. Grange[1,], D.C. Carslaw[1,2]*

[1] Wolfson Atmospheric Chemistry Laboratories, University of York, York, YO10 5DD, United Kingdom
[2] Ricardo Energy & Environment, Harwell, Oxfordshire, OX11 0QR, United Kingdom
* stuart.grange@york.ac.uk

Introduction

The proportion of diesel vehicles which make up the European vehicle fleet has significantly increased since the mid-1990s (ACEA, 2016). This increased dieselisation has caused a number of local air quality issues to arise across Europe, the most significant of which are related to particulate matter (PM) and oxides of nitrogen (NO_x) (Weiss et al., 2012).

NO_x is a regulated pollutant within the vehicular European emission standards framework, usually referred to as the "Euro" standards. NO_x emission limits for new diesel vehicles have been progressively tightened as new Euro standards have been implemented. This progressive tightening of NO_x emission limits has resulted in decreases in ambient NO_x concentrations in most European locations which are influenced by traffic emissions. However, despite reductions in NO_x concentrations, nitrogen dioxide (NO_2) has deceased less than expected (Kiesewetter et al., 2014). NO_2 one component within NO_x but it is the regulated species within the NO_x family, not NO_x itself, in respect to ambient air quality. The lack of decreasing NO_2 concentrations has resulted in many urban areas across Europe not complying to the hourly and annual legal NO_2 limits outlined by the 2008/50/EC Air Quality Directive, especially near roads (Grice et al., 2009).

The disconnect between NO_x and NO_2 trend behaviour and the lack of downward trends in roadside NO_2 concentrations has been attributed to an increase in the amount of directly emitted NO_2 from the tailpipes of diesel vehicles (Williams and Carslaw, 2011; Kiesewetter et al., 2014). This directly emitted component of NO_2 is often called primary NO_2. The reasons why primary NO_2 emissions have increased have been primarily driven by the introduction of new Euro standards. Diesel oxidation catalysts (DOC) were installed to diesel passenger vehicles to meet Euro 3 standards in 2000 which imposed stricter limits on carbon monoxide and hydrocarbon (CO and HC) emissions. Diesel engines often operate under lean conditions, and the excess oxygen in the exhaust stream can oxidise nitrogen oxide (NO) to NO_2 over the catalysts (Carslaw et al., 2016). The introduction of Euro 5 emission standards saw widespread installation of diesel particle filters (DPF) to physically trap particles. To avoid blockage by soot, DPFs are periodically heated and NO_2 generated upstream in the combustion chamber and over the DOC can be used as the soot oxidant. Not all NO_2 is used in this process and this too can increase primary NO_2 emissions. Both of these process increase the amount of directly emitted NO_2 without altering the emissions of total NO_x and is therefore these perturbations are not captured in current vehicle emission testing procedures.

Although the increase in primary NO_2 has been well documented, more recent observations have suggested that primary NO_2 may have started to decrease (Carslaw et al., 2016). If a decrease in primary NO_2 is widespread throughout Europe, this has very significant implications for future air quality management and emission inventories. Despite the importance of such a phenomenon on local air quality, changes in primary NO_2 emissions have been neglected, even after the Volkswagen (VW) diesel emission scandal also known as "dieselgate" broke in late 2015.

Objectives

The primary objective of this study was to determine and explain the trends of primary NO_2 emissions across Europe. Ambient monitoring data across European roadside sites will be used as the source data and the use of data filtering and statistical methods will be used to calculate the primary NO_2 emissions as a NO_2/NO_x emissions ratio to represent the primary NO_2 trend.

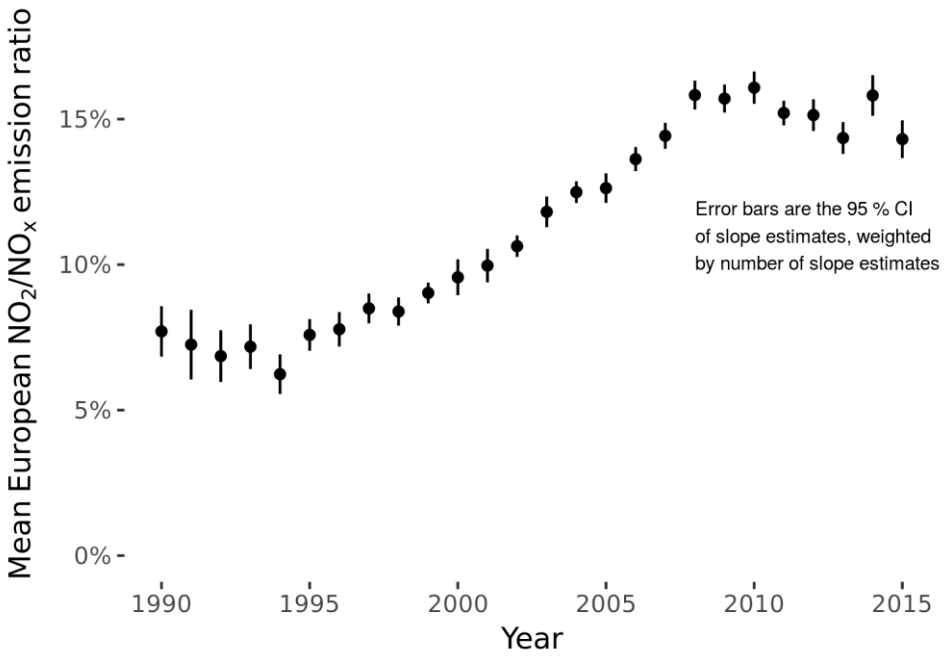

Figure 1. Mean European roadside NO_2/NO_x emission ratio for 61 urban areas between 1999 and 2015.

Methods

Data

Ambient air quality monitoring data from 61 urban areas across Europe between 1990 and 2015 (inclusive) were used for the analysis. These data were sourced from the AirBase and Air Quality e-Reporting (AQER) repositories maintained by the European Environment Agency (EEA) (European Environment Agency, 2014; European Environment Agency, 2016). The data required transformation into a standardised format called **smonitor** due to the repositories' different file formats and data models (Grange, 2016; Grange, 2017). A total of 130 million hourly measurements of NO_x, NO_2, and ozone (O_3) were used from 488 monitoring sites for the analysis.

Filtering and NO_2/NO_x emission ratio estimation

The first step in the analysis was to retrieve spatial polygons for European urban areas. These polygons were mostly found in the AQER "zones" data flow but there was some supplementation by OpenStreetMap when the polygons were not available within the AQER repository. Within a polygon, a representative background O_3 monitoring site was determined. The O_3 time series for this site was used as the typical O_3 concentration for the urban area and were continuous in their nature for the analysis time period (between 1990 and 2015). NO_2 and NO_x observations where then queried for all sites in the urban area's polygon which were classified as traffic, roadside, or kerbside and then immediately filtered to only include observations between 06:00 and 18:00 (time zones depended on the urban area's country), weekdays (Monday to Friday), and when the background O_3 concentrations were less than 10 µg m^{-3} (≈ 5 ppb). These filters had the goal of isolating observations only to times when the NO + O_3 reaction was very small and when the NO_2 detected was dominated by the emissions of the vehicles using the adjacent road.

For each site and for each year, the NO_2/NO_x emission ratio was estimated with a robust linear regression model. The slope of the model was the estimated NO_2/NO_x emission ratio as a molar

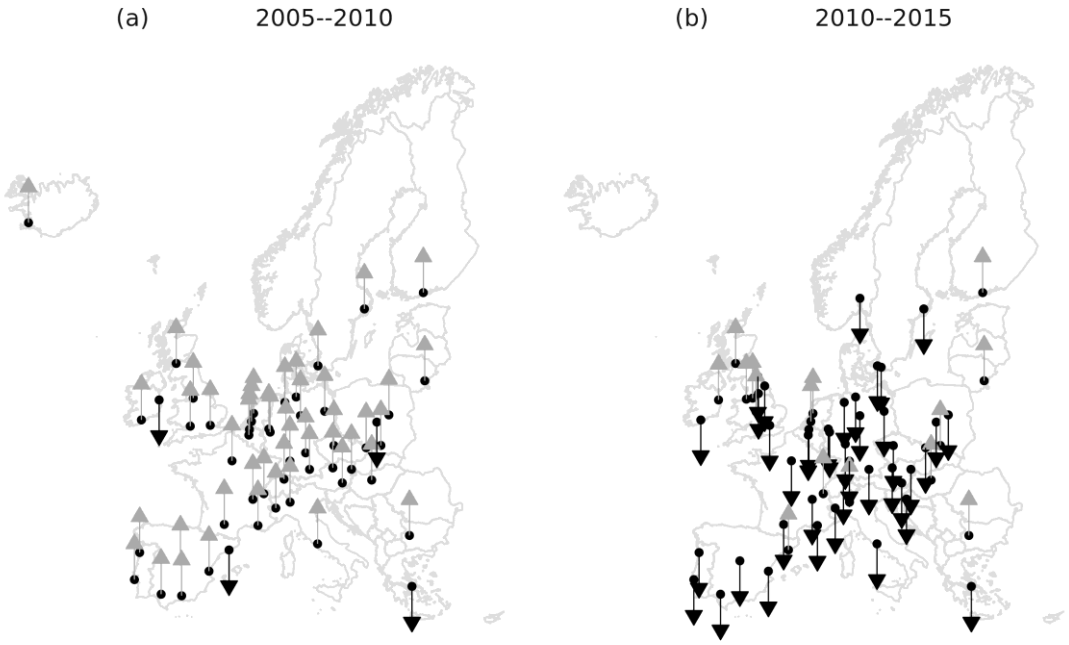

Figure 2. Direction of the NO_2/NO_x emission ratio delta from the European peak year of 2010 for 61 urban areas. Upward and downward arrows indicate increases and decreases in the NO_2/NO_x emission ratio respectively.

volume. The emission ratio estimates where then sequentially aggregated from site, to urban area, to European level to avoid bias towards urban areas with many more monitoring sites. The aggregation function used was the arithmetic mean. This method is referred to in text as "observation filtering".

Results and Discussion

Mean European NO_2/NO_x emission ratio

The mean European NO_2/NO_x emission ratio demonstrated a clear and significant increase between the years of 1995 and 2010 (Figure 1). During the period between 1995 and 2010 the European NO_2/NO_x emission ratio increased from approximately 8 % to 16 % (Figure 1). After 2010, the mean European NO_2/NO_x emission ratio stabilised until in the final year of analysis (2015). In 2015 the ratio was 14.5 %. Pre-2000, the ratio was less than 10 % and the uncertainty was greater due to fewer monitoring sites making up the aggregations, and the mean for the whole analysis period was 11.3 %.

The trend presented in Figure 1 can be broken into three periods where the behaviour of the NO_2/NO_x emission ratio differed. The most striking period was experienced between 1995 and 2008 when the NO_2/NO_x ratio significantly increased. This period coincides with the increased prevalence of passenger diesel vehicles due to promotion and incentivisation of these types of vehicles throughout most European countries. These vehicles were also equipped with DOC for compliance to the Euro 3 and 4 emission standards. Therefore, this period coincides and is consistent with the growth of diesel fuelled passenger cars across Europe and penetration of vehicles with exhaust treatment devices which can increase primary NO_2 emissions (DOCs). However, after the period of significant increase between 2009 and 2015 and after Euro 5 emission standards were introduced, the European NO_2/NO_x ratio stabilised and did not continue to increase. The stabilisation after 2010 was an unexpected feature in the trend and is not currently used in future projections and this is discussed in a later section.

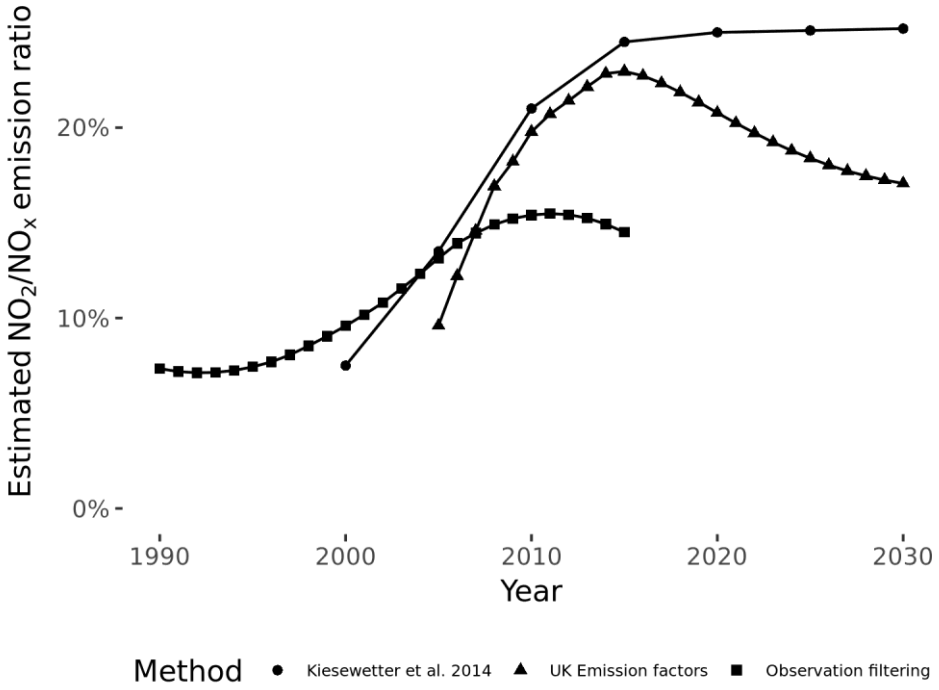

Figure 3. Time series of three methods which estimate roadside primary NO_2 as a NO_2/NO_x emission ratio. The observational filtering is reported in this study and the other two estimates are from Kiesewetter et al., (2014), and UK National Atmospheric Emission Inventory, (2014).

Urban area analysis

When the NO_2/NO_x emission ratios are aggregated to urban area level, the peak ratio at approximately 2010 was experienced in most locations. The mapped deltas in Figure 2 show the reversal in the trend was striking with most European areas analysed conforming to the mean European trend. However, there were a number of urban areas (seven percent of those analysed) which did not experience the same trend as Europe as a whole. These urban areas included: two urban areas in the Netherlands, Barcelona, Dublin, urban areas in central United Kingdom, and Helsinki. These observations suggest that this group of urban areas have experienced other local processes which are not typical of most European cities. Such processes could be specific local bus fleet changes or other changes with the heavy vehicle fleet. Nevertheless, the majority of urban areas demonstrated the pattern seen in Figure 1 which indicates a European-scale effect which is consistent with fleet changes driven by the progressive implementation of passenger vehicle Euro standards and the introduction of emission control devices such as DOCs and DPFs.

Comparison of NO_2/NO_x emission ratio estimates

The stabilisation of the primary NO_2/NO_x emission ratio since 2010 determined by the observational filtering method is currently not used in policy projections, and differs from other estimates of roadside NO_2/NO_x emission ratios. Two other examples which predict the NO_2/NO_x emission ratios are displayed in Figure 3 and demonstrates the difference between the observational record and what is being used in European modelling. The Kiesewetter et al., (2014) European model does not include a decreasing period in the future (up to 2030) while the UK National Emissions Inventory (NAEI) emission factors do decrease, but starting in 2015. Both models use higher NO_2/NO_x emission ratios when compared to what is derived from observations. The higher NO_2/NO_x emission ratios in the models will result in pessimistic European NO_2 future attainment scenarios when used in such a manner.

The differences between what is used in current models and what the observations suggest (Figure 3) can be demonstrated with a simple calculation using the roadside increment of NO_x for European monitoring sites. If the 2015 observational filtering derived ratio of 14.5 % is compared with 23 % (the mean of the other estimates in 2015), the mean European roadside NO_2 delta is 6.6 µg m^{-3} (for the annual mean). The current legal annual NO_2 limit is 40 µg m^{-3} and therefore, this difference is a sixth of the legal limit and would be an important component to consider in many locations. Clearly, this increment and the importance of such a change among monitoring sites and urban areas will vary among Europe. However, it does demonstrate the importance of the differences of what the observational record suggests and what is commonly used in policy projections and suggests that future NO_2 attainment scenarios may be rather pessimistic.

Conclusions

Roadside ambient air quality monitoring data were used to estimate the primary NO_2/NO_x emission ratio across 61 urban areas in Europe. The mean European NO_2/NO_x emission ratio significantly increased from 8 % to 16 % between 1995 and 2010. After 2010 until the final year of analysis (2015), the emission ratio stabilised and did not continue to increase. The stabilisation of the NO_2/NO_x emission ratio has important implications for local air quality and the attainment of the legal limits of NO_2 in Europe. Other, currently used estimates of the European NO_2/NO_x emission ratio are higher and do not show the same trend when compared to the observational record. Therefore, the observations suggest that current models used for European NO_2 attainment scenario predictions are pessimistic.

References

ACEA (2016). Share of Diesel in New Passenger Cars. European Automobile Manufacturers' Association. url: http://www.acea.be/statistics/tag/category/share-of-diesel-in-new-passenger-cars.

Carslaw, David C., Murrells, Tim P., Andersson, Jon, and Keenan, Matthew (2016). Have vehicle emissions of primary NO_2 peaked? *Faraday Discussions* 189, pp. 439–454.

European Environment Agency (2014). AirBase – The European air quality database (Version 8). http://www. eea.europa.eu/data-and-maps/data/airbase-the-european-air-quality-database-8.

European Environment Agency (2016). Eionet Central Data Repository. url: http://cdr.eionet.europa.eu/.

Grange, Stuart K. (2016). **smonitor**: A framework and a collection of functions to allow for maintenance of air quality monitoring data. url: https://github.com/skgrange/smonitor.

Grange, Stuart K. (2017). Technical note: **smonitor** Europe (Version 1.0.1). Tech. rep. Wolfson Atmospheric Chemistry Laboratories, University of York. doi: 10.13140/RG.2.2.20555.49448.

Grice, Susannah, Stedman, John, Kent, Andrew, Hobson, Melanie, Norris, John, Abbott, John, and Cooke, Sally (2009). Recent trends and projections of primary NO_2 emissions in Europe. *Atmospheric Environment* 43.13, pp. 2154–2167.

Kiesewetter, G., Borken-Kleefeld, J., Schopp, W., Heyes, C., Thunis, P., Bessagnet, B., Terrenoire, E., Gsella, A., and Amann, M. (2014). Modelling NO_2 concentrations at the street level in the GAINS integrated assessment model: projections under current legislation. *Atmospheric Chemistry and Physics* 14.2, pp. 813–829.

UK National Atmospheric Emission Inventory (2014). Primary NO_2 Emission Factors for Road Vehicles. August 2014 update.

Weiss, Martin, Bonnel, Pierre, Kühlwein, Jorg, Provenza, Alessio, Lambrecht, Udo, Alessandrini, Stefano, Carriero, Massimo, Colombo, Rinaldo, Forni, Fausto, Lanappe, Gaston, Le Lijour, Philippe, Manfredi, Urbano, Montigny, Francois, and Sculati, Mirco (2012). Will Euro 6 reduce the NO_x emissions of new diesel cars? --- Insights from on-road tests with Portable Emissions Measurement Systems (PEMS). *Atmospheric Environment* 62, pp. 657--665.

Williams, Martin L. and Carslaw, David C. (2011). New Directions: Science and policy — Out of step on NO_x and NO_2? *Atmospheric Environment* 45.23, pp. 3911–3912.

Acknowledgements

The authors thank Anthony Wild with the provision of the Wild Fund Scholarship. This work was also partially funded by the 2016 Natural Environment Research Council (NERC) air quality studentships programme (grant reference number: NE/N007115/1).

Health impact of PM_{10}, $PM_{2.5}$ and BC exposure due to different source sectors in Stockholm, Gothenburg and Umea, Sweden

C. Johansson[1,3], K. Eneroth[1], D. Segersson[2], A. Engström Nylén[1], L. Gidhagen[2], G. Omstedt[2], B. Forsberg[4]

[1]Environment and Health Administration, City of Stockholm, Sweden, christer.johansson@aces.su.se

[2]Swedish Meteorological and Hydrological Institute, Norrköping, Sweden

[3]Department of Environmental Science and Analytical Chemistry, Stockholm University, Stockholm, Sweden

[4]Department of Public Health and Clinical Medicine, Umea University, Sweden

Introduction

Air quality dispersion modelling of population exposures has been used in studies to assess health effects and in many studies the contribution to the exposure from specific anthropogenic sources is separated in order to assess health impacts of abatement strategies (see Segersson et al., 2017 and references therein). As pointed out by WHO (2013a), there is convincing evidence that PM, almost regardless of source, has detrimental health effects. An exception is sea salt, for which there is little indication of harmfulness. Most commonly $PM_{2.5}$ is used as indicator to estimate effects on the mortality, as recommended for cost-benefit analysis by the World Health Organization (WHO) in the HRAPIE project (WHO, 2013b). Also other PM metrics have been used, such as PM_{10} (Forsberg et al, 2005; Gustafsson et al., 2014), EC (elemental carbon) and BC (black carbon) (Keuken et al., 2012; Oxley et al., 2015). An important argument for using BC instead of $PM_{2.5}$ in health impact assessments of local emissions, is that BC is a more specific indicator of the local combustion particles. Recent epidemiological studies indicate that associations between adverse health effects and exposure are stronger for BC than for $PM_{2.5}$ (Janssen et al., 2011; Grahame et al., 2014) and there is more evidence of health effects linked to combustion sources than non-combustion sources.

The objective of this study has been to estimate and evaluate exposure to respirable PM from different sources with appropriate temporal and spatial resolution for use in epidemiological studies and health impact assessments. Also, the consequences of using different indicators for PM exposure and different exposure-response functions for different source categories when performing health impact analysis are investigated. More detailed description of this study is given by Segersson et al. (2017).

Methods

We have applied dispersion modelling to assess annual mean exposure to $PM_{2.5}$, PM_{10} and BC in three major cities included in this study: Stockholm, Gothenburg and Umea, Impact assessments and exposure calculations for were performed for year 2011. The modelling domains were selected to cover the areas with population-based cohorts available for epidemiological studies. The model domains were in size 92.8x112 km^2 (Gothenburg), 174x236 km^2 (Stockholm) and 108.8x182.4 km^2 (Umea), covering the principal cities with suburbs, but also a large number of smaller villages and some rural areas.

The following source categories were defined in order to allow source apportionment and separate impacts of the main contributors to particle emissions in urban areas in Sweden:

- road traffic exhaust
- road traffic non-exhaust
- RWC (residential wood combustion)
- shipping
- other (mainly industrial, energy, off-road machinery, agriculture)

For all three cities, there were local or regional bottom-up emission inventories available (Segersson et al., 2017).

Gaussian models included in the Airviro air quality management system have been used to simulate the annual average PM contributions from different local sources during the year 2011 (SMHI, 2017; Andersson et al., 2015). The long-range transport contributions to each domain were taken from measurements at rural sites outside the calculation domains or determined indirectly. To reduce the time for computations while still maintaining a high resolution in the vicinity of roads and point sources, a quad tree (Finkel and Bentley, 1974) receptor grid was used. Airviro makes use of a diagnostic wind model based on the concept first described by Danard (1977), in which it is assumed that small scale winds can be seen as a local adaptation of large scale winds. For Gothenburg and Umea, dispersion modelling was performed for each hour of the year, while in Stockholm meteorological conditions were based on a climatology (a representative sample) created from 15 years of meteorological measurements.

Exposure has been calculated for population data on a 100x100 m2 grid acquired from Statistics Sweden, representing the year 2012. The population data is based on the coordinates for the home addresses of the total population, but also includes age separated classes: 0-1 years, from 1-5 years and every five year interval up to 85 years, then a final class > 85 years. Both the population data and the calculated concentrations were resampled to a grid with resolution 50x50 m2 in order to calculate the population weighted concentrations. Since grids were aligned and the same map projection was used, no interpolation was necessary when resampling. Baseline mortality representing all natural deaths was acquired from the Swedish Cause of Death Register at The National Board of Health and Welfare. To avoid overestimation, premature deaths due to the pollutant exposure were subtracted from the baseline.

For particles originating from local sources, three different exposure-relationships are used to demonstrate the range of the estimates (table 1). Jerrett et al. (2005), investigated associations within a metropolitan area (Los Angeles), providing relative risk factors for $PM_{2.5}$. Hoek et al. (2013) combined a lot of studies, mostly “between-city comparisons” and also provide risk factors for $PM_{2.5}$. Janssen et al. (2011) provide an estimate for BC and Hoek et al. (2013) for EC, both actually represent a mixture of BC, EC and BS measurements and report the same most probable value for the relative risk (60 % per 10 µg m^{-3}), but slightly different confidence intervals. A European multi-cohort study from the ESCAPE Project (Beelen et al., 2014) with associations resulting from “within-city contrasts” in $PM_{2.5}$, found an estimate closer to the one from Jerrett et al. (2005). Using different relative risk factors for LRT than for local sources can be further justified by the large differences in the composition of PM. For coarse particles, mortality in all ages was used by Meister et al. (2012) and the whole population is therefore used in the calculations.

Table 1. The relative risks used for different sources.

Pollutant	RR (95% CI) per 10 µg m^{-3}	Reference
Long-range contribution ($PM_{2.5}$)	6% (4% - 8%)	WHO (2013), Hoek et al [53]
Local contribution BC	60% (10% – 110%)	Janssen et al. (2011)
Local contribution $PM_{2.5}$	17% (5% - 30%)	Jerrett et al. (2005)
	6% (4% - 8%)	Hoek et al. (2013)
Non-combustion particles ($PM_{2.5-10}$)	1.7% (0.2% - 3%)	Meister et al. (2012)

Results

The modelled concentrations were compared with measurements and the overall r^2 for all data from the three cities were 0.87 and 0.65 for PM_{10} and $PM_{2.5}$, respectively (Figure 1). The overall agreement

is regarded as good considering the uncertainties in both the emission inventories and the dispersion models involved in these calculations.

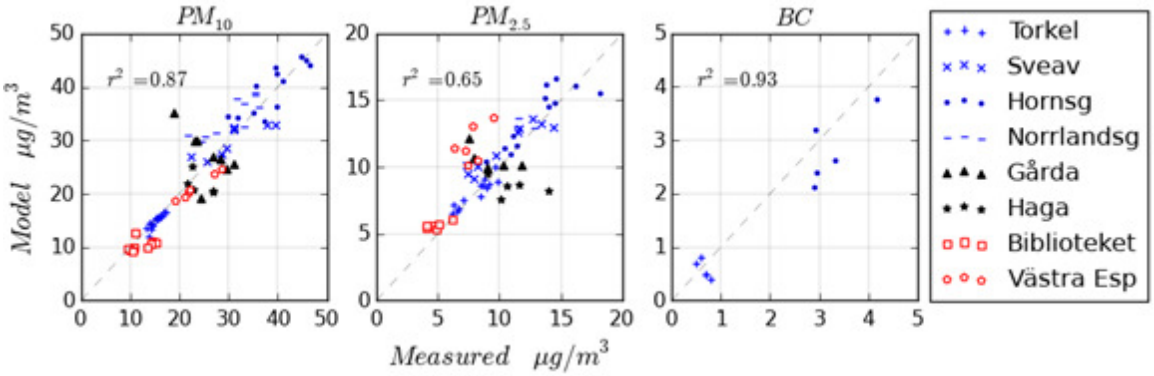

Figure 1. Comparisons between measured and modelled annual average concentrations. The dashed lines are 1:1 lines.

The result of the exposure calculations is presented as population weighted annual mean concentrations for 35x35 km^2 squares centred over the three cities (areas and shown in figure 2).

Figure 2. Annual average of total $PM_{2.5}$ concentration during 2011 presented in 35x35 km^2 areas centred on the main city of each modelling domain. ©Lantmäteriet.

Figure 3 shows population weighted annual average source contributions to PM_{10}, $PM_{2.5-10}$, $PM_{2.5}$ and BC. It can be seen that the coarse mode ($PM_{2.5-10}$) is mainly from LRT and traffic wear particles. For finer particles ($PM_{2.5}$), the contribution from traffic wear is smaller and emissions from combustion sources within the modeling domain have a significant contribution. It is noteworthy that for $PM_{2.5}$, exposure caused by small scale residential heating is comparable to exposure due to road traffic. The contribution from shipping is small for all the evaluated PM-fractions and within all three assessment areas. For BC, traffic exhaust emissions and RWC cause the largest local contribution.

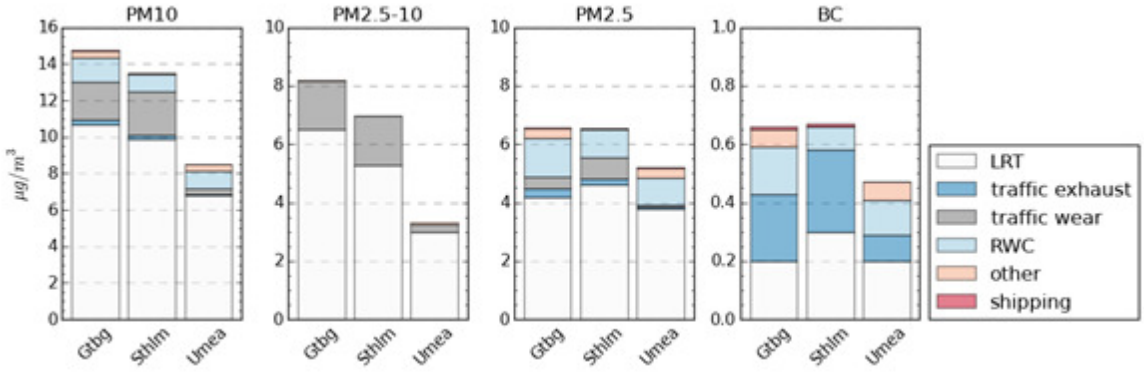

Figure 3. Population weighted exposure (population > 30 years) for the three cities and for the selected sectors. For traffic wear, the whole population is used for consistency with calculations of premature mortality.

Premature mortality for each of the different source categories is presented in figure 4. Since relative risks for the local contribution of $PM_{2.5}$ from road traffic represent both combustion and fine wear particles, the sector is here named "traffic < 2.5 µm" instead of "traffic exhaust" and "traffic wear" is referred to as "traffic wear 2.5-10 2.5 µm". For BC, the local contribution is strictly limited to combustion sources. The results indicate that RWC and road traffic are responsible for the majority of the premature deaths. Using BC instead of $PM_{2.5}$ as an indicator, with relative risk factors according to Janssen et al. (2011), the relative impact of traffic exhaust increases significantly. For Stockholm, the percentage of the premature deaths caused by local sources that are related to "traffic < 2.5µm" is estimated to 66 % when using BC as an indicator and around 40 % using $PM_{2.5}$. In Umea RWC represents 40-60 % of the premature deaths due to local sources. For Gothenburg and Stockholm, RWC is somewhat less important and represents 20%-50 % of the premature deaths related to local sources.

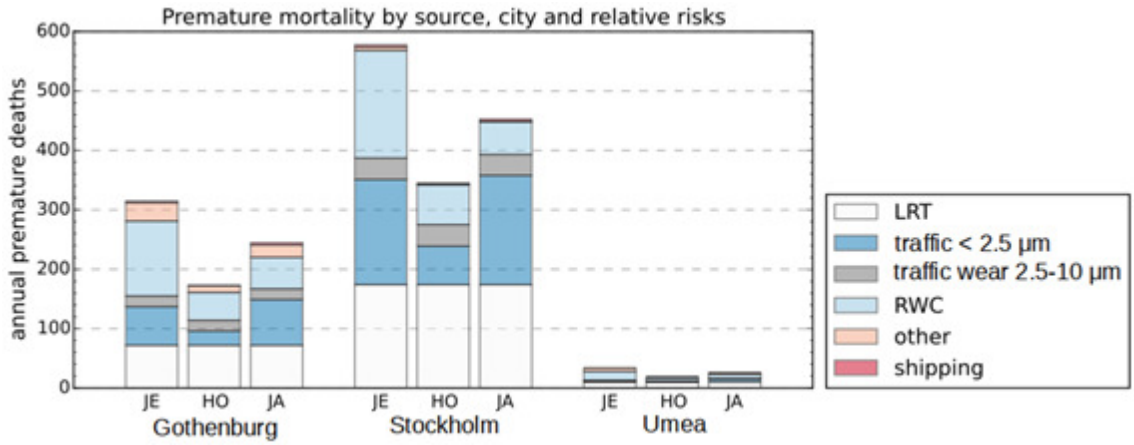

Figure 4. Premature deaths estimated for the different modelling domains. Estimates have been made separately for the source categories. For premature deaths due to local contributions of $PM_{2.5}$ and BC, estimates have been made using relative risks from three different studies: JE: Jerrett et al. 2005, HO: Hoek et al. 2013, JA: Janssen et al. 2011).

In Table 2, the percentage of premature deaths that are attributed to local sources is presented. Both using Jerret et al (2005), representing within-city gradients of $PM_{2.5}$, and Janssen et al. (2011) representing "between-city gradients" of BC, the local sources represent ≥ 60 % of the premature deaths. Using Hoek et al. (2013), long-range transport (LRT) and local sources each represent near half of the premature deaths.

Table 2. Percentage of premature deaths related to local sources compared to long-range transport. For premature deaths due to local contributions to concentrations of $PM_{2.5}$ and BC, separate estimates have been made using relative risks from three different studies: Jerrett et al. (2005), Hoek et al. (2013) and Janssen et al. (2011).

	Gothenburg	Stockholm	Umea
Jerrett et al. (2005)	77	70	69
Hoek et al. (2013)	58	50	46
Janssen et al. (2011)	70	62	60

Discussion

The most important source of uncertainty in the calculated concentrations originates in the emission inventories. However, there is not enough information available to perform a quantitative uncertainty analysis. To provide an indication on the uncertainty, ranges are provided based on judgment of the authors. RWC is one of the largest and also one of the most uncertain emission categories, especially for Gothenburg and Stockholm, where no detailed inventory of stoves and boilers is available. Considering uncertainties in fuel consumption, incomplete information regarding technology and their emission factors, the uncertainty for overall emissions from RWC may be at least 50 %. For road traffic the uncertainty is lower, but could still be as high as 25 % and higher for BC. Emissions from shipping and other sources also have significant uncertainties in the range of 25-50 %, but have a smaller influence on the total concentration.

Considering that most of the uncertainty in local contributions is probably related to uncertainties in the emission inventories, relatively simple Gaussian models have been chosen for the dispersion modelling. An advantage of the Gaussian models applied is their computational efficiency, which makes it possible to use a receptor grid fine enough to resolve the strong concentration gradients in the vicinity of roads and close to other sources. For homes close to major roads, the concentration can often be twice as high as the urban background concentration, even without considering street-canyon effects. Capturing these spatial variations is expected to increase the accuracy of the exposure calculated at homes.

The comparison between model results and measurements verifies that the calculated total concentration is well captured with the applied methodology. It is however more challenging to evaluate the relative contributions of the different source categories. The results indicate that RWC is generally the dominating source behind exposure to combustion particles. With this in mind it is of interest to compare with source assessments based on other methods. Source assessments of the soot aerosol in Gothenburg using a radio-carbon methodology have been reported by Szidat et al. (2009). They estimated the fraction of EC related to wood combustion at the urban background station Femman in Gothenburg to be 10±2 % both during three winter weeks of 2005 and during three summer weeks of 2006. Similar measurements performed at the urban background station Torkel Knutssonsgatan in central Stockholm (Andersson et al., 2011) shows a large variation in the fraction of SC (“soot carbon”) related to combustion of biogenic fuels. Measurements, 4 month in winter and 6 weeks in fall, indicate a fraction of SC related to combustion of non-fossil fuel is in the range 30-50 %, which is significantly higher than for EC found in Gothenburg. The results are not directly comparable since the methodology is somewhat different and all measurements represent relatively short campaigns during different parts of the year. However, they still verify that the RWC can be a significant source of BC, even in the city centers. Even though BC, not EC or SC, was calculated in this study, a comparison of the relative contribution of wood combustion could be considered relevant. The results indicate that the annual average fraction of BC from local wood combustion at the Femman station in Gothenburg is 10 % of the total BC concentration. For Stockholm the corresponding value at the Torkel Knutssongatan site in central Stockholm is 6 %. Since it is likely that also part of the LRT contribution originates from wood combustion, the current study indicates total fractions related to wood combustion above these values.

Exposure at home addresses as an indicator for personal exposure is a common but rather crude estimate. How exposure at home address relates to the actual exposure depends for example on the mobility of each individual as well as the infiltration of PM into the building (Brown et al., 2009). However, there is a lack of relative risk factors from epidemiologic studies based on actual exposure and for this study there was also insufficient information available regarding mobility of the individuals and building properties determining the infiltration of outdoor air. Due to limitations in available data and for consistency with the applied risk factors, ambient exposure at home addresses was considered the best option. Since the relative risks were based on exposure at home addresses, the uncertainty described by the confidence intervals given in Table 1 includes uncertainties related to differences between actual exposure and ambient exposure at homes.

It is noteworthy that even for large Swedish cities the number of premature deaths due to RWC is comparable to those related to road traffic. Thus, a weakness in the present study is the lack of detailed information when describing emissions from RWC in Stockholm and Gothenburg. In order to reduce the uncertainty in the source apportionment, future studies should aim to improve the description of this source category. It is likely that the current trend with improved technology for vehicles, resulting in lower emissions, will continue. At the same time, no significant improvements are

expected within the near future for RWC in Sweden. This means that the relative contribution of RWC will increase.

The presented estimates of premature mortality include the combined uncertainties from the exposure estimates at homes as well as assumptions regarding exposure response functions and applied relative risk factors. With this in mind, the number of deaths should preferably be presented as a range with a confidence interval. This requires more information, e.g. regarding the uncertainty of exposure calculations for specific source categories, as well as further research.

Conclusions

High resolution dispersion models have been used to calculate population exposure to PM_{10}, $PM_{2.5}$ and BC during year 2011 for 35x35 km^2 assessment areas centered on three Swedish cities: Gothenburg, Stockholm and Umea. For each source category, population weighted average concentrations have been calculated and relative risk factors have been applied to estimate premature mortality. Different relative risk factors have been applied for PM from local sources and LRT.

For all three cities, the largest part of the exposure to $PM_{2.5}$ and PM_{10} is due to LRT, while for BC the local contribution is slightly larger than the contribution from LRT. This implies that the use of BC exposure as a health indicator increases the focus on local emissions.

The two dominating local sources are road traffic and RWC. Road traffic is the largest local source of PM_{10}, while RWC is larger for $PM_{2.5}$. For road traffic both exhaust and wear particles are emitted, with wear particles representing the largest local (mass) contribution for both PM_{10} and $PM_{2.5}$. For exposure to BC, traffic exhaust is the most important source in the two larger cities Stockholm and Gothenburg, while in Umea, RWC is larger.

The exposure contribution from shipping is very small, also in Gothenburg, which is the largest port in Sweden. This is expected since only a small number of people live in the direct vicinity of the harbor or the shipping fairways. The exposure contributions from the source category “other” in Umea and Gothenburg are significant. However, the large uncertainties in the spatial distribution of the emissions of this category should be taken into account while assessing their impact.

Among the local sources, RWC and road traffic cause the most premature deaths. Using $PM_{2.5}$ as an indicator attributes most deaths to RWC, while using BC puts more weight on road traffic exhaust. It is also concluded that fine traffic related particles (< 2.5 µm) are likely a more important cause of mortality associated with long-term exposure than the coarser wear related fraction (2.5-10 µm).

A major finding is that using relative risk factors representing within-city comparisons or using BC as an indicator for PM from local combustion sources, the local sources of PM cause more premature deaths as compared to LRT. This is true for all three cities. When risk assessments are instead based on the total PM_{10} or $PM_{2.5}$ concentrations, and using corresponding relative risk factors based on “between-city” comparisons, LRT is normally attributed a larger impact and there is an evident risk of underestimating the impact of local sources. The results emphasize the importance to resolve within-city gradients in the concentration field when assessing population exposure and raise more concern to reduce local PM and BC emissions in our cities.

Acknowledgements

This study forms part of the Swedish Clean Air & Climate Research program, funded by the Swedish Environmental Protection Agency.

References

Andersson, A., Sheesley, R., Kruså, M.; Johansson, C., Gustafsson, O. 14C-Based source assessment of soot aerosols in Stockholm and the Swedish EMEP-Aspvreten regional background site. Atmos Environ 2011, 45, 215-222.

Andersson S., Arvelius J., Gerner A., Danielsson et al. Description of methods and quality of spatially distributed emissions to air during 2015. Swedish EPA, contract no 309 1235. (in Swedish, original title: Metod- och kvalitetsbeskrivning för geografiskt fördelade emissioner till luft under 2015), SMED, 2015.

Beelen R, Raaschou-Nielsen O, Stafoggia M, Andersen ZJ, Weinmayr G, Hoffmann B, et al. Effects of long-term exposure to air pollution on natural-cause mortality: an analysis of 22 European cohorts within the multicentre ESCAPE project. Lancet 2014. 1, 383(9919), 785-95.

Brown K.W., Sarnat J. A., Suh H. H., Coull B. A., Koutrakis P. Factors influencing relationships between personal and ambient concentrations of gaseous and particulate pollutants. Sc Tot Env 2009, 407, 3754-3765.

Danard, M. A simple model for mesoscale effects of topography on surface winds. Monthly Weather Review 1977, 99, 831–839.

Finkel, R.A. & Bentley, J.L. Quad trees a data structure for retrieval on composite keys. Acta Inform 1974, 4: 1. doi:10.1007/BF00288933

Forsberg, B., Hansson, H-C., Johansson, C., Areskoug, H., Persson, K. & Järvholm, B. Comparative health impact assessment of local and regional particulate air pollutants in Scandinavia, Ambio 2005, 34, 11-19.

Grahame, T. J., Klemm, R. and Schlesinger, R. B. Public health and components of particulate matter: The changing assessment of black carbon, J Air Waste Manag Assoc 2014, 64, 620 – 660.

Gustafsson, M., Forsberg, B., Orru, H., Åström, S., Tekie, H., Sjöberg, K. Quantification of population exposure to NO2, $PM_{2.5}$ and PM_{10} and estimated health impacts in Sweden 2010. IVL Report B 2197, IVL Swedish Environmental Research Institute Ltd. P.O. Box 53021 SE-400 14 Göteborg, Sweden, 2014.

Hoek G., Krishnan R. M., Beelen R., Peters A., Ostro B., Brunekreef B., Kaufman J. D. Long-term air pollution exposure and cardio- respiratory mortality: a review, Environ Health 2013, 12:43.

Janssen, N.A.H.; Hoek, G.; Simic-Lawson, M.; Fischer, P.; van Bree, L.; ten Brink, H. et al. Black Carbon as an Additional Indicator of the Adverse Health Effects of Airborne Particles Compared with PM_{10} and $PM_{2.5}$. Environ Health Perspect 2011, 119, 1691-9.

Jerrett M., Burnett R. T., Ma R. J., Pope C. A., Krewski D., Newbold K. B. et al. Spatial analysis of air pollution and mortality in Los Angeles, Epidemiology 2005, 16, 727 – 736.

Keuken, M.,P.,, Jonkers, S., Zandveld, P., Voogt, M., Elshout van den, S. Elemental carbon as an indicator for evaluating the impact of traffic measures on air quality and health. Atmos Environ 2012, 61, 1-8.

Meister, K., Johansson, C., Forsberg, B. Estimated Short-Term Effects of Coarse Particles on Daily Mortality in Stockholm, Sweden. Environ Health Perspect 2012, 120, 431-435.

Oxley T, ApSimon HM, de Nazelle A. Investigating the sensitivity of health benefits to focussed $PM_{2.5}$ emission abatement strategies, Environ Model Softw 2015, 74, 268-283.

Segersson, D., Eneroth, K., Gidhagen, L., Johansson, C., Omstedt, G., Engström Nylén, A., Forsberg, B. Health impact of PM_{10}, $PM_{2.5}$ and BC exposure due to different source sectors in Stockholm, Gothenburg and Umea, Sweden. Int. J. Environ. Res. Public Health 2017, 14(7), 742; doi:10.3390/ijerph14070742.

SMHI, 2017. Swedish Meteorological and Hydrological Institute. Airviro v4.00 User's reference, vol 2 - Working with the Dispersion module. Swedish Meteorological and Hydrological Institute, 601 76 Norrköping, Sweden, 2015, Available online: www.smhi.se/airviro/download (accessed 1 June 2017).

Szidat S., Ruff M., Perron N., Wacker L., Synal H.-A., Hallquist M. et al. Fossil and non-fossil sources of organic carbon (OC) and elemental carbon (EC) in Göteborg, Sweden. Amos Chem Phys 2009, 9, 1521-1535.

WHO, 2013a. World Health Organization. Health risks of air pollution in Europe – HRAPIE project Recommendations for concentration–response functions for cost–benefit analysis of particulate matter, ozone and nitrogen dioxide. WHO Regional Office for Europe, UN City, Marmorvej 51, DK-2100 Copenhagen Ø, Denmark, 2013.

WHO, 2013b. World Health Organizatio. Review of evidence on health aspects of air pollution –REVIHAAP Project. WHO Regional Office for Europe, Scherfigsvej 8, DK-2100 Copenhagen Ø, Denmark, 2013.

Impact of excess NO_x emissions from diesel cars on air quality, public health and eutrophication in Europe

J. E. Jonson [1,5], J. Borken-Kleefeld [2], D. Simpson [1,3], A. Nyíri [1],M. Posch [4], C. Heyes [2]

[1] Norwegian Meteorological Institute, NO-0313, Oslo, Norway
[2] International Institute for Applied Systems Analysis(IIASA), Schlossplatz 1, 2361 Laxenburg, Austria
[3] Department of Space, Earth and the Environment, Chalmers University of Technology, Gothenburg, Sweden
[4] Coordination Centre for Effects(CCE), RIVM, PO Box 1, NL-3720 BA Bilthoven, The Netherlands
[5] Author to whom any correspondence should be addressed

Link to publication:
http://iopscience.iop.org/article/10.1088/1748-9326/aa8850?fromSearchPage=true

Impacts and mitigation of excess diesel-related NO_x emissions in 11 major vehicle markets

S. C. Anenberg, J. Miller, R. Minijares, L. Du, D. K. Henze, F. Lacey, C. S. Malley, L. Emberson, V. Franco, Z. Klimont,, C Heyes

Link to publication:
http://rdcu.be/r0Rg

Assessment of particle emissions from aircraft turbine engines: ground, cruise, and overall flight emissions

L. Durdina[1,2], B.T Brem[1,2], A. Setyan[1,2], F. Siegerist[3], T. Rindlisbacher[4].*

[1] Laboratory for Advanced Analytical Technologies, Empa, Dübendorf, 8600, Switzerland, lukas.durdina@empa.ch
[2] Institute of Environmental Engineering, ETH Zürich, Zürich, 8093, Switzerland
[3]SR Technics Switzerland AG, Kloten, 8302, Switzerland
[4]Swiss Federal Office of Civil Aviation (FOCA), Bern, 3003, Switzerland

Introduction

In the early days of jet airliners more than half a century ago, the loud turbojet engines left the runways in clouds of black smoke. Already back then, due to growing awareness concerning the environmental impacts of aviation (Kuhn, 1970) and prospects of supersonic transport (Johnston, 1971), measures were put in place to get rid of the visible fumes (ICAO, 2008, 2011b). The black smoke was not only a nuisance but a matter of safety – it reduced airport visibility (George et al., 1972). To address this issue, the International Civil Aviation Organization (ICAO) has regulated engine smoke through the smoke number (SN) (Wayson et al., 2009).

SN is determined from the reflectance of a filter paper through which 16.2 kg/m^2 of raw exhaust are drawn (ICAO, 2008). The filter captures particulate matter (PM) in the exhaust, predominantly consisting of black carbon (BC), but is inefficient for particles < 300 nm typical for modern jet engines (Stettler et al., 2013b). For some engine types, SN is virtually undetectable at all power settings (ICAO, 2016). However, invisible plumes are not particle free.

Several recent studies have characterized PM emissions from aircraft jet engines (Beyersdorf et al., 2014; Kinsey et al., 2010; Kinsey et al., 2011; Lobo et al., 2011; Lobo et al., 2015a; Mazaheri et al., 2011; Onasch et al., 2009), but the data are obtained with a variety of sampling and measurement methods, which reduces their potential widespread use for climate and air quality models. For such purposes, researchers have estimated aviation BC emissions from combustion models (Stettler et al., 2013a; Yim et al., 2015) and, most often, from SN (ICAO, 2011a-; Rissman et al., 2013; Unal et al., 2005; Zhu et al., 2011). Besides the inherent uncertainties, these approximations neglect particle losses in the exhaust sampling systems as well as fuel composition (Brem et al., 2015; Durdina et al., 2014). Moreover, none of the approximations resolves particle number concentration, which is a metric relevant for the assessment of health effects of ultrafine particles as well as for the formation of contrails and cirrus clouds (Kärcher et al., 2007; Kärcher and Yu, 2009).

Without up-to-date representative data, impact assessments of aircraft engine BC emissions remain highly uncertain. The emission indices (EIs) used to calculate the BC emission rates from the global fleet typically range from 10 to 50 mg/kg fuel burned (Lee et al., 2010; Petzold et al., 1999). Recent reports claim that aviation BC emissions are underestimated and warm up the atmosphere as much as 1/3 of the aviation's CO2 emissions with an average EI of up to 93 mg/kg fuel (Stettler et al., 2013a; Stettler et al., 2013b). At airports, aircraft BC emissions typically contribute to the suspended fine PM by less than one µg/m^3 (Rissman et al., 2013; Zhu et al., 2011). However, even one µg of aircraft engine BC can contain billions of particles with modes as small as 10 nm (Durdina et al., 2014; Kinsey et al., 2010; Lobo et al., 2015a; Lobo et al., 2015b), a characteristic that makes them a risk factor for severe lung and heart diseases (Block and Calderón-Garcidueñas, 2009; Geiser and Kreyling, 2010; Health Effects Institute, 2013; Peters et al., 2006). The PM emitted is most concentrated near runways and quickly disperses with distance (Hsu et al., 2013; Mazaheri et al., 2011), but is also claimed to raise ambient particle number concentrations fourfold up to 10 km downwind (Hudda et al., 2014; Keuken et al., 2015).

Such air quality and climate impacts can be better assessed through the non-volatile PM (nvPM) emissions standard for commercial jet engines, the first new aviation emissions standard in 40 years (Rindlisbacher and Jacob, 2016). From 2020 onwards, the ICAO emissions databank (ICAO, 2016) will include nvPM number- and mass-based emissions for in-production turbofan engines with rated thrust > 26.7 kN (large business jets and airliners). The nvPM is almost entirely BC, which is the term we use here in the context of the new regulation.

Here, we estimate BC mass and number emissions from a single aisle airliner modeled on the Next-Generation Boeing 737 (almost 1/3 of all 100+ seater airliners in service (Airbus, 2015; The Boeing Company, 2016)) over entire flight missions. We extensively characterized particle properties and determined BC mass and number EIs (EIm and EIn) for two 737NG powerplants in compliance with the new regulation methodology (Miake-Lye and Brem, 2016; Rindlisbacher and Jacob, 2016; SAE International, 2013) as well as measured SN according to the current standard for one of the engines. We first look at the correlation between SN and BC mass. We use the BC data, corrected for particle losses and fuel variability (Brem et al., 2015; Durdina et al., 2014), to calculate the emissions from the standardized ICAO landing and take-off (LTO) cycle, which assesses emissions below 915 m (3000 ft). It defines four thrust settings (static thrust measured on an engine test bed) and time in each mode that roughly represent airport operations: taxiing in and out, take-off, climb at reduced thrust, and approach for landing. We used a calibrated engine performance model for correcting the emissions at the ground to any condition during the flight. Finally, we use our flight mission estimates to answer the question whether modern-day air travel produces more BC per passenger and kilometer than cars and buses.

Materials and Methods

The emission tests were done on two in-service well run-in engines (at 20% and 50% of the typical overhaul cycle, respectively) in the engine test cell of SR Technics at Zurich airport, Switzerland using an nvPM measurement system compliant with the future ICAO nvPM standard (Rindlisbacher and Jacob, 2016). Exhaust samples were extracted at the engine exit plane using a multi-orifice cruciform probe. Upstream of the nvPM measurement system, the sample was diluted with dry synthetic air by a factor of ~10 and drawn through a 24.5 m long trace-heated line (60 °C). The total length of the sample line from the probe inlet to the BC instruments was 34 m. The BC mass concentration was measured with an AVL Micro Soot Sensor (MSS), and the BC number was measured with an AVL Particle Counter Advanced (APC) that contains a two-stage diluter and a volatile particle remover heated to 350°C. The elements of the analysis are shown in Figure 1 and further details can be found in the online supporting information of Durdina et al., 2017.

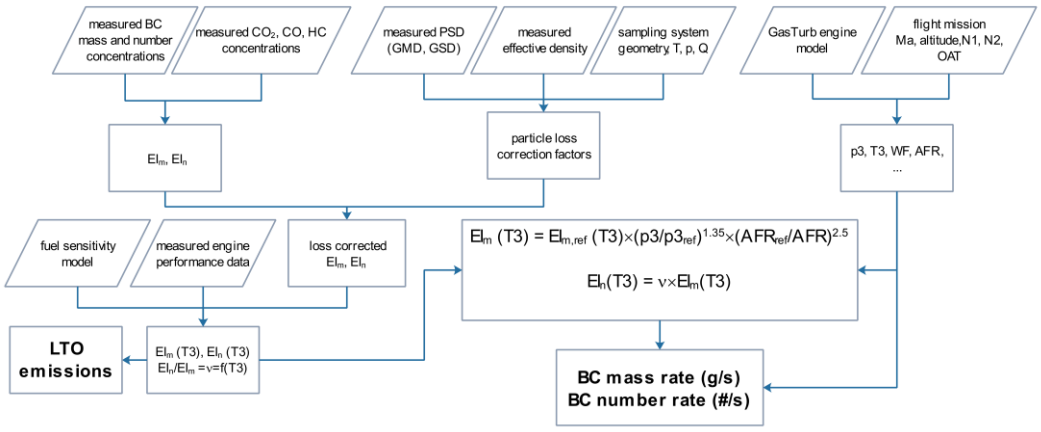

Figure 1: Simplified flow chart visualizing the elements of the analysis.

A substantial fraction of particles entering the sampling system deposits on its inner walls mainly due to diffusion (long sampling lines) and thermophoresis (high thermal gradients). The particles are lost due to thermophoresis mainly in the first seven meters of the sampling system as the sample cools from the exhaust gas temperature (up to 600 °C) to the sample line temperature upstream of the diluter (160 °C). The thermophoretic loss correction factor for this

section of the sampling system was assumed to be independent of particle size and ranged from 1.19 to 1.33.

The diffusional losses depend on particle size and required information about the sampling system penetration, the particle size distributions (PSD), and the relationship between particle size and mass (effective density). The penetration efficiencies of the sampling system and instruments downstream of the probe were modelled using a software tool developed for the particle loss correction in nvPM measurement systems described in the Society of Automotive Engineers (SAE) Aerospace Information Report (AIR) 6504 (SAE International, 2016). We took into account the losses due to diffusion, sample line bends, particle size cut-off as well as the internal losses in the APC (diffusion, thermophoresis, and CPC counting efficiency). We estimated the number-based correction factors by multiplying the modelled PSD based on Scanning Mobility Particle Sizer (SMPS) measurement data by the penetration functions. The number-based correction factors ranged from 2 (take-off) to 11 (idle). For the mass-based losses, we combined the PSD model with particle effective density distributions (Durdina et al., 2014). The mass-based correction factor ranged from 1.1 to 1.7.

Since the BC emissions strongly depend on fuel composition, we estimated the effects of fuel composition variability (fuel aromatics content) using an empirical model developed on the same engine as in this study (Brem et al., 2015). This model uses fuel hydrogen content in mass % (m% H) as the correlating variable. We extrapolated the EIm and EIn for standard fuel used in Europe (14.3 m% H) to the range from 13.8 m% H to 15.0 m% H, which captures the worldwide variability in commercially used jet fuel (Hadaller and Johnson, 2006).

The emissions measured were corrected to flight conditions with the correlation from Döpelheuer and Lecht (Döpelheuer & Lecht, 1999) used in previous cruise BC emission estimates (Peck et al., 2013; Petzold et al., 1999; Stettler et al., 2013a). This correlation corrects the EIm at a reference ground condition to a flight condition, whereas T3ref = T3flight (Figure 1). The reference EIm is corrected for the combustor inlet pressure (p3), the air-fuel ratio (AFR), and adiabatic flame temperature (Tfl) effects. Previous estimates of cruise BC emissions expressed Tfl as linear functions of T3 as well as a function of both T3 and p3 (Peck et al., 2013; Stettler et al., 2013a). We assumed the former, and thus the Tfl term is equal to one. To estimate the EIn, we assumed that the geometric mean diameter (GMD) of the PSD depends only on T3. This assumption is supported by emission measurements of a large turbofan engine at simulated flight altitude conditions (Howard et al., 1996). The data extracted from Howard et al., 1996 show a clear trend of GMD as a function of T3 independent of the simulated flight altitude. Hence, the ratio of EIn to EIm is a unique function of T3.

To determine the p3, T3, and AFR at any flight condition, we developed a detailed engine performance model calibrated to sea level performance data in GasTurb 12, commercial software for gas turbine simulation. We validated the model using in-flight data. Our model predicted the exhaust gas temperature (EGT) within 10 K over a wide range of cruise altitudes and ambient conditions and it also matched the flight recorder data for similar engine and aircraft types. We ran the model using climb and descent rates derived from flight radar data and engine performance limiters based on the Boeing 737-800 Flight Planning and Performance Manual (The Boeing Company, 2006) and Base of Aircraft Data (BADA) tables(Eurocontrol, 2010).

Results and Discussion

The ICAO-recommended method for estimating aircraft engine BC EIs has been the first order approximation version 3.0 (FOA3) that utilizes a correlation of BC mass concentration with SN (ICAO, 2011a). FOA3 is based on data from measurement campaigns of aircraft engine emissions (Wayson et al., 2009). Recently, an alternative correlation has been proposed that predicts up to a factor of 3 higher BC mass concentrations than FOA3 (Stettler et al., 2013b). However, our measured SN and BC mass concentrations corrected for thermophoretic loss agree well with FOA3 (Figure 2).

The data shown in Figure 2 were collected for one engine using the multi-orifice sampling probe as well as a single orifice probe in additional measurements at various thrust levels, mostly above 50%, and various test point durations. All the data points are well below the proposed

updated correlation. Stettler et al.(Stettler et al., 2013b) developed the correlation from SN and total PM mass measurement (instead of BC) of diffusion flame soot. Diffusion flame soot with GMD typical for modern jet engines (< 50 nm) even after thermal treatment may contain as little as 50% BC (Durdina et al., 2016). Thus, correlating total PM with SN, which depends on BC content ("blackness"), leads to an overestimation of the BC mass.

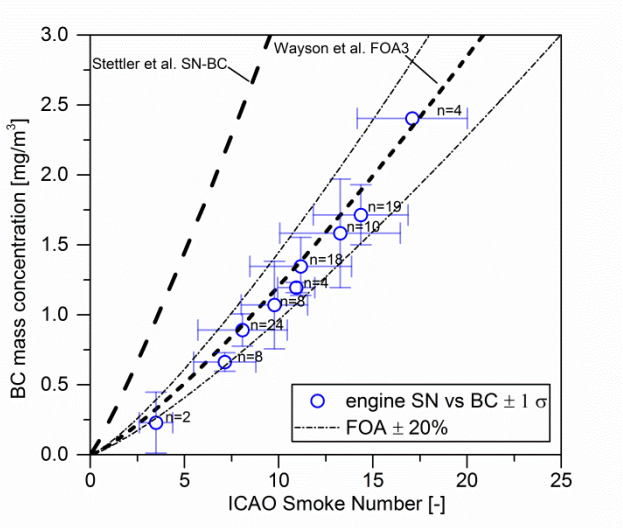

Figure 2: Correlations of BC mass concentration with the ICAO SN. The symbols represent averaged SN and BC mass concentrations at a given engine condition. The measured BC mass concentrations were corrected for dilution and thermophoretic loss as it will be required by the nvPM regulation. The error bars represent one standard deviation.

An improved SN-BC mass correlation can be developed only from standardized measurements of aircraft engine emissions because the PM emission characteristics change with engine power. Typically, BC mass concentration and GMD increase with engine thrust (here, from 10 nm at idle to 40 nm at take-off). SN depends on BC mass loading as well as on GMD as the filter paper used is more efficient for large particles (Stettler et al., 2013b). As engine manufacturers will report their nvPM certification data together with SN (as long as the old SN regulation stays in force), ICAO plans to update the FOA3 (Rindlisbacher and Jacob, 2016). The updated SN-BC mass correlation will be necessary for older out of production engines that are excluded from the nvPM emissions certification scheme but will remain in service for decades to come. For the SN range investigated here, the updated correlation will likely be close to FOA3.

The BC emission characteristics strongly depended on engine operating conditions (Figure 3a, b). The EIn peaked at minimum idle (lowest combustion efficiency), but EIm was extremely low due to the small particle size (GMD at the exit plane ~12 nm). The EIs were the lowest between 15 – 20% thrust (highest AFR), and from there on steeply increased with thrust (decreasing AFR). EIm peaked at maximum thrust, whereas EIn reached the maximum at ~65%. EIn decreased with further thrust increase likely due to particle coagulation within the engine. Such emission characteristics are typical for Rich-Quench-Lean (RQL) combustors, representative of most today's in-service jet engines worldwide.

The EIm and the BC mass emissions calculated for the LTO cycle were mostly overpredicted by methods using SN correlations and combustion models (Figure 3a, c). With respect to the results with nominal fuel (14.3 m% H), they overpredicted the BC mass emissions at taxi by up to a factor of 40. The FOA3 (Wayson et al., 2009) overestimated the low thrust emissions by up to a factor of 12 mainly due to the large uncertainties in the certification SN data (the maximum SN measurement error is estimated to be ± 3 SN (Wayson et al., 2009)). Almost 97% of the total BC mass was emitted during take-off and climb. Thus, any under- or overprediction for these phases has the biggest impact on the estimated total LTO BC emissions. The formation-oxidation (FOX) method (Stettler et al., 2013a) overestimated the total BC mass by up to a factor of 4. On the other hand, the improved FOX (ImFOX) method (Abrahamson et al., 2016) as well as the ICAO-recommended FOA3 underpredicted the BC mass at high thrust by up to

40%, which is a good estimate considering the uncertainties (we estimated 38% uncertainty for the EIm; Durdina et al. 2017). The approximative methods can be potentially improved as standardized BC mass emissions data become available but will remain applicable only to engines that emit maximum BC mass at take-off (FOX and ImFOX) and have measurable SN (SN correlations).

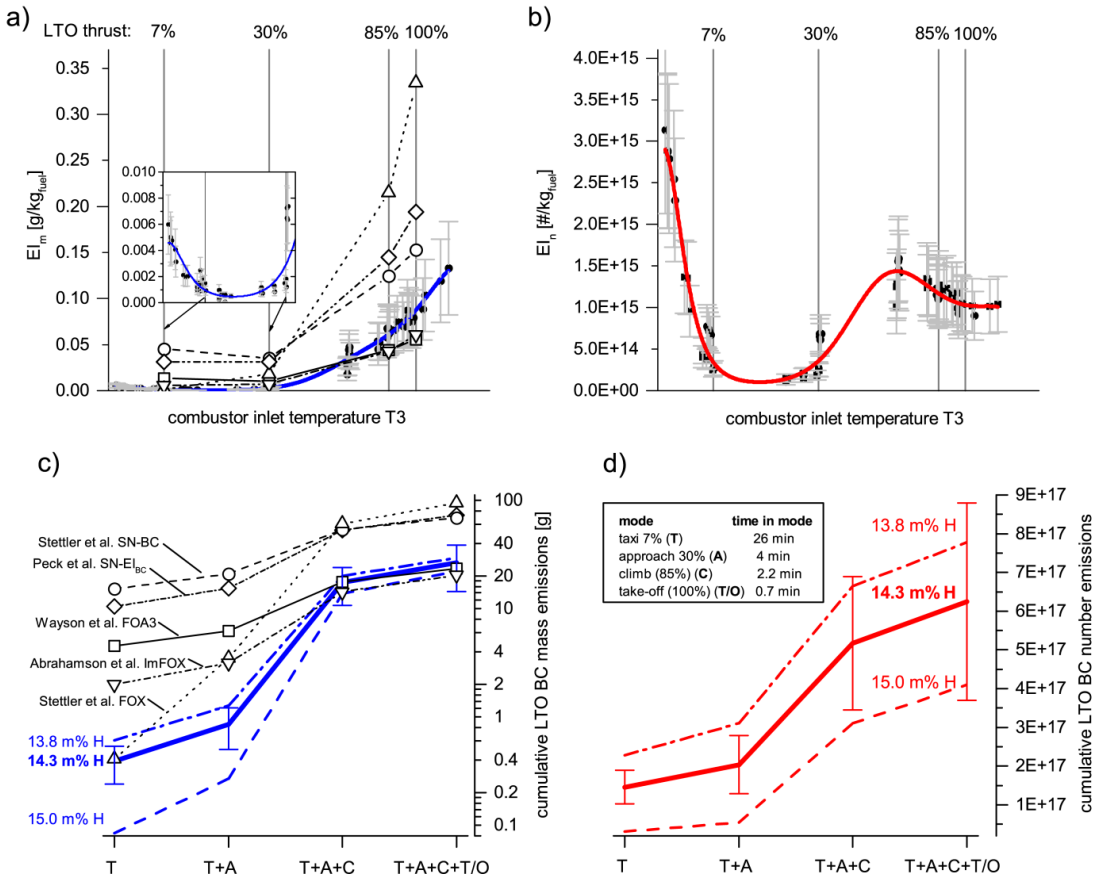

Figure 3: Emission indices of BC mass (a) and BC number (b), and emissions from the LTO cycle per aircraft (2 engines) in terms of BC mass (c) and BC number (d). The error bars represent the estimated EI uncertainty of 38% and 32% in terms of mass and number, respectively.

In contrast to the BC mass emissions, the BC number emissions at taxi constituted up to 30% of the total LTO emissions, depending on the fuel composition (Figure 3d). The fuel composition affects the BC emissions at low power the most. For example, the cumulative taxi and approach emissions with the high aromatics fuel (13.8 m% H) used in North America (Hadaller and Johnson, 2006) and low aromatics fuel (15.0 m% H), typical for a fuel blend of Jet A-1 with synthetic jet fuel (Hadaller and Johnson, 2006), differed by a factor of ~6. The fuel composition negligibly affected the total BC mass emitted from the LTO cycle. However, the total BC number emissions can be readily drastically reduced using fuel blends due to the high contribution of the taxi and approach modes, which would, in turn, improve the airport air quality.

An accurate assessment of the airport air quality is demanding because airport operations differ from the regulatory LTO cycle used for engine technology comparison both in terms of time and engine power used. Except in an emergency, pilots utilize less thrust than the engines are capable of producing. Operators use derated engines (electronically reduced rated thrust) and flexibly reduce take-off thrust as much as conditions permit to extend the engine service life and optimize the overall cost. Since the BC mass emissions of the engine type investigated here peak at maximum thrust, reduced take-off thrust diminishes the total BC mass emissions. For example, a Boeing 737-800 with engines derated by 15% would produce 35% less BC mass per standard LTO cycle. However, the total BC number emissions calculated for the derated engine would be 25% higher, because the taxi condition (7% of the derated take-off thrust)

corresponds to a lower power setting at which the EIn is 60% higher (Figure 3b). In practice, the taxi or idle thrust is lower than 7%. Compared to the LTO taxi setting, the fuel flow of an on-wing engine of a Boeing 737NG at idle with nominal bleed air extraction (cabin air conditioning) is ~10% lower.(Herndon, 2012) Since the EIn peaks at minimum idle, the actual taxi EIn may be up to an order of magnitude higher than at the LTO taxi setting. Thus, the regulatory LTO cycle may underestimate the actual BC mass and number emissions from busy airports with long taxi times.

The EIs at cruise were strongly affected by ambient conditions and fuel composition. For the nominal case (ISA; 35,000 ft altitude; Mach 0.8; 14.3 m% H), we determined EIm of 11 mg/kg fuel and EIn of 6.8×1014/kg fuel (Figure 4). When an aircraft flying with a constant thrust and Mach number encounters warmer air, the engines need to run at a higher rotational speed to compensate for the loss of thrust due to decreasing air density, and T3 and BC emissions increase. Cold air has the opposite effect (Durdina et al., 2017). The cruise EIs varied less due to ambient temperature (±10 K range) than due to fuel composition. The EIs varied with fuel composition by up to 50%, highlighting a possible reduction of aviation BC emissions and their climate impacts at cruise using low-aromatics fuels. These predictions are in line with recent airborne studies (ACCESS I and II campaigns) investigating effects of fuel composition on BC emissions using a similar engine type (Moore et al., 2017).

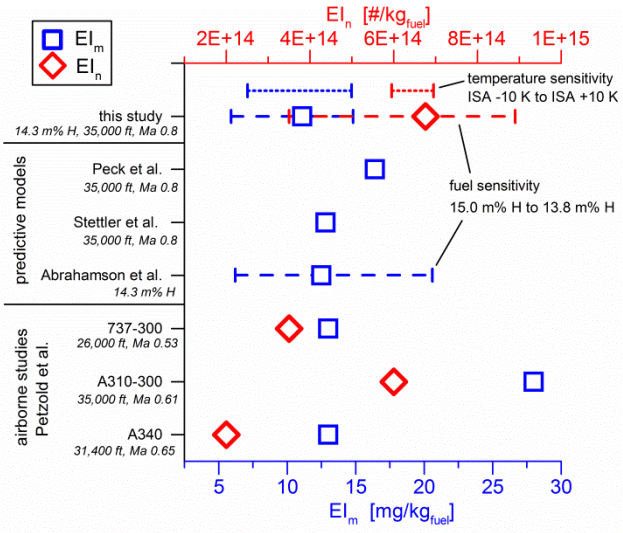

Figure 4: Comparison of cruise emission indices with chase plane studies and estimates obtained by predictive methods.

Our cruise BC estimates are in the range of EIs found during airborne studies of various types of passenger jets in the 1990s (Petzold et al., 1999) (Figure 4). However, those EIm and EIn were calculated from measured particle size distributions. Also, the measurements were done at lower altitude, speed, and weight to accommodate the chase plane. Therefore, the BC emissions were likely lower than at our nominal cruise condition. For example, for the flight conditions of the 737-300 in Figure 4 (26,000 ft and Ma 0.53) we obtained 30% lower fuel burn and EIm of just 3 mg/kg fuel.

The cruise EIm estimates compared to those calculated by previously published methods. The EIm estimates obtained with the methods of Peck et al.(Peck et al., 2013), Stettler et al. (FOX)(Stettler et al., 2013a), and Abrahamson et al. (ImFOX)(Abrahamson et al., 2016) for the fuel flow corresponding to cruise at 35,000 ft and Mach 0.8 were within 50% of our data. However, the method of Peck et al. and FOX predict cruise BC emissions by correcting their ground-based estimates, which we have shown to overestimate our measurements. Using our measured BC mass concentrations for their respective ground reference conditions decreased their cruise estimates by up to a factor of 10. ImFOX, on the other hand, is calibrated to cruise BC measurements of the predecessor of the engine tested here. The ImFOX method also uses fuel hydrogen content for scaling the BC mass concentration. It predicts a range of EIm

overlapping with ours but is limited only to ground and cruise, whereas our model can predict the engine performance parameters at any flight condition.

Since the Boeing 737 aircraft is used worldwide for a broad range of flight missions lasting from under one hour to up to eight hours, the emissions from LTO, climb to cruise altitude, and descent may represent a major fraction of the total emissions depending on the flight time (Figure 5). For a one hour flight, over 70% of the BC mass and number emissions came from the climb phase and over 25% dispersed under 3,000 ft altitude (LTO). The descent phase with engines at flight idle contributed less than 0.5% and 3% in terms of BC mass and number, respectively.With increasing flight time, the cruise BC mass and number emissions reached 50% of the total emissions after four and two hours, respectively. Thus, the climb can much contribute to the total BC emissions of short to medium-haul flights.

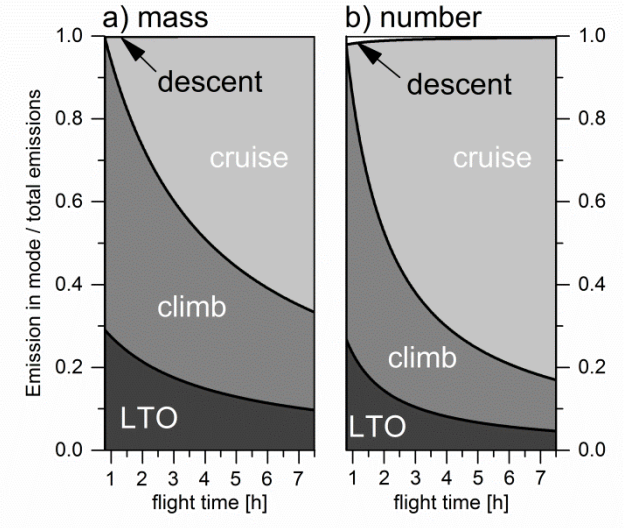

Figure 5: Ratio of the BC mass (a) and number (b) emissions per flight phase and the total emissions as a function of flight time (nominal fuel composition with 14.3 m% H). The flight time on the x-axis is the airborne time above 3,000 ft altitude.

The mission EIm (time-weighted arithmetic means of all flight phases) increased or decreased depending on the cruise EIm for a given fuel composition. The EIn, on the other hand, increased with flight time for all fuel composition cases. For the nominal fuel, the EIn increased from 5.15×10^{14}/kg for a one hour flight to 6.53×10^{14}/kg for a seven-hour flight. For the same interval, the mission EIm moderately decreased from 11.94 mg/kg to 11.20 mg/kg. These estimates are a factor of 2 to 3 lower than the mission EIs used for calculating global fleet emissions (38 mg/kg for the 1992 fleet (Petzold et al., 1999) and 25 mg/kg for the 2000 fleet(Lee et al., 2010)). Given the high number of in-service Boeing 737NG and other aircraft with similar engines (Airbus A320 family), our results are representative of the current fleet of single-aisle airliners (65% of all passenger aircraft (Airbus, 2015)).

The BC emissions per passenger-km of great circle distance decreased with flight time regardless of fuel composition (Figure 6). For the nominal fuel, the normalized BC mass and number emissions decreased with flight distance by up to a factor of 4 and 2, respectively. The drop was most significant in the first three hours of flight, and any longer flight only moderately decreased the emission rates. The range of per passenger-km emission rates increased when we factored in the fuel effects. A short flight using 13.8 m% H fuel produced up to a factor of 9 more BC mass and a factor of 5 more BC number than a long flight using fuel with 15.0 m% H.

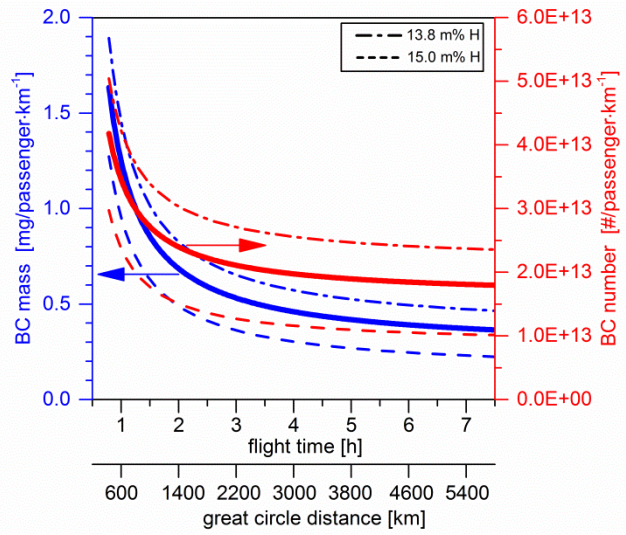

Figure 6: BC mass and number emissions per passenger (assuming 130 people on board of a 737-800 at 80% occupancy) and distance.

We took the ranges of BC emission rates per passenger-km and compared them with road vehicles (Figure 7). We assumed two car passengers and 30 bus passengers and used published data for various engine technologies (Giechaskiel et al., 2012; Hallquist et al., 2013). We note that the BC data for vehicles shown in Figure 7 were obtained with methods different from the nvPM standard methodology. The BC mass was determined by correcting the filter-based total PM mass using the reported upper estimate of the BC content for each vehicle type. The BC number concentration was measured with a particle size cut-off of 23 nm instead of 10 nm used for the aircraft engines. Regarding BC mass, the aircraft engine emissions were in the middle of the range reported for the various vehicle engine technologies (Figure 7a). For a short flight and 13.8 m% H, the BC mass emissions were comparable to a gasoline direct injected (GDI) car, which is characterized by relatively high particle emissions, and decreased with flight distance and increasing fuel hydrogen content to a level of a common port fuel injected (PFI) gasoline car. However, the BC number emissions were as high as a diesel car without a particulate filter (DPF) (Figure 7b). This assessment shows that the mass-based BC emissions per passenger-km of the engine type investigated are relatively low, whereas the number-based BC emissions are considerable. This finding is in line with the general emission characteristics of modern gas turbine engines that produce particles with small GMD and thus low BC mass emissions, but relatively high number-based emissions. At the same time, we note that although these findings are relevant for a large fraction of the current fleet, they would not apply to other engine types, e.g. with lean-burn and staged combustors.

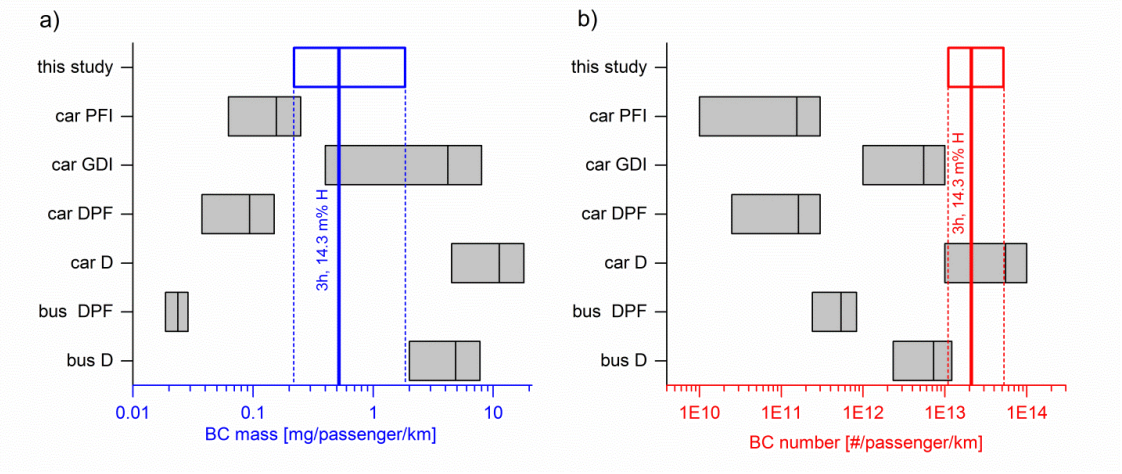

Figure 7: Comparison of the BC mass (a) and number (b) emissions per passenger-km. Vehicle emissions data were taken from Giechaskiel et al. and Hallquist et al. and normalized per two

car passengers and 30 bus passengers. The abbreviations for engine technology are: D – diesel without any emission control, DPF – diesel with a particle filter, PFI – gasoline port fuel injection, and GDI – gasoline direct injection. The solid vertical lines represent values for 3-hour flights and the nominal fuel composition.

Conclusions

In the near future, estimates of aviation BC emissions can be predicted more accurately using standardized BC measurement data. We have shown first such estimates of BC mass and number emissions for all flight phases of the most widely used airliner determined from certification quality data. We have provided updated emission indices for cruise as well as for the flight mission and looked at the sensitivities to fuel composition and ambient temperature. For the representative cruise at ISA conditions with nominal fuel, the determined mission EIm is half the estimate used for the BC emission rates of the global fleet in the year 2000 (Lee et al., 2010) and merely 13% of the average EIm reported by the FOX method for the 2005 fleet(Stettler et al., 2013a). Also, the LTO emissions determined here strongly contrast with recent studies that claim FOA3 to significantly underestimate BC mass emissions from aircraft turbine engines(Stettler et al., 2013a; Stettler et al., 2013b). We found a good agreement with the SN – BC mass correlation used in the FOA3. However, our data also suggest FOA3 may overestimate the mass-based emissions from taxiing aircraft by up to an order of magnitude. Since airports face regulatory limits on ambient PM mass concentration, they need better emission inventories and tools for implementing the best practices with respect to airport air quality. The question remains whether the BC mass concentration is a useful metric for that because it does not capture the considerable number of soot nanoparticles an aircraft turbine engine can emit at the detection limit of the current BC mass instruments while producing no visible smoke.

References

Abrahamson, J.P., Zelina, J., Andac, M.G., and Vander Wal, R.L. (2016). Predictive model development for aviation black carbon mass emissions from alternative and conventional fuels at ground and cruise. *Environmental science & technology, 50* (21), pp 12048–12055.

Airbus (2015). Global Market Forecast 2016-2036. http://www.airbus.com/company/market/forecast/.

Beyersdorf, A.J., Timko, M.T., Ziemba, L.D., Bulzan, D., Corporan, E., Herndon, S.C., Howard, R., Miake-Lye, R., Thornhill, K.L., Winstead, E., Wey, C., Yu, Z., and Anderson, B.E. (2014). Reductions in aircraft particulate emissions due to the use of Fischer–Tropsch fuels. *Atmospheric Chemistry and Physics*, 14, pp. 11–23.

Block, M.L., and Calderón-Garcidueñas, L. (2009). Air pollution. Mechanisms of neuroinflammation and CNS disease. *Trends in Neurosciences*, 32, pp. 506–516.

Brem, B.T., Durdina, L., Siegerist, F., Beyerle, P., Bruderer, K., Rindlisbacher, T., Rocci-Denis, S., Andac, M.G., Zelina, J., Penanhoat, O., and Wang, J. (2015). Effects of Fuel Aromatic Content on Nonvolatile Particulate Emissions of an In-Production Aircraft Gas Turbine. *Environmental science & technology*, 49, pp. 13149–13157.

Döpelheuer, A., and Lecht, M. (1999). Influence of engine performance on emission characteristics. In: *RTO Meeting Proceedings 14*. RTO/NATO: Hull, Canada.

Durdina, L., Brem, B.T., Abegglen, M., Lobo, P., Rindlisbacher, T., Thomson, K.A., Smallwood, G.J., Hagen, D.E., Sierau, B., and Wang, J. (2014). Determination of PM mass emissions from an aircraft turbine engine using particle effective density. *Atmospheric Environment*, 99, pp. 500–507.

Durdina, L., Lobo, P., Trueblood, M.B., Black, E.A., Achterberg, S., Hagen, D.E., Brem, B.T., and Wang, J. (2016). Response of real-time black carbon mass instruments to mini-CAST soot. *Aerosol Science and Technology*, 50, pp. 906–918.

Durdina, L., Brem, B. T., Setyan, A., Siegerist, F., Rindlisbacher, T., & Wang, J. (2017). Assessment of Particle Pollution from Jetliners: From Smoke Visibility to Nanoparticle Counting. *Environmental Science and Technology*, 51(6), 3534–3541.

Eurocontrol (2010). Base of Aircraft Data (BADA) EUROCONTROL's Aircraft Performance Model. http://www.eurocontrol.int/sites/default/files/field_tabs/content/documents/sesar/bada-overview.pdf. Accessed 10 September 2016.

Geiser, M., and Kreyling, W.G. (2010). *Deposition and biokinetics of inhaled nanoparticles*. Particle and fibre toxicology, 7, p. 2.

George, R.E., Nevitt, J.S., and Verssen, J.A. (1972). Jet Aircraft Operations. Impact on the Air Environment. *Journal of the Air Pollution Control Association*, 22, pp. 507–515.

Giechaskiel, B., Mamakos, A., Andersson, J., Dilara, P., Martini, G., Schindler, W., and Bergmann, A. (2012). Measurement of Automotive Nonvolatile Particle Number Emissions within the European Legislative Framework. A Review. *Aerosol Science and Technology*, 46, pp. 719–749.

Hadaller, O.J., and Johnson, J.M. (2006). World fuel sampling program. CRC Reports.

Hallquist, Å.M., Jerksjö, M., Fallgren, H., Westerlund, J., and Sjödin, Å. (2013). Particle and gaseous emissions from individual diesel and CNG buses. *Atmospheric Chemistry and Physics*, 13, pp. 5337–5350.

Health Effects Institute (2013). Understanding the health effects of ambient ultrafine particles. Health Effects Institute: Boston, Massachusetts.

Herndon, S.C. (2012). Measurement of gaseous HAP emissions from idling aircraft as a function of engine and ambient conditions. Transportation Research Board: Washington, D.C.

Howard, R., Hiers, R.S., Whitefield, P.D., Hagen, D.E., Wormhoudt, J.C., Miake-Lye, R.C., and Strange, R. (1996). Experimental characterization of gas turbine emissions at simulated altitude conditions.

Hsu, H.-H., Adamkiewicz, G., Houseman, E.A., Zarubiak, D., Spengler, J.D., and Levy, J.I. (2013). Contributions of aircraft arrivals and departures to ultrafine particle counts near Los Angeles International Airport. *Science of The Total Environment*, pp. 347–355.

Hudda, N., Gould, T., Hartin, K., Larson, T.V., and Fruin, S.A. (2014). Emissions from an international airport increase particle number concentrations 4-fold at 10 km downwind. *Environmental science & technology*, 48, pp. 6628–6635.

ICAO (2008). Environmental Protection. Volume II Aircraft Engine Emissions. ICAO: Montréal, Quebec.

ICAO (2011a-). Airport air quality manual (1st ed.). International Civil Aviation Organization: Montréal.

ICAO (2011b). Environmental Protection. Volume I Aircraft Noise (6th ed.). ICAO: Montréal, Québec.

ICAO (2016). ICAO Aircraft Engine Emissions Databank. http://easa.europa.eu/node/15672.

Johnston, H. (1971). Reduction of stratospheric ozone by nitrogen oxide catalysts from supersonic transport exhaust. *Science*, 173, pp. 517–522.

Kärcher, B., Möhler, O., DeMott, P.J., Pechtl, S., and Yu, F. (2007). Insights into the role of soot aerosols in cirrus cloud formation. *Atmospheric Chemistry and Physics Discussions*, 7, pp. 7843–7905.

Kärcher, B., and Yu, F. (2009). Role of aircraft soot emissions in contrail formation. Geophysical Research Letters, 36.

Keuken, M.P., Moerman, M., Zandveld, P., Henzing, J.S., and Hoek, G. (2015). Total and size-resolved particle number and black carbon concentrations in urban areas near Schiphol airport (the Netherlands). *Atmospheric Environment*, 104, pp. 132–142.

Kinsey, J.S., Dong, Y., Williams, D.C., and Logan, R. (2010). Physical characterization of the fine particle emissions from commercial aircraft engines during the Aircraft Particle Emissions eXperiment (APEX) 1–3. *Atmospheric Environment*, 44, pp. 2147–2156.

Kinsey, J.S., Hays, M.D., Dong, Y., Williams, D.C., and Logan, R. (2011). Chemical characterization of the fine particle emissions from commercial aircraft engines during the Aircraft Particle Emissions eXperiment (APEX) 1 to 3. *Environmental science & technology*, 45, pp. 3415–3421.

Kuhn, P.M. (1970). Airborne Observations of Contrail Effects on the Thermal Radiation Budget. *Journal of the Atmospheric Sciences*, 27, pp. 937–942.

Lee, D.S., Pitari, G., Grewe, V., Gierens, K., Penner, J.E., Petzold, A., Prather, M.J., Schumann, U., Bais, A., and Berntsen, T. (2010). Transport impacts on atmosphere and climate. Aviation. *Atmospheric Environment*, 44, pp. 4678–4734.

Lobo, P., Durdina, L., Smallwood, G.J., Rindlisbacher, T., Siegerist, F., Black, E.A., Yu, Z., Mensah, A.A., Hagen, D.E., Miake-Lye, R.C., Thomson, K.A., Brem, B.T., Corbin, J.C., Abegglen, M., Sierau, B., Whitefield, P.D., and Wang, J. (2015a). Measurement of Aircraft Engine Non-Volatile PM Emissions. Results of the Aviation-Particle Regulatory Instrumentation Demonstration Experiment (A-PRIDE) 4 Campaign. *Aerosol Science and Technology*, 49, pp. 472–484.

Lobo, P., Hagen, D.E., and Whitefield, P.D. (2011). Comparison of PM emissions from a commercial jet engine burning conventional, biomass, and Fischer-Tropsch fuels. *Environmental science & technology*, 45, pp. 10744–10749.

Lobo, P., Hagen, D.E., Whitefield, P.D., and Raper, D. (2015b). PM emissions measurements of in-service commercial aircraft engines during the Delta-Atlanta Hartsfield Study. *Atmospheric Environment*, 104, pp. 237–245.

Mazaheri, M., Johnson, G.R., and Morawska, L. (2011). An inventory of particle and gaseous emissions from large aircraft thrust engine operations at an airport. *Atmospheric Environment*, 45, pp. 3500–3507.

Miake-Lye, R.C., and Brem, B.T. From smoke to nanoparticles: international measurement campaigns for the establishment of a new nvPM regulation. In: *ICAO Environmental Report 2016*, pp. 89–92.

Moore, R.H., Thornhill, K.L., Weinzierl, B., Sauer, D., D'Ascoli, E., Kim, J., Lichtenstern, M., Scheibe, M., Beaton, B., Beyersdorf, A.J., Barrick, J., Bulzan, D., Corr, C.A., Crosbie, E., Jurkat, T., Martin, R., Riddick, D., Shook, M., Slover, G., Voigt, C., White, R., Winstead, E., Yasky, R., Ziemba, L.D., Brown, A., Schlager, H., and Anderson, B.E. (2017). Biofuel blending reduces particle emissions from aircraft engines at cruise conditions. *Nature*, 543, pp. 411–415.

Onasch, T.B., Jayne, J.T., Herndon, S., Worsnop, D.R., Miake-Lye, R.C., Mortimer, I.P., and Anderson, B.E. (2009). Chemical Properties of Aircraft Engine Particulate Exhaust Emissions. *Journal of Propulsion and Power*, 25, pp. 1121–1137.

Peck, J., Oluwole, O.O., Wong, H.-W., and Miake-Lye, R.C. (2013). An algorithm to estimate aircraft cruise black carbon emissions for use in developing a cruise emissions inventory. *Journal of the Air & Waste Management Association*, 63, pp. 367–375.

Peters, A., Veronesi, B., Calderón-Garcidueñas, L., Gehr, P., Chen, L.C., Geiser, M., Reed, W., Rothen-Rutishauser, B., Schürch, S., and Schulz, H. (2006). Translocation and potential neurological effects of fine and ultrafine particles a critical update*. Particle and fibre toxicology*, 3, p. 13.

Petzold, A., Döpelheuer, A., Brock, C.A., and Schröder, F. (1999). In situ observations and model calculations of black carbon emission by aircraft at cruise altitude. *Journal of Geophysical Research: Atmospheres*, 104, pp. 22171–22181.

Rindlisbacher, T., and Jacob, S.D. New particulate matter standard for aircraft gas turbine engines. In: ICAO Environmental Report 2016, pp. 85–88.

Rissman, J., Arunachalam, S., Woody, M., West, J.J., BenDor, T., and Binkowski, F.S. (2013). A plume-in-grid approach to characterize air quality impacts of aircraft emissions at the Hartsfield–Jackson Atlanta International Airport. *Atmospheric Chemistry and Physics*, 13, pp. 9285–9302.

SAE International (2013). AIR 6241 Procedure for the Continuous Sampling and Measurement of Non-Volatile Particle Emissions from Aircraft Turbine Engines.

SAE International (2016). AIR6504 Procedure for the Calculation of Sampling and Measurement System Penetration Functions and System Loss Correction Factors.

Stettler, M.E.J., Boies, A.M., Petzold, A., and Barrett, S.R.H. (2013a). Global civil aviation black carbon emissions. *Environmental science & technology*, 47, pp. 10397–10404.

Stettler, M.E.J., Swanson, J.J., Barrett, S.R.H., and Boies, A.M. (2013b). *Updated Correlation Between Aircraft Smoke Number and Black Carbon Concentration*. Aerosol Science and Technology, 47, pp. 1205–1214.

The Boeing Company (2006). Flight Planning and Performance Manual 737-800 CFM56-7B26 (3rd ed.). Flight Operation Engineering, Boeing Commercial Airplane Group: Seattle, WA, USA.

The Boeing Company (2016). 737 Model Summary Through August 2016. http://active.boeing.com/commercial/orders/displaystandardreport.cfm?cboCurrentModel=737&optReportType=AllModels&cboAllModel=737&ViewReportF=View+Report. Accessed 15 September 2016.

Unal, A., Hu, Y., Chang, M.E., Talat Odman, M., and Russell, A.G. (2005). Airport related emissions and impacts on air quality. Application to the Atlanta International Airport. *Atmospheric Environment*, 39, pp. 5787–5798.

Wayson, R.L., Fleming, G.G., and Iovinelli, R. (2009). Methodology to Estimate Particulate Matter Emissions from Certified Commercial Aircraft Engines. *Journal of the Air & Waste Management Association*, 59, pp. 91–100.

Yim, S.H.L., Lee, G.L., Lee, I.H., Allroggen, F., Ashok, A., Caiazzo, F., Eastham, S.D., Malina, R., and Barrett, S.R.H. (2015). Global, regional and local health impacts of civil aviation emissions. *Environmental Research Letters*, 10, p. 34001.

Zhu, Y., Fanning, E., Yu, R.C., Zhang, Q., and Froines, J.R. (2011). Aircraft emissions and local air quality impacts from takeoff activities at a large International Airport. *Atmospheric Environment*, 45, pp. 6526–6533.

Impact of alternative fuels on the non-volatile particulate matter mass and number emissions of an aero gas turbine

B.T. Brem[1], L. Durdina[1,2], M. Elser[1,2], D. Schönenberger[1,2], A. Setyan[1,2], S. Wyss[3], K Zeyer[3], M. Munoz[1], D. Schreiber[4], A. Liati[4], R. Haag[1], D. Rentsch[5], A. Fischer[3], J. Mohn[3], N.V. Heeb[1]*

[1]Empa, Laboratory for Advanced Analytical Technologies, CH-8600 Dübendorf, Switzerland, benjamin.brem@empa.ch
[2]ETH Zürich, Institute of Environmental Engineering, CH-8093 Zürich, Switzerland
[3]Empa, Laboratory for Air Pollution and Environmental Technology, CH-8600 Dübendorf, Switzerland
[4]Empa, Automotive Powertrain Technologies Laboratory, CH-8600 Dübendorf, Switzerland
[5]Empa, Laboratory for Functional Polymers, CH-8600 Dübendorf, Switzerland

Introduction

Particulate matter (PM) emissions have been identified as a pollutant that has major implications for human welfare and the global climate. Efforts to control and reduce PM emissions in the context of sustainable technology development put PM at the nexus of the prime societal issues of energy, air quality, and climate change. A detailed understanding of pollutant emissions is essential for the establishment of environmental regulation. Even very small amounts of incomplete combustion of hydrocarbon fuels results in emissions of ultrafine carbonaceous non-volatile particulate matter (nvPM) commonly referred to as soot or black carbon. These nvPM emissions are the subject of the 2016 revised ANNEX 16 Appendix 7 to the Chicago Convention which is the only internationally binding regulatory framework that facilitates an environmentally responsible civil aviation growth.

Low-carbon propulsion technology is advancing in all areas of mobility driven by concerns about the environment, climate change and supply security of fossil fuel feedstocks. The non-commercial aviation sector is currently experiencing the dawn of electrical propulsion, but lightweight megawatt-scale drive systems far more powerful and lighter than those currently available for on-road mobility are needed if electric propulsion is ever to succeed in commercial civil aviation. Therefore, the civil aviation sector, in particular intercontinental flights, will likely rely on the combustion of liquid hydrocarbon fuels for decades to come. Major stakeholders such as airlines, the international civil aviation organization (ICAO) and the international air transport association (IATA) consider alternative aviation fuels from non-fossil feedstocks as the most viable way to lower and offset the carbon intensity of the aviation sector. For example IATA envisions a carbon neutral aviation growth by 2020 and to cut aviation carbon emissions by 50% in 2050 in comparison to 2005 levels (IATA, 2011). This is a very ambitious goal when one takes into account that global jet fuel demand has risen steadily at a rate of 3% per year in the last decade and the commercial aircraft fleet is expected to double by 2036 mainly caused by the increased mobility demand in Asia (ICAO, 2015). Renewable alternative fuel can be produced from various feedstocks. Currently, five approved production pathways exist (Braun-Unkhoff, 2017): (1) The Fischer Tropsch Synthetic Paraffinic Kerosene (FT-SPK) process that directly synthesizes biomass or biogas into liquid; (2) Fischer Tropsch Synthetic Kerosene with Aromatics (FT-SKA), which adds an aromatic solvent to FT-SPK product; (3) The Hydroprocessed Esters and Fatty Acids (HEFA) process, which converts vegetable oils and animal fats into hydrocarbons by deoxygenation and hydroprocessing; (4) Synthetic Iso-paraffin from Fermented Hydroprocessed Sugar (SIP), (formerly referred to as Direct-sugar-to-Hydrocarbon (DSHC), converts sugars to a pure paraffin molecule using an advanced fermentation; and (5) the Alcohol to Jet SPK (ATJ-SPK), starts from an alcohol to produce a SPK (through dehydration of the alcohol to an olefinic gas, followed by oligomerization to obtain longer chain length liquid olefins, which are then hydrofractinated). FT and HEFA fuels are Synthetic Paraffinic Kerosene (SPK), consisting of linear or branched alkanes that can be blended at up to 50% in volume with petroleum-derived Jet A-1 fuel to obtain a drop-in fuel. FT-SPK were approved by the by the American Society for Testing and Materials (ASTM) in September 2009, and HEFA-SPK a July 2011. SIP was approved by ASTM in June 2014 for blending ratio up to 10% with conventional jet fuel (ASTM, 2015). Understanding the carbon intensity and the sustainability of the feedstocks of these fuels is of utmost importance and currently a topic of much debate. In addition, the combustion products of these fuels also need careful evaluation.

Complex interactions between fuel chemistry and engine operating conditions determine the non-volatile particulate matter (nvPM) mass and number emissions of aero gas turbines. The link between the chemistry and the sooting propensity of fuels has long been the focus of research (e.g. Richter *et al.*, 2000), and decreased levels of mono-aromatic and naphthenic hydrocarbons in the fuel have been associated with lower soot emissions (Schirmer *et al.*, 1972). Aromatic compounds promote the formation of large polycyclic aromatic hydrocarbons (PAH) and the subsequent soot nucleation and growth in fuel-rich pockets in the combustion zone (Bittner *et al.* 1978). A constant oxidation of these newly formed species takes place in parallel in lean zones; therefore, the engine operating conditions, in particular fuel to air equivalence ratio (FAR) and engine combustor temperature and pressure, are critical for the understanding of fuel effects.

A few aero gas turbine emission datasets indicate a clear thrust dependence of the fuel chemistry effects on nvPM emissions (e.g. Speth *et al.*, 2015). Under high FAR conditions, which concur with high temperatures and pressures in the combustor, fuel chemistry such as changes in the total aromatic content seems to play a minor role. At low FAR conditions, on the other hand, fuel effects on nvPM emissions are clearly distinguishable.

Objective and Significance

This work investigates the impact of alternative Hydro-processed Esters and Fatty Acids (HEFA) fuel originating from used cooking oil at a blending ratio ranging from 5 to 32% with standard Jet A-1 fuel on the emissions and properties of non-volatile particulate matter.

While similar emissions testing with alternative fuels has been performed previously on small gas turbines of helicopters and auxiliary power units, this study uses a modern technology and in-service, high-bypass turbofan. Furthermore, the emissions sampling is performed in a standardized testing facility with a standardized methodology (see next section).

Methods

An in-production, hi-bypass turbofan engine was leased for these measurements. The engine was in an airworthy condition at about three quarters of its expected service life before a major overhaul. Experiments were performed on five test days in April 2017. The tests started with dry motoring followed by a half hour warm-up sequence that included minimum idle, 7%, 65% and 85% relative static sea level thrust levels of 5 minutes each. After the warm-up an engine thrust matrix of 100%, 85%, 65%, 30%, 7% and minimum idle thrust levels running from high to low thrusts was performed. The engine thrust levels were controlled according to the engine combustor inlet temperature (T3, proprietary value) for which the engine manufacturer knows the corresponding thrust levels for international standard atmospheric (ISA) conditions (15 °C, 1013.25 hPa). While the actual thrust is a function of ambient temperature and pressure, manufacturers commonly control the engine by T3 during emissions certification tests and report ISA corrected emissions data. The ambient conditions during the five test days showed some variation with temperatures ranging from 2.2 to 17.6°C and the pressures from 967 to 977 hPa, respectively.

Standard Jet A-1 fuel available at Zurich airport and Jet A-1 fuel blended with HEFA originating from used cooking oil were used for the experiments. Three HEFA blending ratio of 5%, 10% and 32% were tested. The 5% and 10% blending ratio were achieved by using a custom built fuel mixing system that allowed the controlled injection of pure HEFA into the fuel line to the engine. This system has been used previously in other experiments where we blended different aromatic solvents with Jet A-1 fuel (Brem *et al.* 2015). In total 1000L of pure HEFA were used with this system. The 32% HEFA- jet A-1 blend was purchased on the free market from SkyNRG. The purchased 41,985 L of HEFA-Jet A-1 blend became mixed with the tank residue, lowering its original HEFA fraction of 44.4% v/v to 32% v/v when it was completely mixed in the tank. The fuel properties according to ICAO Annex16 Appendix4 were measured by our contractor Intertek. Table 1 shows a subset of the emission relevant fuel properties for the base fuel (Jet A-1), the 32% volume HEFA blend and the pure HEFA. The data for Jet A-1 and the HEFA blend are acquired from samples of the fuel line to the engine, whereas the pure HEFA data originate from the tank connected to the fuel doping system.

Table 1: Fuel properties

Property	Method	Unit	Jet A-1	32% v/v HEFA Blend	Pure HEFA
Tot. Aromatics	ASTM D 1319	% v/v	18.1	11.3	<5
Naphthalenes	ASTM D 1840	% v/v	0.79	0.53	0.01
Hydrogen Mass*	Empa	% m/m	13.8	14.25	15.3
Sulfur Content	ASTM D 5453	ppmm	490	350	<1
Smoke Point	ASTM D 1322	mm	22	24	>35
Density	ASTM D 4052	kg/m3	794.8	781.75	752.45
Spec. Energy	ASTM D 3338	MJ/kg	43.3	43.6	44.2

Table 1 indicates clear differences between the standard Jet A-1 and the HEFA blend. Mixing of HEFA reduces the total aromatics content, as well as the naphthalenes and the sulfur content of the fuel. On the other hand, mixing HEFA into Jet A-1 increases the hydrogen content and the smoke point of the blend. Lastly, the net specific energy is only affected minimally by the blending.

Fuel hydrogen mass content has previously been identified as a suitable parameter to link fuel properties with emissions (*e.g.* Brem *et al.*, 2015). In this study we used nuclear magnetic resonance spectroscopy in addition to the standard method. Figure 2 shows the determined hydrogen content for the NMR and the standard ASTM D5291 method as a function of fuel density. Fuel density is a good correlation variable for assessing the mixtures because it can be determined with a high precision that is better than 0.3 kg/m^3.

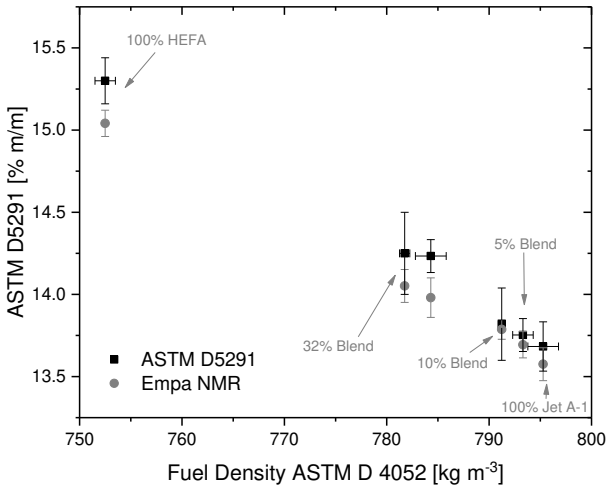

Figure 1: Fuel hydrogen mass content analyzed with the ASTM D5291 and the Empa NMR method as a function of fuel density. Error bars represent the standard deviation of the samples at the same doping level (n = 5)

The maximum change in hydrogen mass content was achieved using the 32% HEFA fuel blend which had an increased hydrogen mass content by 0.48% or 0.57% in comparison to the standard Jet A-1 fuel measured with the NMR method or the traditional ASTM D5291 method, respectively.

The experimental setup deployed in the campaign is shown schematically in Figure 2. Exhaust samples were extracted at the engine exit plane using a single orifice probe at a predefined location. Upstream of the dilutor box, the sample was split into three lines. This work focuses on the results of the standardized nvPM instrumentation. The “PM Line” included an eductor dilutor located as close as reasonably possible to the sampling inlet (5.2m). A suite of instruments were connected to the diluted 24.5m sampling line which included: a photo acoustic micro soot sensor (AVL MSS) for measuring the particle mass and an advanced particle counter (AVL APC) for the determination of the nonvolatile particle number. The MSS instrument was calibrated according to elemental carbon mass by the instrument manufacturer according to the standardized procedure (SAE, 2013). The APC instrument consisted of a first dilution step, a

350°C heated catalytic stripper with a sulfur trap and a second dilution step before a condensation particle counter (CPC). The counting efficiency of the CPC was determined to be 62% and 91% at 10 and 15 nm, respectively. In addition to the mass and number measurements a scanning mobility particle sizer (TSI 3936) was operated in parallel.

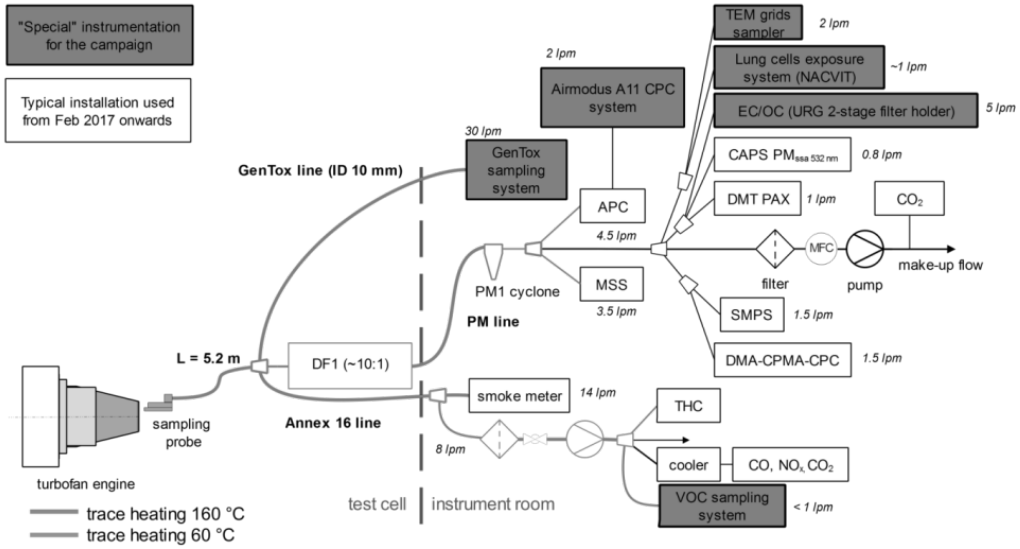

Figure 2: Emission sampling system at SR Technics

More details about the standardized instrumentation and sampling procedures can be found in the published standard (SAE, 2013)

Results and Discussion

Figure 3 shows the effect of HEFA fuel on the nvPM mass and number emissions as a function of engine thrust. The results shown are uncorrected instrument inlet concentrations. Tailpipe emissions are expected to be much higher due to line losses in particular for the nvPM number concentrations.

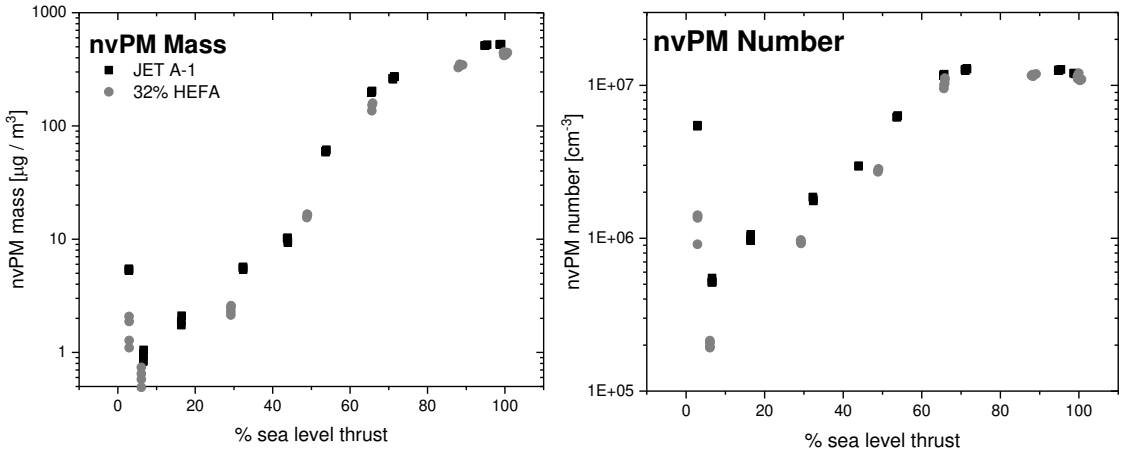

Figure 3: Fuel effect as a function of engine trust on the nvPM mass and number concentrations

A clear thrust dependence of the fuel effect is observed. At high engine thrust levels the emissions of the two fuels are nearly identical whereas at low thrust the emissions of the HEFA-blend can be a factor of two to four lower than for the conventional fuel. Similar thrust dependence has been observed in measurements of a helicopter gas turbine that was operated with different biofuel blends at cruise and idle thrust (DeWitt *et al.*, 2008). The explanation for

this thrust dependence in emissions is that the lower combustor temperatures and pressures at low thrust result in a less efficient combustion of the aromatic species in the rich-burn, quick-quench, lean-burn (RQL) combustor design employed in the engine studied. In such a combustor the fuel is initially burned and pyrolyzed at a FAR with a fast subsequent dilution to overall lean conditions where products of incomplete combustion are consumed. This combustor is optimized for low NOx, because generally lower flame temperatures can be achieved in comparison to traditional designs. Soot emissions are the product of complex reactions and depend on temperature, local FAR and residence time in both zones. While the soot oxidation in the lean zone is not affected by fuel chemistry, the fuel pyrolyzation and decomposition reactions in the rich zone are. The thrust dependence of the fuel effect could be explained by the change in local FAR within the rich zone that decreases from rich conditions at 100% thrust to near stoichiometric conditions at minimum idle. At 100% thrust the additional PAH formation due to the fuel aromatics as explained previously is miniscule in relation to the formation of fuel radicals and products of incomplete combustion that are occurring under such rich FAR conditions. At low thrusts, the FAR is near stoichiometric conditions and the fuel aromatics to PAH to soot reaction pathways become more relevant for the overall soot emissions. Therefore, in addition to the fuel aromatic content, the local FAR in the fuel rich zone is the determining variable for the soot emissions of this engine.

While the HEFA blend contains less total aromatics, the type of fuel aromatics plays an additional role as shown in our previous work (Brem *et al.*, 2015). Using the fuel hydrogen mass content as the correlating variable for the soot emissions is a potential way to account for these chemical differences in aromatic species. Figure 4 shows the reduction of the nvPM mass and number emission index (EI) of the 32% HEFA blend relative to the neat Jet A-1.

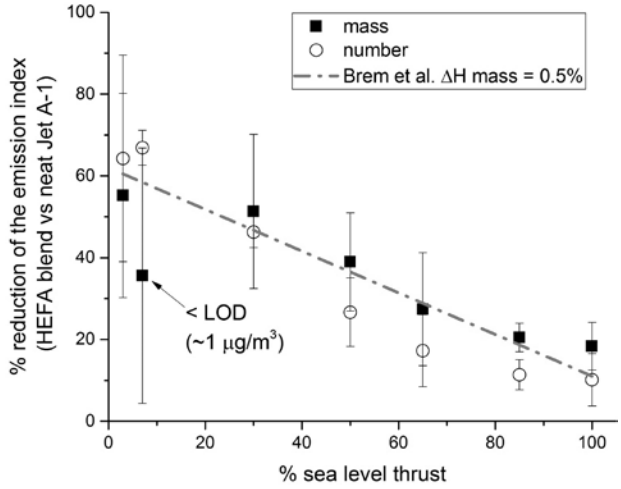

Figure 4: Fuel effect as a function of engine thrust on the nvPM mass and number concentrations

Our previous model: $\Delta Ei_x = (\alpha_0 + \alpha_1 \times F_{\%}) \times \Delta H$, provides a reasonable fit to the data as shown in Figure 4. In this model ΔEI_x corresponds to the percentage change in nvPM number EI, α_0 and α_1 are fitting parameters and corresponded to -119.31 and1.03, respectively, $F_{\%}$ is the percentage of engine thrust and ΔH is the change in hydrogen mass content. The model is comparable to the one used by Speth et al., 2015, that predicts changes in BC mass as a function of fuel aromatic content and engine thrust; however, our model uses the change in hydrogen mass content as one of the independent variables and can be applied to both nvPM mass and number.

Conclusions

This research fills an important gap in the understanding of the effects of alternative fuels on the nvPM mass and number emissions of an in-production aircraft gas turbine engine that is representative of the current fleet. Notable reductions in nvPM emissions by up to 70% are observed at low engine thrust when standard Jet A-1 is blended with 32% by volume of alternative HEFA fuel. This reduction is in line with previous work and the observed link between fuel hydrogen content and nvPM emissions also holds reasonably for alternative fuels.

Since emission reductions of alternative fuels are the greatest at low engine thrusts, potential improvements for local air quality could therefore be expected if such fuels become ubiquitous. However by far larger and more sustainable fuel feedstocks are required which are not in conflict with food security and the climate. To further accurately assess these implications, additional research should cover other engines equipped with more advanced optimized RQL combustor types. In addition, a complementary investigation should be carried out on engines equipped with novel lean burn combustors which might show a different sensitivity to fuels than shown here.

References

ASTM, 2015, Standard D1655.: http://www.astm.org. Accessed 14 Aug 2017

Braun-Unkhoff, M., Riedel, U. & Wahl, C. CEAS Aeronaut J (2017) 8: 167. https://doi.org/10.1007/s13272-016-0230-3

B. T. Brem, L Durdina, F Siegerist, P Beyerle, K Bruderer, T Rindlisbacher, S Rocci-Denis, M. G Andac, J Zelina, O Penanhoat, and J Wang, 2015, Effects of Fuel Aromatic Content on Nonvolatile Particulate Emissions of an In-Production Aircraft Gas Turbine Environmental Science & Technology 2015 49 (22), 13149-13157

Bittner, J. D.; Howard, J. B. Role of aromatics in soot formation Prog. Astronaut. Aeronaut. (U. S.) 1978,

DeWitt, M. J.; Corporan, E.; Graham, J.; Minus, D. Effects of aromatic type and concentration in Fischer– Tropsch fuel on emissions production and material compatibility Energy Fuels 2008, 22 (4) 2411– 2418

ICAO, 2015: http://www.icao.int/environmental-protection/GIACC/Giacc-3/Giacc3_Pres_IndustryGoals.pdf
Accessed: 21 Aug 2017

International Air Transport Association 2011: http://www.iata.org/whatwedo/Documents/economics/Industry-Outlook-Jun2012.pdf. Accessed: 20 Aug 2017

Richter, H.; Howard, J. B. Formation of polycyclic aromatic hydrocarbons and their growth to soot—a review of chemical reaction pathways Prog. Energy Combust. Sci. 2000, 26 (4) 565–608 DOI: 10.1016/S0360-1285(00)00009-5

SAE, 2013: Procedure for the continuous sampling and measurement of non-volatile particle emissions form aircraft turbine engines: Aerospace Information Report 6241; SAE Aerospace: Warrendale, PA, 2013.

Schirmer, R. M. Effect of Fuel Composition on Particulate Emissions from Gas Turbine Engines. In Emissions from Continuous Combustion Systems; Cornelius, W.; Agnew, W., Eds.; Springer: New York, 1972; pp 189– 210.

Speth, R. L.; Rojo, C.; Malina, R.; Barrett, S. R. H. Black carbon emissions reductions from combustion of alternative jet fuels Atmos. Environ. 2015, 105 (0) 37– 42 DOI: 10.1016/j.atmosenv.2015.01.040

Chemical composition and toxicological properties of ambient particles ($PM_{0.25}$) from near-airport and urban road traffic sites

F. Shirmohammadi[1], A. Mousavi[1], M. Sowlat[1], J.J. Schauer[2], R. He[3, 4], F.R. Cassee[3, 4], and C. Sioutas[1]*

[1]University of Southern California, Department of Civil &Environmental Engineering, Los Angeles, CA, USA
[2]University of Wisconsin-Madison, Environmental Chemistry &Technology Program, Madison, WI, USA
[3]National Institute for Public Health and the Environment (RIVM), Utrecht, The Netherlands
[4]Institute of Risk Assessment Sciences of the Utrecht University, Utrecht, The Netherlands

1. Introduction

Among various combustion sources of particulate matter (PM) in urban areas, accurate assessment of airport-related emissions and how they compare to other predominant PM sources such as traffic emissions is essential in understanding the impact of airports on air quality and human health. Airport operations have been shown to significantly contribute to increased PM levels in surrounding communities (Hudda et al., 2014; Westerdahl et al., 2008).

The main objective of this study was to quantify and compare the toxicological properties and chemical composition of ultrafine particles ($PM_{0.25}$) emitted from the Los Angeles International Airport (LAX) versus those emitted from traffic sources in Los Angeles. Airborne $PM_{0.25}$ were collected at 2 selected locations, one near the LAX airport and the other in central Los Angeles, downwind of the I-110 freeway at particle instrumentation unit of University of Southern California (USC). Oxidative potential and pro-inflammatory properties of the PM samples were measured by a variety of cellular and molecular in vitro assays, including an alveolar macrophage assay that quantifies the formation of reactive oxygen species (ROS) (Landreman et al., 2008) in cells, the ability of PM to deplete antioxidants such as ascorbic acid (AA) as well as the ability of PM to induce pro-inflammatory response, IL-8, on human bronchial cells.

2. Methodology

2.1 Sampling location and schedule

Size-fractioned PM samples were collected at two urban background locations in the Los Angeles area. One site represents urban mixed particles, emitted mostly from vehicular sources (Shirmohammadi et al., 2016; Sowlat et al., 2016) was in “central Los Angeles” approximately 150 m to the east and downwind of a major freeway (I-110), at the Particle Instrumentation Unit (PIU) of the University of Southern California. The other site was located near a residential area of Playa del Rey, north-east of LAX and about 600 m from the upper runway, at a South Coast Air Quality Management District (SCAQMD) monitoring station used for monitoring air quality around LAX. This site also experiences a prevailing onshore sea breeze, with no major PM sources upwind of the site other than airport emissions. There are two high schools nearby, which may introduce some bus emissions to the area. However, in general, traffic is very light in this area.

Four parallel Sioutas personal cascade impactor samplers (PCIS) (SKC, Inc., Eighty Four, PA, USA) operating at a flow rate of 9 lpm were used to collect the samples at each site (Misra et al., 2002). Three PCISs were loaded with 37-mm PTFE (Teflon) filters (Pall Life Sciences, 3-µm pore, Ann Arbor, MI) and the other PCIS with 37-mm quartz filters (Whatman International Ltd., Maidstone, England). Particles were collected in three different size ranges (<0.25 µm (quasi-UFP), 0.25–2.5 µm (accumulation) and 2.5–10 µm (coarse PM)) on a weekly basis (i.e., each weekly sample corresponded to 7 days of sampling), continuously from October to December 2016. The focus of this articles is on $PM_{0.25}$.

2.2 Chemical and toxicological analyses

Elemental and organic carbon (EC and OC) content were quantified by analyzing a 1 cm2 punch of the weekly quartz filters using the National Institute for Occupational Safety and Health (NIOSH) Thermal Optical Transmission (TOT) method (Birch and Cary, 1996). The remaining sections of the quartz filters were composited in two and three-week sets in order to supply

sufficient mass for the organic speciation analyses. Water-soluble organic carbon (WSOC) content was quantified using a Sievers 900 Total Organic Carbon Analyzer (Stone et al., 2008); organic species were quantified including Polycyclic Aromatic Hydrocarbons (PAHs), n-alkanes, hopanes, steranes and levoglucosan by Gas Chromatography/Mass Spectrometry (GC/MS). To measure the total elemental composition of the PM by high resolution (magnetic sector) inductively coupled plasma mass spectrometer (SF-ICPMS, Thermo-Finnigan Element 2), a section of each Teflon filter was digested in a mixture of 1.5 mL of 16 M nitric acid, 0.5 mL of 12 M hydrochloric acid and 0.2 mL of hydrofluoric acid using a microwave-aided (Milestone Ethos+) sealed Teflon bomb solubilization protocol.

ROS cell-based assay was conducted on Teflon filters, after extraction with 1.00 ml sterilized Milli-Q water; then the extracts were agitated for 16 hours at room temperature in the dark followed by 30 min of sonication. The ROS assays were then performed by exposing the rat alveolar cell line (NR8383, American Type Culture Collection) to the extracted aqueous PM suspensions.

The effects of particles on pro-inflammatory mediator proteins expression, IL-8 was also determined. 25µL of supernatants after 4h exposure and 20h recovery was analyzed for inflammatory cytokine expression (IL-8) using the Luminex multiplex kit (Millipore, Merck, German). For the IL-8 assay HBSS was used as the negative control.

The ascorbic acid (AA) assay was used to measure the capacity of ascorbic acid consumption of those particle samples, which determines the metal dependent redox activities. Briefly, each sample was measured in 4 wells with 2 wells containing 20µL of 2mM DTPA and the other 2 wells containing 20µL dH2O. All samples were incubated in a spectrophotometer (spectraMAX 190: Molecular Devices, Sunnyvale, USA) for 10 minutes at 37 °C. 20 µl of 2mM ascorbic acid was then added and measured by a microplate reader at 265 nm every 2 minutes for 2 hours. For the AA assay a blank filter extraction, 160 µL of domestic oil burning furnace (DOFA) suspension of 12.5 µg/ml and the dH2O were used as the blank, positive, and negative control, respectively.

2.3 Source apportionment by chemical mass balance (CMB)

A molecular-marker based source apportionment model (CMB software (EPA CMB v8.2)) was used to determine sources of PM0.25 organic carbon (OC) (Schauer et al., 1996). Chemically stable compounds that were detected in the samples, were selected as fitting species, including: EC, nonacosane, hentriacontane, tritriacontane, levoglucosan, 17α(H)-21β(H)-hopane, benzo(b)fluoranthene, benzo(k)fluoranthene, benzo(e)pyrene, indeno(1,2,3-cd)pyrene, benzo(ghi)perylene, vanadium (V), aluminum (Al), titanium (Ti) and calcium (Ca). Input source profiles considered in the model included diesel and gasoline motor vehicles (Kam et al., 2012; Liacos et al., 2012), biomass burning (Fine et al., 2004; Sheesley et al., 2007), vegetative detritus (Rogge et al., 1993), ship emissions (Agrawal et al., 2008; Rogge et al., 1997) and re-suspended dust (Schauer, 1998).

As described in (Shirmohammadi et al., 2017b), source contributions from aircraft emissions were determined indirectly from the “un-apportioned OC fraction”, defined as the residual difference between the measured OC and the sum of all identified primary source contribution estimates as a reliable source profile for jet engine exhaust emissions that includes chemically stable molecular markers from source to receptor was not found within the literature. In a companion paper, Shirmohammadi et al. (2017a) indicated a 2.5-fold larger contribution to daily emissions of EC from LAX airport (6.09 ± 0.41 kg/day) in comparison to the total daily EC emissions from the three adjacent freeways (2.39 ± 0.08 kg/day). As the gasoline and diesel input source profiles were also highly characterized by EC emissions, the EC concentration at LAX was modified using the aforementioned ratio in order to separate the mobile source factor from aircraft emissions in the CMB model. Therefore, EC from traffic emissions was estimated by dividing the measured EC concentration at LAX site by 3.5.

3. Results and discussion

3.1. PM0.25 mass concentration and chemical composition

The average $PM_{0.25}$ mass concentration was comparable at the two study locations with values of 5.05 ± 1.59 µg/m3 and 5.84 ± 2.46 µg/m3 at LAX and central Los Angeles, respectively.

Average OC and EC levels were slightly higher at central Los Angeles, which had values of 1.77 ± 0.65 µg/m3 and 0.64 ± 0.0.24 µg/m3, respectively, compared to the levels at LAX, which were 1.51 ± 0.41 µg/m3 and 0.59 ± 0.22 µg/m3, respectively. The slightly higher concentrations of EC and OC at the central Los Angeles site can be due to the fact that this site is impacted by several sources, particularly traffic emissions.

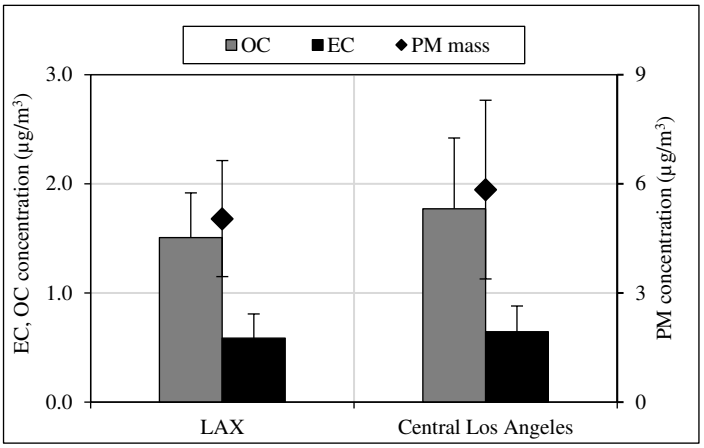

Figure 1. Mass concentration (µg/m3) of quasi-ultrafine PM (PM0.25) as well as carbonaceous species (Organic Carbon (OC), and Elemental Carbon (EC)) concentrations (µg/m3) at the two study locations. Error bars represent standard deviation.

The cumulative concentration of PAHs was higher at the central Los Angeles site (0.67 ± 0.30 ng/m3) in comparison to the LAX site (0.45 ± 0.16 ng/m3), highlighting the stronger PAHs emission source from the nearby freeway compared to the LAX site. While concentration of n-alkanes (C_{21}-C_{34}) was overall comparable at the central Los Angeles (7.02 ± 2.00 ng/m3) and LAX (6.01 ± 0.63 ng/m3) sties.

In the elemental fraction, S, K, Al, Fe, Na and Ca were the most abundant elements at both sampling sites. Among the indicated elements only Na, S, V and As had higher concentrations at LAX in comparison to central Los Angeles, whereas elements associated with abrasion of brake and tire wear (e.g. Ba, Cu, Fe, Mn, Pb and Zn (Pant and Harrison, 2013)) as well as re-suspended road dust (e.g. Al, Ca, K and Ti (Marcazzan et al., 2001)) were higher at the central Los Angeles site.

3.2 Toxicological analyses

The oxidative potential of $PM_{0.25}$, quantified by a macrophage reactive oxygen species was normalized by the total $PM_{0.25}$ mass to represent the intrinsic toxicity of the particles. Mass-normalized ROS activity was slightly higher at LAX (4600.93 ± 1516.98 µg Zymosan/mg PM) than central Los Angeles (4391.22 ± 1902.54 µg Zymosan/mg PM), however this difference was not statistically significant (p = 0.42).

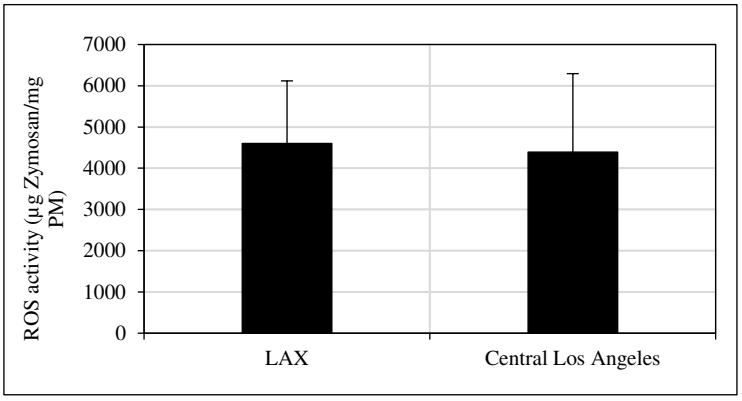

Figure 2. Oxidative potential of $PM_{0.25}$ at the two study locations normalized by the total PM mass (µg Zymosan/mg PM). Error bars represent standard deviation.

The induction of inflammatory mediator's protein expression (IL-8) in 16HBE cells were observed after 24h (4h exposure and 20h recovery), which was illustrated using ratios between samples and negative control (HBSS) (Figure 3). It was indicated that LAX samples induced higher IL-8 by 1.8-fold upregulation compared to USC samples which was 1.3-fold upregulation, respectively. Higher number concentration, a proxy for ultrafine particles, coupled with smaller mean particle size at the LAX site in comparison to the USC site was observed in a companion study (Shirmohammadi et al., 2017a). This can impart explain why the in-vitro assay showed LAX samples are more potent in inducing pro-inflammatory response while oxidative potential per PM mass resulted in comparable levels at the studied sites.

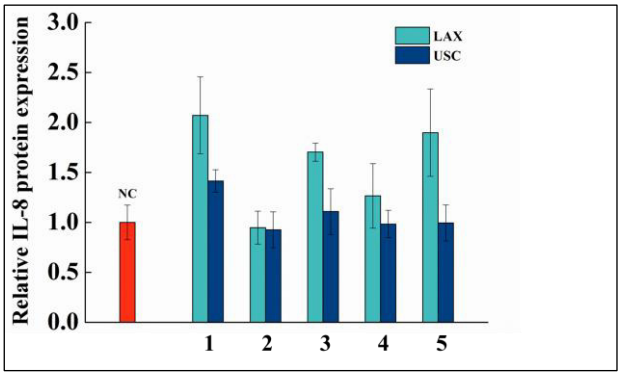

Figure 3. Pro-inflammatory effect in Human Bronchial Cells (IL-8 24h and 10 µg/mL), at sub-cytoxicity levels.

Similar to the ROS activity results AA assay also revealed higher per mass normalized values at USC compared to LAX.

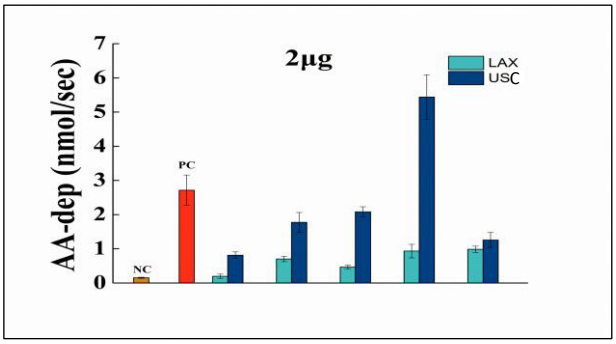

Figure 4. Oxidative potential measured by AA assay (per unit PM mass).

3.3 Chemical mass balance model (CMB) results

The CMB model output was robust for all sites, with an average R^2 of 0.95 and 0.97 for LAX and central Los Angeles, respectively. The central Los Angeles site, which is heavily impacted by the nearby freeway emissions, the mobile primary emissions (from light duty (LDV) and heavy duty vehicles (HDV)) were the dominant sources, contributing to about 82% of the total $PM_{0.25}$ OC (1.55 ± 0.12 µg/m3). The estimated mobile source contribution to $PM_{0.25}$ OC at the LAX site was 28% (0.44 ± 0.06 µg/m3). Biomass burning was the second largest contributor to measured OC, with about 18% (0.28 ± 0.04 µg/m3) and 14% (0.26 ± 0.05 µg/m3) at LAX and central Los Angeles, respectively. The $PM_{0.25}$ re-suspended road dust contribution to OC was estimated as 0.07 ± 0.01µg/m3 and 0.08 ± 0.01 µg/m3 at LAX and central Los Angeles, respectively. The contribution

of “other primary OC,” which is the residual difference between the measured OC and the sum of all source contribution estimates considered in the model, represents the primary contributions from sources not accounted for in the model. The SOC contribution was shown to be minimal (Shirmohammadi et al., 2017b), as discussed in Section 3.1.1 (12.5 ± 2.0% at LAX), and there are no other major sources at the LAX site; thus, the un-apportioned OC fraction can be largely attributed to the aircraft exhaust emissions.

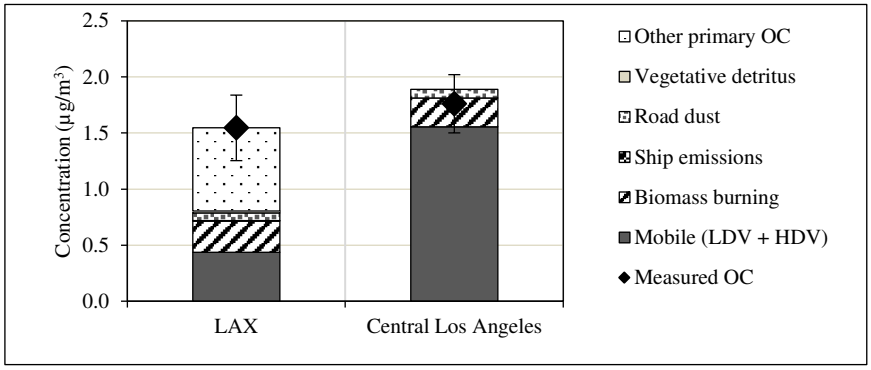

Figure 5. Average source contributions (µg/m3) to $PM_{0.25}$ OC derived from the CMB model.

3.4 Association of species with $PM_{0.25}$ oxidative potential

Bivariate Spearman correlation analysis of AA and ROS activity with that of chemical species revealed significant positive correlations between AA and OP and some traffic-related heavy metals (Mn, Fe, Cu Zn, Ba, and Pb, Spearman *R*: 0.70–0.85; $p < 0.05$); indicating the effect of these sources on PM0.25 oxidative potential at both sites. On the other hand, S and V, which were more abundant at LAX and are the dominant elemental components of aircraft emissions, were also strongly correlated with ROS activity (R > 0.70).

Species	AA	ROS_{4h}	Species	AA	ROS_{4h}
Traffic-related	**0.78***	**0.65***	Ba	**0.85***	**0.65***
Road dust	**0.65***	0.31	Zn	**0.89***	**0.67***
Fe	**0.85***	**0.65***	Cu	**0.87***	**0.71***
Ca	**0.77***	0.50	Ti	**0.71***	0.41
Mg	0.61	0.24	Pb	**0.70***	**0.67***
Al	0.52	0.18	Mn	**0.85***	**0.65***

* means values with $p < 0.05$.

Table 1. Spearman's correlation coefficients (*R*) between the oxidative potential measures (AA and ROS) and chemical species at LAX and USC samples (n=10).

References:

Agrawal, H., Sawant, A.A., Jansen, K., Wayne Miller, J., Cocker III, D.R., 2008. Characterization of chemical and particulate emissions from aircraft engines. Atmos. Environ. 42, 4380–4392. doi:10.1016/j.atmosenv.2008.01.069

Birch, M.E., Cary, R.A., 1996. Elemental Carbon-Based Method for Monitoring Occupational Exposures to Particulate Diesel Exhaust. Aerosol Sci. Technol. 25, 221–241. doi:10.1080/02786829608965393

Fine, P.M., Cass, G.R., Simoneit, B.R.T., 2004. Chemical Characterization of Fine Particle Emissions from the Fireplace Combustion of Wood Types Grown in the Midwestern and Western United States. Environ. Eng. Sci. 21, 387–409. doi:10.1089/109287504323067021

Hudda, N., Gould, T., Hartin, K., Larson, T.V., Fruin, S.A., 2014. Emissions from an International Airport Increase Particle Number Concentrations 4-fold at 10 km Downwind. Environ. Sci. Technol. 48, 6628–6635. doi:10.1021/es5001566

Kam, W., Liacos, J.W., Schauer, J.J., Delfino, R.J., Sioutas, C., 2012. Size-segregated composition of particulate matter (PM) in major roadways and surface streets. Atmos. Environ. 55, 90–97. doi:10.1016/j.atmosenv.2012.03.028

Landreman, A.P., Shafer, M.M., Hemming, J.C., Hannigan, M.P., Schauer, J.J., 2008. A Macrophage-Based Method for the Assessment of the Reactive Oxygen Species (ROS) Activity of Atmospheric Particulate Matter (PM) and Application to Routine (Daily-24 h) Aerosol Monitoring Studies. Aerosol Sci. Technol. 42, 946–957. doi:10.1080/02786820802363819

Liacos, J.W., Kam, W., Delfino, R.J., Schauer, J.J., Sioutas, C., 2012. Characterization of organic, metal and trace element PM2.5 species and derivation of freeway-based emission rates in Los Angeles, CA. Sci. Total Environ. 435–436, 159–166. doi:10.1016/j.scitotenv.2012.06.106

Marcazzan, G.M., Vaccaro, S., Valli, G., Vecchi, R., 2001. Characterisation of PM10 and PM2.5 particulate matter in the ambient air of Milan (Italy). Atmos. Environ. 35, 4639–4650. doi:10.1016/S1352-2310(01)00124-8

Misra, C., Singh, M., Shen, S., Sioutas, C., Hall, P.M., 2002. Development and evaluation of a personal cascade impactor sampler (PCIS). J. Aerosol Sci. 33, 1027–1047. doi:10.1016/S0021-8502(02)00055-1

Pant, P., Harrison, R.M., 2013. Estimation of the contribution of road traffic emissions to particulate matter concentrations from field measurements: A review. Atmos. Environ. 77, 78–97. doi:10.1016/j.atmosenv.2013.04.028

Rogge, W.F., Hildemann, L.M., Mazurek, M.A., Cass, G.R., Simoneit, B.R.T., 1997. Sources of Fine Organic Aerosol. 8. Boilers Burning No. 2 Distillate Fuel Oil. Environ. Sci. Technol. 31, 2731–2737. doi:10.1021/es9609563

Rogge, W.F., Mazurek, M.A., Hildemann, L.M., Cass, G.R., Simoneit, B.R.T., 1993. Quantification of urban organic aerosols at a molecular level: Identification, abundance and seasonal variation. Atmospheric Environ. Part Gen. Top. 27, 1309–1330. doi:10.1016/0960-1686(93)90257-Y

Schauer, J.J., 1998. Source contributions to atmospheric organic compound concentrations : emissions measurements and model predictions (phd). California Institute of Technology.

Schauer, J.J., Rogge, W.F., Hildemann, L.M., Mazurek, M.A., Cass, G.R., Simoneit, B.R.T., 1996. Source apportionment of airborne particulate matter using organic compounds as tracers. Atmos. Environ. 30, 3837–3855. doi:10.1016/1352-2310(96)00085-4

Sheesley, R.J., Schauer, J.J., Zheng, M., Wang, B., 2007. Sensitivity of molecular marker-based CMB models to biomass burning source profiles. Atmos. Environ. 41, 9050–9063. doi:10.1016/j.atmosenv.2007.08.011

Shirmohammadi, F., Hasheminassab, S., Wang, D., Schauer, J.J., Shafer, M.M., Delfino, R.J., Sioutas, C., 2016. The relative importance of tailpipe and non-tailpipe emissions on the oxidative potential of ambient particles in Los Angeles, CA. Faraday Discuss. 189, 361–380. doi:10.1039/C5FD00166H

Shirmohammadi, F., Lovett, C., Sowlat, M.H., Mousavi, A., Verma, V., Shafer, M.M., Schauer, J.J., Sioutas, C., 2018. Chemical composition and redox activity of PM0.25 near Los Angeles International Airport and comparisons to an urban traffic site. Sci. Total Environ. 610–611, 1336–1346. doi:10.1016/j.scitotenv.2017.08.239

Shirmohammadi, F., Sowlat, M.H., Hasheminassab, S., Saffari, A., Ban-Weiss, G., Sioutas, C., 2017. Emission rates of particle number, mass and black carbon by the Los Angeles International Airport (LAX) and its impact on air quality in Los Angeles. Atmos. Environ. 151, 82–93. doi:10.1016/j.atmosenv.2016.12.005

Sowlat, M.H., Hasheminassab, S., Sioutas, C., 2016. Source apportionment of ambient particle number concentrations in central Los Angeles using positive matrix factorization (PMF). Atmos Chem Phys 16, 4849–4866. doi:10.5194/acp-16-4849-2016

Westerdahl, D., Fruin, S.A., Fine, P.L., Sioutas, C., 2008. The Los Angeles International Airport as a source of ultrafine particles and other pollutants to nearby communities. Atmos. Environ. 42, 3143–3155. doi:10.1016/j.atmosenv.2007.09.006

Emission estimation based on cross-sectional traffic data

N. Tsanakas[1], J. Ekström[1] and J. Olstam[1,2]*

[1] Department of Science and Technology, Linköping University, Norrköping, SE-601 74, Sweden
[2] The Swedish National Road and Transport Research Institute, Linköping, SE-581 95, Sweden

1 Introduction

The continuous traffic growth has led to highly congested cities, with negative environmental effects, both related to air quality and climate change. According to the European Environment Agency, transportation remains a significant contributor to the total emissions of the main air pollutants, (EEA, 2016). Specifically, Nitrogen Oxides (NO_x), Carbon Oxide (CO) and fine particulate matter ($PM_{2.5}$) make up 32%, 23% and 8% of the total emissions, respectively. This vigorous impact of vehicular emissions to the urban environmental air quality, raises concerns over the impact of traffic on human health. Therefore, the effective implementation of emission reducing policies, such as traffic control measures or congestion pricing, becomes crucial for many European cities in order to meet the air quality standards and mitigate the human exposure to pollution. To quantify the environmental effects of these measures and demonstrate their effectiveness, a reliable estimation of pollutants concentrations through emission and dispersion modelling is needed.

The estimation of on-road emissions is an important step in an air quality analysis. Emission models are used for the on-road emission estimation, employing traffic related information on vehicle fleet, traffic state and traffic activity, as well as information on other local conditions such as road gradient and ambient temperature. In large urban areas, macroscopic or aggregated emission models are commonly applied, with COPERT (Gkatzoflias, et al., 2007) and HBEFA (Keller, 2010) being the two leading emission models in Europe. The models provide the user with the appropriate emission factor in grams of pollutant per vehicle kilometre. The most significant inputs to the two models are the traffic state and traffic activity, commonly expressed in terms of average speed and flow over a specific time period. The traffic state can be derived from traffic data obtained from sensor measurements (Beevers and Carslaw, 2005; Jing, et al., 2016; Johansson, et al., 2009), traffic models (Borge, et al., 2012; Namdeo, et al., 2002) (Wismans, et al., 2013) or combination between measurements and models (Batterman, et al., 2014; Gately, et al., 2017).

Although, due to the latest years extensive research on intelligent transportation systems, new types of traffic data are becoming accessible, stationary detectors remains a cost-efficient method of collecting traffic data. In the case of limited data, the temporal variations of traffic activity are commonly estimated by applying seasonal factors over the annual average daily traffic flow (AADT). This approach addresses the temporal variation of cross-sectional data, but not the issue of the data being discrete in space. Also, estimations based on AADT will not capture the severity of the most congested days. Using such estimates in air quality analysis, together with time and location specific background pollution and meteorology data, risks to increase the uncertainty of the actual concentration of pollutants. This study investigates the use of cross-sectional data in aggregated emission models and provides some additional insights into the use of AADT data. Additionally, it present alternative techniques for data processing which imply a more consistent level of aggregation of data on traffic, background pollution and meteorology in air quality analysis.

In order to obtain more accurate emission estimates from stationary detector data, we suggest the use a traffic state estimator that is based on filtering and smoothing techniques. Our aim is to obtain temporally and spatially continuous speed and flow fields, capable of capturing the variations in traffic conditions. The paper includes a comprehensive review on emission estimation approaches that use cross-sectional data, and provides a methodology for emission estimation, based on high accuracy traffic data, with limited computational burden, as well as limited number of sensors. Moreover, a comparison of the data processing techniques is presented.

The paper outlines as follows: Section 2 consists a literature review on methods for emission estimations based on sensors measurements. Section 3 provides a description of the methodology of estimating emissions from cross-sectional data by either using AADT estimation

techniques or more sophisticated traffic estimators. Section 4 presents the case study that is a part of the E4 motorway in Stockholm, and provides details about the data collection. The results are presented in Section 5 and finally Section 6 concludes the study and discusses future work.

2 Review of methods for estimating emissions from traffic measurements

Traditionally, aggregated emission models rely on output from macroscopic static traffic assignment models. However, many studies (Aguilera and Lebacque, 2010; Bai, et al., 2007; Bai, et al., 2007) have highlighted the difficulty of using such data as input to emission modelling, since the modelling of traffic dynamics is very limited in these models. Therefore, many researchers have moved towards the exploitation of the increasingly accessible data from traffic sensors, either to be used in combination with traffic models, or on its own as the basis for determining the emission factors. Traffic data are commonly collected and stored for aggregated time periods and homogenous road sections. Traditionally, there are mainly data available from fixed road side sensors, but today there might also be additional sources of data from vehicle probes. A comprehensive overview of traffic sensors and data collection techniques is given in Allström et al. (2016).

It is important to note that new sources of traffic data, such as automated vehicle identification (AVI) or global positioning systems (GPS), mainly contribute to the collection of speeds or travel times, and for the traffic volumes additional sources of data are needed. In Gately, et. al. (2017), emissions are estimated by assimilating GPS data with speed and flow data derived from stationary detectors or a traffic model. Nyhan, et al., (2016) use GPS trajectory data from taxis, available for a large urban area in Singapore, to estimate emissions. However, they conclude that Singapore is a special case, where taxi data can be used to infer general traffic pattern and the total volume, and this is not necessarily true for other urban areas. Jing, et al., (2016) estimate emissions for Beijing based on hourly average segment speed form GPS floating car data. The flow is derived from average speed using a functional relationship between speed and flow. Nevertheless, the floating car data covered only two weeks of data for the entire city. In Ryu, et al., (2015) GPS data is used to obtain speeds as input to the emission calculation, but only for specific vehicles and network routes. Therefore, although, this type of data has become accessible, it is not always possible to have a complete set of both speeds and flows. Additionally, these approaches can be expensive, require significant participation of the drivers and have privacy concerns (Jeng, et al., 2013). On the other hand, cross-sectional data, from stationary detectors (inductive loop detectors or radar sensors), are able to more efficiently provide comprehensive data. However, they only provide this data for specific points in the traffic network, and there is no information on what is happening in between two detectors. An example of the use of cross-sectional data for emission modelling purposes is given by Jeng et al. (2013), where a methodology for estimating emissions using inductive loop signature data to derive flow, space-mean speed and vehicle fleet composition is proposed.

Nevertheless, even in the case of stationary detectors, comprehensive data with respect to time and space, is not always economically feasible. For a reliable emission inventory, the available measured data can be extended in time and space using methods for missing data imputation. A common approach to estimate the traffic activity on a road with missing data or without permanent counting station, is to estimate the annual average daily traffic flow (AADT) and then multiply it by seasonal or hourly variation factors. The seasonal curves and the hourly traffic profiles can be computed with the help of permanent counting stations located in different parts of the network. The roads where those permanent stations are located, are then divided in categories. Each road with missing data, is assigned to the appropriate road category based on short-period measurements, usually using regression models or neural networks, and the corresponding seasonal curves are applied. A detailed review of the traditional methods for estimating missing counts can be found in Zhong et al. (2004). Commonly, only the traffic activity is estimated through AADT, and the traffic state (usually represented by the average speed) is then derived from other sources or through some analytical relationship between speed and flow. There are also examples where flow and capacity ratios are used (e.g. Trafikverket, 2012), to directly determine emission factors. These approaches, however, introduce the problem that there is not a one-to-one mapping between average speed and flows, and the same flow can be measured both at an uncongested (high speed) and a congested (low speed) traffic state.

To improve the accuracy of emission estimations, Fu, et al. (2017) attempt to extend short-period data to AADT using neural networks. Accordingly, Kholod, et al. (2016) derive AADT from video based detection at several locations and types of road while Coelho, et al. (2014) use manual

traffic counts to estimate AADT. In each one of these three studies, GPS data is used to obtain the average speed on each road segment or road category. Alternatively, Lindhjem, et al., (2012) use cross-sectional data to develop temporal allocation profiles for the traffic flow, and speed is derived as a function of flow (using the Bureau of Public Roads travel time functions). In many other recent studies (Batterman, et al., 2014; Batterman, et al., 2015; Basarić, et al., 2014) the estimation of emissions is based on AADT.

With respect to emission modelling, there are two main limitations with using AADT: (1) average conditions do not capture the most congested days, and (2) applying air quality analysis based on average traffic conditions but with specific background pollution and meteorology data risks to underestimate the actual concentration of pollutants. Moreover, all the aforementioned studies focused more on the seasonal, or within day variations, of flow, while average speed was considered as temporally constant. Additionally, cross-sectional measurements is by their nature discrete in space, and by taking the spatial average of such measurement along a homogeneous segment (Ferm and Sjöberg, 2015; Muller-Perriand, 2014), the spatial variations of speed and flow are neglected. Despite the fact that average segment speeds can predict travel times sufficiently accurate, their non-linear relationship to emissions could lead to considerable errors when estimating emissions.

3 Methodology

The ideal situation, for a comprehensive emissions analysis, would be to install permanent traffic sensors on every road segment in the network, obtaining faultless traffic data, 365-days around the year. However, due to limitations such as costs related to installation and maintenance, this is not feasible and actual data sets usually contain a significant percentage of missing data. In this study, we will use and evaluate different techniques for imputation, both in space and time, of traffic data for road segments and/or time periods for which measurements does not exist.

Section 3.1 presents the basis for applying aggregated emission models with traffic data. A methodology for extending data in time, based on annual average daily traffic flows (AADT) estimation is presented in Section 3.2. In order to compute total emissions, it is necessary to extend cross-sectional data in space, and two different approaches are presented in Section 3.3 (spatial averaging) and in Section 3.4 (spatiotemporal interpolation). Note that the spatiotemporal interpolation technique, extending data both in time and space, will provide the most detailed picture of the actual traffic state, assuming a dense deployment of cross-sectional detectors. Hence, the results based on the spatiotemporal interpolation technique is in the case study considered as the ground-truth, when comparing alternative approaches.

3.1 Aggregated emission modelling

In aggregated emission models, emissions are calculated by multiplying the traffic activity with the corresponding emission factor. Emission factors are functional relationships, computing the quantity of a pollutant that a vehicle emits per a specified distance driven. The basic aim of the emission models is to provide the user with the appropriate emission factor for each vehicle and road category. The emission factors can be obtained from dynamometer test or other experimental data corresponding to a specific driving cycle. A detailed review of the experimental approaches that have been used in practice for the development of emission factors can be found in Franco, et al. (2013).

Today, COPERT and HBEFA are the two leading aggregated emission models in Europe. COPERT is an average speed based model, and it is used by several European countries for officially reporting their national inventories of emissions from road transport. The COPERT emission factors depend on vehicle legislative class and road category, and are defined as continuous functions of average speed.

HBEFA is a traffic situation based model, developed on behalf of several European countries (Germany, Austria, Switzerland, Norway and Sweden). The HBEFA database includes emission factors as a discrete function of vehicle legislative class, road category and traffic situation. Traffic situations are defined by indicative flow and speed levels, and HBEFA emission factors rely on the four traffic situations: Free flow, Heavy, Congested, and Stop and go. The road categories are divided by road environment (rural and urban), speed limit and road type (Motorway, Trunk road/ Primary, Distributor/ Secondary, Local/ Collector, Access/ Residential).

In average speed based models (e.g. COPERT) the emission factors are directly determined as a function of speed. The application of a traffic situation based model (e.g. HBEFA), instead, requires definition of the traffic situation in measurable terms. Commonly, average speed and/or flow is used for this. In this paper we will solely base the traffic situation on speed thresholds, and thus, the emission factors can be regarded as function of speed as well in this case. For future reference, $e^p(v)$ will denote the emission factor (in grams per vehicle kilometre) for pollutant *p* as function of speed v (in kilometres per hour).

3.2 Annual average daily traffic

Based on data from permanent stations, here referred as permanent traffic counters (PTC), a time (day/season) variation factor can be computed, describing the average daily flow for a specific type of days and road segment in proportion to the annual average daily flow (AADT). This factor can include characteristics related to specific type of days (e.g. weekdays and weekends) and to seasons (e.g. months).

However, since PTCs can be installed only at some sites of the traffic network, short period traffic counts (SPTC) are commonly available for the rest of the network, providing data for shorter time periods (e.g. weeks or months). The main aim of this method is to predict the AADT for every SPTC site based on the time variation factor derived from a PTC located in the same road category.

For every PTC site α, the AADT can easily be computed, just by finding the mean of the annual daily flow. A key issue is then to group the days of the year into clusters, and group PTCs into road categories, for which we expect the time variation factor to be similar. This can be done using methods such as the k-means clustering (Hartigan and Wong, 1979) or fuzzy C-means clustering (Bezdek, et al., 1984). A common grouping of days is to cluster based on day of week and month of the year. Let I denote the set of road categories, and for a specific road category group $i \in I$, C_i denotes the set of sites belonging to this category. Let J be the set of day clusters. For road category $i \in I$ and day cluster $j \in J$, the time variation factor can be computed as

$$f_{i,j} = \frac{1}{|C_i|} \sum_{\alpha \in C_i} \frac{q_{j,\alpha}^{ADT}}{q_{\alpha}^{AADT}}, \tag{1}$$

where $q_{j,\alpha}^{ADT}$ is the average daily flow at site s for day cluster j, and q_{α}^{AADT} is the annual average daily flow at site s.

The next step is to assign the SPTC sites, to one of the road categories and estimate their average annually flow. This can for instance be done using Artificial Neural Networks (Gastaldi, et al., 2013) or regression models (Zhong, et al., 2004). Once a SPTC site, β, is assigned to a road category group i and the average annually flow, q_{β}^{AADT}, is defined, the average daily flow for the day cluster j can be estimated as

$$q_{j,\beta}^{ADT} = q_{\beta}^{AADT} \cdot f_{i,j} \,. \tag{2}$$

Depending on the use of the AADT, it may be necessary to also include an hourly factor. Emissions are sensitive to temporal traffic variation, and as highlighted in Batterman et al. (2014), they should be estimated in a daily and in an hourly level. As discussed in Tsanakas et al. (2017), one hour is a sufficiently short period to capture the emission estimation effects from traffic temporal variations. The hourly pattern can also be determined from the PTC sites, and can be included in the clustering analysis (Ha and Oh, 2014) and at the estimation procedure as proposed in (Gastaldi, et al., 2013). Therefore, for every road category i, and day cluster j, the hourly factor can be computed as

$$g_{i,j,h} = \frac{1}{|C_i|} \sum_{\alpha \in C_i} \frac{q_{j,h,\alpha}^{HT}}{q_{j,\alpha}^{ADT}}, \tag{3}$$

where $q_{j,h,\alpha}^{HT}$ is the hourly average flow for hour h, on day cluster j, at site α. Using the hourly factor together with estimated AADT and time variation factor, hourly average flows can be computed for all SPTC sites:

$$q_{j,h,\beta}^{HT} = q_{j,\beta}^{ADT} \cdot g_{i,j,h} \,. \tag{4}$$

However, for a comprehensive emission estimation, together with the flow, the temporal variation of speeds should also be included. If we assume that the same type of data as flow from the PTC sites is available also for the average speed, following the same methodology, the corresponding annual average daily speed (AADS) can be calculated. The final output of the method is a coherent set of hourly average speeds $V_{j,h}^{HT}$ and flows $Q_{j,h}^{HT}$, for every h hour of the j day of the year.

3.3 Spatial aggregation methods

Cross-sectional data from stationary detectors needs to be extended in space, before an aggregated emission model can be applied. A common approach for extending the measurements to network links, is to assume that the traffic conditions are homogenous for the whole length of a link, referred to this study average homogenous segment (AHS) approach.

Assume, that S_a is the set of the sensors, s, located in the homogenous link a. Let l_a be the length of link a, and let $V_{j,h,s}^{HT}$ and $Q_{j,h,s}^{HT}$ be the hourly mean speed and flow, of each sensor s. Then, the total emissions, $E_{j,h,a}^{p}$, of pollutant p, during day j and hour h, at link a, can be expressed as

$$E_{j,h,a}^{p} = e^{p}\left(\frac{1}{|S_a|}\sum_{s\in S_a} V_{j,h,s}^{HT}\right)\cdot\frac{1}{|S_a|}\sum_{s\in S_a} Q_{j,h,s}^{HT}\cdot l_a \tag{5}$$

Alternatively, one can assume that each sensor has an area of influence (AOI). This area could, for instance, be the half of the distance between two adjacent sensors. This can easily be achieved by defining link segments so that there is exactly one sensor at each segment. Assume that the sensors s are consecutively numbered based on the their longitudinal position x_s. Then, the total emissions, $E_{j,h,s}^{p}$, of pollutant p, during day d and hour h, at area of influence of sensor s, can be expressed as

$$E_{j,h,s}^{p} = e^{p}\left(V_{j,h,s}^{HT}\right)\cdot Q_{j,h,s}^{HT}\cdot\frac{(x_{s+1}-x_s)+(x_s-x_{s-1})}{2}. \tag{6}$$

3.4 Spatiotemporal interpolation

To obtain a better description of the traffic conditions, including spatial and temporal variations, a traffic state estimator can be applied. Here, the traffic state estimator is based on the spatiotemporal interpolation and smoothing method suggested and described in Treiber & Helbing (2002) and Treiber and Kesting (2013). The adaptive smoothing method (ASM), fully reconstructs the speed and flow field, by both estimating temporally missing data and filling the spatial gaps between stationary sensors. The output of the interpolation is a complete speed $V(x,t)$ and flow $Q(x,t)$ fields as a function of the discretised space and time intervals x, t. In practise there is a need to discretise, because of both computational burden and emission modelling issues. Regarding the latter, an aggregated emission model should be applied on stable traffic conditions, for which the driving cycles can be expected to be valid. Thus, $V_{x,t}$ and $Q_{x,t}$ will denote the discretised speed and flow measurements.

The interpolation method relies on a discrete convolution, with a symmetric exponential function as the weighted kernel, ϕ_0, operating actually as a low-pass filter, smoothing temporal variation and spatial fluctuations. More specifically, the method considers that all the traffic perturbations are propagating either downstream, in free traffic conditions, with a wave speed c_{free}, or upstream, in congested conditions, with a wave speed c_{con}. Assume that $z(x_i, t_j)$, is the value of

the z traffic variable (in our case speed and flow) counted by the stationary sensor i, at position x_i and time t_j, where j denotes the the index of the aggregation time intervals. At each position x and time t, two linear anisotropic low-pass filters $z_{free}$and z_{con} can be computed as

$$z_{free}(x,t) = \frac{\sum_i \sum_j \phi_0\left(x_j - x, t_j - t - \frac{x - x_i}{c_{free}}\right) \cdot z(x_i, t_j)}{\sum_i \sum_j \phi_0\left(x_j - x, t_j - t - \frac{x - x_i}{c_{free}}\right)} \tag{7}$$

and

$$z_{con}(x,t) = \frac{\sum_i \sum_j \phi_0\left(x_j - x, t_j - t - \frac{x - x_i}{c_{con}}\right) \cdot z(x_i, t_j)}{\sum_i \sum_j \phi_0\left(x_j - x, t_j - t - \frac{x - x_i}{c_{con}}\right)}. \tag{8}$$

The Kernel $\phi_0$is given by

$$\phi_0(x,t) = exp\left(\frac{|x|}{\sigma} - \frac{|t|}{\tau}\right), \tag{9}$$

where σ and τ are the spatial and temporal smoothing widths. Finally, the estimated traffic variable consists a superposition of the two low-pass filters

$$z(x,t) = w(x,t)\, z_{con}(x,t) + \big(1 - w(x,t)\big) z_{free}(x,t), \tag{10}$$

with $w(x,t)$ being a weight factor $0 \leq w \leq 1$.

In Wang et al. (2011) the ASM is used in order to estimate emissions from cross-sectional data. They use the ASM based estimation to derive vehicle trajectories for a microscopic emission model. However, the ASM output can be also applied together with an aggregated emission model. As we have mentioned, x and t are associated with the discretised space and time respectively. Given that k and m are the lengths of each space and time interval, in metres and minutes respectively, at each section x and time interval t, emissions can be computed as

$$E_{x,t}^{p} = e\big(V_{x,t}\big) \cdot Q_{x,t} \cdot k \cdot m/(1000 \cdot 60). \tag{11}$$

4 Case study

4.1 Introduction to the study area

For this study we will use traffic data from the city of Stockholm. There are approximately 1500 fixed detectors located all around Stockholm, mainly installed on motorways and arterials (Figure 1 (a)). Almost two third of them are radar sensors, located at the E4 motorway, consisting an integral part of a Motorway Control System on the main highway that passes through Stockholm (Allström, et al., 2011).

In our study, a 23.4 km long section, which is part of the E4, is considered (Figure 1 (b)). The segment consists of 83 network links, which are grouped, based on geographical and other characteristics such as the number of lanes, into 19 homogeneous road segments. Moreover, 92 detector stations, are located every 250-300 metres along this segment of the motorway. Each detector station includes a number of radar sensors equal to the number of lanes at the location that collect one-minute aggregated time mean speed and traffic flow data. Here we use the mean flows and speeds across all lanes, from the first of January 2016 to last of December the same year.

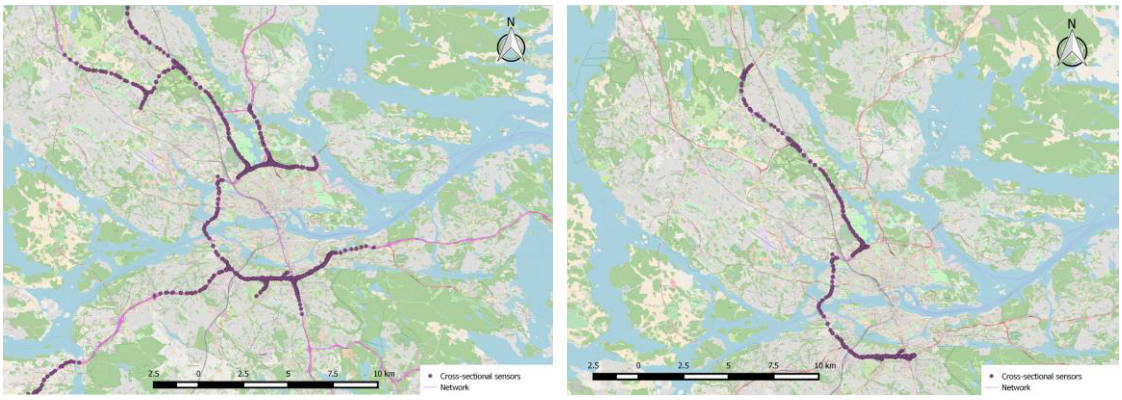

Figure 1: (a) Location of fixed detectors (b) The highway segment under consideration.

4.2 Emission model

In this study we use the HBEFA emission factors, adapted for Swedish roads and traffic conditions. Using information of the Swedish vehicle fleet composition, we calculate the weighted average of the emission factors corresponding to different vehicle classes, fleet mixture and mileage. Finally, our estimations are based on emission factors for the five pollutants HC, CO, NO_x, CO_2 and tail pipe PM and for two different road types (urban motorway with a speed limit of 90 and 70 km/h).

The only existing official description (Trafikverket, 2012), of how the traffic situation in HBEFA should be determined for road in Sweden, is based on the demand to capacity ratio of each network link. This is relevant when applying HBEFA with output from a static traffic model, which allows flow to exceed capacity. However, in our case, where HBEFA is applied together with measured traffic data rather traffic model outputs, we transformed the demand to capacity ratio thresholds to speed thresholds similarly with the method presented in Tsanakas et al. (2017). Finally, we use linear interpolation to describe the emission factors as continuous functions, $e^p(v)$, of average speed v for every pollutant p. The purpose of doing this is to reduce the effect of small changes in speed, on the emission estimation.

4.3 Seasonal, hourly factors and AADT estimation

As mentioned in Section 4.1, each detector station collect one-minute aggregated time mean speed and traffic flow data, which can be used as input for HBEFA emission factors determination. However, the nature of the HBEFA emission factors are not instantaneous, they rather represent an aggregated situation, relying on average conditions during a driving cycle. Hence, the temporal interval of one minute, may not be a sufficiently long interval to describe a HBEFA traffic situation. For this reason, we aggregate the sensors outputs, speed and flow, temporally over an hour. The temporal interval of one hour is more representative for the HBEFA traffic situations and at the same time the speed variations and the demand fluctuations can be sufficiently caught (Tsanakas, et al., 2017).

The flow and the speed data are then aggregated over one hour, and the average hourly data availability for the 92 sensors and the for whole 2016 is 89.9 %, with a 14.4 % standard deviation, the highest data availability for a sensor is 98.2 %, while the lowest 27.4 %. For 38 of the 92 detector stations we managed to create complete AADT and AADS data, and hence the associated to these stations sites are considered as the PTC sites, α, while the corresponding to the remaining 54 detector stations, sites are assumed to be the SPTC, β.

For the grouping of the PTC sites, the Fuzzy C-means algorithm (Bezdek, et al., 1984) is used, similarly to Gastaldi et al. (2013). However, the Fuzzy C-means algorithms requires the optimal number of clusters as input, and for the evaluation of the number of clusters we use the pseudo-F statistic criterion (Calïnski and Harabasz, 1974). Finally, the optimal number of road groups is found to be 3, $|I| = 3$, with respect to both speed and flow. The resulting time variation factors,

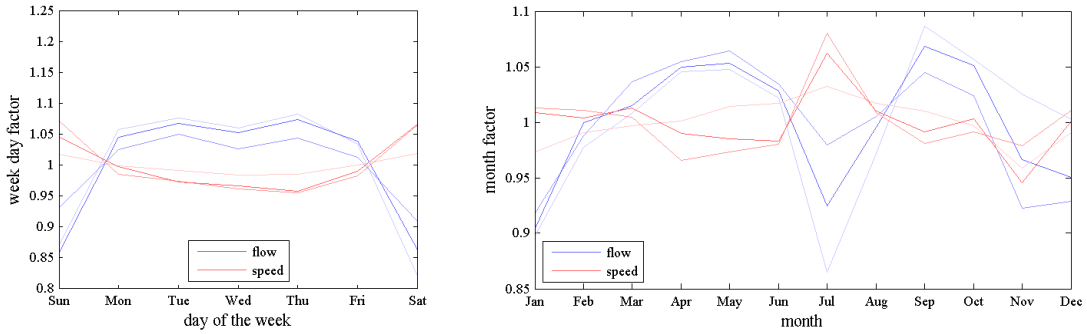

Figure 2: Seasonal factors (a) week day (b) month. The shades of blue and red are associated with different road groups.

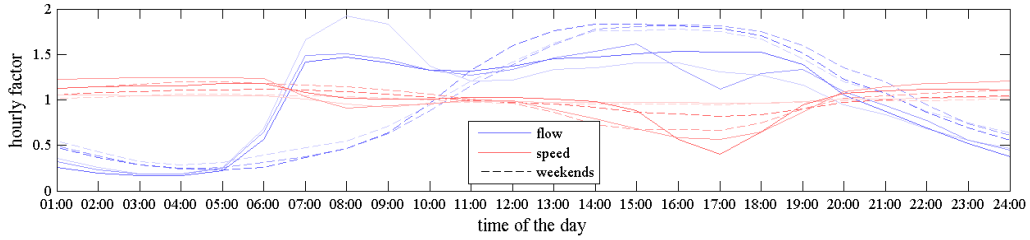

Figure 3: Flow and speed hourly factors, for the different road groups.

$f_{i,j}$ are illustrated by Figure 2, while Figure 3 shows the hourly factors, $g_{d,i,h}$ for each road group i, weekdays and weekends respectively.

For each one of the SPTC sites, β, the annual average daily traffic, $q_{\beta,i}^{AADT}$, is estimated through linear regression, and finally the SPTC site is assigned to a specific road group. The same methodology is used for the estimation of the annual average speed. Finally, the average hourly values that are missing for each detector station and traffic variable are estimated by using the equations (2) and (4).

4.4 Reconstruction of speed and flow filed using the ASM

Figure 4 illustrates the sensors outputs for a typical day of 2016. Note the cross-sectional nature of data and the lack of traffic situation information between sensors. By applying the ASM, based on equations (7), (8), (9) and (10), we can obtain a continuous field, in space and time, of the traffic variables (Figure 5). Finally, emissions for five pollutants are estimated, based on the reconstructed field and using equation (11) with $k = 100$ metres and $m = 5$ minutes. The resulting emissions are illustrated in Figure 6 for NO_x and CO.

5 Results

In this section we will present results for two different cases. The first case considers that the full radar sensors' data is available for the 2016, while the second one assumes that a significant part of the data is missing. For both cases the emissions of the five pollutants were estimated based on the three approaches described in Section 3.

Case 1 (full data): This case considers the complete dataset provided by the radar sensors during 2016. The data availability for the SPTCs is for this case high (84.5 %), resulting in an accurate AADT estimation. Table 1 presents the annual total emissions for the road segment under consideration, based on the three different approaches.

Assuming that ASM provides a complete and reliable space-time field of speed and flow capturing the spatial and temporal variations in traffic conditions, the resulting emission estimates using this method and the full dataset are regarded that represent the ground-truth. In order to evaluate the

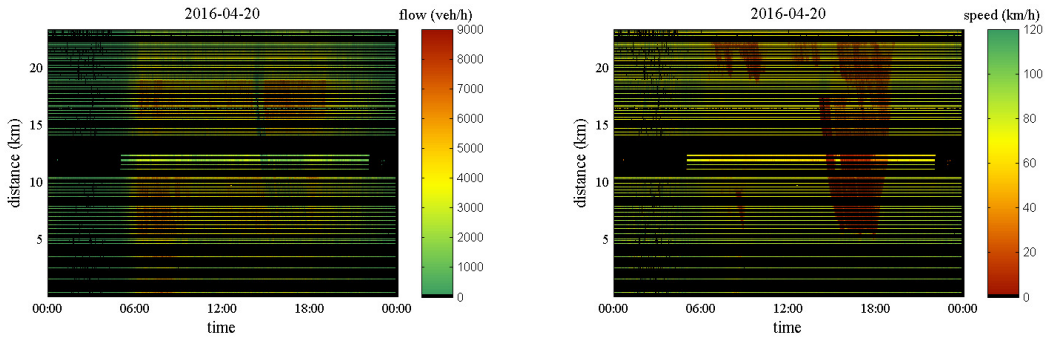

Figure 4: Cross-sectional data from stationary detectors (a) flow, (b) speed.

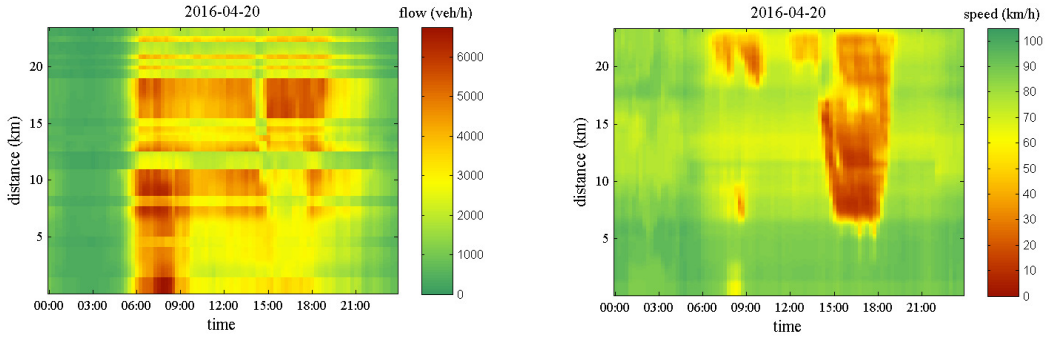

Figure 5: ASM reconstructed field (a) flow, (b) speed.

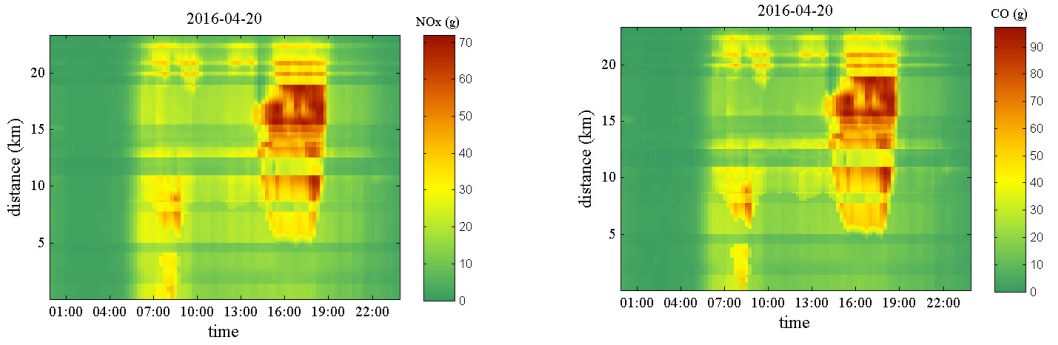

Figure 6: Emission estimation (grams per 100 metres and 15 minutes) for the ASM reconstructed field (a) NO_x, (b) CO.

accuracy of the other two approaches the resulting emissions by these approaches are compared to the emissions estimated based on the ASM data. In Table 1 we notice that at an annual level the differences between the approaches are relatively small, mainly because of the high data availability. However, considering specific days, the differences are high, Table 2 presents the mean, the standard deviation, the minimum and the maximum percentage difference among the 366 days of 2016, between the two approaches (AADT+AHS and AADT+AOI) and the ground-truth for the three pollutants (HC, CO and NO_x) where we noticed the highest differences.

Although, at an annual level the differences between the approaches are not so vital, at a daily level the overestimation could reach to 25.2 % while the underestimation to 22.9 %. However, due to high temporal availability of data, the differences mainly arise due to the dissimilar way of spatially aggregating the cross-sectional data. The spatial allocation of annual emissions, per 100 metres, is illustrated by Figure 7. Despite the fact that the whole segment's annual estimated emissions do not significantly differ between the three approaches, according to Figure 7 their spatial allocation crucially changes. Emissions have local effect and their exact location is important both from a dispersion modelling and from a pedestrians, cyclist and local inhabitants exposure effect point of view.

Case 2 (reduced data): In this case the available data is significantly reduced, by leaving only two weeks counts for 64 sensors. The average sensors' data availability is diminished to 26.3% associated with a standard deviation of 39%. The number of the PTC is reduced from 38 to 14,

Table 1: Annual emissions for case 1.

Case 1: full data	Tones of pollutant emited				
	HC	CO	NO_x	CO_2	PM
ASM	10.500	120.07	103.60	$6.1492 \cdot 10^4$	1.6084
AADT+AHS	10.390	118.80	102.29	$6.0662 \cdot 10^4$	1.5873
AADT+AOI	10.554	120.05	103.35	$6.1283 \cdot 10^4$	1.6016

Table 2: Percentage difference with the ground-truth, at a day level for the case 1.

Case 1	Percentage difference with ground-truth											
	mean			Standard deviation			min			max		
	HC	CO	NO_x	HC	CO	NO_x	HC	CO	NO_x	HC	CO	NO_x
AADT+AHS	-1	-1.1	-1.3	2.9	2.8	2.5	-13.3	-12.0	-11.3	17.2	18.4	14.2
AADT+AOI	0.5	-0.1	-0.2	3.4	3.3	2.7	-22.9	-11.9	-10.9	25.1	25.2	18.8

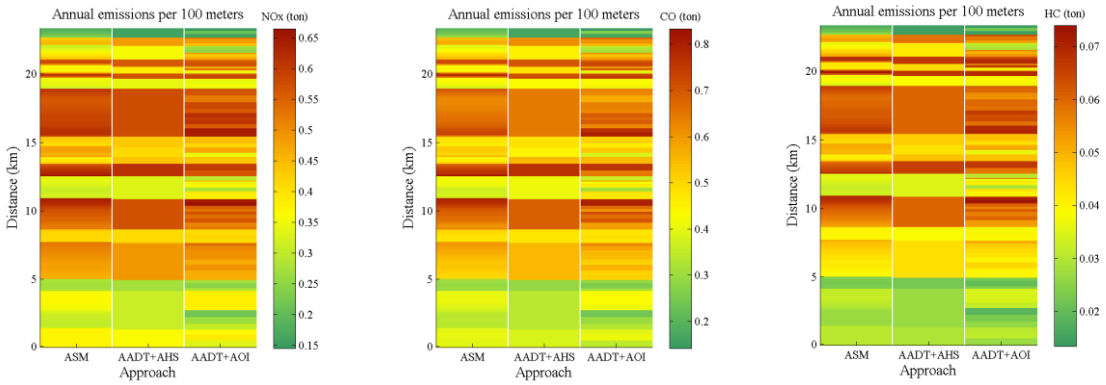

Figure 7: Spatial per 100 metres allocation of the annual emissions considering the case 1, and for the pollutants (a) NO_x, (b) CO, (c) HC.

while the data availability for the STPC sites is declined to 13.5%. For most of the STPC, the assignment into the road groups and the AADT estimation is based on limited measurements with a two weeks duration. Table 3 presents the resulted annual estimated emissions for the three approaches related to this second case, while Table 4 presents the daily variation of the differences.

The level of annual differences between the three approaches and the ground-truth, for this case is again not very high. However, considering the results presented in Table 4, ASM seems to have a better performance when the data is reduced, especially at a daily level. Concerning the other two methods, both of them but especially the AADT+AOI approach, tend to overestimate the total annual emissions compared to the ground-truth. Nevertheless, the most significant difference between the two methods and the ground-truth relies on the temporal, at a day level, variations of the annual emissions.

Figure 8 and Figure 9 illustrate the estimated emissions of CO and NOx, respectively, considering the case 2 (reduced data) versus the ground-truth for each of the three approaches. The results demonstrate that the estimated seasonal curves cannot efficiently capture the traffic variations and consequently the magnitude of the emitted pollutants for some extreme days (either intensely congested or days with sparse traffic). On the contrary, ASM, being capable to estimate the propagation of traffic perturbation, performs better with limited input data.

Table 3: Annual emissions for case 2.

Case 2: reduced data	Tones of pollutant emited				
	HC	CO	NOx	CO2	PM
ASM	10.423	118.59	102.41	$6.0852 \cdot 10^4$	1.5871
AADT+AHS	10.617	121.74	104.74	$6.2139 \cdot 10^4$	1.6251
AADT+AOI	10.292	123.88	106.33	$6.3030 \cdot 10^4$	1.6471

Table 4: Percentage difference with the ground-truth, at a day level for the case 2.

Case 2	Percentage difference with ground-truth											
	mean			Standard deviation			min			max		
	HC	CO	NO_x	HC	CO	NO_x	HC	CO	NO_x	HC	CO	NO_x
ASM	-0.8	-1.3	-1.2	1.9	2	1.8	-5.2	-6.6	-5.1	4.2	3.7	3.1
AADT+AHS	1.1	1.4	1.1	14.5	13.7	11.3	-22.9	-20.0	-16.4	115.8	115.9	93.21
AADT+AOI	3.4	3.2	2.6	16	14.8	11.9	-20.7	-17.9	-14.8	132.7	128.3	101.4

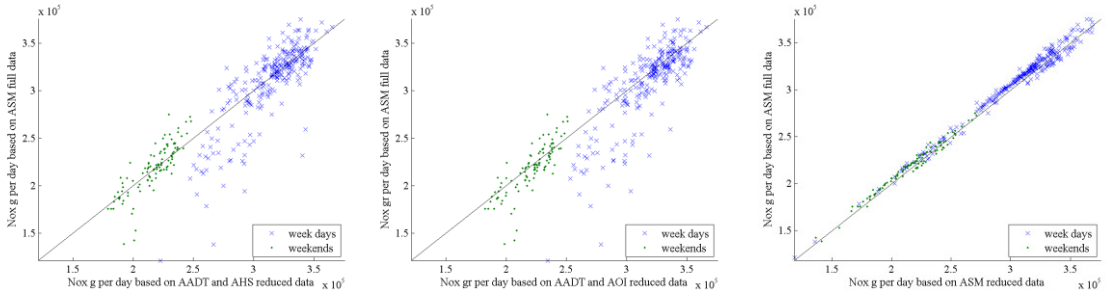

Figure 8: CO estimates based on the three different approaches versus the ground-truth.

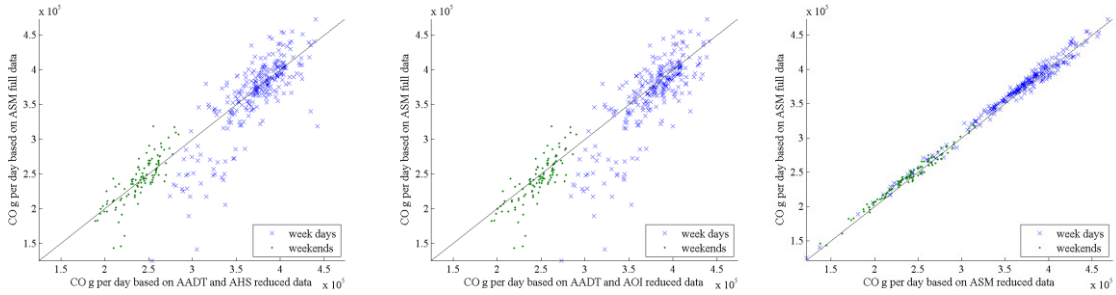

Figure 9: NO_x estimates based on the three different approaches versus the ground-truth.

Table 5: The effect of ASM aggregation level.

Case 2: reduced data	Percentage difference with ASM 100/15						
	HC	CO	NOx	CO2	PM	Computational time	Required memory
ASM 130/25	0.2903	0.4382	0.3078	0.2911	0.3061	-65.178	-52.759
ASM 150/30	0.1240	0.3541	0.2746	0.2784	0.3031	-75.892	-65.170
ASM 160/40	0.0111	0.2831	0.3738	0.4091	0.4293	-83.928	-74.883
ASM 180/50	0.4362	0.7062	0.6888	0.7070	0.6957	-88.392	-81.688
ASM 200/90	1.0132	1.4913	1.8053	1.9365	1.9266	-96.735	-85.445

It is important to notice here that although ASM had a better performance, the computational time and the required computer memory, remain an issue, since they are significantly higher compared to the other two approaches. The computational time of ASM, can be influenced by the input data size, but mainly depends on the length of the space and time discretisation intervals k, m. For that reason, we experiment with different sets of spatiotemporal aggregation values. The accuracy and the efficiency of the aggregation is evaluated based on the emission estimation results. Our most detailed estimation, is based on 100 metre segments and 15 minute time periods (ASM 100/15), and is also associated with the results presented in Table 1 and Table 3 . By gradually increasing the aggregation level, we examined the effect on computational time, data size and annual emissions estimates. The first column in Table 5 describes the considered alternatives regarding the spatial (metres)/temporal (minutes) aggregation levels. The rest columns contain the values of the percentage differences between each alternative and the ASM (100/15).

We can conclude that by modifying the aggregation level, the magnitude of the estimated emissions is not drastically changed, while the computing time and the required memory are significantly decreased. If we compare the estimated emissions from ASM 160/40 to the ground-truth (ASM 100/15 full data), the total annual emissions are underestimated from 0.65% to 1.63% depending on the pollutant, while the standard deviation of this underestimation between the 366 days of the year ranges from 1.7% to 2.2%. Therefore, the ASM even with longer space and time intervals can accurately fill the required for an emission modelling, spatiotemporal gaps of the case's 2 reduced data.

6 Conclusions and future work

Since road emissions is an important contributor to the total emissions of the main air pollutants, their estimation should be accurate, in order to evaluate air pollution mitigation strategies. Emission models are used for this purpose, providing emission factors based on vehicle fleet mixture, road type and traffic activity. The installation of stationary detectors is a cost-efficient method of collecting the traffic activity. However, a temporally comprehensive data set is not always economical feasible for every road of a network and cross-sectional measurements is by their nature non-continuous in space.

Traditionally, during emission estimation analyses, the temporal variations of traffic are estimated by the application of seasonal factors over an estimated AADT, while the spatial variations are aggregated by considering homogeneous segments. Since, from an emission estimation perspective, traffic spatiotemporal variations are a crucial factor, in this study we suggest the use of a traffic state estimator (ASM) to generate inputs for the emission model. The traffic estimator having as input cross-sectional data, provides a continuous time and space field of the traffic variables. The resulted by the ASM approach emission estimates are then compared to the corresponding estimates derived from the aforementioned traditional approaches.

For the first case, with high temporal availability of cross-sectional data, the main differences between the approaches are associated with the temporal and spatial distribution of the total annual emissions. However, despite the fact that the spatial allocation of emissions differs significantly, we noticed convergence among the different approaches regarding the total annual emissions. Concerning the case of reduced temporal data availability, the differences between the variations in terms of daily traffic, are higher, mainly due to the fact that AADT and seasonal factors cannot describe extreme days. ASM showed a better performance, being able to describe more accurately the traffic variations.

Computational time and memory requirements are an issue for ASM, which limits the usage mainly to offline estimation. However, we managed to reduce the computing effort without significant affecting the quality of the results.

Additionally, we should highlight here that our results can be regarded as case specific, since the geographical and other characteristics of each segment are similar. We had a relatively accurate AADT estimation (compared to many real world cases), leading to not so high differences regarding the annual emissions. Furthermore, we used linear regression for the AADT estimation. However, Zhong et al. (2004) conclude that neural networks could have better performance. Furthermore, it would also be interesting to use emission estimates related seasonal factors, instead of the traditional flow and speed seasonal factor estimation.

Moreover, we considered constant vehicle fleet composition, and the emission factors were only depending on average speed and road type. It would be of interest in future to exploit the sensor data for a dynamic and location specific estimation of vehicle fleet composition together with the traffic estimator.

Acknowledgments

This work was supported by the Swedish Energy Agency (grant number 38921-1).

References

Aguilera, A. & Lebacque, M. (2010), Dynamic estimation of traffic emissions in metropolitan road networks. *Proceedings of the 12th WCTR,* Lisbon, Portugal.

Allström, A., Barceló, J., Ekström, J., Grumert, E., Gundlegård, D. and Rydergren, C. (2016) *Traffic Management for Smart Cities*. In Angelakis, V., Tragos, E. Pöhls, H.C., Kapovits, A., Bassi, A. (Eds) *Designing, Developing and Facilitating Smart Cities: Urband Design to IoT Solutions*, Springer International Publishing.

Allström, A., et al. (2011), Mobile Millennium Stockholm. In 2nd International *Conference on Models and Technologies for Intelligent Transportation Systems*. Leuven, Belgium.

Bai, S., Chiu, Y.-C. E., Niemeier, D. A. (2007), A comparative analysis of using trip-based versus link-based traffic data for regional mobile source emissions estimation. *Atmospheric Environment,* 41, 7512-7523.

Bai, S., Nie, Y., Niemeier, D. A. (2007), The impact of speed post-processing methods on regional mobile emissions estimation. *Transportation Research Part D: Transport and Environment,* 12, 307-324.

Basarić, V. et al. (2014), Effects of Traffic on NO 2 and PM 10 Emissions in Novi Sad.. *Polish Journal of Environmental Studies,* 23.

Batterman, S., Chambliss, S., Isakov, V. (2014), Spatial resolution requirements for traffic-related air pollutant exposure evaluations. *Atmospheric environment,* 94, 518-528.

Batterman, S., Cook, R., Justin, T. (2015), Temporal variation of traffic on highways and the development of accurate temporal allocation factors for air pollution analyses. *Atmospheric environment,* 107, 351-363.

Beevers, S. D., Carslaw, D. C. (2005), The impact of congestion charging on vehicle emissions in London. *Atmospheric Environment,* 39, 1-5.

Bezdek, J. C., Ehrlich, R., Full, W. (1984), FCM: The fuzzy c-means clustering algorithm. *Computers & Geosciences,* 10, 191-203.

Borge, R. et al. (2012), Comparison of road traffic emission models in Madrid (Spain). *Atmospheric Environment*, 62, 461-471.

Caliński, T., Harabasz, J. (1974), A dendrite method for cluster analysis. *Communications in Statistics-theory and Methods,* 3, 1-27.

Coelho, M. C. et al. (2014), Assessment of potential improvements on regional air quality modelling related with implementation of a detailed methodology for traffic emission estimation. *Science of the Total Environment,* 470, 127-137.

European Environment Agency (EEA) (2016), Air Quality in Europe -2016, Report. EEA Report No 28/201 ISBN 978-92-9213-847-9, available at https://www.eea.europa.eu/publications/air-quality-in-europe-2016.

Ferm, M., Sjöberg, K. (2015), Concentrations and emission factors for PM 2.5 and PM 10 from road traffic in Sweden. *Atmospheric Environment,* 119, 211-219.

Franco, V., Fontaras, G. Dilara, P., (2012), Towards Improved Vehicle Emissions Estimation in Europe. *Procedia - Social and Behavioral Sciences,* 48, 1304-1313.

Franco, V. et al. (2013), Road vehicle emission factors development: A review. *Atmospheric Environment*, 70, 84-97.

Fu, M., Kelly, J. A., Clinch, J. P. (2017), Estimating annual average daily traffic and transport emissions for a national road network: A bottom-up methodology for both nationally-aggregated and spatially-disaggregated results. *Journal of Transport Geography,* 58, 186-195.

Gastaldi, M., Rossi, R. Gecchele, G., Della Lucia, L., (2013), Annual average daily traffic estimation from seasonal traffic counts. *Procedia-Social and Behavioral Sciences,* 87, 279-291.

Gately, C. K . Hutyra, L. R., Peterson, S., Wing, I. S., (2017), Urban emissions hotspots: Quantifying vehicle congestion and air pollution using mobile phone GPS data, *Environmental Pollution,* 229, 496-504.

Gkatzoflias, D. Kouridis, C., Ntziachristos, L., Samaras, Z., (2007), COPERT 4: Computer programme to calculate emissions from road transport, *European Environment Agency.*

Ha, J.-A., Oh, J.-S. (2014), Estimating Annual Average Daily traffic using Daily Adjustment Factor, *Journal of emerging trends in Computing and Information Sciences,* 580.

Hartigan, J. A., Wong, M. A. (1979), Algorithm AS 136: A k-means clustering algorithm, *Journal of the Royal Statistical Society, Series C (Applied Statistics),* 28, 100-108.

Jeng, S.-T., Nesamani, K. S., Ritchie, S. G. (2013), A new approach to estimate vehicle emissions using inductive loop detector data, *Journal of Intelligent Transportation Systems,* 17, 179-190.

Jing, B. et al. (2016), Development of a vehicle emission inventory with high temporal--spatial resolution based on NRT traffic data and its impact on air pollution in Beijing--Part 1: Development and evaluation of vehicle emission inventory, *Atmospheric Chemistry and Physics,* 16, 3161-3170.

Johansson, C., Burman, L., Forsberg, B. (2009), The effects of congestions tax on air quality and health, *Atmospheric Environment,* 43, 4843-4854.

Keller, M. (2010), *Handbook of emission factors for road transport (HBEFA) 3.1,* Technical report, INFRAS.

Kholod, N. et al. (2016), A methodology for calculating transport emissions in cities with limited traffic data: Case study of diesel particulates and black carbon emissions in Murmansk, *Science of the Total Environment,* 547, 305-313.

Lindhjem, C. E., Pollack, A. K., DenBleyker, A., Shaw, S. L. (2012), Effects of improved spatial and temporal modelling of on-road vehicle emissions, *Journal of the Air & Waste Management Association,* 62, 471-484.

Muller-Perriand, K. (2014), Effects of temporal traffic data aggregation level on the estimation of air pollutant emissions using a COPERT 4 based model: application to A7 motorway (France), *Proceedings of the 5th Transport Research Arena,* Paris, France.

Namdeo, A., Mitchell, G., Dixon, R. (2002), TEMMS: an integrated package for modelling and mapping urban traffic emissions and air quality, *Environmental Modelling & Software,* 17, 177-188.

Nyhan, M. et al. (2016. Predicting vehicular emissions in high spatial resolution using pervasively measured transportation data and microscopic emissions model, *Atmospheric Environment,* 140, 352-363.

Ryu, B. Y., Jung, H. J., Bae, S. H. (2015), Development of a corrected average speed model for calculating carbon dioxide emissions per link unit on urban roads, *Transportation Research Part D: Transport and Environment*, 34, 245-254.

Trafikverket (2012), *Handbok för vägtrafikens luftföroreningar,* Kapitel 6, Emissionsdatabaser.

Treiber, M., Helbing, D. (2002), Reconstructing the spatio-temporal traffic dynamics from stationary detector data, *Cooper@ tive Tr@ nsport@ tion Dyn@ mics,* 1, 3-1.

Treiber, M., Kesting, A. (2013), Traffic flow dynamics, *Traffic Flow Dynamics: Data, Models and Simulation,* Springer-Verlag Berlin Heidelberg.

Tsanakas, N., Ekström, J., Olstam, J. (2017), Reduction of errors when estimating emissions based on static traffic model outputs, *Transportation Research Procedia,* 22, 440-449.

Wang, M., Daamen, W., Hoogendoorn, S., Van Arem, B. (2011), Estimating acceleration, fuel consumption, and emissions from macroscopic traffic flow data, *Transportation Research Record: Journal of the Transportation Research Board,* 123-132.

Wismans, L. et al. (2013), Comparison of estimation of emissions based on static and dynamic traffic assignment.. *Proceedings of the 93rd Annual Meeting of the Trasportation Research Board,* pp. Washington, D.C., USA.

Zhong, M., Lingras, P., Sharma, S. (2004), Estimation of missing traffic counts using factor, genetic, neural, and regression techniques, *Transportation Research Part C: Emerging Technologies,* 12, 139-166.

GNSS data-based approach to monitor real-world exhaust emissions at microscopic resolution

L. Thibault, P. Dégeilh, G. Sabiron, L. Voise, K. Thanabalasingam and G. Corde*

Control, Signal and System Department, IFP New Energies, Rueil-Malmaison, 92500, France
laurent.thibault@ifpen.fr

1. Introduction and Objectives

Real-world driving conditions may have a significant impact on pollutant emissions. So far, real driving emissions knowledge involves installing Portable Emissions Measurement Systems (PEMS), which are too expensive for large scale campaigns of measurement. Large-scale estimation campaigns are usually based on the use of Emissions Factors (EFs). EFs were first developed in the 1990s to achieve national inventories. They are suitable for macroscopic estimations but tend to be limited for a microscopic evaluation. The knowledge of microscopic exhaust emissions, i.e. at the level of small road segments, for large urban areas is a key challenge. It will allow cities to understand the impact of the road infrastructure and regulations and it will help to improve microscopic estimation of the air quality which is now based on the EFs. This paper describes an innovative coupling of information and communication technology and physical modelling to estimate real-world exhaust emissions at a microscopic scale, without adding any sensor to the vehicle. It consists in:

- A smartphone application[1] to measure GNSS (Global Navigation Satellite System) speed and altitude profiles of the vehicle during a trip,
- A cloud-based simulation software, coupled to the driver's smartphone, used to estimate the pollutant emissions, taking into account characteristics of each vehicle.

Real-world Driving emissions sensitivity to the driver behavior may be significant, both for NO_x emissions of Diesel engines (Fonseca, Casanova, & Valdes, 2011) due to the cut of the Exhaust gas recirculation at high load and for CO emissions of gasoline engines due to power enrichment (Samuel, Austin, & Morrey, 2002). This trend is especially true with Euro 5 Diesel engines widely used in Europe without any NO_x after-treatment. This is illustrated in Figure 1 which shows the NO_x exhaust emissions for several repetitions of the same trip, with the same vehicle, and different drivers (each bar corresponding to a driver). It clearly shows that the sensitivity to the driver behavior can be huge, and therefore that there is a potential to improve the air quality by helping the driver to understand and reduce the impact of their driving style.

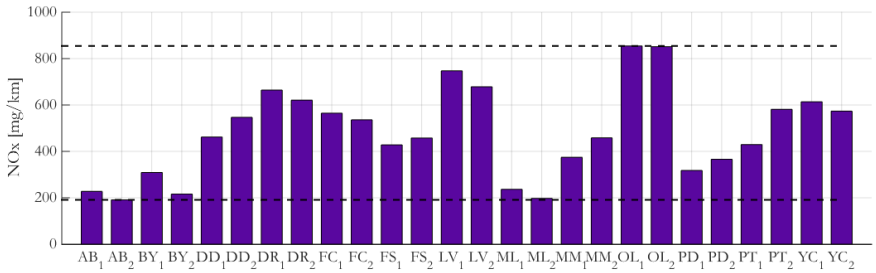

Figure 1: Illustration of the driving style impact

Smartphone applications have a high potential for affordable deployment in large-scale monitoring studies. Thus, they represent a promising solution to aggregate data of real usages and associated emissions into a large database respecting privacy: data are recorded anonymously and only the pollutant level are collected. Smartphone applications offer new opportunities to develop citizen science project in which non-scientists can meaningfully contribute to scientific research. The application benefits both to the driver, by giving a direct feedback of his/her pollutants footprint and personalized advices, and to the regulator, by providing a dynamic monitoring of real-world pollutants emissions. The application is free and interesting people download it to participate to a citizen science project.

[1] Interested readers can download the application, named Geco air, for free on the usual application stores

The two main objectives are:

- Encouraging drivers to improve their driving behavior by offering simple, practical, and personalized advice.
- Raising awareness of the highly polluting nature of some types of journey. For example, on a short journey, there is not enough time for the aftertreatment system to reach its activation temperature. In these instances, drivers are encouraged to use other transport modes.

Once the application is installed, it automatically records the speed and slope profiles of the vehicle using the smartphone GNSS. It is important to recall that these recordings are totally anonymous. The simulation software used for pollutant estimation, with a physical modelling of the vehicle, its engine and its aftertreatment, is too complex for a proper and simple integration on a smartphone. That is the reason why cloud computing is used instead. To keep a small amount of data exchanged between the smartphone and the server, pollutant calculation is made at the end of each trip. To be realistic, the pollutant models are tuned to the specifications of each vehicle, which are retrieved solely based on the license plate number, allowing an automatic tuning of the corresponding models. Indeed with the license plate number it is possible to know the vehicle identification number and then its major technical specifications. After each trip, the driver can see on a personal dashboard his/her emissions and associated driving tips.

The driver is not the only beneficiary of the project. For now, decision-makers use statistical approaches based on global averages of vehicles speeds to monitor and forecast pollutant emissions. As will be explained in part II, this approach greatly miscalculate local reality. Using smartphones as local sensors, it is possible to go a step further by allowing a representation of the fleet and its real use on a much finer mesh both spatially and temporally. The resulting database could help the stakeholders to understand what the most critical sources of pollutant emissions are on their territory, by allowing a wide variety of multi-scale studies, such as:

- Examining the suitability of infrastructure and understand the reasons for local pollutant peaks by a very local analysis.
- Improving the forecast of local phenomena (concentration of particles and nitrogen oxides) thanks to the replacement of average user scenario on a territory by feedback of *in situ* data.

2. State-of-the-Art

For a long time, the environmental impact of vehicles has only been evaluated by the means of dynamometer emission tests. The data derived from such testing is not representative of “real-world” driving conditions (Pelkmans & Debal, 2006). To deal with this issue, Portable Emissions Measurement System have been developed since the 1990s (Breton, 2000). These systems are suitable for measurements on a specific vehicle, but not for a large scale diffusion due to their cost and installation time. A way to measure indirectly real traffic emissions of vehicles is to use air quality sensors but large scale diffusion is limited as well and it is then difficult to relate the pollution to its cause.

The state of the art in terms of vehicle emissions models is made up of two large families, macroscopic and microscopic. It is important to precise that the models suitable for a large scale emissions estimation must not present prohibitive computing time or a too large number of required parameters. Among the macroscopic models, the most widespread approach consider Emission Factors (EF). Emission factors are average values that relate the quantities of a pollutant released to the atmosphere to their sources, car driving in our case. These factors are usually expressed as the mass of pollutant per kilometer. Such factors facilitate estimation of emissions from various sources of air pollution. In most cases, these factors are simply averages of all available data of acceptable quality, and are generally assumed to be representative of long-term averages for all facilities in the source category. The EF can be coupled with real Global Positioning System (GPS) data to estimate vehicle emissions (Liu, Chen, Y., & Han, 2013). The EF approach only considers average vehicles and average driving style. They are suitable for average emissions on long trips but not for real traffic emissions which needs to take into account the local impact of the infrastructure and of the driving style. Their major cause of error comes from the impact of the driving style and slope (Sentoff, Aultman-Hall, & Holmén, 2015). To take into account these phenomena, it is necessary to use a finer level of model, a microscopic model, whose input is generally a 1-Hz vehicle speed profile.

Several microscopic models already exist and the most widespread ones are the Comprehensive Modal Emission Model (CMEM) from University of California (Scora & Barth, 2006), the Passenger car and Heavy duty Emission Model (PHEM) from Graz University of Technology (Hausberger, Rodler, Sturm, & Rexeis, 2003) and the Virginia Tech Microscopic energy and emissions model (VT-Micro) from Virginia Tech (Rakha, Ahn, & Trani, 2004). CMEM is microscopic in the sense that it predicts second-by-second tailpipe emissions and fuel consumption based on different modal operations from in-use vehicle fleet. One of the most important features of CMEM is that it uses a physical, power-demand approach based on a parameterized physical approach that breaks down the entire emission process into components that correspond to the physical events associated with vehicle operation and emission production. The model consists of six modules that predict engine power, engine speed, air-to-fuel ratio, fuel use, engine-out emissions, and catalyst pass fraction. Vehicle and operation variables (e.g., speed, acceleration, and road grade) and model calibrated parameters (e.g., cold start coefficients and an engine friction factor) are model inputs. While the CMEM model was developed as a power-demand model, the VT-Micro model was developed as a regression model from experimentation with numerous polynomial combinations of speed and acceleration levels. A validation of CMEM and PHEM can be found in the literature (Rakha, Ahn, & Trani, 2003 and Nam, Gierczak, & Butler, 2003), showing a good consistency with experimental results. These microscopic models are designed for offline studies. They are often coupled with a traffic simulator such as SUMO or AIMSUN which provide the 1 Hertz speed profile. Unfortunately there is an important gap between simulated and measured speed profiles and therefore pollutant emissions (Nam, Gierczak, & Butler, 2003).

The contribution of this paper consists in coupling a microscopic model with real-world speed profile to estimate on-road pollutant emissions. However it is not possible to use the existing microscopic models for an automated large scale deployment because the input parameters of these models are not available for all vehicles. The modelling approach should be chosen according to the vehicle data available for each car. This is the major reason why it was necessary to develop new microscopic models, suited for the real-world emissions estimation of a large vehicle fleet.

3. Pollutant Emissions Modelling

A model-based approach has been chosen to estimate instantaneous pollutant emissions, namely Nitrogen Oxides (NO_x), Particulate Matter (PM), Carbon Monoxide (CO) and Carbon Dioxide (CO_2.) from the 1Hz GNSS signal of the user smartphone. It relies on mathematical equations describing physical phenomena involved in pollutants formation. A model representative of the vehicle specificities is built using a library of 0D/1D sub-system models. Each sub-model takes into account the impact of calibrations (control-unit strategies), which are essential for real-world emissions modelling. This approach is described in Figure *2*.

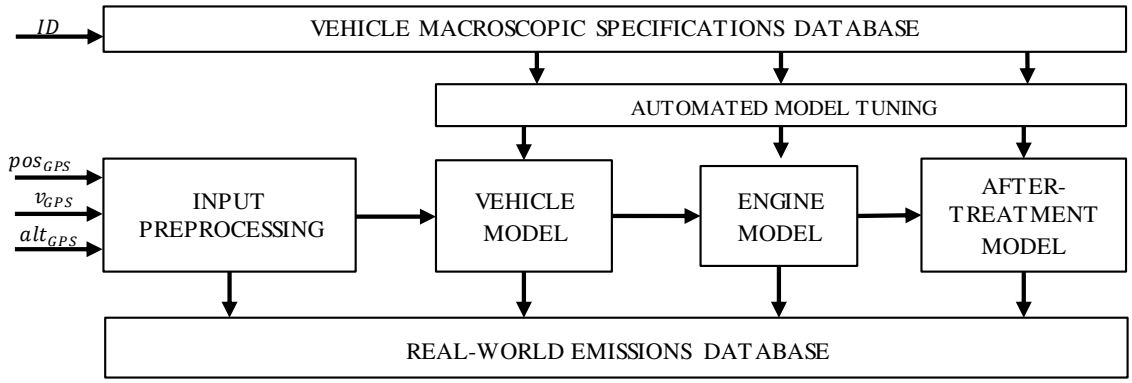

Figure *2:* Global Approach Scheme

The choice of the most suitable modelling level is a trade-off between precision, number of input parameters, and computation time. The desired models should be able to catch the impact of real-world driving conditions and allow to identify situations where pollutant emissions are particularly high or low. Moreover, the model has to be well suited to deal with inputs sampled at low rates, typically 1Hz, as provided by GNSS on most smartphones. This critical point has to be related to physics of pollutant formation which occurs during an engine cycle of only a few milliseconds typically.

An important remark is that the models are not based on the results of a standard driving cycle (such as the NEDC) which often fails to represent real on-road conditions. The models integrate realistic engine and aftertreatment calibrations, which is essential for real-world emissions modelling. The result is that on-road and on-cycle emissions can be widely different for some pollutants depending on engine and aftertreatment technologies used.

A. Vehicle Model

This model relies only on two inputs from the GNSS sensor: vehicle speed and altitude which are used to compute engine speed and torque. The core of the model is based on the longitudinal dynamics equations, which can be written as: $m\frac{dv}{dt} = F_T - F_{res} - F_{slope} - F_{brk}$, where m is the total weight of the vehicle, v the vehicle speed, F_T the traction force of the engine, F_{res} the resistive force comprising the frictions, F_{slope} the gravity force and F_{brk} the braking force. F_{res} can be expressed as a function of the vehicle speed: $F_{res} = a + bv + cv^2$, where a b and c are the coast down coefficients depending on the vehicle. F_{slope} is a function of the vehicle mass and the elevation angle α of the road: $F_{slope} = mg\sin(\alpha)$. These equations allow to compute the engine traction force and then the engine power P_e:

$$P_e = \frac{F_T * v}{\rho_{trans}} = \left(m * \frac{dv}{dt} + F_{res} + F_{slope} + F_{brk}\right) * \frac{v}{\rho_{trans}}$$

where ρ_{trans} is the transmission efficiency. At every time step the model calculates the reduction ratio between the wheel and the engine crankshaft R_{e-w} depending of v and P_e: $R_{e-w} = f(v, P_e)$. It allows to convert the speed and power from the wheel to the engine torque T_e and speed N_e at the crankshaft: $N_e = R_{e-w} * v \; and \; T_e = P_e * \frac{30}{N_e * \pi}$.

B. Hybrid electric powertrain model

In the case of a hybrid vehicle, the engine power is not directly proportional to the actual power required to move the vehicle. The power split between the engine and the electric motor is chosen by a control strategy called the energy management strategy (EMS). This strategy is modelled in our application to take into account the effects of hybridization functionalities, namely: pure electric drive, regenerative braking, and engine operations optimizations.

C. Engine Model

1) Internal physical quantities model

The first step of this model is to evaluate the internal physical quantities for the current engine operating point such as flows, temperatures or concentrations. In a second step, these quantities will then be used to estimate the pollutant emissions, as well as fuel consumption. These quantities are estimated, based on the following basic assumptions:

- Maximum torque curve and air-path architecture are known for the engine;
- Friction Mean Effective Pressure (FMEP) generic law (function of engine speed);
- Constant gross indicated efficiency;
- Fuel air equivalence ratio equal to 1 in SI engine (except at high load where it increases linearly with load), and varying between two values for CI engine;
- EGR (Exhaust gas rate) fraction is known for each point of the engine map.

These assumptions are combined in an iterative algorithm and applied for each point of the engine map to determine the Pumping Mean Effective Pressure (PMEP), to deduce gross Indicated Mean Effective Pressure (IMEP) and fuel consumption, considering the gross

indicated efficiency assumption. Thus, the iterative process is mainly aimed at computing engine fuel consumption and PMEP, which requires to compute for each engine operating point, the air mass flow rate (with equivalence ratio assumption), the exhaust temperatures (an input for the pollutant models), as well as the different pressures and temperatures in the air path. The equations used to determine fuel consumption, total intake mass flow rate, and pressure and temperature conditions in the air path are detailed in (Alix, Dabadie, & Font) for engines without EGR. These equations have been adapted for engines with EGR to improve the exhaust mass flow rate estimation given to the emission model. Basically, this adaptation ensures that: $Q_{exh} = Q_{exh,tot} * (1 - EGR)$ with Q_{exh} the exhaust mass flow rate, $Q_{exh,tot}$ the total exhaust mass flow rate coming from the cylinders and EGR the EGR fraction given for the engine operating point.

2) Engine-out emission models

The estimation of engine-out emissions is made using a physical modelling of the engine using mostly equations from the literature with some adjustments to the available data. This modelling is based on steady state assumptions (i.e. assuming stationary operations) for most parameters but transient phenomena such as the air path settling time, thermal behaviours are included using dynamic models. As stated before, the detail of these models is not the topic of the paper. However, to give an idea of the modelling level used, an example is given for the NO_x emissions of a Diesel engine. It is based on a simplification of a semi-empirical modelling coming from the literature (Gärtner, Hohenberg, Daudel, & Oelschlegel, 2004). The original model was:

$$\log(NO_x) = a_0 + a_1 * COC + a_2 * m_{cyl} + a_3 * m_{O2}$$

With NO_x the mass of NO_x per mass of fuel, COC the centre of combustion (50% energy conversion, from TDC) and m_{cyl} and m_{O2} the in-cylinder air and oxygen mass per stroke and displaced volume and a_0, a_1, a_2, a_3 model coefficients. This model was reduced in

$$\log(NOx) = a_4 + a_5 * R_{BGR}$$

where R_{BGR} is the in-cylinder burnt gas ratio, estimated with the airpath model taking into account engine calibration and the dynamics of the EGR loop. Once engine out emissions estimated, it is necessary to model the aftertreatment impact.

D. Aftertreatment Model

The developed aftertreatment model library is composed of several submodels, each of which representing a physical aftertreatment element of the exhaust line: Diesel Oxidation Catalyst (DOC), Diesel Particulate Filter (DPF), Selective Catalyst Reduction (SCR), Lean NO_x Trap (LNT), Three-Way-Catalyst (TWC) and PIPE (referring to a thermal model of a simple pipe between two elements). These elements can be arranged to describe most existing exhaust line architectures. All the submodels take the physical quantities of gas flow rate, temperature, gas composition) at the element inlet as an input and compute the same quantities at the element outlet as an output. Each variable represent the cross-section-averaged quantity at a given axial location. It is then possible to describe precisely the evolution of the gas temperature and composition through the different elements, and to estimate the tail-pipe pollutants. Going further into details, each element is in fact discretized spatially into several “slices” to account for the non-uniform axial distribution of the properties inside the element itself. This approach is fully consistent with classical models of packed-bed catalysts developed since the 1970s (Depcik & Assanis, 2005). Indeed, the elongated structure of the gas channels is such that it is fairly imprecise to represent such elements by simple CSTRs. In particular, several benefits of this approach make it necessary for our application: it leads to realistic dynamics of pollutants conversion efficiencies during heat-up phases (such as start-up and sudden accelerations) and during transient cool down phases as well (pedal release, slow driving), which would not be captured by a simple map-based model.
Other noteworthy model features included are capturing DOC light-off phenomenon, taking into account SCR and LNT control laws to compute pollutant conversion, handling of the engine shut-off for conventional vehicles and HEV.

MODEL PARAMETERS TUNING

B. Input data description

A key issue to build a representative model of a specific vehicle is to know its technical specifications. It is not possible to ask the driver to fill in all these complex and numerous specifications on a smartphone application. To solve this issue, the models are automatically tuned based on the license plate number of the vehicle. From this unique number, it is possible to get macroscopic specifications of the vehicle such as engine displacement, maximal power, vehicle mass, gearbox type, fuel type, aspiration and type of aftertreatment. The availability and the accuracy of these services vary depending on the driver location, but such databases exist in most countries.

C. Vehicle fleet segmentation

It is not possible to model the emission of a specific pollutant for every vehicle with the same equations. Therefore it has been necessary to divide the cars in circulation into several categories. Each category corresponds to a given vehicle type modelled with specific equations. A vehicle type is the combination of an engine type and a powertrain type. The engine types are obviously different for Diesel and spark-ignition engines. Engine types depend mainly on:

- Air path systems;
- Fuel path technologies;
- Aftertreatment technologies.

In addition to its engine type, each vehicle is described by a powertrain type which corresponds to the level of hybridization of the vehicle, from a conventional vehicle (ICE only) to a plug in hybrid. It allows to take into account the impact of regenerative braking, electric assistance and pure electric drive.

Inside each category, the parameters of the models are tuned specifically depending on the vehicle specifications obtained with the license plate number. When one of these physical specifications is missing, it is computed from the available ones, using physical approaches and heuristic rules inspired from engine calibration methodologies. This allows to take into account the specificity of each vehicle.

Experimental validation

Models were validated experimentally using PEMS, engine and roller test beds, on a representative sample of 28 vehicles from different technologies and emission standards.

Table 1: Experimental data used for models validation

	Seg-ment	Mass [kg]	Fuel type	AFT Device	Power [cv]	Certif.	Capacity	Engine maps	Engine test bed	Roller test bed	PEMS
1	A	850	Gasoline	-	68	€ 4	1.0L	X		X	
2	A	1020	Gasoline	-	85	€ 5	0.9L	X		X	
3	C	1204	Gasoline	-	125	€ 5	1.0L	X		X	
4	B	1050	Gasoline	-	82	€ 5	1.2L			X	
5	C	1296	Gasoline	-	140	€ 5	1.4L			X	
6	B	1150	Gasoline	-	157	€ 5	1.6L	X		X	
7	C	1250	Gasoline	-	155	€ 5	1.6L	X		X	
8	D	1430	Gasoline	-	170	€ 6	1.8L	X		X	X
9	D	1472	Gasoline	-	204	€ 6	2.0L	X		X	
10	C	1250	Diesel	EGR	85	€ 4	1.5L			X	
11	C	1300	Diesel	EGR	110	€ 4	1.6L	X	X	X	
12	A	1080	Diesel	EGR	90	€ 5	1.4L				X
13	B	1200	Diesel	EGR	90	€ 5	1.5L			X	
14	C	1300	Diesel	EGR	114	€ 5	1.6L			X	
15	C	1130	Diesel	EGR	92	€ 5	1.6L			X	

16	E	1506	Diesel	EGR	150	€ 5	2.0L				X
17	SUV	1445	Diesel	EGR	140	€ 5	2.0L				X
18	Van	1776	Diesel	EGR	140	€ 5	2.0L				X
19	SUV	1660	Diesel	EGR	163	€ 5	2.0L			X	
20	C	1350	Diesel	EGR	115	€ 6	1.5L				X
21	C	1328	Diesel	EGR + LNT	120	€ 6	1.5L				X
22	E	1522	Diesel	EGR + LNT	160	€ 6	1.6L				X
23	D	1415	Diesel	EGR + SCR	150	€ 6	2.0L	X		X	
24	C	1430	Diesel	EGR + SCR	150	€ 6	2.0L				X
25	C	1417	Diesel	EGR + SCR	150	€ 6	2.0L				X
26	C	1300	Diesel	EGR + LNT	184	€ 6	2.0L	X		X	X
27	C	1410	Diesel	EGR	140	€ 6	2.2L				X
28	E	1525	Diesel	EGR	175	€ 6	2.2L				X

Laboratory test data (here engine and roller test bed) allow to evaluate the accuracy of each submodel thanks to detailed and precise measurements given by extra sensors. In particular, it allows to evaluate separatly the accuracy of vehicle, engine, and after-treatment models. PEMS data, which only contain tail-tipe pollutants, speed and slope profiles are a good complement because they are more representative of real world conditions. As a consequence, PEMS data are used to evaluate only the global accuracy of the full model. This validation is essential to demonstrate that models take correctly into account real-world operations of the vehicle, and specific behaviors due to different control strategies between laboratory and real-world testing.

This experimental campaign of RDE tests on eight Euro 5 and 6 Diesel vehicles showed a mean precision of the models on the cumulative values of 92% for CO_2 and 82% for NOx. The details per vehicle are given in Figure 3. It is interesting to focus on the case of the vehicle 24 and 25 which have equivalent technical main specifications (Table 2) and are compared on the same itinerary (87 km RDE test). By considering different levels of efficiency of the aftertreament systems due to specific strategies, models successfully catch the specific behavior of each vehicle and the associated exhaust emissions, varying from 60 mg/km to around 400mg/km for NOx emissions. It shows that the models are able to represent the wide range of behaviors of recent Diesel vehicles in real-world situation.

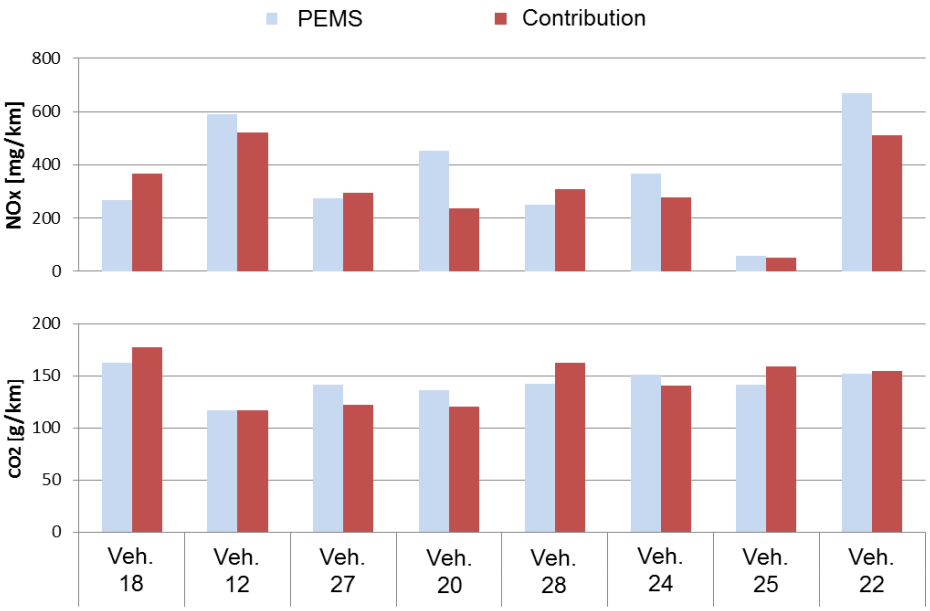

Figure 3: Estimated vs. PEMS measured NOx and CO2 emissions on 8 Euro 5-6 Diesel vehicles

In addition to being able to estimate cumulative emissions over the entire trip, the models are used to determine the instantaneous emissions at 1 Hz. Figure 4 shows an example of instantaneous performances of the fuel consumption and NOx models for an Euro 6 Diesel car.

The capture of these emissions peaks is essential for the study of the critical zones, which will be developed in the last part of this paper.

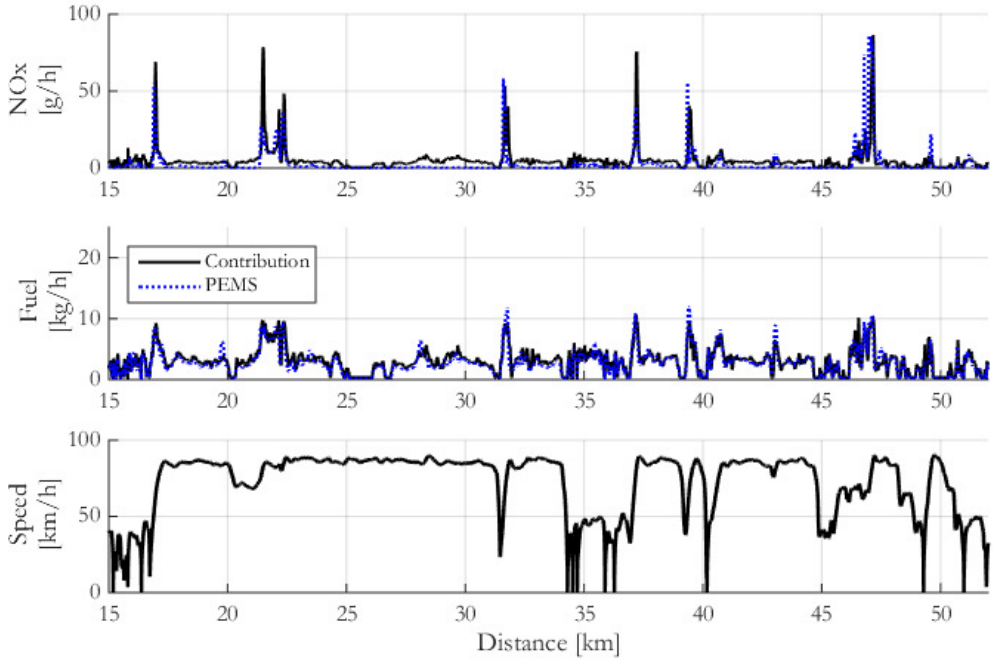

Figure 4: Example of instantaneous precision for NOx and fuel consumption – Vehicle 24 (Euro 6 2.0L 150cv)

Comparison with Emission factors on real-world driving profiles

For now the estimation of exhaust emissions of large scale fleet is mainly made using emission factors. Air quality models are based on emission factors for the contribution of traffic (Vardoulakis, Fisher, Pericleous, & Gonzalez-Flesca, 2003). This can be limited to achieve modelling at a microscopic scale. Today a lot of dispersion models claim resolution below ten meters but still use emission factors as inputs. If emission factors are quite precise at a macroscopic scale, they lead to significant errors at the scale of a road link. This is illustrated in Figure 5 which compares the contribution of this paper, microscopic modelling with measurements made with PEMS and COPERT Emissions Factors (EFs) for a Euro 6 Diesel vehicle with a SCR after-treatment. The comparison was made on road testing, in terms of instantaneous NO_x and CO_2 emissions. On the two last figures, the exhaust emissions have been aggregated on road segment of 400 meters length. EFs have been computed using the measured average speed on each segment.

The first interesting fact is that NO_x emissions can increase significantly during specific driving events such as strong acceleration or slope. The model, contribution of this paper, is able to catch this sensitivity whereas emissions factors, which are only based on the average speed are not. The estimation of CO_2 and NO_x emissions demonstrates a good precision level and reproduces the significant events responsible for pollutant emissions, while EF only give a single mean value throughout the trip. In addition to the microscopic resolution, the microscopic models allows to take into account the impact of real-world driving behaviour, accelerations and slopes. It is interesting to note that even in extra-urban conditions where the vehicle speed is quite constant, EFs can lead to significant errors due to the impact of the slope. Furthermore, the contribution allows to take into account more precisely the impact of the vehicle and its control strategy. This is a key issue for modern Diesel vehicles because of the great variability of their pollutant emissions (Franco, Sánchez, German, & Mock, 2014). Both tested vehicles are Diesel, Euro 6 2.0L with an SCR (details given in Table 2) and have therefore the same emissions factors. However their NO_x emissions are significantly different, due to different control strategies. Those strategies are taken into account by the model.

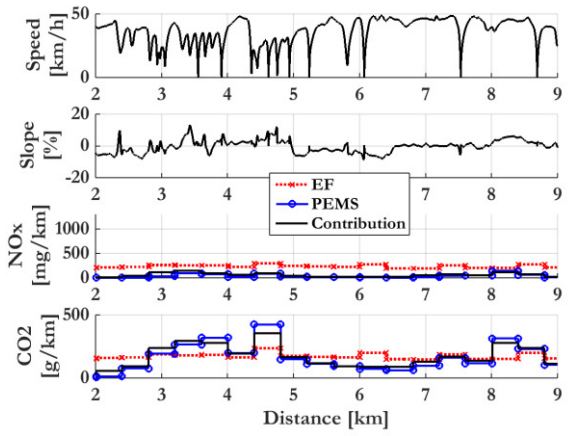

a. Urban on-road test with vehicle A

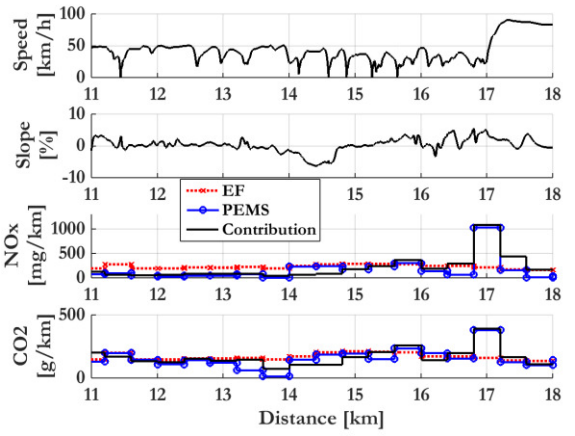

b. Urban on-road test with vehicle B

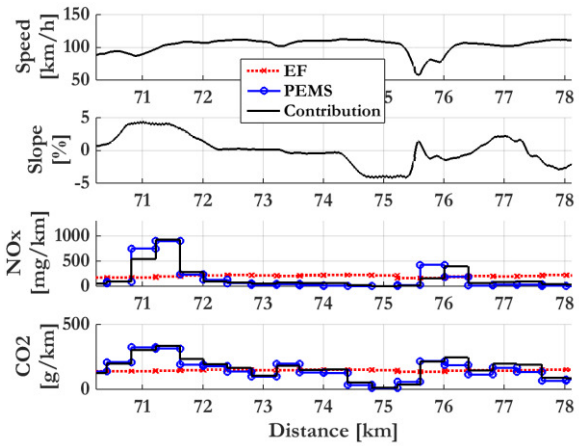

c. Extra-urban on-road test with vehicle A

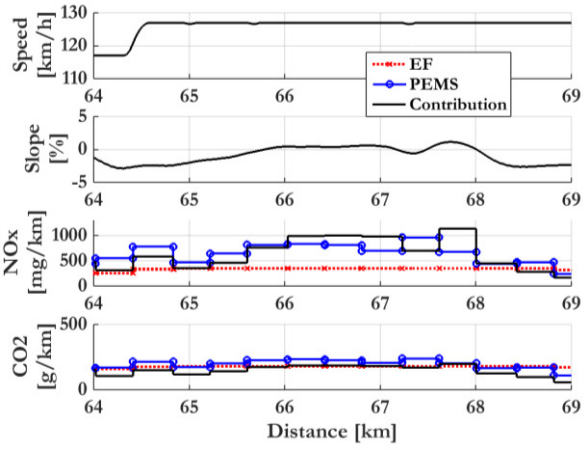

d. Extra-urban on-road test with vehicle B

Figure 5: Comparison of the microscopic emission model ("Contribution") with measurements ("PEMS"), and emission factors ("EF") for on-road tests

Table 2: Vehicle specifications

	Vehicle A	Vehicle B
Engine Type	Diesel	Diesel
Classification	Euro 6	Euro 6
Engine Displacement	2000cc	2000cc
Engine Power	150cv	150cv
Vehicle Mass	1430kg	1417kg
Aftertreatment	DOC+DPF+SCR	DOC+DPF+SCR

A new tool to give a feedback on real-world emissions

The application has been launched in the beginning of 2017 and there are 5000 active users and more than 6 million kilometers traveled. If we combine the database of the previous application (Geco, focused on CO_2 emissions) we have a total of 30 000 users and 20 millions kilometers of 1Hz real-world driving profiles. These data give a dynamic feedback of real world emissions. The purpose of this section is to show the potential of what can be achieved with this database with two examples.

Identifying real-world driver best practices

As mentioned in introduction and illustrated by Figure 1, the level of emissions is highly dependent of the driver behaviour. The objective of the smartphone application is to collect data from real-world about this different behaviour, in order to analyse good and bad practices, quantify the part of the pollutant emissions that could by avoid by a better driving style and finally give personalized advices to reach this "green" driving style.

What is a "green" driving style?

Thanks to the database of real-world driving profiles, it is possible to analyse the drivers behaviour and identify the best practices. One of the major criterion of a "green" driving style is to limit the power demand, which is generally achieved by a good anticipation and soft accelerations. Some drivers demonstrated very low emissions levels by a very contained power demand, i.e. a quite low Vehicle Specific Power (VSP) during all their trips. Figure 6 presents an example of two drivers using the same car, respectively mainly on city and extra-urban areas. It represents 1Hz operating points of the engine during their 45 last trips. Both of them are on the best driver list, and these figures show how they limit the high power demands (more than 20 kW/t) that are mainly causing emissions. Further analyses are on-going on the real-world driving database to identify specific good and bad practices associated to specific situations or locations.

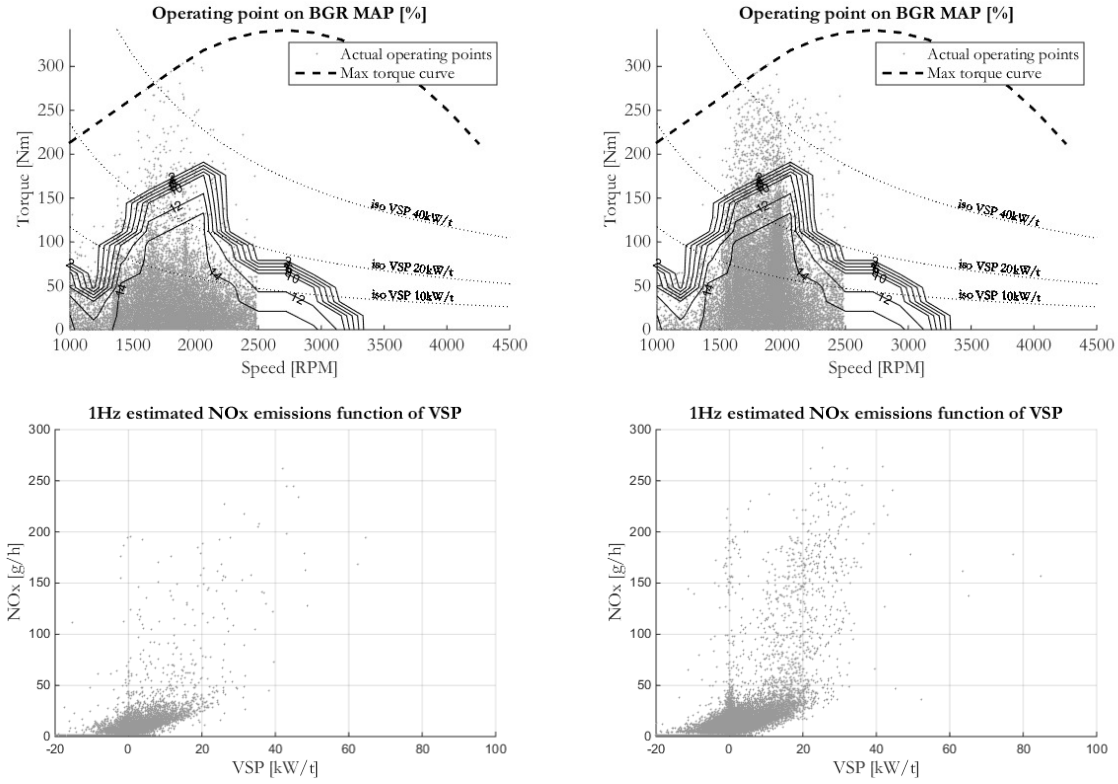

a. 45 trips, mainly city conditions

b. 45 trips, mainly extra-urban area

Figure 6: 1Hz operating points (Engine speed, torque and VSP) and NOx sensitivity

Identifying critical areas in terms of pollutant emissions

By aggregating pollutant acquisitions, a real-world emissions database is created to identify high pollutant emissions zones. Since the release of the application, 20M kilometers of real-world driving have already been recorded and it is already possible to give the first dynamic emissions maps as illustrated in Figure 7 for the city of Lyon in France.

Figure 7: Map of Lyon (France) with aggregated exhaust emissions (NO_x).

This valuable database allows to analyse finely the infrastructure impact on local pollution. Indeed, one can extract high emission roads and find a logical explanation such as important slopes, highway entrance, change in speed limitations in order to give feedback to urban planning actors.

A methodology was designed in order to process the large amount of data already available on the database:

1) The area and time window of interest are selected (multi-scale capabilities: street, city, region, country, world).
2) All trips of this area have to be fed to the vehicle model in order to process 1Hz pollutant emissions. This step is the corner stone of the micro-pollutant-estimation framework. Depending on the expected outcome, the modelled vehicle can be either, the actual vehicle used for each of the recordings, a different one or a mix of several vehicle representative of a given car fleet.
3) A map matching algorithm is applied in order to aggregate all measurements on road segments. The length of a road segment is selected according to the expected input of the study with a minimal value of ten meters.
4) Once each measurement is attached to a single road segment, a statistical analysis is performed to estimate the average emission profile on this segment for each vehicle studied. Depending on the objective of the study, if the number of measurements is not sufficient, a model can be used to estimate speed profiles from existing Geographic Information Systems (GIS) data.
5) Once again, depending on the expected outcome of the study, the average emissions of each vehicle of the study on each road segment can be multiplied by the corresponding vehicle flow to represent actual traffic and diminish spatial sampling related issues (small road segment with numerous measurements vs. large road with fewer recordings).
6) The result is a map of exhaust emissions of a given fleet with a microscopic resolution. This map takes into account all the factors influencing real world emissions, namely congestion, road slopes, driving style, traffic signs…

Two examples are given below that correspond to an acceleration zone on the highway for the first one and a positive slope area on an highway with constant speed for the latter.

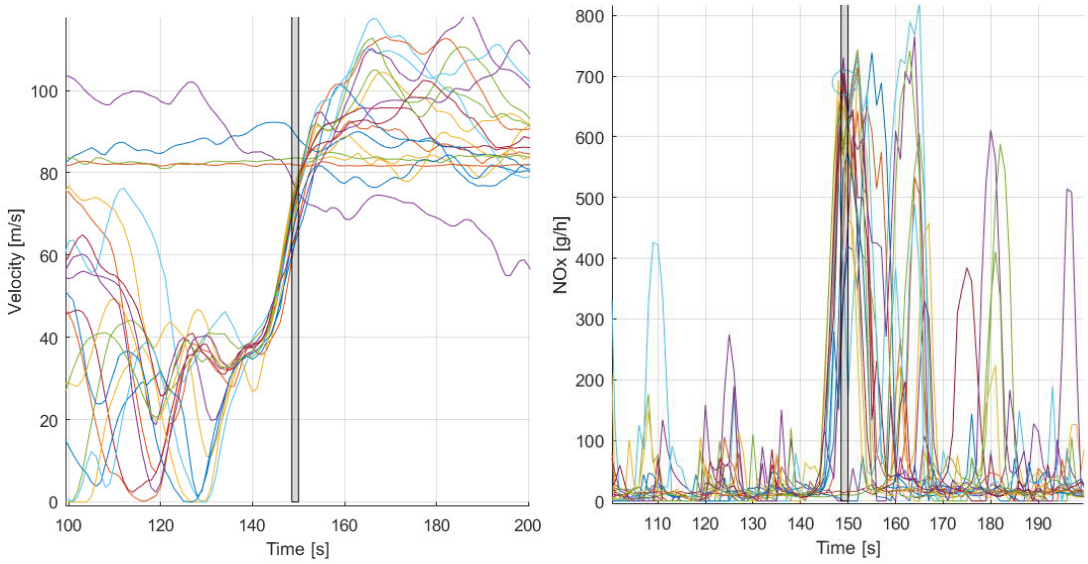

Figure 8: Velocity and NO_x profiles of all trips recorded on a road segment (lat/long 45.7197/4.936) corresponding to a highway acceleration area.

One can see that drivers already on the highway (green and red curves at 90km/h) do not generate NOx emission peak while driving at constant speed meanwhile all other drivers entering the highway and accelerating from 40 to 100 km/h generate a very high NO_x peak with high repeatability.

Secondly, with a sharp increase in the road slope around 150s, drivers maintaining their speed around 90 km/h, vehicles generate a fairly high NO_x emission peak that spreads along the area with a strong slope.

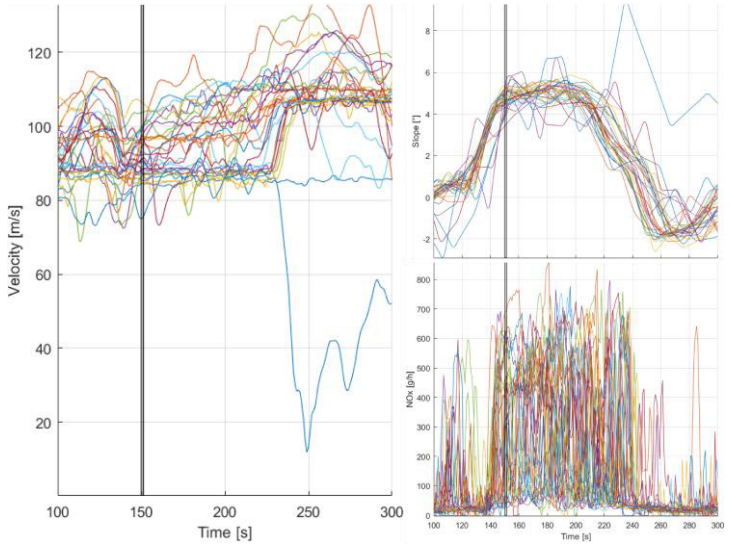

Figure 9: Velocity slope and NO_x profiles of all trips recorded on a road segment (lat/long 45.8069/4.92219) corresponding to an important slope on an highway with constant speed.

Assessment of the real-world efficiency of driving restrictions

As presented in the last section, the large scale recording of real-world driving profiles gives a feedback on the impact of the infrastructure on exhaust emissions. With the same approach, it is also possible to assess the real-world impact of driving restrictions, such as speed limits reduction, partial driving restriction and alternate-day travel. Real-world impact of such restrictions on driving conditions (measuring congestion) and exhaust emissions can thus be studied. By simulating the exhaust emissions of different car fleets, it is also possible to assess the impact of the fleet renewal.

Conclusion

Coupling real-world velocity profiles with microscopic exhaust models offers new tools to improve the knowledge of on-road pollutant emissions for a large vehicle fleet. A device, as common as a smartphone, can be turned into a virtual remote sensor of exhaust emissions. On one hand, it gives drivers the opportunity of a direct feedback on the pollutant footprint of their own mobility and personalized tips to reduce it. On the other hand, it allows a large citizen science campaign to assess and reduce real-world exhaust emissions. Indeed, each trip recorded with the application is anonymously aggregated to build a large database of real-world driving conditions with instantaneous emissions. Since the beginning of the study, 20 million kilometers of 1Hz driving profiles have been recorded with the associated GNSS coordinates. This database allows cities to identify and explain the most critical areas in terms of exhaust emissions. It is important to highlight the fact that most approaches presented in this paper can be used independently from the smartphone application and its database. A first interesting example consists in coupling the exhaust emissions models with data provided by Geographic Information Systems (GIS), which are available all around the world. Another ongoing extension of this work consists in using the microscopic emissions models to feed an atmospheric dispersion model in order to enhance Emissions Factors and achieve microscopic air quality modelling.

References

Alix, G., Dabadie, J., & Font, G. (n.d.). An ICE Map Generation Tool Applied to the Evaluation of the Impact of Downsizing on Hybrid Vehicle Consumption,. SAE Technical Paper(2015-24-2385).

Barth, M., An, F., Younglove, T., Scora, G., Levine, C., Ross, M., et al. (2000). Comprehensive Modal Emission Model (CMEM), version 2.0 user's guide. Riverside: University of California.

Breton, L. (2000, Nov 21). Patent No. 6,148,656. US.

Depcik, C., & Assanis, D. (2005). One-dimensional automotive catalyst modelling. Progress in Energy and Combustion Science, 31(4), 308-369.

Fonseca, N., Casanova, J., & Valdes, M. (2011). Influence of the stop/start system on CO 2 emissions of a diesel vehicle in urban traffic. Transportation Research Part D: Transport and Environment, 16(2), 194-200.

Franco, V., Sánchez, F. P., German, J., & Mock, P. (2014). Real-world exhaust emissions from modern diesel cars. communications, 49(30), 847129-102.

Gärtner, U., Hohenberg, G., Daudel, H., & Oelschlegel, H. (2004). Development and application of a semi-empirical NO_x model to various HD diesel engines. In Thermo-and Fluid Dynamic Processes in Diesel Engines 2 (pp. 285-312). Springer Berlin Heidelberg.

Hausberger, S., Rodler, J., Sturm, P., & Rexeis, M. (2003). Emission factors for heavy-duty vehicles and validation by tunnel measurements. Atmospheric Environment, 37(37), 5237-5245.

Liu, H., Chen, X., Y., W., & Han, S. (2013). Vehicle Emission and Near-Road Air Quality Modelling for Shanghai, China: Based on Global Positioning System Data from Taxis and Revised MOVES Emission Inventory. Transportation Research Record: Journal of the Transportation Research Board, 38-48.

Nam, E. K., Gierczak, C. A., & Butler, J. W. (2003). A Comparison of real-world and modeled emissions under conditions of variable driver aggressiveness. 82nd Annual Meeting of the Transportation Research Board. Washington, DC.

Pelkmans, L., & Debal, P. (2006). Comparison of on-road emissions with emissions measured on chassis dynamometer test cycles. Transportation Research Part D: Transport and Environment, 11(4), 233-241.

Rakha, H., Ahn, K., & Trani, A. (2003). Comparison of MOBILE5a, MOBILE6, VT-MICRO, and CMEM models for estimating hot-stabilized light-duty gasoline vehicle emissions. Canadian Journal of Civil Engineering, 30(6), 1010-1021.

Rakha, H., Ahn, K., & Trani, A. (2004). Development of VT-Micro model for estimating hot stabilized light duty vehicle and truck emissions. Transportation Research Part D: Transport and Environment, 9(1), 49-74.

Samuel, S., Austin, L., & Morrey, D. (2002). Automotive test drive cycles for emission measurement and real-world emission levels-a review. Proceedings of the Institution of Mechanical Engineers, Part D: Journal of Automobile Engineering, 216(7), 555-564.

Scora, G., & Barth, M. (2006). Comprehensive modal emissions model (cmem), version 3.01. User guide. Riverside: Centre for Environmental Research and Technology. University of California.

Sentoff, K. M., Aultman-Hall, L., & Holmén, B. A. (2015). Implications of driving style and road grade for accurate vehicle activity data and emissions estimates. Transportation Research Part D: Transport and Environment, 35, 1756188.

University, L., Astronomy, D. R., research, S. N., & KNMI Royal Netherlands Meteorological Institute, a. R. (2016, 05 11). ISPEX Project Website. Retrieved from http://ispex-eu.org/

Vardoulakis, S., Fisher, B. E., Pericleous, K., & Gonzalez-Flesca, N. (2003). Modelling air quality in street canyons: a review. Atmospheric environment, 37(2), 155-182.